

A taxonomic review of the order Mantodea in Korea based on morphology and DNA barcodes

Jaeil Shim^{1,2}, Jeong-Hun Song¹ 

¹ Department of Agricultural Biology, National Institute of Agricultural Sciences, Wanju 55365, Republic of Korea

² Department of Biology, Chungnam National University, Daejeon 34134, Republic of Korea

Corresponding author: Jeong-Hun Song (jeonghuns@korea.kr)

Abstract

A taxonomic study of Korean Mantodea using morphological and molecular characters (COI) is presented. Eight species [*Amantis nawai* (Shiraki, 1908), *Acromantis japonica* Westwood, 1889, *Mantis religiosa sinica* Bazyluk, 1960, *Statilia maculata* (Thunberg, 1784), *Tenoderangustipennis* Saussure, 1869, *T. sinensis* Saussure, 1871, *Hierodula chinensis* Werner, 1929, *H. patellifera* (Audinet-Serville, 1838)] belonging to six genera in three families are recognized. Interspecific genetic divergence of COI using uncorrected *p*-distance ranged from 6.7% to 22.4%, while intraspecific divergence ranged from 0% to 2.2% among eight Korean Mantodea species. All eight species were each strongly supported as a single lineage using COI on both neighbor-joining and parsimony trees. An illustrated key, redescriptions, habitus photographs, and illustrations of diagnostic characters of the species of Korean Mantodea are provided to facilitate identification.

Key words: DNA barcodes, Korea, Mantodea, review, taxonomy



Academic editor:

Christian Jürgen Schwarz

Received: 18 March 2024

Accepted: 10 May 2024

Published: 2 July 2024

ZooBank: <https://zoobank.org/DADFFEB5-DC8C-4A87-BA92-87C503E4F9C4>

Citation: Shim J, Song J-H (2024)

A taxonomic review of the order Mantodea in Korea based on morphology and DNA barcodes.

ZooKeys 1206: 1–43. <https://doi.org/10.3897/zookeys.1206.123355>

Copyright: © Jaeil Shim & Jeong-Hun Song.
This is an open access article distributed under terms of the Creative Commons Attribution License (Attribution 4.0 International – CC BY 4.0).

Introduction

The order Mantodea comprise approximately 2,400 species in 460 genera, making it a distinctive group of predatory insects (Ehrmann 2002; Otte et al. 2024). They exhibit remarkable diversity in morphology, hunting strategies, and habitat specialization and are widely distributed in tropical and subtropical regions (Otte et al. 2024). Members of this order are generally characterized by a carnivorous diet, mimetic behavior, triangular head, large compound eyes, raptorial foreleg with elongated forecoxa, forefemur and foretibia with characteristic spines, femoral brush for grooming, elongated pronotum, male subgenital plate (coxosternite IX), asymmetrical male genitalia, female subgenital plate (coxosternite VII), and ootheca covered by a secretion (Klass 2001; Klass and Meier 2006; Yager and Svenson 2008; Wieland 2013; Svenson et al. 2015; Hashimoto et al. 2016; Brannoch et al. 2017).

Prior to 1995, only a few entomologists had recorded four species of Mantodea on the Korean peninsula, *Mantis religiosa* Linnaeus, 1758, *Statilia maculata* (Thunberg, 1784), *Tenoderangustipennis* Saussure, 1869, and *T. aridifolia*

(Stoll, 1813) (Okamoto 1924; Bey-Bienko 1930; Doi 1932; Shiraki 1932; Cho 1959; Bazyluk 1960; Ju 1969; ESK and KSAE 1994). Kwon et al. (1996) recorded *Amantis nawai* (Shiraki, 1908), and Jeon et al. (1999) added three species, *Acromantis japonica* Westwood, 1889, *Hierodula patellifera* (Audinet-Serville, 1838), and *S. nemoralis* (Saussure, 1870), with descriptions and illustrations. Additionally, Shim et al. (2021a) reported the giant Asian mantis *Hierodula chinensis* Werner, 1929, with a diagnosis and illustrations. To date, nine species of Mantodean insects have been reported in Korea (Kim 2010, 2021; Shim et al. 2021a). While some species have been previously described, accurate identification of species within this group is challenging due to a lack of available morphological information.

In this paper, we present a taxonomic reassessment of Korean Mantodea, recognizing eight species belonging to six genera in three families, including *A. nawai* (Shiraki, 1908), *Ac. japonica* Westwood, 1889, *M. religiosa sinica* Bazyluk, 1960, *S. maculata* (Thunberg, 1784), *T. angustipennis* Saussure, 1869, *T. sinensis* Saussure, 1871, *H. chinensis* Werner, 1929, and *H. patellifera* (Audinet-Serville, 1838). Re-descriptions incorporate salient morphological features critical for accurate identification of these species, including the male genitalia. We also used molecular criteria including genetic divergence and gene tree monophyly using a COI barcode region as a multiple lines of evidence approach for the species identification. Our taxonomic review of Korean Mantodea provides redescriptions, habitus photographs, an interactive key, and diagnoses.

Materials and methods

Studied specimens were mostly collected from inland and the islands of the Korean peninsula. Specimens were collected by direct sweeping, scanning, shifting leaf litter and light trapping. If nymphs or oothecae were found, samples were reared until the adult insect emerged. The collected specimens were killed by freezing to prevent discoloration and were moved to a drying chamber for dehydration at 60 °C for 10 days until completely hardened. The subsequent sample preparation followed methods by Brannoch et al. (2017) and Shim et al. (2021b). Briefly, the male genitalia were incubated overnight in 10% potassium hydroxide (KOH), and washed with distilled water, then 75% ethanol, before storage in glycerol. Depository of specimens examined is as follows: National Institute of Agricultural Sciences Insect Collection (**NASIC**, Wanju, Korea); Kunsan National University (KsNU, Gunsan, Korea); National Institute of Biological Resources (**NIBR**, Incheon, Korea).

The specimens were examined with a stereomicroscope (MS5, Leica Microsystem, Wetzlar, Germany). Images were obtained using a Canon DSLR (EOS 5D; Tokyo, Japan) with an attached Canon MP-E 65 mm f/2.8 1–5× lens. Several layers of photographs were combined in Helicon Focus 5.3 software (Helicon Soft Ltd, Kharkov, Ukraine) and edited using Adobe Photoshop CC 2020 (Adobe, San Jose, CA, USA). Measurements were recorded in millimeters using digital Vernier calipers (CD-15APX; Mitutoyo, Saka-do, Japan). The terminology of taxonomic characters and measurements of specimens mainly followed Wieland (2013) and Brannoch et al. (2017)

for external morphology, and Klass (1997) and Schwarz and Roy (2019) for male genitalia.

The following abbreviations are used for the foreleg spination formula and male genitalia: spination formula: **Avfs** = anteroventral femoral spines; **Avts** = anteroventral tibial spines; **Ds** = discoidal spines of forefemur; **Pvfs** = posteroventral femoral spines; **Pvts** = posteroventral tibial spines. Male genitalia: **afa** = anterior process of left phallomere (phalloid apophysis); **aafa** = anterior lobe of phalloid apophysis; **fda** = posterior lobe of right phallomere; **loa** = posterior membranous lobe of left phallomere; **pafa** = posterior lobe of phalloid apophysis; **L4B** = a sclerite of left phallomere, mostly spoon-shaped; **maa** = medial arm process of right phallomere; **paa** = elongated process of left phallomere, titillator; **pia** = process arising from the midlength of the ventral wall of right phallomere, located posterolateral area of pva, strongly sclerotized; **pva** = process arising from midlength of the ventral wall of right phallomere, located anteromesal area of pia, strongly sclerotized; **sdpl** = lateral secondary distal process; **sdpm** = median secondary distal process.

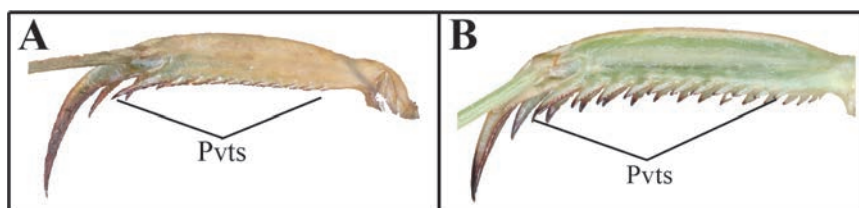
The following abbreviations are used for the provinces of Korean peninsula (Specimens examined): **GW**: Gangwon-do; **GG**: Gyeonggi-do; **CB**: Chungcheongbuk-do; **CN**: Chungcheongnam-do; **GB**: Gyeongsangbuk-do; **GN**: Gyeongsangnam-do; **JB**: Jeollabuk-do; **JN**: Jeollanam-do; **JJ**: Jeju-do (Is.).

For the study of molecular characters, we included a total of 74 specimens for DNA extraction in the dataset and the specimens used are listed in Suppl. material 1. DNA extraction, sequencing and alignments follow the methods described by Shim et al. (2021b). The mitochondrial COI was selected. Primers and amplification strategies are provided in Shim et al. (2021b). Data from GenBank for 50 foreign specimens were incorporated into the study, as indicated in Suppl. material 1. Parsimony (PA) analyses were conducted using MEGA X (Kumar et al. 2018) with 1000 bootstrap replications. A neighbor-joining analysis (NJ) was performed in MEGA X (Kumar et al. 2018) using the Kimura-2-Parameter (K2P) model (Kimura 1980). Bootstrap support values for each node were evaluated via MEGA X with 1000 replicates. Intra- and inter-specific distances in the different taxonomic levels were calculated using an uncorrected pairwise distance method (Srivathsan and Meier 2012).

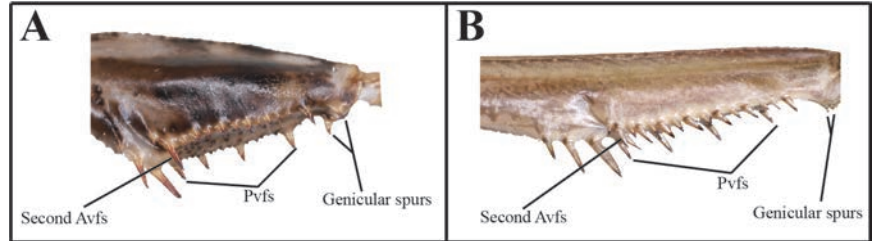
Taxonomic accounts

Key to species of Mantodea in Korea

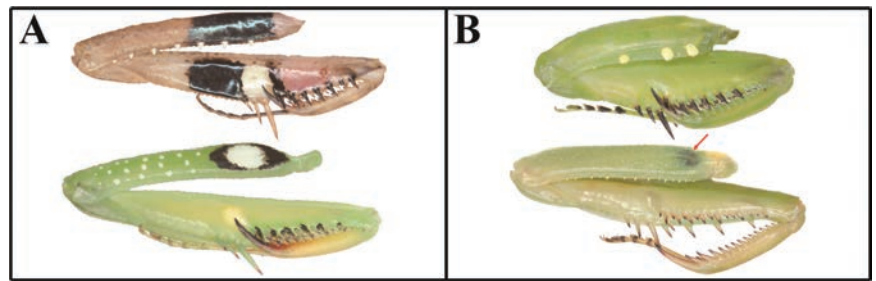
- 1 (A) Pvts fully decumbent *Acromantis japonica*
- (B) Pvts not fully decumbent 2



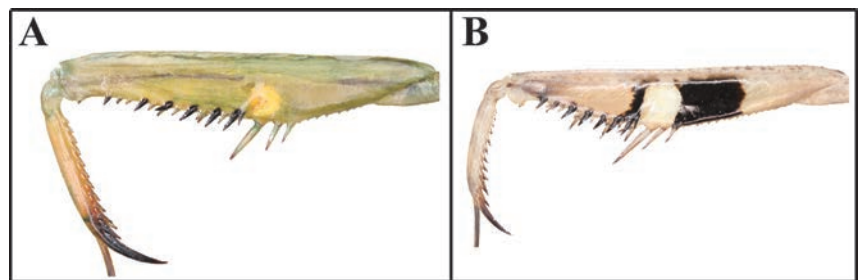
- 2 (A) Genicular spurs length as long as Pvfs; second Avfs greatly enlarged. ***Amantis nawai***
- (B) Genicular spurs length clearly shorter than Pvfs; second Avfs not enlarged **3**



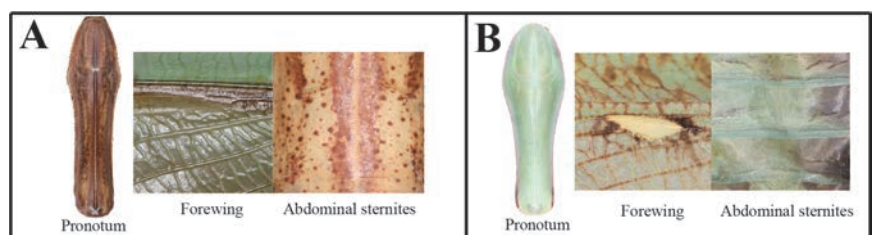
- 3 (A) Forecoxa with a distinct dark or eye spot covering ~ 1/4 to 2/5 of the total length..... **4**
- (B) Forecoxa without spot or a faint dark spot covering ~ 1/9 of the total length **5**



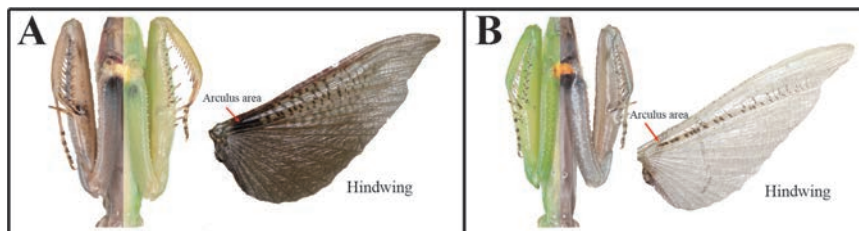
- 4 (A) Tibial spur groove only with yellow spot or no spot at all..... ***Mantis religiosa sinica***
- (B) Tibial spur groove with white spot, and dark patch either side ***Statilia maculata***



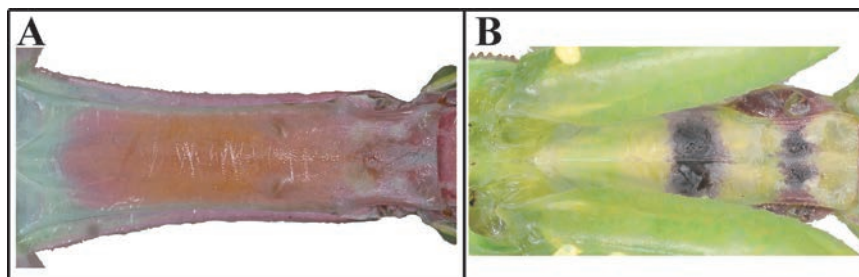
- 5 (A) Pronotum long and robust; forewing without stigma pattern; abdominal sternites with longitudinally striped pattern..... **6**
- (B) Pronotum clavate in shape; forewing with stigma pattern; abdominal sternites without striped pattern..... **7**



- 6 (A) Forecoxa base color yellow (in life); hindwing, area of arculus near cells colored dark brown, subcostal to cubitus area brown to dark brown. *Tenodera sinensis*
 – (B) Forecoxa base color orange (in life); hindwing, area of arculus near cells transparent, subcostal to cubitus area reddish *T. angustipennis*



- 7 (A) Furcasternite without pattern *Hierodula chinensis*
 – (B) Furcasternite with two-band pattern *H. patellifera*



Species descriptions

Family *Gonypetidae* Westwood, 1889
Subfamily *Iridopteryginae* Giglio-Tos, 1915

Genus *Amantis* Giglio-Tos, 1915

Cimantis Giglio-Tos, 1915: 154 (synonymized by Beier 1935: 28).
Shirakia Beier, 1935: 47.

Type species. *Mantis (Oxypilus) reticulata* De Haan, 1842.

Diagnosis. Very small sized mantises. Body with mottled dark spot pattern. Pronotum short, kite- shaped, its dorsal surface with longitudinal striped pattern. Genicular spurs length as long as Pvfs length. Second Avfs is as long as second Ds, much longer than the neighboring spines. Wings brachypterous or macropterous.

***Amantis nawai* (Shiraki, 1908)**

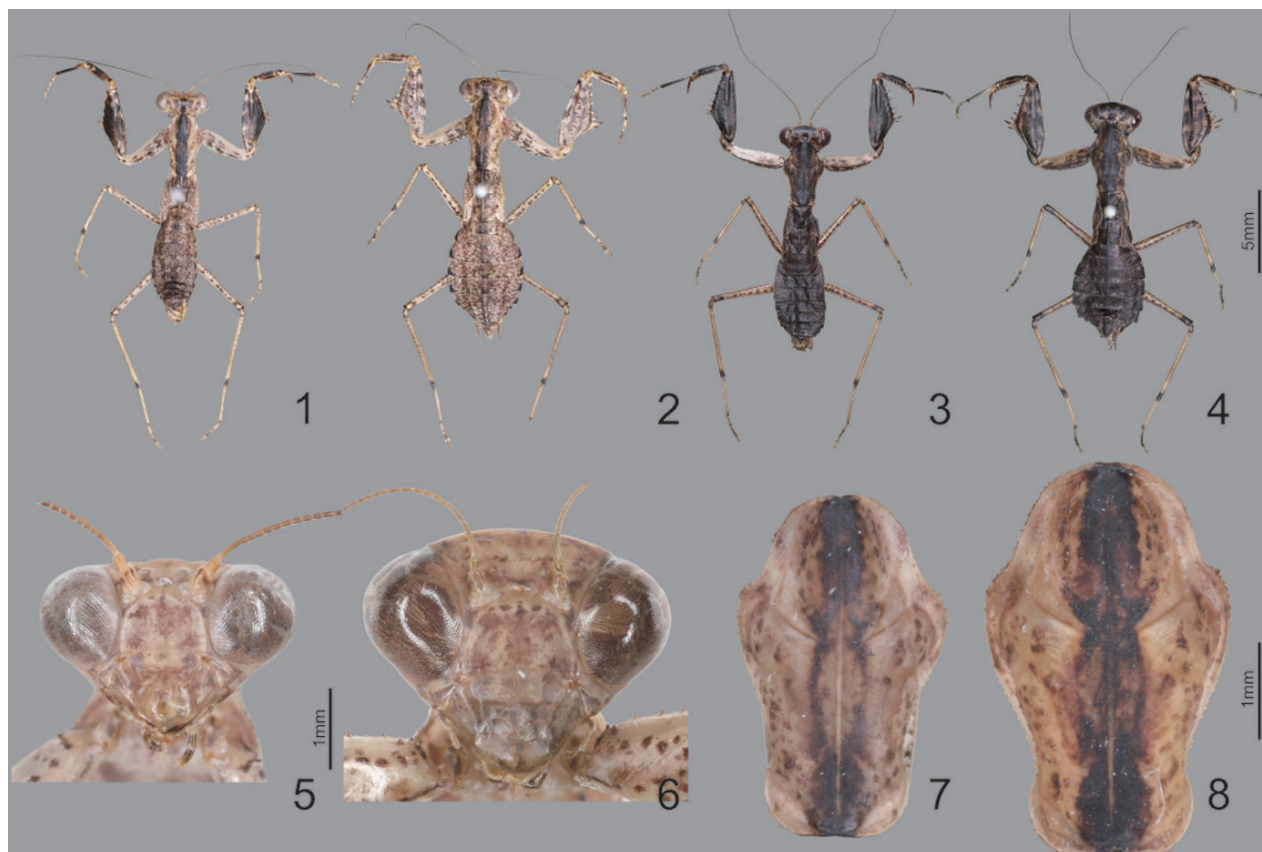
Figs 1–19

Gonypeta nawai Shiraki, 1908: 47.
Gonypeta maculata Shiraki, 1911: 318.
Amantis nawai (Shiraki, 1908): ESK and KSAE 1994: 44; Kim 2010: 31; Kim 2021: 65. Korean record.

Iridopteryx maculatus (Shiraki, 1911): Kwon et al. 1996: 221. Korean record.

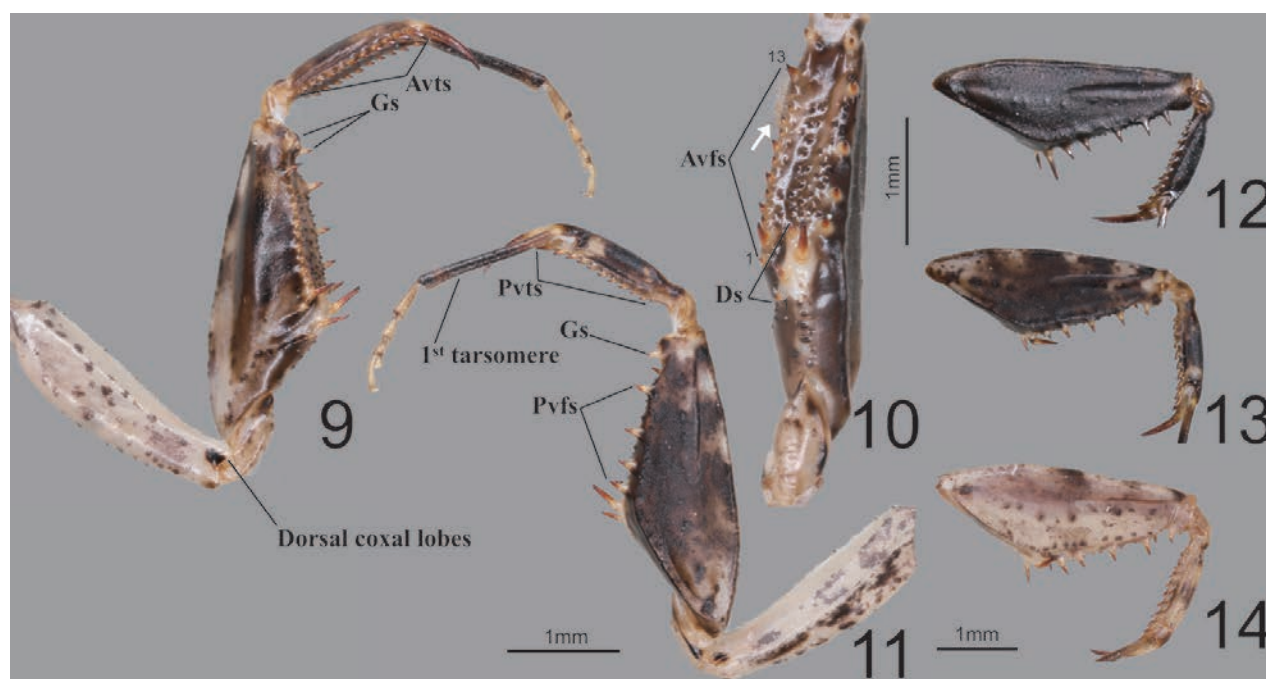
Specimens examined. [NASIC] SOUTH KOREA: GN: 1♂1♀, Mt. Noja, Dongbu-myeon, Island Geojedo, Geoje-si, 7 VIII 2019, Yeong-Hun Kim; 3♂3♀, Mt. Noja, Dongbu-myeon, Island Geojedo, Geoje-si, 7 VIII 2019, Woojin Jang; **JN:** 3♂1♀, Island Yeoseodo, Yeoseo-ri, Cheongsan-myeon, Wando-gun, 26 I 2019, Jaeil shim (reared from Ootheca); **JJ:** 1♀, Andeok Valley, Seogwipo-si, Jeju-do, X 2019, Do-yoon Kim; 2♂1♀, Donnaeko, Seogwipo-si, Jeju-do, 9 IX 2020, Yeong-Hun Kim; 3♂2♀, Seonheul-ri, Jocheon-eup, Jeju-si, Jeju-do, 19 V 2023, Jaeil Shim (reared from ootheca); 2♀, Gamsan-ri, Andeok-myeon, Seogwipo-si, Jeju-do, 23 IX 2023, Jaeil Shim; 1♀, Gamsan-ri, Andeok-myeon, Seogwipo-si, Jeju-do, X 2023, Jisung Kim; **JAPAN:** 1♂, Yanbaru, Okinawa, 1–4 I 2020, Wonjun Seong, Forest.

Redescription. Measurements (mm): Body length ♂ 12.1–13.0, ♀ 13.8–15.2; head width ♂ 2.2, ♀ 3.3; head length ♂ 2.9, ♀ 3.9; pronotum width ♂ 2.1, ♀ 2.5; pronotum length ♂ 3.3, ♀ 3.9; forewing (tegmina) length ♂♀ 1.6. **Male** (Figs 1, 3, 5, 7, 9–17). Very small sized mantises. **Coloration** (Figs 1, 3): Body color bright brown to dark brown. Body surface with irregular dark brown spots. **Head** (Fig. 5): Triangular, slightly broader than pronotum maximum width. Head length 1.3× width. Antenna filiform. Antenna nearly 3× as long as pronotum. Vertex nearly flat, posterior area (Figs 1, 3) with five dark spots. Compound eye slightly protruding, its surface glossy and brown moire pattern (in live specimens). Ocelli small, all of the same shape and size. Epistomal



Figures 1–8. Habitus, head and pronotum of *Amantis nawai* **1** male dorsal aspect (Geojedo island) **2** female dorsal aspect (Geojedo island) **3** male dorsal aspect (Jeju) **4** female dorsal aspect (Jeju) **5** male face **6** female face **7** male pronotum **8** female pronotum.

sulcus weakly concave. **Prothorax** (Fig. 7): Dorsal surface with dark brown longitudinal stripe pattern. Pronotum very short, kite-shaped, lateral margin with minute denticulation. Pronotum length 1.4× as long as maximum width. Metazone nearly 2× as long as prozone. **Forelegs (Prothoracic legs)** (Figs 9–17): Coxa and femur slightly longer than pronotum. Coxa dorsal margin (Figs 9, 11) with 9–13 minute forecoxal spines. Dorsal and ventral coxal lobes (Fig. 9) fully divided from each other; dorsal coxal lobes with dark brown spot. Femur, tibia, and first tarsomere darker than body color (Figs 1, 3, 11). Femur interior surface (Fig. 10) with numerous denticles. Genicular spurs (Figs 9, 11) well-developed, as long as Pvts length. Spination formula (Figs 9–11): Avts = 10–12; Pvts = 12–13; Avfs = 11–14; Pvfs = 4; Ds = 4. In 13 Avfs (Figs 9, 10): spines 2 and 13 larger than remaining Avfs; spines 10, 11, and 12 smallest of Avfs. **Meso- and metathoracic legs:** Meso- and metathoracic legs long and slender, apical area of tibia and first tarsomere dark brown. Tarsi 5-segmented. First tarsomere of mesotarsus subequal to combined length of remaining segments, first tarsomere of metatarsus longer than remaining segments combined. **Wings:** Brachypterous. Wing venation faded. **Abdomen:** Cerci setose, not flattened, with nine or ten segments. Male subgenital plate (coxosternite IX) (Fig. 15) nearly rhombus, inter-stylar margin slightly convex; stylus rather short. **Male genitalia** (Figs 16, 17): Right phallomere with C-shaped pva (Fig. 16); pia sclerotized and weakly wrinkled; fda distal edge margin rounded, surface with few setae. Left phallomere with short and curved paa; afa sclerotized, rectangular (slightly concave at the middle), shape of distal end variable, surface weakly granulated; Korean populations with two types of afa: dorsally curved type (Fig. 16) and posteriorly decumbent type (Fig. 17); loa mostly invisible. Ventral phallomere nearly oblong; sdpm very weakly developed; sdpl slightly expanded (digitiform), right margin of sdpl conspicuously concave. **Female** (Figs



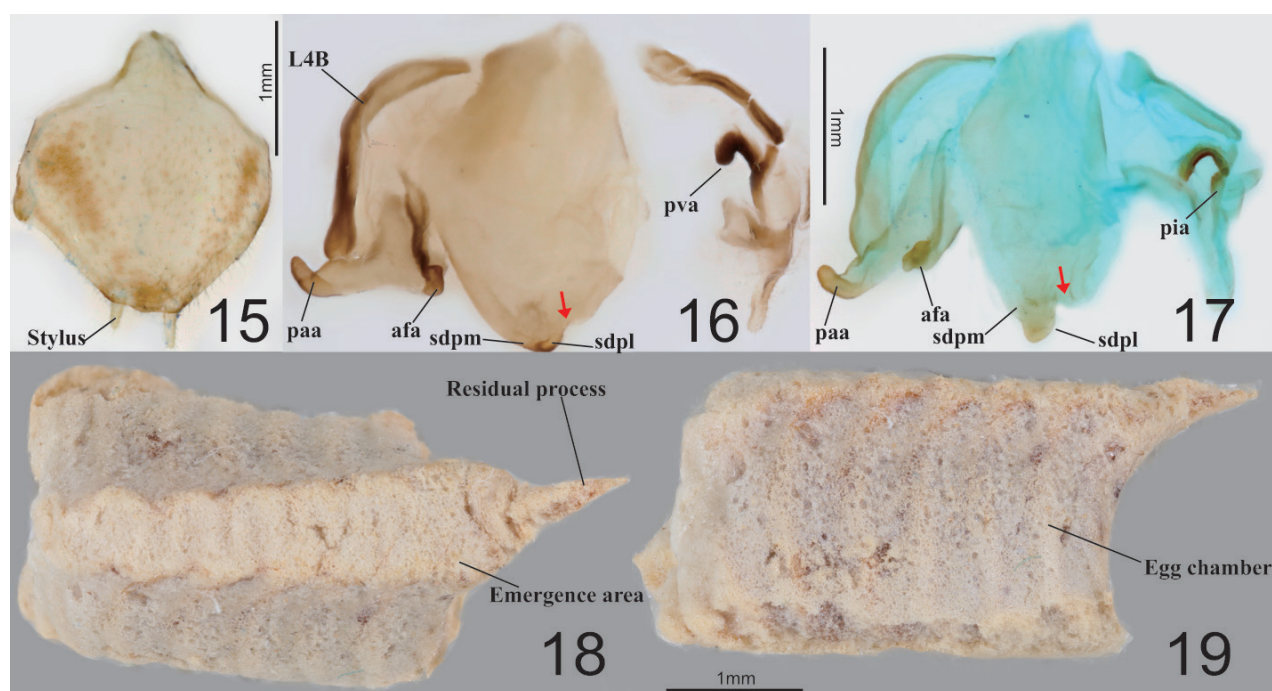
Figures 9–14. Male foreleg of *Amantis nawai* **9** ventral aspect **10** interior aspect **11** dorsal aspect **12** foreleg dorsal aspect (Jeju) **13** foreleg dorsal aspect (Geojedo island) **14** foreleg dorsal aspect (Yeoseodo island). White arrow = femoral brush.

2, 4, 6, 8). Similar to male, with following differences. **Head** (Fig. 6): length 1.2× width. Antenna nearly 2× as long as pronotum. Vertex swollen. **Prothorax** (Fig. 8): Pronotum length 1.5× maximum width. Narrowest width on posterior one-third of pronotum. **Forelegs (Prothoracic legs)** (Figs 2, 4): Femur color generally same as body color. First tarsomere distal end area dark brown. **Abdomen**: Post-lateral margin of tergite with dark brown spot. **Ootheca** (Figs 18, 19). **Measurements (mm)**: Length 3.2–5.3; width 2.8–3.4; height 2.7–3.4; length of emergence area 3.9–6.4; width of emergence area 1.0–1.6. **Identification**: Prism-shaped, triangular in cross-section. Ootheca attached by ventral surface. External wall colored russet. External coating (Figs 18, 19) beige, consisting of a very thin layer and frothy material, lateral surface and emergence area fully covered. Exhibiting ~ 4–8 egg chambers (Fig. 19). Lateral surface with longitudinal parallel ridges (boundaries). Distal end of ootheca truncate and rough. Distal flap area with long residual process (Fig. 18). **Nymph. First instar nymph**: Body surface shiny, reddish brown with brightly colored transverse pattern on body segments and legs; postero-medial edge of pro-, meso-, and metathorax tergite slightly protruding.

Biological notes. *Amantis nawai* is distributed throughout the southern islands of the Korean peninsula, as reported by Kwon et al. (1996). This species is commonly found beneath the litter layer in shaded areas and typically lays its oothecae under dead leaves or between stones on the ground. The species exhibits unique behaviors, including the vibration of its antenna and swinging of its forelegs. The first instar nymphs usually hatch between mid-June and early July, while adults emerge in mid-August.

Distribution. China, Japan, Taiwan, South Korea.

Remarks. *Amantis nawai* occurs in East Asia (Yamasaki 1981; Chou 2006; Patel and Singh 2016; Oshima 2018). Korean populations of *A. nawai* exhibit



Figures 15–19. Male genitalia and ootheca of *Amantis nawai* **15** subgenital plate **16** male genitalia (Jeju) **17** male genitalia (Yeoseodo island) **18** ootheca (dorsal aspect) **19** ootheca (lateral aspect). Red arrows = concave area.

two distinct male genitalia structures, distinguished by the ‘afa’ structure (Figs 16, 17), as well as variable forefemur color patterns (Figs 12–14). The Yeoseodo Island population features a posteriorly decumbent ‘afa’ structure (Fig. 17), and the male forefemur color matches their body color (Fig. 14). In contrast, the Geojedo and Jeju Island populations exhibit a dorsally curved ‘afa’ structure (Fig. 16), and the forefemur color of most male samples is darker than their body color (Figs 1, 3). However, there is no significant intraspecific genetic divergence (COI) between the Yeoseodo and Geojedo Island populations. Additionally, the Jeju population shows only a 0.3% divergence from the other islands.

Family Hymenopodidae Giglio-Tos, 1915

Subfamily Acromantinae Brunner de Wattenwyl, 1893

Genus *Acromantis* Saussure, 1870

Type species. *Mantis oligoneura* De Haan, 1842

Diagnosis. Small-sized mantises. Compound eye with stripe pattern (in live specimens). Anterior area of vertex and lower frons slightly protruding. Pronotum metazone middle area with flat bulge. Genicular spurs clearly shorter than the shortest Pvfs length. Pvts fully decumbent. Meso- and metathoracic femora with weakly expanded postero-ventral femoral lobe. Posterior margins of sternites with a medial lip. Hindwing apex distally truncate.

Acromantis japonica Westwood, 1889

Figs 20–33

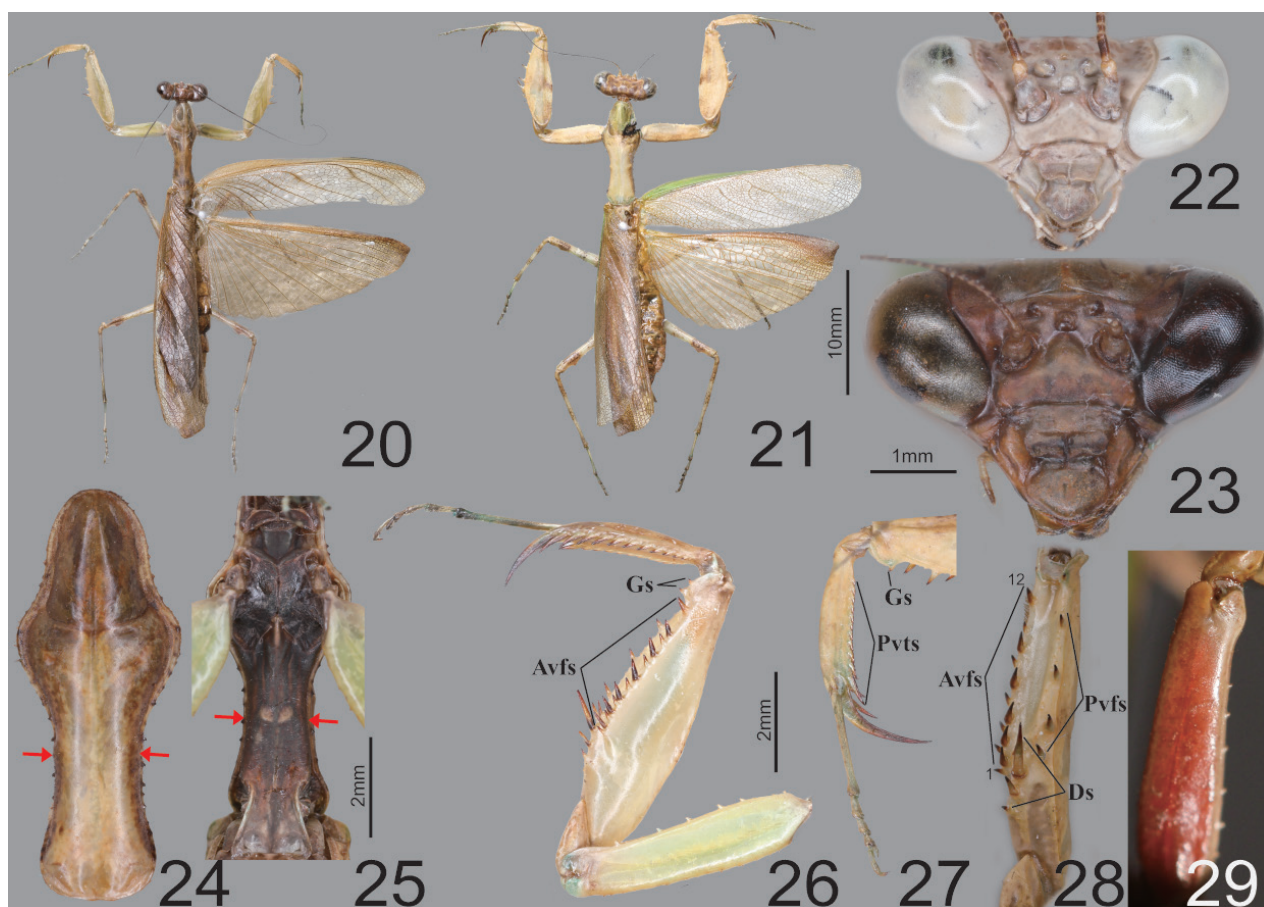
Acromantis japonica Westwood, 1889: 43.

Acromantis japonica Westwood, 1889: Jeon et al. 1999: 226 (South Korea); Kim 2021: 65. Korean records.

Specimens examined. [NASIC] SOUTH KOREA: GN: 2♀, Mt. Noja, Dongbu-myeon, Island Geojedo, Geoje-si, 10 IX 2016, Jaeil Shim; 1♂, Mt. Wangjo, Nambu-myeon, Tappo-ri, Island Geojedo, Geoje-si, 23 XII 2019, Jun-Ho Lee; 2♀, Mt. Noja, Dongbu-myeon, Island Geojedo, Geoje-si, 29 IX 2016, Byeongmin Jeong; **JN:** 3♂, Jeongdo-ri, Wando-gun, 10 I 2019, JaeDong Gim (reared from ootheca); 3♂, Jeongdo-ri, Wando-gun, 26 II 2019, Jaeil Shim (reared from ootheca); 8♂6♀, Is. Bogil-do, Bogil-myeon, Wando-gun, 2 III 2023, Jaeil Shim (reared from ootheca); **JJ:** 1♂, Mt. Sambang, Namjeju-gun, Jeju-si 28 IX 2000, Miae Kim; 1♂, Hwasun-ri, Andeok-myeon, Seogwipo-si, 12–13 IX 2023, Jaeil Shim; 8♂1♀, Sumang-ri, Namwon-eup, Seogwipo-si, 13–14 IX 2023, Jaeil Shim.

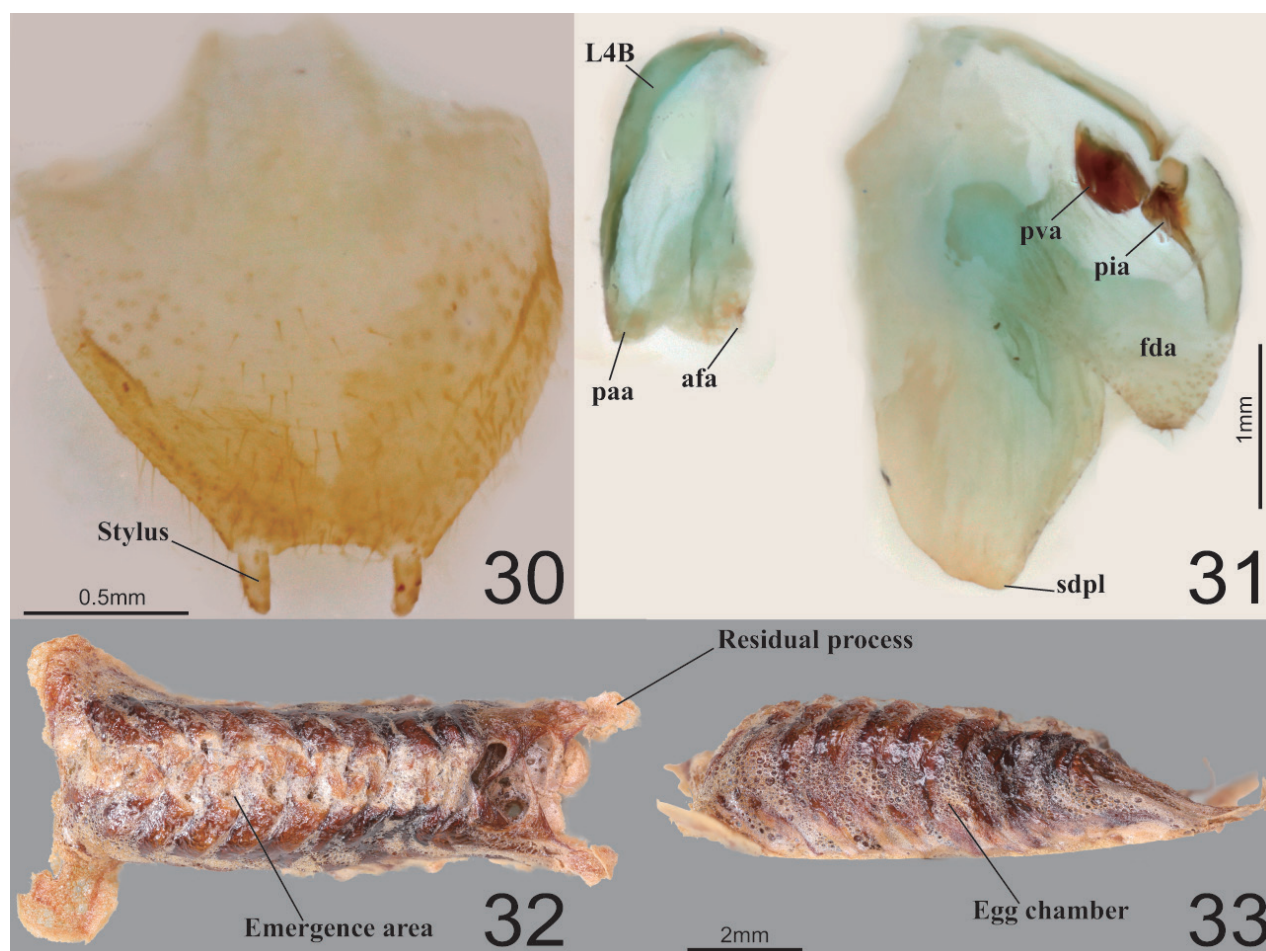
Redescription. Measurements (mm): Total length (vertex to tip of abdomen) ♂ 23.3–26.2, ♀ 28.4–32.2; head width ♂ 4.1–4.2, ♀ 5.0–5.1; head length ♂ 2.4, ♀ 3.4; pronotum width ♂ 2.6–2.7, ♀ 3.4; pronotum length ♂ 6.5–7.0, ♀ 8.2–8.4; forewing (tegmina) length ♂ 17.4–20.0, ♀ 17.0–18.5. **Male** (Figs 20, 22, 24–28, 30, 31). Small sized mantises. **Coloration** (Fig. 20): Body greenish brown to brown. **Head** (Fig. 22): Triangular; width 1.7× length. Antenna > 2× as long as pronotum. Vertex nearly flat, anterior vertex with weakly pronounced spurs. Postocellar tubercle weakly pronounced. Compound eye globular, slightly protruding laterally;

compound eye with brightly coloured moire pattern (in live specimens). Ocelli larger than female, middle ocellus nearly globular, lateral two ocelli oblong. Posterior apex of lower frons (Fig. 22) with protruding spur. **Prothorax** (Figs 24, 25): Pronotum length 2.5–2.6× maximum width. Pronotum (Fig. 24) surface smooth, lateral margin with few denticles; metazone > 2× longer than prozone; middle of metazone with flat bulge (pair); metazone lateral margin slightly concave. Furcasternite (Fig. 25) very slightly convex, middle area with flat protuberance. **Forelegs (Prothoracic legs)**: Foreleg (Figs 20, 26) surface smooth and shiny, pale green. Coxa dorsal margin with 6–10 spines. Dorsal and ventral coxal lobes (Fig. 26) fully divided from each other. Femur dorsal margin (Figs 20, 26) slightly convex at the middle, distal half of margin very slightly concave. Genicular spurs (Fig. 26) well developed, conspicuously shorter than Pvfs, postero-ventral genicular spurs weakly curved outward. Pvts (Fig. 27) fully decumbent. Spination formula: Avts = 12–13; Pvts = 12; Avfs = 10–13; Pvfs = 4; Ds = 4. In 12 Avfs (Fig. 26, 28): spines 2, 4, 6, 8, 10, and 12 size larger than remaining Avfs, dark brown. Ds 2 and 3 dark brown in live specimens. **Meso- and metathoracic legs**: Meso- and metathoracic legs with transverse dark pattern. Meso- and metathoracic femora (Fig. 20) with weakly expanded postero-ventral femoral lobe. Tarsi 5-segmented. **Wing**: Wings completely surpassing the end of abdomen (Fig. 20). Forewing cos-



Figures 20–29. Habitus, head, pronotum and foreleg of *Acromantis japonica* **20** male dorsal aspect **21** female dorsal aspect **22** male face **23** female face **24** female pronotum **25** male furcasternite **26** male foreleg ventral aspect **27** foreleg tibia and tarsus (dorsal aspect) **28** foreleg interior aspect **29** female coxa ventral aspect (live specimens). Red arrows = bulge and protuberance.

tal area bright brown or green, discoidal area brownish and transparent, cubitus brown. Forewing with oblique brown stripes. Hindwing costal area brown, discoidal area brownish and transparent; hindwing apex brown, truncate. **Abdomen:** Sternites III–VII posterior margin with a medial lip, process slightly expanded. Cerci setose, 13 segments. Male subgenital plate (coxosternite IX) (Fig. 30) irregularly rounded rhomboidal in shape, inter-stylar margin generally concave, but medial area occasionally slightly convex. Ventral surface of subgenital plate with numerous setae. Styli rather short. **Male genitalia** (Fig. 31): Right phallomere pia sclerotized and surface with few denticles; fda nearly triangular in shape, its surface with few setae. Left phallomere, paa nearly absent (very blunt); afa weakly sclerotized, and distal end bulbous; loa invisible. Ventral phallomere nearly elliptical, without any melanized structures, distal margin truncate or weakly bilobed (sdpm and sdpl may be expanded). **Female** (Figs 21, 23, 29). Similar to male, with following differences. **Head** (Fig. 23): width 1.5× length. Antenna as long as pronotum. **Prothorax:** Pronotum length 2.4× maximum width. **Forelegs (Prothoracic legs):** Foreleg dorsal surface brown, coxa ventral surface (Fig. 29) red in live specimens. **Wings** (Fig. 21): Forewing costal area color green. **Ootheca** (Figs 32, 33). **Measurements (mm):** Length 10.7–14.8; maximum width 4.3–4.8; maximum height 3.6–4.3; length of emergence area 7.8–10.4; width of emergence area 1.5–2.4. **Identification:** Nearly rectangular dorsally, hemispherical



Figures 30–33. Male genitalia and ootheca of *Acromantis japonica* **30** subgenital plate **31** male genitalia **32** ootheca (dorsal aspect) **33** ootheca (lateral aspect).

in cross-section, each edge with slightly expanded attachment area (Fig. 32). Ootheca attached on ventral surface. External wall color brown (Fig. 33). External coating bright brown but surface weakly covered. Exhibiting ~ 10–15 egg chambers (Fig. 33) clearly delimited by prominently visible curved lips. Distal end softly truncate and weakly rough. **Nymph. First instar nymph:** Body color black and surface shiny (ant mimic); compound eye with white stripes (moiré pattern); posterior margin of pro-, meso-, and metathoracic tergite with white lines; tarsus of meso- and metathoracic legs white. **Second to last instar nymph:** Body brown to dark brown with brightly colored mottled pattern; vertex spurs well developed; abdomen with expanded lamellar process (lip) in the middle of sternites.

Biological notes. *Acromantis japonica* is found in the southern islands of the Korean Peninsula (Jeon et al. 1999; An 2011). They occur in leaf litter, under broad leaves and on tree trunks. Adults exhibit positive phototaxis, and oothecae are typically laid under stones and the bark of rotten logs. This species overwinters in the egg stage inside their oothecae (Taniguchi 1987; Befu 1992). They exhibit behaviors such as vibrating their antennae and swinging forelegs. Nymphs fold their abdomens back during rest. The first instar nymphs hatch from the end of May to early June, while adults emerge beginning from the end of August.

Distribution. China, Japan, Taiwan, North Korea, South Korea.

Remarks. The genus *Acromantis* has characteristic stripe patterns on their compound eyes when they are alive (see Nakamine et al. 2017: figs 2, 3), weakly pronounced postocellar tubercles and truncated hindwings (Vyjayandi et al. 2010; Mukherjee et al. 2017; Shcherbakov and Anisyutkin 2018). They occur in East Asia to Australasia (Jeon et al. 1999; Nakamine 2016; Patel et al. 2016).

Family Mantidae Latreille, 1802

Subfamily Mantinae Latreille, 1802

Genus *Mantis* Linnaeus, 1758

Mantes Geoffroy, 1762: 399.

Type species. *Gryllus (Mantis) religiosa* Linnaeus, 1758

Diagnosis. Medium to large sized mantises. Body color mostly bright green, yellow, brown. Male antenna reddish, conspicuously thicker than the female's. Vertex swollen. Forecoxal proximal area with dark spot, ventral surface with numerous yellow spots. Tibial spur groove area with yellow spot. Furcasternite with numerous spots. Metathoracical episternum with a dark lateral spot. Male inter-stylar margin notched.

Mantis religiosa sinica Bazyluk, 1960

Figs 34–51

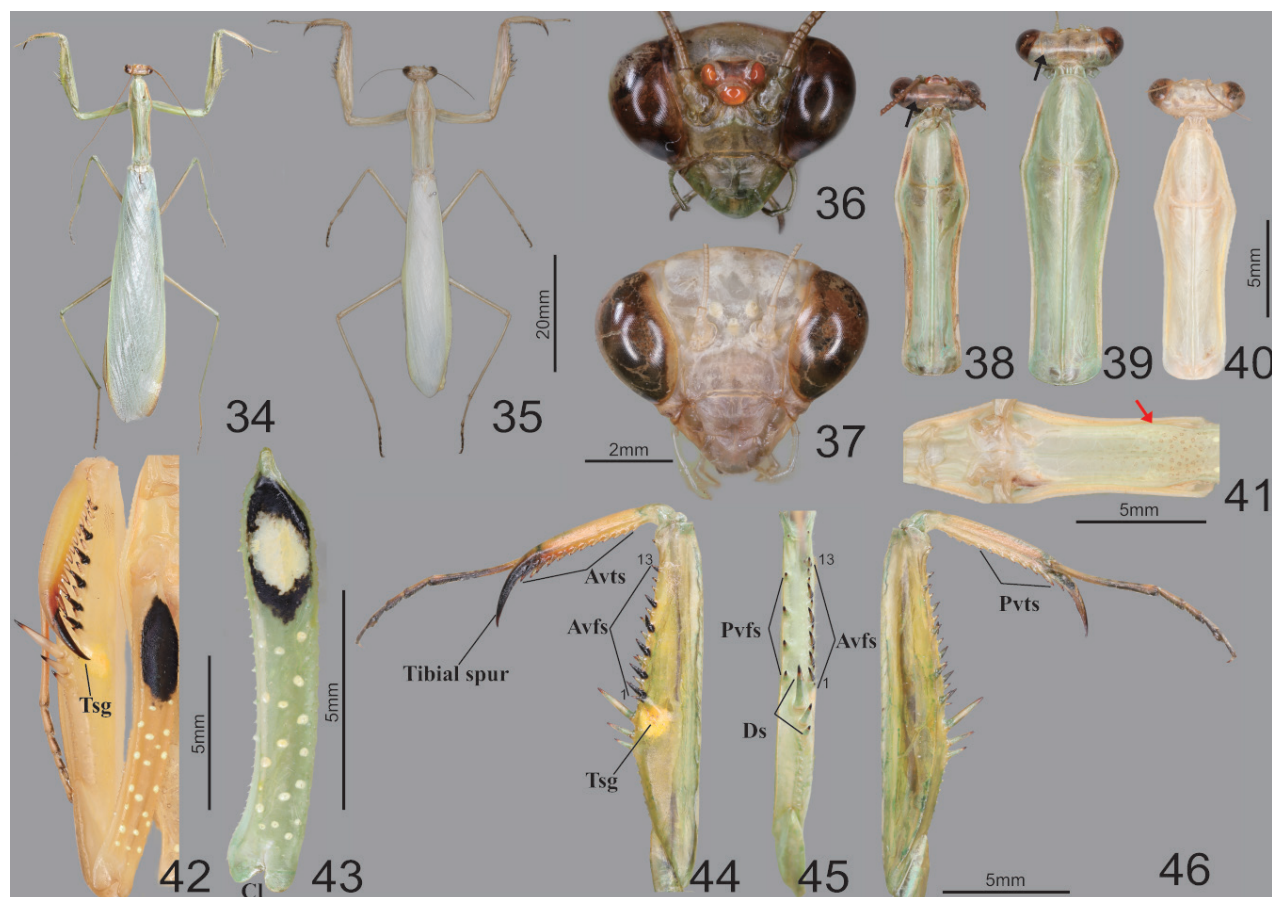
Mantis religiosa sinica Bazyluk, 1960: 255.

Mantis religiosa sinica Bazyluk, 1960: 255; Kim 2010: 31; Kim 2021: 65. Korean record.

Mantis religiosa (Linnaeus, 1758): ESK and KSAE 1994: 44. Korean record.

Specimens examined. [NASIC] SOUTH KOREA: GW: 3♂, Hotel Ramada, Daegwal-lyeong Pass, Pyeongchang-gun, 22 VIII 2019, JuHyeong Sohn; **GG:** 1♀, Jeong-gok-eup, Yeoncheon-gun, 22 VIII 84, Sunhee Jang; 1♀, Mt. Acha, Gwangjin-gu, Seoul, 8 IX 1977, Sunhee Yoon, Sungshin Univ.; 1 Nymph 1♂4♀, Island Gureopdo, Gureop-ri, Deokjeok-myeon, Incheon, 17 VII 2019, Byeongmin Jeong (reared from nymph); 2♂1♀, Island Gureopdo, Gureop-ri, Deokjeok-myeon, Incheon, 28 VI 2023, Jaeil Shim, Wonjun Sung (reared from nymph); **CN:** 1♂1♀, Coastal Dune, Sindu-ri, Wonbuk-myeon, Taeon-gun, 1 IX 2001, Haechul Park, near the grassland; 4♂6♀, Sonhwang-ri, Woongcheon-eup, Boryeong-si, 12 VII 2023, Jaeil Shim, near the grassland (reared from nymph); 2♂3♀, Coastal Dune, Sindu-ri, Wonbuk-myeon, Taeon-gun, 12 VIII 2023, Jaeil Shim, near the grassland; **GB:** 2♂, Mt. Angi, Songhyeon-dong, Andong-si, VIII 2022, Jaeil Shim; 3 Nymphs, Gyeongjeong Beach, Gyeongjeong-ri, Chuksan-myeon, Yeongdeok-gun, 20 VII 2023, Jaeil Shim; **GN:** 2♀, Mt. Noja, Dongbu-myeon, Island Geojedo, Geoje-si, 15 IX 2021, Jaeil Shim; **JB:** 1♂, Byeonsan-myeon, Buan-gun, VIII 1999, Jeonbuk Nat. Univ; 1♂, Mt. Jeok-sang, Muju-gun, 8 IX 1999, Taewoo Kim; 1♀, Kunsan Nat. Univ., Gunsan-si, 31 VIII 2019, JuHyeong Sohn; 6♂8♀, Is. Yamido, Okdo-myeon, Gunsan-si, 5 VII 2023, Jaeil Shim (reared from nymph); **JJ:** 3 Nymphs, Gwangchigi Beach, Goseong-ri, Seongsan-eup, Seogwipo-si, 16 V 2021, Jaeil Shim; **HUNGARY: *Mantis religiosa religiosa***, 1♂, Mt. Csakyar, Vertes, 23 VIII 2003, J.C. Sohn, Haraszt hegy 250m.

Redescription. Measurements (mm): Total length (vertex to tip of abdomen) ♂ 42.3–55.2, ♀ 50.8–72.4; head width ♂ 5.1–5.4, ♀ 6.2–6.5; head length ♂ 3.8–4.2, ♀ 5.4–5.6; pronotum width ♂ 4.0–4.2, ♀ 5.6–6.0; pronotum length ♂ 13.2–14.0, ♀ 16.6–18.0; forewing (tegmina) length ♂ 38.4–43.2, ♀ 36.1–47.7. **Male** (Figs 34, 36, 38, 42–49) Medium to large sized mantises. **Coloration** (Figs 34, 35): Body bright green, brown and yellow. **Head** (Fig. 36): width 1.3× length. Vertex swollen; with pale transverse magenta line along dorsal apex (in live specimens) (Fig. 38). Compound eye globular, anteriorly protruding; dorsal surface with two transverse stripes (in live specimens). Ocelli large, oval, pale yellow. Antenna filiform; pedicel, scape and initial flagellum pale, remaining flagellum orangish to reddish brown (Figs 34, 36). Antenna length > 2× as long as pronotum, conspicuously thicker than in female. Lower frons posterior apex weakly protruding; pale transverse line at posterior one-third of lower frons (in live specimens). Epistomal sulcus transverse. **Prothorax** (Fig. 38): Pronotum flattened dorso-ventrally, its length 3.3× as long as maximum width. Prozone lateral margin with small denticles. Metazone 3× as long as prozone; lateral margin smooth. Medial keel protruding. Furcaster-nite (Fig. 41) posterior area with numerous dark spots. **Forelegs (Prothoracic legs)** (Figs 42–46): Coxa dorsal margin with 6–11 spines (Fig. 43), small denticles located between its spines. Coxa ventral surface (Figs 42, 43) with large oblong black spot or eye spot in proximal area; remaining surface with 15–24 yellow spots, center of each spot with small seta. Coxal lobes fully divided from each other. Tibial spur groove (Figs 42, 44) with yellow spotted (blotch) pattern. Genicular spurs minute. Ventral surface of tibia (Fig. 44) yellow to orange. Spination formula (Figs 44, 45): Avts = 12–13; Pvts = 7; Avfs = 12–13; Pvfs = 4; Ds = 4. In 13 Avfs (Figs 44, 45): spines 2, 4, 6, 8, 10, 12 and 13 larger and black, spines with black spot at the base. Tarsus with ventral area brownish. **Meso- and metathorax and legs:** Metathorax episternum (Fig. 47) with dark triangular spot. Meso- and metathoracic legs long and slender;



Figures 34–46. Habitus, head, pronotum and foreleg of *Mantis religiosa sinica* **34** male dorsal aspect **35** female dorsal aspect **36** male face **37** female face **38** male pronotum **39** female pronotum (inland) **40** female pronotum (Gureopdo island) **41** furcasternite **42** foreleg ventral aspect (live specimens) **43** coxa ventral aspect **44** foreleg ventral aspect **45** foreleg interior aspect **46** foreleg dorsal aspect. Abbreviation: Tsg = tibial spur groove. Red arrows = dark spots of furcasternite.

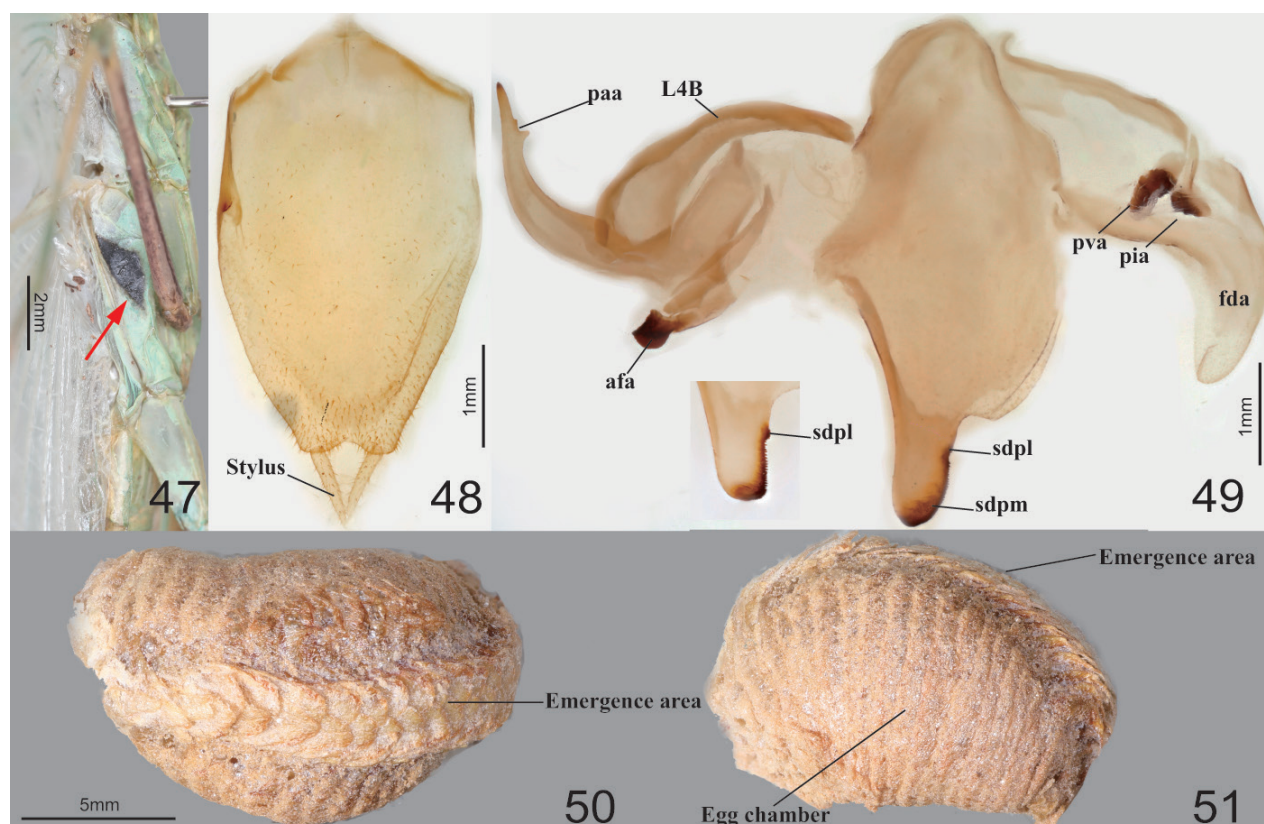
tarsi 5-segmented. **Wings:** Forewing completely surpassing the end of abdomen. Stigma elongate, slightly protruding; color same as forewing venation. Forewing anterior margin brown, discoidal area mostly hyaline. Hindwing transparent but apex brownish. **Abdomen:** Cerci setose, elongated, and thick, not flattened, brown; 17 segments. Male subgenital plate (coxosternite IX) (Fig. 48) irregularly elliptical in shape, inter-stylar margin notched in V-shape. Styli rather long. **Male genitalia** (Fig. 49): Right phallosome smooth, forming a C-shaped pva; pia sclerotized and weakly wrinkled; fda triangular. Left phallosome with elongate and curved paa, its distal end sharp and sclerotized, paa anterior margin one-fourth to one-third with one or two short projections; afa strongly sclerotized, rounded, anterior margin obliquely curved dorsally, surface granulated; L4B curved spoon-shaped. Ventral phallosome (Fig. 49) nearly rhomboidal; sdpm elongated, blunt finger-like and slightly curved dorsally, distal end and right margin sclerotized and surface with numerous denticulation; sdpl slightly protruding (blunt projection). **Female** (Figs 35, 37, 39, 40). Similar to male, with following differences. **Head** (Fig. 37): Vertex convex. Head width 1.1× as long as length. Antenna as long as pronotum. **Prothorax** (Figs 39, 40): Pronotum length 2.9–3.0× as long as maximum width. Metazone 2–3× as long as prozone. **Ootheca** (Figs 50, 51). **Measurements (mm):** Length 17.2–25.1; maximum width 11.4–14.3; maximum height 9.3–10.5;

length of emergence area 17.0–21.6; width of emergence area 3.2–5.3. **Identification:** Oblong, nearly hemispherical in cross-section. External wall bright brown to brown (Fig. 50). External coating beige on egg chamber surface, pale on emergence area (flap). Exhibiting ~ 20–30 egg chambers (Fig. 51) clearly delimited by visible slightly curved lips. Distal end of ootheca narrowed into residual process; residual process attached to substrate. **Nymph. First instar nymph:** Body brown, vertex dorsal apex with pair of dark spots. **Mid to last instar nymph:** In brown morph, dorsal surface of body with a few stripes.

Biological notes. *Mantis religiosa sinica* is sparsely distributed on the Korean Peninsula. This species prefers broad grasslands and bushy areas, comprised of shrubs and grass in sandy fields as its habitat. It exhibits positive phototaxis, meaning it is attracted to light. When threatened, it makes a hissing sound by rubbing its hindwings against the abdomen. The first instar nymphs hatch from the end of May onwards while the adults emerge in August.

Distribution. China, Japan, South Korea.

Remarks. *Mantis religiosa* (Linnaeus) is a widely distributed Palearctic and Holarctic species (Lia 2007; Patel and Singh 2016; Otte et al. 2024). Bazyluk (1960) and Roy (1968) provided illustrations of the sdpm variations and Schwarz and Roy (2019) presented figures of male genitalia. Additional morphological information was provided by Ehrmann and Borer (2015), Shcherbakov and Anisyutkin (2018), and Shcherbakov and Govorov (2020). Bazyluk (1960) classified this species as the subspecies *M. religiosa sinica*, which is



Figures 47–51. Metathorax, male genitalia and ootheca of *Mantis religiosa sinica* **47** metathorax episterum **48** subgenital plate **49** male genitalia (small box = variation of sdpl) **50** ootheca (dorsal aspect) **51** ootheca (lateral aspect). Red arrow = dark pattern.

found in East Asia including Korea. The population on Gureopdo Island exhibits a shorter pronotum, smaller body size, and shorter forewing length compared to inland populations. However, there are minimal genetic differences in the partial COI regions (0%–0.2%). Furthermore, all specimens were supported as a single lineage using COI on both NJ and PA trees (Fig. 138).

Genus *Statilia* Stål, 1877

Type species. *Pseudomantis nemoralis* Saussure, 1870

Diagnosis. Medium sized mantises. Vertex nearly flat. Pronotum slender. Ventral surface of foreleg shiny, densely patterned, forcoxa proximal area with dark pattern. Tibial spur groove with whitish yellow to yellow spots. Male inter-stylar margin notched. Male genitalia: sdpl and sdpm well developed, angled at 90°.

Statilia maculata (Thunberg, 1784)

Figs 52–70

Mantis maculata Thunberg, 1784: 61.

Pseudomantis haanii Saussure, 1871a: 37, 1871b: 400.

Statilia maculata var. *hyalina* Giglio-Tos, 1927: 410.

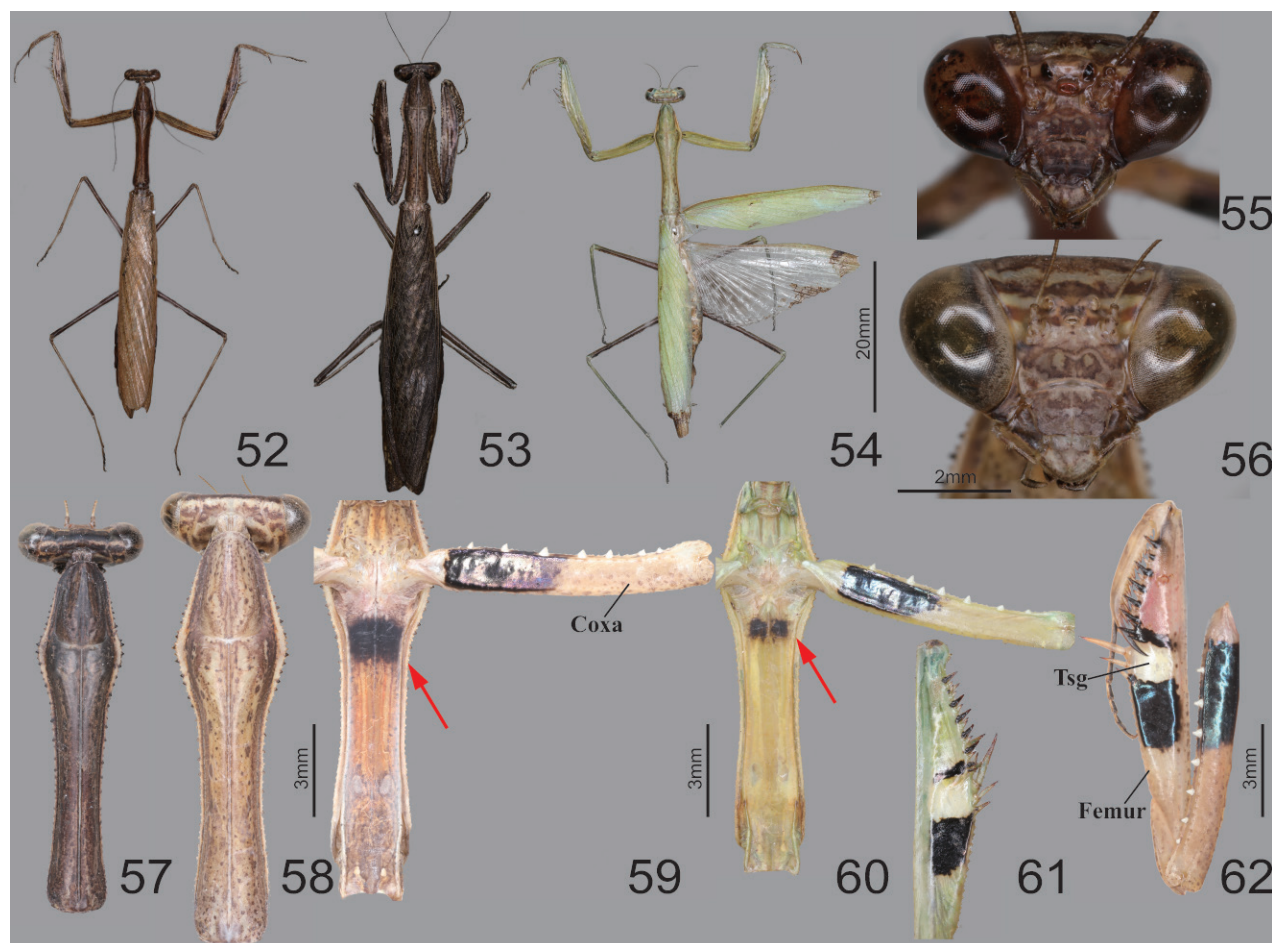
Statilia haani var. *major* Werner, 1922: 154.

Statilia maculata continentalis Werner, 1935: 495.

Statilia maculata (Thunberg, 1784): ESK and KSAE 1994: 44; Kim 2010: 31; Kim 2021: 65. Korean record.

Statilia nemoralis (Saussure, 1870): Jeon et al. 1999: 227 (misidentification); Kim 2010: 31 (misidentification). Korean record.

Specimens examined. [KsNU] SOUTH KOREA: **CN:** 1♂, Mt. Bongsoo, Dae-chung-myeon, Yesan-gun, 18 V 2017 Hongjoon Choi; **JB:** 1♀, Eunpa Lake, Jigok-dong, Gunsan-si, 3 IX 2016; Donghwan Na; 1♀, Miryong-dong, Gunsan-si, 27 VI 2017, Eunhye Jeon; [NASIC] SOUTH KOREA: **GW:** 1♂, Ssangyong, Yeongwol-gun, 30 IX 1999, Miae Kim; **GG:** 1♀, Mt. Umyeon, Seocho-gu, Seoul, 1 IX 1991, Jiyung Oh; 1♀, Jamsil 6-dong, Songpa-gu, Seoul, 20 X 1997, Soyeon Kim; 1♀, Mt. Nam, Hada-ri, Heungcheon-myeon, Yeosu-si, 3 IX 2000, Yeongbo Lee; 1♀, Seodun-dong, Suwon-si, 4 IX 2000, Taewoo Kim; 1♂, Seodun-dong, Suwon-si, 20 IX 2000, Taewoo Kim; 1♂, Seodun-dong, Suwon-si, 20 IX 2001, Jeonghun Hwang; 1♂, Haguidong, Uiwang-si, 24 IX 2003, Jeongsun Lee; 1♂, Mt. Gwanggyo, Jang-gu, Suwon-si, 10 X 2003, Mikyeong Ahn; **CB:** 1♀, Mt. Nam, Cheongju-si, 8 VIII 2000, Hyea Lee; 1♂, Geumseok-ri, Geumwang-eup, Eumseong-gun, 14 IX 2019, Seong-Gyu Lee; **CN:** 1♂1♀, Coastal Dune, Sindu-ri, Wonbuk-myeon, Taean-gun, 1 IX 2005, Yeongbo Lee; **GB:** 1♀, Mt. Sobaek, Punggi-gun, 5 IX 2000, Miae Kim; 1♂3♀, Mt. Angi, Songhyeon-dong, Andong-si, VIII 2022, Jaeil Shim; 2♂6♀, Hotel Interburgo, Manchon-dong, Suseong-gu, Daegu-si 29 X 2023, Jaeil Shim; **GN:** 1♂, Sinhyeon-ri, Geoje island, Geoje-si, 11 IX 2002, Miae Kim; 2♂1♀, Mundong Waterfall, Geoje-si, 19 IX 2006, Miae Kim; ♀1 (green), Recreational Forest, Dongbu-myeon, Geojedo, Geoje-si, 29 IX 2020, Wonjun Sung; **JB:** 2♂4♀,

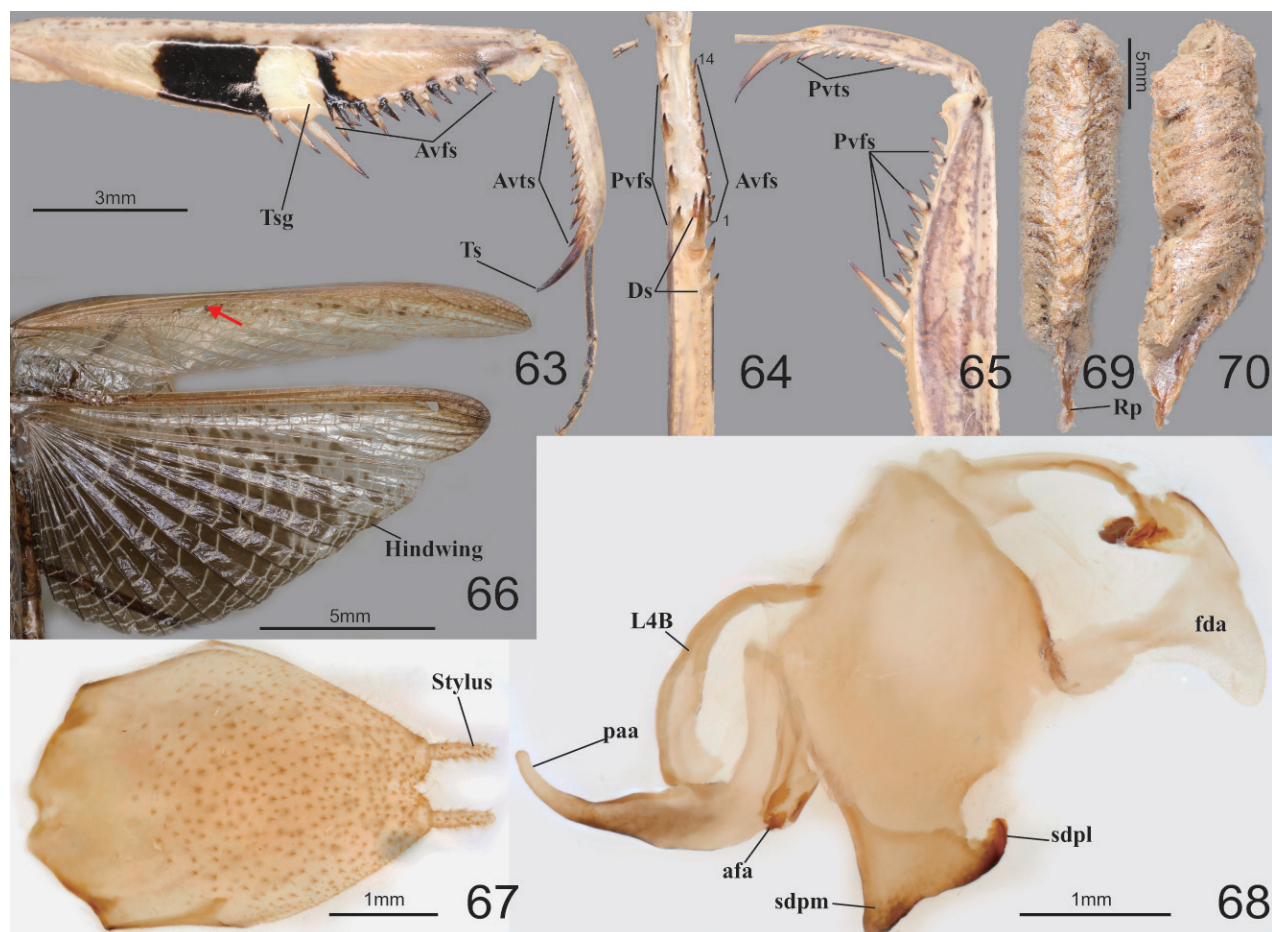


Figures 52–62. Habitus, head, pronotum and foreleg of *Statilia maculata* 52 male dorsal aspect 53 female dorsal aspect 54 female dorsal aspect (green morpho-type) 55 male face 56 female face 57 male pronotum 58 female pronotum 59 furcasternite (brown morpho-type) 60 furcasternite (green morpho-type) 61 femur ventral aspect (green morpho-type) 62 foreleg ventral aspect (live specimens). Abbreviation: Tsg = tibial spur groove. Red arrows = dark spot of furcasternite.

Gueok, Yongjin-myeon, Wanju, 13 VIII 2013, Hanjun Bae; 1♂, Iseo-myeon, Wanju-gun, 26 VII 2016, Taeman Han; 1♀, Iseo-myeon, Wanju-gun, 29 VII 2014, Kyusuk Lee; 1♂1♀, Apartment, Iseo-myeon, Wanju-gun, 6 VIII 2015, Kyusuk Lee; 1♀ (green), National Institute of Agricultural Sciences, Iseo-myeon, Wanju-gun, 24 VIII 2016, Hyeop Lee; 1♀, Miryong-dong, Gunsan-si, 27 VI 2017, Eunhye Jeon; 2♂, Iseo-myeon, Wanju-gun, 23 VIII 2019, Jaeil Shim; 1♂2♀, Mt. Moak, Gui-myeon, Wanju-gun, 7 IX 2019, Jaeil Shim; 7♂5♀, Jangsu-eup, Jangsu-gun, 5 IX 2019, Jaeil Shim; **JN**: 3♀, Geumgok-dong, Buk-gu, Gwangju-si, 20 III 2021, Jaeil Shim; 4♀, Near Yeosu Airport, Sinpung-ri, Yulchon-myeon, Yeosu-si, IX 2021, Byeongmin Jeong; 2♂1♀, Is. Bogil-do, Bogil-myeon, Wando-gun, 2 III 2023, Jaeil Shim (reared from ootheca); 8♂9♀, Island Yeoseodo, Yeoseo-ri, Cheongsan-myeon, Wando-gun, VI 2023, Jaeil Shim (reared from Ootheca); **JJ**: 1♂, Seonheul-ri, Jeju-si, 28 IX 2000, Taewoo Kim; 1♂, Sinae 1-ri, Jeju-si, 18 X 2001, Mikyeong Ahn; 1♂, Bijarim Forest, Jeju-si, 22 IX 2006, Miae Kim; **JAPAN**: 1♂, Asakura, Kyushu, 24 VIII 2013, Sangwook Park; **[NIBR] SOUTH KOREA**: **GG**: 1♀, Namhansanseong, Seongnam, 28 IX 1997, Jeong Yun Chang.

Redescription. Measurements (mm): Total length (vertex to tip of abdomen) ♂ 35.2–43.1, ♀ 43.7–57.7; head width ♂ 4.5–5.0, ♀ 5.4–5.8; head length ♂ 2.9–3.2, ♀ 4.1–4.3; pronotum width ♂ 2.9–3.2, ♀ 4.4–4.6; pronotum length ♂ 12.1–

14.0, ♀ 14.0–15.3; forewing (tegmina) length ♂ 26.4–31.2, ♀ 33.1–36.1. **Male** (Figs 52, 55, 57, 63–68) Medium sized, body slender. **Coloration** (Figs 52, 53): Beige to dark brown. **Head** (Fig. 55): Triangular. Head width 1.5–1.6× length. Vertex flat; dark transverse stripe on dorsal apex. Vertex and juxtaocular bulge with sparse, pale, transversely striped pattern. Compound eye large, globular, protruding laterally; in live specimens, dorsal and lateral surface with two brightly colored lines. Ocelli large, oblong. Antenna filiform, slightly longer than pronotum. Lower frons posterior apex protruding very slightly. Epistomal sulcus slightly concave. **Prothorax** (Fig. 57): Pronotum slender, narrow; length 4.1–4.3× as long as maximum width; dorsal surface smooth. Pronotum lateral margin with numerous denticles. Medial keel protruding. Metazone 3× as long as prozone. Membranous area between basis of forecoxa attachment, shiny and pinkish pearl in color (in live specimens). Furcasternite (Fig. 59) anterior area with rectangular dark spot, remaining posterior area reddish brown to magenta. **Forelegs (Prothoracic legs)** (Figs 62–65): Coxa very slender, triangular; dorsal margin (Figs 59, 62) with 6–8 white spines; proximal area of ventral surface (Fig. 59) with large and shiny rectangular black spot. Coxal lobes divided from each other. Femur ventral surface shiny, with two black spots (Figs 62, 63), large rectangular spot preceding the tibial spur groove, linear spot (transverse line) distad to tibial spur grooves; tibial spur groove (Fig. 63) with white or whitish yellow pattern; distal area of ventral surface (Fig. 62) pale pink to magenta (in live specimens). Spination formula: Avts = 11; Pvts = 6–7; Avfs = 14; Pvfs = 4; Ds = 4. Tarsomere ventral surface (euplantula) dark brown. Basal rim of Pvts with dark spot. In 14 Avfs (Figs 63, 64): spines 2, 4, 6, 8, 10, 12, and 14 larger in size than remaining Avfs; spines 1, 2, 4, 6, 8, 10, 12, and 14 black, with small dark spot at the base. **Meso- and metathoracic legs**: Tarsi 5-segmented. **Wings** (Fig. 66): Forewing completely surpassing the end of abdomen. Stigma elongate, slightly protruding. Hindwing costal area reddish brown; discoidal area with darkish smoky mottled pattern but cross veins clearly transparent. **Abdomen**: Cerci setose, not flattened, brown, with 14 segments. Male subgenital plate (coxosternite IX) (Fig. 67) irregular rhomboidal, inter-stylar margin deeply notched in V-shape. Styli rather long. **Male genitalia** (Fig. 68): Right phallomere forming a V-shape pva; pia sclerotized and weakly wrinkled; fda triangular. Left phallomere with elongate and curved paa, surface smooth, distal end blunt and slightly swollen; afa sclerotized, small and irregularly rough, surface weakly granulated; L4B C-shaped. Ventral phallomere (Fig. 68) irregular rhomboidal; sdpm sclerotized, wide triangular; sdpl anteriorly curved hook-shaped with blunt apex, margin between sdpm and sdpl flat or slightly concave. **Female** (Figs 53, 56, 58, 59). Similar to male, with following differences. **Coloration** (Fig. 53): Body and forewing color beige to dark brown. **Head** (Fig. 56): width 1.3× as long as length. Antenna 2× longer than prozone length. **Prothorax** (Figs 58): Pronotum length 3.1–3.3× as long as maximum width. **Green morphotype female** (Figs 54, 60, 61). **Prothorax**: Rectangular black spot (Fig. 60) of furcasternite absent or very weakly developed, remaining posterior area greenish. **Forlegs (Prothoracic legs)** (Figs 60, 61): Tibial spur grooves (Fig. 61) with rectangular pale spotted pattern. Distal area of femur ventral surface pale pink or green. **Wings** (Fig. 54): Hindwing transparent or anal area with few mottled dark spots. **Ootheca** (Figs 69, 70). **Measurements (mm)**: Length 20.4–28.9; maximum width 6.1–10.2; maximum height 6.4–8.3; length of emergence area 15.3–24.2; width of emergence area



Figures 63–70. Foreleg, wings, male genitalia and ootheca of *Statilia maculata* **63** foreleg ventral aspect **64** foreleg interior aspect **65** foreleg dorsal aspect **66** wings **67** subgenital plate **68** male genitalia **69** ootheca (dorsal aspect) **70** ootheca (lateral aspect). Abbreviation: Ts = tibial spur Tsg = tibial spur groove. Red arrow = stigma.

2.2–3.5. **Identification:** Fusiform in shape, nearly hemispherical in cross-section. Proximal end with medial elevation of emergence area. Ootheca attached by its ventral surface. External wall bright brown. External coating weakly covering lateral zone of emergence area; beige in color. Exhibiting ~ 25–50 egg chambers clearly delimited by visible prominently oblique lips (Fig. 70). Distal end of ootheca narrowed into residual process, greatly elongated, and attached to substrate. **Nymph. First instar nymph:** Body dark brown, leg with few brightly colored stripes. **Mid to last instar nymph:** Forefemur distal area (pale pink to magenta) covered by mottled black or brown spots.

Biological notes. *Statilia maculata* is found throughout the Korean Peninsula. This species has shown a remarkable adaptability to urban and suburban environments, and is often observed on building walls and streetlights, exhibiting positive phototaxis. They are known to deposit their oothecae under stones and in cracks of tree bark. Notably, *S. maculata* is capable of producing a hissing sound by rubbing its hindwings and abdomen together. This species typically hatches in early June, with adults emerging in the middle of August.

Distribution. China, Japan, Nepal, South Korea, Taiwan. Invasive in Eastern USA and Russia.

Remarks. *Statilia maculata* is predominantly found in the eastern Palearctic regions (*S. maculata* has also been introduced to Eastern USA and Russia),

whereas *S. nemoralis* is described from the Philippines and, erroneously, from various Southeast Asian countries (Ehrmann 2002; Patel and Singh 2016; Schwarz et al. 2018). These two species, with *S. nobilis* (Brunner de Wattenwyl, 1893), are frequently confused in the taxonomic literature, leading to numerous misidentifications (see details in Schwarz et al. 2018); for example, both *S. nobilis* and *S. maculata* have been erroneously reported as *S. nemoralis* (Wang 1993; Jeon et al. 1999; Oshima 2017; Schwarz et al. 2018; Oshima 2020; Shcherbakov and Govorov 2020). Notably, the green morph is relatively uncommon in female *S. maculata* (Fig. 54) but prevalent in both sexes of *S. nobilis* and *S. nemoralis* (Zhu et al. 2012; Ehrmann and Borer 2015; Schwarz et al. 2018).

Jeon et al. (1999) initially reported *S. nemoralis* in Korea based on two female specimens lacking black spots on the furcasternite. Differences in the male genitalia, specifically the margins of the sdpl and sdpm, are reliable for distinguishing between *S. maculata* and *S. nobilis* (Schwarz et al. 2018). On the other hand, the lack of a black spot on the furcasternite is a common feature of the green morph of *S. maculata*. The occurrence of the Philippine *Statilia nemoralis* is continental SE Asia needs confirmation. Subsequent examinations revealed that the specimens initially identified by Jeon et al. (1999) as *S. nemoralis* were, in fact, misidentifications of *S. maculata*.

Subfamily Tenoderinae Brunner de Wattenwyl, 1893

Genus *Tenodera* Burmeister, 1838

Mantis (*Tenodera*) Burmeister, 1838: 534.

Paratenodera Rehn, 1903: 705.

Type species. *Mantis fasciata* Manuel, 1797

Diagnosis. Large sized mantises. Male body slender, female robust. Ventral surface of forefemur patterned with minute spots. Area between forecoxae attachment point of yellow to orange in color. Hindwing with dark mottled pattern. Abdominal sternites with yellowish longitudinal stripes at middle. Male genitalia: aafa and pafa well developed, pafa spoon- or blade-shaped; loa elongate (Jensen et al. 2010).

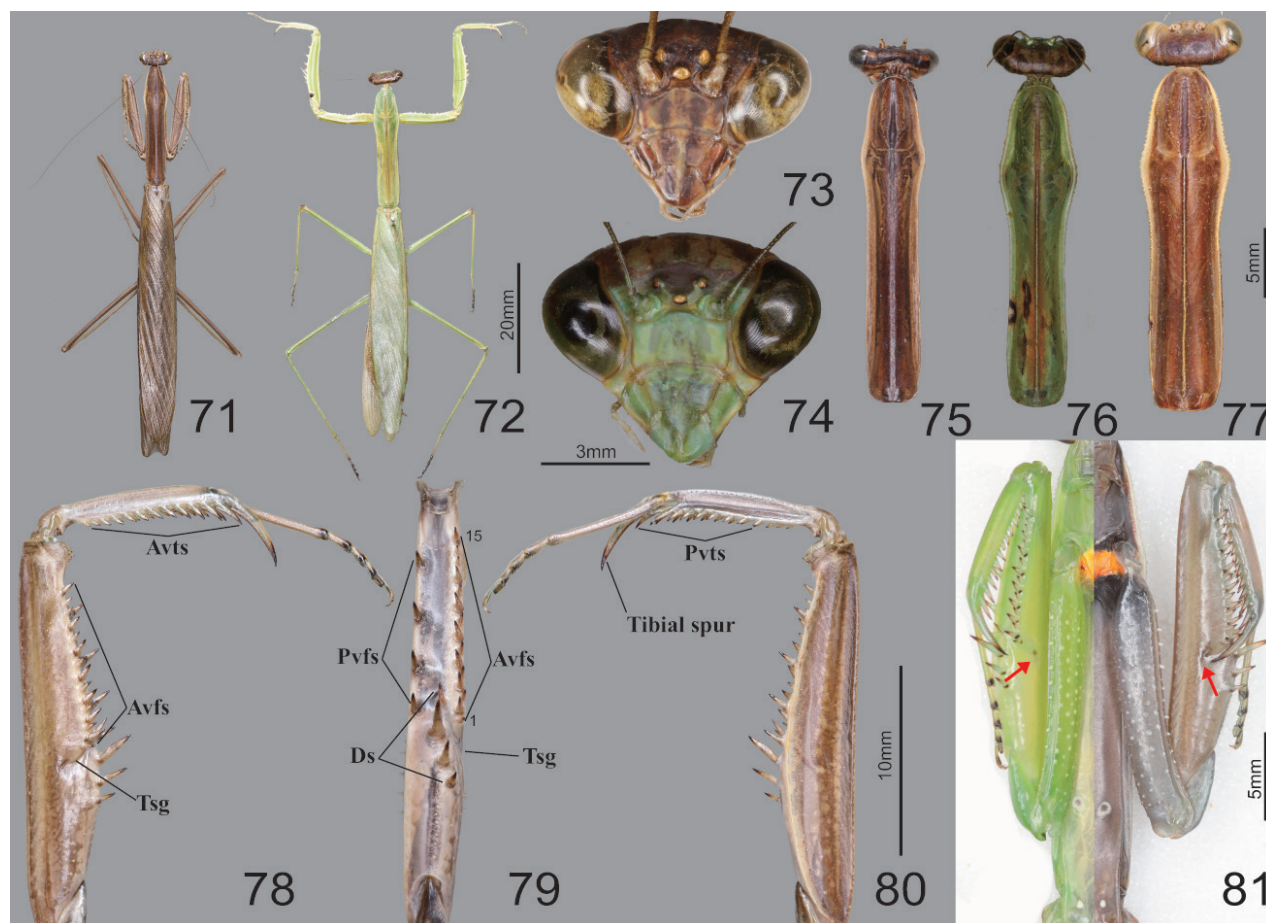
Tenodera angustipennis Saussure, 1869

Figs 71–87

Tenodera angustipennis Saussure, 1869: 69.

Tenodera angustipennis Saussure, 1869: ESK and KSAE 1994: 44; Kim 2010: 31; Kim 2021: 65. Korean record.

Specimens examined. [KsNU] **SOUTH KOREA:** **JB:** 1♀, River Geumgang, Gunsan-si, 15 IX 2012, Hyojoong Kim, near the river mouth; 1♂, Kunsan Nat. Univ., Gunsan-si, 15 X 2015, Soyeon Kim; 1♀, Eunpa Lake, Gunsan-si, 10 V 2016, Si-hyun Kim; 1♀, Kunsan Nat. Univ., Gunsan-si, 20 VIII 2017, Juyeong Oh; [NASIC] **SOUTH KOREA:** **GW:** 1♂, Songjuk Coastal area, Ganseong-eup, 19 IX 2001, Miae Kim; **GG:** 1♂, Gaepo-dong, Seoul, 1 IX 1991, Hyeonjeong Jo; 2 Nymphs,



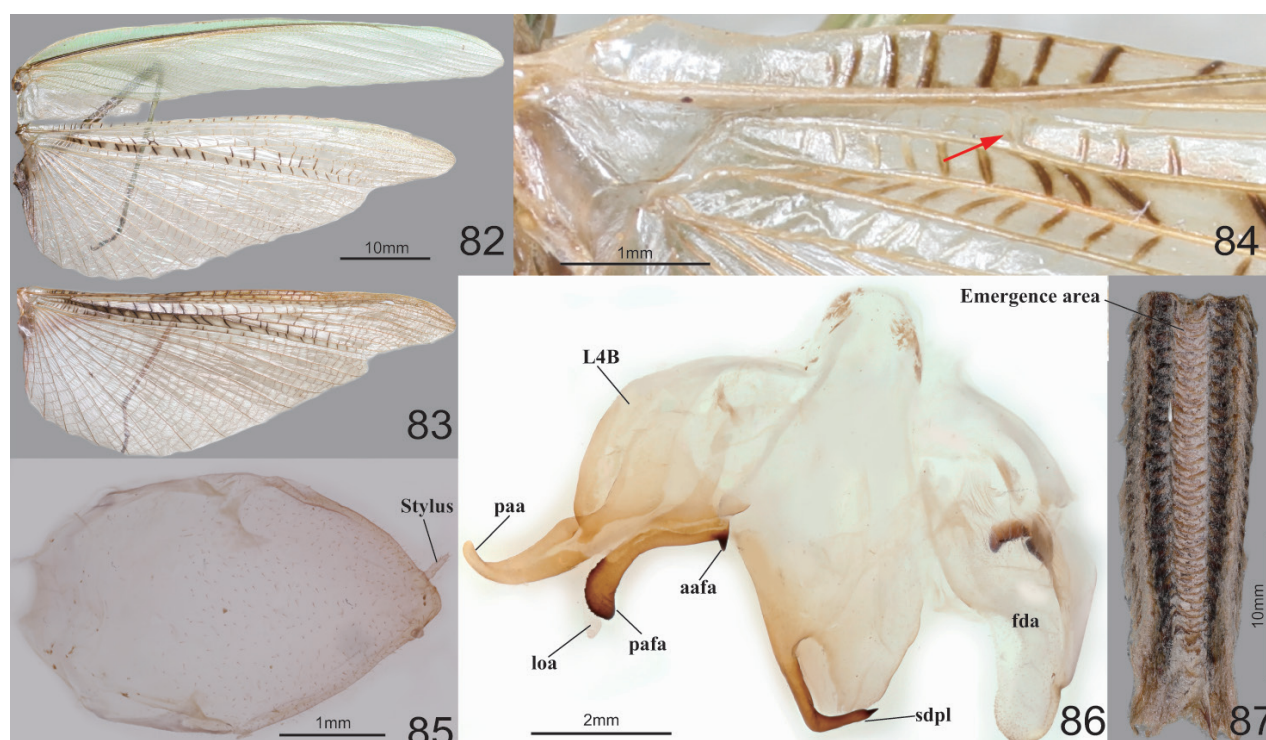
Figures 71–81. Habitus, head, pronotum and foreleg of *Tenodera angustipennis* 71 male dorsal aspect 72 female dorsal aspect 73 male face 74 female face 75 male pronotum 76 female pronotum (small sized) 77 female pronotum (large sized) 78 foreleg ventral aspect 79 foreleg interior aspect 80 foreleg dorsal aspect 81 ventral aspect of foreleg and furcasternite (live specimens). Abbreviation: Tsg = tibial spur groove. Red arrows = dark spot near the tibial spur groove.

Seodun-dong, Suwon-si, 13 VIII 1998, Graduate School of Korea Univ.; 1♂, Gosaek-dong, Suwon-si, 20 VIII 1998, Seongsun Jang, ridge of rice field; 1♂, Yulgeuk 2-ri, Heungcheon-myeon, Yeosu-si, 24 VIII 1998, Yeongbo Lee, ridge of rice field; 1♂, Seodun-dong, Suwon-si, 11 IX 1998, Graduate School of Korea Univ.; 1♂1♀, Yulgeuk 2-ri, Heungcheon-myeon, Yeosu-si, 30 IX 1999, Yeongbo Lee, ridge of rice field; 1 Nymph, Seodun-dong, Suwon-si, 6 VII 2000, Taewoo Kim; 3 Nymphs, Seodun-dong, Suwon-si, 20 VII 2000, Taewoo Kim; 2♂1♀, Seodun-dong, Suwon-si, 20 IX 2000, Taewoo Kim; 5 Nymphs, Shihwa, Siheung-si, 30 VII 2003, Jaecheon Son; 1♂, Sinheung College, Howon-dong, Uijeongbu-si, 26 IX 2005, Jindong Yeo; 5 Nymphs, World Cup Park, Seongsan-dong, Mapo-gu, Seoul, 20 VII 2013, Yeongbo Lee; **CB**: 1♀, Mt. Nam, Cheongju-si, 24 VIII 2000, Heeah Lee; 1♀, Maebong peak, Mt. Songni, Boeun-gun, 17 IX 2002, Yeongbo Lee; 1♀, Maebong peak, Mt. Songni, Boeun-gun, 18 IX 2002, Haechul Park; 1♀, Box office, Mt. Songni, Jangam-ri, Boeun-gun, 30 IX 2002, Jaecheon Son; 1♂1♀, Gamgok-myeon, Eumseong-gun, 31 VIII 2019, Byeongmin Jeong; 1♀, Parking area of Cheongju Airport, Ipsang-ri, Naesu-eup, Cheongwon-gu, Cheongju-si, 15 IX 2023, Jaeil Shim; **CN**: 1♂, Sindu-ri, Wonbuk-myeon, Taean-gun, 1 IX 2001, Haechul Park, grassland; 1 Nymph, Sindu-ri, Wonbuk-myeon, Taean-gun, 1 IX 2005, Jaecheon Son; 2♀, Coastal Dune, Sindu-ri, Wonbuk-myeon, Taean-gun,

12 VIII 2023, Jaeil Shim, near the grassland; **GB**: 1♂, Rest area of expressway, Chilgok-gun, 8 IX 2000, Taewoo Kim; 2♀, Mt. Palgong, Daegu, 1 IX 2014, Taeman Han; 2♂1♀, Gomo station, Suseong-gu, Daegu, 3 IX 2016, Jaeil Shim; 1♂, Gomo station, Suseong-gu, Daegu, 14 IX 2019, Jaeil Shim; 1♂6♀, Mangudang park, Hyomok-dong, Daegu-si 29 X 2023, Jaeil Shim; **GN**: 2♀, Yonggang-ri, Hwagae-myeon, Hadong-gun, 15 IX 2023, Jaeil Shim; **JB**: 1♀, Jeonbuk Nat. Univ., Jeonju-si, 17 X 2017, Sunyeong Park; 1♀, Jinan-Maisan Rest area of expressway, Jinan-gun, 22 VIII 2019, Jaeil Shim; 1♂, National Institute of Agricultural Sciences, Iseo-myeon, Wanju-gun, 31 VIII 2019, Jaeil Shim; 1♀, Jangsu-eup, Jangsu-gun, 5 IX 2019, Jaeil Shim; 2♂5♀, Mt. Moak, Gui-myeon, Wanju-gun, 7 IX 2019, Jaeil Shim; 1♂, Temple Geumsansa, Gimje-gun, Gimje-si, 5 IX 2020, Jaeil Shim; **JN**: 2♀, Myeongsasimni, Coastal Dune, Island Bigeumdo, Sinan-gun, 22 IX 2001, Haechul Park; **JJ**: 1♀, Island Udo, Jeju-si, 10 X 1999, Taewoo Kim.

Redescription. Measurements (mm): Total length (vertex to tip of abdomen) ♂ 44.2–63.3, ♀ 51.2–86.6; head width ♂ 5.9–6.5, ♀ 6.9–7.8; head length ♂ 4.5–4.9, ♀ 5.6–6.7; pronotum width ♂ 4.3–4.9, ♀ 4.9–6.4; pronotum length ♂ 18.0–22.3, ♀ 19.2–25.0; forewing (tegmina) length ♂ 38.4–48.2, ♀ 38.1–55.2. **Male** (Figs 71, 73, 75, 78–80, 82–86). Large sized, body slender. **Coloration** (Figs 71, 82): Body and forewing discoidal area green, greenish brown and brown. **Head** (Fig. 73): Triangular. Head width 1.3× as long as head length. Vertex slightly convex, brown; apex with a bright brown transverse line. Compound eye globular. Ocelli large, oblong. Antenna filiform; antenna length nearly 1.5× as long as pronotum. Lower frons posterior apex slightly protruding. Epistomal sulcus slightly concave. Lower frons with three, clypeus and labrum with two dark longitudinal stripes. **Prothorax** (Fig. 75): Pronotum long and slender, flattened dorso-ventrally, dorsal surface smooth; length 4.1–4.4× as long as maximum width. Prozone lateral margin with few denticulations in large sized specimens. Metazone color orangish in green morph; lateral margin smooth; metazone 3.4–4.7× as long as prozone. Between basis of forecoxa attachment membranous surface (Fig. 81) orange (in live specimen). Postcervical plate and anterior area of furcasternite with gradational dark pattern in brown morph (Fig. 81) and occasionally in green morph. Medial keel brownish (Fig. 76). **Forelegs (Prothoracic legs)** (Figs 78–81): Coxa (Fig. 81) dorsal margin with pale color, 7–10 whitish spines, conical or blunt; ventral surface with pale and dark pattern on proximal area in brown morph; remaining surface with numerous white spots. Tibial spur groove (Figs 78, 81) with faint dark spot. Spination formula (Figs 78–80): Avts = 12–17; Pvts = 9; Avfs = 14–16; Pvfs = 4; Ds = 4. In 15 Avfs (Figs 78, 79): spines 2, 4, 6, 8, 10, 12, and 15 larger than remaining Avfs; spines 1, 2, 4, 6, 8, 10, 12, and 14 with dark brown spot at the base. Each tarsomere (Fig. 78) distal area dark brown. Tarsi 5-segmented. **Wings** (Figs 82–84): Forewing completely surpassing end of abdomen; costal area green, discoidal area transparent. Forewing (Fig. 82) subcosta and radius brown, its color obviously darker than other veins. Hindwing anal area hyaline and nearly transparent in green morph (Fig. 82), brownish and smoky spotted pattern in brown morph (Fig. 83); arculus veins (Fig. 84) and nearby cells mostly transparent; cross veins of subcostal and cubitus area brown to dark brown. **Abdomen**: A longitudinal yellow stripe in middle of abdominal sternites; abdominal sternites with brightly colored mottled pattern. Cerci setose, not flattened, with 17 segments. Male subgenital plate (coxosternite IX) (Fig. 85) irregular rhom-

boidal, inter-stylar margin extremely convex; ventral surface with numerous setae. Styli rather short. **Male genitalia** (Fig. 86): Right phallomere forming nearly V-shaped pva; pia sclerotized and weakly wrinkled; posterior surface of pia with weakly expanded membranous area, surface with minute denticulation; fda elongate lobed shape. Left phallomere (Fig. 86) with elongate and curved paa, its distal apex rounded; aafa sclerotized, straight spike shape; pafa sclerotized, curved at more than 45° arch, wide blade-shaped, outer margin with numerous decumbent spines; loa membranous, elongate finger-shaped, longer than pafa; L4B curved spoon-shaped. Ventral phallomere irregular rhomboidal, posterior margin prominently expanded; sdpl (Fig. 86) more than 90° angle at the middle. **Female** (Figs 72, 74, 77). Similar to male, with following differences. **Head** (Fig. 74): width 1.1 to 1.2× as long as head length. Vertex convex. Antenna as long as head to pronotum length. **Prothorax** (Figs 76, 77): Pronotum length 3.8–3.9× as long as maximum width; lateral margin with numerous denticles. Prozone dorsal surface with numerous blunted denticles. Metazone 2.8–3.1× as long as prozone. Medial keel protruding, pale brown or occasionally green in green morph. **Forelegs (Prothoracic legs)**: Coxa dorsal margin with 7–13 large conical spines, small denticles located between them. **Wings**: Forewing often reaching end of abdomen; discoidal area semi-transparent. **Ootheca** (Fig. 87). **Measurements (mm)**: Length 21.8–39.7; maximum width 10.1–13.7; maximum height 7.1–11.0; length of emergence area 15.0–31.0; width of emergence area 3.2–4.3. **Identification**: Fusiform, nearly hemispherical in cross-section. Proximal end with medial elevation of emergence area. Ootheca attached by ventral surface or fully encircling a thin substrate such as sticks. External wall bright brown. External coating covering almost entire surface of ootheca except later-



Figures 82–87. Wings, male genitalia and ootheca of *Tenoderangustipennis*. **82** wings (green morpho-type) **83** hindwing (brown morpho-type) **84** hindwing venations **85** subgenital plate **86** male genitalia **87** ootheca (dorsal aspect). Red arrow = arcular area.

al zone of emergence area; beige. Lateral side of emergence area prominently concave (Fig. 87). Exhibiting ~ 18–29 egg chambers clearly delimited by visible prominently oblique lips; lips occasionally invisible on new oothecae due to covering by external coating. Distal end of ootheca narrowed to residual process; greatly elongate and attached to substrate. **Nymph. Mid to last instar nymph:** Avfs 1 and last Avfs base to tibial spur groove with dark spotted pattern; between forecoxa basis membranous attachment surface orange.

Biological notes. *Tenodera angustipennis* occurs throughout the Korean peninsula and both adults and oothecae can be commonly found on trees and shrubs. First instar nymphs hatch from late May to mid-June, and adults emerge in mid-August.

Distribution. China, India, Japan, Java, South Korea. Invasive in NE USA and Hawaii.

Remarks. *Tenodera angustipennis* is morphologically similar to *T. sinensis* in Korea but can be distinguished by their more slender bodies, the pronotum length/width ratio, the orange coloration between the forecoxa base (Oshima 2018) (Fig. 81), lack of reddish coloration on the hindwing radius area (Figs 82–84), and the pointed, perpendicular apex of the aafa (Fig. 86).

***Tenodera sinensis* Saussure, 1871**

Figs 88–102

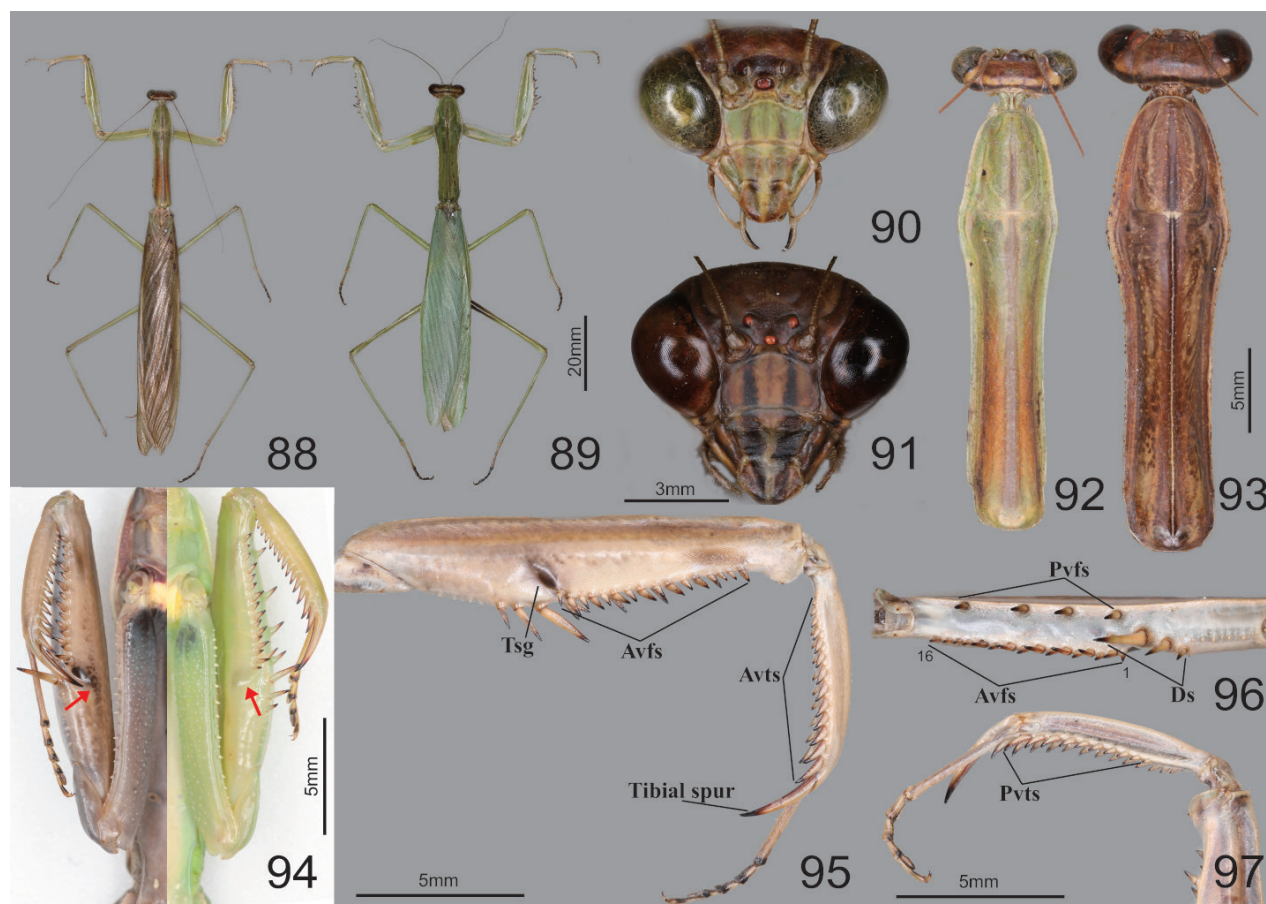
Mantis mandarinea Saussure, 1871a: 289.

Tenodera aridifolia var. *sinensis* Saussure, 1871b: 417.

Tenodera aridifolia (Stoll, 1813): ESK and KSAE 1994: 44 (misidentification). Korean record.

Tenodera sinensis Saussure, 1871: Kim 2010: 31; Kim 2021: 65. Korean record.

Specimens examined. [KsNU] SOUTH KOREA: JB: 1♂, Eunpa Lake, Gunsan-si, 8 XI 2016, Donghwan Na; **[NASIC] SOUTH KOREA: GW:** 2 Nymphs, Balsan 2-ri, Chuncheon-si, 12 VI 1998, Sungsoon Jang; 1♀, Jinburyeong, Jinbu-myeon, Pyeongchang-gun, 29 IX 2000, Taehwa Kang; 1 Nymph, Ingye-ri, Okgye-myeon, Gangneung-si, 15 VIII 2002, Jingoo Yeo; 3♂, Mt. Odae, Hongcheong-gun, 29 VIII 2019, Jaeil Shim; **GG:** 1♂, Mijang-ri, Samjuk-myeon, Anseong-si, 17 IX 2000, Yeongbo Lee; 1♂, Mt. Cheolma, Incheon, 26 VIII 2001, Taewoo Kim; 1 Nymph, Shihwa, Siheung-si, 30 VII 2003, Jaecheon Son; 1 Nymph, Temple Jeondeungsa, Onsu-ri, Gilsang-myeon, Ganghwa-gun, Incheon, 4 IX 2009, Yeongbo Lee; 1♀, Jikdong-ri, Sohol-eup, Pocheon-si, 7 IX 2011, Yeongbo Lee; 2 Nymphs, Temple Bogwangsa, Gwangtan-myeon, Paju-si, 10 VII 2013, Yeongbo Lee; 3 Nymphs, World Cup Park, Seongsan-dong, Mapo-gu, Seoul, 21 VII 2013, Yeongbo Lee; 2 Nymphs, Noel Park, Sangam-dong, Mapo-gu, Seoul, 30 VII 2013, Yeongbo Lee;); 1♂, Island Gureopdo, Gureop-ri, Deokjeok-myeon, Incheon, 28 VI 2023, Jaeil Shim, Wonjun Sung (reared from nymph); **CB:** 1 Nymph, Magok-ri, Bongyang-eup, Jecheon-si, 13 VII 2005, Taehwa Kang; 1♀, Gamgok-myeon, Eumseong-gun, 31 VIII 2019, Byeongmin Jeong; 3♂, Geumseok-ri, Geumwang-eup, Eumseong-gun, 14 IX 2019, Seong-Gyu Lee; 1♂, Jeongbang-ri, Annae-myeon, Okcheon-gun, 12 X 2000, Yeongbo Lee; **CN:** 1♀, Mt. Sikjang, Daejeon, 14 VIII 2019, Geonheyok Kim (reared from nymph); 4♂, Coastal Dune, Sindu-ri, Wonbuk-myeon, Taean-gun,

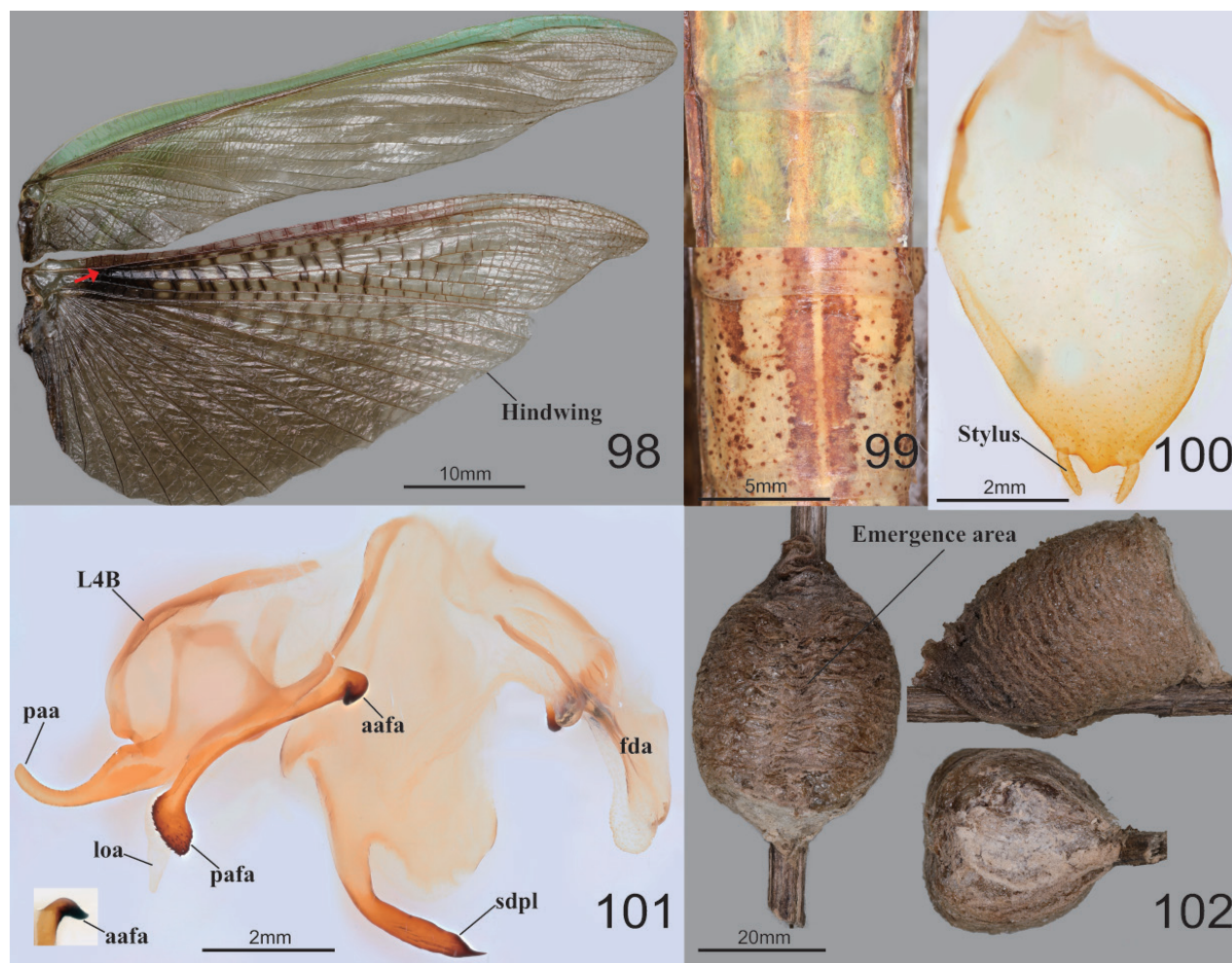


Figures 88–97. Habitus, head, pronotum and foreleg of *Tenodera sinensis* **88** male dorsal aspect **89** female dorsal aspect **90** male face **91** female face **92** male pronotum **93** female pronotum **94** ventral aspect of foreleg and furcasternite (live specimens) **95** foreleg ventral aspect **96** foreleg interior aspect **97** foreleg tibia and tarsus (dorsal aspect). Abbreviation: Tsg = tibial spur groove. Red arrows = dark spot near the tibial spur groove.

12 VIII 2023, Jaeil Shim, near the grassland; **GB**: 1 Nymph, Geumgok-ri, Byeonggok-myeon, Yeongdeok-gun, 1 VII 2009, Yeongbo Lee, Hoyeon Jeong; **GN**: 4♀, Mt. Noja, Dongbu-myeon, Island Geoje-do, Geoje-si, 15 IX 2021, Jaeil Shim; **JB**: 1♀, Hoyja 3-dong, Wansan-gu, Jeonju-si, 28 VIII 2014, Taeman Han; 1♂, Deokjin Park, Deokjin-gu, Jeonju-si, 6 IX 2018, Junhee Park; 1♀, Jeonju river-side, Jeonju-si, 15 IX 2018, Jaeil Shim; 1♂, Mt. Moak, Gui-myeon, Wanju-gun, 6 X 2018, Hyeon-Ha Yoo; 1♂, Jinan-Maisan Rest area of expressway, Jinan-gun, 22 VIII 2019, Jaeil Shim; 1♀, Jeonju Univ., Jeonju-si, 4 IX 2019, Jaeil Shim; 1♂, Jangsu-eup, Jangsu-gun, 5 IX 2019, Jaeil Shim; 11♂2♀, Mt. Moak, Gui-myeon, Wanju-gun, 7 IX 2019, Jaeil Shim; 3♂, Temple Geumsansa, Gimje-gun, Gimje-si, 5 IX 2020, Jaeil Shim; **JN**: 1♂, Myeongsasimni, Coastal Dune, Island Bigeumdo, Sinan-gun, 22 IX 2001, Haechul Park; 1♀, Island Gogyeumdo, Wando-gun, 3 IX 2003, Mikyung Ahn; 1♂1♀, Bukyi-myeon, Jangseong-gun, 20 VIII 2021, Jaeil Shim;); 2♂1♀, Island Yeoseodo, Yeoseo-ri, Cheongsan-myeon, Wando-gun, VI 2023, Jaeil Shim (reared from nymph); **JJ**: 1♀, Ihotewau Beach, Jeju-si, 26 VIII 2014, Taeman Han, windbreak forest; 2 Nymphs, Gwangchigi Beach, Goseong-ri, Seongsan-eup, Seogwipo-si, 16 V 2021, Jaeil Shim.

Redescription. Measurements (mm): Total length (vertex to tip of abdomen) ♂ 54.2–89.1, ♀ 58.2–100.8; head width ♂ 5.9–6.5, ♀ 6.9–7.8; head length ♂ 4.5–4.9, ♀ 5.6–6.7; pronotum width ♂ 4.3–5.6, ♀ 4.9–7.4; pronotum length ♂

18.0–24.3, ♀ 19.2–27.0; forewing (tegmina) length ♂ 38.4–55.2, ♀ 38.1–63.2. **Male** (Figs 88, 90, 92, 95–101). Large to very large. **Coloration** (Figs 88, 98): Body and forewing discoidal area green to greenish brown or brown. **Head** (Fig. 90): Triangular. Head width 1.2× as long as head. Vertex slightly convex, brownish; apex with a bright brown transverse line (in live specimens). Ocelli large, oblong. Antenna nearly 1.5× as long as pronotum. Epistomal sulcus slightly concave. Lower frons, clypeus, and labrum with two darkish longitudinal stripes. **Prothorax** (Fig. 92): Pronotum long but robust, flattened dorso-ventrally, dorsal surface smooth; pronotum length 3.8–4.0× as long as maximum width. Prozone lateral margin and dorsal surface with minute denticles. Metazone (Fig. 92) often orangish; lateral margin smooth; 3.0–3.2× as long as prozone. Between forecoxa basis membranous attachment surface yellow (Fig. 94). Postcervical plate reddish in brown morph (Fig. 94), anterior area of furcasternite with gradational dark pattern in brown morph, its pattern occasionally occurring in green morph. **Forelegs (Prothoracic legs)** (Figs 94–97): Coxa dorsal margin with 14–17 whitish conical spines; ventral surface of coxa proximal area with gradational dark pattern (Fig. 94); remaining surface with numerous small white spots. Tibial spur groove with faint dark spot (Fig. 94). Spination formula (Figs 95–97): Avts = 14–15; Pvts = 8–10; Avfs = 14–17; Pvfs = 4; Ds = 4. In 16 Avfs (Figs 95, 96): spines 2, 4, 6, 8, 10, 12, and 16 larger than remaining Avfs. Tarsomere distal end dark brown. Tarsi 5-segmented. **Wings** (Fig. 98): Forewing completely surpassing the end of abdomen. Forewing costal area green, discoidal area transparent. Hindwing venation brown, cross veins and cells of subcostal to radius area reddish to magenta; radius to cubitus proximal area, near cells of arculus veins dark brown (Fig. 98); anal area with dark brownish smoky pattern. **Abdomen** (Figs 99, 100): Middle of the abdominal sternites with longitudinal yellow stripe pattern (Fig. 99). Cerci setose, not flattened, with 17–20 segments. Male subgenital plate (coxosternite IX) (Fig. 100) irregular rhomboidal, inter-stylar margin convex at the middle; ventral surface with numerous setae. Styli rather short. **Male genitalia** (Fig. 101): Right phallomere forming nearly V-shaped pva; pia sclerotized and weakly wrinkled; posterior surface of pia (Fig. 101) with membranous wide hump, surface with minute denticulation; fda elongate lobe shape. Left phallomere (Fig. 101) with elongated and curved paa, its apex round; aafa sclerotized, surface smooth, weakly bulbous spike-shaped basally, apically curved dorso-laterally; pafa sclerotized, nearly 90° angle, arched wide blade-shaped (apex expanded), posterior and apical margin of pafa with numerous spines; loa membranous, elongate finger-shaped, much longer than pafa; L4B curved spoon-shaped. Ventral phallomere irregular rhomboidal; posterior margin prominently expanded; sdpl hardly sclerotized, curved at ~45° at middle, its distal half slightly thicker and more sclerotized and melanized than basal, point of sdpl tips shallowly concave. **Female** (Figs 89, 91, 93, 94). Similar to male, with following differences. **Head** (Fig. 91): width 1.1× as long as head length. Vertex convex. Antenna as long as pronotum. Ocelli smaller than male. **Prothorax** (Fig. 93): Pronotum length 2.8–2.9× as long as maximum width; lateral margin with numerous denticles. Prozone with numerous blunt denticles on dorsal surface. Medial keel protruded. **Forelegs (Prothoracic legs)**: Coxa dorsal margin (Fig. 94) with 14–20 large conical spines (with sharp tips), small denticles located between them. **Wings**: Forewing occasionally reaching end of abdomen. **Abdomen**: Elongate oval, much broader than in male. Cerci with 15–17 segments.



Figures 98–102. Wings, abdomen, male genitalia and ootheca of *Tenodera sinensis* **98** wings **99** male abdominal sternites (above: green morpho-type below: brown morpho-type) **100** subgenital plate **101** male genitalia (small box = lateral aspect of aafa) **102** ootheca (left: dorsal aspect right above: lateral aspect right below: distal aspect). Red arrow = arcus area.

Ootheca (Fig. 102). **Measurements (mm):** Length 30.0–42.2; maximum width 22.2–27.6; maximum height 20.7–24.9; length of emergence area 18.4–32.8; width of emergence area 5.2–5.5. **Identification:** Barrel-like shape, mostly circular in cross-section. Ootheca attached to flat substrate by its ventral surface or fully encircling substrates such as sticks. External wall with very thick air-filled area, colored beige to bright brown. External coating covering entire surface of ootheca; beige in color. Emergence area depressed. Exhibiting ~ 15–29 egg chambers; lips invisible due to very thick air-filled layer of ootheca. Distal end of ootheca obliquely truncate. **Nymph. Mid to last instar nymph:** Avfs 1 base (near femoral brush), last Avfs base to tibial spur groove area with dark spotted pattern; between forecoxa basis attachment membranous surface yellow.

Biological notes. *Tenodera sinensis* occurs throughout the Korean peninsula and has adapted well to urban, suburban, and riverside environments. It spawns ootheca in various locations, such as on stones, tree trunks, and branches. First instar nymphs hatch from mid-April to mid-May, while adult mantises typically emerge in mid-August.

Distribution. China, Nepal, Japan, Russia, Thailand, South Korea. Invasive in Canada and the USA.

Remarks. *Tenodera sinensis* was originally described as a variation of the widely distributed species *Tenodera aridifolia* (Stoll, 1813), and treated as a subspecies for quite a long time (Saussure 1871b; Rehn 1903; Shiraki 1932; Beier 1932; Tinkham 1937; Bazyluk 1977; Iwasaki 1996; Bruins 1999), but already Giglio-Tos (1927) and Ehrmann (2002) considered *T. sinensis* as a valid species. *Tenodera aridifolia* and *T. sinensis* are extremely close and morphologically very similar (Ehrmann and Borer 2015), but Jensen et al. (2010) provide differences in male genitalia of *T. sinensis* and *T. aridifolia*. According to Jensen et al. (2010), it is a distinctly divided sister species pair based on phylogeny using nuclear genes (histone III, wingless gene) and mitochondrial genes (large and small rRNA, cytochrom oxidase II). *Tenodera aridifolia* is found in tropical and subtropical regions but is replaced by *T. sinensis* in temperate habitats. Our study used one male West Javan *T. aridifolia* specimen to comparatively examine and recovered remarkable characters from *T. sinensis* including the narrow pronotum (length/maximum width = 5.1) and forewing, a smaller head proportional to body size, short and stout aafa, pafa, and sdpl curved at ~ 45° (Mukherjee et al. 1995; Jensen et al. 2010).

Subfamily Hierodulinae Brunner de Wattenwyl, 1893

Genus *Hierodula* Burmeister, 1838

Parhierodula Giglio-Tos, 1912: 108.

Type species. *Hierodula membranacea* Burmeister, 1838

Diagnosis. Pronotum clavate. Furcasternite in Korean specimens with spotted pattern or reddish coloration. Forewing stigma triangular, whitish to yellow. Hindwing transparent (Fig. 115). Male subgenital plate margin with numerous black spines. Male genitalia: afa hook- or boat-shaped; maa well developed.

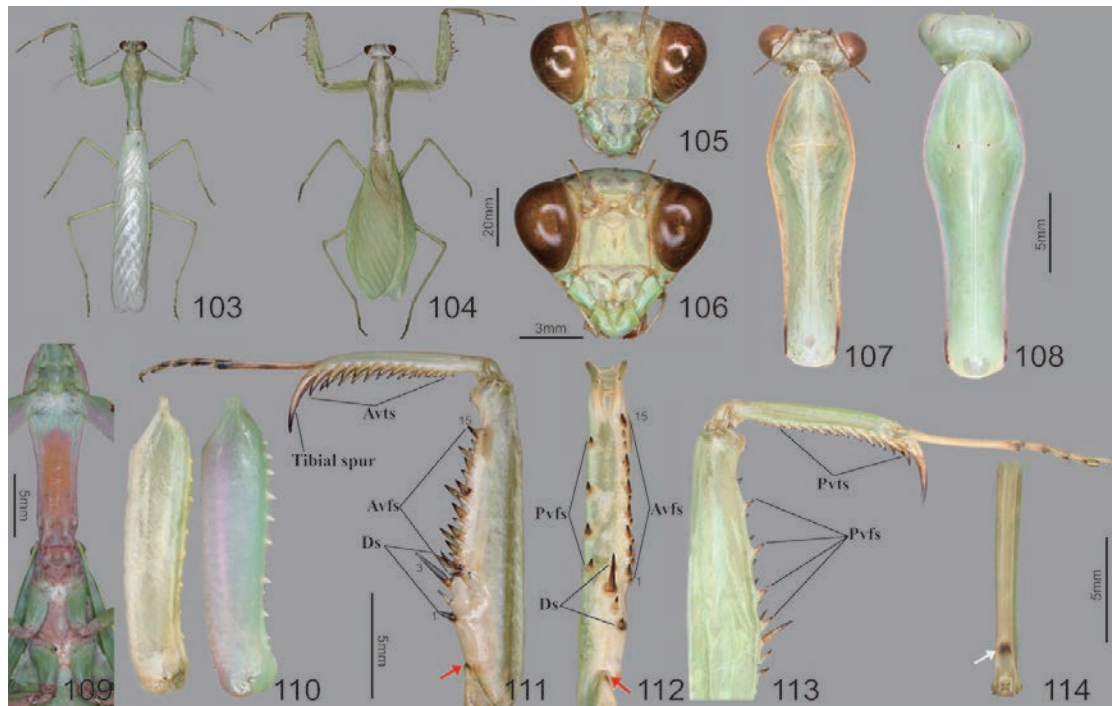
Hierodula chinensis Werner, 1929

Figs 103–120

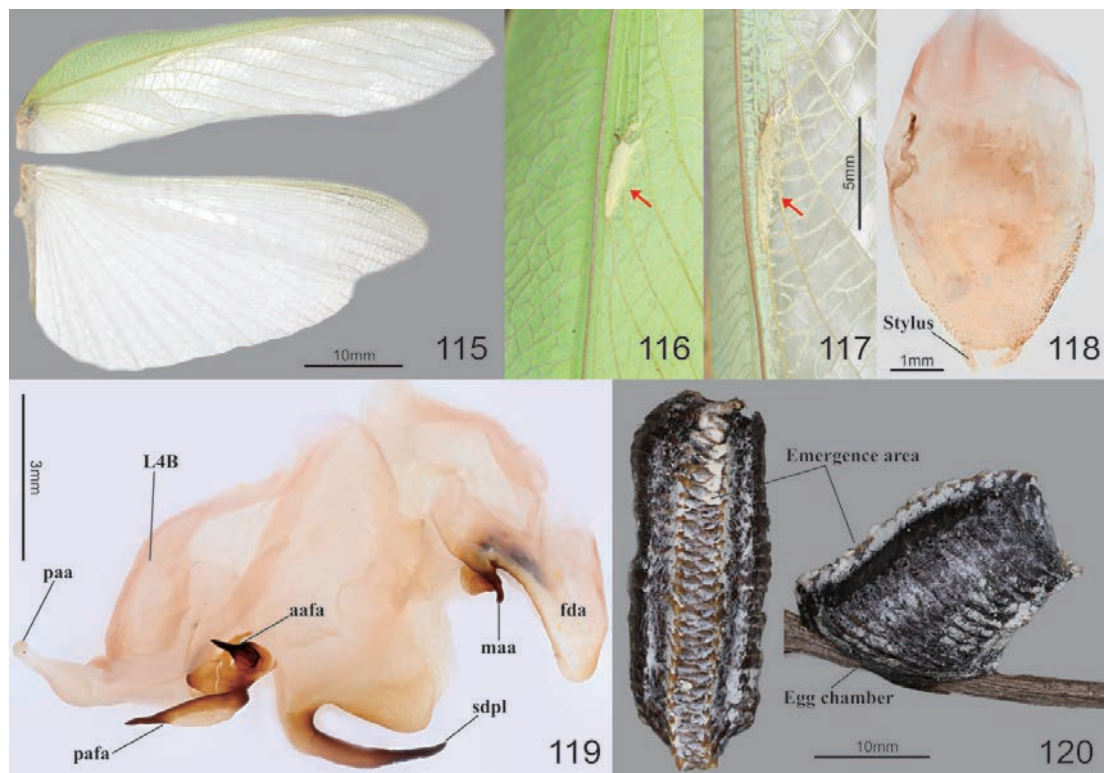
Hierodula chinensis Werner, 1929: 75.

Hierodula chinensis Werner, 1929: Shim et al. 2021a: 121. Korean record.

Specimens examined. [NASIC] SOUTH KOREA: CB: 1 Nymph, Sannam-dong, Seowon-gu, Cheongju-si, 18 VII 2023, NASIC; **GB:** 1 ♀, Namtong-dong, Gumi-si 10 X 2023, Jaeil Shim; 1 ♀, Mangudang park, Hyomok-dong, Daegu-si 29 X 2023, Jaeil Shim; **GN:** 2 ♀, Yonggang-ri, Hwagae-myeon, Hadong-gun, 15 IX 2023, Jaeil Shim; **JB:** 3 ♂ 1 ♀, Jeonbuk Art Museum, Gui-myeon, Wanju-gun, 9 IX 2018, Jaeil Shim; 1 ♂, Mt. Moak, Gui-myeon, Wanju-gun, 13 IX 2018, Jaeil Shim; 5 ♂ 3 ♀ Mt. Moak, Gui-myeon, Wanju-gun, 7 IX 2019, Jaeil Shim; 6 ♀, Jeonbuk Art Museum, Gui-myeon, Wanju-gun, 5 IX 2020, Jaeil Shim; 3 ♂, Jeonbuk Art Museum, Gui-myeon, Wanju-gun, 19 IX 2020, Jaeil Shim; 5 ♂ 2 ♀, National Institute of Agricultural Sciences, Iseo-myeon, Wanju-gun, 20 IX 2023, Jaeil Shim; **JN:** 2 Nymphs 1 ♂, Cheongso-ri, Seo-myeon, Suncheon-si, 17 VIII 2019, Jaeil Shim; 2 Nymphs, Haesan-dong, Yeosu-si, 20 VII 2022, Jaeil Shim.



Figures 103–114. Habitus, head, pronotum, foreleg and hindleg of *Hierodula chinensis* **103** male dorsal aspect **104** female dorsal aspect **105** male face **106** female face **107** male pronotum **108** female pronotum (live specimens) **109** furcasternite (live specimens) **110** foreleg coxa ventral aspect (right: male left: live female) **111** foreleg ventral aspect **112** foreleg interior aspect **113** foreleg dorsal aspect **114** hindleg femur (interior aspect). Red arrows = dark spot of foreleg trochanter. White arrow = dark spot of joint.



Figures 115–120. Wings, male genitalia and ootheca of *Hierodula chinensis* **115** wings of male **116** female forewing stigma **117** male forewing stigma **118** male subgenital plate **119** male genitalia **120** ootheca (left: dorsal aspect right: lateral aspect). Red arrows = stigma.

Description. See Shim et al. (2021a) for detailed diagnosis and description.

Biological notes. *Hierodula chinensis* is sparsely distributed in the Korean peninsula, primarily inhabiting wooded areas with shrubs and tall trees. It typically lives under tree leaves throughout its lifespan and deposits its oothecae on tree branches. Nymphs have the ability to camouflage themselves by folding their abdomens backwards. The first instar nymphs of *H. chinensis* hatch in early July, with adult mantises typically emerging at the end of August.

Distribution. China. Invasive in Japan and South Korea.

Remarks. *Hierodula chinensis* was recently reported in the Korean peninsula by Shim et al. (2021a). This species was previously recorded in China by Werner (1929) and Beier (1932) and was recently reported in Japan (Yamasaki et al. 2022). However, this species has been erroneously confused with *H. membranacea* Burmeister and *H. macrodentata* Wang, Zhou & Zhang, 2020 by some authors, including Tinkham (1937), Wang (1993), and Zhu et al. (2012). Recent studies by Wang et al. (2020) and Liu et al. (2020) have provided a redescription of *H. chinensis*, clarifying its taxonomic status. See Shim et al. (2021a) for detailed description.

***Hierodula patellifera* (Audinet-Serville, 1838)**

Figs 121–136

Mantis patellifera Audinet-Serville, 1838: 185.

Mantis bipapilla Audinet-Serville, 1838: 188.

Hierodula assamensis Mukherjee et al., 1995: 185.

Hierodula manillensis Saussure, 1870: 233.

Hierodula raptoria Stål, 1877: 38.

Hierodula dispar Kirby, 1900: 146.

Hierodula saussurei Kirby, 1904: 245.

Hierodula manillana Giglio-Tos, 1912: 96.

Hierodula (Hierodula) manillana Giglio-Tos, 1927: 448.

Hierodula yunnanensis Wang, 1993: 137.

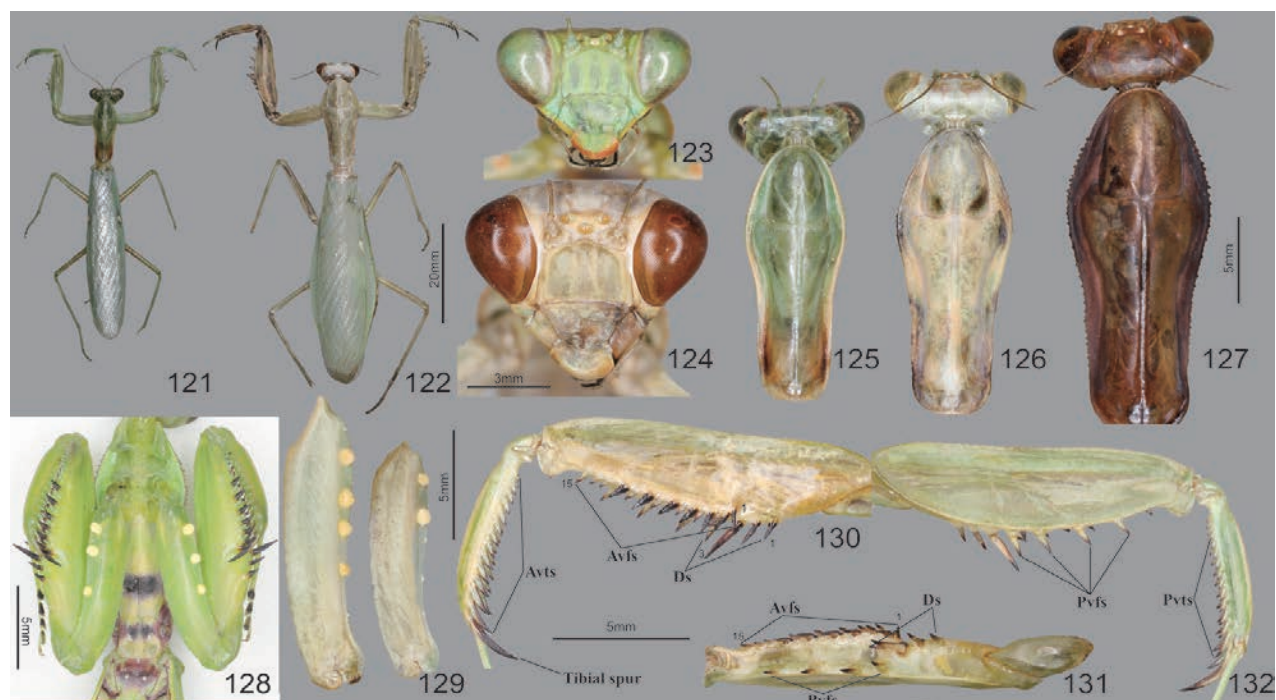
Hierodula xishaensis Wang, 1993: 140.

Hierodula multispina Wang, 1993: 141.

Hierodula daqinshanensis Wang, 1993: 143.

Hierodula patellifera (Audinet-Serville, 1838): Jeon et al. 1999: 226 (South Korea); Kim 2010: 31; Kim 2021: 65; Shim et al. 2021b: 149. Korean record.

Specimens examined. [NASIC] SOUTH KOREA: GG: 1♀, Seodun-dong, Suwon-si, 2 IX 1999, Taewoo Kim; 1♂, Seodun-dong, Suwon-si, 13 IV–17 VIII 2001, Taewoo Kim (reared); 4♂1♀, SETEC, Daechi-dong, Gangnam-gu, Seoul, 8 VI 2023, Jaeil Shim (reared from nymph); **CB:** 1♂5♀, Parking area of Cheongju Airport, Ipsang-ri, Naesu-eup, Cheongwon-gu, Cheongju-si, 15 IX 2023, Jaeil Shim; **CN:** 1♂, Rest area, Geumsan-gun, 10 IX 2013, Haechul Park; 1♂, Mt. Gubong, Gwanjeo-dong, Seo-gu, Daejeon, 1 IX 2014, Taekyu Kim; 1♀, Chungnam Nat. Univ., Yuseong-gu, Daejeon, 27 IX 2015, Taeman Han; 4♂2♀, Samsong-ri, Haemi-myeon, Seosan-si, 24 IV 2023, Jaeil Shim (reared from oothecae); 4♂9♀, Chungnam Nat. Univ., Yuseong-gu, Daejeon-si, 19 VIII 2023, Jaeil Shim; **GB:** 2♀, Street near Gomo station (Gomo-ro), Suseong-gu, Daegu, 14 IX 2019, Jaeil Shim; 8♀, Hyomok Elementary Scholl, Hyomok-dong, Daegu-si 29 X 2023, Jaeil Shim; **GN:**

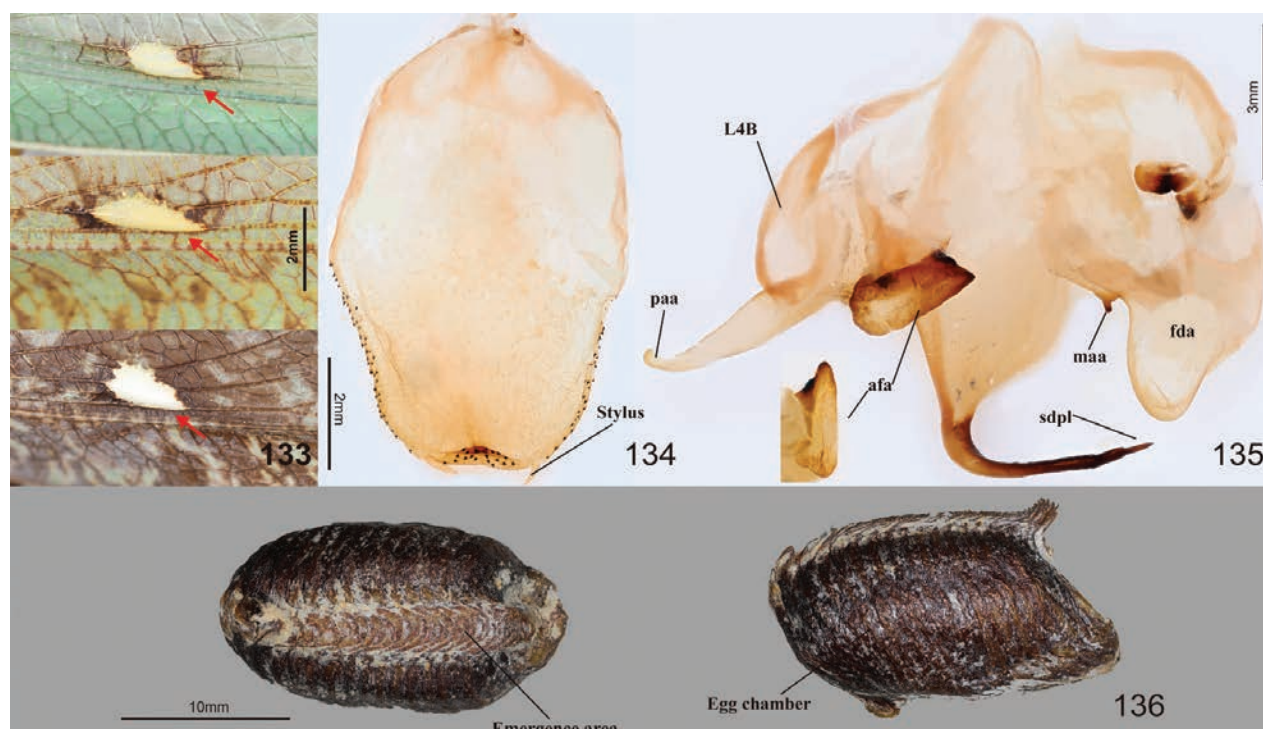


Figures 121–132. Habitus, head, pronotum and foreleg of *Hierodula patellifera* **121** male dorsal aspect **122** female dorsal aspect **123** male face **124** female face **125** male pronotum (small sized) **126** male pronotum (large sized) **127** female pronotum **128** ventral aspect of foreleg and furcasternite (live specimens) **129** foreleg coxa ventral aspect (right: female with 4 forecoxal spines left: male with 2 forecoxal spines) **130** foreleg ventral aspect **131** foreleg interior aspect **132** foreleg dorsal aspect.

1♀, Mt. Mang, Island Geojedo, Geoje-si, 23 VII 2019, Jun-Gi Lee, Jun-Ho Lee; **JB**: 2♂2♀, Jeonbuk Nat. Univ., Jeonju-si, 21 VIII 2017, Jaeil Shim; 3♀, National Institute of Agricultural Sciences, Iseo-myeon, Wanju-gun, 4 VII 2018, Jaeil Shim (reared from nymph); 2♂, Jangsu-eup, Jangsu-gun, 5 IX 2019, Jaeil Shim; 2♂3♀, Mt. Moak, Gui-myeon, Wanju-gun, 7 IX 2019, Jaeil Shim; 2♂, Jeonbuk Art Museum, Gui-myeon, Wanju-gun, 21 IX 2019, Jaeil Shim; 4♂6♀, Jeonbuk Art Museum, Gui-myeon, Wanju-gun, 22 IX 2019, Jaeil Shim; 2♂10♀, Iseo-myeon, Wanju-gun, 10 IX 2021, Jaeil Shim; 5♂3♀, Eunpa Lake, Gunsan-si, VI 2022, Jaeil Shim, JuHyeong Sohn (reared from nymph); 2♀, Byeonsan-myeon, Buan-gun, VIII 2022, Jeonbuk Jaeil Shim; 1♂1♀, Hyangga-ro, Pungsan-myeon, Sunchang-gun, 26 VII 2023, Jaeil Shim (reared from nymph); **JN**: 1♂1♀, Near the Korea Coast Guard Academy (KCGA), Yeosu-si, 1 IX 2019, Byeongmin Jeong; 1♂1♀, Dal-dong, Mokpo-si, VIII 2020, Jaeil Shim; **JJ**: 1♀, Jeju Airport, Jeju-si, Jeju-do, 22 IX 2023, Jaeil Shim; 1♂3♀, Donnaeko, Seogwipo-si, Jeju-do, 22 IX 2023, Jaeil Shim; **GUAM**: 1♀, Guam, USA, 19 VII 2017, Yeong-Hun Kim; **JAPAN**: 1♂1♀, Yanabaru, Okinawa, Japan, 1–4 I 2020, Wonjun Sung; **JAVA**: 1♂1♀, Mt. Argopuro, East Java, Indonesia, V 2019, Jaeil Shim (purchase) **VIETNAM**: 1♂, Quang Trung, Bao Loc, Lam Dong, 20 II 2012, Lam Dong Agro-Forestry Research and Experiment Center.

Redescription. Measurements (mm): Total length (vertex to tip of abdomen) ♂ 44.3–57.8, ♀ 54.3–74.2; head width ♂ 6.6–7.5, ♀ 8.4–9.7; head length ♂ 5.1–5.7, ♀ 7.3–8.1; pronotum width ♂ 5.1–6.0, ♀ 6.7–8.6; pronotum length ♂ 12.9–15.1, ♀ 16.1–20.2; forewing (tegmina) length ♂ 33.8–40.9, ♀ 36.8–47.5. **Male** (Figs 121, 123, 125–126, 129, 133–135). Medium to large sized, body robust. **Coloration** (Fig. 121): Bright green to green or bright brown to darkish brown. **Head** (Fig. 123): Triangular. Head width 1.3× as long as length. Vertex flat. Compound eye

globular, inverse drop-shaped. Ocelli large, oblong. Antenna filiform; length nearly 1.2× as long as pronotum. Lower frons with two very weakly protruding parallel vertical ridges, lower frons width 1.5× as long as height. Epistomal sulcus transverse. Lateral margin of compound eye, mandible, and gena yellow. In live specimens, labrum posterior margin orangish. **Prothorax** (Figs 125, 126): Pronotum short, clavate, flatted dorso-ventrally; pronotum dorsal surface smooth and covered in waxy secretion; pronotum length 2.5× maximum width. Prozone lateral margin with numerous denticles. Metazone lateral margin weakly expanded. Medial keel very weakly protruding. Furcasternite (Fig. 128) with two thick transverse and purple markings, larger one at furcasternite medial area and smaller one at posterior one-fourth of furcasternite. **Forelegs (Prothoracic legs)** (Figs 128–132): Coxa dorsal margin (Figs 128, 129) with 2–5 large spines, rounded triangular or round tooth-like shape, yellow; occasionally 1–3 very minute, white, blunt spines located between large spines. Dorsal and ventral coxal lobes continuous, lacking space between them. Spination formula (Figs 130–132): Avts = 13–15; Pvts = 10–12; Avfs = 14–16; Pvfs = 4; Ds = 4. In 15 Avfs (Figs 130, 131): spines 2, 4, 6, 8, 10, 12 and 15 size larger than remaining Avfs; spines 1, 2, 4, 6, 8, 10 and 12 black. Ds (Fig. 130) 1–3 interior surface black. Tarsomere distal end black. **Meso- and metathorax and their legs**: Mesothorax sternite anterior area with purple pattern. Meso- and metathoracic legs simple, long, and slender. Tarsi 5-segmented. First tarsomere of midleg slightly shorter than remaining segments combined, first tarsomere of hindleg slightly longer than remaining segments combined. **Wings** (Figs 121, 133): Forewing completely surpassing end of abdomen; costal area thick, discoidal area transparent; discoidal area occasionally with brightly colored (yellow, beige, brown) mottled pattern. Stigma (Fig. 133) triangular, white to



Figures 133–136. Wings, male genitalia and ootheca of *Hierodula patellifera* **133** stigma of forewing (3 variations) **134** male subgenital plate **135** male genitalia (small box = variation of afa) **136** ootheca (left: dorsal aspect right: lateral aspect). Red arrows = stigma.

whitish yellow; rimmed with dark pattern. Hindwing hyaline. **Abdomen:** Fusiform. Tergites bright yellow to green. Cerci setose, not flattened, with 17 or 18 segments. Male subgenital plate (coxosternite IX) (Fig. 134) irregularly rhomboidal; inter-stylar margin slightly convex and protruding dorsally, margin with 14–20 black spines; ventral surface of subgenital plate with numerous setae; left margin with 41–56 black spines, right margin with 16–28 black spines. Styli rather short. **Male genitalia** (Fig. 135): Pia sclerotized and weakly wrinkled; fda triangular; maa short and stout, surface covered by minute spines. Left phallomere (Fig. 135) with elongate and curved paa, its surface smooth, distal area curved dorso-laterally, apex round; afa (aafa+pafa) weakly sclerotized, wide trapezoidal, surface densely covered in minute denticles; anterior margin area of afa, basal one-third with stout dark decumbent projection (aafa); on dorsal surface of afa with long longitudinal groove; posterior apex mostly rounded; loa membranous, weakly humped; L4B curved spoon-shaped. Ventral phallomere (Fig. 135) irregular rhomboidal; sdpl hardly sclerotized, spear and hook-like in shape, curved at basal one-sixth by little more than 90°, remaining distal area long and straight. **Female** (Figs 122, 124, 127–133). Similar to male, with following differences. Body (Fig. 122) robust. **Head** (Fig. 124): Vertex slightly convex. Head width 1.1 to 1.2× as long as length. Ocelli smaller than male. Antenna slightly shorter than pronotum. Lower frons width 1.3–1.4× as long as height. **Prothorax** (Fig. 127): Pronotum length 2.3–2.4× as long as maximum width; lateral margin with numerous denticles. Medial keel protruding. **Forelegs (Prothoracic legs)** (Figs 128–132): Large forecoxal spines more pronounced than in male. Number of Avfs = 14–17. **Wings** (Figs 122, 133): Forewing occasionally reaching end of abdomen. **Ootheca** (Fig. 136). **Measurements (mm):** Length 21.4–29.0; maximum width 11.2–15.6; maximum height 11.3–13.5; length of emergence area 15.1–21.3; width of emergence area 3.0–3.9. **Identification:** Oblong, nearly elliptical (mostly dorso-ventrally compressed) in cross-section. Ootheca attached to flat substrate by ventral surface or fully encircling substrate such as sticks. External wall (Fig. 136) dark green to brown. External coating comes off easily in the wild, colored beige. Exhibiting ~ 15–27 egg chambers clearly delimited by visible slightly curved lips. Distal end of ootheca truncate and surface rough.

Biological notes. *Hierodula patellifera* occurs throughout the Korean peninsula. This species is well-adapted to urban and suburban environments, and can be easily found near mountains, expressway rest areas, and parks. It typically lives under tree leaves throughout its life cycle and lays its oothecae on tree branches, trunks, and building walls near trees. Nymphs fold their abdomens back to camouflage themselves. First instar nymphs hatch in early June and adult mantises emerge in mid-August.

Distribution. China, Guam, India, Japan, Java, New Guinea, Philippines, Sumatra, Taiwan, Thailand, Vietnam, Korea. Invasive in France, Italy, and Hawaii.

Remarks. *Hierodula patellifera* is a widely distributed species (Ehrmann and Borer 2015; Patel and Singh 2016; Shcherbakov and Anisyutkin 2018; Battiston et al. 2019; Moulin 2020). The species exhibits a high degree of morphological variation, which has led to the recognition of numerous synonyms (Audinet-Serville 1838; Wang 1993, Schwarz et al. 2018). Morphological variation, including differences in the number of forecoxal spines, and shapes of forewing stigma and afa, have been observed among *H. patellifera* populations, including those in Korea. Shim et al. (2021b) discuss the challenges

of species delimitation in *H. patellifera* in detail and emphasize the need for a comprehensive analysis of both morphological and molecular data to resolve taxonomic uncertainties.

DNA barcoding of Korean Mantodea

In total, 56 new sequences from seven species in six genera were generated (657 bp of COI). All new sequences were deposited in GenBank under the accession numbers OQ826709–OQ826764 (Suppl. material 1). Table 1 and Fig. 137 present the *p*-distances of COI regions for specimens at each taxonomic level. Intraspecific distances from eight species were either identical or very similar (0%–2.2%). The minimum interspecific genetic distance between congeners (6.7%) was ~ 3× higher than the maximum intraspecific genetic distance (2.2%), indicating a significant barcoding gap. All eight species were supported as a single lineage using COI on both NJ and PA trees, respectively (Fig. 138).

Table 1. Inter- and intraspecific genetic differences in Korean Mantodea species at each taxonomic level for COI (657 bp) calculated using *p*-distance.

Taxonomic level	Mean	SD	Max	Min
Intraspecific distances	0.007	0.006	0.022	0.000
Interspecific distances	0.150	0.025	0.224	0.067
Interspecific distances of congeners	0.101	0.033	0.146	0.067
Interspecific distances in family	0.146	0.023	0.188	0.067

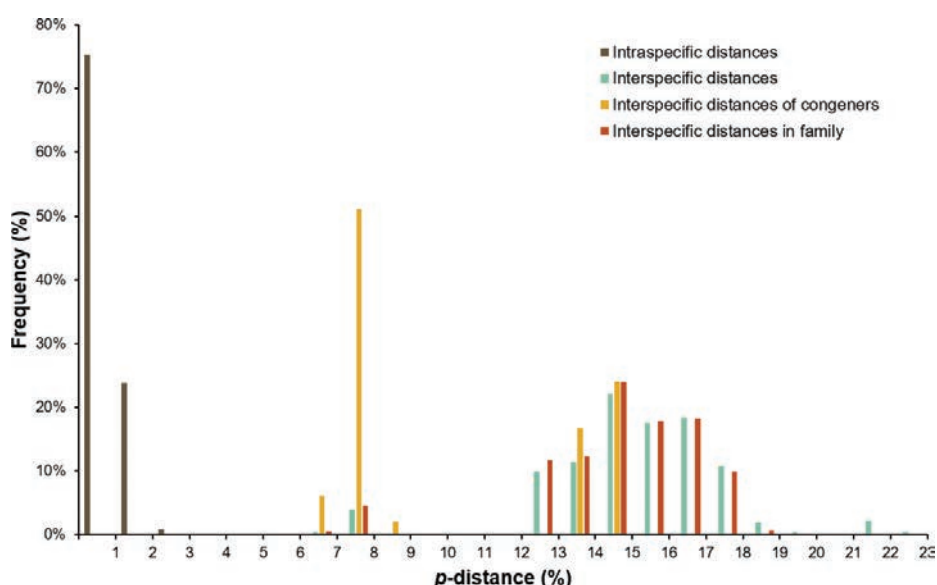


Figure 137. Intra- and interspecific uncorrected distances of partial COI gene sequences for each taxonomic level of Mantodea.

Discussion

This study presents the first comprehensive taxonomic review of the Mantodea species in Korea, recognizing eight species based on morphology and DNA barcodes. In contrast to previous studies that primarily focused on the documentation of unrecorded species, our study meticulously examined 494 specimens, encompassing all eight species that have been recorded in Korea. Notably,

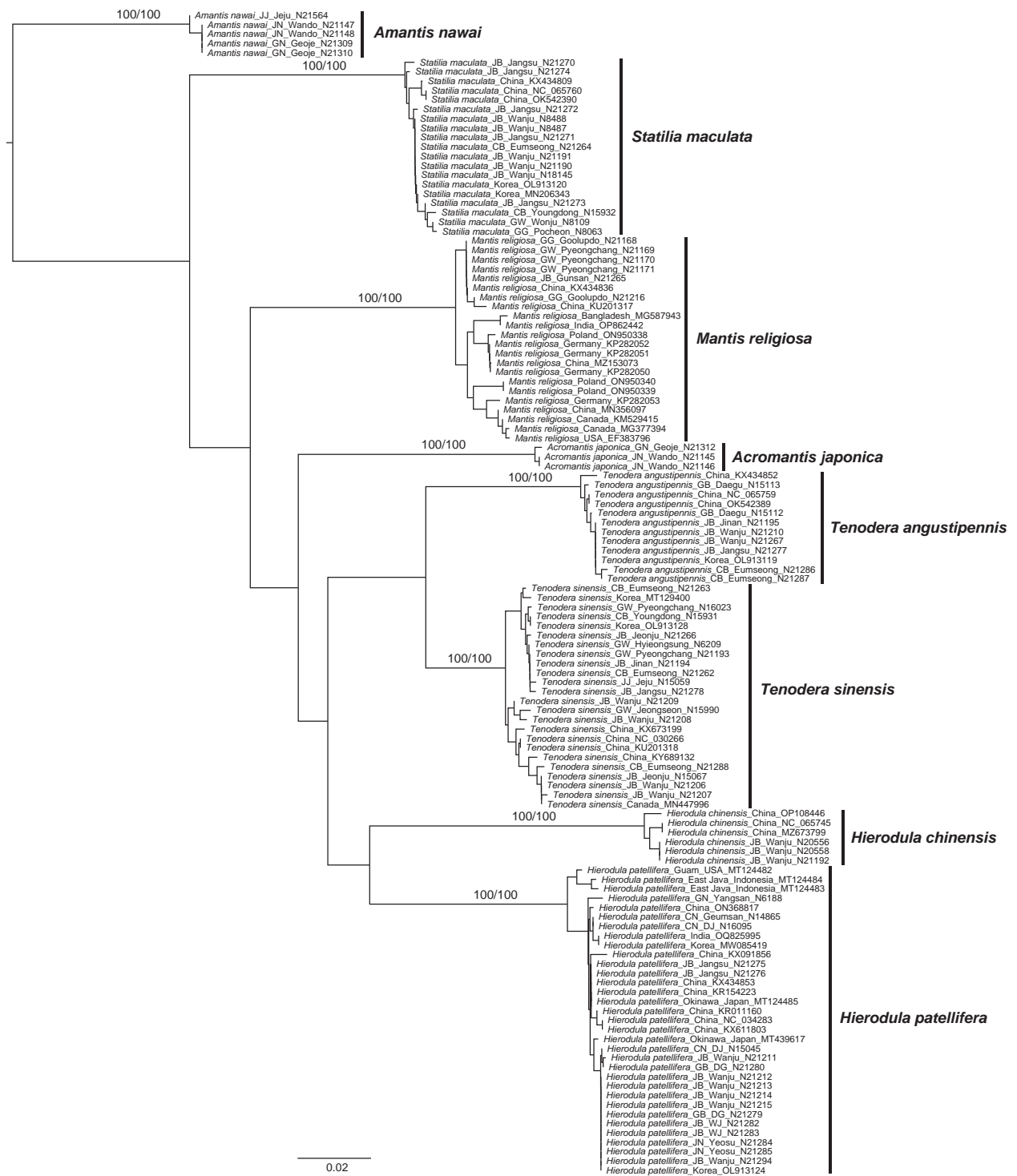
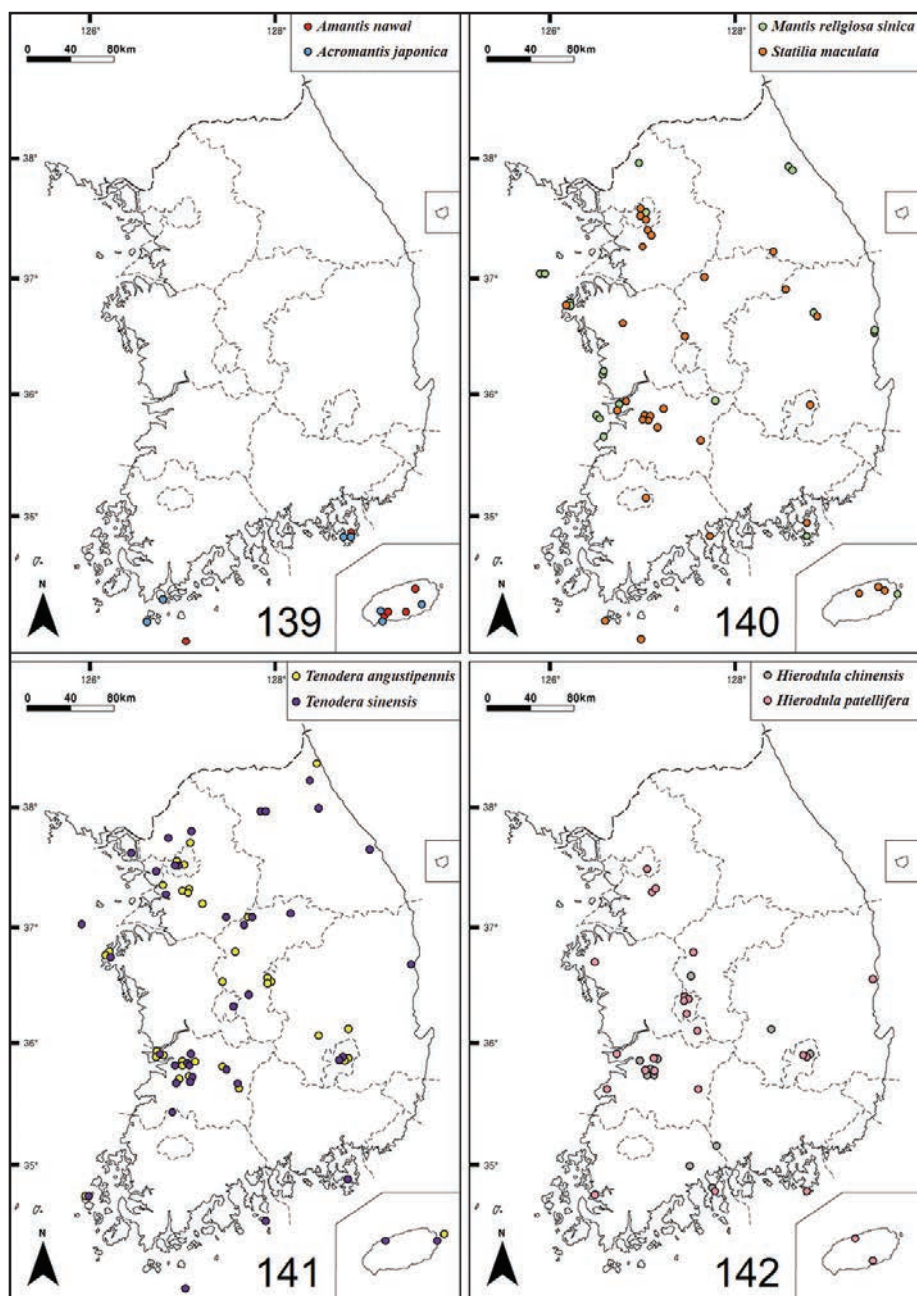


Figure 138. Neighbor-joining tree of Korean Mantodea species based on partial COI gene sequences with bootstrap values (left) and Parsimony analysis bootstrap values (right). Scale bar indicates the expected number of substitutions per site.

while the majority of species exhibit a broad distribution across the Korean peninsula (Figs. 139–142), the genera *Amantis* and *Acromantis* are confined to the southern islands of Korea (Fig. 139). Furthermore, *Hierodula chinensis*, initially documented in Jeonbuk Province in 2021 (Shim et al. 2021a), has been found in more locations since (Fig. 142).

The morphology of male genitalia is a crucial diagnostic feature for species identification and delineation in mantids, supporting the monophyly of high-



Figures 139–142. Distribution maps **139** *Amantis nawai*, *Acromantis japonica* **140** *Mantis religiosa sinica*, *Statilia maculata* **141** *Tenodera angustipennis*, *T. sinensis* **142** *Hierodula chinensis*, *H. patellifera*.

er taxa (Schwarz and Roy 2019; Liu et al. 2021). However, it is important to note that misidentification at the species level may occur in some cases due to afa structural variations in male genitalia, which can occur intraspecifically in mantids, even under sympatric conditions (Svenson and Roy 2011; Svenson and Vollmer 2014; Shim et al. 2021b). For example, the Korean populations of *Amantis nawai* exhibit two morphotypes of afa structural variations at the intra-specific level, which could lead to confusion at the species level (Figs. 16, 17). This situation makes it challenging to determine whether the observed variation in male genitalia represents a cryptic species or a morphological variation. However, the genetic divergence between the two morphotypes based on COI barcode data were not significantly different (0.3%, Table 1), and they were also

supported as a single lineage (Fig. 138). This is consistent with our findings that the intraspecific genetic divergence ranges from 0% to 2.2%, while interspecific divergence among congeners ranges from 6.7% to 14.6% (Tables 1, 2; Fig. 137). Furthermore, Mantodea species are each formed as distinct lineages on NJ (Fig. 138) and PA trees (not shown). Consequently, we consider all of them as separate and valid species, given that they exhibit morphological differences as discussed above.

Although the diversity of Mantodea in Korea is relatively modest when compared to the high species diversity and endemism observed in neighboring China and Japan (Otte et al. 2024), this study substantially advances our understanding of mantodean diversity within Korea. To further elucidate the diversity of Mantodea across the Korean peninsula, it is imperative that future research initiatives prioritize intensified specimen collection efforts, particularly targeting areas that have been under-sampled to date.

Table 2. Inter- and intraspecific genetic differences among Korean Mantodea species for COI (657 bp) calculated using *p*-distance.

	<i>Amantis nawai</i>	<i>Acromantis japonica</i>	<i>Mantis religiosa</i>	<i>Statilia mculata</i>	<i>Tenodera angustipennis</i>	<i>T. sinensis</i>	<i>Hierodula chinensis</i>	<i>H. patellifera</i>
<i>Amantis nawai</i>	0–0.003							
<i>Acromantis japonica</i>	0.165–0.170	0–0.003						
<i>Mantis religiosa</i>	0.159–0.193	0.146–0.178	0–0.022					
<i>Statilia mculata</i>	0.155–0.182	0.153–0.160	0.140–0.164	0–0.011				
<i>Tenodera angustipennis</i>	0.179–0.188	0.152–0.161	0.139–0.168	0.168–0.188	0–0.009			
<i>T. sinensis</i>	0.165–0.177	0.131–0.143	0.123–0.150	0.142–0.164	0.067–0.083	0–0.017		
<i>Hierodula chinensis</i>	0.196–0.204	0.169–0.176	0.146–0.159	0.165–0.182	0.172–0.181	0.143–0.154	0–0.011	
<i>H. patellifera</i>	0.210–0.224	0.142–0.153	0.150–0.173	0.163–0.179	0.138–0.154	0.122–0.145	0.134–0.146	0–0.020

Acknowledgements

We are grateful to A.L. Suzumura (Graduate School of Agriculture Hokkaido University) for her English editing and T. Kim (National Institute of Biological Resources) for providing us with valuable specimens. Comments and suggestions by reviewer E. Shcherbakov (Lomonosov Moscow State University, Russia) and subject editor C.J. Schwarz (Ruhr University Bochum, Germany) significantly improved the manuscript.

Additional information

Conflict of interest

The authors have declared that no competing interests exist.

Ethical statement

No ethical statement was reported.

Funding

This work was carried out with the support of the 'Cooperative Research Program for Agriculture Science and Technology Development (Project No. PJ01727703)' and the 2024 Collaborative Research Program between University and Rural Development Administration, Republic of Korea.

Author contributions

Conceptualization: JHS. Data curation: JS. Formal analysis: JHS, JS. Supervision: JHS. Visualization: JS. Writing - original draft: JS. Writing - review and editing: JHS.

Author ORCIDs

Jeong-Hun Song  <https://orcid.org/0000-0003-0317-1457>

Data availability

All of the data that support the findings of this study are available in the main text or Supplementary Information.

References

- An SL (2011) Current Status of Research about Insect Fauna of Natural Reserves in Korea. *Journal of Korean Nature* 4(4): 273–285. <https://doi.org/10.7229/jkn.2011.4.4.273>
- Audinet-Serville JG (1838) *Histoire naturelle des insectes: Orthoptères*. Librairie Encyclopédique de Roret, Paris XVIII, 776 pp. <https://doi.org/10.5962/bhl.title.16081>
- Battiston R, Leandri F, di Pietro W, Andria S (2019) *Mantis, Hierodula e Sphodromantis*: aggiornamento su conoscenze e identificazione delle mantidi (Mantodea: Mantinae) native ed aliene presenti in Italia. *Scienze e storia dell' ambiente padano* 38: 89–96.
- Bazyluk W (1960) Die geographische Verbreitung und Variabilität von *Mantis religiosa* (L.) (Mantodea, Mantidae), sowie Beschreibungen neuer Unterarten. *Annales Zoologici (Wars.)* 18: 231–272.
- Bazyluk W (1977) Fauna Polski, Blattodea et Mantodea (Insecta). *Polska Akademia Nauk, Warszawa* 6: 1–175. [Mantodea: 109–167]
- Befu T (1992) Notes on some ecological traits of *Acromantis japonica* and *A. satsumensis*. *Battarigisu* 93: 23. [in Japanese]
- Beier M (1932) Beiträge zur Fauna sinica. Herausgegeben von R. Mell, Berlin. XIII. Die Mantodeen Chinas. *Mitteilungen aus dem Museum für Naturkunde in Berlin. Zoologisches Museum und Institut für Spezielle Zoologie (Berlin)* 18: 322–337. <https://doi.org/10.1002/mmzn.19320180304>
- Beier M (1935) Mantodea. Subfamilie: Mantinae. In: Wytzman P (Ed.) *Genera Insectorum, Fascicule* 203, 1–146.
- Bey-Bienko G (1930) XLIX. Further studies on the Dermaptera and Orthoptera of Manchuria. *Annals & Magazine of Natural History* 10(29): 493–500. <https://doi.org/10.1080/00222933008673159>
- Brannoch SK, Wieland F, Rivera J, Klass KD, Béthoux O, Svenson GJ (2017) Manual of praying mantis morphology, nomenclature, and practices (Insecta, Mantodea). *ZooKeys* 696: 1–100. <https://doi.org/10.3897/zookeys.696.12542>
- Bruins E (1999) *Terrarien Enzyklopädie*. Karl Müller Verlag, Erlangen, 320 pp.
- Brunner de Wattenwyl K (1893) Révision du système des Orthoptères et description des espèces rapportées par M. Leonardo Fea de Birmanie. *Annali, Museo Civico de Storia Naturale Giacomo Doria, Genova, Serie 2* 13: 230. <https://doi.org/10.5962/bhl.title.5121>
- Burmeister H (1838) Frangschrecken. Mantodea. In: Burmeister H (Ed.) *Handbuch der Entomologie. Zweiter Band. Besondere Entomologie. Zweite Abtheilung. Kaukerfe, Gymnognatha (Erste Hälfte; vulgo Orthoptera)*. Enslin, Berlin, 517–552.
- Cho PS (1959) A manual of the Orthoptera of Korea. *Journal of Colleague Livial Arts Natrual Science of Korea Univsity* 4: 131–198.

- Chou HY (2006) Wing dimorphism of *Amantis nawai* (Shiraki, 1908) (Mantodea: Mantidae): male *A. nawai* in Taiwan possesses two wing morphs. (Doctoral dissertation). Unpublished D. Thesis. National Taiwan University's Institute of Entomology.
- De Haan W (1842) Bijdragen tot de Kennis der Orthoptera. In: Temmink CJ (Ed.) Verhandelingen over de Natuurlijke Geschiedenis der Nederlansche Overzeesche Bezittingen. Natuurkundige Commissie in Indie, Leiden, 248 pp. [23 pls]
- Doi H (1932) Miscellaneous of Insects. Journal of Chosen Natural History Society 13: 33–39.
- Ehrmann R (2002) Mantodea, gottesanbeterinnen der Welt. Natur und Tier, Münster, 519 pp.
- Ehrmann R, Borer M (2015) Mantodea (Insecta) of Nepal: An annotated checklist. Biodiversität und Naturlausstattung im Himalaya 5: 227–274.
- ESK and KSAE (The Entomological Society of Korea and Korean Society of Applied Entomology) (1994) Check List of Insects from Korea. Kon-Kuk University Press, Seoul.
- Geoffroy M (1762) Histoire abrégée des insectes, dans laquelle ces animaux sont rangés suivant un ordre méthodique. Delalain 1, Paris, 28+523 pp. [Mantodea: pp. 399–400] <https://doi.org/10.5962/bhl.title.154767>
- Giglio-Tos E (1912) Mantidi esotici. V. Mantes, Tenoderae, Hierodulae et Rhomboderae. Bollettino della Società Entomologica Italiana 43: 3–167.
- Giglio-Tos E (1915) Mantidi esotici. Generi e specie nuove. Bollettino della Società Entomologica Italiana 46: 134–200.
- Giglio-Tos E (1927) Das Tierreich. Orthoptera-Mantidae. Walter de Gruyter & Co., Berlin, 707 pp. <https://doi.org/10.1515/9783111430669>
- Hashimoto K, Suzuki K, Hayashi F (2016) Unique set of copulatory organs in mantises; Concealed female genital opening and extremely asymmetric male genitalia. Entomological Science 19(4): 383–390. <https://doi.org/10.1111/ens.12219>
- Iwasaki T (1996) Comparative Studies on the life histories of two praying mantises, *Tenodera aridifolia* (Stoll) and *Tenodera angustipennis* Saussure (Mantodea: Mantidae): I. temporal pattern of egg hatch and nymphal development. Applied Entomology and Zoology 31(3): 345–356. <https://doi.org/10.1303/aez.31.345>
- Jensen D, Svenson GJ, Song H, Whiting MF (2010) Phylogeny and evolution of male genitalia within the praying mantis genus *Tenodera* (Mantodea: Mantidae). Invertebrate Systematics 23(5): 409–421. <https://doi.org/10.1071/IS09004>
- Jeon JB, Lee SH, Lee SM (1999) Notes on the Praying Mantids (Mantodea) in Korea. Insecta Koreana 16: 225–229.
- Ju DR (1969) Check list of insect classification. Gwahakwon Publish, Pyeongyang.
- Kim TW (2010) Dictyoptera. In: Paek MK (Ed.) Checklist of Korean Insects. Nature and Ecology, Seoul, 31 pp.
- Kim TW (2021) Mantodea. In: Park JK, Lee JE et al. (Eds) Checklist of Insects from Korea. Korean Society of Applied Entomology & The Entomological Society of Korea. Paper and Pencil, Daegu, 65 pp.
- Kimura M (1980) A simple method for estimating evolutionary rates of base substitutions through comparative studies of nucleotide sequences. Journal of Molecular Evolution 16(2): 111–120. <https://doi.org/10.1007/BF01731581>
- Kirby WF (1900) Mantodea, in: Andrews CW (Ed.) A monograph of Christmas Island (Indian Ocean): physical Features and geology by Charles W Andrews. With descriptions of the fauna and flora by numerous contributors. Lonemans, London, 146–147.
- Kirby WF (1904) A synonymic catalogue of Orthoptera. Euplexoptera, Cursoria (Forficulidae, Hemimeridae, Blattidae, Mantidae, Phasmidae). Print of the Trust, British Museum, London 1: I–X+501 pp. [Mantodea: pp. 207–316]

- Klass KD (1997) External male genitalia and phylogeny of Blattaria and Mantodea. *Zoologisches Forschungsinstitut* 42: 1–341.
- Klass KD (2001) Morphological evidence on blattarian phylogeny: “phylogenetic histories and stories” (Insecta, Dictyoptera). *Deutsche Entomologische Zeitschrift* 48: 223–265. <https://doi.org/10.1002/mmnd.4800480203>
- Klass KD, Meier R (2006) A phylogenetic analysis of Dictyoptera (Insecta) based on morphological characters. *Entomologische Abhandlungen* 63: 3–50.
- Kumar S, Stecher G, Li M, Knyaz C, Tamura K (2018) MEGA X: Molecular Evolutionary Genetics Analysis across computing platforms. *Molecular Biology and Evolution* 35(6): 1547–1549. <https://doi.org/10.1093/molbev/msy096>
- Kwon YJ, Suh SJ, Huh EY (1996) Insect diversity of Pogil island in Korea. Report on the survey of Natural Environment in Korea 11: 213–261.
- Latreille PA (1802) Histoire, générale et particulière des Crustacés et des Insectes. Sonnini CS Vol. 3. Dufart, Paris, XII + 467 pp. <https://doi.org/10.5962/bhl.title.15764>
- Lia A (2007) Distribution of *Mantis religiosa* (L.) and its changes in Poland. *Fragmenta Faunistica* 50(2): 91–125. <https://doi.org/10.3161/00159301FF2007.50.2.091>
- Linnaeus C (1758) Systema naturae per regna tria naturae, secundum classes, ordines, genera, species, cum characteribus, differentiis, synonymis, locis. Tomus 1, editio decima, reformata. Holmiae, Laurentii Salvii, Stockholm, 847 pp. <https://doi.org/10.5962/bhl.title.542>
- Liu QP, Liu ZJ, Chen ZT, Yuan ZL, Shi Y (2020) A new species and two new species records of Hierodulinae from China, with a revision of *Hierodula chinensis* (Mantodea: Mantidae). *Oriental Insects* 55(1): 99–118. <https://doi.org/10.1080/00305316.2020.1754954>
- Liu QP, Liu ZJ, Wang G, Yin Z (2021) Taxonomic revision of the praying mantis subfamily Hierodulinae of China (Mantodea: Mantidae). *Zootaxa* 4951(3): 401–433. <https://doi.org/10.11646/zootaxa.4951.3.1>
- Manuel B (1797) Histoire Naturelle, Insectes– Mantes. *Encyclopédie Méthodique*. 7: 619–642.
- Moulin N (2020) When Citizen Science highlights alien invasive species in France: The case of Indochina mantis, *Hierodula patellifera* (Insecta, Mantodea, Mantidae). *Biodiversity Data Journal* 8: e46989. <https://doi.org/10.3897/BDJ.8.e46989>
- Mukherjee TK, Ghosh AK, Hazra AK (1995) The mantid fauna of India (Insecta: Mantodea). *Oriental Insects* 29(1): 185–358. <https://doi.org/10.1080/00305316.1995.10433744>
- Mukherjee TK, Iyer G, Chatterjee P (2017) Twenty-three new records of mantodea (Insecta) from some states of India. *Journal of Threatened Taxa* 9(2): 9829–9839. <https://doi.org/10.11609/jott.1936.9.2.9829-9839>
- Nakamine H (2016) Mantodea. In: Orthopterological Society of Japan (Ed.) The standard of Polyneoptera in Japan. Gakken Plus, Tokyo, 198–205.
- Nakamine H, Yamasaki K, Naka H (2017) The number of stripes on the compound eyes reflects each instar in *Acromantis satsumensis* (Mantodea: Hymenopodidae). *Applied Entomology and Zoology* 52(1): 135–138. <https://doi.org/10.1007/s13355-016-0445-0>
- Okamoto H (1924) The insect Fauna of Quelpat island (Saishiu-to). *Bulletin of the Agricultural Experiment Station. Government General of Chosen* 1, iv+47–223.
- Oshima K (2017) New records of *Statilia nemoralis* and *Tenodera fasciata* from Kume Island, the Ryukyus, Japan. *Journal of Entomology, New Series* 20: 129–131. [in Japanese] https://doi.org/10.20848/kontyu.20.3_129

- Oshima K (2018) New records of six species of Mantodea from some islands adjacent to Okinawa-jima Island, the Ryukyus, Japan. *Journal of Entomology, New Series* 21: 151–160. (in Japanese). https://doi.org/10.20848/kontyu.21.2_151
- Oshima K (2020) Confirmation of the presence of *Statilia maculata* (Thunberg) (Mantodea, Mantidae) in Taiwan, with notes on its morphology. *Nodai Entomology* 2: 1–4.
- Otte D, Spearman L, Stiewe MBD (2024) Mantodea Species File Online. Version 5.0/5.0. <http://mantodea.speciesfile.org>
- Patel S, Singh R (2016) Updated checklist and distribution of Mantidae (Mantodea: Insecta) of the World. *International Journal of Research Studies in Zoology* 2(4): 17–54. <https://doi.org/10.20431/2454-941X.0204003>
- Patel S, Singh G, Singh R (2016) Checklist of global distribution of Hymenopodidae (Mantodea: Dictyoptera: Insecta). *International Journal of Current Research* 8: 42047–42054.
- Rehn JAG (1903) Studies in Old World Mantidae (Orthoptera). *Proceedings. Academy of Natural Sciences of Philadelphia* 55: 701–718.
- Roy R (1968) Compléments à la connaissance du genre Mantis: L'identité de *M. nobilis* et *M. octospilota*. *Bulletin de la Société Entomologique de France* 73(7): 174–176. <https://doi.org/10.3406/bsef.1968.21013>
- Saussure HD (1869) Essai d'un Système des Mantides. *Mitteilungen der Schweizerische Entomologische Gesellschaft* 3: 49–73.
- Saussure HD (1870) Additions au système des Mantides. *Mitteilungen der Schweizerische Entomologische Gesellschaft* 3: 221–244.
- Saussure HD (1871a) Mélanges Orthoptérologiques, III^{me} Fascicule. IV. Mantides. *Mémoires de la Société de Physique et d'Histoire naturelle de Genève* 21: 1–214. [pl. 4–6]
- Saussure HD (1871b) Mélanges Orthoptérologiques, Supplément au III^{me} Fascicule. H. Georg, Genève & Bâle, 363–460. [pl. 7]
- Schwarz C, Roy R (2019) The systematics of Mantodea revisited: an updated classification incorporating multiple data sources (Insecta: Dictyoptera). *Annales de la Société entomologique de France (N.S.)* 55: 101–196. <https://doi.org/10.1080/00379271.2018.1556567>
- Schwarz C, Ehrmann R, Borer M, Monnerat C (2018) Mantodea (Insecta) of Nepal: Corrections and annotations to the checklist. *Biodiversität und Naturlausstattung im Himalaya* 6: 201–247.
- Shcherbakov E, Anisyutkin L (2018) Update on the praying mantises (Insecta: Mantodea) of South-East Vietnam. *Annales de la Société entomologique de France (N.S.)* 54: 119–140. <https://doi.org/10.1080/00379271.2018.1447394>
- Shcherbakov E, Govorov V (2020) *Statilia maculata* (Thunberg, 1784) the first invasive praying mantis (Mantodea, Mantidae) in the fauna of Russia. *Annales de la Société entomologique de France (N.S.)* 56: 189–202. <https://doi.org/10.1080/00379271.2020.1785941>
- Shim J, Park H, Ju HJ, Song JH (2021a) The giant Asian mantis *Hierodula chinensis* Werner (Mantodea: Mantidae) new to Korea. *Journal of Asia-Pacific Biodiversity* 14(1): 121–126. <https://doi.org/10.1016/j.japb.2020.11.001>
- Shim J, Park H, Kim S, Ju HJ, Song JH (2021b) Species delimitation of the praying mantis *Hierodula patellifera* (Audinet-Serville) based on morphological and molecular characters (Mantodea: Mantidae). *Zootaxa* 4951(1): 147–158. <https://doi.org/10.11646/zootaxa.4951.1.7>
- Shiraki T (1908) *Gonypeta nawai*. Shiraki. *Insect World* 12: 47–50. [in Japanese]

- Shiraki T (1911) Phasmiden und Mantiden Japans. The Zoological Society of Japan. 7: 291–331.
- Shiraki T (1932) Orthoptera of the Japanese Empire Part III. Insecta Matsumurana 22: 113–123.
- Srivathsan A, Meier R (2012) On the inappropriate use of Kimura-2-parameter (K2P) divergences in the DNA-barcoding literature. Cladistics 28(2): 190–194. <https://doi.org/10.1111/j.1096-0031.2011.00370.x>
- Stål C (1877) Systema Mantodeorum. Essai d'une systematisation nouvelle des Mantodées. Bihang till kőngliche Svenska Vetenskaps Akademien Handlingar, Stockholm 4: 1–91.
- Svenson GJ, Roy R (2011) Taxonomic treatment of the endemic Malagasy praying mantis genus *Hyalomantis* Giglio-Tos, 1915, with a new synonymy and the description of three new species (Mantodea, Iridopterygidae, Tropidomantinae). Zootaxa 2777(1): 1–24. <https://doi.org/10.11646/zootaxa.2777.1.1>
- Svenson GJ, Vollmer W (2014) A case of the higher-level classification of praying mantises (Mantodea) obscuring the synonymy of *Majangella* Giglio-Tos, 1915 (Liturgusidae, Liturgusinae) and *Ephippiomantis* Werner, 1922 (Hymenopodidae, Acromantinae). Zootaxa 3797(1): 103–119. <https://doi.org/10.11646/zootaxa.3797.1.10>
- Svenson GJ, Hardy NB, Cahill Wightman HM, Wieland F (2015) Of flowers and twigs: phylogenetic revision of the plant-mimicking praying mantises (Mantodea: Empusidae and Hymenopodidae) with a new suprageneric classification. Systematic Entomology 40(4): 789–834. <https://doi.org/10.1111/syen.12134>
- Taniguchi I (1987) Notes on breeding *Acromantis japonica*. Insectarium 24: 24–25. [in Japanese]
- Thunberg CP (1784) Dissertatio entomologica novae insectorum specis sistens, III. Mantodea. Edmann, Jahan. Novae Insectorum Species, Uppsala 3: 53–68.
- Tinkham ER (1937) Studies in Chinese Mantidae (Orthoptera). Lingnan Science Journal 16: 481–499.
- Vjayandi MC, Rajeesh RS, John PS, Dhanasree MM (2010) On a collection of praying mantids (Insecta: Mantodea) from Goa, India, with new distribution records. Journal of Threatened taxa 1325–1329. <https://doi.org/10.11609/JoTT.o2188.1325-9>
- Wang TQ (1993) Synopsis on the classification of Mantodea from China. Shanghai Scientific and Technological, Literature Publishing House, Shanghai.
- Wang Y, Zhou S, Zhang Y (2020) Revision of the genus *Hierodula* Burmeister (Mantodea: Mantidae) in China. Entomotxonomia 42: 1–21.
- Werner F (1922) Philippine mantids, or praying insects. Philippine Journal of Science 21: 147–157.
- Werner F (1929) Über einige Mantiden aus China (Expedition Stötzner) und andere neue oder seltene Mantiden des Museum Dresden. Entomologische Zeitung 90: 74–78. [in German]
- Werner F (1935) Farther communication on Indian mantids or praying insects. Proceedings of the Zoological Society of London 105(3): 495–498. <https://doi.org/10.1111/j.1096-3642.1935.tb01676.x>
- Westwood JO (1889) Revisio Insectorum Familiae Mantidarum speciebus novis aut minus cognitis descriptis et delineatis. Gurney and Jackson, London.
- Wieland F (2013) The phylogenetic system of Mantodea (Insecta: Dictyoptera). Species. Phylogeny and Evolution 3: 3–222. <https://doi.org/10.17875/gup2013-711>
- Yager DD, Svenson GJ (2008) Patterns of praying mantis auditory system evolution based on morphological, molecular, neurophysiological, and behavioural data.

Biological Journal of the Linnean Society 94: 541–568. <https://doi.org/10.1111/j.1095-8312.2008.00996.x>

Yamasaki T (1981) The taxonomic status of "*Iridopteryx maculata*" (Mantodea, Mantidae) with notes on its distribution. *Memoirs of the National Museum of Nature and Science, Tokyo* 14: 95–102.

Yamasaki K, Schütte K, Nawa T (2022) New record of Chinese reddish mantis, *Hierodula chinensis* Werner, 1929 (Mantodea, Mantidae) from Japan. *Check List* 18(1): 147–150. <https://doi.org/10.15560/18.1.147>

Zhu X, Wu C, Yuan Q (2012) *Mantodea in China*. Xiyuan Publishing House, Beijing.

Supplementary material 1

List of species with their locality data, voucher numbers, and GenBank accession numbers

Authors: Jaeil Shim, Jeong-Hun Song

Data type: xlsx

Explanation note: Asterisks indicate new addition.

Copyright notice: This dataset is made available under the Open Database License (<http://opendatacommons.org/licenses/odbl/1.0/>). The Open Database License (ODbL) is a license agreement intended to allow users to freely share, modify, and use this Dataset while maintaining this same freedom for others, provided that the original source and author(s) are credited.

Link: <https://doi.org/10.3897/zookeys.1206.123355.suppl1>

Seven new species of the subgenus *Homoneura* Malloch (Diptera, Lauxaniidae, *Homoneura*) from Jiangjin District, southwestern Chongqing, China

Xulong Chen¹, Pengyan You², Wenliang Li², Zhisheng Zhang¹

1 Key Laboratory of Eco-environments in Three Gorges Reservoir Region (Ministry of Education), School of Life Sciences, Southwest University, Chongqing 400715, China

2 College of Horticulture and Plant Protection, Henan University of Science and Technology, Luoyang, Henan 471023, China

Corresponding authors: Wenliang Li (wenliangli@haust.edu.cn); Zhisheng Zhang (zhangzs327@qq.com)

Abstract

Seven new species of the subgenus *Homoneura* are described, *Homoneura* (*Homoneura*) *biconica* Chen & Li, **sp. nov.**, *Homoneura* (*Homoneura*) *dilatata* Chen & Li, **sp. nov.**, *Homoneura* (*Homoneura*) *jiangjinensis* Chen & Li, **sp. nov.**, *Homoneura* (*Homoneura*) *microtricha* Chen & Li, **sp. nov.**, *Homoneura* (*Homoneura*) *multisetata* Chen & Li, **sp. nov.**, *Homoneura* (*Homoneura*) *serrulata* Chen & Li, **sp. nov.**, *Homoneura* (*Homoneura*) *simianshana* Chen & Li, **sp. nov.**, which were collected from Jiangjin District, southwestern Chongqing, China and are assigned to the *henanensis* group. A key to all of the 53 species of this species group in China is presented.

Key words: Homoneurinae, illustration, morphology, new taxon, taxonomy



Academic editor: Owen Lonsdale

Received: 7 April 2024

Accepted: 11 May 2024

Published: 2 July 2024

ZooBank: <https://zoobank.org/A39A64C8-5BE5-4643-AA43-03026F8DD268>

Citation: Chen X, You P, Li W, Zhang Z (2024) Seven new species of the subgenus *Homoneura* Malloch (Diptera, Lauxaniidae, *Homoneura*) from Jiangjin District, southwestern Chongqing, China. ZooKeys 1206: 45–80. <https://doi.org/10.3897/zookeys.1206.124892>

Copyright: © Xulong Chen et al.
This is an open access article distributed under terms of the Creative Commons Attribution License (Attribution 4.0 International – CC BY 4.0).

Introduction

The Lauxaniid fauna in southwestern China is relatively well-known, but new species are continuously discovered in the humid parts and especially in southern Yunnan and southwestern Guizhou, where significantly higher species richness and endemism are found (Gao and Yang 2002, 2005; Shi et al. 2009, 2017a, 2020; Li and Yang 2012, 2013, 2015; Shi and Yang 2015; Li et al. 2019, 2020a, 2020b, 2020c, 2020d, 2020e, 2020f, 2021a, 2021b, 2023; Zhao et al. 2022). Compared to these areas, research on the diversity of lauxaniid flies in Chongqing is relatively weak, and currently only nine species in five genera are known; four *Homoneura* species were described more recently by You et al. (2023) from Yintiaoling Nature Reserve, Chongqing, China.

Jiangjin District is located in southwestern Chongqing, adjacent to Guizhou Province to the southeast and Sichuan Province to the west and southwest. The geographical coordinates are between 105°49'–106°38' east longitude and 28°28'–29°28' north latitude. It has a subtropical humid monsoon climate, with a mild climate and abundant precipitation, high vegetation abundance and rich humus and fungi, providing a good environment for the habitat and reproduction of many organisms.

Homoneura (Homoneura) Malloch, 1927 is the largest subgenus of genus *Homoneura* Wulp, 1891 with more than 700 species distributed worldwide. The Chinese fauna of *H. (Homoneura)* is richly represented with more than 220 species, which are sorted into 21 species groups based on external characters and male genitalia morphology (Shi and Yang 2014). Seven new species described in this paper are assigned to the *henanensis* group of the subgenus *Homoneura* Malloch by the wing having five brown spots, which are respectively located between the r-m and apical spot on R_{4+5} , crossvein dm-cu and the tips of R_{2+3} , R_{4+5} , and M_1 .

At present, there are 46 known species of *henanensis* group in China (Kertész 1915; Matsumura 1916; Malloch 1926; Yang et al. 1999, 2001, 2003; Gao and Yang 2002, 2003, 2004, 2005; Wang et al. 2012; Papp and Gaimari 2013; Shi and Yang 2014; Shi et al. 2017b; Gao and Shi 2019; Chen and Li 2022; You et al. 2023). Seven new species were found among recently collected specimens from Jiangjin District, Chongqing in southwestern China. In present paper, the descriptions and illustrations of male genitalia of these new species are provided, increasing the number of species of the *Homoneura henanensis* group to 53 species in China, with 11 in Chongqing.

Materials and methods

General terminology follows Cumming and Wood (2017) and Gaimari and Miller (2021). Genitalia preparations were made by removing and macerating the apical portion of the abdomen in pancreatin for six hours (Álvarez-Padilla and Hormiga 2007), then rinsing them with distilled water for dissection and study. After examination in glycerin, they were transferred to fresh glycerin and stored in a microvial pinned below the specimen. Specimens examined were deposited in the Henan University of Science and Technology, Luoyang, Henan, China (HAUST).

Taxonomy

Key to species of *Homoneura (Homoneura) henanensis* group in China (modified from Gao and Shi 2019; You et al. 2023)

- 1 Wing with brown spot at tip of Sc and R_1 elongating along costal margin.... 2
- Wing without brown spot at tip of Sc and R_1 3
- 2 Basal edge of brown apical spot on R_{2+3} behind vertical level as crossvein dm-cu; wing with brown spot at tip of Sc and R_1 slightly elongating along costal margin; surstylus claviform with 3 long setulae, postgonite long coniform with 5 short setulae..... ***H. (H.) hirayamae* (Matsumura, 1916)**
- Basal edge of brown apical spot on R_{2+3} at same vertical level as crossvein dm-cu; wing with brown spot at tip of Sc and R_1 , extending closely to brown apical spot on R_{2+3} along costal margin; surstylus without long setula, short claviform with a subapical concavity in posterior view; postgonite hook-like and sharp at apex..... ***H. (H.) similicurvata* Gao & Shi, 2019**
- 3 Basal edge of brown apical spot on R_{2+3} at same vertical level as crossvein dm-cu 4
- Basal edge of brown apical spot on R_{2+3} behind vertical level as crossvein dm-cu 15

- 4 Palpus yellow except for black at tip; surstylus broad, sheet-like with short apical setulae in lateral view and curved apically in posterior view..... ***H. (H.) dadongshanica* Shi & Yang, 2014**
- Palpus entirely yellow; surstylus not as above **5**
- 5 Mesonotum with acrostichal setulae in 6 irregular rows..... **6**
- Mesonotum with acrostichal setulae in 8–10 irregular rows..... **7**
- 6 Arista with longest ray slightly < 1/2 height of first flagellomere; surstylus with a small triangular process with several setulae in lateral view ***H. (H.) dagupingensis* Gao & Shi, 2019**
- Arista with longest ray as long as height of first flagellomere; surstylus with a long digitiform process in lateral view and without subapical concavity ***H. (H.) wuxica* You, Chen & Li, 2023**
- 7 Mesonotum with acrostichal setulae in 8 irregular rows..... ***H. (H.) brevis* Gao & Yang, 2004**
- Mesonotum with acrostichal setulae in 10 irregular rows **8**
- 8 Wing with brown apical spots on R_{2+3} , R_{4+5} and M_1 entirely separated (Fig. 22) ***H. (H.) jiangjinensis* sp. nov.**
- Wing with brown apical spots on R_{2+3} , R_{4+5} and M_1 confluent, or brown apical spots on R_{4+5} and M_1 confluent, separated from apical spot on R_{2+3} **9**
- 9 Subcostal cell hyaline (Fig. 42)..... ***H. (H.) multiseta* sp. nov.**
- Subcostal cell pale brown..... **10**
- 10 Ultimate and penultimate sections of M_1 in proportion of 1.2: 1 ***H. (H.) yaromi* Yang, Hu & Zhu, 2001**
- Ultimate and penultimate sections of M_1 in proportion of 1: 1 **11**
- 11 Brown apical spots on R_{4+5} and M_1 confluent, separated from apical spot on R_{2+3} **12**
- Brown apical spots on R_{2+3} , R_{4+5} and M_1 slightly confluent and forming pale brown connecting area between 3 apical spots..... **13**
- 12 Abdominal tergites 2–5 without brown posterior margin; syntergosternite with 2 or 3 setulae around spiracle; surstylus consisting of wide knife-like process and triangular process in lateral view; postgonites symmetrical in ventral view ***H. (H.) stepheni* Shi, Gao & Shen, 2017**
- Abdominal tergites 2–5 each with brown posterior margin; syntergosternite without setula around spiracle; surstylus long and furcated in lateral view; postgonites asymmetrical in ventral view ***H. (H.) anadaequata* Gao & Shi, 2019**
- 13 Male tergites 2–5 each with blackish brown posterior margin (Fig. 55); ctenidium with 14 short setae on fore femur; inner process of surstylus evaginable apically with serrulate margin in posterior view (Fig. 57)..... ***H. (H.) serrulata* sp. nov.**
- Male tergites 2–5 each with brown posterior margin; ctenidium with 18–20 short setae on fore femur; surstylus not as above **14**
- 14 Fore femur with 8 posterior dorsal setae, 6 posterior ventral setae; mid femur with 6 or 7 anterior setae; brown apical spots on R_{2+3} longer, at least 2/3 length of ultimate section of M_1 ; brown median spot on R_{4+5} at middle point of distance between r-m and dm-cu.... ***H. (H.) shunhuangshana* Chen & Li, 2022**
- Fore femur with 9 posterior dorsal setae, 4 posterior ventral setae; mid femur with 5 anterior setae; brown apical spots on R_{2+3} shorter, as long as 1/2 length of ultimate section of M_1 (Fig. 62); brown median spot on R_{4+5}

- behind middle point of distance between r-m and dm-cu (Fig. 62)
 ***H. (H.) simianshanica* sp. nov.**
- 15 Basal edge of brown apical spot on R_{2+3} at same vertical level as apical spot on R_{4+5} ; apical spot on R_{4+5} close to brown spot on crossvein dm-cu or at least 2/3 length of ultimate section of M_1 **16**
- Basal edge of brown apical spot on R_{4+5} behind vertical level as apical spot on R_{2+3} ; apical spot on R_{4+5} far from brown spot on crossvein dm-cu and < 2/3 length of ultimate section of M_1 **19**
- 16 Apical spot on R_{4+5} close to brown spot on crossvein dm-cu; ctenidium with 16 short setae on fore femur; surstylus apically acute in lateral view; pregonite absent; postgonite consisting of a furcated process and a subuliform process in ventral view ***H. (H.) denticulata* Shi & Yang, 2014**
- Apical spot on R_{4+5} ~ 2/3 length of ultimate section of M_1 , not close to brown spot on crossvein dm-cu; ctenidium with 12–14 short setae on fore femur; surstylus apically blunt in lateral view, pregonite with inverse U-shaped process and postgonite consisting a pair of subuliform processes in ventral view **17**
- 17 Hypandrium with a short ventral process; pregonite with a pair of inverse U-shaped processes in ventral view; postgonite short and acute, but pregonite longer than postgonite in ventral view **18**
- Hypandrium with a long ventral process; shape of pregonite and postgonite not as above, but pregonite shorter than postgonite in ventral view
 ***H. (H.) pseudograndis* Papp & Gaimari, 2013**
- 18 Phallus with a pair of lateral teeth subapically in ventral view; 2 arms of inverse U-shaped pregonite asymmetrical distinctly
 ***H. (H.) simigrandis* Shi & Yang, 2014**
- Phallus without a pair of lateral teeth subapically in ventral view; 2 arms of inverse U-shaped pregonite almost symmetrical in length
 ***H. (H.) grandis* (Kertész, 1915)**
- 19 Wing with brown string-like spot on R_{2+3} and apical spots on R_{4+5} and M_1 ; epandrium slender and surstylus apically acute with a long seta in lateral view ***H. (H.) curvispina* Gao & Yang, 2003**
- Wing with round, elliptical or quadrate spot on R_{2+3} , R_{4+5} and M_1 ; epandrium and surstylus not as above **20**
- 20 Wing with brown apical spots on R_{2+3} , R_{4+5} and M_1 entirely confluent, or slightly confluent and forming pale brown connecting area between apical spots on R_{2+3} , R_{4+5} and M_1 **21**
- Wing with brown apical spots on R_{4+5} and M_1 confluent, separated from apical spot on R_{2+3} , or apical spots on R_{2+3} , R_{4+5} and M_1 entirely separated **27**
- 21 Brown medial spot on R_{4+5} separated from brown cloud on crossvein dm-cu **22**
- Brown medial spot on R_{4+5} confluent with brown cloud on crossvein dm-cu **25**
- 22 Abdominal tergites 2–5 without blackish brown posterior margin; syntergosternite with long hairs around spiracle **23**
- Abdominal tergites 2–5 with blackish brown posterior margin; syntergosternite without long hair around spiracle **24**
- 23 Mesonotum with acrostichal setulae in 8 irregular rows; fore femur with 3 posterior ventral setae; syntergosternite without ventral process; surstylus

- blunt apically; phallapodeme normal apically
 ***H. (H.) martini* Shi, Gao & Shen, 2017**
- Mesonotum with acrostichal setulae in 10 rows (Fig. 14); fore femur with 5 posterior ventral setae (Fig. 13); syntergosternite with a trapeziform ventral process (Fig. 18); surstylus furcated into 2 curved, short processes in lateral view (Fig. 16); phallapodeme expanded apically (Fig. 20)
 ***H. (H.) dilatata* sp. nov.**
- 24 Mesonotum with acrostichal setulae in 8 irregular rows; fore femur with 10 posterior dorsal setae and ctenidium with 12 short setae; subcostal cell pale brown apically; surstylus with concavity apically in lateral view ...
 ***H. (H.) apiconcava* You, Chen & Li, 2023**
- Mesonotum with acrostichal setulae in 10 irregular rows (Fig. 4); fore femur with 8 posterior dorsal setae and ctenidium with 16 short setae (Fig. 3); subcostal cell hyaline (Fig. 2); surstylus consisting of a longer subuliform process and a shorter subuliform process in lateral view (Fig. 6).....
 ***H. (H.) biconica* sp. nov.**
- 25 Fore femur with 4 posteroventral setae; syntergosternite circular **26**
- Fore femur with 6 posteroventral setae; syntergosternite semicircular
 ***H. (H.) yangi* Gao & Yang, 2005**
- 26 Abdominal tergites 2–5 without blackish brown posterior margin; surstylus indistinct, blunt apically; hypandrium Y-shaped; phallus without triangular median process in ventral view..... ***H. (H.) guizhouensis* Gao & Yang, 2002**
- Abdominal tergites 2–5 with blackish brown posterior margin; surstylus distinctly digitiform in lateral view; hypandrium H-shaped; phallus with a pair of triangular median process in ventral view
 ***H. (H.) yintiaolingica* You, Chen & Li, 2023**
- 27 Wing with brown apical spot on R_{4+5} and M_1 slightly confluent and forming pale brown connecting area between 2 apical spots; apical spot on R_{2+3} distinctly separated from apical spot on R_{4+5} **28**
- Wing with brown apical spots on R_{2+3} , R_{4+5} , and M_1 entirely separated **42**
- 28 Mesonotum with acrostichal setulae in 10 rows **29**
- Mesonotum with acrostichal setulae in 6–8 rows **32**
- 29 Subcostal cell hyaline **30**
- Subcostal cell pale brown or brown apically **31**
- 30 Surstylus bulged claviform, with long setulae in lateral view; abdominal tergites 2–5 with pale brown posterior margin; arista with longest ray as long as height of first flagellomere; ctenidium with 16 or 17 short setae on fore femur; hypandrium Y-shaped..... ***H. (H.) bispinalis* Yang, Hu & Zhu, 2001**
- Surstylus T-shaped and rounded apically in lateral view; abdominal tergites 2–5 without pale brown posterior margin; arista with longest ray shorter than height of first flagellomere; ctenidium with 10 short setae on fore femur; hypandrium H-shaped ***H. (H.) fujianensis* Yang, Zhu & Hu, 2003**
- 31 Mesoscutum with 1 square or oval brown spot before scutoscutellar suture, scutellum with 1 square brown spot at middle; fore femur with 7 or 8 posterior dorsal setae, ctenidium with 22 short setae; surstylus long and spine-like in lateral view, without inner process
 ***H. (H.) maculiscutellata* Chen & Li, 2022**
- Mesoscutum without spot before scutoscutellar suture, scutellum without brown spot; fore femur with 5 posterior dorsal setae, ctenidium with

- 12 short setae; surstylus with 1 short, claviform inner process in lateral view ***H. (H.) tianeensis* Gao & Yang, 2004**
- 32 Abdomen yellow or pale brown, at least tergites 2–5 with black or brown posterior margin **33**
- Abdomen yellow, tergites 1–6 without brown posterior margin **35**
- 33 Abdomen pale brown; surstylus straight and claviform in lateral view
..... ***H. (H.) serrata* Gao & Yang, 2002**
- Abdomen yellow; surstylus subuliform in lateral view **34**
- 34 Arista with longest ray as long as 1/2 height of first flagellomere; ultimate section of CuA₁ ~ 1/9 of penultimate; hypandrium inverse U-shaped; postgonite short, with 2 teeth-like processes in lateral view; phallus curved backwards apically and acute at apex in lateral view
..... ***H. (H.) longiacutata* Gao & Shi, 2019**
- Arista with longest ray as long as height of first flagellomere (Fig. 31); ultimate section of CuA₁ ~ 1/5 of penultimate (Fig. 32); hypandrium H-shaped (Fig. 39); postgonite long spine-like in lateral view (Fig. 40); phallus not curved backwards apically, without acute tip in lateral view (Fig. 40)
..... ***H. (H.) microtricha* sp. nov.**
- 35 Mid femur with 5 or 6 anterior setae **36**
- Mid femur with 4 anterior setae **39**
- 36 Mesonotum with acrostichal setulae in 6 rows **37**
- Mesonotum with acrostichal setulae in 8 rows **38**
- 37 Arista with longest ray as long as 4/5 height of first flagellomere; surstylus long and curved at apex in lateral view ***H. (H.) longicurve* Gao & Shi, 2019**
- Arista with longest ray slightly shorter than height of first flagellomere; surstylus short and narrow in lateral view
..... ***H. (H.) chongqingensis* You, Chen & Li, 2023**
- 38 Fore femur with 6 posterior dorsal setae, 2 posterior ventral setae and ctenidium with 12 short setae; surstylus consisting of a small acute apical process, directed downward and a slender knife-like process with dense setulae on dorsal margin in lateral view ***H. (H.) henanensis* Yang, Zhu & Hu, 1999**
- Fore femur with 8 posterior dorsal setae, 4 posterior ventral setae and ctenidium with 15–17 short setae; surstylus claviform in lateral view
..... ***H. (H.) pangae* Shi, Gao & Shen, 2017**
- 39 Wing with a brown spot between r-m and apical spot on R₄₊₅ distinctly or slightly confluent with brown spot on crossvein dm-cu; surstylus claviform or digitiform **40**
- Wing with a brown quadrate spot between r-m and apical spot on R₄₊₅ separated from brown spot on crossvein dm-cu; surstylus not as above **41**
- 40 Ctenidium with 15 short setae on fore femur; surstylus absent; pregonite short, broad, and acute apically in ventral view; postgonite consisting of a furcated process and a subuliform process in ventral view
..... ***H. (H.) curvispinosa* Yang, Hu & Zhu, 2001**
- Ctenidium with 13 short setae on fore femur; surstylus digitiform with long setulae in lateral view; pregonite and postgonite furcated apically, pregonite shorter than postgonite in ventral view
..... ***H. (H.) zonalis* Yang, Zhu & Hu, 1999**
- 41 Fore femur with 3 posteroventral setae; epandrium blunt triangular apically; surstylus separated from epandrium and originated from anterior

	ventral corner of epandrium, with dense tiny setulae on apical 2/3	
	<i>H. (H.) tianjingshanica</i> Shi & Yang, 2014
–	Fore femur with 4 posteroventral setae; epandrium and surstylus fused, blunt round apically	<i>H. (H.) tianmushana</i> Yang, Hu & Zhu, 2001
42	Ctenidium with 17–19 short setae on fore femur	43
–	Ctenidium with 10–16 short setae on fore femur	44
43	The first flagellomere ~ 1.8 × longer than high; surstylus narrow and columnar in lateral view and broad with tiny setulae in posterior view; postgonites triangular with sharp apex in lateral view	
	<i>H. (H.) zhangjiagensis</i> Shi & Yang, 2014
–	The first flagellomere ~ 2.3 × longer than high; surstylus light color and narrow at base while dark yellow and broad at apex, nearly trapeziform with 2 long setulae in lateral view; postgonite hook-like in lateral view	
	<i>H. (H.) bicolorata</i> Gao & Shi, 2019
44	Pregonite and postgonite subuliform in ventral view or short and triangular in lateral view	45
–	Pregonite and postgonite not as above	47
45	Surstylus without acute or triangular process, blunt and rounded apically and slightly rolled up with several setulae in lateral view	
	<i>H. (H.) miaoae</i> Gao & Shi, 2019
–	Surstylus with acute or triangular process, not as above in lateral view ...	46
46	Surstylus very broad ball-like with a triangular process apically in lateral view; hypandrium H-shaped; phallus acute subapically in lateral view	
	<i>H. (H.) kuankuoshuiensis</i> Wang & Yang, 2012
–	Surstylus narrow, acute apically in lateral view; hypandrium Y-shaped; phallus blunt and subapically rounded in lateral view	
	<i>H. (H.) chinensis</i> Malloch, 1926
47	Subcostal cell hyaline or pale yellow apically	48
–	Subcostal cell dark apically	50
48	Mesonotum with acrostichal setulae in 6 regular rows; surstylus curved and knife-like in lateral view; postgonite absent	
	<i>H. (H.) spectabilis</i> Gao & Shi, 2019
–	Mesonotum with acrostichal setulae in 10 irregular rows; surstylus not as above	49
49	Basal edge of brown apical spot on R ₄₊₅ at same vertical level as apical spot on M ₁ ; surstylus consisting of a slender knife-shaped process and a furcated process with several setulae on subapical and apical margin and a small tooth on lateral margin in lateral view	
	<i>H. (H.) caoi</i> Wang & Yang, 2012
–	Basal edge of brown apical spot on R ₄₊₅ behind vertical level as apical spot on M ₁ ; surstylus short and broad, with a row of long apical setulae	
	<i>H. (H.) jiangxiensis</i> Shi, Gao & Shen, 2017
50	Synergosternite elliptic without sternal part flat; surstylus broad and slightly curved apically in lateral view	<i>H. (H.) platimarginata</i> Gao & Shi, 2019
–	Synergosternite circular, but with sternal part flat; surstylus not as above	51
51	Mesonotum with acrostichal setulae in 8 rows	
	<i>H. (H.) curvata</i> Yang, Zhu & Hu, 1999
–	Mesonotum with acrostichal setulae in 10 irregular rows	52

- 52 A brown elliptical spot present between r-m and apical spot on R_{4+5} ; mid femur with 6–8 anterior setae; surstylus curved knife-like, acute apically in lateral view; postgonite longer than phallus, elongate subuliform, curved forwards apically in lateral view *H. (H.) longispina* Gao & Yang, 2004
- A brown square spot present between r-m and apical spot on R_{4+5} ; mid femur with 4 anterior setae; surstylus short, triangular, and acute apically, with several long setae on dorsal margin and a row of short setulae on ventral margin in lateral view; both pregonite and postgonite shorter subuliform, $\sim \frac{1}{2}$ length of phallus in ventral view *H. (H.) acutata* Yang, Zhu & Hu, 1999

Species descriptions

Homoneura (Homoneura) biconica Chen & Li, sp. nov.

<https://zoobank.org/FA24E555-3C34-4BC7-8DBA-8C8BCA604CC2>

Figs 1–10

Chinese name: 双锥同脉缟蝇

Type material. *Holotype*: ♂, CHINA, Chongqing City, Jiangjin District, Simianshan Natural Reserve, Zhengqiangou, 28°36'59.54"N, 106°26'25.88"E, 1273 m, 14.VI.2022, leg. Xulong Chen. *Paratypes*: 6♂♂, same data as holotype; 1♂, CHINA, Chongqing City, Jiangjin District, Simianshan Natural Reserve, Dahonghai, 28°35'34.27"N, 106°26'34.93"E, 1144 m, 15.VII.2022, leg. Xulong Chen.

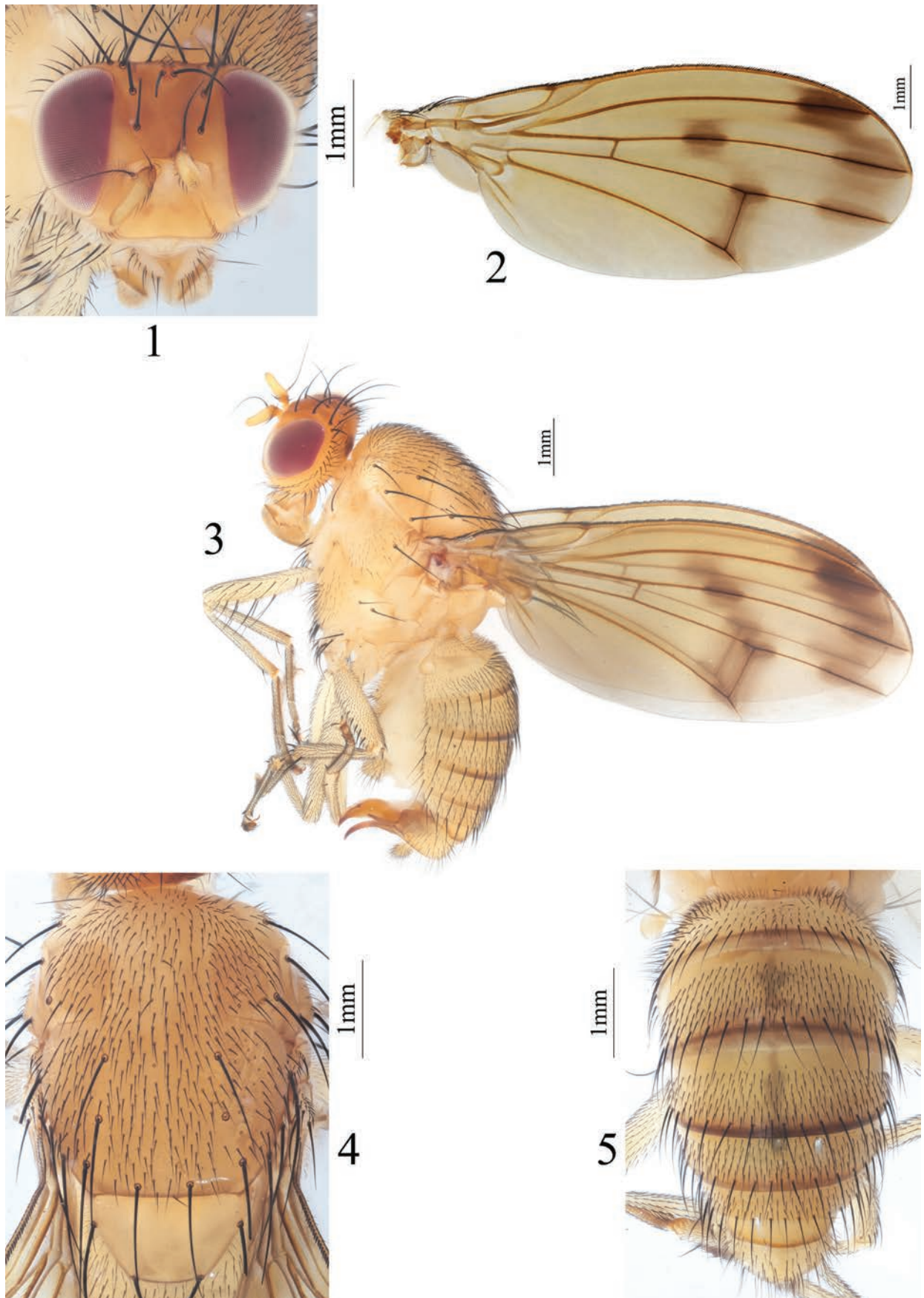
Etymology. The specific name comes from the combination of the prefix *bi-* (meaning two) and the Latin word, *conica* (meaning cone-shaped), referring to the surstylus consisting of two subuliform processes in lateral view.

Diagnosis. Mesonotum with acrostichal setulae in ten irregular rows. Basal margin of brown apical spot on R_{2+3} behind vertical level as crossvein dm-cu; brown apical spots on R_{2+3} , R_{4+5} , and M_1 slightly confluent; subcostal cell hyaline. Male tergites 2–5 with blackish brown posterior margin. Surstylus consisting of two subuliform processes in lateral view. Pregonite and postgonite inwardly curved, pregonite with one long setula. Phallus long and knife-like with an acute subapical tooth in lateral view.

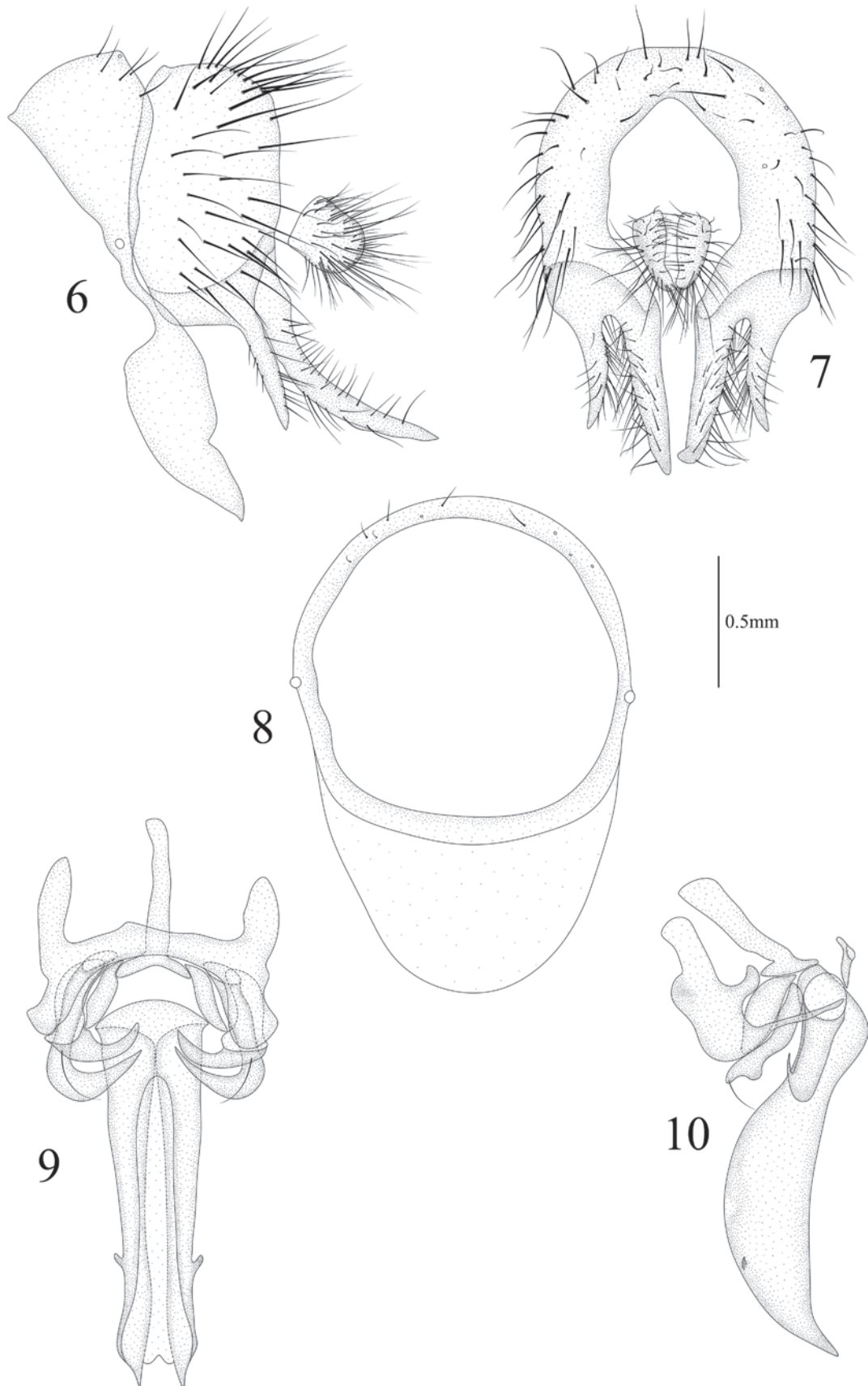
Description. Male. Body length 8.4–8.6 mm, wing length 8.3–8.4 mm.

Head (Fig. 1) yellow. Frons as long as wide and parallel-sided; ocellar triangle yellow, ocellar seta developed, longer than anterior fronto-orbital seta, anterior fronto-orbital seta shorter than posterior fronto-orbital seta. Gena $\sim 1/7$ height of eye. Antenna yellow, first flagellomere $\sim 2.0 \times$ longer than high; arista black except pale brown at base, long plumose, with longest ray as long as height of first flagellomere. Proboscis and palpus yellow.

Thorax (Fig. 4) yellow, with gray pruinosity. 0+3 dorsocentral setae, anteriormost postsutural dorsocentral seta far from scutal suture, acrostichal setulae in ten irregular rows. Legs yellow. Fore femur with eight posterior dorsal setae, five posterior ventral setae and ctenidium with 16 short setae; fore tibia with one dorsal preapical seta and one short apical ventral seta. Mid femur with five or six anterior setae and one apical posterior seta; mid tibia with one dorsal preapical seta and three strong apical ventral setae. Hind femur with several weak anterior ventral setae and one preapical anterior dorsal seta; hind tibia with one weak dorsal preapical seta and one short apical ventral seta. Wing (Fig. 2) slightly yellow, basal margin of brown apical



Figures 1–5. *Homoneura (Homoneura) biconica* sp. nov. male **1** head, anterior view **2** wing **3** habitus, lateral view **4** thorax, dorsal view **5** abdomen, dorsal view.



Figures 6–10. *Homoneura (Homoneura) biconica* sp. nov. male **6** syntergosternite and epandrium, lateral view **7** epandrial complex, posterior view **8** syntergosternite, anterior view **9** phallic complex, ventral view **10** phallic complex, lateral view. Scale bar: 0.5 mm.

spot on R_{2+3} behind vertical level as crossvein dm-cu; brown apical spots on R_{2+3} , R_{4+5} , and M_1 slightly confluent and forming pale brown connecting area between apical spots on R_{2+3} , R_{4+5} , and M_1 ; brown median spot on R_{4+5} separated from brown cloud-like spot on crossvein dm-cu; subcostal cell hyaline; eight short hairs present at base of R_{4+5} ; costa with 2nd (between R_1 and R_{2+3}), 3rd (between R_{2+3} and R_{4+5}), and 4th (between R_{4+5} and M_1) sections in proportion of 4: 1: 0.8; r-m before middle of discal cell; ultimate and penultimate sections of M_1 in proportion of 3.5: 3.3; ultimate section of CuA_1 ~ 1/8 of penultimate. Haltere yellow.

Abdomen (Fig. 5) yellow, tergites 2–5 with blackish brown posterior margin. Male genitalia (Figs 6–10): syntergosternite circular, with a triangular ventral process and with several dorsal setulae. Epandrium broad in lateral view; surstylus consisting of a longer subuliform process and a shorter subuliform process in lateral view. Hypandrium H-shaped. Pregonite and postgonite curved inwards, pregonite with one long setula. Phallus long, knife-like, and with an acute subapical tooth in lateral view. Phallapodeme shorter than phallus.

Female. Unknown.

Distribution. China (Chongqing).

Remarks. The new species resembles *Homoneura (Homoneura) apiconcava* in the habitus and abdominal tergites 2–5 with blackish brown posterior margin [see You et al. 2023: figs 3, 5], but it can be distinguished from the latter by the following: mesonotum with acrostichal setulae in ten irregular rows; fore femur with eight posterior dorsal setae and ctenidium with 16 short setae; subcostal cell hyaline; surstylus consisting of a longer subuliform process and a shorter subuliform process in lateral view. In *H. (H.) apiconcava*, mesonotum with acrostichal setulae in eight irregular rows; fore femur with ten posterior dorsal setae and ctenidium with 12 short setae; subcostal cell pale brown apically; surstylus with concavity apically in lateral view [see You et al. 2023: figs 2–6].

***Homoneura (Homoneura) dilatata* Chen & Li, sp. nov.**

<https://zoobank.org/8E80C793-E526-48DD-B79B-88B1DF3D89BF>

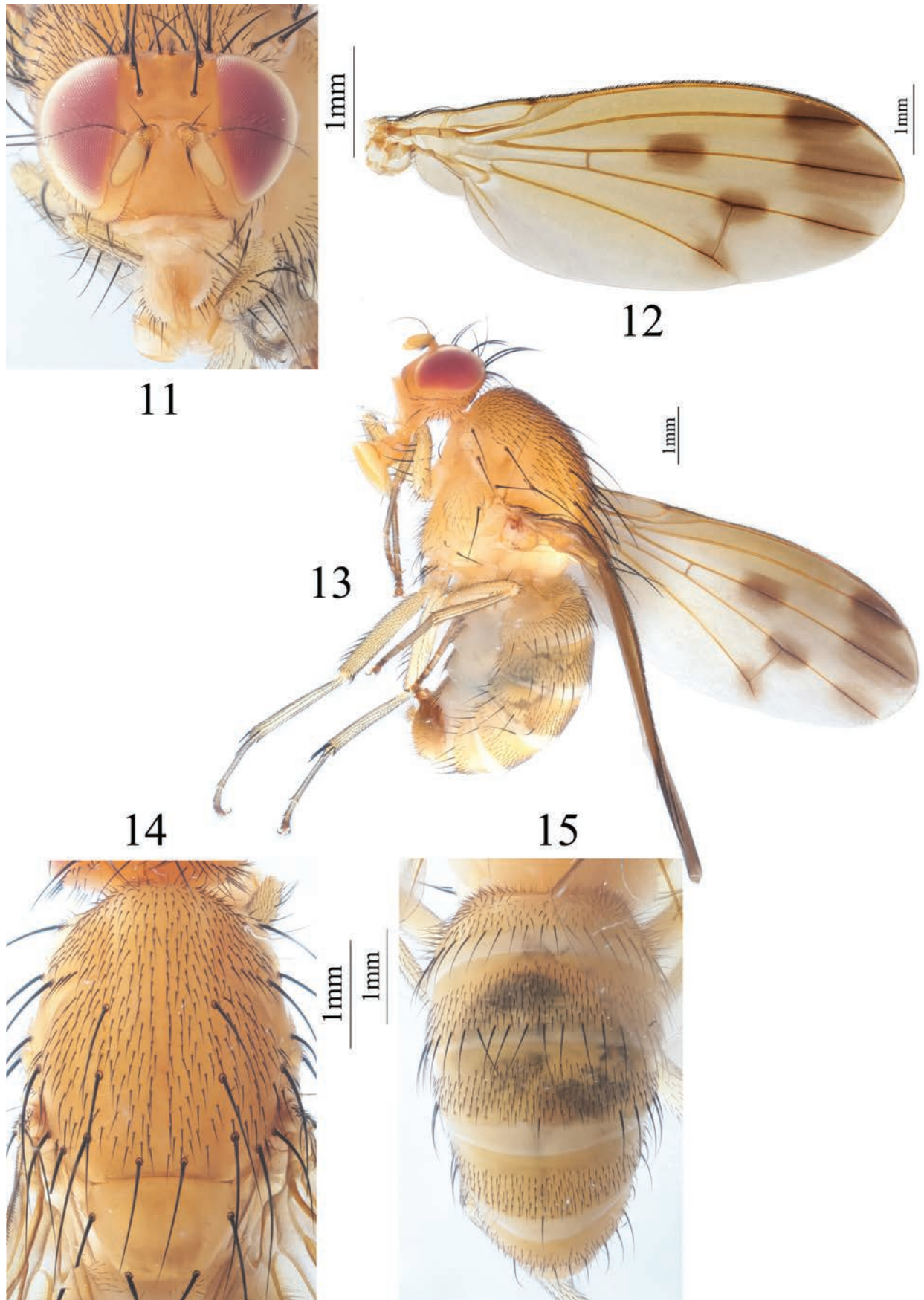
Figs 11–20

Chinese name: 膨突同脉缟蝇

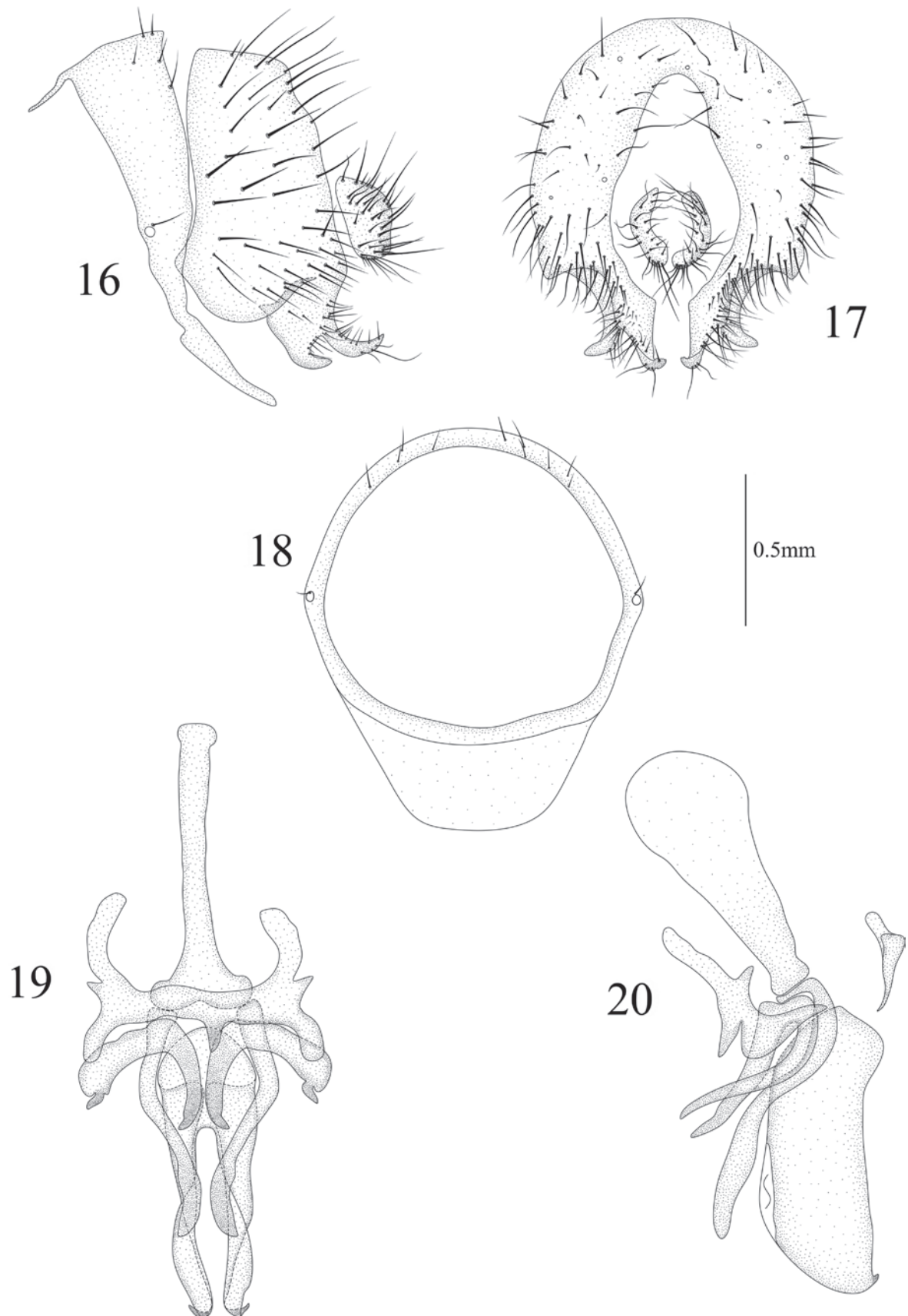
Type material. Holotype: ♂, CHINA, Chongqing City, Jiangjin District, Simianshan Natural Reserve, Zhengqiangou, 28°36'59.54"N, 106°26'25.88"E, 1273 m, 14.VI.2022, leg. Xulong Chen. **Paratypes:** 1♂, CHINA, Chongqing City, Jiangjin District, Simianshan Natural Reserve, Dawopu, 28°34'11.28"N, 106°20'26.96"E, 1007 m, 6.IX.2022, leg. Xulong Chen.

Etymology. The specific name refers to the phallapodeme expanded apically in lateral view.

Diagnosis. Mesonotum with acrostichal setulae in ten irregular rows. Basal margin of brown apical spot on R_{2+3} behind vertical level as crossvein dm-cu; brown apical spots on R_{2+3} , R_{4+5} , and M_1 slightly confluent. Syntergosternite with a setula around spiracle. Surstylus furcated into two short, curved processes in lateral view. Hypandrium with one short subuliform ventral process. Phallapodeme expanded apically in lateral view.



Figures 11–15. *Homoneura (Homoneura) dilatata* sp. nov. male 11 head, anterior view 12 wing 13 habitus, lateral view 14 thorax, dorsal view 15 abdomen, dorsal view.



Figures 16–20. *Homoneura (Homoneura) dilatata* sp. nov. male **16** syntergosternite and epandrium, lateral view **17** epandrial complex, posterior view **18** syntergosternite, anterior view **19** phallic complex, ventral view **20** phallic complex, lateral view. Scale bar: 0.5 mm.

Description. Male. Body length 7.7–8.1 mm, wing length 7.9–8.0 mm.

Head (Fig. 11) yellow. Frons as long as wide and parallel-sided; ocellar triangle yellow, ocellar seta developed, as long as anterior fronto-orbital seta, anterior fronto-orbital seta shorter than posterior fronto-orbital seta. Gena ~ 1/8 height of eye. Antenna yellow, first flagellomere ~ 2.0 × longer than high; arista black except pale brown at base, long plumose, with longest ray as long as height of first flagellomere. Proboscis and palpus yellow.

Thorax (Fig. 14) yellow, with gray pruinosity. 0+3 dorsocentral setae, anteriormost postsutural dorsocentral seta far from scutal suture, acrostichal setulae in ten irregular rows. Legs pale yellow. Fore femur with nine posterior dorsal setae, five posterior ventral setae and ctenidium with 16 short setae; fore tibia with one dorsal preapical seta and one short apical ventral seta. Mid femur with five anterior setae and one apical posterior seta; mid tibia with one dorsal preapical seta and three strong apical ventral setae. Hind femur with several weak anterior ventral setae and one preapical anterior dorsal seta; hind tibia with one weak dorsal preapical seta and one short apical ventral seta. Wing (Fig. 12) slightly yellow, basal margin of brown apical spot on R_{2+3} behind vertical level as crossvein dm-cu; brown apical spots on R_{2+3} , R_{4+5} , and M_1 slightly confluent and forming pale brown connecting area between apical spots on R_{2+3} , R_{4+5} , and M_1 ; brown median spot on R_{4+5} separated from brown cloud-like spot on crossvein dm-cu; subcostal cell pale brown apically; three short hairs present at base of R_{4+5} ; costa with 2nd (between R_1 and R_{2+3}), 3rd (between R_{2+3} and R_{4+5}), and 4th (between R_{4+5} and M_1) sections in proportion of 10.5: 2.7: 2.2; r-m before middle of discal cell; ultimate and penultimate sections of M_1 in proportion of 1: 1; ultimate section of CuA_1 ~ 1/6 of penultimate. Haltere yellow.

Abdomen (Fig. 15) yellow. Male genitalia (Figs 16–20): sytergosternite circular with a trapeziform ventral process, with several dorsal setulae and a setula around spiracle. Epandrium broad in lateral view; surstylus hairy, furcated into two short, curved processes in lateral view. Hypandrium H-shaped, with one short subuliform ventral process. Pregonite V-shaped in ventral view, acute apically, postgonite curved, claviform. Phallus with one small, curved hook in lateral view. Phallapodeme expanded apically in lateral view, slightly shorter than phallus.

Female. Unknown.

Distribution. China (Chongqing).

Remarks. The new species resembles *Homoneura (Homoneura) martini* in brown apical spots on R_{2+3} , R_{4+5} , and M_1 slightly confluent, abdominal tergites 2–5 without blackish brown posterior margin and sytergosternite with long hairs around spiracle [see Shi et al. 2017b: figs 10, 13, 14, 16], but it can be distinguished from the latter by the following: mesonotum with acrostichal setulae in ten rows; fore femur with five posterior ventral setae; sytergosternite with a trapeziform ventral process; surstylus furcated into two short, curved processes in lateral view; phallapodeme expanded apically. In *H. (H.) martini*, mesonotum with acrostichal setulae in eight irregular rows; fore femur with three posterior ventral setae; sytergosternite without ventral process; surstylus blunt apically; phallapodeme normal apically [see Shi et al. 2017b: figs 12, 16, 17, 19].

***Homoneura (Homoneura) jiangjinensis* Chen & Li, sp. nov.**

<https://zoobank.org/5EEEC111-1B29-44FD-89EC-8F7616B7D0D1>

Figs 21–30

Chinese name: 江津同脉缟蝇

Type material. *Holotype*: ♂, CHINA, Chongqing City, Jiangjin District, Simianshan Natural Reserve, Zhengqiangou, 28°36'59.54"N, 106°26'25.88"E, 1273 m, 14.VI.2022, leg. Xulong Chen. *Paratypes*: 1♂, same data as holotype.

Etymology. The specific name refers to the type locality Jiangjin District.

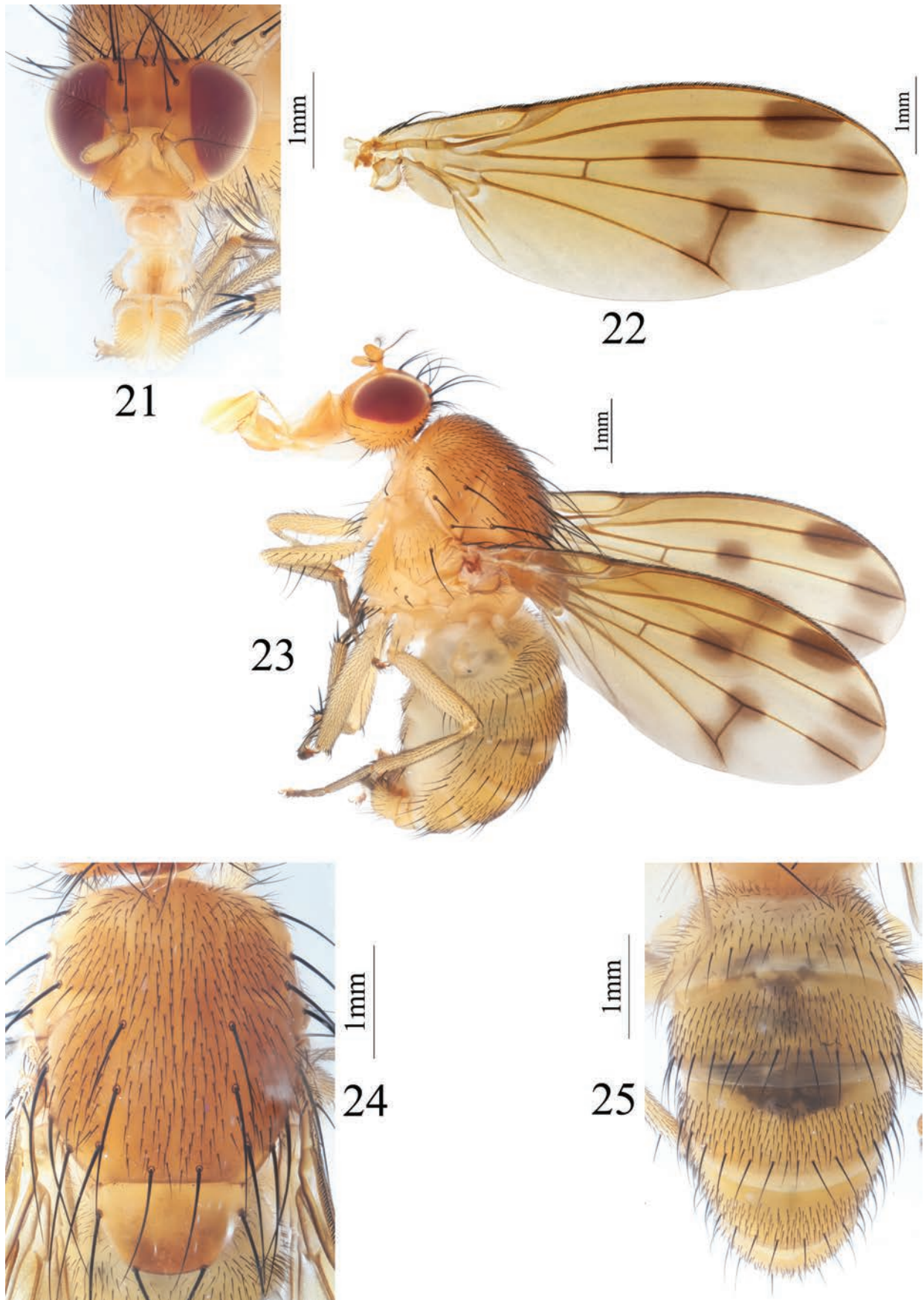
Diagnosis. Basal margin of brown apical spot on R_{2+3} at same vertical level as crossvein dm-cu; brown apical spots on R_{2+3} , R_{4+5} and M_1 entirely separated. Syntergosternite with several setulae above right spiracle, ventral process with several hairs at middle. Surstylus consisting of a long spinous process and a hairy blunt process in lateral view. Hypandrium with a pair of tooth-like ventral processes at middle. Pregonite consisting of a short spinous process and a long curved spinous process, postgonite curved and spine-like in lateral view. Phallus with a subapical tooth in lateral view.

Description. Male. Body length 7.0–7.1 mm, wing length 6.9 mm.

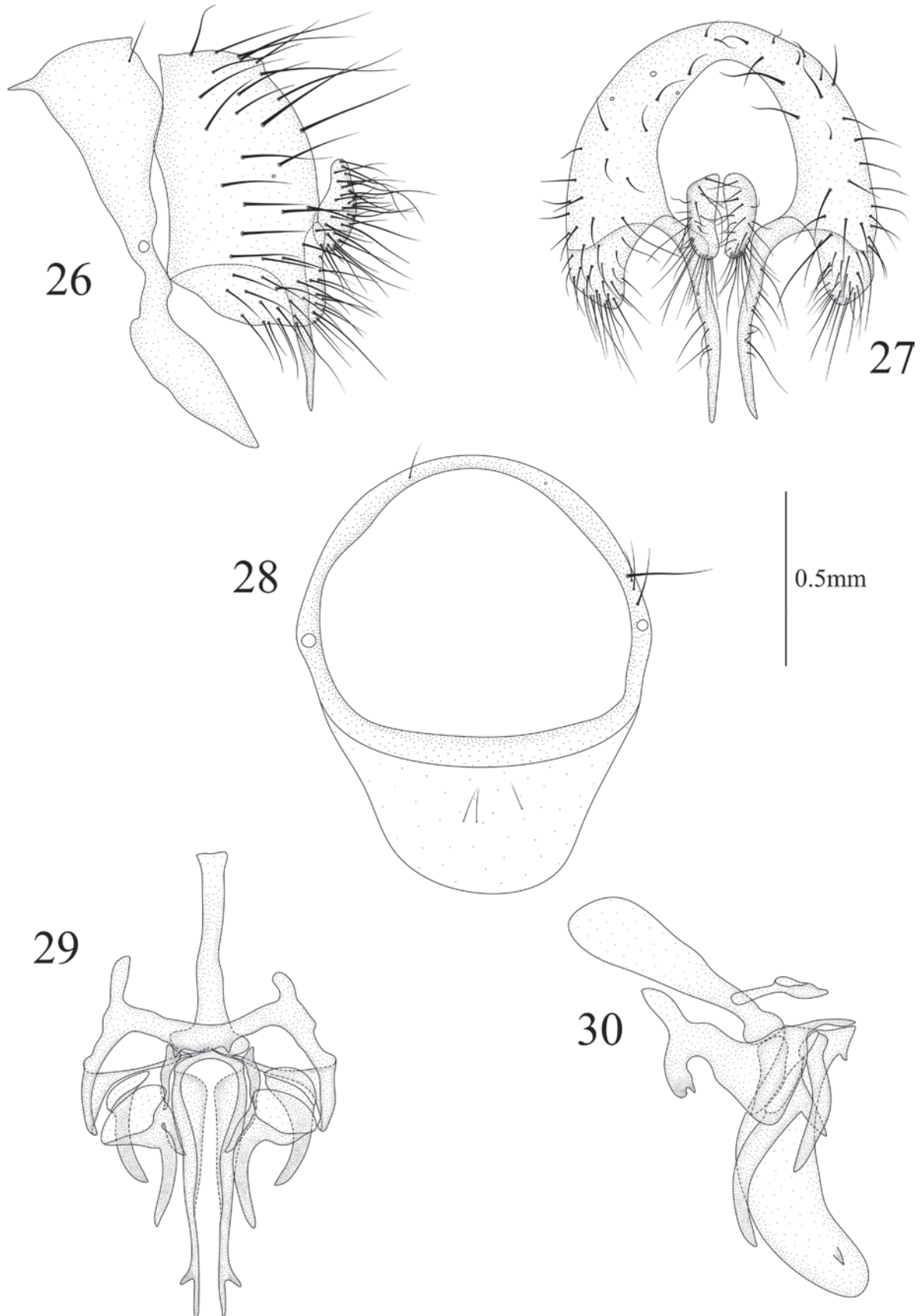
Head (Fig. 21) yellow. Frons as long as wide and parallel-sided; ocellar triangle yellow, ocellar seta developed, longer than anterior fronto-orbital seta, anterior fronto-orbital seta shorter than posterior fronto-orbital seta. Gena ~ 1/8 height of eye. Antenna yellow, first flagellomere ~ 2.0 × longer than high; arista black except yellow at base, long plumose, with longest ray as long as height of first flagellomere. Proboscis and palpus yellow.

Thorax (Fig. 24) yellow, with gray pruinosity. 0+3 dorsocentral setae, anterior-most postsutural dorsocentral seta far from scutal suture, acrostichal setulae in ten irregular rows. Legs yellow. Fore femur with ten posterior dorsal setae, five or six posterior ventral setae and ctenidium with 16 short setae; fore tibia with one dorsal preapical seta and one short apical ventral seta. Mid femur with five anterior setae and one apical posterior seta; mid tibia with one dorsal preapical seta and three strong apical ventral setae. Hind femur with several weak anterior ventral setae and one preapical anterior dorsal seta; hind tibia with one weak dorsal preapical seta and one short apical ventral seta. Wing (Fig. 22) slightly yellow, basal margin of brown apical spot on R_{2+3} at same vertical level as crossvein dm-cu; brown apical spots on R_{2+3} , R_{4+5} and M_1 entirely separated; brown median spot on R_{4+5} separated from brown cloud-like spot on crossvein dm-cu; subcostal cell pale brown apically; costa with 2nd (between R_1 and R_{2+3}), 3rd (between R_{2+3} and R_{4+5}), and 4th (between R_{4+5} and M_1) sections in proportion of 4: 1.2: 0.8; r-m before middle of discal cell; ultimate and penultimate sections of M_1 in proportion of 1.1: 1; ultimate section of CuA_1 ~ 1/7 of penultimate. Haltere yellow.

Abdomen (Fig. 25) yellow. Male genitalia (Figs 26–30): syntergosternite circular with a trapeziform ventral process, with several dorsal setulae and several setulae above right spiracle, ventral process with several hairs at middle. Epandrium broad in lateral view; surstylus consisting of a long spinous process and a blunt and hairy process in lateral view. Hypandrium H-shaped, with a pair of tooth-like ventral processes at middle. Pregonite consisting of a short spinous process and a long curved spinous process, postgonite curved and spine-like



Figures 21–25. *Homoneura (Homoneura) jiangjinensis* sp. nov. male **21** head, anterior view **22** wing **23** habitus, lateral view **24** thorax, dorsal view **25** abdomen, dorsal view.



Figures 26–30. *Homoneura (Homoneura) jiangjinensis* sp. nov. male **26** syntergosternite and epandrium, lateral view **27** epandrial complex, posterior view **28** syntergosternite, anterior view **29** phallic complex, ventral view **30** phallic complex, lateral view. Scale bar: 0.5 mm.

in lateral view. Phallus curved backwards, with a subapical tooth in lateral view. Phallapodeme shorter than phallus.

Female. Unknown.

Distribution. China (Chongqing).

Remarks. The new species resembles *Homoneura (Homoneura) caoi* in the habitus, mesonotum with acrostichal setulae in ten irregular rows and brown apical spots on R_{2+3} , R_{4+5} and M_1 entirely separated [see Wang et al. 2012: figs 12, 14, 15], but it can be distinguished from the latter by the following: fore femur with ten posterior dorsal setae and ctenidium with 16 short setae; subcostal cell pale brown apically; abdominal tergites 2–5 without brown posterior margin; syntergosternite with several setulae above right spiracle; surstylus consisting of a long spinous process and a blunt hairy process in lateral view; hypandrium with a pair of tooth-like ventral processes at middle; pregonite consisting of a short spinous process and a long curved spinous process, postgonite curved and spine-like in lateral view. In *H. (H.) caoi*, fore femur with seven or eight posterior dorsal setae and ctenidium with 12 or 13 short setae; subcostal cell hyaline; abdominal tergites 2–5 with brown posterior margin; syntergosternite without setula around spiracle; surstylus trifurcated; gonopod with three inwardly curved arc-shaped processes [see Wang et al. 2012: figs 12, 15, 16, 19, 20, 21].

***Homoneura (Homoneura) microtricha* Chen & Li, sp. nov.**

<https://zoobank.org/3070733C-4EF9-48F9-BBC2-45424FC52630>

Figs 31–40

Chinese name: 微毛同脉缟蝇

Type material. Holotype: ♂, **CHINA**, Chongqing City, Jiangjin District, Simianshan Natural Reserve, Zhengqiangou, 28°36'59.54"N, 106°26'25.88"E, 1273 m, 15.VI.2022, leg. Xulong Chen. **Paratypes:** 43♂♂6♀♀, **CHINA**, Chongqing City, Jiangjin District, Simianshan Natural Reserve, Zhengqiangou, 28°36'59.54"N, 106°26'25.88"E, 1273 m, 14.VI.2022, leg. Xulong Chen; 1♂, **CHINA**, Chongqing City, Jiangjin District, Simianshan Natural Reserve, Zhengqiangou, 28°36'59.54"N, 106°26'25.88"E, 1273 m, 26.VI.2022, leg. Pengyan You; 3♂♂8♀♀, **CHINA**, Chongqing City, Jiangjin District, Simianshan Natural Reserve, Dahonghai, 28°35'34.27"N, 106°26'34.93"E, 1144 m, 15.VII.2022, leg. Xulong Chen; 5♂♂, **CHINA**, Chongqing City, Jiangjin District, Simianshan Natural Reserve, Mohuayan, 28°35'15.67"N, 106°22'7.36"E, 1017 m, 14.VII.2022, leg. Xulong Chen; 2♂♂1♀, **CHINA**, Chongqing City, Jiangjin District, Simianshan Natural Reserve, Zhenzhutan, 28°35'50.74"N, 106°25'25.70"E, 1226 m, 15.VII.2022, leg. Xulong Chen; 2♂♂2♀♀, **CHINA**, Chongqing City, Jiangjin District, Simianshan Natural Reserve, Tudiyan, 28°37'24.45"N, 106°24'6.69"E, 1126 m, 15.VII.2022, leg. Xulong Chen; 1♂2♀♀, **CHINA**, Chongqing City, Jiangjin District, Simianshan Natural Reserve, Chaoyuanguan, 28°38'53.38"N, 106°20'23.84"E, 920 m, 14.VII.2022, leg. Xulong Chen; 1♂, **CHINA**, Chongqing City, Jiangjin District, Taihe Management and Protection Station, Heishenmiao, 28°48'9.21"N, 106°15'46.04"E, 836 m, 14.VII.2022, leg. Xulong Chen; 1♂, **CHINA**, Chongqing City, Jiangjin District, Dayuandong National Forest Park, Kongzimiao, 28°53'9.68"N, 106°15'24.28"E, 709m, 12.VII.2022, leg. Xulong Chen; 1♂1♀, **CHINA**, Chongqing City, Jiangjin District, Dayuandong National Forest

Park, Shuijingwan, 28°53'10.96"N, 106°14'19.32"E, 717 m, 13.VII.2022, leg. Xulong Chen; 2♂♂1♀, **CHINA**, Chongqing City, Jiangjin District, Dayuandong National Forest Park, Tian'ehu, 28°52'54.45"N, 106°15'14.53"E, 728 m, 13.VII.2022, leg. Xulong Chen; 4♂♂12♀♀, **CHINA**, Chongqing City, Jiangjin District, Dayuandong National Forest Park, Diaojiaolou, 28°53'5.89"N, 106°15'42.18"E, 731 m, 13.VII.2022, leg. Xulong Chen.

Etymology. The specific name comes from the combination of the prefix *micro-* (meaning small) and the Latin word, *tricha* (meaning hair), referring to the surstylus covered by small hairs.

Diagnosis. Mesonotum with acrostichal setulae in eight irregular rows. Brown apical spots on R_{4+5} and M_1 slightly confluent, separated from apical spot on R_{2+3} ; brown median spot on R_{4+5} slightly fused with brown cloud-like spot on crossvein dm-cu. Surstylus subuliform in lateral view. Pregonite knife-like in ventral view, connected with postgonite; postgonite long and spine-like in lateral view. Phallus with two pairs of subapical teeth in lateral view.

Description. Male. Body length 5.8–6.3 mm, wing length 5.6–6.1 mm.

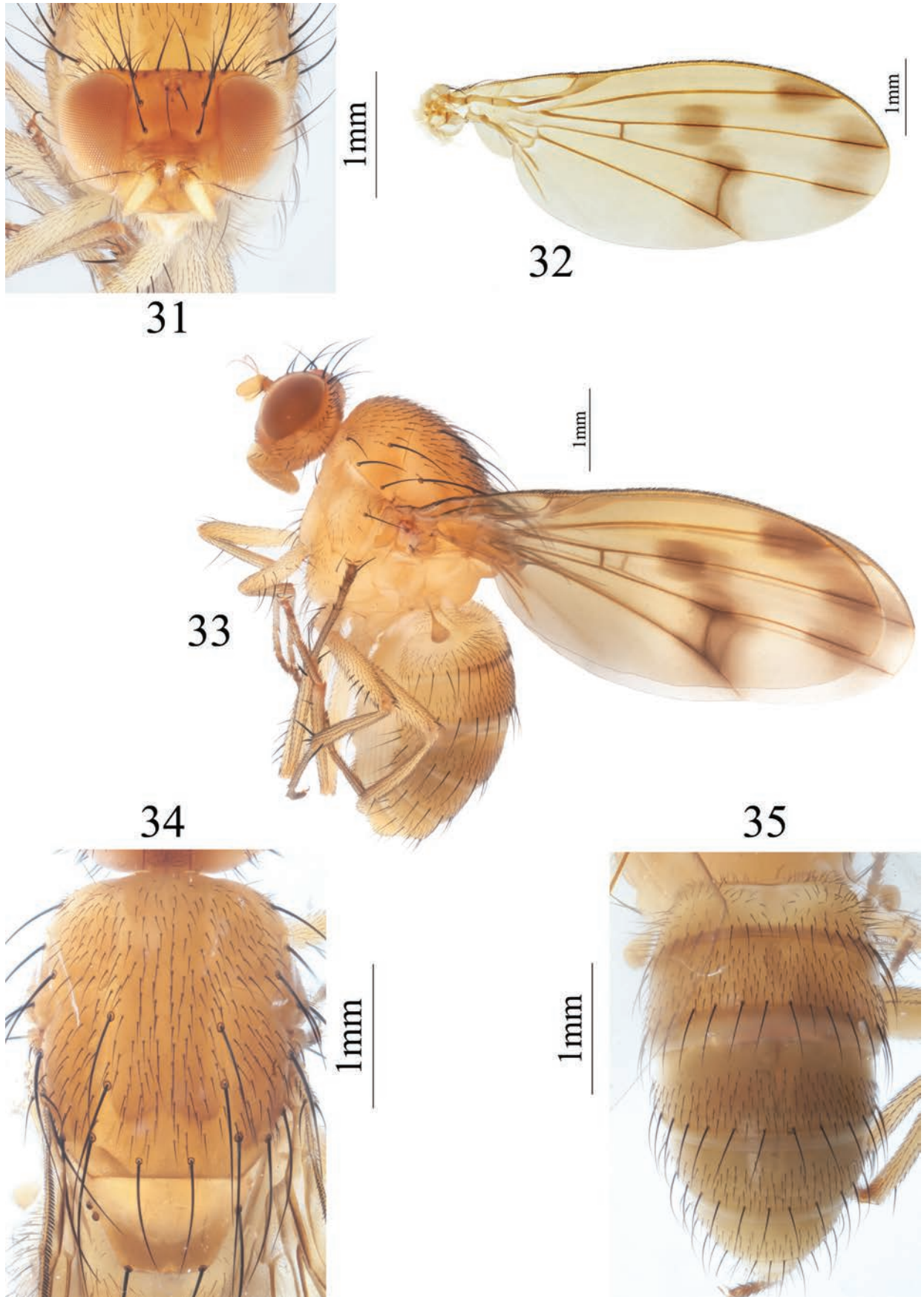
Head (Fig. 31) yellow. Frons as long as wide and parallel-sided; ocellar triangle yellow, ocellar seta developed, longer than anterior fronto-orbital seta, anterior fronto-orbital seta shorter than posterior fronto-orbital seta. Gena ~ 1/8 height of eye. Antenna yellow, first flagellomere ~ 2.0 × longer than high; arista black except yellow at base, long plumose, with longest ray slightly shorter than height of first flagellomere. Proboscis pale yellow, palpus yellow.

Thorax (Fig. 34) yellow, with gray pruinosity. 0+3 dorsocentral setae, anterior-most postsutural dorsocentral seta far from scutal suture, acrostichal setulae in eight irregular rows. Legs yellow. Fore femur with seven posterior dorsal setae, four posterior ventral setae, and ctenidium with 14 or 15 short setae; fore tibia with one dorsal preapical seta and one short apical ventral seta. Mid femur with four or five anterior setae and one apical posterior seta; mid tibia with one dorsal preapical seta and three strong apical ventral setae. Hind femur with one preapical anterior dorsal seta; hind tibia with one weak dorsal preapical seta and one short apical ventral seta. Wing (Fig. 32) slightly yellow, basal margin of brown apical spot on R_{2+3} behind vertical level as crossvein dm-cu; brown apical spots on R_{4+5} and M_1 slightly confluent, separated from apical spot on R_{2+3} ; brown median spot on R_{4+5} slightly fused with brown cloud-like spot on crossvein dm-cu; subcostal cell pale brown apically; costa with 2nd (between R_1 and R_{2+3}), 3rd (between R_{2+3} and R_{4+5}), and 4th (between R_{4+5} and M_1) sections in proportion of 9.7: 2.7: 2; r-m before middle of discal cell; ultimate and penultimate sections of M_1 in proportion of 3: 2.3; ultimate section of CuA_1 ~ 1/5 of penultimate. Haltere pale brown.

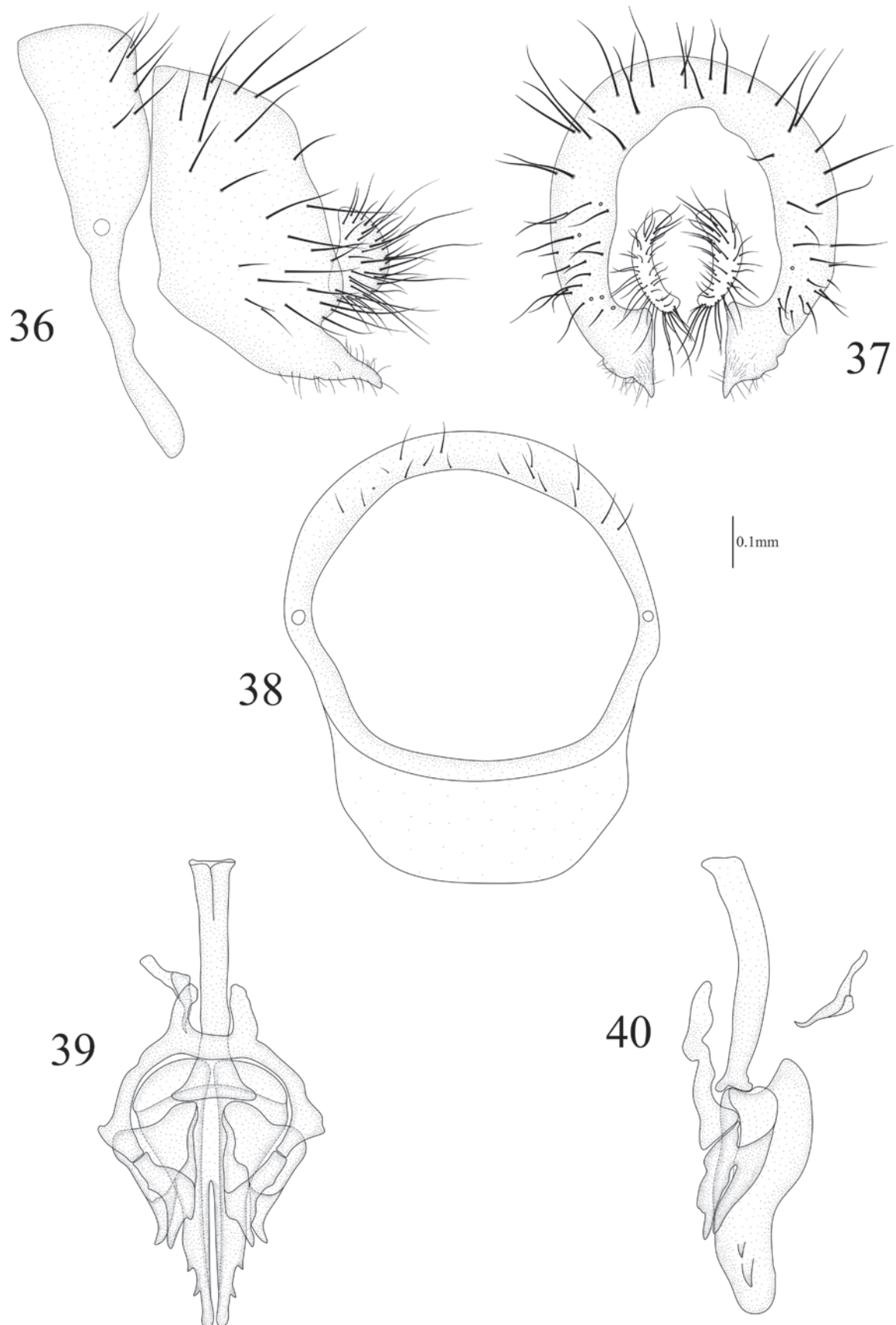
Abdomen (Fig. 35) yellow, tergites 2–5 with pale brown posterior margin. Male genitalia (Figs 36–40): syntergosternite circular, with a trapeziform ventral process and with several dorsal setulae. Epandrium broad in lateral view; surstylus hairy, subuliform in lateral view. Hypandrium H-shaped. Pregonite knife-like in ventral view, connected with postgonite; postgonite long and spine-like in lateral view. Phallus with two pairs of subapical teeth in lateral view. Phallapodeme as long as phallus.

Female. Body length 5.9–6.3 mm, wing length 6.0–6.2 mm.

Distribution. China (Chongqing).



Figures 31–35. *Homoneura (Homoneura) microtricha* sp. nov. male 31 head, anterior view 32 wing 33 habitus, lateral view 34 thorax, dorsal view 35 abdomen, dorsal view.



Figures 36–40. *Homoneura (Homoneura) microtricha* sp. nov. male **36** syntergosternite and epandrium, lateral view **37** epandrial complex, posterior view **38** syntergosternite, anterior view **39** phallic complex, ventral view **40** phallic complex, lateral view. Scale bar: 0.1 mm.

Remarks. The new species resembles *Homoneura (Homoneura) longiacutata* in the habitus and surstylus that is subuliform in lateral view [see Gao and Shi 2019: figs 35, 41–42], but it can be distinguished from the latter by the following: arista with longest ray as long as height of first flagellomere; ultimate section of CuA_1 ~ 1/5 of penultimate; hypandrium H-shaped; postgonite long and spine-like in lateral view; phallus not curved backwards apically, without acute tip in lateral view. In *H. (H.) longiacutata*, arista with longest ray as long as 1/2 height of first flagellomere; ultimate section of CuA_1 ~ 1/9 of penultimate; hypandrium inverse U-shaped; postgonite short, with two teeth-like processes in lateral view; phallus curved backwards apically and acute at apex in lateral view [see Gao and Shi 2019: figs 36, 40, 44, 45].

***Homoneura (Homoneura) multiseta* Chen & Li, sp. nov.**

<https://zoobank.org/8749E02C-8EC1-4C65-93E8-6478A74D82D4>

Figs 41–50

Chinese name: 多鬃同脉缟蝇

Type material. *Holotype*: ♂, **CHINA**, Chongqing City, Jiangjin District, Simianshan Natural Reserve, Dahonghai, 28°35'34.27"N, 106°26'34.93"E, 1144 m, 15.VII.2022, leg. Xulong Chen. *Paratypes*: 1♂, **CHINA**, Chongqing City, Jiangjin District, Simianshan Natural Reserve, Zhengqiangou, 28°36'59.54"N, 106°26'25.88"E, 1273 m, 14.VI.2022, leg. Xulong Chen.

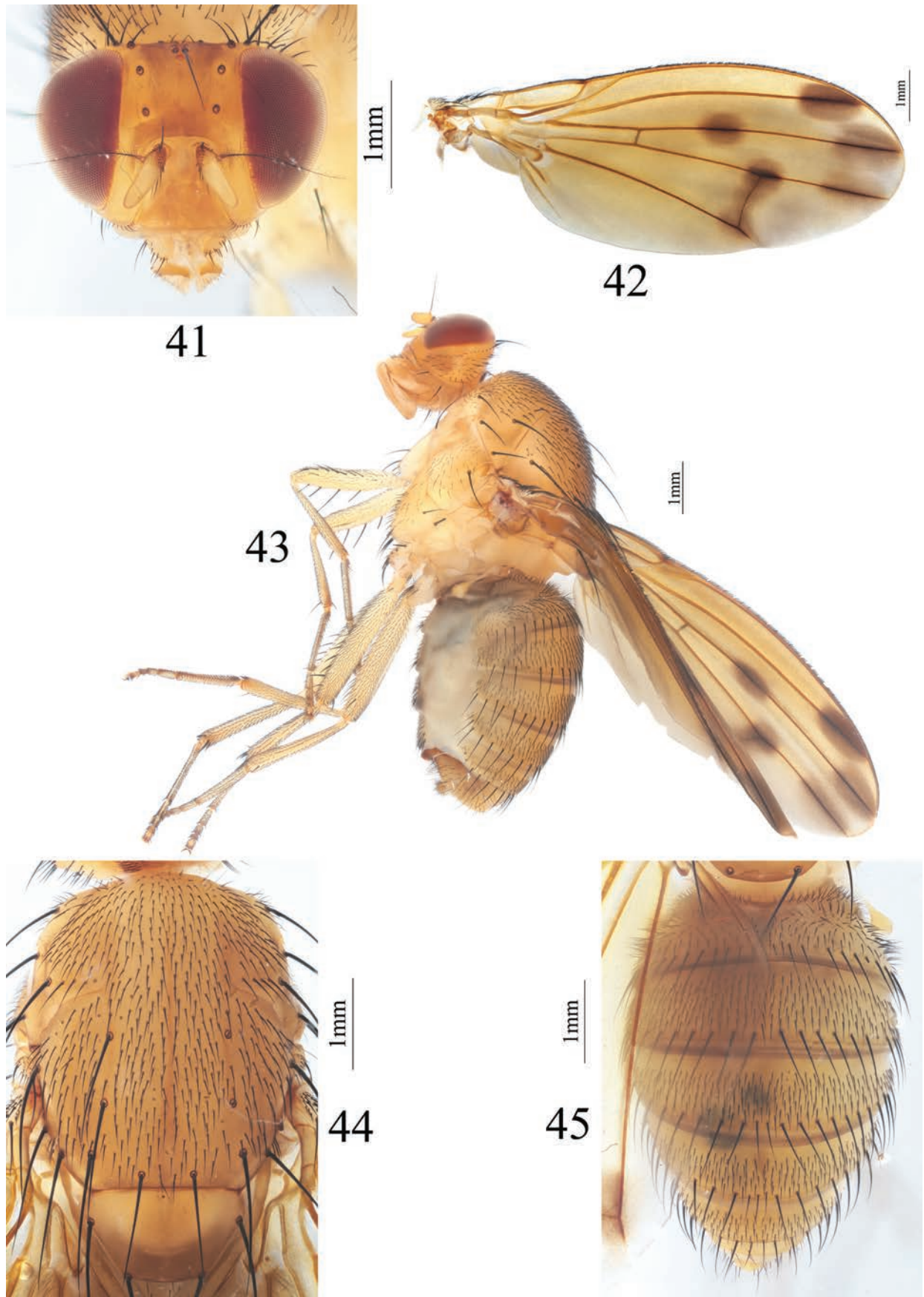
Etymology. The specific name comes from the combination of the prefix *multi* and the Latin *seta*, referring to the epandrium covered by many setae.

Diagnosis. Basal margin of brown apical spot on R_{2+3} at same vertical level as crossvein dm-cu; brown apical spots on R_{2+3} , R_{4+5} , and M_1 slightly confluent. Male tergites 2–5 with brown posterior margin. Surstylus blunt and rolled up in ventral view. Hypandrium U-shaped. Pregonite broad and postgonite long, spine-like. Phallus with small sharp process in lateral view.

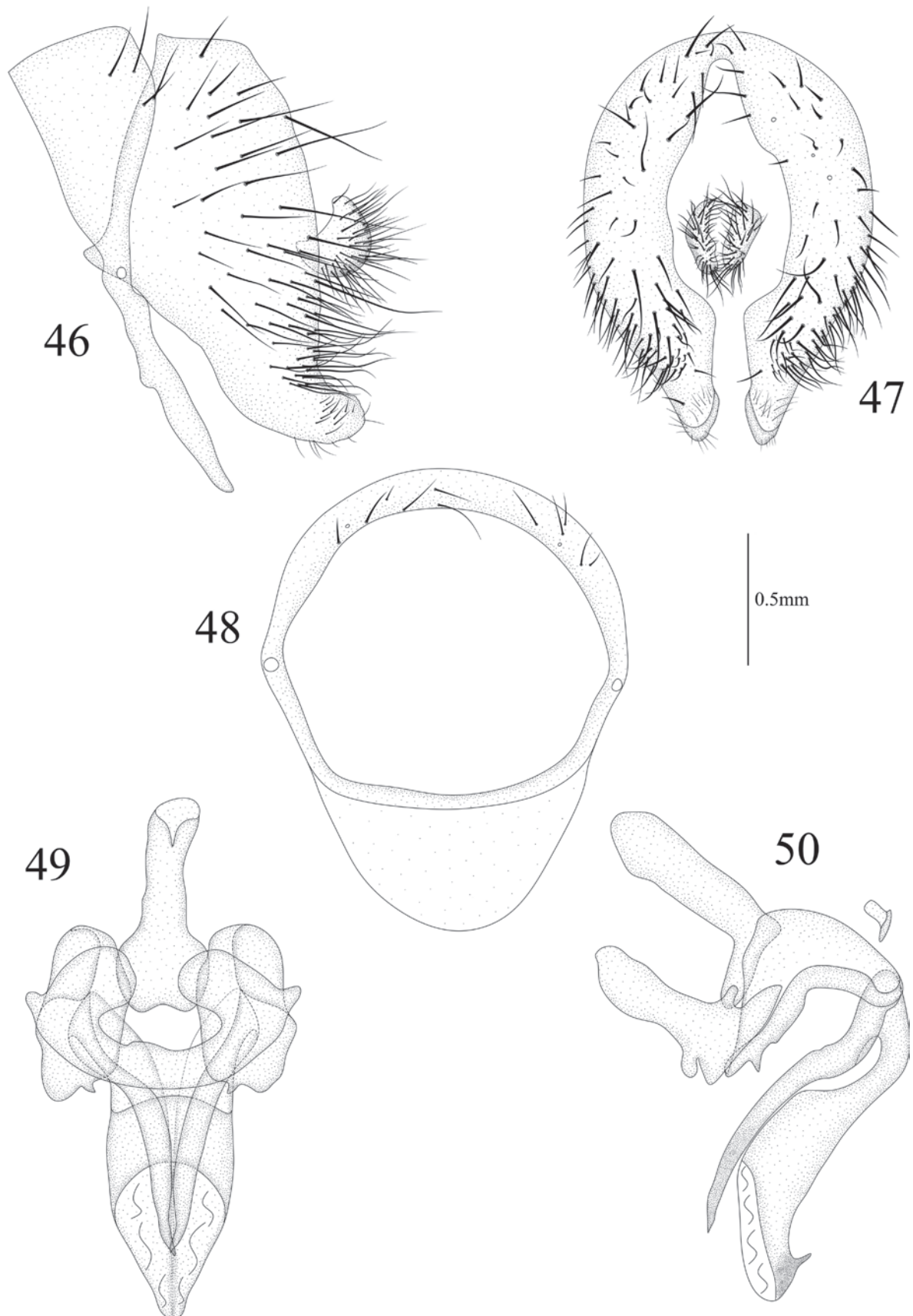
Description. Male. Body length 8.7–8.8 mm, wing length 8.5 mm.

Head (Fig. 41) yellow. Frons as long as wide and parallel-sided; ocellar triangle yellow, ocellar seta developed. Gena ~ 1/8 height of eye. Antenna yellow, first flagellomere ~ 2.0 × longer than high; arista black except yellow at base, long plumose, with longest ray shorter than height of first flagellomere. Proboscis and palpus yellow.

Thorax (Fig. 44) yellow, with gray pruinosity. 0+3 dorsocentral setae, anterior-most postsutural dorsocentral seta far from scutal suture, acrostichal setulae in ten rows. Legs yellow. Fore femur with nine posterior dorsal setae, four posterior ventral setae and ctenidium with 18 short setae; fore tibia with one dorsal preapical seta and one short apical ventral seta. Mid femur with five or six anterior setae and one apical posterior seta; mid tibia with one dorsal preapical seta and three strong apical ventral setae. Hind femur with several weak anterior ventral setae and one preapical anterior dorsal seta; hind tibia with one weak dorsal preapical seta and one short apical ventral seta. Wing (Fig. 42) slightly yellow, basal margin of brown apical spot on R_{2+3} at same vertical level as crossvein dm-cu; brown apical spots on R_{2+3} , R_{4+5} , and M_1 slightly confluent and forming pale brown connecting area between apical spots on R_{2+3} , R_{4+5} , and M_1 ; brown median spot on R_{4+5} separated from brown cloud-like spot on crossvein dm-cu; subcostal cell hyaline;



Figures 41–45. *Homoneura (Homoneura) multiseta* sp. nov. male 41 head, anterior view 42 wing 43 habitus, lateral view 44 thorax, dorsal view 45 abdomen, dorsal view.



Figures 46–50. *Homoneura (Homoneura) multiseta* sp. nov. male **46** syntergosternite and epandrium, lateral view **47** epandrial complex, posterior view **48** syntergosternite, anterior view **49** phallic complex, ventral view **50** phallic complex, lateral view. Scale bar: 0.5 mm.

seven short hairs present at base of R_{4+5} : costa with 2nd (between R_1 and R_{2+3}), 3rd (between R_{2+3} and R_{4+5}), and 4th (between R_{4+5} and M_1) sections in proportion of 4: 1: 0.8; r-m before middle of discal cell; ultimate and penultimate sections of M_1 in proportion of 1: 1; ultimate section of $CuA_1 \sim 1/7$ of penultimate. Haltere yellow.

Abdomen (Fig. 45) yellow, tergites 2–5 with brown posterior margin. Male genitalia (Figs 46–50): syntergosternite circular with a trapeziform ventral process, with several dorsal setulae. Epandrium broad in lateral view; surstylus blunt in lateral view, hairy and rolled up in ventral view. Hypandrium U-shaped. Pregonite broad, with a small tooth apically, postgonite long spine-like. Phallus curved backwards, with a small sharp process in lateral view. Phallapodeme shorter than phallus.

Female. Unknown.

Distribution. China (Chongqing).

Remarks. The new species resembles *Homoneura (Homoneura) shunhuangshana* in the habitus, basal margin of brown apical spot on R_{2+3} at same vertical level as crossvein dm-cu and mesonotum with acrostichal setulae in ten rows [see Chen and Li 2022: figs 7B–D], but it can be distinguished from the latter by the following: subcostal cell hyaline; brown apical spots on R_{2+3} shorter, as long as 1/2 length of ultimate section of M_1 ; brown median spot on R_{4+5} behind middle point of distance between r-m and dm-cu; surstylus blunt, rolled up in ventral view; hypandrium U-shaped. In *H. (H.) shunhuangshana*, subcostal cell pale brown apically; brown apical spots on R_{2+3} longer, at least 2/3 length of ultimate section of M_1 ; brown median spot on R_{4+5} at middle point of distance between r-m and dm-cu; surstylus horn-shaped in lateral view; hypandrium H-shaped [see Chen and Li 2022: figs 7B, 8A, D].

***Homoneura (Homoneura) serrulata* Chen & Li, sp. nov.**

<https://zoobank.org/0D01DD62-421D-43DC-8745-9EE3F678F714>

Figs 51–60

Chinese name: 锯缘同脉缟蝇

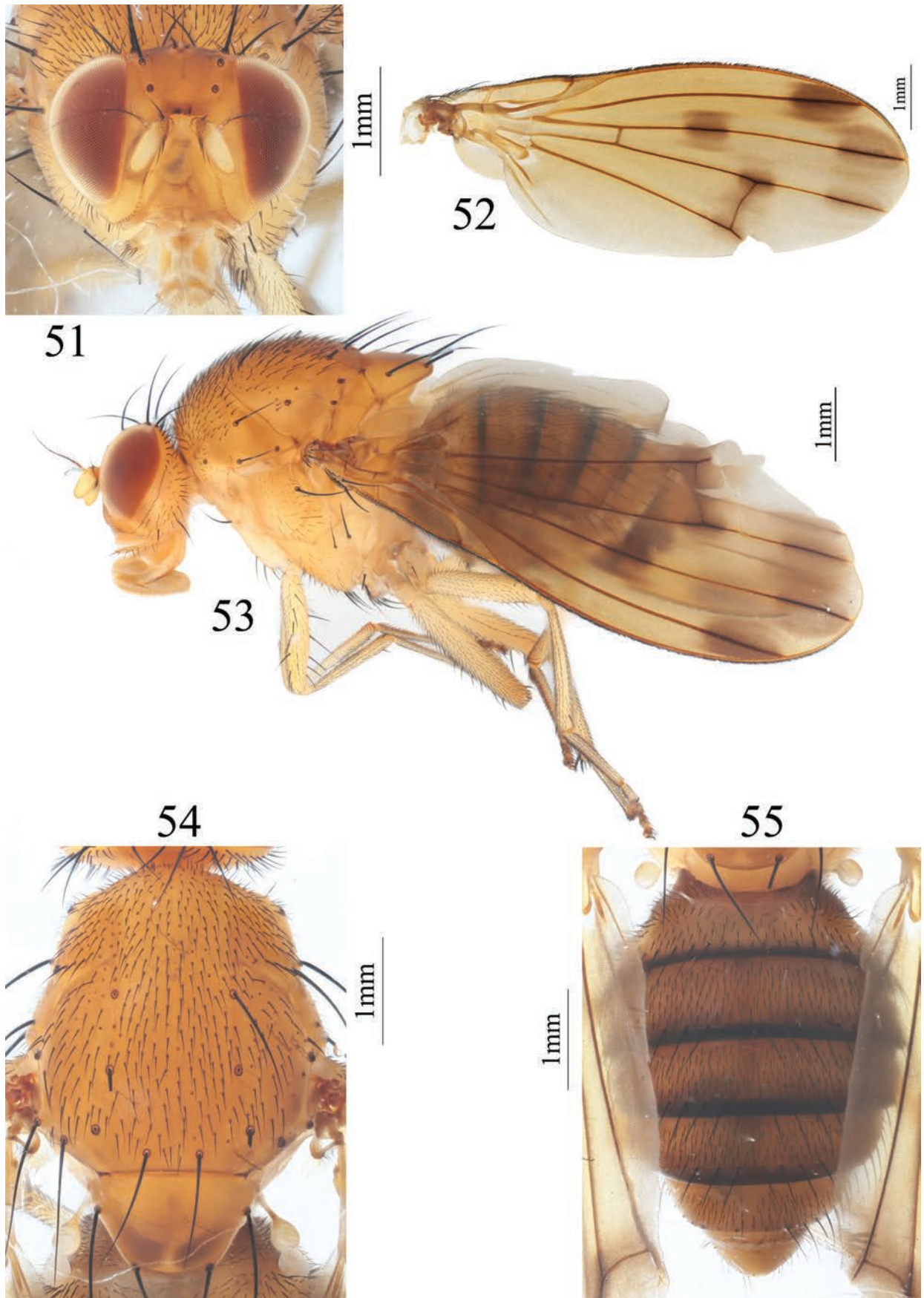
Type material. Holotype: ♂, CHINA, Chongqing City, Jiangjin District, Dayuandong National Forest Park, Shuijingwan, 28°53'10.96"N, 106°14'19.32"E, 717 m, 13.VII.2022, leg. Xulong Chen. **Paratypes:** 1♂, CHINA, Chongqing City, Jiangjin District, Dayuandong National Forest Park, Tian'ehu, 28°52'54.45"N, 106°15'14.53"E, 728 m, 13.VII.2022, leg. Xulong Chen.

Etymology. The specific name refers to the inner process of surstylus with serrulate margin in posterior view.

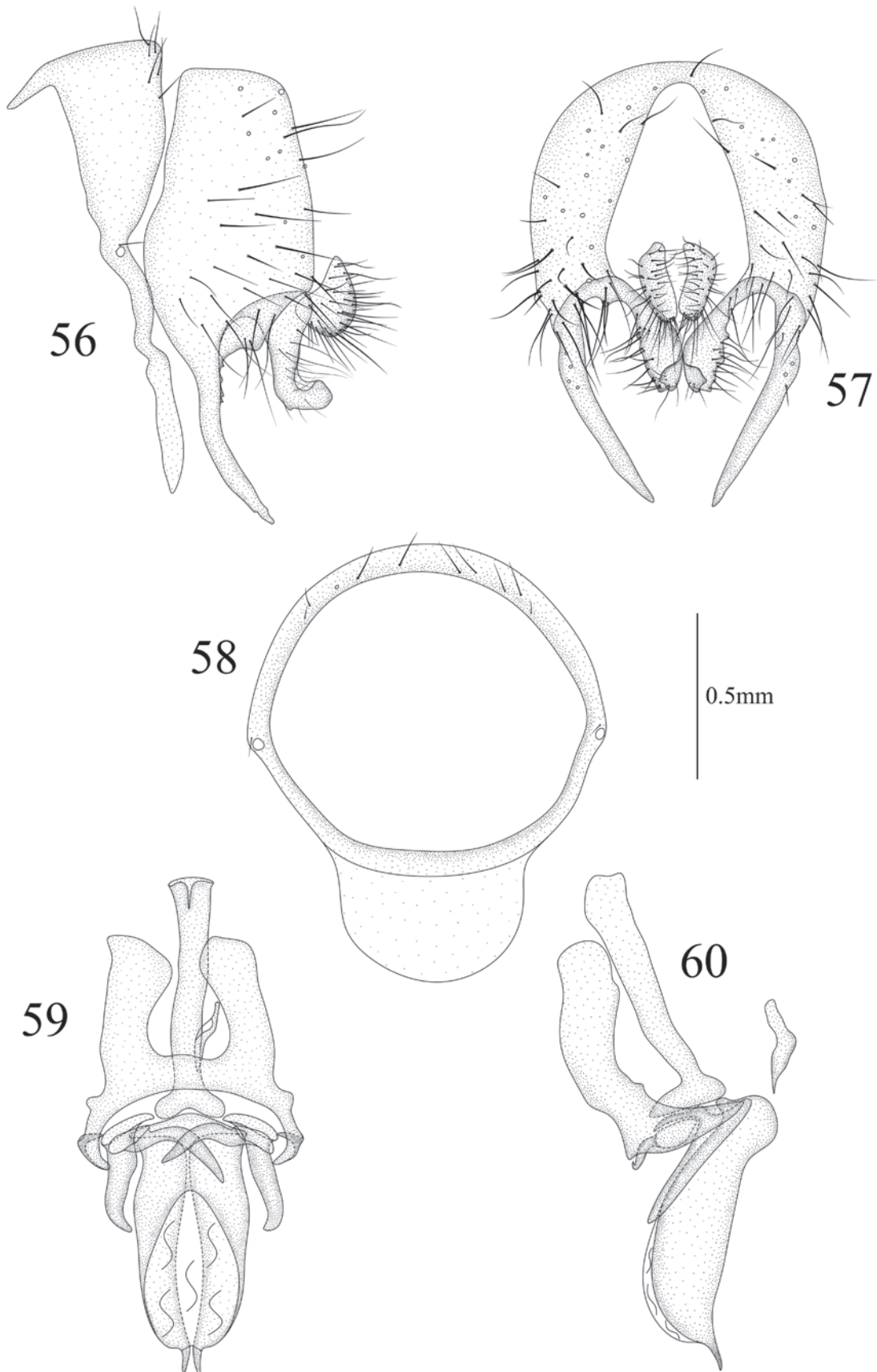
Diagnosis. Basal margin of brown apical spot on R_{2+3} at same vertical level as crossvein dm-cu. Male tergites 2–5 with blackish brown posterior margin. Syntergosternite with a setula around spiracle. Inner process of surstylus evaginable apically with serrulate margin in posterior view, outer process long spine-like. Pregonite crossed at front of phallus in ventral view, postgonite digitiform and curved apically. Phallus tapering apically in lateral view.

Description. Male. Body length 7.7 mm, wing length 7.8–7.9 mm.

Head (Fig. 51) yellow. Frons as long as wide and parallel-sided; ocellar triangle yellow, ocellar seta developed. Gena $\sim 1/10$ height of eye. Antenna yellow, first flagellomere $\sim 2.0 \times$ longer than high; arista black except yellow at base, long plumose, with longest ray as long as height of first flagellomere. Proboscis pale yellow, palpus yellow.



Figures 51–55. *Homoneura (Homoneura) serrulata* sp. nov. male 51 head, anterior view 52 wing 53 habitus, lateral view 54 thorax, dorsal view 55 abdomen, dorsal view.



Figures 56–60. *Homoneura (Homoneura) serrulata* sp. nov. male **56** syntergosternite and epandrium, lateral view **57** epandrial complex, posterior view **58** syntergosternite, anterior view **59** phallic complex, ventral view **60** phallic complex, lateral view. Scale bar: 0.5 mm.

Thorax (Fig. 54) yellow, with gray pruinosity. 0+3 dorsocentral setae, anterior-most postsutural dorsocentral seta far from scutal suture, acrostichal setulae in ten rows. Legs yellow. Fore femur with eight posterior dorsal setae, four or five posterior ventral setae and ctenidium with 14 short setae; fore tibia with one dorsal preapical seta and one short apical ventral seta. Mid femur with five or six anterior setae and one apical posterior seta; mid tibia with one dorsal preapical seta and three strong apical ventral setae. Hind femur with several weak anterior ventral setae and one preapical anterior dorsal seta; hind tibia with one weak dorsal preapical seta and one short apical ventral seta. Wing (Fig. 52) slightly yellow, basal margin of brown apical spot on R_{2+3} at same vertical level as crossvein dm-cu; brown apical spots on R_{2+3} , R_{4+5} and M_1 slightly confluent and forming pale brown connecting area between apical spots on R_{2+3} , R_{4+5} and M_1 ; brown median spot on R_{4+5} separated from brown cloud-like spot on crossvein dm-cu; subcostal cell pale brown apically; seven short hairs present at base of R_{4+5} ; costa with 2nd (between R_1 and R_{2+3}), 3rd (between R_{2+3} and R_{4+5}), and 4th (between R_{4+5} and M_1) sections in proportion of 7.5: 2: 1.5; r-m before middle of discal cell; ultimate and penultimate sections of M_1 in proportion of 1.1: 1.2. Haltere yellow.

Abdomen (Fig. 55) yellow, tergites 2–5 with blackish brown posterior margin. Male genitalia (Figs 56–60): sytergosternite circular with a trapeziform ventral process, with several dorsal setulae and setula around spiracle. Epandrium broad in lateral view; surstylus consisting of inner process and outer process, inner process evaginable apically with serrulate margin in posterior view, outer process long spine-like. Hypandrium H-shaped. Pregonite acute apically, crossed at front of phallus in ventral view, postgonite digitiform and curved apically. Phallus tapering apically in lateral view. Phallapodeme shorter than phallus.

Female. Unknown.

Distribution. China (Chongqing).

Remarks. The new species resembles *Homoneura (Homoneura) anadaequata* in the habitus, basal margin of brown apical spot on R_{2+3} at same vertical level as crossvein dm-cu and mesonotum with acrostichal setulae in ten rows [see Gao and Shi 2019: figs 1, 4, 7], but it can be distinguished from the latter by the following: brown apical spots on R_{2+3} , R_{4+5} and M_1 slightly confluent; sytergosternite with a setula around spiracle; inner process of surstylus evaginable apically with serrulate margin in posterior view; postgonites symmetrical in ventral view. In *H. (H.) anadaequata*, brown apical spots on R_{4+5} and M_1 confluent, separated from apical spot on R_{2+3} ; sytergosternite without setula around spiracle; surstylus long and furcated in posterior view; postgonites asymmetrical in ventral view [see Gao and Shi 2019: figs 7, 9, 10, 11].

***Homoneura (Homoneura) simianshana* Chen & Li, sp. nov.**

<https://zoobank.org/10AC3A27-80B5-41BD-8E58-221DAE4F0838>

Figs 61–70

Chinese name: 四面山同脉缟蝇

Type material. **Holotype:** ♂, CHINA, Chongqing City, Jiangjin District, Simianshan Natural Reserve, Dawopu, 28°34'11.28"N, 106°20'26.96"E, 1007 m, 6.IX.2022, leg. Xulong Chen. **Paratypes:** 3♂♂, same data as holotype; 4♂♂1♀, CHINA, Chongqing City, Jiangjin District, Simianshan Natural Reserve, Zhengq-

iangou, 28°36'59.54"N, 106°26'25.88"E, 1273 m, 14.VI.2022, leg. Xulong Chen; 4♂♂3♀♀, **CHINA**, Chongqing City, Jiangjin District, Simianshan Natural Reserve, Tudiyan, 28°37'23.62"N, 106°24'4.02"E, 1128 m, 7.IX.2022, leg. Xulong Chen; 1♂, **CHINA**, Chongqing City, Jiangjin District, Simianshan Natural Reserve, Qinjiagou, 28°37'6.32"N, 106°23'53.40"E, 1131 m, 15.VII.2022, leg. Xulong Chen; 1♂, **CHINA**, Chongqing City, Jiangjin District, Simianshan Natural Reserve, Zhenzhutan, 28°35'50.74"N, 106°25'25.70"E, 1226 m, 15.VII.2022, leg. Xulong Chen; 1♂, **CHINA**, Chongqing City, Jiangjin District, Simianshan Natural Reserve, Dahonghai, 28°35'34.27"N, 106°26'34.93"E, 1144 m, 15.VII.2022, leg. Xulong Chen; 1♂1♀, **CHINA**, Chongqing City, Jiangjin District, Dayuandong National Forest Park, Diaojiaolou, 28°52'16.19"N, 106°15'18.47"E, 759 m, 8.IX.2022, leg. Xulong Chen; 1♂, **CHINA**, Chongqing City, Jiangjin District, Dayuandong National Forest Park, Diaojiaolou, 28°53'5.89"N, 106°15'42.18"E, 731 m, 13.VII.2022, leg. Xulong Chen.

Etymology. The specific name refers to the type locality Simianshan Natural Reserve.

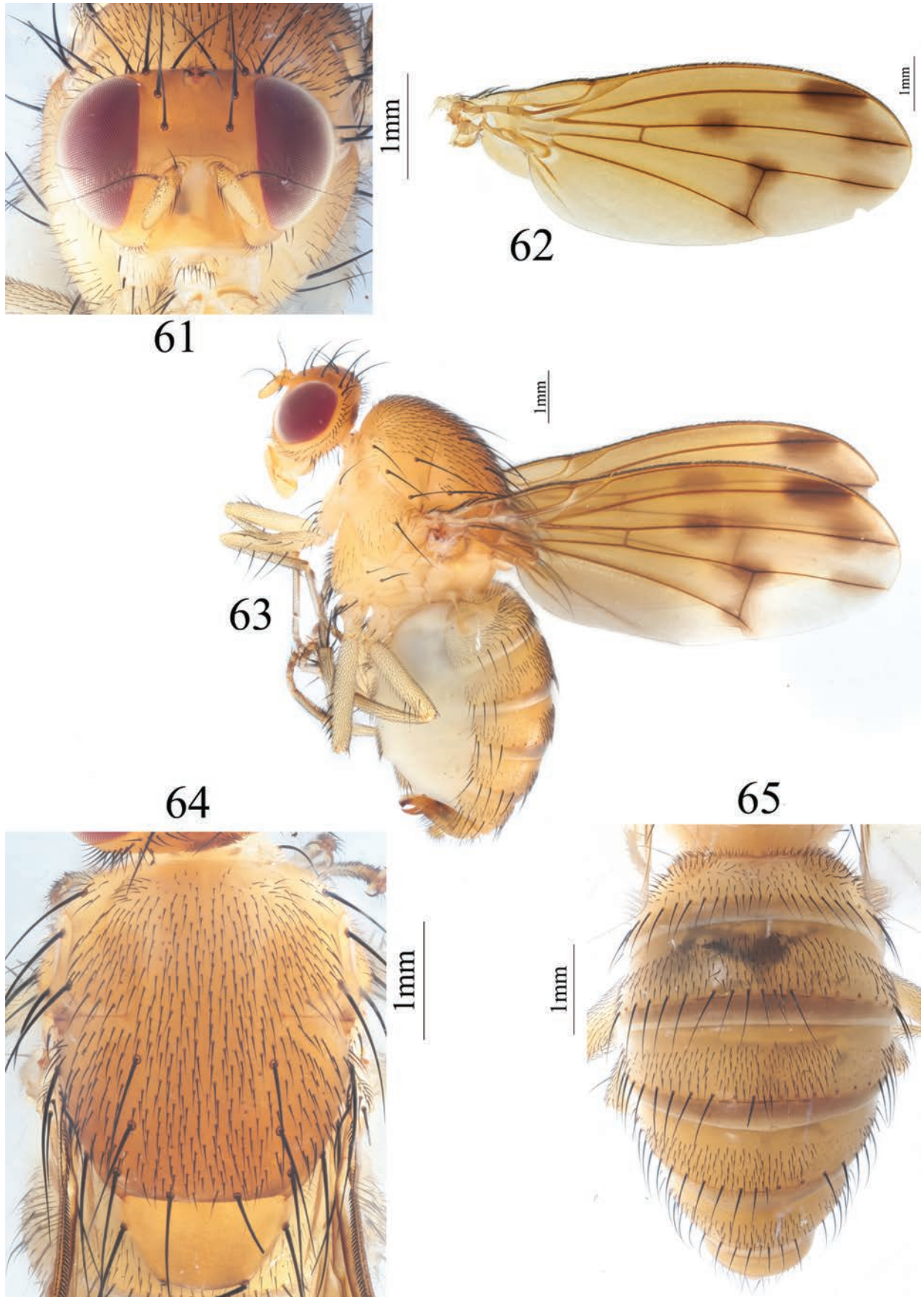
Diagnosis. Basal margin of brown apical spot on R_{2+3} at same vertical level as crossvein dm-cu; brown apical spots on R_{2+3} , R_{4+5} , and M_1 slightly confluent. Male tergites 2–5 with brown posterior margin. Surstylus inwardly curved apically in posterior view. Postgonite consisting of a pair of asymmetric sclerites, furcated in lateral view.

Description. Male. Body length 8.6–8.8 mm, wing length 8.5–8.6 mm.

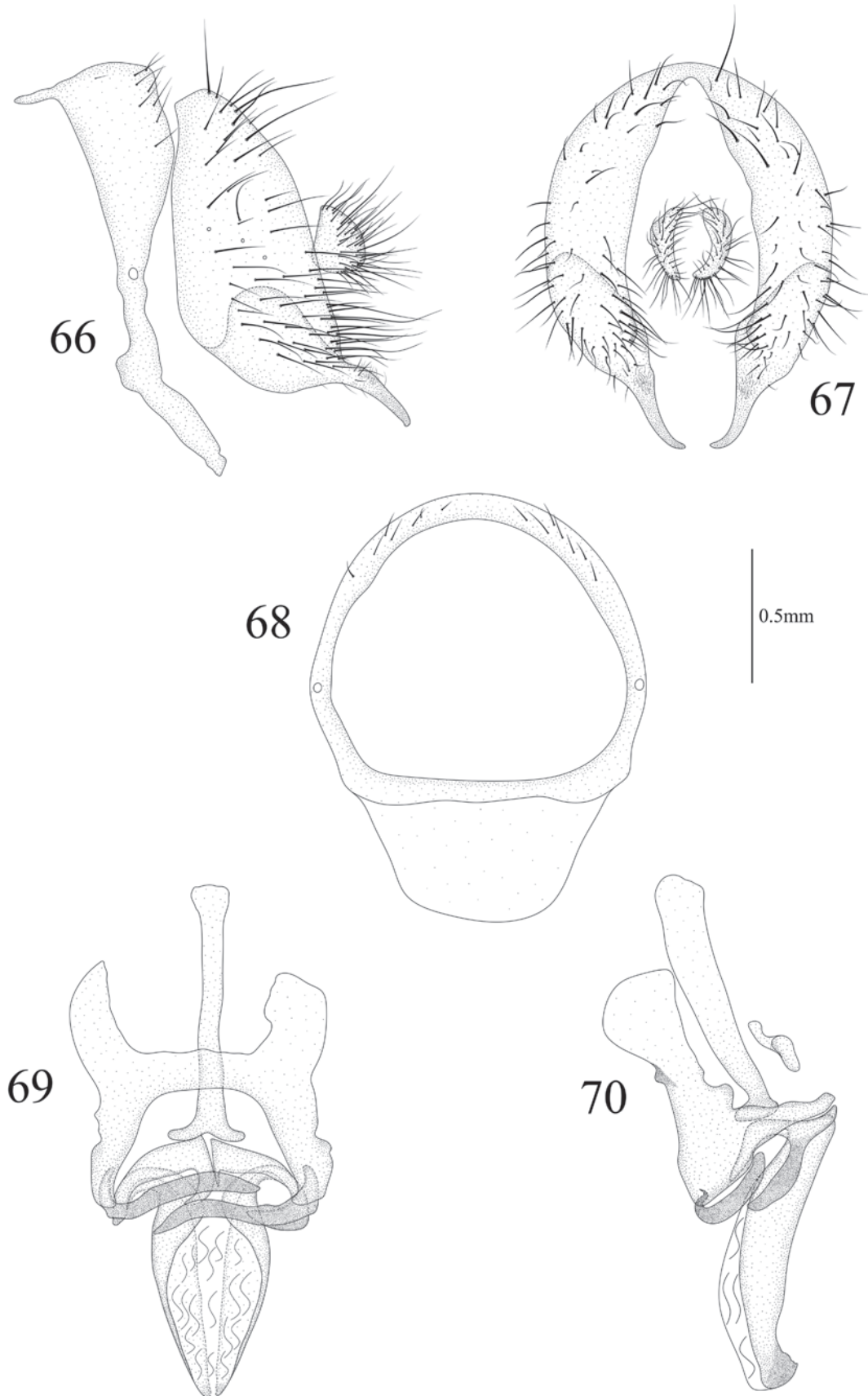
Head (Fig. 61) yellow. Frons as long as wide and parallel-sided; ocellar triangle yellow, ocellar seta developed, slightly longer than anterior fronto-orbital seta, anterior fronto-orbital seta shorter than posterior fronto-orbital seta. Gena ~ 1/6 height of eye. Antenna yellow, first flagellomere ~ 2.0 × longer than high; arista black except brown at base, long plumose, with longest ray slightly shorter height of first flagellomere. Proboscis pale yellow; palpus yellow.

Thorax (Fig. 64) yellow, with gray pruinosity. 0+3 dorsocentral setae, anterior-most postsutural dorsocentral seta far from scutal suture, acrostichal setulae in ten irregular rows. Legs yellow. Fore femur with nine posterior dorsal setae, four posterior ventral setae, and ctenidium with 18–20 short setae; fore tibia with one dorsal preapical seta and one short apical ventral seta. Mid femur with five anterior setae and one apical posterior seta; mid tibia with one dorsal preapical seta and three strong apical ventral setae. Hind femur with several weak anterior ventral setae and one preapical anterior dorsal seta; hind tibia with one dorsal preapical seta and one short apical ventral seta. Wing (Fig. 62) slightly yellow, basal margin of brown apical spot on R_{2+3} at same vertical level as crossvein dm-cu; brown apical spots on R_{2+3} , R_{4+5} , and M_1 slightly confluent and forming pale brown area between apical spots on R_{2+3} , R_{4+5} , and M_1 ; brown median spot on R_{4+5} separated from brown cloud-like spot on crossvein dm-cu; subcostal cell pale brown apically; four short hairs present at base of R_{4+5} , costa with 2nd (between R_1 and R_{2+3}), 3rd (between R_{2+3} and R_{4+5}), and 4th (between R_{4+5} and M_1) sections in proportion of 5.5: 1.5: 1; r-m before middle of discal cell; ultimate and penultimate sections of M_1 in proportion of 1: 1; ultimate section of CuA_1 ~ 1/8 of penultimate. Haltere yellow.

Abdomen (Fig. 65) yellow, tergites 2–5 with brown posterior margin. Male genitalia (Figs 66–70): syntergosternite circular, with a trapeziform ventral process and with several dorsal setulae. Epandrium broad in lateral view; surstylus long digitiform in lateral view, inwardly curved apically in posterior view. Hypandrium H-shaped. Pregonite long digitiform and curved apically in ventral view,



Figures 61–65. *Homoneura (Homoneura) simianshana* sp. nov. male 61 head, anterior view 62 wing 63 habitus, lateral view 64 thorax, dorsal view 65 abdomen, dorsal view.



Figures 66–70. *Homoneura (Homoneura) simianshana* sp. nov. male **66** syntergosternite and epandrium, lateral view **67** epandrial complex, posterior view **68** syntergosternite, anterior view **69** phallic complex, ventral view **70** phallic complex, lateral view. Scale bar: 0.5 mm.

postgonite consisting of a pair of asymmetric sclerites, furcated in lateral view. Phallus curved backwards in lateral view. Phallapodeme as long as phallus.

Female. Body length 8.8 mm, wing length 8.5–8.6 mm.

Distribution. China (Chongqing).

Remarks. The new species resembles *Homoneura (Homoneura) shunhuangshana* in the habitus, mesonotum with acrostichal setulae in ten rows, basal margin of brown apical spot on R_{2+3} at same vertical level as crossvein dm-cu and tergites 2–5 each with brown posterior margin [see Chen and Li 2022: figs 7B–E], but it can be distinguished from the latter by the following: fore femur with nine posterior dorsal setae, four posterior ventral setae; mid femur with five anterior setae; brown apical spots on R_{2+3} shorter, as long as 1/2 length of ultimate section of M_1 ; brown median spot on R_{4+5} behind middle point of distance between r-m and dm-cu. In *H. (H.) anadaequata*, fore femur with eight posterior dorsal setae, six posterior ventral setae; mid femur with six or seven anterior setae; brown apical spots on R_{2+3} longer, at least 2/3 length of ultimate section of M_1 ; brown median spot on R_{4+5} at middle point of distance between r-m and dm-cu [see Chen and Li 2022: fig. 7B, C].

Discussion

Homoneura (Homoneura) henanensis species group is species rich in Oriental and Palearctic species, with 53 described species, and is now the largest group of the subgenus *Homoneura*. The species of the *henanensis* group are almost unified in external morphological characters (i.e., large body size, antennal first flagellomere $\sim 2.0 \times$ longer than high, wing with five large brown spots), but are not sufficient for species identification. Interestingly, the male genitalia of *henanensis* group are extremely complex and variable, and different species exhibit distinctive shapes and forms; therefore, the male genitalia structures can provide the most reliable diagnostic characters for species delimitation, while the value of the female genitalia is relatively limited for species identification. Seven new species of the *henanensis* group are described in this paper, of which six species have extremely characteristic male genitalia, except for *H. (H.) microtricha* sp. nov. that resembles *H. (H.) longiacutata* in the shape of surstylus, but the new species can be separated from the latter by the following male genitalia characters: 1) the H-shaped hypandrium; 2) the long spine-like postgonite in lateral view; 3) the not curved phallus, blunt and round apically. In *H. (H.) longiacutata*, the hypandrium is U-shaped, the postgonite is short and the middle part depressed, and the phallus is curved backwards apically and acute at the apex.

The *henanensis* group is diverse in Chinese moist and shaded herb habitats (Fig. 71; including Shaanxi, Chongqing, Henan, Guangdong, Guangxi, Zhejiang), and suitable habitats can attract a large number of species that survive and reproduce here, which may be the reason they are abundant in collections, as well as contribute to the discovery of new species. However, it is surprising that only one species of this group has been found in Yunnan province, which has the highest species richness of lauxaniid flies in China; such distributional gaps may be the result of insufficient sampling for this group. There is no doubt that additional species await discovery in unsampled primary forests throughout southwestern China.



Figure 71. Habitat and plants in Simianshan Natural Reserve, Zhengqiangou.

Acknowledgements

Thanks are due to the editor and reviewers for their comments that improved this paper.

Additional information

Conflict of interest

The authors have declared that no competing interests exist.

Ethical statement

No ethical statement was reported.

Funding

The research was funded by the National Natural Science Foundation of China (32070477).

Author contributions

All authors have contributed equally.

Author ORCIDs

Xulong Chen  <https://orcid.org/0000-0003-0787-3333>

Pengyan You  <https://orcid.org/0000-0002-7485-8056>

Wenliang Li  <https://orcid.org/0000-0001-9019-1223>

Zhisheng Zhang  <https://orcid.org/0000-0002-9304-1789>

Data availability

All of the data that support the findings of this study are available in the main text.

Reference

- Álvarez-Padilla F, Hormiga G (2007) A protocol for digesting internal soft tissues and mounting spiders for scanning electron microscopy. *The Journal of Arachnology* 35(3): 538–542. <https://doi.org/10.1636/Sh06-55.1>
- Chen XL, Li WL (2022) Four new species of the subgenus *Homoneura* from Hunan Province, China (Diptera: Lauxaniidae: *Homoneura*). *Oriental Insects* 56(4): 437–462. <https://doi.org/10.1080/00305316.2021.2022546>
- Cumming JM, Wood DM (2017) 3. Adult morphology and terminology. In: Kirk-Spriggs AH, Sinclair BJ (Eds) *Manual of Afrotropical Diptera: Vol. 1. Suricata 4. South African National Biodiversity Institute, Pretoria*, 89–133.
- Gaimari SD, Miller RM (2021) 74. Lauxaniidae (Lauxaniid flies). In: Kirk-Spriggs AH, Sinclair BJ (Eds) *Manual of Afrotropical Diptera. Vol. 3. Brachycera—Cyclorrhapha, excluding Calyptratae. Suricata 8. South African National Biodiversity Institute, Pretoria*, 1757–1781.
- Gao XF, Shi L (2019) Nine new species of genus *Homoneura* from Qinling mountains in China (Diptera: Lauxaniidae). *Zootaxa* 4608(3): 401–432. <https://doi.org/10.11646/zootaxa.4608.3.1>
- Gao CX, Yang D (2002) A review of the genus *Homoneura* from Guizhou, China (Diptera: Lauxaniidae). *Annales Zoologici* 52(2): 293–296.
- Gao CX, Yang D (2003) A revision of the genus *Homoneura* from Tibet, China (Diptera, Lauxaniidae). *Deutsche Entomologische Zeitschrift* 50(2): 243–248. <https://doi.org/10.1002/mmnd.20030500208>
- Gao CX, Yang D (2004) A review of the genus *Homoneura* from Guangxi, China (Diptera: Lauxaniidae). *The Raffles Bulletin of Zoology* 52(2): 351–364.
- Gao CX, Yang D (2005) Notes on genus *Homoneura* from Guizhou, China (Diptera: Lauxaniidae). *Zootaxa* 1010(1): 15–24. <https://doi.org/10.11646/zootaxa.1010.1.2>
- Kertész K (1915) H. Sauter's Formosa Ausbeute. Lauxaniidae (Dipt). II. *Annales Musei Nationali Hungarici* 13: 491–534.
- Li WL, Yang D (2012) Eleven new species of the *Homoneura* (*Homoneura*) *beckeri* group from Yunnan, China (Diptera, Lauxaniidae). *Zootaxa* 3537(1): 1–28. <https://doi.org/10.11646/zootaxa.3537.1.1>
- Li WL, Yang D (2013) Four new species of *Homoneura* s. str. from Yunnan, China (Diptera, Lauxaniidae). *Revue Suisse de Zoologie* 120(4): 549–561.
- Li WL, Yang D (2015) Species of the subgenus *Neohomoneura* Malloch from Yunnan, China (Diptera, Lauxaniidae). *Transactions of the American Entomological Society* 141(1): 27–44. <https://doi.org/10.3157/061.141.0104>
- Li WL, Qi L, Yang D (2019) First record of the genus *Trypetisoma* Malloch, 1924 (Diptera, Lauxaniidae) for China with nine species. *Zootaxa* 4608(1): 035–064. <https://doi.org/10.11646/zootaxa.4608.1.2>
- Li WL, Chen XL, Yang D (2020a) Five new species of the genus *Noeetomima* Enderlein (Diptera: Lauxaniidae) from China, with a key to world species. *Zootaxa* 4768(4): 499–516. <https://doi.org/10.11646/zootaxa.4768.4.3>
- Li WL, Chen XL, Yang D (2020b) Four new species of the subgenus *Minettiella* from China (Diptera, Lauxaniidae, *Minettia*). *ZooKeys* 932: 93–111. <https://doi.org/10.3897/zookeys.932.50763>

- Li WL, Qi L, Yang D (2020c) Four new species of the subfamily Homoneurinae (Diptera, Lauxaniidae) from southwestern China. *ZooKeys* 953: 119–136. <https://doi.org/10.3897/zookeys.953.53976>
- Li WL, Qi L, Yang D (2020d) First Chinese record and the second species of the genus *Pleurigona* Malloch, 1929 (Diptera: Lauxaniidae). *Revue Suisse de Zoologie* 127(2): 245–248. <https://doi.org/10.35929/RSZ.0018>
- Li WL, Qi L, Yang D (2020e) Four species of the genus *Lauxania* Latreille, 1804 (Diptera: Lauxaniidae) from China. *Oriental Insects* 54(3): 417–432. <https://doi.org/10.1080/00305316.2019.1665595>
- Li WL, Qi L, Yang D (2020f) Four new species of the subgenus *Frendelia* Collin, 1948 (Diptera: Lauxaniidae: *Minettia*) from China. *Annales Zoologici* 70(2): 273–284. <https://doi.org/10.3161/00034541ANZ2020.70.2.007>
- Li WL, Chen XL, Feng KL, Zhao SJ, Yang D (2021a) Four new species of the genus *Luzonomyza* Malloch (Diptera, Lauxaniidae) from China. *ZooKeys* 1074: 43–59. <https://doi.org/10.3897/zookeys.1074.68392>
- Li WL, Qi L, Yang D (2021b) Three new species of the genus *Noonamyia* Stuckenberg 1971 (Diptera: Lauxaniidae) from China. *Oriental Insects* 55(1): 119–132. <https://doi.org/10.1080/00305316.2020.1754955>
- Li WL, Bai YM, Yang D (2023) The genus *Minettia* Robineau-Desvoidy, 1830 (Diptera: Lauxaniidae: Lauxaniinae) from the Oriental Region with descriptions of seventeen new species. *Zootaxa* 5256(3): 201–249. <https://doi.org/10.11646/zootaxa.5256.3.1>
- Malloch JR (1926) A new species of Sapromyzidae from China (Diptera). *Bulletin of the Brooklyn Entomological Society* 21: 176.
- Malloch JR (1927) Fauna sumatrensis. Sapromyzidae (Diptera). *Supplementa Entomologica* 15: 102–110.
- Matsumura S (1916) Thousand Insects of Japan. *Additamenta*. 2 (Diptera): 185–474.
- Papp L, Gaimari SD (2013) The holotype of *Homoneura grandis* (Kertész, 1915) with description of a new species from Taiwan (Diptera, Lauxaniidae). *Acta Zoologica Academiae Scientiarum Hungaricae* 59(1): 31–39.
- Shi L, Yang D (2014) Supplements to species groups of the subgenus *Homoneura* in China (Diptera: Lauxaniidae: *Homoneura*), with descriptions of twenty new species. *Zootaxa* 3890(1): 1–117. <https://doi.org/10.11646/zootaxa.3890.1.1>
- Shi L, Yang D (2015) Two new species of the genus *Luzonomyza* from China (Diptera, Lauxaniidae). *Zootaxa* 3964(1): 087–094. <https://doi.org/10.11646/zootaxa.3964.1.5>
- Shi L, Li WL, Yang D (2009) Five new species of the genus *Dioides* from China (Diptera: Lauxaniidae). *Annales Zoologici* 59(1): 93–105. <https://doi.org/10.3161/000345409X432600>
- Shi L, Gaimari SD, Yang D (2017a) Five new species of the genus *Tetroxyrhina* Hendel from China (Diptera, Lauxaniidae). *Zootaxa* 4247(3): 246–280. <https://doi.org/10.11646/zootaxa.4247.3.2>
- Shi L, Gao XF, Shen RR (2017b) Four new species of the subgenus *Homoneura* from Jiangxi Province, China (Diptera: Lauxaniidae: *Homoneura*). *Zootaxa* 4365(3): 361–377. <https://doi.org/10.11646/zootaxa.4365.3.5>
- Shi L, Liu M, Hu ZK (2020) A new species of the genus *Noeetomima* Enderlein (Diptera, Lauxaniidae) from Guizhou, China with a key to worldwide species. *ZooKeys* 1000: 107–123. <https://doi.org/10.3897/zookeys.1000.57577>
- Wulp FM van der (1891) Eenige uitlandsche Diptera. *Tijdschrift voor Entomologie* 34: 193–218. [1890–1891]

- Wang JC, Gao CX, Yang D (2012) Three new species of the *Homoneura* (*Homoneura*) *henanensis* species group (Diptera, Lauxaniidae), with a key to Chinese species. *Zootaxa* 3262(1): 35–45. <https://doi.org/10.11646/zootaxa.3262.1.3>
- Yang D, Zhu F, Hu XY (1999) New species of Lauxaniidae from Henan (Diptera: Acalyptratae). 211–217. In: Shen XC, Shi ZY (Eds) *Fauna and Taxonomy of Insects in Henan: Vol. 4*: 211–217. China Agricultural Sciencetech Press, Beijing, 404 pp.
- Yang D, Hu XY, Zhu F (2001) Diptera: Lauxaniidae. 446–453. In: Wu H, Pan CW (Eds) *Insects of Tianmushan National Nature Reserve*: 446–453. Science Press, Beijing, 764 pp.
- Yang D, Zhu F, Hu XY (2003) Diptera: Lauxaniidae. 555–558. In: Huang BK (Ed.) *Fauna of Insects in Fujian Province of China*. 8. Fujian Science and Technology Publishing House, Fuzhou, 706 pp.
- You PY, Chen XL, Li WL (2023) Four new species of the subgenus *Homoneura* from Yintiaoling Nature Reserve, China (Diptera: Lauxaniidae: *Homoneura*). *Zootaxa* 5257(1): 143–159. <https://doi.org/10.11646/zootaxa.5257.1.11>
- Zhao SJ, Chen XL, Li WL, Yang D (2022) Two new species of the genus *Melanopachycerina* (Diptera: Lauxaniidae) from China, with a key to known species worldwide. *Annales Zoologici* 72(4): 943–950. <https://doi.org/10.3161/00034541ANZ2022.72.4.010>

The first two complete mitochondrial genomes for the genus *Anagyrus* (Hymenoptera, Encyrtidae) and their phylogenetic implications

Cheng-Hui Zhang¹, Hai-Yang Wang¹, Yan Wang¹, Zhi-Hao Chi¹, Yue-Shuo Liu¹, Guo-Hao Zu¹

¹ College of Horticulture and Landscape, Tianjin Agricultural University, Tianjin 300392, China
Corresponding author: Guo-Hao Zu (zuguohao@tjau.edu.cn)

Abstract

Anagyrus, a genus of Encyrtidae (Hymenoptera, Chalcidoidea), represents a successful group of parasitoid insects that attack various mealybug pests of agricultural and forestry plants. Until now, only 20 complete mitochondrial genomes have been sequenced, including those in this study. To enrich the diversity of mitochondrial genomes in Encyrtidae and to gain insights into their phylogenetic relationships, the mitochondrial genomes of two species of *Anagyrus* were sequenced, and the mitochondrial genomes of these species were compared and analyzed. Encyrtid mitochondrial genomes exhibit similarities in nucleotide composition, gene organization, and control region patterns. Comparative analysis of protein-coding genes revealed varying molecular evolutionary rates among different genes, with six genes (*ATP8*, *ND2*, *ND4L*, *ND6*, *ND4* and *ND5*) showing higher rates than others. A phylogenetic analysis based on mitochondrial genome sequences supports the monophyly of Encyrtidae; however, the two subfamilies, Encyrtinae and Tetracneminae, are non-monophyletic. This study provides valuable insights into the phylogenetic relationships within the Encyrtidae and underscores the utility of mitochondrial genomes in the systematics of this family.

Key words: Encyrtid, genome structure, mitogenome, protein-coding genes, phylogenetic analyses, Tetracneminae



Academic editor: Zachary Lahey
Received: 29 February 2024
Accepted: 12 June 2024
Published: 5 July 2024

ZooBank: <https://zoobank.org/C6737E11-5992-4B82-B0C1-48C6C32DF550>

Citation: Zhang C-H, Wang H-Y, Wang Y, Chi Z-H, Liu Y-S, Zu G-H (2024) The first two complete mitochondrial genomes for the genus *Anagyrus* (Hymenoptera, Encyrtidae) and their phylogenetic implications. ZooKeys 1206: 81–98. <https://doi.org/10.3897/zookeys.1206.121923>

Copyright: © Cheng-Hui Zhang et al.
This is an open access article distributed under terms of the Creative Commons Attribution License (Attribution 4.0 International – CC BY 4.0).

Introduction

Encyrtidae is a large hymenopteran family in the superfamily Chalcidoidea, comprising 518 known genera, of which 495 are recognized as valid (totaling more than 4830 species), along with 23 fossil genera (26 species) worldwide (Simutnik et al. 2022; Simutnik et al. 2023; Simutnik and Perkovsky 2023; Wang et al. 2023). The genus *Anagyrus* Howard, 1986 is one of the largest genera in Encyrtidae, comprising 289 valid species (Noyes 2019). This genus was established by Howard and Ashmead (1896) based on the type species, *Anagyrus greeni* Howard, 1896. Diagnostics for the genus include a broadened, flattened scape (normally 2–3× as long as broad), funicle segments longer than broad, occipital margin normally quite sharp but often rounded, postmarginal vein normally not longer than the stigma vein, and ovipositor at least half the length of

the mid tibia (Noyes 1980; Noyes and Hayat 1994). *Anagyrus* species are primary parasitoids of Pseudococcidae; for example, *Anagyrus galinae* has been utilized in classical biocontrol and integrated pest management of *Trionymus copiosus* (Japoshvili and Hansen 2015; Noyes 2019).

Insect mitochondrial genomes are usually small, circular molecules containing 37 genes: 13 protein-coding genes (PCGs), two ribosomal RNA genes (rRNAs), and 22 transfer RNA genes (tRNAs), as well as a large non-coding element known as the A+T-rich or control region (CR), which regulates transcription and replication (Wolstenholme 1992a, 1992b; Boore 1999; Cameron 2014). Due to their distinct characteristics, including gene-content conservation, maternal inheritance, and rapid evolutionary rate, mitogenome sequences serve as valuable molecular markers for various evolutionary studies (Boore 1999; Krzywinski et al. 2006). Although the mitochondrial genome of Chalcidoidea exhibits structural resemblance to other insects, significant rearrangements characterize it, along with a relatively high A+T content in its sequence composition, deviating from the presumed ancestral pattern (Brown et al. 1979; Cameron and Whiting 2008).

The exploration of hymenopteran mitochondrial genomes commenced with the sequencing of *CYTB* and *ATP8* genes of *Apis mellifera*, and it was not until 1993 that the first complete mitochondrial genome was deciphered (Crozier and Crozier 1992, 1993). The first comprehensive phylogenetic analysis of Chalcidoidea based on molecular data was conducted using 18S and 28S rDNA (Munro et al. 2011). Subsequently, Heraty et al. (2013) conducted an in-depth exploration of the phylogenetic relationships within Chalcidoidea based on both morphological and molecular data. Zhang et al. (2020a) further reconstructed the phylogenetic relationships within Chalcidoidea using transcriptome data, providing valuable insights for achieving more accurate phylogenetic relationships. Recently, Cruaud et al. (2024) conducted a comprehensive phylogenetic study using data from PCGs and ultra-conserved elements (UCEs), while Zhu et al. (2023) conducted a comprehensive phylogenetic study using 139 mitochondrial genomes from the main clades of Chalcidoidea. These studies have significantly advanced our understanding of the phylogenetic relationships within Chalcidoidea. However, to obtain a more accurate reconstruction of evolutionary relationships, it is necessary to expand the sampling range to include more understudied species. This approach will help construct a more comprehensive and precise phylogenetic tree, revealing deeper levels of phylogenetic relationships. Additionally, integrating different types of data, such as rDNA genes, mitochondrial genomes, and UCEs, is crucial. By comprehensively utilizing morphological, biological, and molecular data and conducting multidimensional phylogenetic analyses, we can improve the accuracy of classification and phylogenetic research. Such integrative approaches will provide a more robust framework for understanding the evolutionary relationships within Hymenoptera.

At present, there are only morphology-based classification systems for Encyrtidae (Noyes and Hayat 1984, 1994; Trjapitzin 1989), lacking auxiliary verification from molecular data, particularly from the mitochondrial genome (mitogenome). Consequently, the monophyly and phylogenetic relationships of Encyrtidae have been controversial for a long time. Problems that are difficult to distinguish in taxonomy indicate the requirement for using various molecular data to understand the systematic position and the monophyly of Encyrtidae in

Chalcidoidea. Mitogenome data seem sufficient to solve these problems (Wei et al. 2010; Li et al. 2016; Liu et al. 2023). There are currently only 1291 complete mitochondrial genomes of Hymenoptera on GenBank, and the number of encyrtid genomes is small (Sayers et al. 2024). This limited data negatively impacts our ability to resolve potential systematic ambiguity within Encyrtidae.

In this study, we conducted the sequencing and annotation of the mitogenomes of *Anagyrs galinae* (accession number: OR652687) and *Anagyrs jenniferae* (accession number: OR790122), analyzing their respective characteristics. In addition, we reconstructed the molecular phylogenetic relationships of these two new mitochondrial genomes and other species of Encyrtidae. The molecular data presented in this study will contribute to a better understanding of the characteristics of the Encyrtidae mitogenome. Further, a phylogenetic analysis was performed, including 19 uploaded mitogenomes together with our newly acquired data, which represented Encyrtidae. The goal of our study was to place two new species of *Anagyrs* within the context of the known mitogenome diversity of Encyrtidae by performing mitogenomic and phylogenetic analyses.

Materials and methods

Sample collection, DNA extraction and sequencing

The specimens, *A. galinae* and *A. jenniferae*, were collected from Tianjin Agricultural University (39°5'21"N, 117°5'38"E), Xiqing District, Tianjin City, China, in September 2022. Freshly collected specimens were promptly immersed in 100% ethanol for initial preservation and subsequently stored at -40 °C in the Insect Herbarium of Tianjin Agricultural University. Following morphological identification, total DNA from each specimen was extracted from the body, excluding the abdomen, using the DNeasy Blood & Tissue Kit (Qiagen, Hilden, Germany) according to the manufacturer's instructions. The purity and concentration of the extracted total DNA were assessed through 1% agarose gel electrophoresis and optical density value detection. The total DNA of two encyrtids underwent sequencing using the Illumina NovaSeq 6000 platform with a 350 bp insert size and a paired-end 150 bp sequencing strategy. Sequencing was conducted by Novogene Co., Ltd. (Beijing, China).

Mitogenome assembly, annotation and analysis

After initial data acquisition, with adapter sequences removed, additional filtering was carried out using fastp 0.23.4 (Chen et al. 2018) to filter low-quality reads (quality value <30), ensuring that each sample retained clean data of no less than 4 Gb. The software MitoZ v. 3.6 (Meng et al. 2019) and GetOrganelle v. 1.7.7.0 (Jin et al. 2020) were used for the de novo assembly of mitogenomes. Homologous sequences of other Encyrtidae species from GenBank were used for comparison, and the mitogenomes were annotated using the Mitos WebServer (Donath et al. 2019). The secondary structures of tRNAs were predicted using Mitos WebServer and further visualized using VARNA v. 3.9 (Darty et al. 2009). The structures of the mitochondrial genome were mapped using the online tool CGview Server. The nucleotide composition and relative synonymous codon usage (RSCU) of protein-coding genes were calculated and analyzed by

MEGA v. 11.0.13 (Tamura et al. 2021). The skew analysis of nucleotide composition was calculated using the formulas: AT-skew = $(A-T)/(A+T)$ and GC-skew = $(G-C)/(G+C)$, where A, T, G and C were the base contents of the same chain (Perna and Kocher 1995; Hassanin et al. 2005). The nonsynonymous mutation rate (Ka) and synonymous mutation rate (Ks) of protein coding genes were calculated using DnaSP 6.12.03 (Rozas et al. 2017). Tandem repeats in the CR were identified by Tandem Repeats Finder (Benson 1999).

Molecular phylogenetic analyses

A total of 21 mitogenomes from two families of Chalcidoidea, including 20 Encyrtidae species and a Aphelinidae species as outgroup, were used for the phylogenetic analysis (Table 1). The phylogenetic trees were reconstructed using both maximum-likelihood (ML) and Bayesian-inference (BI) methods. For this, each PCG was individually aligned using the MAFFT 7 online service with the L-INS-i strategy, followed by optimization using MACSE (Ranwez et al. 2018; Katoh et al. 2019). The individual PCG alignments were trimmed using GBlocks and concatenated into a PCG dataset using PhyloSuite v. 1.2.3 (Talavera and Castresana 2007; Zhang et al. 2020b). The best nucleotide substitution model was obtained using ModelFinder v. 2.2.0 with Bayesian Information Criterion (BIC) (Kalyanamorthy et al. 2017). BI analysis was performed using MrBayes v. 3.2.7a with four chains (Ronquist et al. 2012). Two independent runs of

Table 1. GenBank accession numbers of species used in phylogenetic reconstruction and their original publications.

Superfamily	Family	Species	Accession Number	References
Chalcidoidea	Aphelinidae	<i>Encarsia formosa</i>	MG813797	Zhu et al. 2018
	Encyrtidae	<i>Aenasius arizonensis</i>	NC_045852	Ma et al. 2019
		<i>Anagyrus galinae</i>	OR652687	This study
		<i>Anagyrus jenniferae</i>	OR790122	This study
		<i>Blastothrix speciosa</i>	NC_082111	Unpublished
		<i>Cheiloneurus chinensis</i>	NC_084192	Unpublished
		<i>Cheiloneurus elegans</i>	NC_071192	Unpublished
		<i>Diaphorencyrtus aligarhensis</i>	NC_046058	Du et al. 2019
		<i>Encyrtus aurantii</i>	OR120384	Unpublished
		<i>Encyrtus eulecaniumiae</i>	NC_051459	Rudoy et al. 2022
		<i>Encyrtus infelix</i>	NC_041176	Xiong et al. 2019
		<i>Encyrtus rhodococcusiae</i>	NC_051460	Rudoy et al. 2022
		<i>Encyrtus sasakii</i>	NC_051458	Rudoy et al. 2022
		<i>Exoristobia philippinensis</i>	NC_084171	Unpublished
		<i>Lamennaisia ambigua</i>	NC_082113	Unpublished
		<i>Lamennaisia nobilis</i>	NC_061411	Unpublished
		<i>Leptomastidea bifasciata</i>	OR790123	Unpublished
		<i>Metaphycus eriococci</i>	NC_056349	Zhou et al. 2021
		<i>Ooencyrtus plautus</i>	NC_068223	Xing et al. 2022
		<i>Psyllaephagus</i> sp.	OP787025	Unpublished
		<i>Tassonia gloriae</i>	NC_082112	Unpublished

2,000,000 generations were carried out with sampling every 1,000 generations. The first 25% of trees were discarded as burn-in. After the average standard deviation of split frequencies fell below 0.01 and the potential scale reduction factor (PSRF) approached 1.0, stationarity was assumed. ML analysis was performed using IQ-TREE v. 2.2.0 (Nguyen et al. 2015) under the standard bootstrap approximation approach with 1,000 replicates.

Results

Mitogenome organization and nucleotide composition

The assembled mitochondrial genome of *A. galinae* was a 15,364 bp, and the *A. jenniferae* mitochondrial genome was 15,396 bp, which both had the same gene organization, including 13 PCGs, 22 tRNAs, two rRNAs and a control region located between *trnM* and *trnI* (Fig. 1). For the mitogenomes of two species, the majority strand (J-strand) encodes 10 PCGs (*ND3*, *CO3*, *ATP6*, *ATP8*, *CO2*, *CO1*, *ND5*, *ND4*, *ND4L*, *ND1*), 15 tRNAs (*trnI*, *trnY*, *trnS1*, *trnC*, *trnR*, *trnG*, *trnD*, *trnL2*, *trnF*, *trnH*, *trnP*, *trnL1*, *trnA*, *trnV*, *trnM*) and 2 rRNAs (*lrRNA*, *srRNA*), while the remaining three PCGs (*ND2*, *ND6*, *CYTB*) and seven tRNAs (*trnW*, *trnN*, *trnK*, *trnE*, *trnT*, *trnS2*, *trnQ*) are located on the minority strand (Table 2). Two mitogenomes both obtained 13 overlapping nucleotides, and up to 53 bp ranging from 1 to 16 bp. The longest overlap was located between *CO1* and *trnE* in *A. jenniferae*. There were 17 and 16 intergenic spacers each from *A. galinae* and *A. jenniferae*, totaling 171 bp and 115 bp, ranging 1 to 77 bp and 1 to 27 bp, respectively.

The nucleotide composition of the mitogenome from *A. galinae* was biased toward A and T, with 83.12% of A+T content (A = 45.12%, T = 38.00%, C = 10.82%, G = 6.05%), A+T content was 82.94%, 87.20% in PCGs and

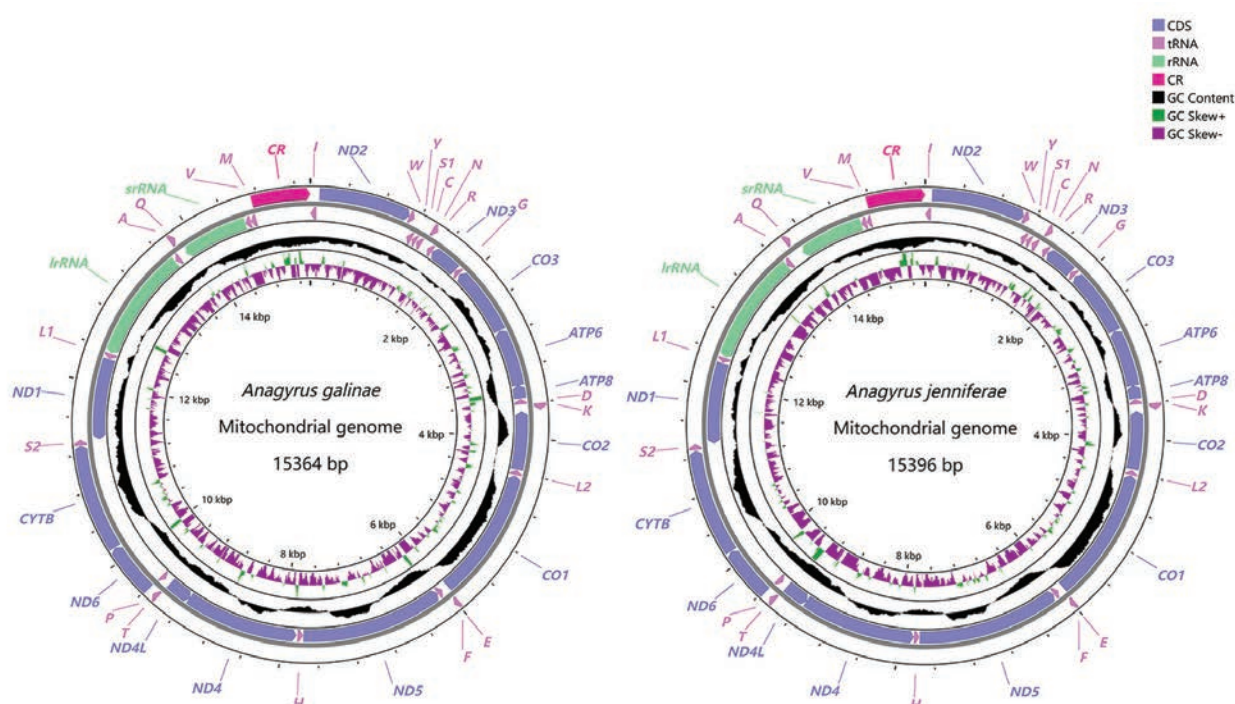


Figure 1. Circular map of the mitochondrial genome of *Anagyrus galinae* and *Anagyrus jenniferae*.

Table 2. Gene organization of the mitochondrial genomes of *Anagyris galinae* and *Anagyris jenniferae*.

Gene	Direction		Anticodon	<i>Anagyris galinae</i>				<i>Anagyris jenniferae</i>				
				Position	Length	Start codon	Stop codon	Intergenic Nucleotides	Position	Length	Start codon	Stop codon
<i>trnI</i>	-	GAU	1-70	70				1-67	67			
<i>ND2</i>	+		98-1087	990	ATT	TAA	27	74-1081	1008	ATT	TAA	6
<i>trnW</i>	+	UCA	1087-1149	63			-1	1080-1146	67			-2
<i>trnY</i>	-	GUA	1155-1221	67			5	1148-1212	65			1
<i>trnS1</i>	-	UCU	1222-1280	59			0	1216-1275	60			3
<i>trnC</i>	-	GCA	1283-1348	66			2	1293-1361	69			17
<i>trnN</i>	+	GUU	1369-1434	66			20	1368-1431	64			6
<i>trnR</i>	-	UCG	1433-1497	65			-2	1439-1504	66			7
<i>ND3</i>	-		1498-1842	345	ATT	TAA	0	1505-1858	354	ATA	TAA	0
<i>trnG</i>	-	UCC	1843-1906	64			0	1856-1919	64			-3
<i>CO3</i>	-		1911-2714	804	ATG	TAA	4	1925-2710	786	ATG	TAA	5
<i>ATP6</i>	-		2715-3387	673	ATG	T	0	2710-3383	674	ATG	TA	-1
<i>ATP8</i>	-		3381-3542	162	ATT	TAA	-7	3377-3538	162	ATC	TAA	-7
<i>trnD</i>	-	GUC	3543-3608	66			0	3539-3602	64			0
<i>trnK</i>	+	UUU	3612-3683	72			3	3606-3676	71			3
<i>CO2</i>	-		3688-4365	678	ATT	TAG	4	3678-4355	678	ATT	TAA	1
<i>trnL2</i>	-	UAA	4369-4434	66			3	4365-4428	64			9
<i>CO1</i>	-		4440-5987	1548	ATT	TAA	5	4431-5969	1539	ATG	TAA	2
<i>trnE</i>	+	UUC	5972-6036	65			-16	5972-6034	63			2
<i>trnF</i>	-	GAA	6036-6102	67			-1	6034-6099	66			-1
<i>ND5</i>	-		6102-7769	1668	ATA	TAA	-1	6099-7763	1665	ATT	TAG	-1
<i>trnH</i>	-	GUG	7767-7833	67			-3	7764-7829	66			0
<i>ND4</i>	-		7844-9169	1326	ATG	TAG	10	7829-9156	1328	ATG	TA	-1
<i>ND4L</i>	-		9163-9450	288	ATT	TAA	-7	9150-9437	288	ATT	TAA	-7
<i>trnT</i>	+	UGU	9453-9518	66			2	9440-9505	66			2
<i>trnP</i>	-	UGG	9520-9582	63			1	9506-9574	69			0
<i>ND6</i>	+		9584-10151	568	ATG	T	1	9575-10143	569	ATG	TA	0
<i>CYTB</i>	+		10152-11300	1149	ATG	TAA	0	10143-11285	1143	ATG	TAA	-1
<i>trnS2</i>	+	UGA	11300-11365	66			-1	11290-11354	65			4
<i>ND1</i>	-		11356-12291	936	ATT	TAG	-10	11345-12283	939	ATA	TAG	-10
<i>trnL1</i>	-	UAG	12292-12358	67			0	12284-12348	65			0
<i>lrRNA</i>	-		12364-13674	1311			5	12353-13654	1302			4
<i>trnA</i>	-	UGC	13682-13744	63			7	13651-13719	69			-4
<i>trnQ</i>	+	UUG	13761-13831	71			16	13797-13864	68			77
<i>srRNA</i>	-		13831-14602	772			-1	13891-14646	756			26
<i>trnV</i>	-	UAC	14602-14669	68			-1	14646-14710	65			-1
<i>trnM</i>	-	CAU	14668-14735	68			-2	14709-14770	62			-2
CR			14736-15364	629			0	14771-15396	626			0

rRNAs, respectively. The nucleotide composition of the mitogenome from *A. jenniferae* was biased toward A and T, with 82.64% of A+T content (A = 46.41%, T = 36.23%, C = 11.33%, G = 6.02%), A+T content was 82.32%, 85.20% in PCGs and rRNAs, respectively. The values of AT-skew and GC-

Table 3. Nucleotide features of the mitochondrial genome across *Anagyryrus galinae* and *Anagyryrus jenniferae*.

Feature	Length (bp)	T%	C%	A%	G%	A+T%	AT-Skew	GC-Skew
Whole genome	15364/15396	38.00/36.23	10.82/11.33	45.12/46.41	6.05/6.02	83.12/82.64	0.086/0.123	-0.283/-0.306
<i>ATP6</i>	673/674	46.66/47.63	7.43/8.01	34.92/34.27	11.00/10.09	81.58/81.90	-0.144/-0.163	0.194/0.115
<i>ATP8</i>	162/162	48.77/48.77	4.32/4.94	43.83/36.42	3.09/9.88	92.59/85.19	-0.053/-0.145	-0.167/0.333
<i>CO1</i>	1524/1539	45.41/46.39	10.37/10.98	29.86/27.23	14.37/15.40	75.26/73.62	-0.207/-0.260	0.162/0.167
<i>CO2</i>	678/678	45.58/45.72	8.55/8.41	33.04/33.19	12.83/12.68	78.61/78.91	-0.159/-0.159	0.200/0.203
<i>CO3</i>	804/786	46.64/49.75	7.84/8.52	32.21/29.90	13.31/11.83	78.86/79.64	-0.183/-0.249	0.259/0.163
<i>CYTB</i>	1149/1143	43.69/41.91	14.36/14.7	32.64/34.82	9.31/8.57	76.33/76.73	-0.145/-0.092	-0.213/-0.263
<i>ND1</i>	936/939	46.47/48.35	7.05/6.71	32.37/31.31	14.1/13.63	78.85/79.66	-0.179/-0.214	0.333/0.340
<i>ND2</i>	990/1008	50.10/47.52	9.19/9.62	37.58/39.19	14.10/13.63	87.68/86.71	-0.143/-0.096	-0.492/-0.448
<i>ND3</i>	345/351	51.01/52.99	5.22/5.41	33.91/31.34	9.86/10.26	84.93/84.33	-0.201/-0.257	0.308/0.309
<i>ND4</i>	1326/1328	50.08/52.41	4.98/5.20	34.01/30.20	10.94/12.20	84.09/82.61	-0.191/-0.269	0.374/0.403
<i>ND4L</i>	288/288	53.13/53.82	2.78/2.08	34.03/36.46	10.07/7.64	87.15/90.28	-0.219/-0.192	0.568/0.571
<i>ND5</i>	1665/1665	50.81/51.11	5.77/5.77	33.09/32.61	10.33/10.51	83.90/83.72	-0.211/-0.221	0.284/0.292
<i>ND6</i>	568/569	46.13/45.34	8.45/10.54	42.25/41.48	3.17/2.64	88.38/86.82	-0.044/-0.045	-0.455/-0.600
<i>srRNA</i>	772/756	44.30/44.84	4.15/4.10	43.52/40.08	8.03/10.98	87.82/84.92	-0.009/-0.056	0.319/0.456
<i>lrRNA</i>	1311/1302	44.55/46.08	4.27/4.15	42.03/39.40	9.15/10.37	86.58/85.48	-0.029/-0.078	0.364/0.429
CR	629/626	42.61/40.57	7.15/8.47	46.26/48.72	3.98/2.24	88.87/89.29	0.041/0.091	-0.285/-0.582

skew were often used to indicate the nucleotide composition of the mitochondrial genome. In this study, the nucleotide features of two new mitogenomes were investigated by calculating the percentages of AT-skew and GC-skew (Table 3). The skew analysis showing the mitogenome of *A. galinae* had a positive AT-skew (0.086) and a negative GC-skew (-0.283), and the mitogenome of *A. jenniferae* had a positive AT-skew (0.123) and a negative GC-skew (-0.306).

Protein-coding genes and codon usage

By comparing the known mitochondrial genome structure of Encyrtidae, we found that the sequence of 13 PCGs was consistent, except for *ND3* rearranged in *Diaphorencyrtus aligarhensis* and *Leptomastidea bifasciata*. The sequence of PCGs in these mitochondrial genomes were the same (Fig. 2). Additionally, this arrangement is consistent with the mitochondrial gene order in other Encyrtidae, which is also consistent with inferred ancestry.

The total lengths of 13 PCGs are 11,108 bp in *A. galinae*, 11,130 bp in *A. jenniferae*. In these mitochondrial genomes, the length of each PCG ranges from 162 bp (*ATP8*) to 1665 bp (*ND5*). Two mitogenomes of *Anagyryrus* exhibited similar start and stop codons. All the initiation codons of PCGs were ATN (ATA, ATG and ATT). Three kinds of stop codons existed on the new mitogenomic sequences: TAA, TAG and truncated termination codons (TA existed on *ATP6*, *ND4*, *ND6* in *A. jenniferae*, T existed on *ATP6*, *ND6* in *A. galinae*), TAA were the most frequently used. Truncated termination codons are commonly used in metazoan mitogenomes, which could be completed by post-transcriptional poly-adenylation (Ojala et al. 1981).

<i>Aenasius arizonensis</i>	J	ND2	W	N	Y	SI	C	R	ND3	G	CO3	ATP6	ATP8	D	K	CO2	L2	COI	F	E	NDS	H	ND4	ND4L	P	T	ND6	CYTB	S2	ND1	LI	rRNA	A	Q	rRNA	V	M	
<i>Anagyrus galinae</i>	J	ND2	W	I	SI	C	N	R	ND3	G	CO3	ATP6	ATP8	D	K	CO2	L2	COI	E	F	NDS	H	ND4	ND4L	T	P	ND6	CYTB	S2	ND1	LI	rRNA	A	Q	rRNA	V	M	CR
<i>Anagyrus jenniferae</i>	J	ND2	W	I	SI	C	N	R	ND3	G	CO3	ATP6	ATP8	D	K	CO2	L2	COI	E	F	NDS	H	ND4	ND4L	T	P	ND6	CYTB	S2	ND1	LI	rRNA	A	Q	rRNA	V	M	CR
<i>Blastothrix speciosa</i>	ND2	W	SI	N	R	I	Y	C	ND3	Q	CO3	ATP6	ATP8	D	K	CO2	L2	COI	E	F	NDS	H	ND4	ND4L	T	P	ND6	CYTB	S2	ND1	LI	rRNA	A	Q	rRNA	V	M	CR
<i>Cheiloneurus elegans</i>	V	M	CR	Y	I	ND2	G	R	N	ND3	CO3	ATP6	ATP8	D	K	CO2	L2	COI	E	F	NDS	H	ND4	ND4L	T	P	ND6	CYTB	S2	ND1	LI	rRNA	A	Q	rRNA	V	M	CR
<i>Cheiloneurus chinensis</i>	CR	I	ND2	R	Q	ND3	SI	N	Y	G	CO3	ATP6	ATP8	D	K	CO2	L2	COI	E	F	NDS	H	ND4	ND4L	T	P	ND6	CYTB	S2	ND1	LI	rRNA	A	Q	rRNA	V	M	CR
<i>Diaphorencyrtus aligarhensis</i>	ND2	W	SI	Y	C	Q	G	CO3	ATP6	ATP8	D	K	CO2	L2	COI	E	F	NDS	H	ND4	ND4L	T	P	ND6	CYTB	S2	ND1	LI	rRNA	A	Q	rRNA	V	M	CR	J		
<i>Encyrtus aurantii</i>	N	SI	Y	C	W	I	ND2	R	ND3	G	CO3	ATP6	ATP8	D	K	CO2	L2	COI	E	F	NDS	H	ND4	ND4L	T	P	ND6	CYTB	S2	ND1	LI	rRNA	A	Q	rRNA	V	M	CR
<i>Encyrtus eulecaniumiae</i>	N	SI	Y	C	W	I	ND2	R	ND3	G	CO3	ATP6	ATP8	D	K	CO2	L2	COI	E	F	NDS	H	ND4	ND4L	T	P	ND6	CYTB	S2	ND1	LI	rRNA	A	Q	rRNA	V	M	CR
<i>Encyrtus infelix</i>	N	SI	Y	C	W	I	ND2	R	ND3	G	CO3	ATP6	ATP8	D	K	CO2	L2	COI	E	F	NDS	H	ND4	ND4L	T	P	ND6	CYTB	S2	ND1	LI	rRNA	A	Q	rRNA	V	M	CR
<i>Encyrtus rhodococcidae</i>	N	SI	Y	C	W	I	ND2	R	ND3	G	CO3	ATP6	ATP8	D	K	CO2	L2	COI	E	F	NDS	H	ND4	ND4L	T	P	ND6	CYTB	S2	ND1	LI	rRNA	A	Q	rRNA	V	M	CR
<i>Encyrtus sasakii</i>	N	SI	Y	C	W	I	ND2	R	ND3	G	CO3	ATP6	ATP8	D	K	CO2	L2	COI	E	F	NDS	H	ND4	ND4L	T	P	ND6	CYTB	S2	ND1	LI	rRNA	A	Q	rRNA	V	M	CR
<i>Exoristobia philippinensis</i>	J	ND2	C	N	R	SI	Q	Y	ND3	G	CO3	ATP6	ATP8	D	K	CO2	L2	COI	E	F	NDS	H	ND4	ND4L	T	P	ND6	CYTB	S2	ND1	LI	rRNA	A	Q	rRNA	V	M	CR
<i>Lamennaisia ambigua</i>	ND2	I	Y	R	SI	ND3	C	Q	G	N	CO3	ATP6	ATP8	D	K	CO2	L2	COI	E	F	NDS	H	ND4	ND4L	T	P	ND6	CYTB	S2	ND1	LI	rRNA	A	Q	rRNA	V	M	CR
<i>Lamennaisia nobilis</i>	Q	SI	R	C	W	ND2	I	Y	ND3	G	CO3	ATP6	ATP8	D	K	CO2	L2	COI	E	F	NDS	H	ND4	ND4L	T	P	ND6	CYTB	S2	ND1	LI	rRNA	A	Q	rRNA	V	M	CR
<i>Leptomastidea bifasciata</i>	CR	I	ND2	W	Y	C	Q	SI	R	A	CO3	ATP6	ATP8	D	K	CO2	L2	COI	E	F	NDS	H	ND4	ND4L	T	P	ND6	CYTB	S2	ND1	LI	rRNA	A	Q	rRNA	V	M	CR
<i>Metaphycus eriococi</i>	J	ND2	W	Y	SI	N	C	R	ND3	G	CO3	ATP6	ATP8	D	K	CO2	L2	COI	E	F	NDS	H	ND4	ND4L	T	P	ND6	CYTB	S2	ND1	LI	rRNA	A	Q	rRNA	V	M	CR
<i>Ooencyrtus plautus</i>	ND2	R	Q	N	W	C	SI	Y	ND3	G	CO3	ATP6	ATP8	D	K	CO2	L2	COI	E	F	NDS	H	ND4	ND4L	T	P	ND6	CYTB	S2	ND1	LI	rRNA	A	Q	rRNA	V	M	CR
<i>Psyllaphagus sp.</i>	I	ND2	W	N	SI	Y	R	C	ND3	G	CO3	ATP6	ATP8	D	K	CO2	L2	COI	E	F	NDS	H	ND4	ND4L	T	P	ND6	CYTB	S2	ND1	LI	rRNA	A	Q	rRNA	V	M	CR
<i>Tassonia glorieae</i>	R	N	I	SI	W	ND2	Q	C	ND3	G	CO3	ATP6	ATP8	D	K	CO2	L2	COI	E	F	NDS	H	ND4	ND4L	T	P	ND6	CYTB	S2	ND1	LI	rRNA	A	Q	rRNA	V	M	CR

Figure 2. Gene order of mitochondrial genomes of different Encyrtidae species.



Figure 3. Relative synonymous codon usage in mitochondrial genomes of *Anagyrus galinae* and *Anagyrus jenniferae*.

The codon UUA (Leu2) was the most commonly used in both mitogenomes. Mitochondrial protein coding genes have obvious bias towards A and T, and for mitochondrial protein-coding gene of *A. galinae* the three most frequently used codons were UUA (Leu2) 469 times, AUU (Ile) 440 times and UUU (Phe) 432 times. For *A. jenniferae*, the three most used codons were UUA (Leu2) 463 times, UUU (Phe) 431 times and AUU (Ile) 393 times. Mitochondrial protein-coding genes in Encyrtidae prefer A and U in the third codon, which is like some hymenopteran insects (Fan et al. 2017; Peng et al. 2017). The RSCU values of *A. galinae* and *A. jenniferae* are shown in Fig. 3.

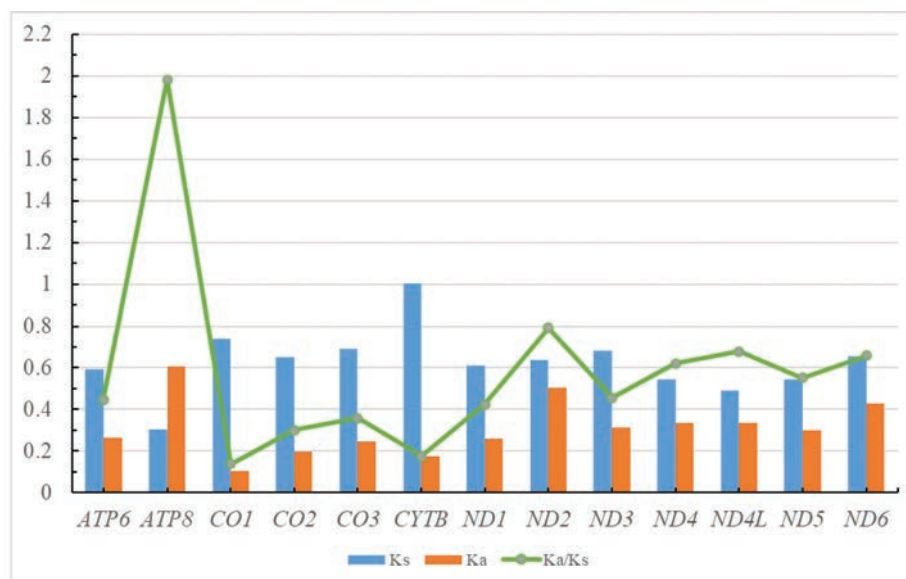


Figure 4. Evolutionary rates of protein-coding genes in the mitochondrial genomes of Encyrtidae.

In this study, based on 20 mitochondrial genomes of Encyrtidae, DnaSP was used to calculate the non-synonymous substitution rate, synonymous substitution, and Ka/Ks ratio of 13 PCGs in the mitochondrial genome and then to compare the evolution rate between genes (Fig. 4). The results showed that among the 13 protein-coding genes in the mitochondrial genome of encyrtids, *CYTB* had the highest Ks, whereas *ATP8* had the highest Ka and Ka/Ks value, and *ATP8* had the largest variation and *COI* had the slowest evolution rate. The evolution rate of 13 genes was in the order of *ATP8* > *ND2* > *ND4L* > *ND6* > *ND4* > *ND5* > *ND3* > *ATP6* > *ND1* > *CO3* > *CO2* > *CYTB* > *CO1*.

Ka/Ks values of 12 PCGs (all PCGs except *ATP8*) were far lower than 1.0, indicating that they were subject to purifying selection, a phenomenon first discovered in Chalcidoidea. In addition, the Ka/Ks value of *ATP8* is higher than 1.0, higher value of *ATP8* was also found in other species (Ma et al. 2019; Jia et al. 2020; Xu et al. 2021). The reason for this phenomenon may be that the evolution speed of a gene is related to its function (Wang et al. 2011).

Transfer RNA genes, ribosomal RNA genes, and control region

The mitochondrial genomes of the two species both included 22 tRNA genes, and the total lengths of the tRNAs of *A. galinae* and *A. jenniferae* are 1455 bp and 1445 bp, respectively. The length of tRNA genes in two *Anagyrus* species ranged from 59 to 72 bp. The secondary structures of the 22 tRNAs of the two species are shown in Suppl. materials 1, 2. The 22 tRNA genes in the mitochondrial genome are identical with the anticodon of tRNA corresponding to the mitochondrial genome of other Hymenoptera, except that *trnL* and *trnS* have two tRNA structures, and the others only have one corresponding tRNA structure. Most tRNAs could be folded into a typical clover-leaf structure, except for *trnS1* which lost a dihydrouridine (DHU) arm and became a simple loop. A lack of the DHU arm in *trnS1* was found in the mitochondrial genomes of most insects (Downton et al. 2002). Changes in the length of the DHU and TΨC arms led to

differences in the size of the tRNA sequence (Shao et al. 2001). In addition, the anticodon of *trnS1* became UCU instead of the more common GCU. In addition to typical Watson-Crick pairings (A-U and G-C), G-U pairings also exist, which are called atypical pairings or wobble base pairs. A total of 30 mismatched base pairs were found in the arm structures of the tRNAs.

Hymenopteran mitochondria have a high rearrangement rate, which mainly occurs in A+T-rich regions, *ND2*, *ND2-CO2*, *CO2-ATP8*, and *ND3-ND5* regions (Wei 2009). The gene arrangement of the suborder Symphyta was conserved and less rearranged than that of suborder Apocrita. However, there are a large number of rearrangements in the Apocrita, including displacement, inversion in situ, and ectopic inversion (Song 2015; Zhao et al. 2021). The rearrangement of mitochondrial genomes in Encyrtidae species was compared (Fig. 2), and the rearrangement was mainly found in tRNA genes. The rearrangement of tRNA occurred at many sites, and the pattern was complicated. Except that *trnD-trnK* (*trnK-trnD* in *Ooencyrtus plautus*), *trnL2*, *trnE-trnF* (*trnF-trnE* in *Aenasius arizonensis* and *Diaphorencyrtus aligarhensis*), *trnH*, *trnT-trnP* (*trnP-trnT* in *Aenasius arizonensis* and *Lamennaisia ambigua*), *trnS2* and *trnL1* are stable between *ATP8* to *lrRNA*, there was no exclusion, and the other tRNA genes had been rearranged.

As for the rRNAs of two *Anagyrs* species, both *lrRNA* and *srRNA* genes are encoded on the N-strand and have a heavy AT nucleotide bias. The lengths of *lrRNA* and *srRNA* in *A. galinae* are 1311 bp and 772 bp, with the different A+T contents of 86.58% and 87.82%, and in *A. jenniferae* are 1302 bp and 756 bp, with the different A+T contents of 85.48% and 84.92%.

In the mitogenome, the largest non-coding region is normally the A+T-rich region, also known as the control region, which regulates the replication and transcription of mitochondrial DNA (Boore 1999; Cameron 2014). In the mitogenomes of the two *Anagyrs* species sequenced in this study, the CR is located between *trnM* and *trnI* (Fig. 5). The length of the CR is 629 bp in *A. galinae* and 626 bp in *A. jenniferae*. The A+T content is 88.87% and 89.29% in the CR of *A. galinae* and *A. jenniferae*. Analysis of AT-skew and CG-skew indicates that both *Anagyrs* species exhibit A and C usage bias. Three structural elements were found in each CR of two *Anagyrs* species: (1) a leading sequence adjacent to *trnM*; (2) four tandem repeats (TPs); (3) the remaining area of the control region.

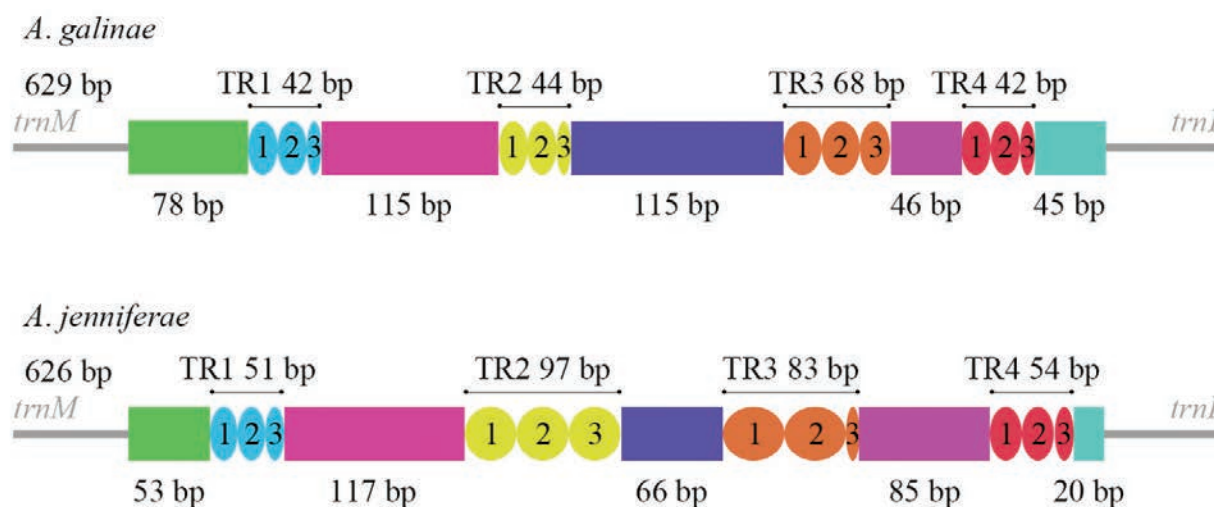


Figure 5. Control region structure of two *Anagyrs* species. TR, tandem repeat.

Phylogenetic relationships

The phylogenetic analysis of the concatenated dataset was conducted using BI and ML, which were shown in Fig. 6. With *Encarsia formosa* as an outgroup, the phylogenetic trees of Encyrtidae were constructed based on 13 protein-coding gene sequences of the 21 mitochondrial genomes, including NCBI data and the two newly sequenced *Anagyrus* genomes reported in this study.

The result of maximum-likelihood and Bayesian analysis both indicate that the taxonomic relationship of each genus of Encyrtidae is (*Metaphycus* + *Aenasius*) + (((*Anagyrus* + *Leptomastidea*) + *Encyrtus*) + ((*Blastothrix* + *Psyllaephagus*) + (((*Cheiloneurus* + *Tassonia*) + *Diaphorencyrtus*) + (*Ooencyrtus* + (*Exoristobia* + *Lamennaisia*)))))).

Overall, the phylogenetic trees reconstructed by both methods indicate that species belonging to the same tribe are clustered into one or adjacent clades, while species belonging to the same genus are clustered into the same clade, consistent with the morphological classification system. At the subfamily level, according to the morphological classification system, Encyrtidae is divided into two subfamilies: Tetracneminae and Encyrtinae. *Aenasius*, *Anagyrus*, and *Leptomastidea* all belong to Tetracneminae, while the remaining genera belong to Encyrtinae. However, in the phylogenetic trees reconstructed in this study, the results of both methods show that, except for *Encyrtus* and *Metaphycus*, Encyrtidae is divided into two main parts, which essentially conforms to the morphological classification system. *Metaphycus* and *Aenasius* form a monophyletic clade as sister groups, which is consistent with the previous phylogenetic results (Zhao et al. 2021; Xing et al. 2022).

While the *Anagyrus* species were not clustered on one branch with *Aenasius arizonensis* but clustered with *Encyrtus*, this may be due to different dietary habits. The five genera *Metaphycus*, *Aenasius*, *Anagyrus*, *Leptomastidea*, and *Encyrtus* exclusively parasitize scale insects within Hemiptera. In contrast, other species of Encyrtinae have a broader host range, including species from Lepidoptera, Diptera, Coleoptera, Hymenoptera, and more families within Hemiptera (Noyes 2019). Specifically, *Anagyrus jenniferae* parasitizes *Phenacoccus indicus*, *Anagyrus galinae* parasitizes *Trionymus copiosus*, and *Leptomastidea bifasciata*

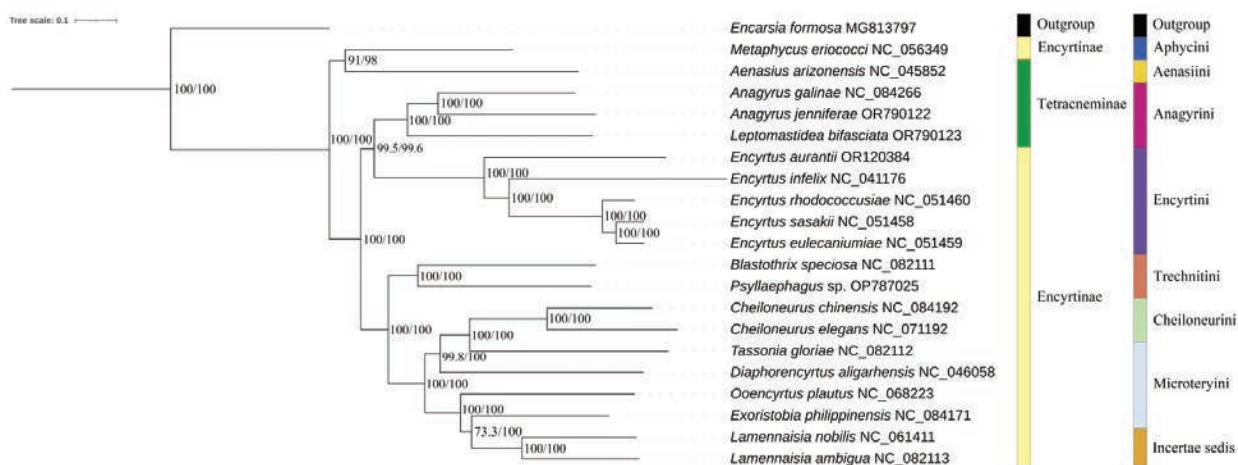


Figure 6. Phylogenetic tree of Encyrtidae based on nucleotide sequence of PCGs. Numbers at the nodes are Bayesian posterior probabilities (left) and ML bootstrap values (right). Each color block represents the corresponding family and tribe.

parasitizes *Phenacoccus aceris* and *Planococcus vovae* (Noyes and Hayat 1994; Japoshvili and Hansen 2015; Trjapitzin 1989; Zhang and Xu 2009). These Anagyrini species, which exclusively parasitize the Pseudococcidae, form a distinct clade in both phylogenetic trees. The hosts of *Encyrtus sasakii* include *Takahashia japonica* and *Eulecanium kuwanai*; *Encyrtus eulecaniumiae* parasitizes *Eulecanium kuwanai* and *Eulecanium giganteum*; *Encyrtus rhodococcusiae* targets *Rhodococcus sariuoni*; and *Encyrtus infelix* parasitizes *Ceroplastes destructor*, *Saissetia coffeae*, and *Saissetia oleae* (Trjapitzin 1989; Öncüer 1991; Noyes and Hayat 1994; Zhang and Huang 2001; Gupta and Poorani 2009; Wang et al. 2016), which were exclusively parasitize the Coccidae. Additionally, *Encyrtus aurentii* can parasitize members of the Coccidae (*Saissetia coffeae*), Eriococcidae (*Eriococcus buxi*), and Pseudococcidae (*Planococcus citri*) (Hayat et al. 2003). Consequently, in the phylogenetic trees, the clustering of Anagyrini and Encyrtini species together in the phylogenetic analysis might be attributed to the close genetic relationship between Coccidae and Pseudococcidae (Cook et al. 2002). This phenomenon also indicates the need for further mitochondrial genome sequencing of Encyrtidae species to obtain a more accurate classification status.

Discussion

In this study, we determined two newly sequenced mitogenomes, which are from *A. galinae* and *A. jenniferae*, then found them consistent with previously reported mitogenomes of Encyrtidae. Two new mitogenomes exhibited quite similar features in the genome size, base content, AT nucleotide bias, AT-skew, GC-skew, codon usage of protein genes, secondary structure of tRNAs and gene rearrangement. The BI and ML phylogenetic analysis among the major lineages based on the concatenated datasets yielded well-resolved topologies with moderate to high support for most branches. These results provide a relatively holistic framework and valuable data toward the future resolution of phylogenetic relationships in Encyrtidae. This study provided insights into the phylogenetic relationships of certain taxa within Encyrtidae, the limited sample size and scarcity of molecular evidence remain challenges. Therefore, future studies should aim to augment the number of sampled species and expand the dataset of mitochondrial genomes, utilizing a broader range of data for robust phylogenetic analysis and a comprehensive assessment of the taxonomic status within Encyrtidae.

Acknowledgments

We extend our heartfelt gratitude to Tao Wang from the College of Life Sciences, Nankai University, China, for providing valuable assistance in software analysis. Special thanks also go to Miss Zi-Yan Wang from the University of Sheffield, UK, as well as Mr. Shuai Zhang and Mr. Mark Sharples from the University of Manchester, UK, for their dedicated efforts in reviewing and revising the article. Their contributions have significantly enriched the quality and clarity of our work.

Additional information

Conflict of interest

The authors have declared that no competing interests exist.

Ethical statement

No ethical statement was reported.

Funding

No funding was received for conducting this study.

Author contributions

Conceptualization: GHZ, CHZ. Data curation: YW, CHZ. Formal analysis: CHZ. Investigation: CHZ, HYW. Methodology: CHZ, YW. Project administration: YW, CHZ, HYW. Resources: GHZ. Software: CHZ, YSL, ZHC. Supervision: GHZ, CHZ. Validation: CHZ, HYW. Visualization: CHZ. Writing – original draft: YW, CHZ, HYW. Writing – review and editing: CHZ, HYW.

Author ORCIDs

Cheng-Hui Zhang  <https://orcid.org/0000-0001-8234-0903>

Hai-Yang Wang  <https://orcid.org/0009-0007-5665-2111>

Yan Wang  <https://orcid.org/0000-0002-5001-975X>

Zhi-Hao Chi  <https://orcid.org/0009-0006-0447-6948>

Guo-Hao Zu  <https://orcid.org/0000-0002-9892-2171>

Data availability

Data presented in this study are openly available in the NCBI repository with accession numbers: OR652687, OR790122.

References

- Benson G (1999) Tandem repeats finder: A program to analyze DNA sequences. *Nucleic Acids Research* 27(2): 573–580. <https://doi.org/10.1093/nar/27.2.573>
- Boore JL (1999) Animal mitochondrial genomes. *Nucleic Acids Research* 27(8): 1767–1780. <https://doi.org/10.1093/nar/27.8.1767>
- Brown WM, George Jr M, Wilson AC (1979) Rapid evolution of animal mitochondrial DNA. *Proceedings of the National Academy of Sciences of the United States of America* 76(4): 1967–1971. <https://doi.org/10.1073/pnas.76.4.1967>
- Cameron SL (2014) Insect mitochondrial genomics: Implications for evolution and phylogeny. *Annual Review of Entomology* 59(1): 95–117. <https://doi.org/10.1146/annurev-ento-011613-162007>
- Cameron SL, Whiting MF (2008) The complete mitochondrial genome of the tobacco hornworm, *Manduca sexta*, (Insecta: Lepidoptera: Sphingidae), and an examination of mitochondrial gene variability within butterflies and moths. *Gene* 408(1–2): 112–123. <https://doi.org/10.1016/j.gene.2007.10.023>
- Chen SF, Zhou YQ, Chen YR, Gu J (2018) fastp: An ultra-fast all-in-one FASTQ preprocessor. *Bioinformatics (Oxford, England)* 34(17): i884–i890. <https://doi.org/10.1093/bioinformatics/bty560>
- Cook LG, Gullan PJ, Trueman HE (2002) A preliminary phylogeny of the scale insects (Hemiptera: Sternorrhyncha: Coccoidea) based on nuclear small-subunit ribosomal DNA. *Molecular Phylogenetics and Evolution* 25(1): 43–52. [https://doi.org/10.1016/S1055-7903\(02\)00248-8](https://doi.org/10.1016/S1055-7903(02)00248-8)
- Crozier RH, Crozier YC (1992) The cytochrome *b* and ATPase genes of honeybee mitochondrial DNA. *Molecular Biology and Evolution* 9(3): 474–482. <https://doi.org/10.1093/oxfordjournals.molbev.a040729>

- Crozier RH, Crozier YC (1993) The mitochondrial genome of the honeybee *Apis mellifera*: Complete sequence and genome organization. *Genetics* 133(1): 97–117. <https://doi.org/10.1093/genetics/133.1.97>
- Craud A, Rasplus JY, Zhang JX, Burks R, Delvare G, Fusu L, Gumovsky A, Huber JT, Janšta P, Mitroiu MD, Noyes JS, van Noort S, Baker A, Böhmová J, Baur H, Blaimer BB, Brady SG, Bubeníková K, Chartois M, Copeland RS, Dale-Skey Papilloud N, Dal Molin A, Dominguez C, Gebiola M, Guerrieri E, Kresslein RL, Krogmann L, Lemmon E, Murray EA, Nidelet S, Nieves-Aldrey JL, Perry RK, Peters RS, Polaszek A, Sauné L, Torrén J, Triapitsyn S, Tselikh EV, Yoder M, Lemmon AR, Woolley JB, Heraty JM (2024) The Chalcidoidea bush of life: Evolutionary history of a massive radiation of minute wasps. *Cladistics* 40(1): 34–63. <https://doi.org/10.1111/cla.12561>
- Darty K, Denise A, Ponty Y (2009) VARNA: Interactive drawing and editing of the RNA secondary structure. *Bioinformatics (Oxford, England)* 25(15): 1974–1975. <https://doi.org/10.1093/bioinformatics/btp250>
- Donath A, Jühling F, Al-Arab M, Bernhart SH, Reinhardt F, Stadler PF, Middendorf M, Bernhart M (2019) Improved annotation of protein-coding genes boundaries in metazoan mitochondrial genomes. *Nucleic Acids Research* 47(20): 10543–10552. <https://doi.org/10.1093/nar/gkz833>
- Downton M, Castro LR, Austin AD (2002) Mitochondrial gene rearrangements as phylogenetic characters in the invertebrates: The examination of genome ‘morphology’. *Invertebrate Systematics* 16(3): 345–356. <https://doi.org/10.1071/IS02003>
- Du YM, Song X, Liu XJ, Zhong BL (2019) Mitochondrial genome of *Diaphorencyrtus aligarhensis* (Hymenoptera: Chalcidoidea: Encyrtidae) and phylogenetic analysis. *Mitochondrial DNA. Part B, Resources* 4(2): 3190–3191. <https://doi.org/10.1080/23802359.2019.1667913>
- Fan XL, Gong YJ, Chen PY, Tan QQ, Tan JL, Wei SJ (2017) Next-generation sequencing of the mitochondrial genome of *Dolichovespula panda* (Hymenoptera: Vespidae) with a phylogenetic analysis of Vespidae. *Journal of Asia-Pacific Entomology* 20(3): 971–976. <https://doi.org/10.1016/j.aspen.2017.07.009>
- Gupta A, Poorani J (2009) Taxonomic studies on a collection of Chalcidoidea (Hymenoptera) from India with new distribution records. *Journal of Threatened Taxa* 1(5): 300–304. <https://doi.org/10.11609/JoTT.o1861.300-4>
- Hassanin A, Léger N, Deutsch J (2005) Evidence for multiple reversals of asymmetric mutational constraints during the evolution of the mitochondrial genome of Metazoa, and consequences for phylogenetic inferences. *Systematic Biology* 54(2): 277–298. <https://doi.org/10.1080/10635150590947843>
- Hayat M, Narendran TC, Remadevi OK, Manikandan S (2003) Parasitoids (Hymenoptera: Chalcidoidea; Ceraphronoidea) reared mainly from Coccoidea (Homoptera) attacking Sandalwood, *Santalum album* L. *Oriental Insects* 37(1): 309–334. <https://doi.org/10.1080/00305316.2003.10417352>
- Heraty JM, Burks RA, Craud A, Gibson GAP, Liljebblad J, Munro J, Rasplus JY, Delvare G, Janšta P, Gumovsky A, Huber J, Woolley JB, Krogmann L, Heydon S, Polaszek A, Schmidt S, Darling DC, Gates MW, Mottern J, Murray E, Dal Molin A, Triapitsyn S, Baur H, Pinto JD, van Noort S, George J, Yoder M (2013) A phylogenetic analysis of the megadiverse Chalcidoidea (Hymenoptera). *Cladistics* 29: 466–542. <https://doi.org/10.1111/cla.12006>
- Howard LO, Ashmead WH (1896) On some reared parasitic hymenopterous insects from Ceylon. *Proceedings of the United States National Museum* 18(1092): 633–648. <https://doi.org/10.5479/si.00963801.18-1092.633>

- Hurst LD (2002) The Ka/Ks ratio: diagnosing the form of sequence evolution. *Trends in Genetics* 18(9): 486–487. [https://doi.org/10.1016/S0168-9525\(02\)02722-1](https://doi.org/10.1016/S0168-9525(02)02722-1)
- Japoshvili O, Hansen LO (2015) New records of Encyrtidae (Hymenoptera, Chalcidoidea) from Norway VI. *Norwegian Journal of Entomology* 62(2): 174–179.
- Jia CH, Zhang XM, Xu SY, Yang TY, Yanagimoto T, Gao TX (2020) Comparative analysis of the complete mitochondrial genomes of three rockfishes (Scorpaeniformes, Sebastiscus) and insights into the phylogenetic relationships of Sebastidae. *Bioscience Reports* 40(12): BSR20203379. <https://doi.org/10.1042/BSR20203379>
- Jin JJ, Yu WB, Yang JB, Song Y, dePamphilis CW, Yi TS, Li DZ (2020) GetOrganelle: A fast and versatile toolkit for accurate de novo assembly of organelle genomes. *Genome Biology* 21(1): 241. <https://doi.org/10.1186/s13059-020-02154-5>
- Kalyaanamoorthy S, Minh BQ, Wong TKF, von Haeseler A, Jermiin LS (2017) ModelFinder: Fast model selection for accurate phylogenetic estimates. *Nature Methods* 14(6): 587–589. <https://doi.org/10.1038/nmeth.4285>
- Katoh K, Rozewicki J, Yamada KD (2019) MAFFT online service: Multiple sequence alignment, interactive sequence choice and visualization. *Briefings in Bioinformatics* 20(44): 1160–1166. <https://doi.org/10.1093/bib/bbx108>
- Krzywinski J, Grushko OG, Besansky NJ (2006) Analysis of the complete mitochondrial DNA from *Anopheles funestus*: An improved dipteran mitochondrial genome annotation and a temporal dimension of mosquito evolution. *Molecular Phylogenetics and Evolution* 39(2): 417–423. <https://doi.org/10.1016/j.ympev.2006.01.006>
- Li Q, Wei SJ, Tang P, Wu Q, Shi M, Sharkey MJ, Chen XX (2016) Multiple Lines of Evidence from Mitochondrial Genomes Resolve Phylogenetic Relationships of Parasitic Wasps in Braconidae. *Genome Biology and Evolution* 8(9): 2651–2662. <https://doi.org/10.1093/gbe/evw184>
- Liu MD, Luo YF, Jallow BJJ, Meng FM (2023) Characterization of Complete Mitochondrial Genome and Phylogenetic Analysis of a Nocturnal Wasps – *Provespa barthelemyi* (Hymenoptera: Vespidae). *Current Issues in Molecular Biology* 45(12): 9368–9377. <https://doi.org/10.3390/cimb45120587>
- Ma Y, Zheng BY, Zhu JC, Tang P, Chen XX (2019) The mitochondrial genome of *Aenasius arizonensis* (Hymenoptera: Encyrtidae) with novel gene order. *Mitochondrial DNA. Part B, Resources* 4(1): 2023–2024. <https://doi.org/10.1080/23802359.2019.1617052>
- Meng GL, Li YY, Yang CT, Liu SL (2019) MitoZ: A toolkit for animal mitochondrial genome assembly, annotation and visualization. *Nucleic Acids Research* 47(11): e63. <https://doi.org/10.1093/nar/gkz173>
- Munro JB, Heraty JM, Burks RA, Hawks D, Mottern J, Cruaud A, Rasplus JY, Janšta P (2011) A Molecular Phylogeny of the Chalcidoidea (Hymenoptera). *PLOS ONE* 6(11): e27023. <https://doi.org/10.1371/journal.pone.0027023>
- Nguyen LT, Schmidt HA, von Haeseler A, Minh BQ (2015) IQ-TREE: A fast and effective stochastic algorithm for estimating maximum-likelihood phylogenies. *Molecular Biology and Evolution* 32(1): 268–274. <https://doi.org/10.1093/molbev/msu300>
- Noyes JS (1980) A review of the genera of Neotropical Encyrtidae (Hymenoptera: Chalcidoidea). *Bulletin of the British Museum of Natural History* 41: 107–253.
- Noyes JS (2019) Universal Chalcidoidea Database. World Wide Web electronic publication. <http://www.nhm.ac.uk/chalcidoids>. [Accessed on 27 Jul 2023]
- Noyes JS, Hayat M (1984) A review of the genera of Indo-Pacific Encyrtidae (Hymenoptera: Chalcidoidea). *Bulletin of the British Museum of Natural History* 48: 131–395.
- Noyes JS, Hayat M (1994) Oriental mealybug parasitoids of the Anagyrini (Hymenoptera: Encyrtidae). CAB International, Wallingford, 554 pp.

- Ojala D, Montoya J, Attardi G (1981) tRNA punctuation model of RNA processing in human mitochondria. *Nature* 290(5806): 470–474. <https://doi.org/10.1038/290470a0>
- Öncüer C (1991) A catalogue of the parasites and predators of insect pests of Turkey. Ege University Agricultural Faculty Press No. 505, Izmir, 204 pp.
- Peng Y, Chen B, Li TJ (2017) Sequencing and analysis of the complete mitochondrial genome of *Parapolybia crocea* (Hymenoptera: Vespidae). *Acta Entomologica Sinica* 60(4): 464–474. <https://doi.org/10.16380/j.kcxb.2017.04.011>
- Perna NT, Kocher TD (1995) Patterns of nucleotide composition at fourfold degenerate sites of animal mitochondrial genomes. *Journal of Molecular Evolution* 41(3): 353–358. <https://doi.org/10.1007/BF01215182>
- Ranwez V, Douzery EJP, Cambon C, Chantret N, Delsuc F (2018) MACSE v2: Toolkit for the Alignment of Coding Sequences Accounting for Frameshifts and Stop Codons. *Molecular Biology and Evolution* 35(10): 2582–2584. <https://doi.org/10.1093/molbev/msy159>
- Ronquist F, Teslenko M, van der Mark P, Ayres DL, Darling A, Höhna S, Larget B, Liu L, Suchard MA, Huelsenbeck JP (2012) MrBayes 3.2: Efficient Bayesian phylogenetic inference and model choice across a large model space. *Systematic Biology* 61(3): 539–542. <https://doi.org/10.1093/sysbio/sys029>
- Rozas J, Ferrer-Mata A, Sánchez-DelBarrio JC, Guirao-Rico S, Librado P, Ramos-Onsins SE, Sánchez-Gracia A (2017) DnaSP 6: DNA sequence polymorphism analysis of large data sets. *Molecular Biology and Evolution* 34(12): 3299–3302. <https://doi.org/10.1093/molbev/msx248>
- Rudoy A, Zhu CD, Ferrari RR, Zhang YZ (2022) Integrative taxonomy based on morphometric and molecular data supports recognition of the three cryptic species within the *Encyrtus sasakii* complex (Hymenoptera, Encyrtidae). *Journal of Hymenoptera Research* 90: 129–152. <https://doi.org/10.3897/jhr.90.75807>
- Sayers EW, Cavanaugh M, Clark K, Pruitt KD, Sherry ST, Yankie L, Karsch-Mizrachi I (2024) GenBank 2024 Update. *Nucleic Acids Research* 52(D1): D134–D137. <https://doi.org/10.1093/nar/gkad903>
- Shao RF, Campbell NJH, Barker SC (2001) Numerous gene rearrangements in the mitochondrial genome of the Wallaby Louse, *Heterodoxus macropus* (Phthiraptera). *Molecular Biology and Evolution* 18(5): 858–865. <https://doi.org/10.1093/oxfordjournals.molbev.a003867>
- Simutnik SA, Perkovsky EE (2023) Description of a new genus and species of Encyrtidae (Hymenoptera: Chalcidoidea) from Danish amber, based on a male specimen featuring an antenna with a distinct anellus. *Zootaxa* 5369(3): 437–445. <https://doi.org/10.11646/zootaxa.5369.3.7>
- Simutnik SA, Perkovsky EE, Vasilenko DV (2022) *Electronoyesella antiqua* Simutnik, gen. et sp. nov. (Chalcidoidea, Encyrtidae) from Rovno amber. *Journal of Hymenoptera Research* 94: 105–120. <https://doi.org/10.3897/jhr.94.94773>
- Simutnik SA, Perkovsky EE, Pankowski MV (2023) A new genus and species of Encyrtidae (Hymenoptera: Chalcidoidea) with a four-segmented funicle from late Eocene Baltic amber. *Zootaxa* 5389(1): 119–127. <https://doi.org/10.11646/zootaxa.5389.1.6>
- Song SN (2015) Comparative mitogenomics and phylogeny of the Microsatrinae (Hymenoptera: Braconidae). PhD Thesis, Zhejiang University, Hangzhou, China.
- Talavera G, Castresana J (2007) Improvement of Phylogenies after Removing Divergent and Ambiguously Aligned Blocks from Protein Sequence Alignments. *Systematic Biology* 56(4): 564–577. <https://doi.org/10.1080/10635150701472164>

- Tamura K, Stecher G, Kumar S (2021) MEGA11: Molecular Evolutionary Genetics Analysis Version 11. *Molecular Biology and Evolution* 38(7): 3022–3027. <https://doi.org/10.1093/molbev/msab120>
- Trjapitzin VA (1989) Parasitic Hymenoptera of the Fam. Encyrtidae of Palaearctics. Nauka, Leningrad, 489 pp.
- Wang DP, Fei L, Wang L, Huang S, Yu J (2011) Nonsynonymous substitution rate (Ka) is a relatively consistent parameter for defining fast-evolving and slow-evolving protein-coding genes. *Biology Direct* 6(1): 13. <https://doi.org/10.1186/1745-6150-6-13>
- Wang Y, Zhou QS, Qiao HJ, Zhang AB, Yu F, Wang XB, Zhu CD, Zhang YZ (2016) Formal nomenclature and description of cryptic species of the *Encyrtus sasakii* complex (Hymenoptera: Encyrtidae). *Scientific Reports* 6(1): 34372. <https://doi.org/10.1038/srep34372>
- Wang HY, Zhang CH, Xue H, Xi CX, Yang ZN, Zu GH (2023) Encyrtidae (Hymenoptera: Chalcidoidea) from China, with the description of two new species. *Zootaxa* 5361(2): 237–251. <https://doi.org/10.11646/zootaxa.5361.2.5>
- Wei SJ (2009) Characterization and evolution of hymenopteran mitochondrial genomes and their phylogenetic utility. PhD Thesis, Zhejiang University, Hangzhou, China.
- Wei SJ, Shi M, Sharkey MJ, van Achterberg C, Chen XX (2010) Comparative mitogenomics of Braconidae (Insecta: Hymenoptera) and the phylogenetic utility of mitochondrial genomes with special reference to Holometabolous insects. *BMC Genomics* 11(1): 371. <https://doi.org/10.1186/1471-2164-11-371>
- Wolstenholme DR (1992a) Genetic novelties in mitochondrial genomes of multicellular animals. *Current Opinion in Genetics & Development* 2(6): 918–925. [https://doi.org/10.1016/S0959-437X\(05\)80116-9](https://doi.org/10.1016/S0959-437X(05)80116-9)
- Wolstenholme DR (1992b) Animal mitochondrial DNA: Structure and evolution. *International Review of Cytology* 141: 173–216. [https://doi.org/10.1016/S0074-7696\(08\)62066-5](https://doi.org/10.1016/S0074-7696(08)62066-5)
- Xing ZP, Liang X, Wang X, Hu HY, Huang YX (2022) Novel gene rearrangement pattern in mitochondrial genome of *Ooencyrtus plautus* Huang & Noyes, 1994: New gene order in Encyrtidae (Hymenoptera, Chalcidoidea). *ZooKeys* 1124: 1–21. <https://doi.org/10.3897/zookeys.1124.83811>
- Xiong M, Zhou QS, Zhang YZ (2019) The complete mitochondrial genome of *Encyrtus infelix* (Hymenoptera: Encyrtidae). *Mitochondrial DNA. Part B, Resources* 4(1): 114–115. <https://doi.org/10.1080/23802359.2018.1537727>
- Xu W, Lin SP, Liu HY (2021) Mitochondrial genomes of five *Hyphessobrycon* tetras and their phylogenetic implications. *Ecology and Evolution* 11(18): 12754. <https://doi.org/10.1002/ece3.8019>
- Zhang YZ, Huang DW (2001) Two new Encyrtid parasites (Hymenoptera: Chalcidoidea) from China. *Oriental Insects* 35(1): 311–319. <https://doi.org/10.1080/00305316.2001.10417310>
- Zhang YZ, Xu ZH (2009) A review of Chinese species of *Leptomastidea* Mercet (Hymenoptera: Encyrtidae). *Acta Entomologica Sinica* 52(4): 420–423.
- Zhang JX, Lindsey ARI, Peters RS, Heraty JM, Hopper KR, Werren JH, Martinson EO, Woolley JB, Yoder MJ, Krogmann L (2020a) Conflicting signal in transcriptomic markers leads to a poorly resolved backbone phylogeny of chalcidoid wasps. *Systematic Entomology* 45(4): 783–802. <https://doi.org/10.1111/syen.12427>
- Zhang D, Gao FL, Jakovlić I, Zou H, Zhang J, Li WX, Wang GT (2020b) PhyloSuite: An integrated and scalable desktop platform for streamlined molecular sequence data

- management and evolutionary phylogenetics studies. *Molecular Ecology Resources* 20(1): 348–355. <https://doi.org/10.1111/1755-0998.13096>
- Zhao HF, Chen Y, Wang ZT, Chen HF, Qin YG (2021) Two complete mitogenomes of Chalcididae (Hymenoptera: Chalcidoidea): genome description and phylogenetic implications. *Insects* 12(12): 1049. <https://doi.org/10.3390/insects12121049>
- Zhou QS, Xiong M, Luo AR, Zhang YZ, Zhu CD (2021) The complete mitochondrial genome of *Metaphycus eriococci* (Timberlake) (Hymenoptera: Encyrtidae). *Mitochondrial DNA. Part B, Resources* 6(2): 550–552. <https://doi.org/10.1080/23802359.2021.1872450>
- Zhu JC, Tang P, Zhou BY, Wu Q, Wei SJ, Chen XX (2018) The first two mitochondrial genomes of the family Aphelinidae with novel gene orders and phylogenetic implications. *International Journal of Biological Macromolecules* 118(A): 386–396. <https://doi.org/10.1016/j.ijbiomac.2018.06.087>
- Zhu JC, Xiao H, Tang P, Li XF, Li XK, Zhu CD, Wu Q, Xiao JH, van Achterberg C, Huang DW, Chen XX (2023) Evolutionary timescale of chalcidoid wasps inferred from over one hundred mitochondrial genomes. *Zoological Research* 44(3): 467–482. <https://doi.org/10.24272/j.issn.2095-8137.2022.379>

Supplementary material 1

Secondary structures of 22 tRNA genes of *Anagyrus galinae*

Authors: Cheng-Hui Zhang, Hai-Yang Wang, Yan Wang, Zhi-Hao Chi, Yue-Shuo Liu, Guo-Hao Zu

Data type: jpg

Explanation note: Blue gene names indicate that in the major strand, and red names indicate that in the minor strand.

Copyright notice: This dataset is made available under the Open Database License (<http://opendatacommons.org/licenses/odbl/1.0/>). The Open Database License (ODbL) is a license agreement intended to allow users to freely share, modify, and use this Dataset while maintaining this same freedom for others, provided that the original source and author(s) are credited.

Link: <https://doi.org/10.3897/zookeys.1206.121923.suppl1>

Supplementary material 2

Secondary structures of 22 tRNA genes of *Anagyrus jenniferae*

Authors: Cheng-Hui Zhang, Hai-Yang Wang, Yan Wang, Zhi-Hao Chi, Yue-Shuo Liu, Guo-Hao Zu

Data type: jpg

Explanation note: Blue gene names indicate that in the major strand, and red names indicate that in the minor strand.

Copyright notice: This dataset is made available under the Open Database License (<http://opendatacommons.org/licenses/odbl/1.0/>). The Open Database License (ODbL) is a license agreement intended to allow users to freely share, modify, and use this Dataset while maintaining this same freedom for others, provided that the original source and author(s) are credited.

Link: <https://doi.org/10.3897/zookeys.1206.121923.suppl2>

Revision of *Troporhogas* Cameron (Hymenoptera, Braconidae, Rogadinae) with six new species from India and Thailand

Donald L. J. Quicke¹, A. P. Ranjith^{1,2}, Marisa K. Loncle¹, Cornelis van Achterberg^{3,4},
Khuat Dang Long⁵, Buntika A. Butcher¹

1 Integrative Insect Ecology Research Unit, Department of Biology, Faculty of Science, Chulalongkorn University, Phayathai Road, Pathumwan, Bangkok 10330, Thailand

2 Ashoka Trust for Research in Ecology and the Environment (ATREE), Royal Enclave, Srirampura, Jakkur Post, Bangalore 560064, India

3 Department of Terrestrial Zoology, Naturalis Biodiversity Center, Darwinweg 2, 2333 CR Leiden, Netherlands

4 Zhejiang University, Hangzhou 310058, China

5 Institute of Ecology & Biological Resources (IEBR), Vietnam Academy of Science & Technology (VAST), 18 Hoang Quoc Viet Road, Cau Giay, Hanoi, Vietnam

Corresponding author: Buntika A. Butcher (buntika.a@chula.ac.th)

Abstract

The genus *Troporhogas* Cameron, 1905 from the Indo-Malayan region is reviewed. Six new species, *Troporhogas alboniger* Quicke, Loncle & Butcher, **sp. nov.**, *T. benjamini* Quicke, Loncle & Butcher, **sp. nov.**, *T. hugoolseni* Quicke, Loncle & Butcher, **sp. nov.**, *T. rafaelnadali* Quicke, Loncle & Butcher, **sp. nov.**, and *T. rogerfedereri* Quicke, Loncle & Butcher, **sp. nov.** from Thailand, and *T. anamikae* Ranjith, **sp. nov.** from India are described and illustrated photographically, bringing the total number of species of the genus known from the Indo-Malayan Region to 19. *Troporhogas* is recorded for the first time from India. A key is included to differentiate *Troporhogas* species. A four-gene ML tree based on COI, Cytb, 16S and 28S is reconstructed, representing the six new species. *Troporhogas contrastus* Long, 2014, originally described from Vietnam, is recorded from Thailand for the first time. The holotypes of the type species, *Troporhogas tricolor* Cameron, 1905 and that of its junior synonym *Iporhogas* are illustrated, and photographs are presented of all the species known only from China and Sri Lanka. Sexual colour dimorphism of males of several species is described for the first time. Drawings summarising the different patterns of black marks on the metasoma that aid species recognition are presented.

Key words: Checklist, *Iporhogas*, ML phylogeny, new species, Rogadinae, Southeast Asia, *Troporhogas*



Academic editor:

Mostafa Ghafouri Moghaddam

Received: 13 February 2024

Accepted: 22 May 2024

Published: 5 July 2024

ZooBank: <https://zoobank.org/39B52383-4713-4F9D-B7C6-96C9A7F05184>

Citation: Quicke DLJ, Ranjith AP, Loncle MK, van Achterberg C, Long KD, Butcher BA (2024) Revision of *Troporhogas* Cameron (Hymenoptera, Braconidae, Rogadinae) with six new species from India and Thailand. ZooKeys 1206: 99–136. <https://doi.org/10.3897/zookeys.1206.120824>

Copyright: © Donald L. J. Quicke et al.
This is an open access article distributed under terms of the Creative Commons Attribution License (Attribution 4.0 International – CC BY 4.0).

Introduction

The cosmopolitan Rogadinae Förster, 1863 is one of the most diverse subfamilies of Braconidae, with more than approximately 1,200 described species and 54 genera worldwide (Yu et al. 2016; Quicke et al. 2021). Of these, 16 Rogadinae genera occur in the New-World regions and 50 in the Old World tropics. Regarding its described species, it is the third most diverse subfamily in South East Asia (SEA) with 196 species known for Thailand (Songvorawit et al. 2021), while in contrast, only 36 species were reported for India (Yu et al. 2016; Ranjith

et al. 2018, 2022; Rishabanu et al. 2021); the large former number is largely due to a single revisionary work on one huge genus by Butcher et al. (2012).

Rogadine wasps are koinobiont endoparasitoids that attack caterpillars in several groups (Zaldivar-Riverón et al. 2008; Quicke et al. 2021). When the rogadine wasp has completed its development, the host caterpillar is easily recognised because it is mummified and usually found attached to its host plant (van Achterberg 1991; Zaldivar-Riverón et al. 2008; Quicke 2015). This biological trait makes the subfamily particularly useful for the study of host-parasitoid associations, because the caterpillar's remains can often be identified based on morphology (van Achterberg et al. 2020) or molecular techniques (Quicke et al. 2012). Unfortunately, there are no biological data as yet for the genus *Troporhogas*.

Until recently, specimens from the Indo-Malayan region were referred to under the generic name *Iporhogas* Granger, 1949, which was originally described from Madagascar based on a single species. *Troporhogas* Cameron, 1905, was originally described from Sri Lanka; however, it was subsequently referred to only in catalogues, and species from SEA and southern China were described under the name *Iporhogas*. The two genera were formally synonymised by Quicke et al. (2021) based on a molecular phylogenetic study in which a Sri Lankan specimen of *T. ruficeps* Cameron, closely related to *T. tricolor*, the type species of *Troporhogas*, was deeply nested in a clade with species that had been assigned to *Iporhogas* (Chen and He 1997; Long 2014). We illustrate here the type species of the genera *Troporhogas* and *Iporhogas* here in Fig. 1. The type species of *Troporhogas*, *T. tricolor*, has a distinct mid-longitudinal carina on the median area of the metanotum (Fig. 1E), whereas this is absent in the type species of *Iporhogas* (Fig. 1O).

Troporhogas was originally described based on seven species, all from Sri Lanka, viz.: *T. albipes*, *T. lateralis*, *T. maculipennis*, *T. ruficeps*, *T. spilonotus*, *T. tricolor*, and *T. trimaculatus* (Figs 2, 3). Of these, *T. maculipennis* was transferred to *Megarhogas* by Baltazar (1972). *Troporhogas spilonotus* was transferred to *Pseudogyroneuron* Baker, 1917, by Baltazar (1972) and then to *Canalirogas* van Achterberg & Chen, 1996, by Quicke and Shaw (2005) and subsequently treated as a senior synonym of *C. balgooyi* van Achterberg & Chen, 1996 (van Achterberg and Chen 1996) by Long and van Achterberg (2015). *Troporhogas lateralis* was formally transferred to *Rogas*, often regarded as a senior synonym of *Aleiodes*, and then to *Aleiodes* by Broad (2021); in the same paper, Broad designated a lectotype for *T. trimaculata*.

Members of *Troporhogas* can be recognised by the key provided in Chen and He (1997) in which they will key to *Iporhogas*. Many *Troporhogas* species have a distinctive habitus together with a bicoloured metasoma, black medially on some tergites (mainly on TT1–5) and white, especially on the anterolateral areas of the tergites (Long 2014), but in others it may be uniformly honey-coloured to ochraceous.

Chen and He (1997) recorded the genus for the first time from China, and described five new species, and Long (2014) recorded it from Vietnam and described an additional four species, all of these under the generic name *Iporhogas*.

Here we describe six more new species, *T. anamikae* sp. nov. from India, and *T. alboniger* sp. nov., *T. benjamini* sp. nov., *T. hugoolseni* sp. nov., *T. rafaelnadali* sp. nov., and *T. rogerfedereri* sp. nov. from Thailand, bringing the total number of *Troporhogas* species known worldwide to 20. This is the first report of *Troporhogas* from India and *T. contrastus* (Long 2014) and *T. tricoloratus* (Long 2014)

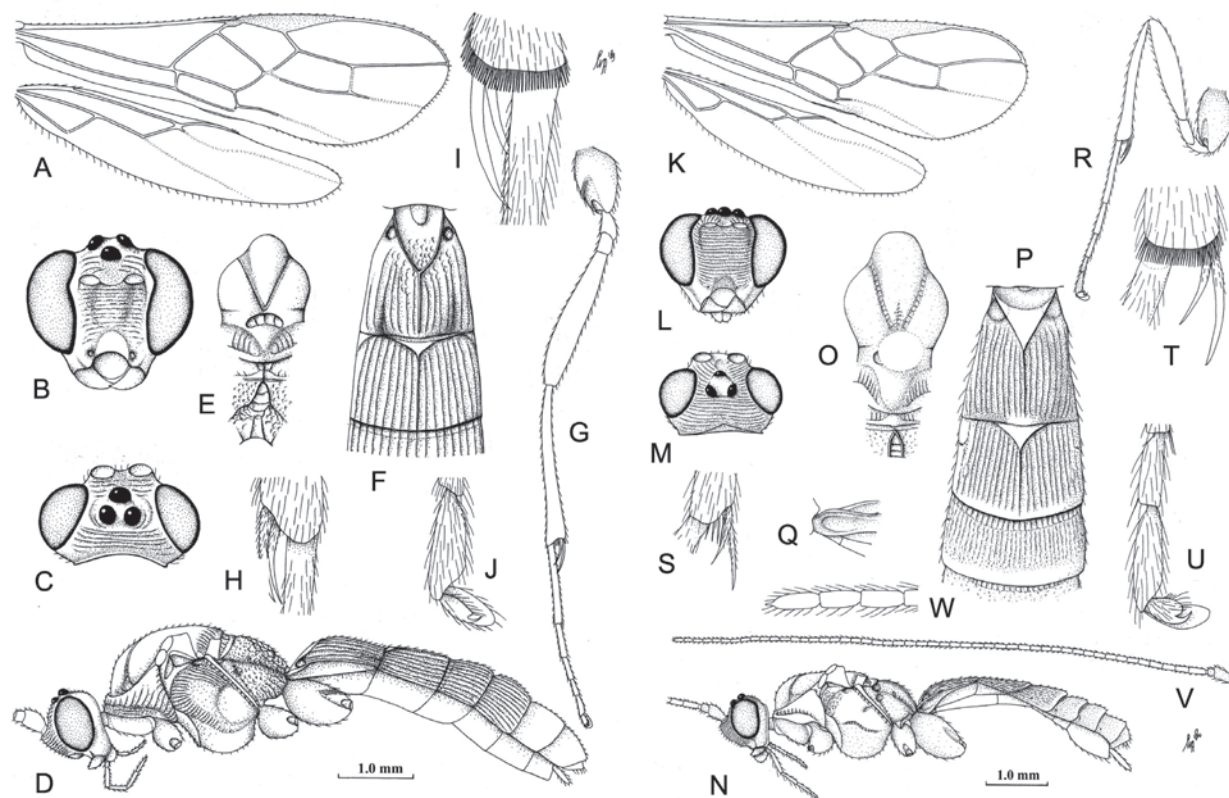


Figure 1. Drawings of lectotypes of **A–J** *Troporhogas tricolor* Cameron, the type species of the genus, and **K–W** *T. infuscaticipennis* (Granger), type species of *Iporhogas* **A** wings **B** head, anterior view **C** head, dorsal view **D** habitus, lateral view **E** mesosoma, dorsal view **F** metasomal tergites 1 and 2, dorsal view **G** hind legs **H** middle tibial spurs **I** hind tibial spurs, inner aspect **J** outer hind claw **K** wings **L** head, anterior view **M** head, dorsal view **N** habitus, lateral view **O** mesosoma, dorsal view **P** metasomal tergites 1–3, dorsal view **Q** base of first tergite, lateral view **R** hind leg **S** middle tibial spurs, inner aspect **T** hind tibial spurs, inner aspect **U** outer hind claw **V** antenna **W** apical three flagellomeres.

are recorded from Thailand for the first time. A key is provided to enable recognition of all non-Afrotropical species. Further, since the original descriptions of the Chinese species, despite being quite thorough, were only illustrated with a few line drawings, we present photographs of the type specimens to facilitate use of the key. Phylogenetic relationships among all species of *Troporhogas* for which DNA data are available were also reconstructed based on four gene markers: cytochrome *c* oxidase subunit 1 (COI), cytochrome *b* (Cyt *b*), 16S rDNA, and the D2-D3 expansion region of 28S rDNA.

Materials and methods

Specimens were collected with light traps at Doi Phu Kha National Park, Nan and Nakhon Ratchasima, with Malaise traps at Khao Yai National Park, Thailand, and by sweep net from secondary forests at Janakikkad, Kerala, south India.

The holotypes of *T. alboniger* sp. nov., *T. benjamini* sp. nov., *T. hugoolseni* sp. nov., *T. rafaelnadali* sp. nov. and *T. rogerfedereri* sp. nov. were imaged using a Leica M205 C with Montage multifocus, interactive measurement and fusion optics stereo microscope, using the Leica Application Suite (LAS). Holotype images of *T. anamikae* sp. nov. were taken using a Keyence VHX-6000 digital microscope. Raw figures were edited with the program GIMP v. 2.10.

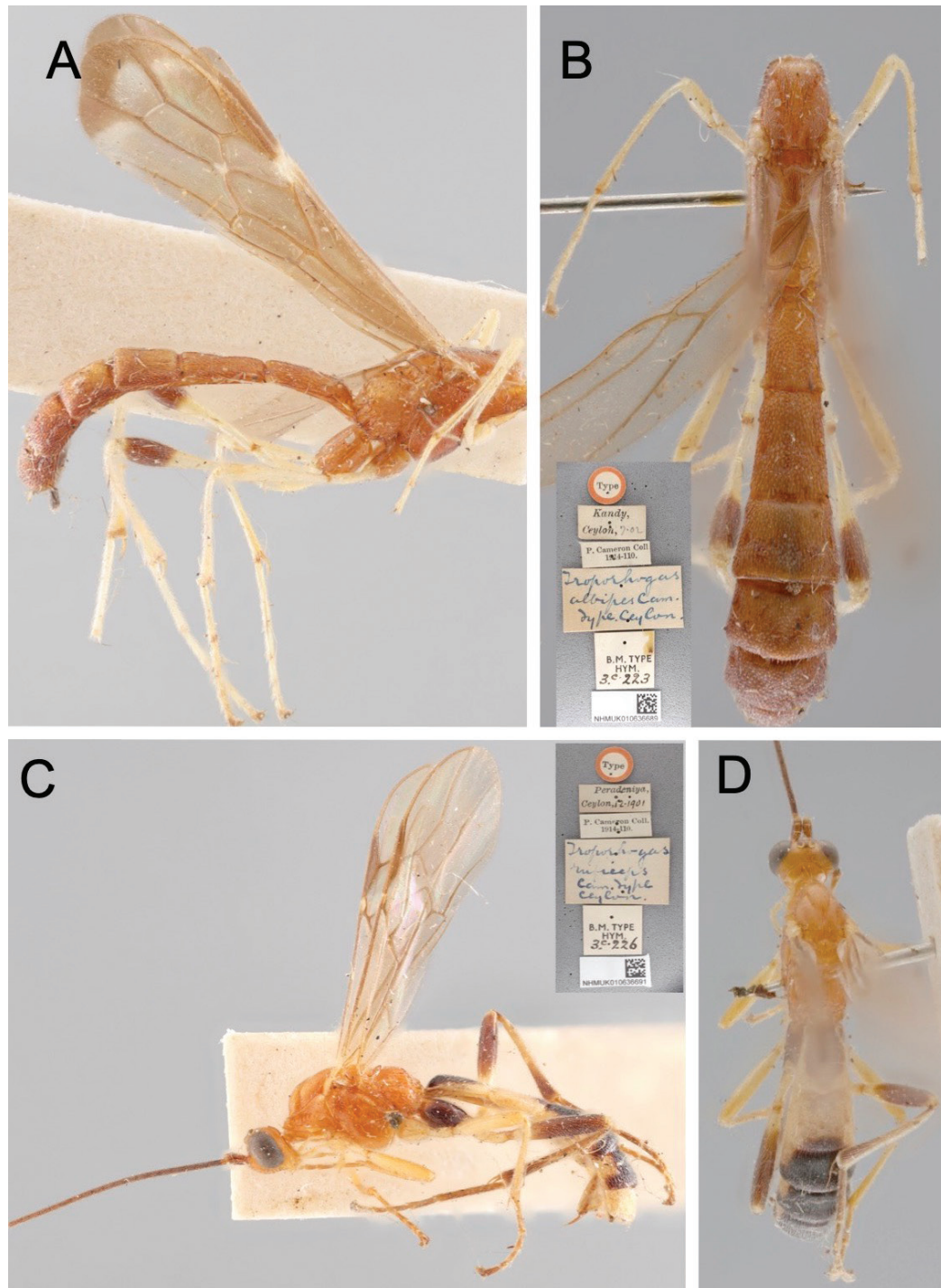


Figure 2. Light micrographs of ♀ holotypes of *Troporhogas* species described by Cameron (1905) **A** *T. albipes* Cameron, lateral view **B** *T. albipes*, dorsal view (labels inset) **C** *T. ruficeps* Cameron, lateral view (labels inset) **D** *T. ruficeps*, dorsal view.

Repositories

- AIMB** ATREE Insect Collection, Ashoka Trust for Research in Ecology and the Environment, Bengaluru, Karnataka, India
- CUMZ** Insect Museum, Chulalongkorn University Museum of Natural History, Bangkok, Thailand
- NHMUK** Natural History Museum, London
- QSBG** Queen Sirikit Botanic Garden, Chiang Mai, Thailand

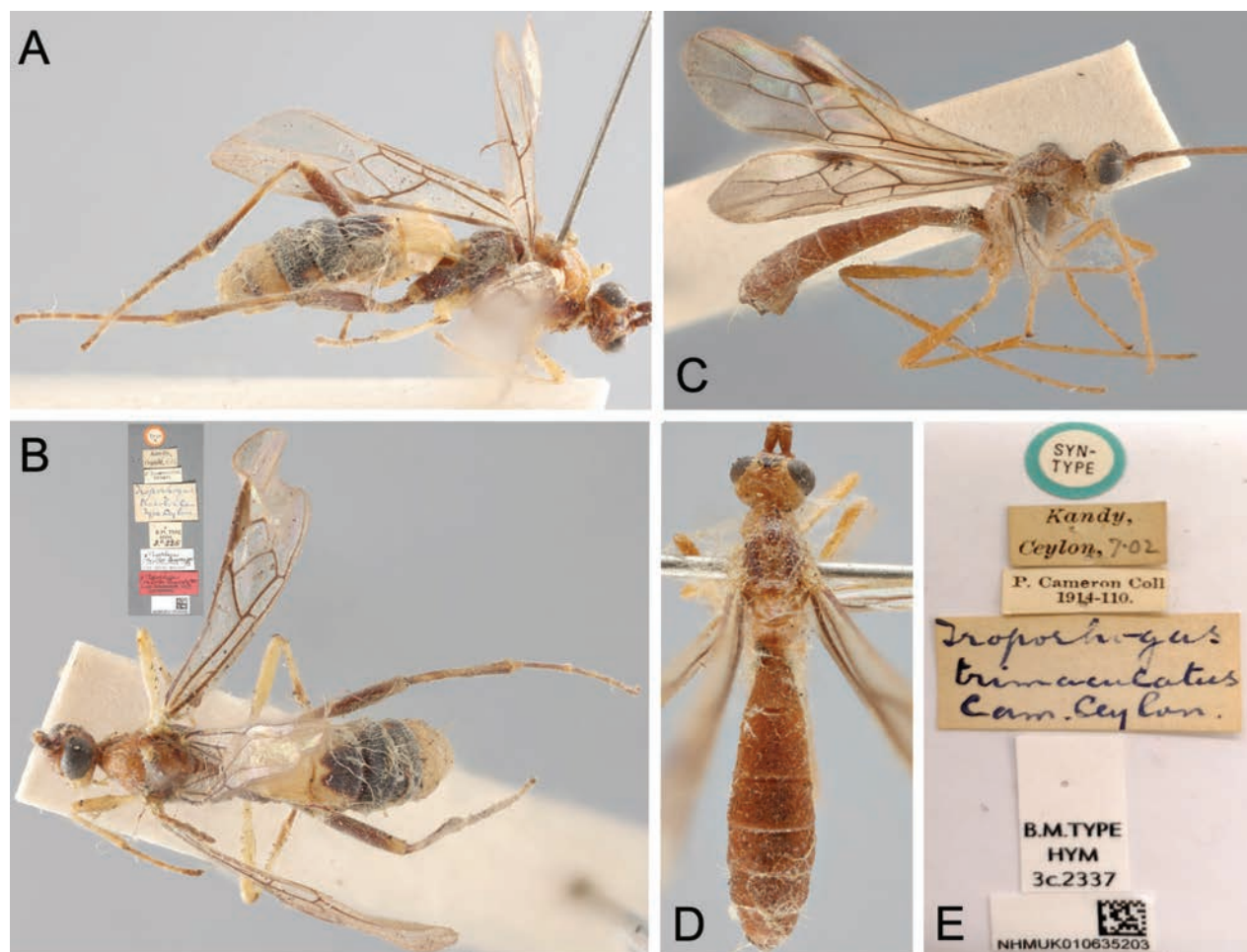


Figure 3. Light micrographs of *Troporhogas* **A** *T. tricolor* Cameron lectotype ♀, lateral view **B** *T. tricolor* lectotype, dorsal view **C** *T. trimaculatus* Cameron syntype ♀, lateral view **D** *T. trimaculatus* syntype, dorsal view **E** labels of *T. trimaculatus* syntype.

Terminology follows van Achterberg (1988) except for wing venation which follows Sharkey and Wharton (1997) and Butcher and Quicke (2023). Metasomal tergite/tergites are abbreviated as **T/TT**.

Molecular methods

A molecular data matrix was created comprising up to four gene regions: barcoding region of cytochrome oxidase c subunit 1 (COI), cytochrome b (386 base pairs) (Cytb), regions IV and V of the mitochondrial 16S rRNA gene from H2507 to H1792' (~ 650 bp), and the D2-D3 expansion region of 28S rDNA (28S). Most sequences (one sequence of the new species *T. benjamini*, *T. rafaelnadali*, and *T. rogerfedereri* and sequences of *T. contrastus*, *T. ruficeps*, *T. tricoloratus*, *Troporhogas* spp. 1–5, *Papuarogas dameni*, *Rogasodes* spp. 1 and 2, and *Rogasella* sp. 3) are taken from Quicke et al. (2021) and were generated from wasp legs by the Centre for Biodiversity Genomics, University of Guelph, based on standard protocols as described in Hebert et al. (2003), Park et al. (2010), and Quicke et al. (2023). In addition, we included sequences from representatives of three closely related species belonging to the genera *Papuarogas* Quicke, 2021, *Rhogasella* Baker, 1917, and *Rogasodes* Chen & He, 1997 as outgroups based on the large phylogeny presented by Quicke et al. (2021). Most of the Cytb sequences are newly generated.

Alignment of both COI and cytochrome b sequences was trivial as there were no indels. The length-variable 28S sequences were aligned according to the secondary structure model of Gillespie et al. (2005) as in other studies (Butcher et al. 2014; Quicke et al. 2016) and the length-variable 16S sequences were aligned according to the secondary structure models (Buckley et al. 2000; Wu et al. 2014). For both COI and Cytb, the three codon positions were each treated as a separate partition. For both 16S and 28S, only confidently aligned base pairs were included and each was treated as a single partition.

Maximum likelihood (ML) trees were constructed using RAxML v. 7.0.4 (Stamatakis 2014) with the GTRGAMMA model and a rapid bootstrap (100 replicates) using the options -m GTRGAMMA -f a -# 100 command. Tree was visualised using FigTree v. 1.4.4. (Rambaut 2018).

Provenances of sequenced specimens, DNA barcode index numbers (BINs), and GenBank accessions numbers are given in Suppl. material 1. In addition, the colour pattern on metasomal tergite of *Troporhogas* is provided in Fig. 21.

Results

Checklist and distribution of *Troporhogas* species worldwide

Troporhogas anamikae Ranjith, sp. nov., India

Troporhogas albilateralis (Long, 2014) (= *Iporhogas albilateralis* Long, 2014), Vietnam, Thailand)

Troporhogas albipes Cameron, 1905, Sri Lanka

Troporhogas alboniger Quicke, Loncle & Butcher, sp. nov., Thailand

Troporhogas benjamini Quicke, Loncle & Butcher, sp. nov., Thailand

Troporhogas chinensis (Chen & He, 1997), (= *Iporhogas chinensis* Chen & He, 1997), China

Troporhogas contrastus (Long, 2014), (= *Iporhogas contrastus* Long, 2014), Vietnam, Thailand

Troporhogas flavistigma (Chen & He, 1997), (= *Iporhogas flavistigma* Chen & He, 1997), China

Troporhogas guangxiensis (Chen & He, 1997), (= *Iporhogas guangxiensis* Chen & He, 1997), China, Vietnam

Troporhogas hugoolseni Quicke, Loncle & Butcher, sp. nov., Thailand

Troporhogas infuscatipennis (Granger, 1949), (= *Iporhogas infuscatipennis* Granger, 1949), Madagascar

Troporhogas rafaelnadali Quicke, Loncle & Butcher, sp. nov., Thailand

Troporhogas rogerfedereri Quicke, Loncle & Butcher, sp. nov., Thailand

Troporhogas ruficeps Cameron, 1905, Sri Lanka

Troporhogas rugivertex (Chen & He, 1997), (= *Iporhogas rugivertex* Chen & He, 1997), China

Troporhogas simulatus (Long, 2014), (= *Iporhogas simulatus* Long, 2014), Vietnam

Troporhogas tricolor Cameron, 1905, Sri Lanka

Troporhogas tricoloratus (Long, 2014), (= *Iporhogas tricoloratus* Long, 2014), Vietnam

Troporhogas trimaculatus Cameron, 1905, Sri Lanka

Troporhogas unicolor (Chen & He, 1997), (= *Iporhogas unicolor* Chen & He, 1997), China, Thailand

Phylogeny

The maximum likelihood tree obtained is shown in Fig. 4. *Troporhogas* was recovered as monophyletic with 100% bootstrap support. The circles at nodes indicate rapid bootstrap clade support. The genus comprised two separate clades each with 100% bootstrap support, one including all the Afrotropical species and the other all Indo-Australian species. Six of the Thai species and the one from India form a monophyletic group with 79% bootstrap support.

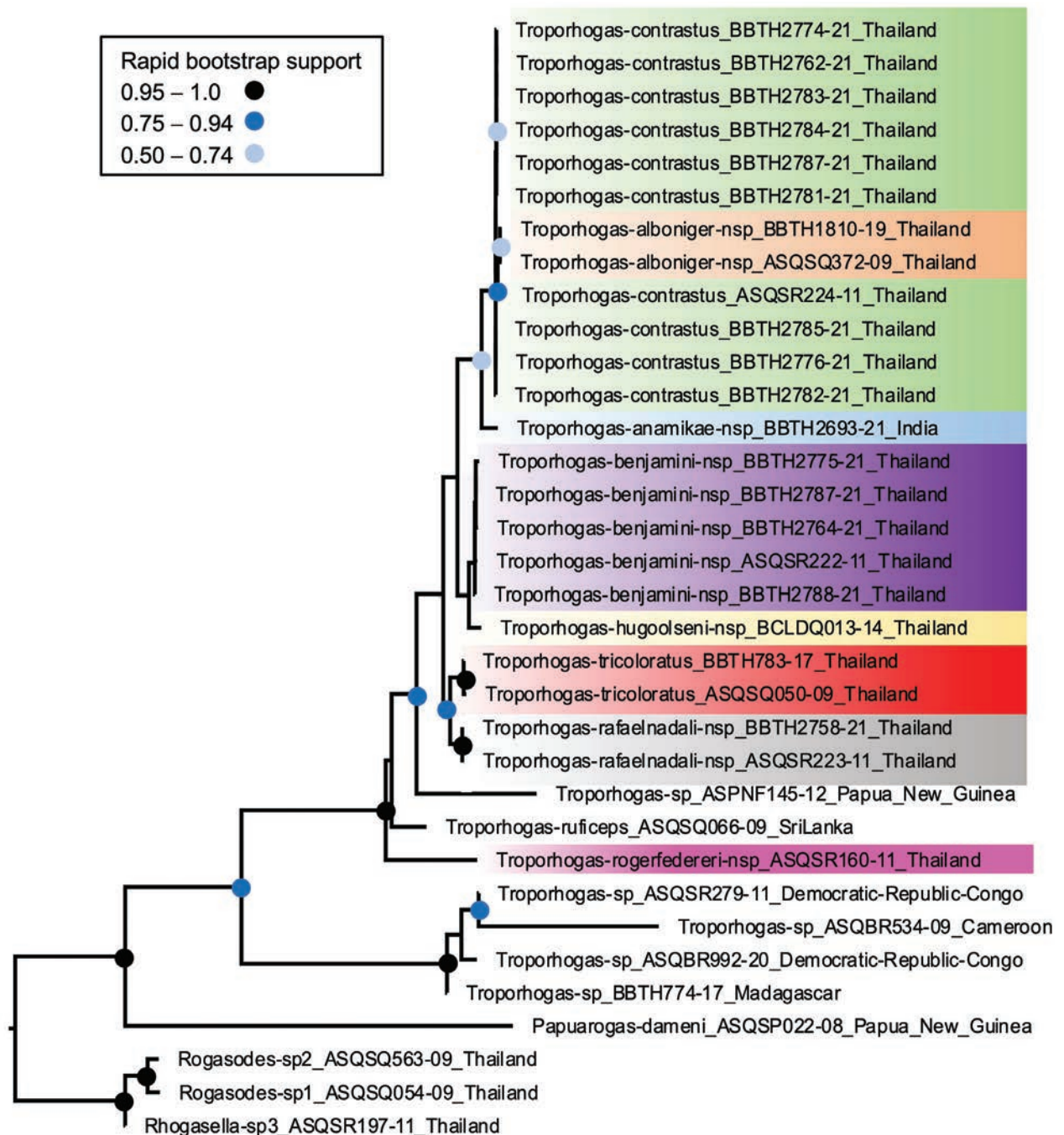


Figure 4. Maximum likelihood tree based on combined analysis of four gene fragments (COI, Cytb, 16S, 28S) using GTR+G parameter model with *Troporhogas* represented by 31 BINS. Support values at nodes are rapid bootstrap and indicated by coloured dots.

Of these, *T. rafaelnadali* sp. nov. and *T. tricoloratus* were both supported $\geq 99\%$. The most basal member of the Asian clade was *T. rogerfedereri* sp. nov., a species that appears most closely related, on the basis of morphology, to the Chinese *T. flavistigma*, both sharing five carinae in the scutellar sulcus and anteriorly widely-separated submedial longitudinal propodeal carinae anteriorly (Figs 16G, 19F). However, within the remainder of this clade there was little support for the additional species recognised by morphological characters, especially for *T. alboniger* sp. nov. and *T. contrastus* Long and our reasons for recognising this new species are dealt with below.

Systematics

Class Insecta Linnaeus, 1758

Order Hymenoptera Linnaeus, 1758

Family Braconidae Nees, 1811

Subfamily Rogadinae Foerster, 1863

***Troporhogas* Cameron, 1905**

Troporhogas Cameron, 1905: 92 (type species *Troporhogas tricolor* Cameron, 1905).

Iporhogas Granger 1949: 167; synonymised by Quicke et al. 2021: 16.

Generic diagnosis. Antenna usually $\sim 1.5 \times$ fore wing length; palpi normal; face at least with some transverse striation; malar suture shallow; eyes emarginate; temple with fine striation; frons rather flat, usually with transverse or oblique striation, usually with a pair of carinae running posteriorly from the lateral margins of antennal sockets and then converging more or less joining anterior to median ocellus separating frons into anterior and posterior portions (Figs 15B, C, 17B); occipital carina complete, joining hypostomal carina ventrally well-removed from base of mandible; mesosoma largely smooth shiny; notauli moderately deep and crenulate, converging but not uniting posteriorly, not reaching posterior margin of mesoscutum; prepectal carina complete or nearly so; precoxal sulcus present; scutellar sulcus wide with single mid-longitudinal carina; metanotum with mid-longitudinal carina at least posteriorly, though sometimes indistinct; propodeum areolate, with at least a trace of submedial carinae close together anteriorly, gradually diverging posteriorly; tarsal claws usually with small to large, pointed or angulate basal lobe (except absent in *T. guangxiensis* and *T. simulatus*); fore wing vein 1m-cu antefurcal, slightly curved, gradually merging into vein 1CUB; 2nd submarginal cell elongate, vein 2RS $> 1.7 \times$ width of cell; hind wing vein 1M straight, approximately as long as M+CU; hind wing vein RS weakly curved basally and only short basal stub, tubular and sclerotised; hind wing vein m-cu absent; hind wing veins M+CU and 1M of approximately same length; middle tibial spurs largely setose and nearly straight; apex of hind tibia with distinct comb of specialised setae medially; hind tibial spurs curved and at least apical half glabrous; T1 not widened basally, with large dorsope, dorsal carinae united behind level of spiracles to form complete mid-longitudinal carina, and without pair of submedial carinae; T2 with distinct mid-basal

triangular area, giving rise to complete or nearly complete mid-longitudinal carina; TT3–6 without mid-longitudinal carina; TT2–5 with sharp lateral crease, largely finely longitudinally striate; hypopygium large, ventrally slightly convex and apically truncate; ovipositor sheath rather slender.

Type species. *Troporhogas tricolor* Cameron, 1905 (Fig. 3).

Diagnosis. Antenna longer than body, slender, setose, 40–50 flagellomeres. Eyes large, clearly emarginated on inner side; malar space short (Fig. 3B). Maxillary palp very long, slender, setose, 4–5 jointed (Fig. 3D). Temple short, oblique. Occiput sharply margined, transverse (Fig. 3C). Metanotum with two roundly diverging carina basally (Fig. 3E). Mesopleuron with a depression ventrally (Fig. 3D). Legs long and slender; femora narrowed basally (Fig. 3J). Fore wing 2nd submarginal cell 2.0 × longer than wide, of equal width throughout; anal vein not interstitial (Fig. 3A); vein (RS+M)b short; vein r-rs less half the length of 3RSa; vein 3RSb longest and curved upwards (Fig. 3A). Tarsi longer than tibiae; basitarsus longer than two following joints combined (Fig. 3J). Hind tibial spurs glabrous (Fig. 1I). Metasoma 2.0 × as long as mesosoma (Fig. 3D); TT1–3 closely longitudinally striated (Fig. 3G); TT4–6 with posterior transverse furrows; base of TT4–6 depressed, apex of TT4–6 raised and clearly separated from the base. Hypopygium large, cultriform; ovipositor shortly projecting, the sheaths stout (Fig. 3D). Head rufous; mesosoma largely orange with propodeum largely piceous; metasoma cream-white with medial black mark on T2, with larger black marks on TT3 and 4 which reach lateral margins posteriorly.

Key to the species of Indo-Malayan *Troporhogas*

- 1 Tarsal claws simple, without lobe; hind tibial spurs entirely glabrous .. **2**
- Tarsal claws with minute to large lobe; hind tibial spurs setose basally ... **3**
- 2(1) Occipital carina in dorsal view angularly concave; stemmaticum without any dark mark; hind wing vein SC+Ra almost straight apically; vein SC+Rb of hind wing quadrate; TT1–3 ochreous yellow, 4–6 paler yellow. Vietnam..... ***T. simulatus* Long**
- Occipital carina in dorsal view roundly concave; propodeum without areola and with basal carina; hind wing vein SC+Ra distinctly curved apically; hind wing vein SC+Rb subquadrate, swollen apically; metasomal tergites yellowish with pale brown patches anteromedially (Fig. 19H). China, Vietnam ***T. guangxiensis* Chen & He**
- 3(1) Metasoma honey to brownish yellow with or without darker marks or paler marks (Figs 2A, B, 3D, 19B, D, H)..... **4**
- Metasoma white or pale cream with black marks (Fig. 20)..... **7**
- 4(3) Wing membrane patterned hyaline and grey (Figs 2A, 3C) **5**
- Wing membrane plain and uniform (e.g. Figs 5D, 9B) **6**
- 5(4) Hind femur robust (Fig. 2A); hind leg boldly patterned, white with distal 0.7 femur dark brown (Fig. 2A); mesoscutum uniformly brown-yellow (Fig. 2B). Sri Lanka ***T. albipes* Cameron**
- Hind femur slender (Fig. 3C); hind leg uniformly brown-yellow (Fig. 3C); mesoscutum with three dark marks (Fig. 3D). Sri Lanka ***T. trimaculatus* Cameron**

- 6(4) Occipital carina in dorsal view strongly angularly (Fig. 19C); vertex smooth; fore wing veins all pale yellow. China..... ***T. unicolor* Chen & He**
- Occipital carina in dorsal view weakly rounded; vertex transversely rugose; fore wing veins 1M, 1Cub and 1cu-a darker brown than remaining venation. China..... ***T. rugivertex* Chen & He**
- 7(3) Submedial propodeal carinae anteriorly forming a wide inverted 'U'-shape (Figs 16G, 19F); scutellar sulcus with five carinae between outer borders (Figs 16G, 19F); T5 variable, often largely or entirely cream-white (Fig. 18D, F); vertex largely smooth except immediately posterior to stemmaticum..... **8**
- Submedial propodeal carinae anteriorly running closer together and forming an inverted narrow or wider V-shape (Fig. 14A); scutellar sulcus usually with three carinae between outer borders (Figs 14A, 15F, 19B); T5 largely black except for anterolateral areas (Figs 2C, D, 15G, 16D, 17H, 18C); vertex variable..... **9**
- 8(7) Occipital carina medially forming a point (Fig. 19G); vertex largely smooth except immediately posterior to stemmaticum; pterostigma largely yellow-brown and venation pale (Fig. 19G); dark mark on T1 not reaching posterior margin (Fig. 19H). China ***T. flavistigma* Chen & He**
- Occipital carina medially more rounded (Fig. 16C); vertex (extending well towards temples) strongly transversely striate (Fig. 16D); pterostigma black (Fig. 16I); dark mark on T1 reaching posterior margin (Fig. 19H). Thailand..... ***T. rogerfedereri* sp. nov.**
- 9(7) T1 entirely white (Figs 3A, B, 6B, 9D) **10**
- T1 with a well-developed black mark at least anteriorly (Figs 2C, D, 13A, 16D)..... **14**
- 10(9) Head, mesosoma entirely black except for white tegulae (Figs 5A, 6A); T2 entirely white (Fig. 6B). Thailand ***T. alboniger* sp. nov.**
- Head, mesoscutum and pronotum with yellow marks, at least at mid-posterior of mesoscutum and scutellar sulcus (Figs 12C) or mesosoma largely pale (Fig. 3B)..... **11**
- 11(10) T4 medially and T5 entirely white (Fig. 9A, B). India ***T. anamikae* sp. nov.**
- TT4 and 5 almost entirely black except for white anterolateral areas..... **12**
- 12(11) T5 largely whitish (Fig. 3A, B). Sri Lanka ***T. tricolor* Cameron**
- T5 black (Figs 12B, 17B)..... **13**
- 13(12) Vertex and temples finely transversely striate (Fig. 11C); mesoscutum mainly black except medial-posteriorly white (Fig. 12A). Thailand ***T. benjamini* sp. nov.**
- Vertex and temples polished, without conspicuous striation; mesoscutum laterally black, middle lobe entirely brownish yellow (occasionally piceous on anterior half). Thailand, Vietnam ***T. contrastus* Long**
- 14(9) Dark markings on TT1–5 contiguous (Figs 19D, 21D); vertex finely transversely sculptured. China ***T. chinensis* Chen & He**
- Dark markings on TT1–5 not contiguous; vertex sculpture variable..... **15**
- 15(14) Vertex with setiferous punctation but without distinct transverse striation (Fig. 13C). Thailand ***T. hugoolseni* sp. nov.**
- Vertex transversely striate (Fig. 18D) **16**

- 17(16) Raised oblique area of mesopleuron immediately below subalar depression strongly finely striate (Fig. 15E). Thailand.....
..... *T. rafaelnadali* sp. nov.
- Raised oblique area of mesopleuron immediately below subalar depression smooth, without striation. Thailand, Vietnam.....
..... *T. tricoloratus* Long

Descriptions

Troporhogas alboniger Quicke, Loncle & Butcher, sp. nov.

<https://zoobank.org/1ED0F077-8612-4593-878F-A39CEEFCD34A>

Figs 5, 6, 7A–C, 21J

Type material. Holotype ♀. THAILAND, Nan province, Doi Phu Kha National Park, 19°12.164'N, 101°04.473'E, 19.vi.2019, M.V. light trap, col. M. Loncle (CUMZ).

Paratype THAILAND: ♂ Loei province, Phu Ruea National Park, 17°28.826'N, 101°21.330'E, 19–26.vii.2006, Malaise trap, col. N. Jareonchai (QSBG).

Diagnosis. *Troporhogas alboniger* sp. nov. can be differentiated from all other species by its colour pattern, the female being bicoloured (black and white), its body without any yellow or brownish yellow colouration. Head black except area around the mouthparts including palps white. The mesosoma is completely black except for white tegular area. Metasoma bicoloured: TT1, 2, and 6 white, TT3–5 black (with white spot on the middle of posterior area of fifth tergite). Molecularly (Fig. 1) and morphologically it is closest to *T. contrastus* (originally described from Vietnam) which displays a very different colour pattern, having the head and anterior mesosoma yellow. Apart from colouration, *T. alboniger* sp. nov. differs from *T. contrastus* in (1) having fewer flagellomeres (41 cf. 45, 46); (2) anterior margin of mesopleuron a little below antescutal depression with zone of fine subvertical striation with (Fig. 7B, E; white arrows) compared with a few, irregular somewhat longitudinal rugae (Fig. 7B, E; white arrows); (3) posteromedial part of mesopleuron above precoxal sulcus with more or less round setiferous pits (Fig. 7B, E; yellow arrows) compared with distinctly elongate pits (Fig. 7B, E; yellow arrows); (4) anteromedial area of propodeum adjacent to anterior areola with smaller and more widely spaced setiferous punctures (Fig. 7C) compared with a denser zone of deep large setiferous punctures (Fig. 7F).

Description. Holotype, female, body length 5.5 mm; fore wing 4.6 mm; ovipositor sheath 0.6 mm.

Head. Antenna with 41 flagellomeres. Terminal flagellomere acuminate, 4 × longer than wide, 1.3 × longer than penultimate flagellomere. First flagellomere 1.1 × and 1.25 × longer than second and third, respectively, the latter 2.1 × longer than wide. Width of head: width of face: height of eye = 2.3: 1.0: 1.1. Face and clypeus rugose with sparse setosity laterally. Inter-tentorial distance 2.2 × tentorio-ocular distance. Shortest distance between posterior ocelli: transverse diameter of posterior ocellus: shortest distance between posterior ocellus and eye = 1.0: 2.3: 2.0. Vertex and temple smooth and shiny, with distinct mid-longitudinal groove. Occipital carina very weakly curved dorsally, a distinct transverse groove present immediately anterior to it.

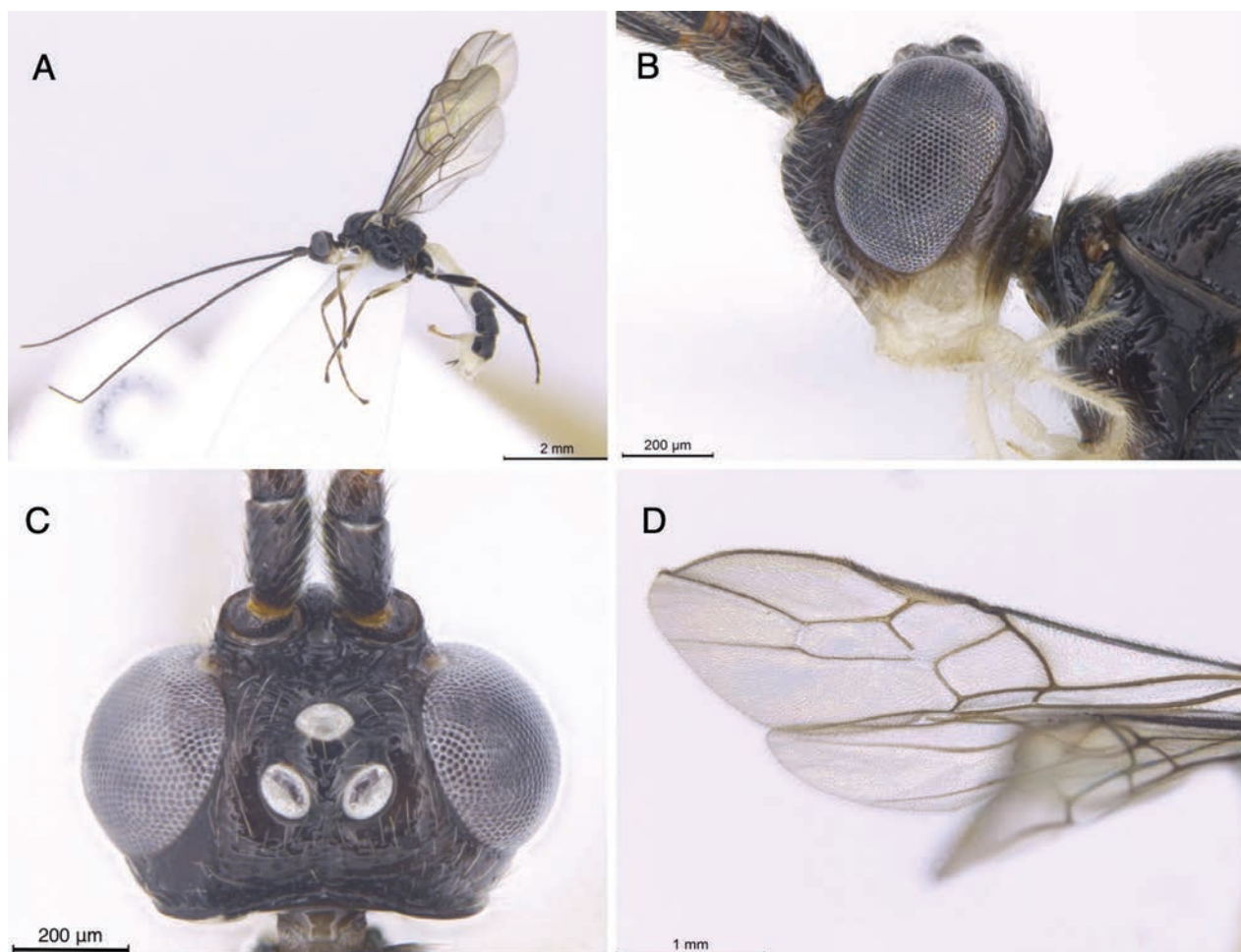


Figure 5. Light micrographs of holotype female *T. alboniger* sp. nov. **A** habitus, lateral view **B** head, lateral view **C** head, dorsal view **D** fore wing.

Mesosoma. Mesosoma 1.6 × longer than high. Notauli crenulate becoming foveate posteriorly. Scutellar sulcus with three well-developed carinae between outer pair. Axilla with ~ 6 sinuous carinae carina. Mesopleuron and metapleuron setose, precoxal sulcus a short deep groove with a broad area of irregular striation extending below it. Propodeum with submedial carinae weak, uniting anteriorly in a narrow U-shape, lateral to this with long setae, arising from distinct small punctures.

Wings. Fore wing. Length ratios of fore wing veins r-rs: 3RSa: 3RSb = 1.0: 3.2: 5.1. Length ratios of vein 2RS: 3RSa: rs-m = 2.2: 2.9: 1.0.

Legs. Length ratios of fore femur: fore tibia: fore tarsus = 1.1: 1.0: 1.1. Length ratios of hind femur: hind tibia: hind tarsus = 1.0: 1.0: 1.0. Length of hind femur and tibia 4.5 × and 8.6 × as long as medially wide, respectively. Tarsal claws with large acutely pointed basal lobe.

Metasoma. T1 1.2 × longer than posteriorly wide. T2 1.4 × longer than third. TT1 and 2 with mid-longitudinal carina dorsally, sparsely striate. Ovipositor sheath straight and shorter than hind basitarsus, ~ 0.3 × length hind femur (including trochantellus).

Colour. Bicoloured body; scapus, pedicellus and antennal segments black. Head brownish black, but mouthpart area and palps white, stemmaticum black. Mesosoma dark brown to black except for white tegulae. Metasoma bicoloured; TT1,2, and 6 white, TT3–5 black with white spot on the middle of

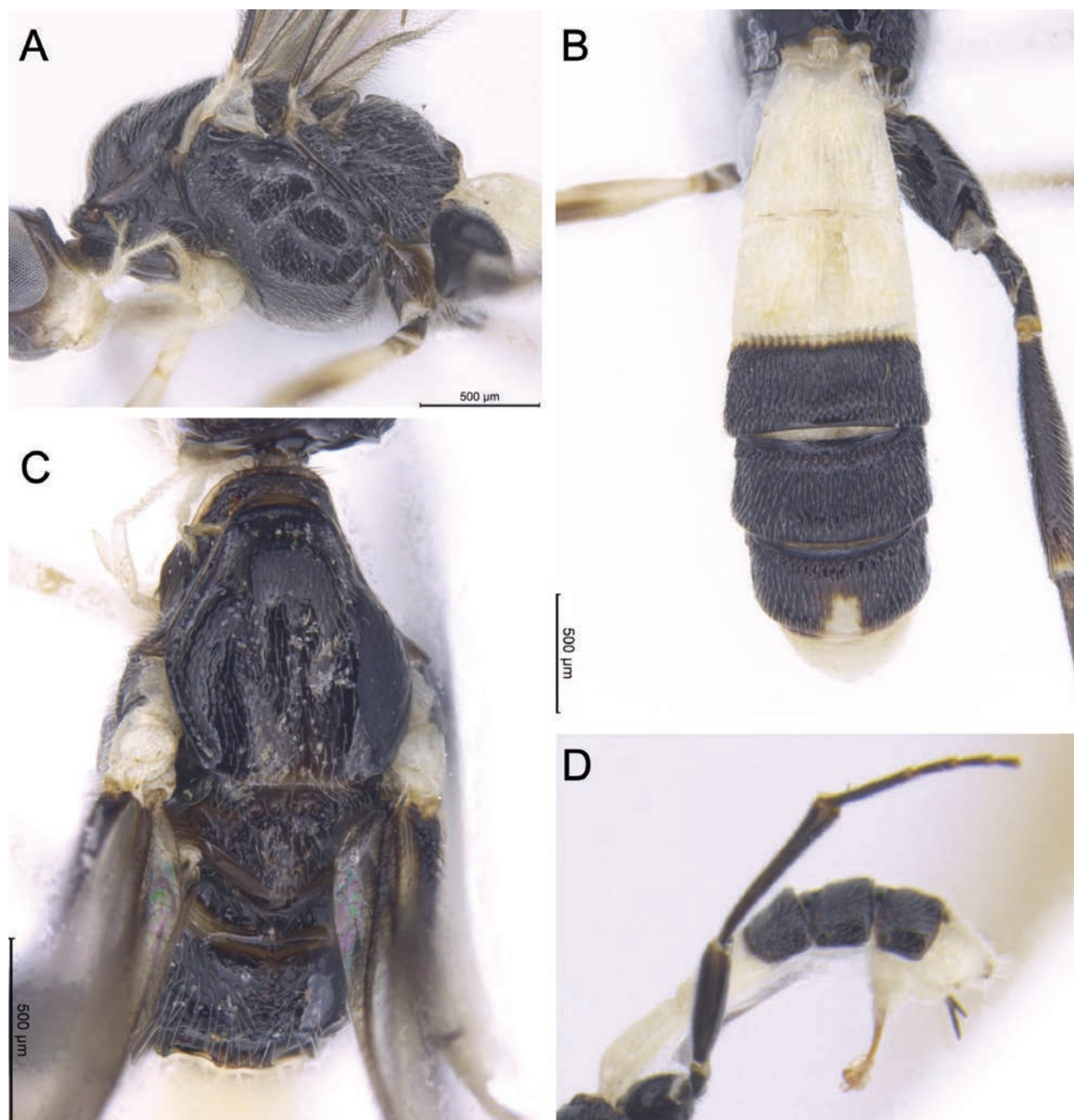


Figure 6. Light micrographs of holotype female *T. alboniger* sp. nov. **A** mesosoma, lateral view **B** metasoma, dorsal view **C** mesosoma, dorsal view **D** metasoma, lateral view.

posterior area of T5, hypopygium white. Wings hyaline with brown venation, pterostigma brown becoming paler posteriorly. Fore and mid legs pale brown, paler posteriorly, and coxa and trochantellus white; hind legs entirely black. Ovipositor sheath black.

Male. Length of body 4.6 mm, of fore wing 4.1 mm. Antenna incomplete, with at least 34 flagellomeres. Occipital carina distinctly pointed medially. Head and mesosoma yellow. Metasomal tergites white except TT3 and 4 which each have a pair of black submedial, somewhat triangular marks.

Distribution. North and east Thailand.

Biology. Unknown.

Etymology. From Latin *alboniger* referring to the white and black colouration.

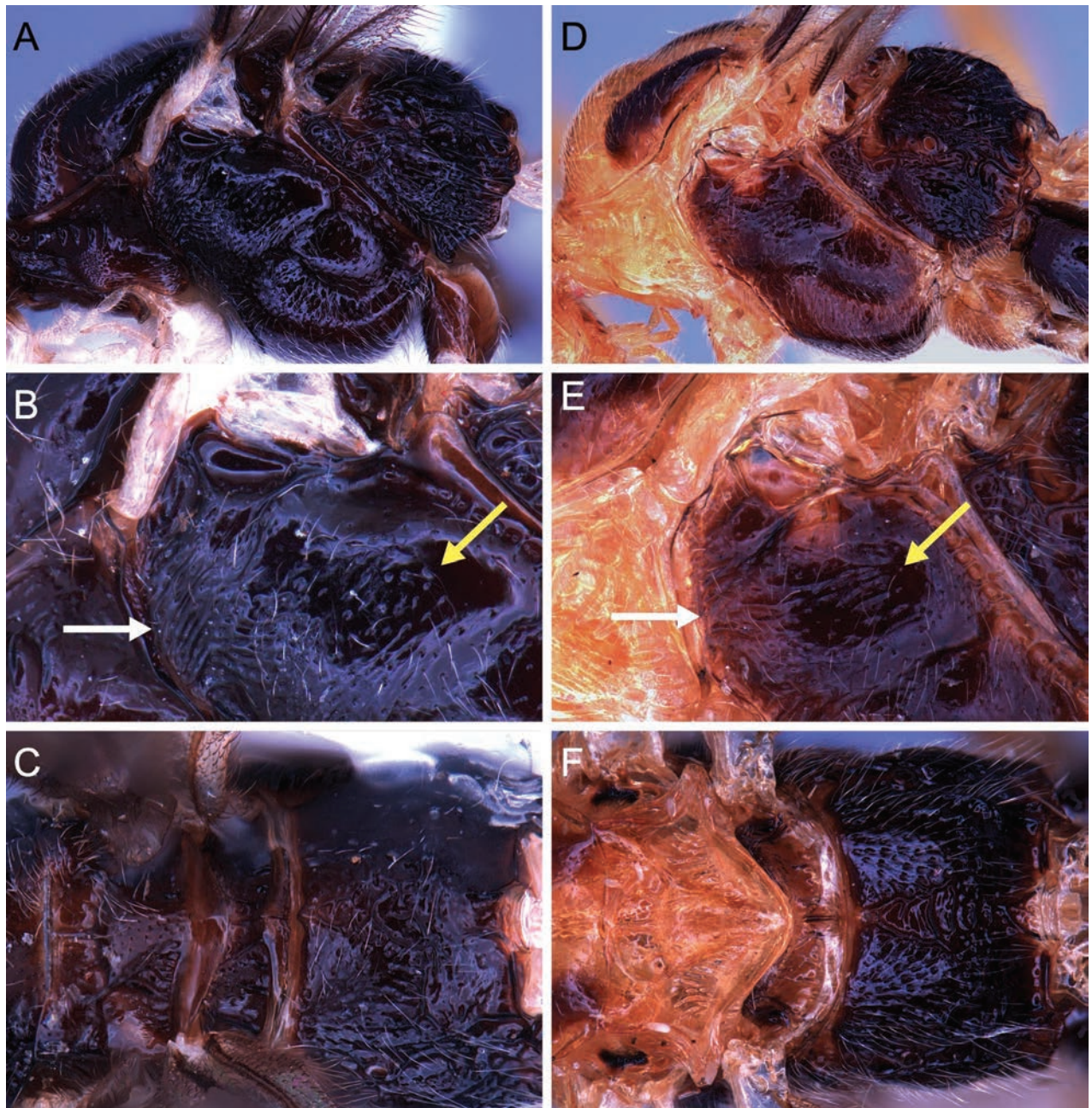


Figure 7. Light micrographs of holotype female *T. alboniger* sp. nov. comparing with Thai specimen of *T. contrastus* **A** mesosoma of *T. alboniger* sp. nov., lateral view **B** mesopleuron of *T. alboniger* sp. nov. **C** scutellum and propodeum of *T. alboniger* sp. nov., dorsal view **D** mesosoma of *T. contrastus*, lateral view **E** mesopleuron of *T. contrastus* **F** scutellum and propodeum of *T. contrastus*, dorsal view.

***Troporhogas anamikae* Ranjith, sp. nov.**

<https://zoobank.org/79017778-9048-4E70-92CE-371F07A6176C>

Figs 8–10, 21K

Type material. Holotype ♀, INDIA • Kerala, Kozhikode, Janakikkad, 3.i.2020, 11°37.309'N, 75°47.308'E, sweep net, col. Ranjith, A.P. (AIMB).

Diagnosis. *Troporhogas anamikae* sp. nov. is similar to *T. tricolor* Cameron in having a more or less similar colour pattern but the new species differs in having notauli distinct only in the basal half of mesoscutum (vs notauli complete in



Figure 8. Light micrographs of holotype female *T. anamikae* sp. nov. **A** habitus, lateral view **B** head, anterior view **C** head, dorsal view **D** head, lateral view **E** mesosoma, lateral view **F** propodeum dorsal view.

T. tricolor), mesosoma yellow dorsally (vs black in *T. tricolor*), pterostigma mostly yellow (vs completely black in *T. tricolor*), face with smooth longitudinal area antero-medially (vs completely striated in *T. tricolor*), ocello-ocular area smooth (vs striated in *T. tricolor*), midbasal triangular area of propodeum smooth (vs irregularly reticulated in *T. tricolor*), T5 longitudinally striated (vs punctate in *T. tricolor*).

Description. Holotype, female, body length 6.2 mm, fore wing 5.1 mm, ovipositor sheath 0.4 mm.



Figure 9. Light micrographs of holotype female *T. anamikae* sp. nov. **A** propodeum, dorsal view **B** wings **C** metasoma, lateral view **D** metasoma, dorsal view.

Head. Antenna with 45 flagellomeres. First flagellomere $1.6 \times$ longer than second and third, respectively. Width of head: width of face: height of eye = 2.75: 1.0: 1.5. Shortest distance between posterior ocelli: transverse diameter of posterior ocellus: shortest distance between posterior ocellus and eye = 0.7: 2.0: 1.0. Face transversely striate with a smooth longitudinal area antero-medially. Clypeus smooth with sparse setosity laterally. Vertex and temple finely transversely striate. Occipital carina complete, very weakly curved dorsally.

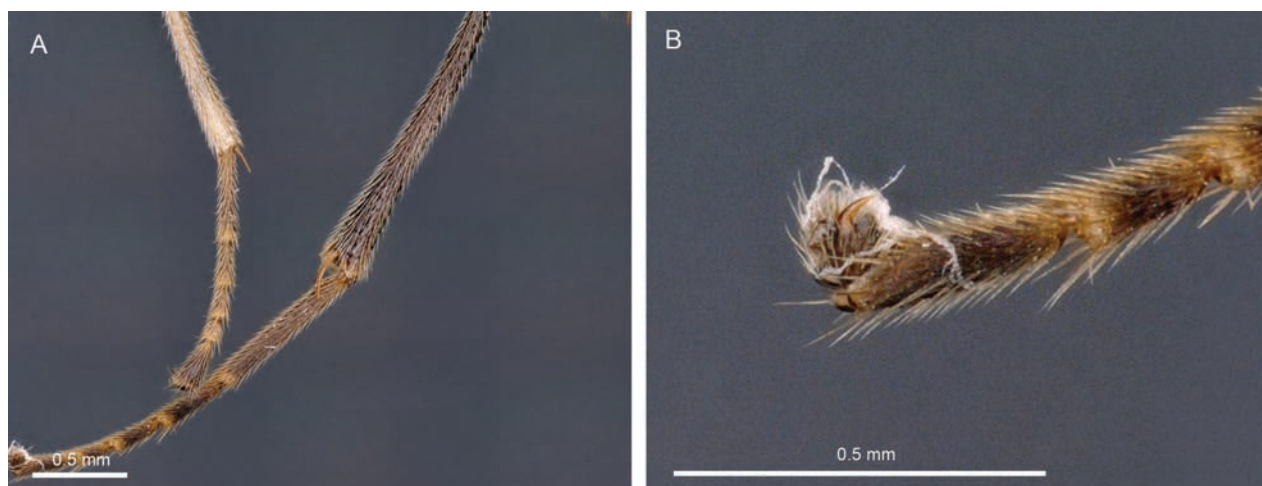


Figure 10. Light micrographs of holotype female *T. anamikae* sp. nov. **A** hind tibia **B** hind tarsus.

Mesosoma. Mesosoma 1.5 × longer than high, more or less smooth to coriaceous and setose. Mesoscutum smooth without groove medially, notauli present, crenulated. Scutellar sulcus smooth with seven carinae. Mesopleuron and metapleuron setose, precoxal sulcus broad, upwardly curving, and striate. Propodeum reticulate with long setae and without a mid-longitudinal carina.

Wings. Fore wing. Lengths of fore wing veins r-rs: 3RSa: 3RSb = 1.0: 2.5: 5.0. Lengths of vein 2RS: 3RSa: rs-m = 1.3: 2.4: 1.0.

Legs. Lengths of fore femur: fore tibia: fore tarsus = 1.0: 1.1: 1.1. Lengths of hind femur: hind tibia: hind tarsus = 1.0: 1.2: 1.5. Length of hind femur and tibia 5.0 × and 8.5 × as long as wide, respectively. Tarsal claws with large acutely pointed basal lobe.

Metasoma. T1 as long as posteriorly wide. T2 1.6 × longer than third tergite. TT1 and 2 with medial longitudinal carina dorsally, distinctly striate. TT3 and 4 distinctly striate, TT5 and 6 finely longitudinally striate. Ovipositor sheath straight and shorter than hind basitarsus, ~ 0.2 × length of hind femur (including trochantellus).

Colour. Body mostly yellow except antenna, eye, face medially, tip of mandible, frons, ocellar region, occiput, mesopleuron posterior 0.7, metapleuron, propodeum, wing venation, hind leg except trochanter, T2 with bilobed black mark mid-posteriorly, T3 largely except anterolateral areas, T4 with pair of large black marks submedially which reach posterior and posterolateral margin of tergite. Ovipositor sheath brown.

Male. Unknown.

Distribution. Kerala (India).

Host. Unknown.

Etymology. APR dedicates this species to his friend Ms Anamika Menon, for her constant support and encouragement.

***Troporhogas benjamini* Quicke, Loncle & Butcher, sp. nov.**

<https://zoobank.org/47B75022-5A59-4CE5-9333-C72AE3E58B9A>

Figs 11, 12, 21H

Material. Holotype ♀, THAILAND, Nakhon Ratchasima province, Wang Nam Khaew district, Sakaerat Environmental Research Station (SERS), 26.vii.2021,

14°60.755'N, 101°82.761'E, M.V. light trap, col. K. Chansri (CUMZ). **Paratypes** THAILAND: 1♂, Nakhon Ratchasima province, Wang Nam Khaew district, Sakaerat Environmental Research Station (SERS), 26.vii.2021, 14°60.755'N, 101°82.761'E, M.V. light trap, col. K. Chansri (CUMZ); 1♀, Nakhon Ratchasima province, Wang Nam Khaew district, Sakaerat Environmental Research Station (SERS), 25.i.2021, 14°49.672'N, 101°91.615'E, aerial net, col. K. Chansri (CUMZ); 1♀, Nakhon Ratchasima province, Wang Nam Khaew district, Sakaerat Environmental Research Station (SERS), 30.viii.2021, 14°49.630'N, 101°91.600'E, Malaise trap, col. K. Chansri (CUMZ); 1♀, Phetchaburi province, Kaeng Krachan National Park, 3–10. iv.2009, 12°48.107'N, 99°26.669'E, Malaise trap, col. Sirichai (CUMZ).

Diagnosis. *Troporhogas benjamini* sp. nov. can be differentiated from others species by its colour pattern, which is mainly dark brownish red with ivory white on mouthparts including palps, tegula (Fig. 12C) and TT1 and 2 (anteriorly and laterally) and T6. Metasoma bicoloured: T1 and T6 ivory, T2 anteriorly and laterally ivory with black mark in the middle, TT3–5 mainly black except for small anterolateral areas.

Description. Holotype, female body length 5.5 mm; fore wing 4.9 mm; ovipositor sheath 0.05 mm.

Head. Antenna with 50 flagellomeres. Terminal flagellomere acuminate, $3.7 \times$ longer than wide, $1.4 \times$ longer than penultimate flagellomere. First flagellomere $1.2 \times$ longer than second and third, respectively. Width of head: width of face: height of eye = 3.2: 1.5: 1.0. Inter-tentorial distance $3.2 \times$ tentorio-ocular distance. Face and clypeus rugose with sparse setosity laterally. Frons with

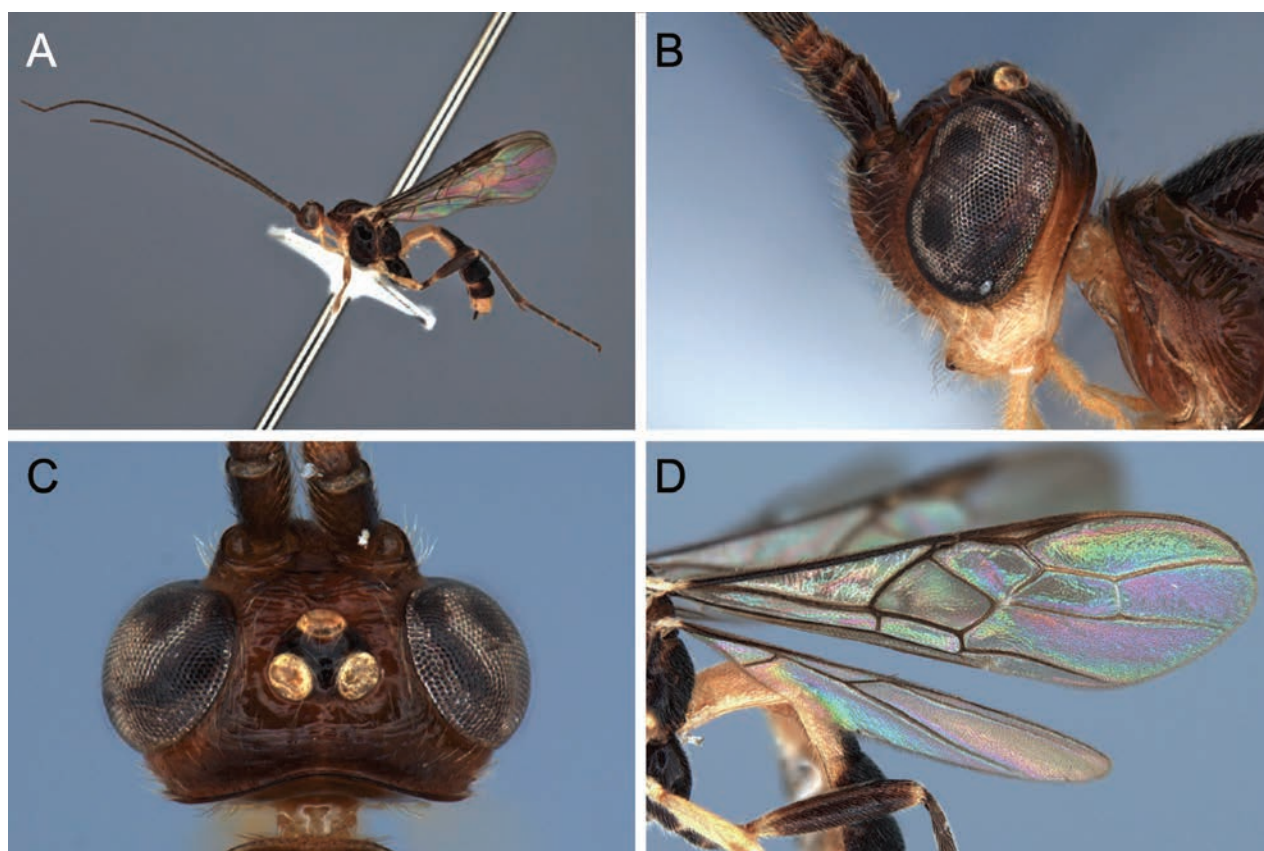


Figure 11. Light micrographs of holotype female *T. benjamini* sp. nov. **A** habitus, lateral view **B** head, lateral view **C** head, dorsal view **D** fore wing.

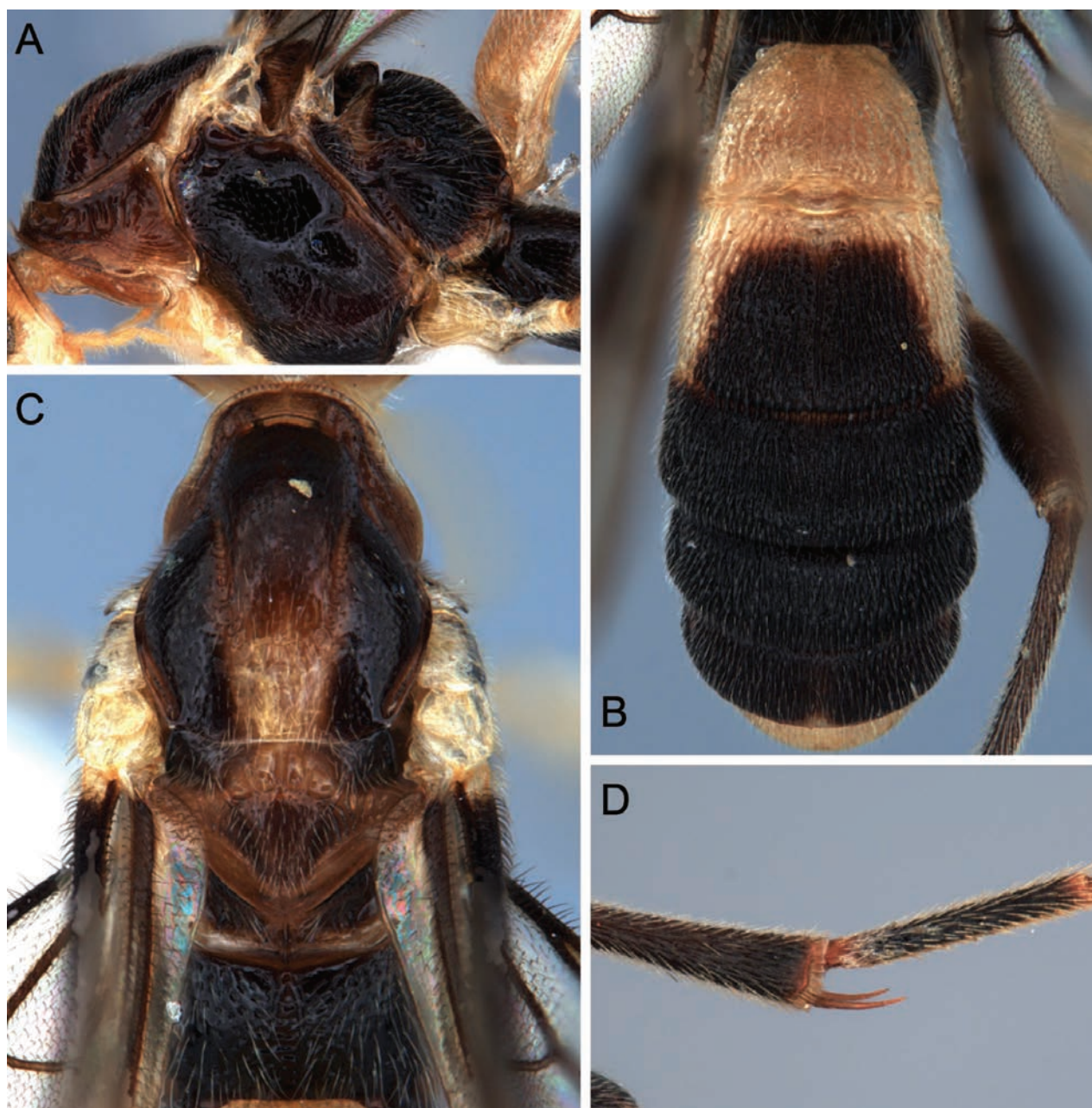


Figure 12. Light micrographs of holotype female *T. benjamini* sp. nov. **A** mesosoma, lateral view **B** metasoma, dorsal view **C** mesosoma, dorsal view **D** hind tibial spurs.

strong transverse striation that obscure the transverse carina arising from outer part of antennal sockets. Shortest distance between posterior ocelli: transverse diameter of posterior ocellus: shortest distance between posterior ocellus and eye = 1.0: 1.8: 1.8. Vertex and temple shiny and with sparse setosity, with mid-longitudinal groove. Occipital carina weakly curved dorsally.

Mesosoma. Mesosoma 2.0 × longer than high. Entire mesosoma coriaceous and setose. Mesopleuron and metapleuron setose. Mesoscutum shiny, without groove medially, sparsely punctate, notauli present. Scutellar sulcus smooth with strong medial carina and a pair of incomplete submedial carinae. Axillae narrow, finely striate. Raised anterodorsal area of mesopleuron below subalar depression with strong punctures tending to merge into distinct diagonal striate anteriorly. Precoxal sulcus complete, sinuate, transversely striate, broad

and weakly impressed anteriorly becoming narrower and deeper to posterior margin of mesopleuron. Propodeum with submedial carinae anteriorly weakly curved and converging posteriorly; with strong setiferous punctures lateral to them, reticulate with long setae and without a mid-longitudinal carina.

Wings. Fore wing. Lengths of fore wing veins r-rs: 3RSa: 3RSb = 1.0: 2.7: 3.7. Lengths of vein 2RS: 3RSa: rs-m = 1.7: 2.0: 1.0.

Legs. Lengths of fore femur: fore tibia: fore tarsus = 1.1: 1.0: 1.1. Lengths of hind femur: hind tibia: hind tarsus = 1.0: 1.1: 1.4. Length of hind femur and tibia 2.7 × and 6.8 × as long as wide, respectively. Hind tibial spurs with long setae on basal 0.3. Tarsal claws with large acutely pointed basal lobe.

Metasoma. T1 1.5 × longer than posteriorly wide. T2 1.5 × as long as T3. TT1 and 2 with mid-longitudinal carina dorsally, sparsely striate. TT3–6 with distinct striate sculpture. Ovipositor sheath straight and much shorter than hind basitarsus, ~ 0.2 × length hind femur (including trochantellus).

Colour. Bicoloured body; scapus, pedicellus and flagellar segments dark brown. Head brownish black, but mouthparts area ivory, stemmaticum dark brown. Mesosoma dark brown to black except for ivory tegulae. Metasoma bicoloured; T1 and T6 ivory, T2 anteriorly and laterally ivory with black mark in the middle, TT3–5 mainly black, hypopygium white. Wings hyaline with dark brown venation, pterostigma brown. Fore legs and mid legs bicoloured brownish and white, hind legs entirely black. Ovipositor and ovipositor sheath black.

Male. Length of body 5.9 mm, of fore wing 4.9. Antenna incomplete, with at least 38 flagellomeres. Sculpture on frons less strong. Occipital carina distinctly pointed medially. Head yellow, darker dorsally. Mesosoma orange-yellow except mesopleuron, mesosternum, metapleuron and propodeum which are largely brown to piceous. Metasoma cream-white except T3 behind anterior transverse groove with pair or large black marks the join narrowly across midline and project to posterolateral margin, and T4 which same pattern as T3 except black marks not connected medially.

Variation (female). Antennae with 49–52 flagellomeres.

Distribution. Northern Thailand and Eastern Thailand.

Hosts. Unknown.

Etymology. This species is named after the third author's husband.

***Troporhogas hugoolseni* Quicke, Loncle & Butcher, sp. nov.**

<https://zoobank.org/3A8D97AC-40B4-44E9-9C4E-DE3734416B3E>

Figs 13, 14, 21B

Type material. *Holotype* ♀, THAILAND, Nakhon Ratchasima province, Khoa Yai National Park, 19.iv.2007, 14°25.535'N, 101°23.442'E, Malaise trap, col. S. Warat (QSBG).

Diagnosis. *Troporhogas hugoolseni* sp. nov. can be differentiated from others with similar colour pattern (orangish mesosoma, T1 with black mark anteriorly, T2 largely and T6 entirely white) by having the vertex smooth except for small setiferous punctures and the raised oblique area of mesopleuron immediately below subalar depression moderately densely punctate but without oblique striation.

Description. Holotype, female body length 6.2 mm; fore wing 5.5 mm; ovipositor sheath 0.5 mm.

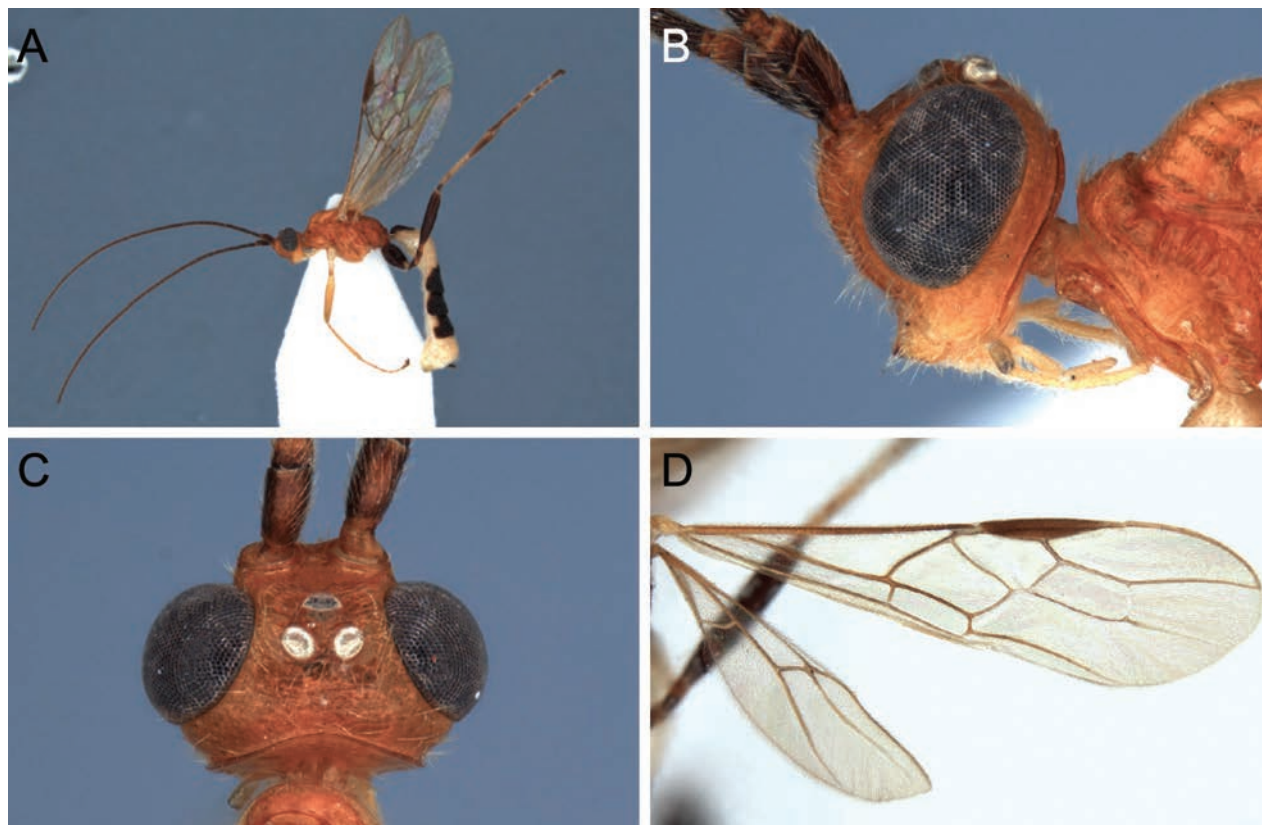


Figure 13. Light micrographs of holotype female *T. hugoalseni* sp. nov. **A** habitus, lateral view **B** head, lateral view **C** head, dorsal view **D** fore wing.

Head. Antenna incomplete, with at least 40 flagellomeres. First flagellomere $2.0 \times$ longer than second and third, respectively. Width of head: width of face: height of eye = 3.1: 1.6: 1.0. Shortest distance between posterior ocelli: transverse diameter of posterior ocellus: shortest distance between posterior ocellus and eye = 1.0: 1.4: 1.6. Face and clypeus rugose with sparse setosity laterally. Vertex and temple shiny and with sparse setosity. Occipital carina complete, curved dorsally.

Mesosoma. Mesosoma $1.6 \times$ longer than high. Mesoscutum shiny, sparsely punctate, with narrow foveate longitudinal groove mid-posteriorly. Scutellar sulcus with three carinae between outer pair. Axillae striate. Raised anterodorsal area of mesopleuron below subalar depression with diagonal striation. Precoxal sulcus short, broad, and shallow, with weak irregular striation. Mid-longitudinal carina of metanotum strong and roundly protruding posteriorly, weak anteriorly. Propodeum reticulate with long setae, with submedial carinae meeting medially in V-shape connected by ladder of variably developed transverse crenulations, lateral to these with moderately dense, small setiferous punctures.

Wings. Fore wing. Lengths of fore wing veins r-rs: 3RSa: 3RSb = 1.0: 2.8: 4.7. Lengths of vein 2RS: 3RSa: rs-m = 1.1: 1.9: 1.0.

Legs. Lengths of fore femur: fore tibia: fore tarsus = 1.0: 1.1: 1.5. Lengths of hind femur: hind tibia: hind tarsus = 1.0: 1.3: 1.6 Length of hind femur and tibia $5.0 \times$ and $8.3 \times$ as long as wide, respectively. Hind tibial spurs glabrous. Tarsal claws with large acutely pointed basal lobe.

Metasoma. T1 $1.1 \times$ longer than posteriorly wide. T2 $1.5 \times$ as long as T3. TT1 and 2 with mid-longitudinal carina dorsally, sparsely striate. TT3–6 with distinct striate

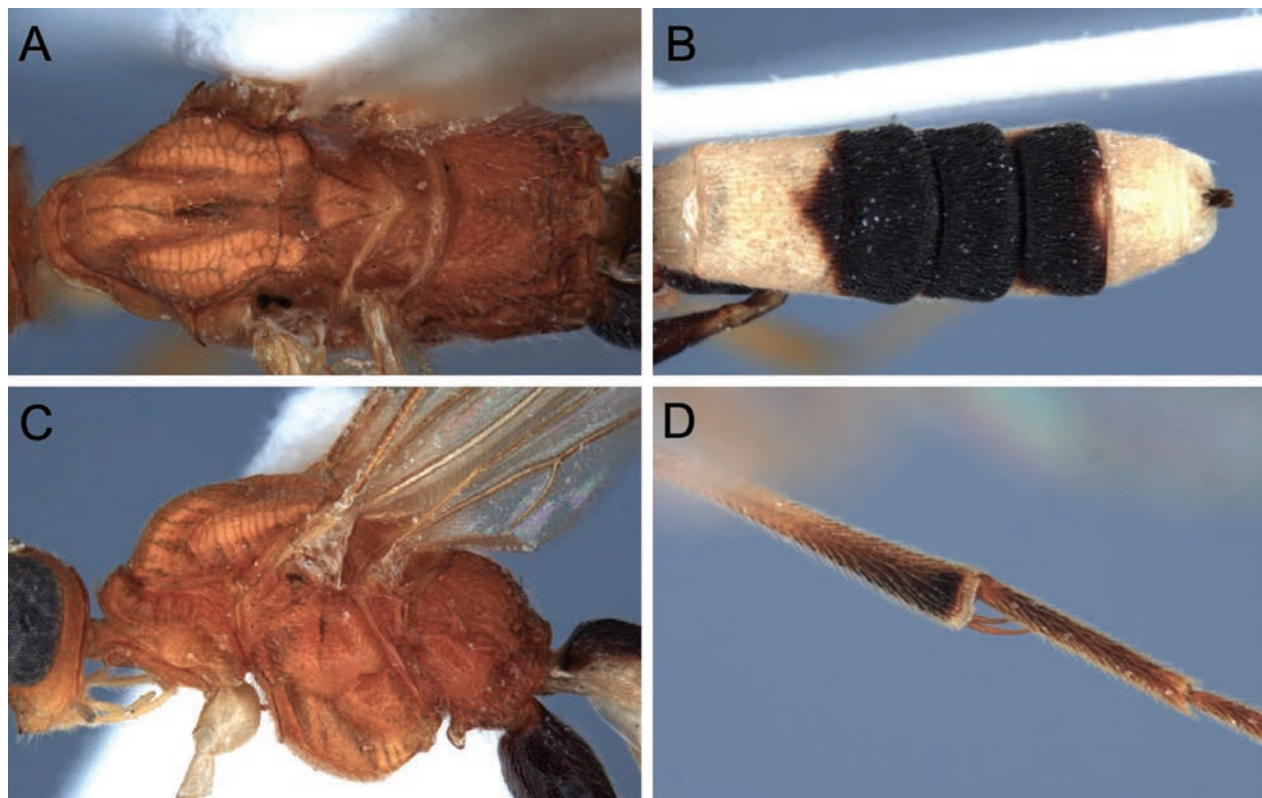


Figure 14. Light micrographs of holotype female *T. hugoolseni*, sp. nov., **A**, mesosoma, dorsal view **B** metasoma, dorsal view **C** mesosoma, lateral view **D** hind tibial spurs.

sculpture and without medial longitudinal carina. Ovipositor sheath straight and shorter than hind basitarsus, $\sim 0.3 \times$ length hind femur (including trochantellus).

Colour. Body tricoloured; scapus, pedicellus and flagellar segments dark brown. Head including stemmaticum orange-red, mouthparts paler brownish yellow. Mesosoma and tegulae ochraceous. Metasoma bicoloured; TT1, 2, and 6 white but T1 and T6 with small black marks anteriorly and posteriorly, TT3–5 black with small white anterolateral areas and with small white spot on the mid-posterior margin of T5, hypopygium white. Wings hyaline with dark brown venation, pterostigma brown. Fore legs and mid legs yellow, hind legs mainly dark brown. Ovipositor and ovipositor sheath black.

Male. Unknown.

Distribution. Central Thailand.

Hosts. Unknown.

Etymology. This species named after Mr Hugo Olsen, Norwegian marathoner and a special friend of the corresponding author.

***Troporhogas rafaelnadali* Quicke, Loncle & Butcher, sp. nov.**

<https://zoobank.org/58BBFD86-4131-40ED-8D99-C900717A8B48>

Figs 15, 21G

Type material. *Holotype* ♀, THAILAND, Nakhon Ratchasima province, Khao Yai National Park, 22.xii.2002, 19°14.459'N, 101°04.373'E, Malaise trap, col. S. Pong (QSBG).

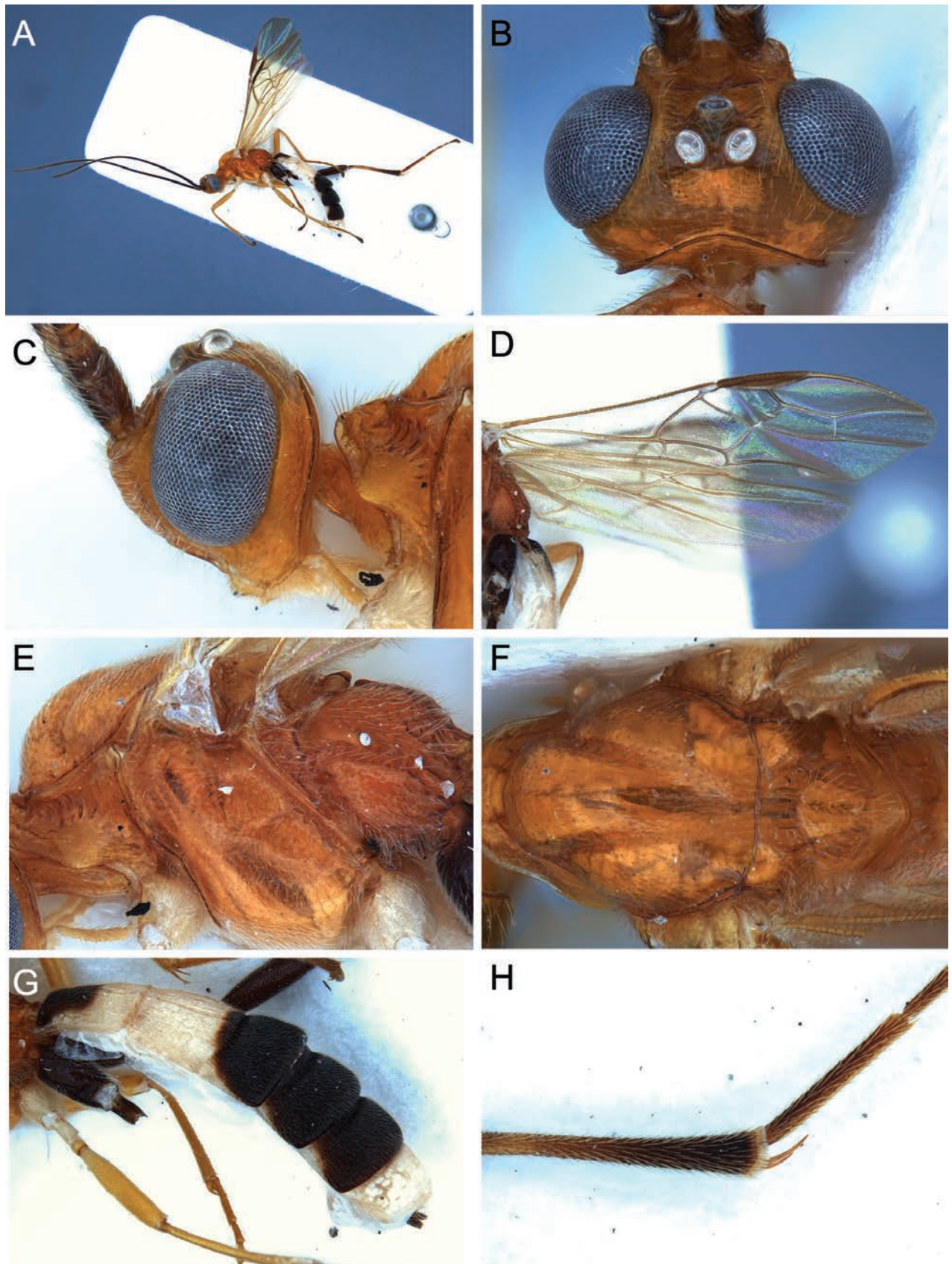


Figure 15. Light micrographs of holotype female *T. rafaelnadali* sp. nov., **A**, habitus, lateral view **B** head, dorsal view **C** head, lateral view **D** wings **E** mesosoma, lateral view **F** mesosoma, dorsal view **G** metasoma, oblique dorsal view **H** hind tibial spurs.

Diagnosis. *Troporhogas rafaelnadali* sp. nov. can be distinguished from other members of the genus with similar colour pattern (orangish mesosoma, T1 with black mark anteriorly, T2 largely and T6 entirely white) by having the vertex transversely striate and the raised oblique area of mesopleuron immediately below subalar depression strongly finely striate.

Description. Holotype, female, body length 6.0 mm; fore wing 4.2 mm; ovipositor sheath 0.5 mm.

Head. Antenna with 48 flagellomeres. First flagellomere 1.6 × longer than second and third, respectively. Width of head: width of face: height of eye = 3.6: 1.8: 1.0. Shortest distance between posterior ocelli: transverse diameter of posterior ocellus: shortest distance between posterior ocellus and eye = 1.0: 2.3: 1.3. Face and clypeus rugose with sparse setosity laterally. Vertex and temple shiny and smooth. Occipital carina completely present, slightly pointed dorsally.

Mesosoma. Mesosoma 1.7 × longer than high. Antescutal depression relatively well developed. Mesoscutum smooth and shiny, sparsely punctate, with narrow, foveate groove mid-posteriorly. Scutellar sulcus smooth with three carinae between outer margins. Mesopleuron and metapleuron setose. Precoxal sulcus shallow, long narrow and down-curving anteriorly, with narrow band of crenulation. Median area of metanotum with strong, roundly protruding mid-longitudinal carina over median area, but carina weak anteriorly. Propodeum with submedial carinae anteriorly forming a narrow 'V'-shape and at extreme anterior, a short mid-longitudinal carina, lateral to this with dense small setiferous punctation.

Wings. Fore wing. Lengths of fore wing veins r-rs: 3RSa: 3RSb = 1.0: 1.2: 2.0. Lengths of vein 2RS: 3RSa: rs-m = 1.7: 2.0: 1.0.

Legs. Lengths of fore femur: fore tibia: fore tarsus = 1.0: 1.1: 1.4. Lengths of hind femur: hind tibia: hind tarsus = 1.0: 1.1: 1.9. Length of hind femur and tibia 3.6 × and 6.3 × as long as wide, respectively. Hind tibial spurs glabrous. Tarsal claws with large acutely pointed basal lobe.

Metasoma. T1 1.1 × longer than posteriorly wide. T2 1.3 × longer than third tergite, 0.5 × as long as T3. TT1 and 2 with mid-longitudinal carina dorsally, sparsely striate. TT1–3 with distinct striate sculpture and without medial longitudinal carina. Ovipositor sheath straight and shorter than hind basitarsus, ~ 0.1 × length hind femur (including trochantellus).

Colour. Body tricoloured body orange-yellow, black, and white. Scapus, pedicellus, and flagellar segments brown. Head and mouthparts, including palps, orange-yellow. Mesosoma completely orange-yellow except for whitish tegula. Metasoma tricoloured: TT1 and 2 white with small black mark anteriorly, TT3–5 black except for small white anterolateral areas, T6 white. Wings hyaline with dark brown venation distally becoming paler basally, pterostigma dark brown. Fore and mid legs brownish yellow with coxa and trochanter white, hind leg black except basal 0.6 of tibia brown.

Male. Unknown.

Distribution. Central Thailand.

Biology. Unknown.

Etymology. This species is named after a Spanish professional tennis player, Rafael Nadal who has been ranked world No. 1 in singles by the ATP (Association of Tennis Professionals).

***Troporhogas rogerfedereri* Quicke, Loncle & Butcher, sp. nov.**

<https://zoobank.org/04E5147A-1A14-463F-9C6C-8B2BC83D7A54>

Figs 16, 21E

Type material. *Holotype* ♀, THAILAND, Surat Thani province, Khao Sok NP, Klong Morg unit, 23.vi.2009, 84m, Malaise trap, coll. Pongphan (QSBG).

Diagnosis. *Troporhogas rogerfedereri* sp. nov. is the only Thai species known with the submedial propodeal carinae forming a wide U-shape anteriorly (Fig. 16G). It differs from the only other known species with this feature, *T. flavistigma*, in having the vertex strongly transversely striate.

Description. Holotype, female, body length 6.0 mm; fore wing 4.2 mm; ovipositor sheath 0.5 mm.

Head. Antenna with 40 flagellomeres. Terminal flagellomere acuminate, 4.5 × longer than wide. Penultimate flagellomere 3.0 × longer than wide. First flagellomere 1.0 × and 1.05 × longer than the second and third, respectively, the latter 2.4 × longer than wide. Width of face: width of head: height of eye = 1.0: 2.3: 1.4. Face transversely striate with a smooth longitudinal ridge medially. Inter-tentorial distance 2.3 × tentorio-ocular distance. Carina running from anterior margins of antennal sockets well-developed and uniting medially anterior of median ocellus. Shortest distance between posterior ocelli: transverse diameter of posterior ocellus: shortest distance between posterior ocellus and eye = 1.0: 1.4: 1.0. Vertex and temple transversely striate. Occipital carina strong, more or less evenly and weakly curved, with deep transverse groove immediately in front of it.

Mesosoma. Mesosoma 1.5 × longer than high. Antescutal depression narrow. Mesopleuron and metapleuron setose. Mesoscutum shiny, without groove posteromedially, sparsely punctate. Scutellar sulcus with five carinae between outer pair. Raised anterodorsal area of mesopleuron below subalar depression with diagonal striation. Precoxal sulcus shallow, short, upcurved posteriorly, with weak irregular sculpture. Propodeum with pair of submedial carinae forming a wide inverted 'U'-shape anteriorly; lateral to the carinae anteriorly with deep punctures that form close longitudinal rows, posteriorly with coarse irregular reticulations.

Wings. Fore wing. Lengths of fore wing veins r-rs: 3RSa: 3RSb = 1.0: 3.0: 5.3. Lengths of vein 2RS: 3RSa: rs-m = 1.2: 2.3: 1.0.

Legs. Lengths of fore femur: fore tibia: fore tarsus = 1.0: 1.1: 1.2. Lengths of hind femur: hind tibia: hind tarsus = 1.0: 1.1: 1.3. Length of hind femur and tibia 5.8 × and 15.0 × as long as medially wide, respectively. Hind tibial spurs distinctly setose on basal third. Tarsal claws with large acutely pointed basal lobe.

Metasoma. T1 as long as posteriorly wide, T2 1.4 × longer than T3. TT1 and 2 sparsely striate, with mid-longitudinal carina. TT3–6 with distinct striate sculpture. Ovipositor sheath straight and shorter than hind basitarsus, ~ 0.3 × length of hind femur (including trochantellus).

Colour. Body tricoloured; scapus, pedicellus and flagellar segments dark brown to black. Head orange-red, and mouthparts paler ochraceous, stemmaticum ochraceous. Mesosoma orange-red, tegulae paler ochraceous. Front and middle legs brownish yellow, except coxae and trochanters white, fore tarsus somewhat darker; hind leg largely black, tarsus paler. Wings hyaline with dark brown venation that becomes distinctly more yellowish towards wing base,

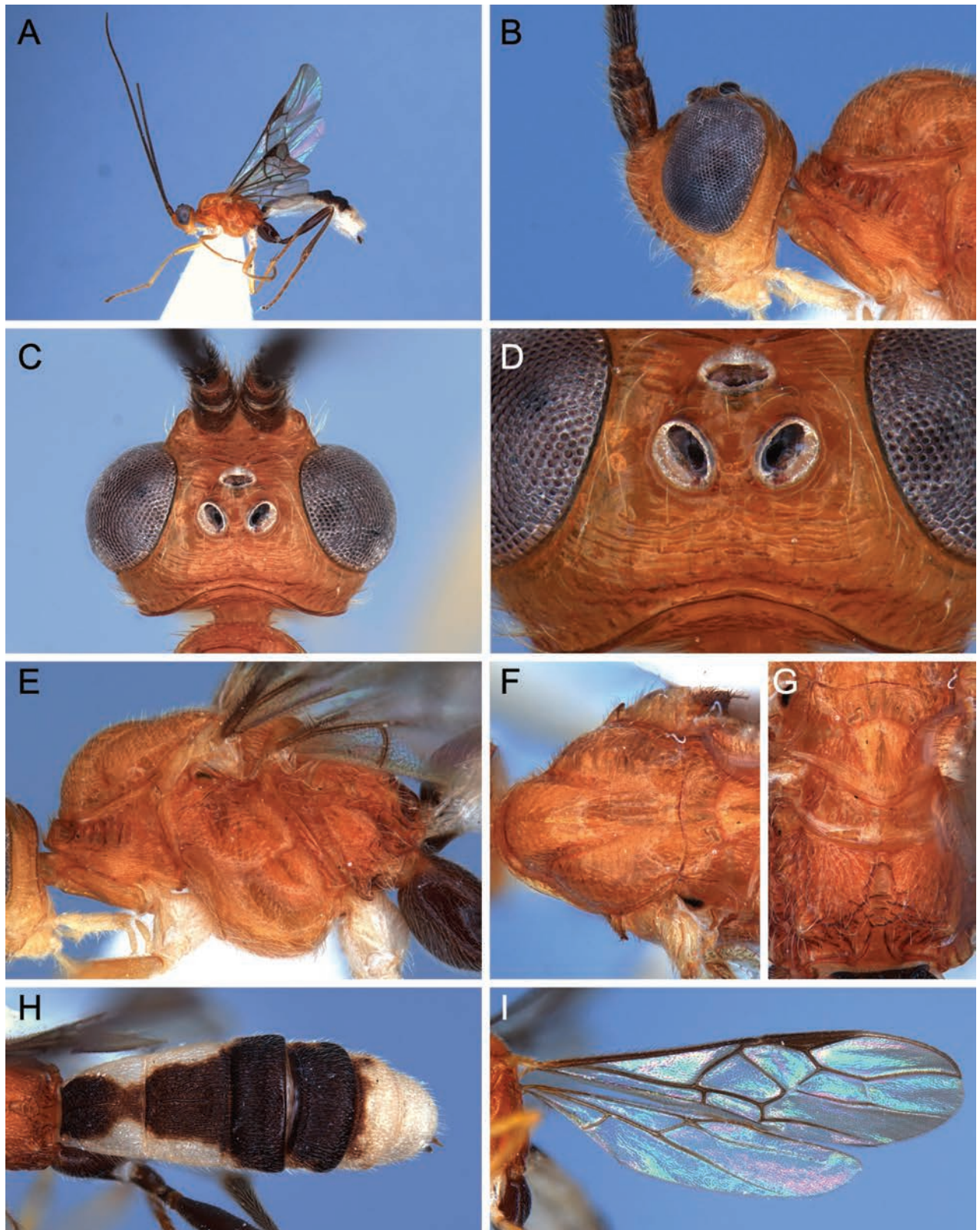


Figure 16. Light micrographs of holotype female *T. rogerfedereri* sp. nov. **A** habitus, lateral view **B** head and anterior mesosoma, lateral view **C** head, dorsal view **D** stemmaticum and vertex, detail **E** mesosoma, lateral view **F** anterior mesosoma, dorsal view **G** scutellum and propodeum, dorsal view **H** metasoma, dorsal view **I** wings.

pterostigma dark brown. Metasoma bicoloured; TT1–4 white with contiguous medial piceous to black marks that are narrowest at the junction of TT1 and 2; T5 largely except anteriorly, and T6 entirely ivory white; hypopygium white.

Male. Unknown.

Distribution. Peninsular Thailand.

Biology. Unknown.

Etymology. This species is named after a Swiss former professional tennis player, Dr. Roger Federer who was ranked world No.1 in singles by the ATP.

New record of *Troporhogas* from Thailand

Two new species records for Thailand were identified by key to species of the genus from Vietnam (Long 2014) and then, detailed comparison the specimens with original photographs of the type specimens from Vietnam.

***Troporhogas contrastus* (Long, 2014)**

Figs 17, 211

Material. THAILAND, **Nakorn Ratchasima province**, 6♀ Sakaerat Environmental Research Station (SERS); Light trap; 10–13.v.2021, 17 iii 2021 (CUMZ); **Nakorn Ratchasima province**, 3♂ Sakaerat Environmental Research Station (SERS), light trap; 17.ii–20.iii.2021 (CUMZ); **Chiang Mai province**, 1♂ Doi Chiangdao, 9–16.xi.2007, Malaise trap, (CUMZ); 1♀; Doi Phahompok, 11–18 vii 2007, Malaise trap (CUMZ); **Uthai Thani province**, 1♀; Khao Yong Rum, 6–8.vi.1986, 400 m, coll. J.M. Allen (NHMUK).

Diagnosis. Female. Body length 6.4–7.4 mm, length of fore wing 5.4–5.5 mm, antenna 7.9 mm; head in dorsal view occipital carina weakly curved, compound eyes large, lateral view temple and malar space small, face with median carina, frons smooth with sparse setae, maxillary palp 5-segmented; mesoscutum shiny and smooth with fine setae, notauli deep, propodeum areolate medially, rugose anteriorly and reticulated posteriorly; fore wing: pterostigma pale brown, vein r-rs arising slightly before the middle of pterostigma, (RS+M) a straight, hind wing: m-cu absent, cu-a reclivous; length of inner hind tibial spur < 1/3 of basitarsus, hind tarsal claw with large lobe; TT1 and 2 with dorsal longitudinal carina enclosing a triangular area at the base, metasomal tergites densely striate, ovipositor short; head yellow but stemmaticum black, mesosoma yellow except for meso- and metapleuron and propodeum black, legs yellow but hind legs brown, metasoma ivory, except for TT3–5 blackish brown, T2 with black spot posteriorly.

Male. Length of body 5.0–5.1 mm, of fore wing 4.9. Antenna with 36–39 flagellomeres. Sculpture on frons less strong. Occipital carina more or less rounded medially. Head and mesosoma orange-yellow except mesopleuron sometimes with dark medial mark, metapleuron largely piceous or black, propodeum black. Hind leg largely black but tarsus dark brown. Metasoma cream-white except TT3 and 4 which variably have a piceous to black mark submedially, to largely black behind anterior transverse groove with a weak break indicated anteriorly.

Variation. One female specimen has the anterior third of middle lobe of mesoscutum piceous.

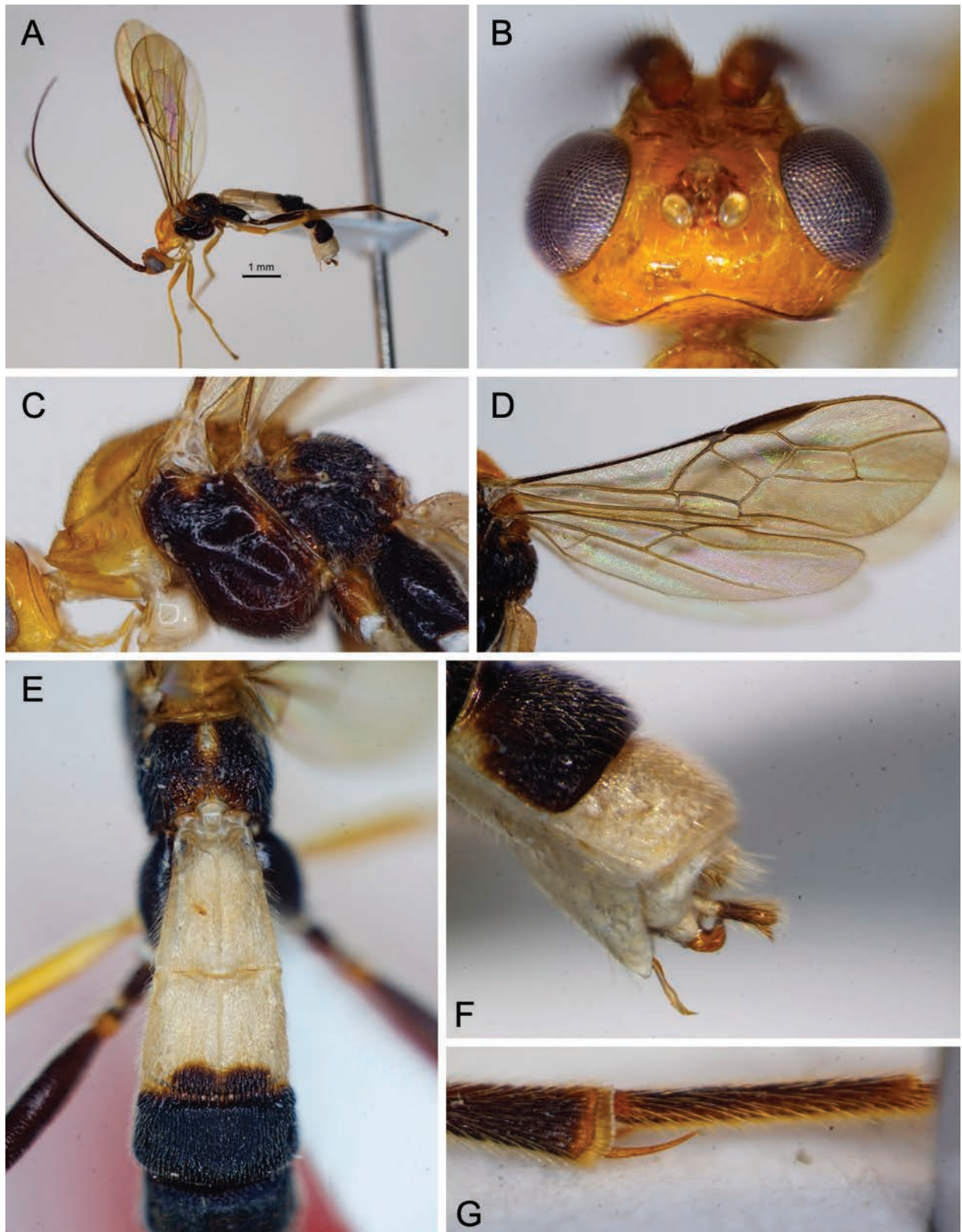


Figure 17. Light micrographs *T. contrastus* holotype female from Vietnam **A** habitus, lateral view **B** head, dorsal view **C** mesosoma, lateral view **D**, wings **E** propodeum and anterior metasoma, dorsal view **F** T5 and 6, lateral view **G** hind tibial spurs.

General distribution. North central and north west Vietnam (Long 2014), north and central Thailand.

Biology. Unknown.

***Troporhogas tricoloratus* (Long, 2014)**

Figs 18, 21D

Material. THAILAND • 1♀, Phetchabun province, Nam Nao National Park, 16°13.103'N, 101°33.836'E, 28.iv.2007, Malaise trap, col. J. Leng (QSBG); 1♂, Sara Buri province, Kaeng Khoi, Chulalongkorn University Campus, 27.xii.2016, 15.589°N, 101.011°E, light trap, col. Mudang Marissa (CUMZ).

Re-description. Female, body length 7.1 mm; fore wing 5.0 mm; ovipositor sheath 0.6 mm.

Head. Antenna with 45 flagellomeres. First flagellomere 1.4 × longer than second and third, respectively. Width of head: width of face: height of eye = 2.6: 1.2: 1.0. Shortest distance between posterior ocelli: transverse diameter of posterior ocellus: shortest distance between posterior ocellus and eye = 1.0: 1.8: 1.8. Face and clypeus rugose with sparse setosity laterally. Vertex and temple shiny and with striate sculptured. Occipital carina completely present, curved dorsally.

Mesosoma. Mesosoma 1.5 × longer than high, smooth and shiny. Mesopleuron and metapleuron setose. Mesoscutum shiny, with narrow, punctate median groove posteriorly, sparsely punctate. Scutellar sulcus smooth without carina. Axillae striate. Raised anterodorsal area of mesopleuron below subalar depression smooth. Precoxal sulcus, short and crenulate. Propodeum with submedial carinae anteriorly forming very narrow, sharp V-shape, lateral to this with rather dense and strong setiferous punctation.

Wings. Fore wing. Lengths of fore wing veins r-rs: 3RSa: 3RSb = 1.0: 2.2: 4.3. Lengths of vein 2RS: 3RSa: rs-m = 1.0: 2.2: 1.2.

Legs. Lengths of fore femur: fore tibia: fore tarsus = 1.3: 1.2: 1.0. Lengths of hind femur: hind tibia: hind tarsus = 1.0: 1.3: 1.6. Length of hind femur and tibia 4.0 × and 7.5 × as long as wide, respectively. Hind tibial spurs glabrous. Tarsal claws with large acutely pointed basal lobe.

Metasoma. T1 1.3 × longer than posteriorly wide. T2 1.4 × longer than tergite 3. TT1 and 2 with mid-longitudinal carina, sparsely striate. TT3–6 with distinct striate sculpture and without medial longitudinal carina. Ovipositor sheath straight and shorter than hind basitarsus, ~ 0.2 × length hind femur (including trochantellus).

Colour. Body tricoloured: scapus, pedicellus and flagellar segments brown. Head and mouthparts area ochraceous, stemmaticum ochraceous. Mesosoma and tegulae ochraceous yellow colour. Metasoma bicoloured; TT1, 2, and 6 white but first tergite with small black marks anteriorly and sixth with very small black mark posteriorly, TT3–5 black (with a small anterolateral areas and spot on middle of posterior area margin of tergite 5 white), hypopygium white. Wings hyaline with dark brown venation, pterostigma brown. Fore legs and mid legs yellow, hind legs entirely black and dark brown. Ovipositor and ovipositor sheath black.

Male. Head and mesosoma orange-yellow. Metasoma ivory-white with black markings: TT1 and 2 with black marks meso-anteriorly, TT3 and 4 with large black marks reach anterior margin anteriorly and posterolateral corners posteriorly, but with large ivory antero-lateral areas, TT5 and 6 ivory-white. Wings hyaline with dark brown pterostigma and venation. Fore and mid legs orange-brown with coxa white and tarsus brown. Hind coxa black with large whitish dorsal patch, hind trochantellus white, hind femur white on basal 0.4, distally black, hind tibia white on basal 0.75, distally black, hind tarsus dark brown.

Distribution. Northern Vietnam and northern Thailand and Eastern Thailand.

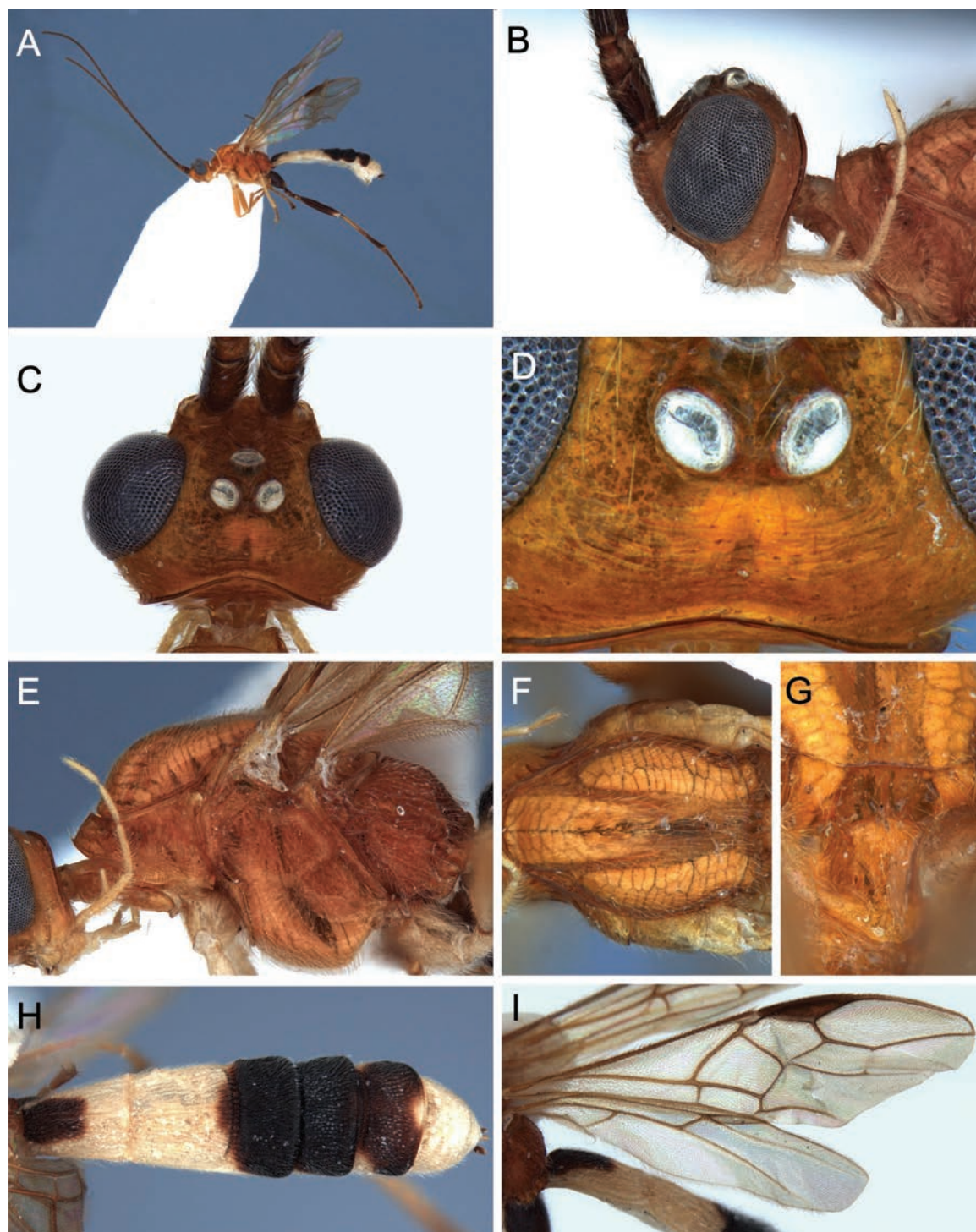


Figure 18. Light micrographs of female Thai specimen of *T. tricoloratus* **A** habitus, lateral view **B** head, lateral view **C** head, dorsal view **D** vertex, dorsal view **E** mesosoma, lateral view **F** mesoscutum, dorsal view **G** scutellar sulcus **H** metasoma, dorsal view **I** wings.

Hosts. Unknown.

Notes. The female Thai specimen agrees very well with the original description except that the dark mark at posterior of T2 is smaller and there is a small pale spot on the mid posterior margin of T2. Thus, given that there is some colour variation in nearly all the species represented by multiple individuals of the same sex, we believe them to be conspecific.

Notes on *Troporhogas* from China

Troporhogas chinensis (Chen & He, 1997)

Figs 19A, B, 21B

Comments. Known only from the holotype female from the southerly island of Hainan. It differs from *T. albilateralis* which also has contiguous black markings on TT1–5 in that the whitish anterolateral areas of the tergites are distinctly smaller (Fig. 21B cf. 21A), and the fore wing vein 1cu-a is virtually interstitial.

Troporhogas flavistigma (Chen & He, 1997)

Figs 19D–F, 21F

Comments. Known from the holotype female, two female paratypes, and a male paratype collectively from locations in Fujian, Guangxi, and Yunnan. The original description notes some variation in colour with TT1 and 2 sometimes being largely yellow and T5 sometimes largely black but does not specify whether or not these variants reflect sexual dimorphism.

Troporhogas guangxiensis (Chen & He, 1997)

Fig. 20E–H

Comments. This is one of two predominantly brown-yellow species that have a simple rounded, not produced, basal lobe to the claws (Chen and He 1997: fig. 324). The other known species with this unusual character is *T. simulatus*, thus far known only from Vietnam (Long 2014: fig. 31).

Troporhogas rugivertex (Chen & He, 1997)

Fig. 20A, B

Comments. Known only from holotype female from Yunnan. It is the only known entirely ochreous yellow species with uniformly hyaline wings and a dorsomedially pointed occipital carina.

Troporhogas unicolor (Chen & He, 1997)

Fig. 20C, D

Comments. Known only from a single male specimen from Yunnan. The holotype has a distinctively coloured metasoma, ochreous yellow with some darker medial spots but, given the sexual dimorphism in colour pattern in the boldly coloured species (*T. benjamini* sp. nov. and *T. contrastus*), it is impossible to know whether this would be useful for recognising females of the species.

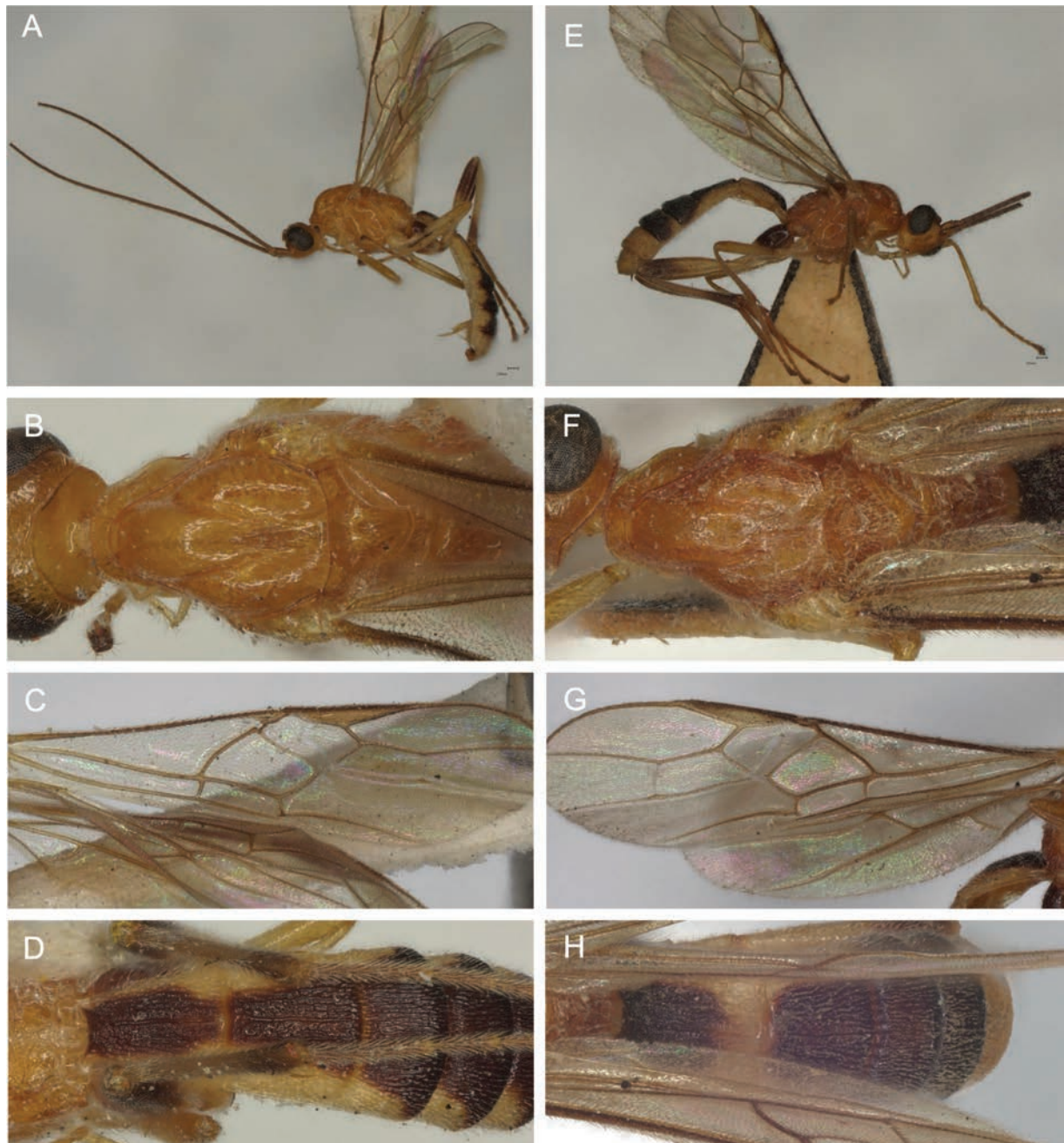


Figure 19. Light micrographs of Chinese species of *Troporhogas*. **A–D** *T. chinensis*, ♀ holotype **A** habitus, lateral view **B** posterior of head and mesosoma, dorsal view **C** fore wing **D** metasoma, dorsal view **E–H** *T. flavistigma* ♀ holotype **E** habitus, lateral view **F** posterior of head and mesosoma, dorsal view **G** fore wing **H** metasoma, dorsal view.

Discussion

The molecular phylogenetic analysis (Fig. 4) shows that *Troporhogas alboniger* sp. nov. is nested within the *T. contrastus* clade, their barcode sequences differing by only one base pair. Hence all specimens of these two species fall into the same BIN (Ratnasingham and Hebert 2013), and they are undoubtedly closely related and presumably have speciated quite recently. Unfortunately for the new species we were only able to obtain sequences from the barcode gene and not from the other three markers. There are three reasons we recognise these as different species. Firstly, we identified three consistent differences in mesosomal sculpture,

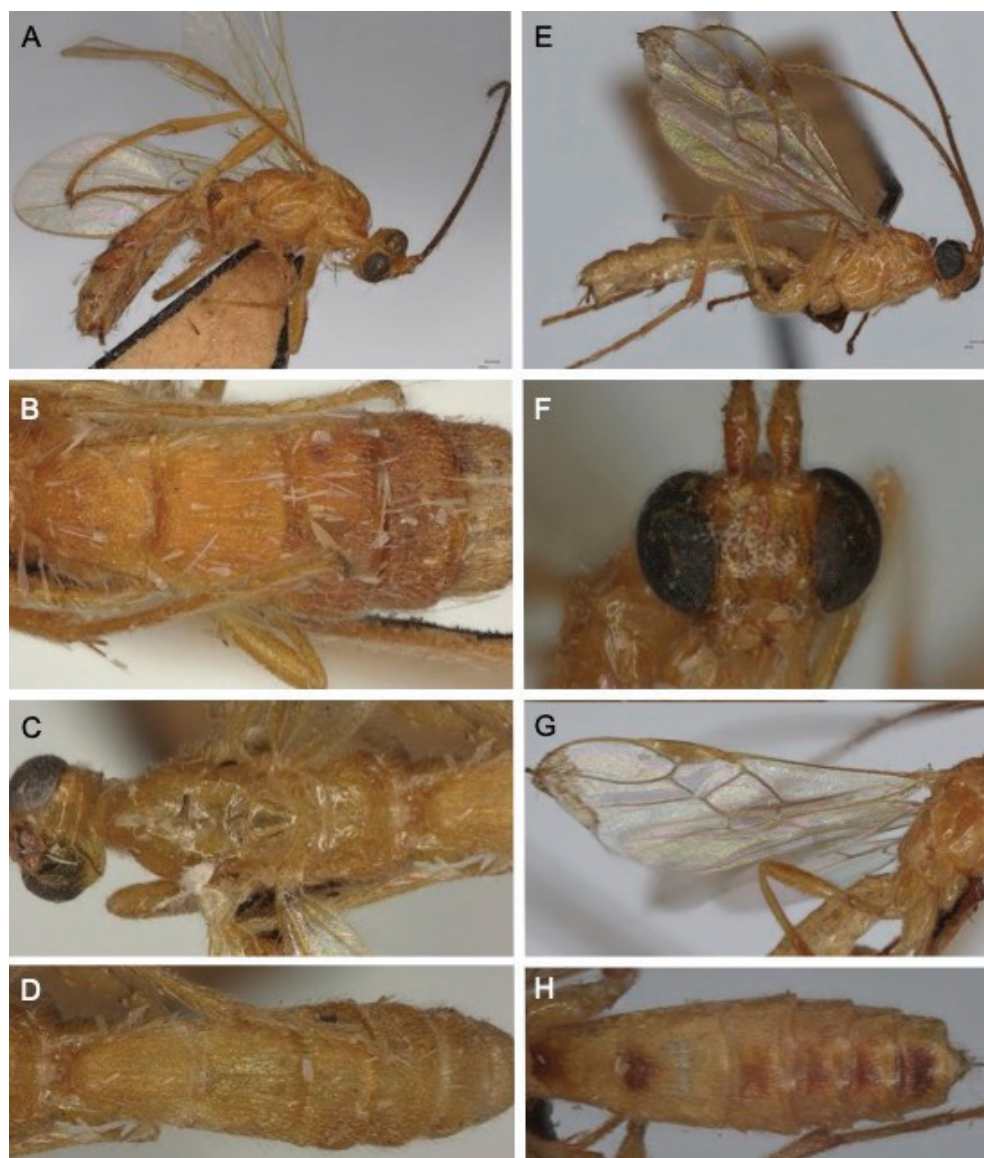


Figure 20. Light micrographs type specimens of Chinese species of *Troporhogas* **A, B** *T. rugiventris* **A** habitus, lateral view **B** metasoma, dorsal view **C, D** *T. unicolor* **C** head and mesosoma, dorsal view **D** metasoma, dorsal view **E–H** *T. guangxiensis* **E** habitus, lateral view **F** head, anterior view **G** fore wing **H** metasoma, dorsal view.

and importantly, the vertical striation in the new species at the anterior of the mesopleuron is not simply a matter of an increase in density of a feature as there is no indication of such sculpture in *T. contrastus*. Secondly, the difference in colouration is also not simply a matter of intensity. The available material of *T. contrastus* displays a small amount of colour variation, with some having the mesoscutum more orange-red and others black with piceous orange, but none show the pure blackness of *T. alboniger* sp. nov. The head, including mouthparts and palps, of *T. contrastus* are orange-yellow whereas in the new species the head is bicoloured with a sharp demarcation between the pure black upper parts and the virtually pure white malar area, mouthparts, and palps. Thirdly, there is very little variation in colour pattern in either of the two species that are represented in our collection based on multiple female specimens *T. benjamini* sp. nov. and *T. contrastus*.

Although a fairly gradual variation (especially in degree of melanisation) is not uncommon in the Braconidae, and examples are known of temperature, latitudinal

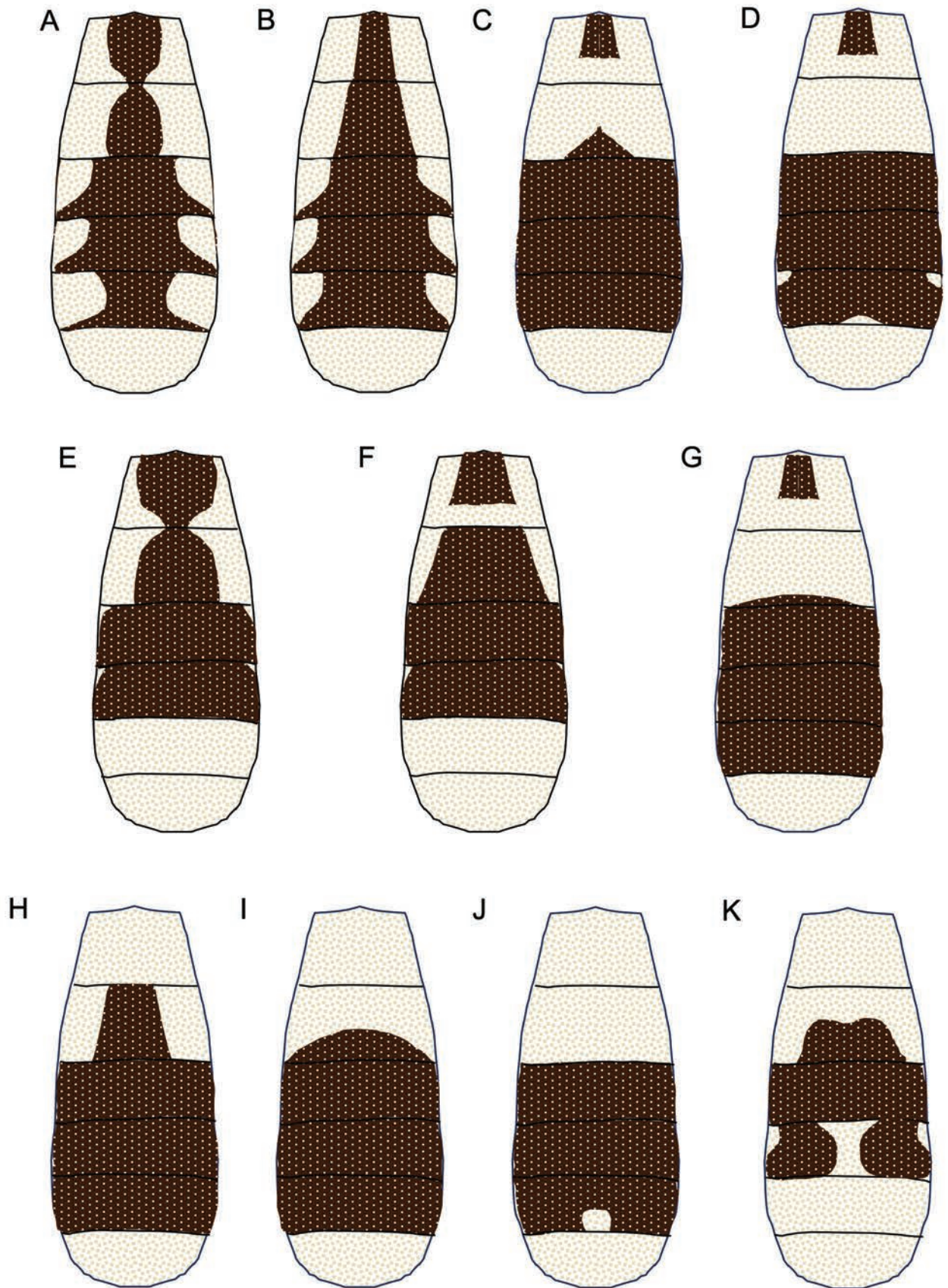


Figure 21. Drawings of metasomal colour patterns of females of *Troporhogas* species **A** *T. albilateralis* **B** *T. chinensis* **C** *T. hugoolseni* sp. nov. **D** *T. tricoloratus* (Thai specimen) **E** *T. rogerfedereri* sp. nov. **F** *T. flavistigma* **G** *T. rafaelnadali* sp. nov. **H** *T. benjamini* sp. nov. **I** *T. contrastus* **J** *T. alboniger* sp. nov. **K** *T. anamikae* sp. nov.

(Ito et al. 2015), or host-induced colour differences, again in degree of melanisation: there are very few examples where genuine pattern polymorphism has been found (Tucker and Sharkey 2016). We are not aware of any examples involving the replacement of one colour with two quite different colours such as that seen in the difference between *T. contrastus* and *T. alboniger* sp. nov., and therefore we believe that collectively the evidence supports that these are two distinct species.

Acknowledgements

We would like to gratefully thank Gavin Broad for photographs of the type specimens of *Troporhogas* described by Cameron from the Natural History Museum (London), and Prof. Pu Tang for the photographs of the type specimens of Chinese species to compare with the new species. Mr. Kittipum Chansri kindly allowed us to study and include his specimens. We would like to thank Mr. Chatchai Yothawut, Director of Doi Phu Kha National Park, the specimen collecting site, and Mr. Phasin Inkeaw for providing facilities, and their cooperation during a year of insect collecting field trips. APR acknowledges Department of Biotechnology, Government of India for financial assistance through a major research project on “Bio-resource and Sustainable livelihoods in North East India” (BT/01/17/NE/TAX) which was instrumental for completion of this study. APR was supported by a postdoctoral fellowship from the Rachadaphiseksomphot Fund, Graduate School, Chulalongkorn University. Finally, we are very grateful to the subject editor and three referees for their many helpful comments and suggestions.

Additional information

Conflict of interest

The authors have declared that no competing interests exist.

Ethical statement

No ethical statement was reported.

Funding

This research is funded by Thailand Science Research and Innovation Fund Chulalongkorn University and Chulalongkorn University and RSPG Chula to BAB; DLJQ was supported by a senior postdoctoral fellowship from the Rachadaphiseksomphot Fund, Graduate School, Chulalongkorn University. MKL was supported by C2F Fellowship, Chulalongkorn University.

Author contributions

Conceptualization: DLJQ, BAB. Data curation: APR, MKL, CVA, KDL. Formal analysis: MKL, DLJQ. Funding acquisition: BAB. Investigation: APR, DLJQ. Methodology: MKL, DLJQ. Project administration: BAB. Resources: MKL, KDL, CVA, APR. Supervision: BAB, DLJQ. Validation: APR, DLJQ, BAB. Visualization: DLJQ, BAB, CVA, APR, KDL. Writing – original draft: MKL. Writing – review and editing: DLJQ, APR, BAB.

Author ORCIDs

Donald L. J. Quicke  <https://orcid.org/0000-0003-4471-6775>

A. P. Ranjith  <https://orcid.org/0000-0001-7061-9659>

Marisa K. Loncle  <https://orcid.org/0000-0002-6221-7331>
Cornelis Van Achterberg  <https://orcid.org/0000-0002-6495-4853>
Khuat Dang Long  <https://orcid.org/0000-0002-9237-7344>
Buntika A. Butcher  <https://orcid.org/0000-0002-0541-0709>

Data availability

All of the data that support the findings of this study are available in the main text or Supplementary Information.

References

- Baltazar CR (1972) Reclassification of some Indo-Australian and African Braconinae and Rogadinae (Braconidae, Hymenoptera). *Philippine Journal of Science* 98: 259–277.
- Broad GR (2021) Taxonomic changes in Ichneumonoidea (Hymenoptera), and notes on certain type specimens. *Zootaxa* 4941(4): 511–541. <https://doi.org/10.11646/zootaxa.4941.4.3>
- Buckley TR, Simon C, Flook PK, Misof B (2000) Secondary structure and conserved motifs of the frequently sequenced domains IV and V of the insect mitochondrial large subunit rRNA gene. *Insect Molecular Biology* 9(6): 565–580. <https://doi.org/10.1046/j.1365-2583.2000.00220.x>
- Butcher BA, Quicke DLJ (2023) *Parasitoids Wasps of South East Asia*. CABI, Wallingford, 440 pp. <https://doi.org/10.1079/9781800620605.0000>
- Butcher BA, Smith MA, Sharkey MJ, Quicke DLJ (2012) A turbo-taxonomic study of Thai *Aleiodes* (*Aleiodes*) and *Aleiodes* (*Arcaleiodes*) (Hymenoptera: Braconidae: Rogadinae) based largely on COI bar-coded specimens, with rapid descriptions of 179 new species. *Zootaxa* 3457(1): 1–232. <https://doi.org/10.11646/zootaxa.3457.1.1>
- Butcher BA, Zaldivar-Riverón A, Van de Kamp T, Dos Santos Rolo T, Baumbach T, Quicke DLJ (2014) Extension of historical range of Betylobraconinae (Hymenoptera: Braconidae) into Palaearctic region based on a Baltic amber fossil, and description of a new species of *Mesocentrus* Szépligeti from Papua New Guinea. *Zootaxa* 3860(5): 449–463. <https://doi.org/10.11646/zootaxa.3860.5.4>
- Cameron P (1905) On the phytophagous and parasitic Hymenoptera collected by Mr. E. Ernest Green in Ceylon. *Spolia Zeylanica* 3: 67–143.
- Chen X-X, He J-H (1997) Revision of the subfamily Rogadinae (Hymenoptera: Braconidae) from China. *Zoologische Verhandlungen* 308: 1–187.
- Gillespie JJ, Yoder MJ, Wharton RA (2005) Predicted secondary structure for 28S and 18S rRNA from Ichneumonoidea (Insecta: Hymenoptera: Apocrita): impact on sequence alignment and phylogeny estimation. *Journal of Molecular Evolution* 61(1): 114–137. <https://doi.org/10.1007/s00239-004-0246-x>
- Granger C (1949) Braconides de Madagascar. *Memoires de l'Institut Scientifique de Madagascar (A)* 2: 1–428.
- Hebert PDN, Cywinska A, Ball SL, de Waard JR (2003) Biological identification through DNA barcodes. *Proceedings of the Royal Society of London Series A: Biological Sciences* 270: 96–99. <https://doi.org/10.1098/rspb.2002.2218>
- Ito M, Watanabe K, Maeto K (2015) Molecular evidence resolving the confusion of two species of *Spilopteron* (Hymenoptera: Ichneumonidae) caused by marked geographical color variation. *European Journal of Entomology* 112(3): 543–556. <https://doi.org/10.14411/eje.2015.068>

- Long KD (2014) New records of genus *Iporhogas* Granger (Hymenoptera, Braconidae, Rogadinae) from Vietnam, with description of four new species. *ZooKeys* 428: 79–96. <https://doi.org/10.3897/zookeys.428.7729>
- Long KD, van Achterberg C (2015) Review of the genus *Canalirogas* van Achterberg & Chen (Hymenoptera, Braconidae, Rogadinae) from Vietnam, with description of ten new species. *ZooKeys* 506: 27–59. <https://doi.org/10.3897/zookeys.506.9247>
- Park DS, Suh SJ, Oh HW, Hebert PDN (2010) Recovery of the mitochondrial COI barcode region in diverse Hexapoda through tRNA-based primers. *BMC Genomics* 11(1): 1–7. <https://doi.org/10.1186/1471-2164-11-423>
- Quicke DLJ (2015) *The Braconid and Ichneumonid Parasitic Wasps: Biology, Systematics, Evolution and Ecology*. Wiley Blackwell, Oxford, 688 pp. <https://doi.org/10.1002/9781118907085>
- Quicke DLJ, Shaw MR (2005) First host records for the rogadine genera *Rogasodes* Chen and He and *Canalirogas* van Achterberg and Chen (Hymenoptera: Braconidae) with description of a new species and survey of mummy types within Rogadinae s. str. *Journal of Natural History* 39(40): 3525–3542. <https://doi.org/10.1080/00222930500392782>
- Quicke DLJ, Smith MA, van Achterberg C, Miller SE, Hrcek J (2012) A new genus and three new species of parasitoid wasp from Papua New Guinea and redescription of *Trigonophatnus* Cameron (Hymenoptera, Braconidae, Rogadinae). *Journal of Natural History* 46(21–22): 1369–1385. <https://doi.org/10.1080/00222933.2012.658585>
- Quicke DLJ, Belokobylskij SA, Smith MA, Rota J, Hrcek J, Butcher BA (2016) A new genus of rhyssoline wasp (Hymenoptera: Braconidae) with modified wing venation from Africa and Papua New Guinea, parasitoid on Choreutidae (Lepidoptera). *Annales Zoologici* 66(2): 173–192. <https://doi.org/10.3161/00034541ANZ2016.66.2.003>
- Quicke DLJ, Fagan-Jeffries EP, Jasso-Martínez JM, Zaldivar-Riverón A, Shaw MR, Janzen DH, Hallwachs W, Smith MA, Hebert PDN, Hrcek J, Miller S, Sharkey MJ, Shaw SR, Butcher BA (2021) A molecular phylogeny of the parasitoid wasp subfamily Rogadinae (Ichneumonoidea: Braconidae) with descriptions of three new genera. *Systematic Entomology* 46(4): 1019–1044. <https://doi.org/10.1111/syen.12507>
- Quicke DLJ, Ranjith AP, Priyadarsanan DR, Nasser M, Hebert PDN, Butcher BA (2023) Two new genera and one new species of the tribe Adeshini (Hymenoptera, Braconidae, Braconinae) from India and South Africa. *ZooKeys* 1166: 235–259. <https://doi.org/10.3897/zookeys.1166.105589>
- Rambaut A (2018) *Figtree 1.4.4*. Institute of Evolutionary Biology, University of Edinburgh, Edinburgh.
- Ranjith AP, Rajan PD, Nasser M (2018) Revision of *Cystomastacoides* van Achterberg (Hymenoptera: Braconidae, Rogadinae) with the description of two new species from south India. *Zootaxa* 4387(2): 365–374. <https://doi.org/10.11646/zootaxa.4387.2.7>
- Ranjith AP, Quicke DLJ, Belokobylskij SA, Priyadarsanan DR (2022) *Kerevata* Belokobylskij (Hymenoptera: Braconidae: Rogadinae) is no longer a Papua New Guinean endemic with descriptions of three new species from the Indomalayan Region. *Zootaxa* 5091(2): 341–356. <https://doi.org/10.11646/zootaxa.5091.2.6>
- Ratnasingham S, Hebert PDN (2013) A DNA-based registry for all animal species: The Barcode Index Number (BIN) system. *PLoS One* 8(7): e66213. <https://doi.org/10.1371/journal.pone.0066213>
- Rishabanu K, Binoy C, Santhosh S (2021) Description of a new species of *Yelicones* Cameron, 1887 (Braconidae: Rogadinae) from Southern India. *Zootaxa* 5016(2): 294–298. <https://doi.org/10.11646/zootaxa.5016.2.10>

- Sharkey MJ, Wharton RA (1997) Morphology and terminology. In: Wharton RA, Marsh PM, Sharkey MJ (Eds) Manual of the New World Genera of the Family Braconidae (Hymenoptera). Allen Press, Lawrence, Kansas, 19–37.
- Songvorawit N, Quicke DLJ, Butcher BA (2021) Taxonomic progress and diversity of Ichneumonoid wasps (Hymenoptera: Ichneumonoidea) in Southeast Asia. *Tropical Natural History* 21: 79–93.
- Stamatakis A (2014) RAxML version 8: a tool for phylogenetic analysis and post-analysis of large phylogenies. *Bioinformatics* 30(9): 1312–1313. <https://doi.org/10.1093/bioinformatics/btu033>
- Tucker EM, Sharkey MJ (2016) Deserters of *Cremnops desertor* (Hymenoptera: Braconidae: Agathidinae): delimiting species boundaries in the *C. desertor* species-complex. *Systematics and Biodiversity* 14(4): 385–393. <https://doi.org/10.1080/14772000.2016.1150362>
- van Achterberg C (1988) Revision of the subfamily Blacinae Foerster (Hymenoptera: Braconidae). *Zoölogische Verhandelingen* 249: 1–324.
- van Achterberg C (1991) Revision of the genera of the Afrotropical and W. Palaearctic Rogadinae Foerster (Hymenoptera: Braconidae). *Zoölogische Verhandelingen* 273: 1–102.
- van Achterberg C, Chen X (1996) *Canalirogas*, a new genus of the subfamily Rogadinae Foerster (Hymenoptera: Braconidae) from the Indo-Australian region. *Zoologische Mededelingen Leiden* 70(3): 63–92.
- van Achterberg C, Shaw MR, Quicke DLJ (2020) Revision of the western Palaearctic species of *Aleiodes* Wesmael (Hymenoptera, Braconidae, Rogadinae). Part 2: Revision of the *A. apicalis* group. *ZooKeys* 919: 1–259. <https://doi.org/10.3897/zookeys.919.39642>
- Wu Q-L, Li Q, Gu Y, Shi B-C, van Achterberg C, Wei S-J, Chen X-X (2014) The complete mitochondrial genome of *Taeniogonalos taihorina* (Bischoff) (Hymenoptera: Trigonalyidae) reveals a novel gene rearrangement pattern in the Hymenoptera. *Gene* 543(1): 76–84. <https://doi.org/10.1016/j.gene.2014.04.003>
- Yu DSK, van Achterberg C, Horstmann K (2016) Taxapad 2016, Ichneumonoidea 2015. Nepean, Ontario, Canada. <http://www.taxapad.com> [database on flash-drive]
- Zaldivar-Riverón A, Shaw MR, Saez AG, Mori M, Belokobylskij SA, Shaw SR, Quicke DLJ (2008) Evolution of the parasitic wasp subfamily Rogadinae (Braconidae): Phylogeny and evolution of lepidopteran host ranges and mummy characteristics. *BMC Evolutionary Biology* 8(1): 329. <https://doi.org/10.1186/1471-2148-8-329>

Supplementary material 1

Provenances of sequenced specimens, DNA barcode index numbers (BINs), and GenBank accessions number

Authors: Donald L. J. Quicke, A. P. Ranjith, Marisa K. Loncle, Cornelis Van Achterberg, Khuat Dang Long, Buntika A. Butcher

Data type: docx

Copyright notice: This dataset is made available under the Open Database License (<http://opendatacommons.org/licenses/odbl/1.0/>). The Open Database License (ODbL) is a license agreement intended to allow users to freely share, modify, and use this Dataset while maintaining this same freedom for others, provided that the original source and author(s) are credited.

Link: <https://doi.org/10.3897/zookeys.1206.120824.suppl1>

Integrative taxonomic study of mononchid nematodes from riparian habitats in Bulgaria. I. Genera *Mononchus* Bastian, 1865 and *Coomansus* Jairajpuri & Khan, 1977 with the description of *Mononchus pseudoaquaticus* sp. nov. and a key to the species of *Mononchus*

Stela Altash¹, Aneta Kostadinova¹ , Vlada Peneva¹

¹ Institute of Biodiversity and Ecosystem Research, Bulgarian Academy of Sciences, 2 Gagarin Street, 1113 Sofia, Bulgaria
Corresponding author: Vlada Peneva (esn.2006@gmail.com)



Academic editor: Sergei Subbotin
Received: 30 March 2024
Accepted: 12 May 2024
Published: 5 July 2024

ZooBank: <https://zoobank.org/C1AC9890-1735-4929-B1D5-2056B7E8AFBE>

Citation: Altash S, Kostadinova A, Peneva V (2024) Integrative taxonomic study of mononchid nematodes from riparian habitats in Bulgaria. I. Genera *Mononchus* Bastian, 1865 and *Coomansus* Jairajpuri & Khan, 1977 with the description of *Mononchus pseudoaquaticus* sp. nov. and a key to the species of *Mononchus*. ZooKeys 1206: 137–180. <https://doi.org/10.3897/zookeys.1206.124237>

Copyright: © Stela Altash et al.
This is an open access article distributed under terms of the Creative Commons Attribution License (Attribution 4.0 International – CC BY 4.0).

Abstract

The species diversity of the genera *Mononchus* Bastian, 1865 and *Coomansus* Jairajpuri & Khan, 1977 was assessed in a study of the mononchid nematodes from a wide range of riparian habitats in Bulgaria. Four species were identified based on morphological and morphometric data: *Coomansus parvus* (de Man, 1880), *Mononchus truncatus* Bastian, 1865, *Mononchus pseudoaquaticus* sp. nov., and *Mononchus* sp. The first three species were characterised both morphologically and molecularly (18S and 28S rRNA gene sequences) and the integration of these data and phylogenetic analyses provided support for their distinct species status. This paper provides detailed descriptions, morphometric data for multiple species populations, drawings and photomicrographs, and the first taxonomically verified sequences for *C. parvus* ($n = 6$), *M. truncatus* (sensu stricto) ($n = 4$) and *M. pseudoaquaticus* sp. nov. ($n = 3$). Comparative sequence and phylogenetic analyses suggested that the utility of the 18S rRNA gene for species delimitation is rather limited at least for some species complexes within the genus *Mononchus*. At the generic and suprageneric level, the 18S and 28S rDNA phylogenies both recovered the three genera represented by two or more species (*Mononchus*, *Mylonchulus*, and *Parkellus*) as monophyletic with strong support, the Mononchidae as paraphyletic, the Anatonchidae as monophyletic, and there was no support for a sister-group relationship between *Mylonchulus* and *Mononchus*. A key to the species of *Mononchus* is provided to facilitate the identification of the currently recognised 31 species.

Key words: Distribution, Mononchidae, morphology, phylogeny, riverine, taxonomy, 18S rDNA, 28S rDNA

Introduction

Riparian zones, i.e., the ecotones between aquatic and terrestrial ecosystems, represent areas of high biodiversity caused by the diversity of habitats and heterogeneous environmental conditions they provide. Both plant and animal diversity are high in these areas with impressive levels of faunal diversity in

riparian soils (Décamps et al. 2009). Soils in these functionally unique ecosystems are also important for sustaining diverse nematode communities, e.g., Décamps et al. (2009) estimated the number of species of nematodes in riparian soils to be greater than 5000. Because soil nematodes are abundant and functionally diverse, they can serve as useful indicators of food-web structure and complexity (Bongers and Ferris 1999; Ferris et al. 2001; Neher 2001; Ferris 2005); nematode communities are also important for ecosystem functions. These features justify the increased interest in studying free-living nematode communities and the ecosystem functions they perform in both undisturbed and disturbed riparian zones and riparian corridors (e.g., Young-Mathews et al. 2010; Briar et al. 2012; Hodson et al. 2014). Notably, nematodes are usually identified to the genus/family level in these ecological studies due to difficulties in the identification based on morphological characters and/or the lack of taxonomic expertise, so there is a lack of species-level assessments on larger-scale processes in riparian zones (Bardgett et al. 2001).

Sequence-based tools such as barcoding have proven successful in accelerating identification of previously characterised species or in detecting cryptic species (Palomares-Rius et al. 2014, 2022; Archidona-Yuste et al. 2023). Currently, two nuclear loci are considered to be most relevant to barcoding of nematodes, the small subunit ribosomal RNA gene (SSU or 18S) and the large subunit ribosomal RNA gene (LSU or 28S), the first being the best sampled gene in nematodes, and the second being the subject of increased interest. However, key for the successful application of barcoding for nematodes is the availability of a database of taxonomically verified sequences, i.e., associated with species identification based on detailed morphological characterisation and morphological vouchering (physical and “virtual” vouchers sensu De Ley et al. 2005). Although the number of species of the order Mononchida Jairajpuri, 1969 with sequences available for both nuclear loci indicated above is limited, a recent trend towards building a combined evidence database is promising (Kim et al. 2018; Tabolin and Kolganova 2020; van Rensburg et al. 2021; Vu 2021; Vu et al. 2021a, 2021b; Shokoohi and Moyo 2022).

In a study of the free-living nematodes from a wide range of riparian habitats in Bulgaria, we have collected several species of three families of the order Mononchida. These have been characterised both morphologically and molecularly. This paper presents the results of the integrative taxonomic study of the species of *Coomansus* Jairajpuri & Khan, 1977 and *Mononchus* Bastian, 1865 (family Mononchidae Chitwood, 1937), and phylogenetic analyses that delineate the species and establish their relationships within the suborder Mononchina Kirjanova & Krall, 1969 based on partial sequences of the 28S and 18S rRNA genes.

Species of the order Mononchida occur in both aquatic and terrestrial habitats. Species of the genus *Mononchus* are aquatic nematodes, occasionally occurring in wet terrestrial habitats (Zullini and Peneva 2006; Andrásy 2009) unlike the species of the second genus considered here, *Coomansus*, which predominantly dwell in terrestrial habitats. Currently, the genus *Mononchus* contains 30 species (Andrásy 2011a; Shah and Hussain 2016; Gagarin and Naumova 2017; Ishaque et al. 2022). According to Andrásy (2009) the number of valid species of *Coomansus* is 28. Subsequently, five new species have been described (Andrásy 2011b; Shah and Hussain 2015; Vu 2021). Ahmad and Jairajpuri (2010)

transferred the species of the *Coomansus* “*zschokkei*-group” to the genus *Parkellus* Jairajpuri, Tahseen & Choi, 2001; however, the validity of *Parkellus* is not widely accepted (e.g., Zullini and Peneva 2006; Andr ssy 2009, 2011b).

In Bulgaria, two species of the genus *Coomansus*, *C. parvus* (de Man, 1880) Jairajpuri & Khan, 1977 and *Coomansus zschokkei* (Menzel, 1913) Jairajpuri & Khan, 1977 have been reported (Iliev and Ilieva 2016). Two further species of the genus *Mononchus*, *M. truncatus* Bastian, 1865 and *M. aquaticus* Coetzee, 1968 have also been recorded; however, morphological data have not been provided (Andr ssy 1958; Katalan-Gateva 1962, 1965; Stoichev 1996; Lazarova et al. 2004; Stoichev and Chernev 2011; Stoichev and Varadinova 2011). Only the latter two species have been reported in aquatic habitats.

Materials and methods

Sampling, nematode isolation, and processing

More than 150 soil and litter samples were collected at 76 localities in different riparian zones in Bulgaria. Multiple core soil samples (3 per site) were collected at a depth of 40–60 cm from each habitat (sampling site of 15 × 15 m or along the riverbank) around the roots of the dominant tree species; litter samples were collected simultaneously.

Nematodes were extracted from soil (at least 400 g) and litter (at least 20 g) samples using a decanting and sieving technique and a modified Baerman funnel method with 48 h of exposition and counted alive. Thereafter, the nematodes were gently heated at 63 °C for 2 min and fixed in 4% formaldehyde, 1% glycerine, dehydrated, and mounted on permanent slides in anhydrous glycerine with paraffin as a support for the cover slide (Seinhorst 1959). Morphological examination was carried out and measurement taken under a light microscope (Olympus BX41, Tokyo, Japan) equipped with a digitising tablet (CalComp Drawing Board III) and using the DIGITRAK 1.0 f program (Philip Smith, the John Hutton Institute, Dundee, UK). Drawings were prepared using an Olympus BX51 compound microscope with differential interference contrast (DIC). Photomicrographs were taken with Axio Imager.M2 microscope (Carl Zeiss, Oberkochen, Germany) equipped with a digital camera (ProgRes C7) and CapturePro 2.8 software (Jenoptic).

All measurements in the descriptions and tables are in micrometres unless stated otherwise and are given as the mean ± standard deviation followed by the range in parentheses. A standard set of De Man indices was calculated for each specimen as follows: *L*, body length; *V*, distance from vulva to anterior end of body as % of body length; *a*, body length/greatest body diameter; *b*, body length/distance from anterior end to pharyngo-intestinal valve; *c*, body length/tail length; *c'* tail length/tail diameter at anus; *G1* anterior female gonad length as % of body length; *G2* posterior female gonad length as % of body length (De Man 1876, 1880).

DNA isolation, amplification, and sequencing

Specimens intended for the molecular study were identified on temporary mounts; a standard set of photomicrographs was taken for each specimen. Genomic DNA (gDNA) was isolated using 5% suspension of deionised water

and Chelex®, containing 0.1 mg/ml proteinase K; samples were incubated at 56 °C for 3 h or overnight, boiled at 90 °C for 8 min, and centrifuged at 14,000× g for 10 min. Two genetic markers were sequenced, the small (18S) and the large (28S) ribosomal subunit RNA coding regions.

Partial fragments of the 28S rRNA gene (domains D1-D3; ~ 1000 bp) were amplified using the forward primer LSU5 (5'-TAG GTC GAC CCG CTG AAY TTA AGC A-3') (Littlewood et al. 2000) and the reverse primer 1500R (5'-GCT ATC CTG AGG GAA ACT TCG-3') (Tkach et al. 1999). Nearly complete (~ 1600–1700 bp) fragments of the 18S rRNA gene were amplified in two partially overlapping fragments using the primer sets 988F (forward: 5'-CTC AAA GAT TAA GCC ATG C-3') and 1912R (reverse: 5'-TTT ACG GTC AGA ACT AGG G-3') for the first fragment, and 1813F (forward: 5'-CTG CGT GAG AGG TGA AAT-3') and 2646R (reverse: 5'-GCT ACC TTG TTA CGA CTT TT-3') for the second fragment (Holterman et al. 2006).

PCR amplifications were performed in a total volume of 25 µl using Illustra™ PuReTaq™ Ready-To-Go™ PCR beads (GE Healthcare, Chicago, USA; Cat. # 27-9559-01). In the case of poor amplification, the PCR reactions were performed with 2× MyFi™ DNA Polymerase mix (Bioline Inc., Taunton, USA; Cat. # BIO-25049) in a total volume of 20 µl, containing 8 pmol of each primer and ~ 50 ng of gDNA. The amplification profile for 28S rDNA comprised an initial denaturation at 94 °C for 5 min (or 3 min when using MyFi™ DNA Polymerase mix) followed by 40 cycles (30 s at 94 °C; 30 s at 55 °C; and 2 min at 72 °C), and a final extension step at 72 °C for 7 min. The following amplification profile was used for 18S rDNA: initial denaturation at 94 °C for 5 min, followed by 5 cycles (30 s at 94 °C; 30 s at 45 °C; 70 s at 72 °C) and 35 cycles (30 s at 94 °C; 30 s at 54 °C; 70 s at 72 °C), and a final extension step at 72 °C for 5 min. PCR amplicons were purified and sequenced directly for both strands using the PCR primers (and in some cases the internal primers 300F, ECD2 and LSU1200R (Littlewood et al. 2000) for 28S rDNA) at Macrogen Europe (Amsterdam, the Netherlands). Contiguous sequences were assembled, quality checked, and edited manually using MEGA7 (Kumar et al. 2016) and subjected to a BLASTn search on the NCBI GenBank database.

Phylogenetic analyses

The newly generated 18S rDNA and 28S rDNA sequences were aligned separately using MUSCLE implemented in MEGA7 (Kumar et al. 2016) with representative sequences available in the GenBank database. First, an exploratory neighbour-joining (NJ) analysis was carried out on an untrimmed 28S rDNA alignment (domains D1-D3), including representative sequences for *Mononchus* spp. and *Coomansus* spp. to assess the associations of the newly generated sequences from riparian nematode populations sampled in Bulgaria.

Secondly, two alignments were constructed comprising sequences for species of three families of the suborder Mononchina: Anatonchidae Jairajpuri, 1969, Mononchidae, and Mylonchulidae Jairajpuri, 1969. These alignments were trimmed to the length of the shortest sequence. The 28S rDNA alignment (domains D2-D3) contained 33 sequences for representatives of ten genera

of the three families and the 18S rDNA alignment contained 32 sequences for representatives of ten genera of the three families.

Phylogenetic relationships were estimated by conducting maximum likelihood (ML) analyses as implemented in MEGA7. Prior to analyses, the best-fitting models of nucleotide substitution were estimated based on the Akaike information criterion (AIC); these were the Tamura 3-parameter model (T92) including estimates of invariant sites and among-site rate heterogeneity (T92+I+G) for the 18S rDNA alignment and the Kimura 2-parameter model (K2) with among-site rate heterogeneity (K2+G) for the 28S rDNA alignment. Nodal support was estimated by performing 1000 bootstrap pseudoreplicates. *Mermis nigrescens* Dujardin, 1842 was used as the outgroup in the analyses of both alignments based on the phylogeny published by Holterman et al. (2006). Genetic distances (number of nucleotide positions and uncorrected p-distance) were calculated in MEGA7.

Results

Overview of the morphological identification and the novel molecular and distributional data

A total of 17 populations of *Coomansus* spp. and *Mononchus* spp. were collected in soil and litter samples from habitats with various vegetation types along 12 rivers (Arda, Danube, Devinska, Dyavolska, Grafaska, Lopushnitsa, Maritsa, Rezovska, Shirokoleshka, Trigradska, Vedena, and Veleka) in eight provinces in Bulgaria (Burgas, Kardzhali, Lovech, Montana, Plovdiv, Silistra, Smolyan, and Sofia). In each locality, the nematode populations were recovered around the roots of the dominant tree species (predominantly *Salix* spp., but also *Alnus glutinosa* (L.), *Carpinus betulus* L., *Fagus sylvatica* L., *Fraxinus excelsior* L., *Populus* sp., *Ulmus laevis* Pall., and *Ulmus* sp.) (Table 1).

Four species were identified based on morphological data: *C. parvus* (4 populations), *M. truncatus* (7 populations), *Mononchus pseudoaquaticus* sp. nov. (5 populations), and *Mononchus* sp. (1 population). The geographical distribution of *Mononchus* spp. (9 localities) did not overlap that of the single species of *Coomansus* recovered during the study (4 localities) (Table 1). Of note, populations of the two widespread species of *Mononchus*, *M. truncatus* and *M. pseudoaquaticus* sp. nov., co-occurred in four localities (along riverbanks of the rivers Danube, Maritsa, Shirokoleshka, and Veleka).

Although an attempt was made to obtain representative 28S rDNA sequences for all species populations, the success rate was generally low. A total of nine sequences were generated, four for *C. parvus* (1017–1037 bp), three for *M. truncatus* (987–1041 bp), and two for *M. pseudoaquaticus* sp. nov. (910–1042 bp). Four of the sequenced populations were selected for generating representative 18S rDNA sequences (1630–1682 bp; 2 for *C. parvus*, 1 for *M. truncatus*, and 1 for *M. pseudoaquaticus* sp. nov.). No sequences were generated for *Mononchus* sp. The newly generated 28S rDNA sequences showed very low intraspecific genetic divergence (0–2 nt positions, i.e., 0.2% for sequences for *C. parvus* and *M. truncatus*, and identical sequences for *M. pseudoaquaticus* sp. nov.); the two 18S rDNA sequences for *C. parvus* were also identical.

Table 1. Summary data for the populations of *Coomansus parvus* and *Mononchus* spp. studied in 17 riparian habitats in Bulgaria.

Species	River	Locality	Coordinates	Elevation (m) ^a	Associated tree species (habitat)	Date (Collector)
<i>Coomansus parvus</i> (de Man, 1880)	Lopushnitsa (Balkan Mountains)	Near Kaleytsa, Lovech Province	42°55'34"N, 24°38'38"E	~ 440	<i>Acer</i> sp. (litter)	9.05.2021 (VP)
	Arda (Rhodope Mountains)	Dyavolski Most, Kardzhali Province	41°37'14"N, 25°06'53"E	~ 460	<i>Ulmus</i> sp. (soil)	29.08.2020 (VP)
			41°37'22"N, 25°06'54"E	~ 440	<i>Populus</i> sp. (soil)	
	Vedena (Vitosha Mountain)	Near Zheleznya, Sofia Province	42°32'05"N, 23°20'57"E	~ 1200	<i>Fagus sylvatica</i> L. (litter)	4.04.2022 (SA, VP)
Devinska (Rhodope Mountains)	Near Devin, Smolyan Province	41°45'21"N, 24°20'02"E	~ 880	<i>Carpinus betulus</i> L. (soil)	20.05.2019 (SA)	
<i>Mononchus truncatus</i> Bastian, 1865	Shirokoleshka (Rhodope Mountains)	Shiroka Laka, Smolyan Province	41°40'26"N, 24°35'51"E	~ 1120	<i>Salix</i> sp. (soil)	23.05.2019 (SA)
	Maritsa (Upper Thracian Plain)	Near Plovdiv, Plovdiv Province	42°09'N, 25°50'E	~ 153	<i>Salix</i> sp. (soil)	18.10.1995 (VP)
	Trigradska (Rhodope Mountains)	Teshel, Smolyan Province	41°40'18"N, 24°21'13"E	~ 860	<i>Salix</i> sp. (litter)	23.05.2019 (SA)
	Dyavolska (Strandzha Mountains)	Near Primorsko, Burgas Province	42°15'34"N, 27°44'18"E	~ 10	<i>Fraxinus excelsior</i> L. (soil)	6.06.2019 (SA)
	Rezovska (Strandzha Mountains)	Slivarovo, Burgas Province	41°57'N, 27°40'E	~ 240	<i>Ulmus laevis</i> Pall. (soil)	22.10.2008 (RS)
	Danube (Southern Dobruja)	Vetren, Silistra Province	44°08'24"N, 27°01'47"E	~ 20	<i>Salix</i> sp. (soil)	5.07.2021 (VP)
	Veleka	Brodilovo, Burgas Province	42°04'53"N, 27°51'33"E	~ 15	<i>Alnus glutinosa</i> (L.) (soil)	4.06.2019 (SA)
	<i>Mononchus pseudoaquaticus</i> sp. nov.	Shirokoleshka (Rhodope Mountains)	Shiroka Laka, Smolyan Province	41°40'26"N, 24°35'51"E	~ 1120	<i>Salix</i> sp. (soil)
Maritsa (Upper Thracian Plain)		Near Plovdiv, Plovdiv Province	42°09'N, 25°50'E	~ 153	<i>Salix</i> sp. (soil)	18.10.1995 (VP)
Veleka		Brodilovo, Burgas Province	42°04'53"N, 27°51'33"E	~ 15	<i>Alnus glutinosa</i> (L.) (soil)	4.06.2019 (SA)
Danube (Southern Dobruja)		Vetren, Silistra Province	44°08'24"N, 27°01'47"E	~ 20	<i>Salix</i> sp. (soil) ^b	5.07.2021 (VP)
Danube (Southern Dobruja)		Komluka Island, Silistra Province	44°08'03"N, 27°03'40"E	~ 20	<i>Populus</i> sp. (soil)	5.07.2021 (VP)
<i>Mononchus</i> sp.	Grafska, inflow of River Kopilovtsi (Balkan Mountains)	Waterfall "Durshin skok", near Kopilovtsi, Montana Province	43°19'40"N, 22°51'01"E	~ 1048	<i>Fagus sylvatica</i> L. (soil)	27.07.2000 (VP)

Abbreviations: RS, Rabia Soufi; SD, Stela Altash; VP, Vlada Peneva.

^a Metres above sea level.^b Type-population.

Taxonomy

Genus *Coomansus* Jairajpuri & Khan, 1977

Coomansus parvus (de Man, 1880) Jairajpuri & Khan, 1977

Figs 1, 2

Description. Female [Based on 10 specimens from 3 localities; see Table 2 for measurements]. Body short, 0.70–1.15 mm, J- or C-shaped upon relaxation,

body diameter at mid-body 47–53. Cuticle smooth under light microscope (very faint striation observed in one specimen, Fig. 2H), 2–3 thick along most of body, 3–4 thick in post-anal region. Lip region offset, cephalic and labial papillae prominent, conical, of almost same size. Amphid apertures oval, 5 ± 0.4 (4–5) ($n = 6$) wide, situated anterior to dorsal tooth apex, at 10–14 from anterior end. Buccal capsule oval, somewhat flattened at base, 1.6–1.9 as long as wide or 0.9–1.2 times as long as lip region width; its ventral wall 1.5–2.5 thick, dorsal wall posterior to dorsal tooth ~ 3 thick. Dorsal tooth small, its anterior margin 3.0 ± 0.5 (2–4) wide, located near middle of buccal capsule, tooth apex at 9 ± 1 (8–11) from anterior end of buccal capsule. Nerve-ring at 97 ± 6 (90–103) ($n = 6$) from anterior end of body. Excretory pore posterior to nerve-ring, small, well visible. Reproductive system amphidelphic. Genital branches almost symmetrical; anterior branch 134 ± 50 (80–253) ($n = 9$) long; posterior branch 115 ± 19 (80–133) ($n = 9$) long. Ovaries well developed; anterior ovary 60–105 ($n = 7$) long; posterior ovary 70–140 ($n = 7$) long. Oviduct with marked *pars dilatata oviductus*, ~ 30 wide. Uteri very short. Two uterine eggs present in one female measuring 81×40 and 90×38 . Vagina with straight walls, its length representing 25–33% of corresponding body width; *pars refringens vaginae* as 2 oval to drop-shaped smooth sclerotised pieces, 3–4 long and 2–3 wide; *pars distalis vaginae* ~ 3 long. Vulva a transverse slit; *pars refringens vaginae* protruding in some specimens (Fig. 2I). Rectum 0.7–0.8 times as long as body diameter at anus. Tail conoid, ventrally arcuate, with finely rounded tip. Caudal glands and spinneret absent. Caudal pores two pairs. **Male:** Not found.

Voucher material. Ten specimens are deposited in the Nematological Collection of the Institute of Biodiversity and Ecosystem Research, Bulgarian Academy of Sciences, Bulgaria, under the accession numbers IBER-BAS NC 49/1, IBER-BAS NC 51/2, IBER-BAS PN 68/4 litter, IBER-BAS NC 88/4, IBER-BAS NC 88/7-9. Photovouchers for the sequenced specimens are provided in Suppl. material 1: figs S1–S3.

Habitats and localities. Soil around *Ulmus* sp., *Populus* sp., and *C. betulus* and litter around *F. sylvatica* and *Acer* sp. along riverbanks of the rivers Arda, Lopushnitsa, Vedena, and Devinska (see Table 1 for details).

Representative DNA sequences. 28S rRNA gene (GenBank: PP768895–PP768898); 18S rRNA gene (GenBank: PP768899 and PP768900).

Distribution. Almost cosmopolitan, except in Australia (Andrássy 2009). In Bulgaria, *C. parvus* has been reported with no morphological evidence supporting identification in soil samples from an oak forest in Burgas Province (Aleksiev et al. 1998), from beech forests in Strandzha Mountain (Strandzha Nature Park, protected zones “Bjalata prust” and “Propada”; Iliev and Ilieva 2014), and from arable lands in Sofia (Katalan-Gateva 1968) and Kazanlak provinces (Katalan-Gateva et al. 1981). Iliev and Ilieva (2016) described and illustrated *C. parvus* based on a large population of females in soil samples from one habitat in the Rhodope Mountains. The present study provides the second documented record of *C. parvus* in Bulgaria, the first record of this species in litter samples, and four new localities in three provinces (Tables 1, 2).

Remarks. Morphologically, the present material belongs to and was identified as *C. parvus*. Some variation was detected in the present material with single specimens from three populations sampled in the Rhodope and Balkan Mountains showing lower values for *L*, *a*, *G1*, *G2*, the length of the genital branches,

Table 2. Morphometric data for females of *Coomansus parvus* collected in four riparian localities in Bulgaria.

Locality	Near Kaleytsa, Lovech Province	Dyavolski Most, Kardzhali Province		Near Zheleznița, Sofia Province
River	Lopushnitsa (Balkan Mountains)	Arda (Rhodope Mountains)		Vedena (Vitosha Mountain)
Habitat	<i>Acer</i> sp. (litter)	<i>Ulmus</i> sp. (soil)	<i>Populus</i> sp. (soil)	<i>Fagus sylvatica</i> (litter)
<i>n</i>	(<i>n</i> = 1)	(<i>n</i> = 1)	(<i>n</i> = 2)	(<i>n</i> = 6)
<i>L</i> (mm)	1.05	0.70	0.90, 1.07	0.96 ± 0.14 (0.83–1.15)
<i>a</i>	18.7	12.9	17, 17	19.0 ± 2.5 (16.2–21.7)
<i>b</i>	3.6	3.7	3.5, 3.5	3.2, 3.4, 3.5 (<i>n</i> = 3)
<i>c</i>	14.8	11.7	12.2, 12.9	12.7 ± 1.1 (11.5–14.0)
<i>c'</i>	2.3	2.1	2.4, 2.3	2.3 ± 0.3 (2.0–2.7)
<i>V</i> (%)	62.0	59.9	61.3, 62.2	62.5 ± 1.6 (59.6–64.5)
<i>G1</i> (%)	9.2	11.4	12.2, 10.5	13.8 ± 2.4 (12.0–17.3) (<i>n</i> = 5)
<i>G2</i> (%)	12.6	11.3	10.2, 11.4	12.6 ± 1.5 (11.6–15.1) (<i>n</i> = 5)
Buccal capsule length	24	22	23, 26	26 ± 1 (25–27)
Buccal capsule width	14	14	14, 15	15 ± 0.4 (14–15)
Tooth apex from anterior end of buccal capsule	9	11	8, 8	9 ± 0.4 (9–10)
Position of tooth apex (%) ^a	38	–	36, 32	35 ± 2 (33–38)
Excretory pore from anterior end	116	–	110, 113	117 ± 15 (97–131)
Nerve-ring from anterior end	92	–	90, –	100 ± 4 (94–103) (<i>n</i> = 4)
Pharynx length	294	189	258, 302	303, 324, 324 (<i>n</i> = 3)
Lip region height	8	7	8, 8	8 ± 1 (7–10) (<i>n</i> = 4)
Lip region width	25	23	25, 25	24 ± 3 (22–28) (<i>n</i> = 4)
Amphid from anterior end	11	14	14, 11	10 (<i>n</i> = 2)
Maximum body diameter	56	54	53, –	50 ± 2 (48–53)
Body diameter at pharynx base	49	49	51, –	46 ± 3 (43–50) (<i>n</i> = 5)
Body diameter at mid-body	49	53	51, –	50 ± 2 (48–53)
Body diameter at vagina	56	54	53, –	50 ± 2 (48–53)
Body diameter at anus	31	28	31, 36	33 ± 2 (31–36)
Anterior genital branch length	96	80	110, 112	161 ± 53 (118–253) (<i>n</i> = 5)
Posterior genital branch length	132	80	92, 122	122 ± 11 (106–133) (<i>n</i> = 5)
Anterior ovary length	90	70	60, 80	100, 105, 105
Posterior ovary length	105	75	70, 100	86, 110, 140
Vagina length	17	17	16, 18	14 ± 2 (12–16) (<i>n</i> = 5)
Rectum length	23	21	24; 26	23 ± 2 (21–25)
Tail length	71	60	74; 83	75 ± 8 (66–85)

^a Distance from tooth apex to anterior end of buccal capsule as % of buccal capsule length from its anterior

ovaries, and tail, and greater values for the distance of the amphid from anterior end compared with the population from Vitosha Mountain (Table 2). We consider these small metrical differences to represent intraspecific variation; this was confirmed by the very low levels of genetic divergence (see above).

The morphometric data for the present material fall within the range given by Andr assy (2011b), except for the slightly greater values for the width of the buccal capsule (14–15 vs 10–12 μ m). Comparisons with published descriptions

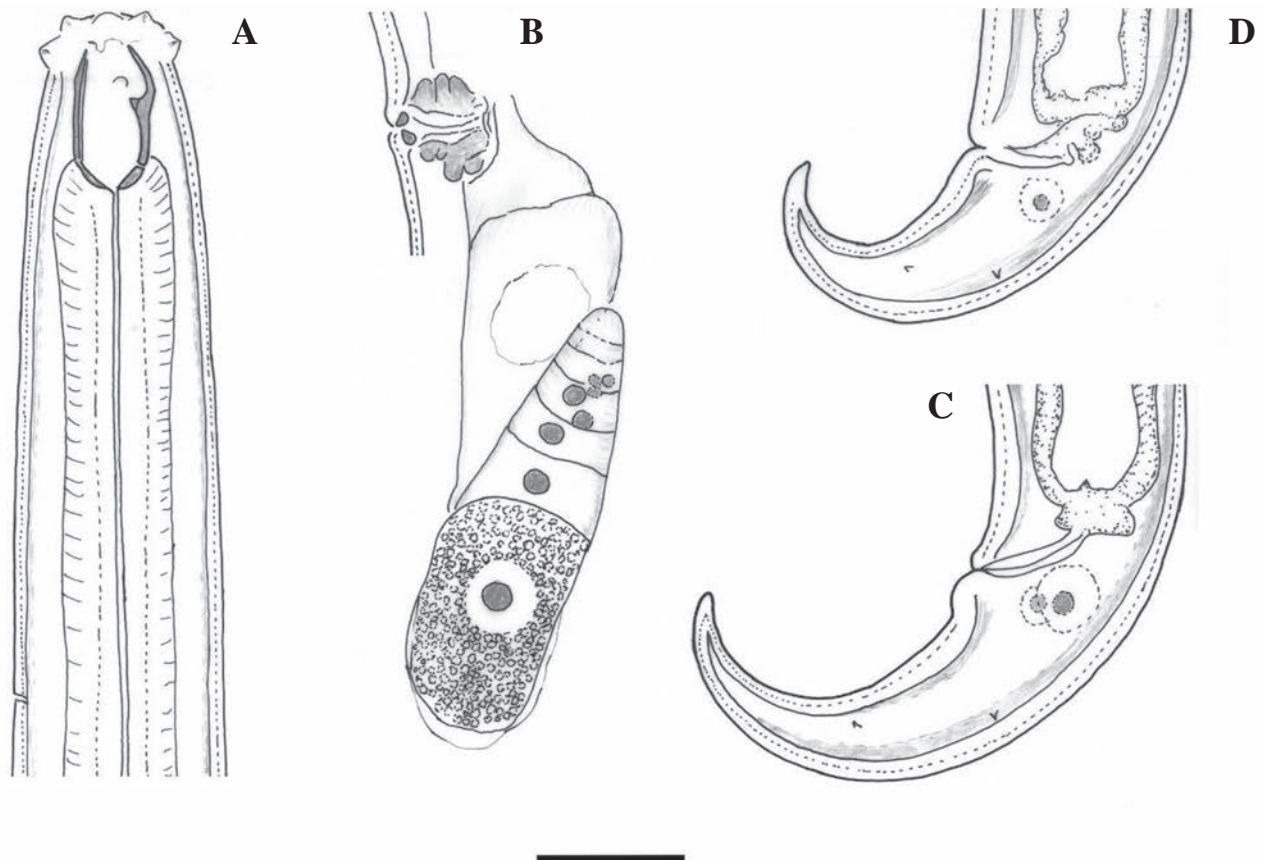


Figure 1. Line drawings of *Coomansus parvus* (de Man, 1880) Jairajpuri & Khan, 1977. Female specimens from populations collected from riverbanks of the rivers Vedena (**A, B, D**) and Arda (**C**): **A** anterior region **B** posterior genital branch **C, D** tail end. Scale bar: 25 μ m.

of *C. parvus* revealed an overlap with the morphometric data of the present material but also a greater variation with higher upper limits of variation for the published ranges of body length (Zullini et al. 2002; Ahmad and Jairajpuri 2010; Ishaque et al. 2022) and most of the indices, and lower ranges for the width of the buccal capsule in four populations falling below the range recorded in the present specimens (Suppl. material 2: table S1). It is worth noting that there was an overall good agreement with the descriptions and morphometric data for a population of *C. parvus* collected in Bulgaria by Iliev and Ilieva (2016) and especially with a population used for generating 18S rDNA and 28S rDNA sequences for this species described by Tabolin and Kolganova (2020).

However, the material described by Ishaque et al. (2022) showed little overlap with the published descriptions and the present material, with ranges for a number of characters falling outside the known ranges for *C. parvus*: outside the upper limits of variation (*L*, *V*, buccal capsule length and width, lip region width, and rectum length); and outside the lower limits of variation (*G1*, *G2*, and position of tooth apex) (Suppl. material 2: table S1). This material keys down to *C. indicus* Jairajpuri & Khan, 1982 in the key to species of *Coomansus* by Andr assy (1993, 2009) and to *C. ulsani* Choi, Khan & Lee, 1999 in the key by Vu (2021) but does not agree completely with the data for these species. Clearly, the material of Ishaque et al. (2022) does not belong to *C. parvus* but definite identification is not possible based on the available data and illustrations (also see comments in Suppl. material 2: table S1).

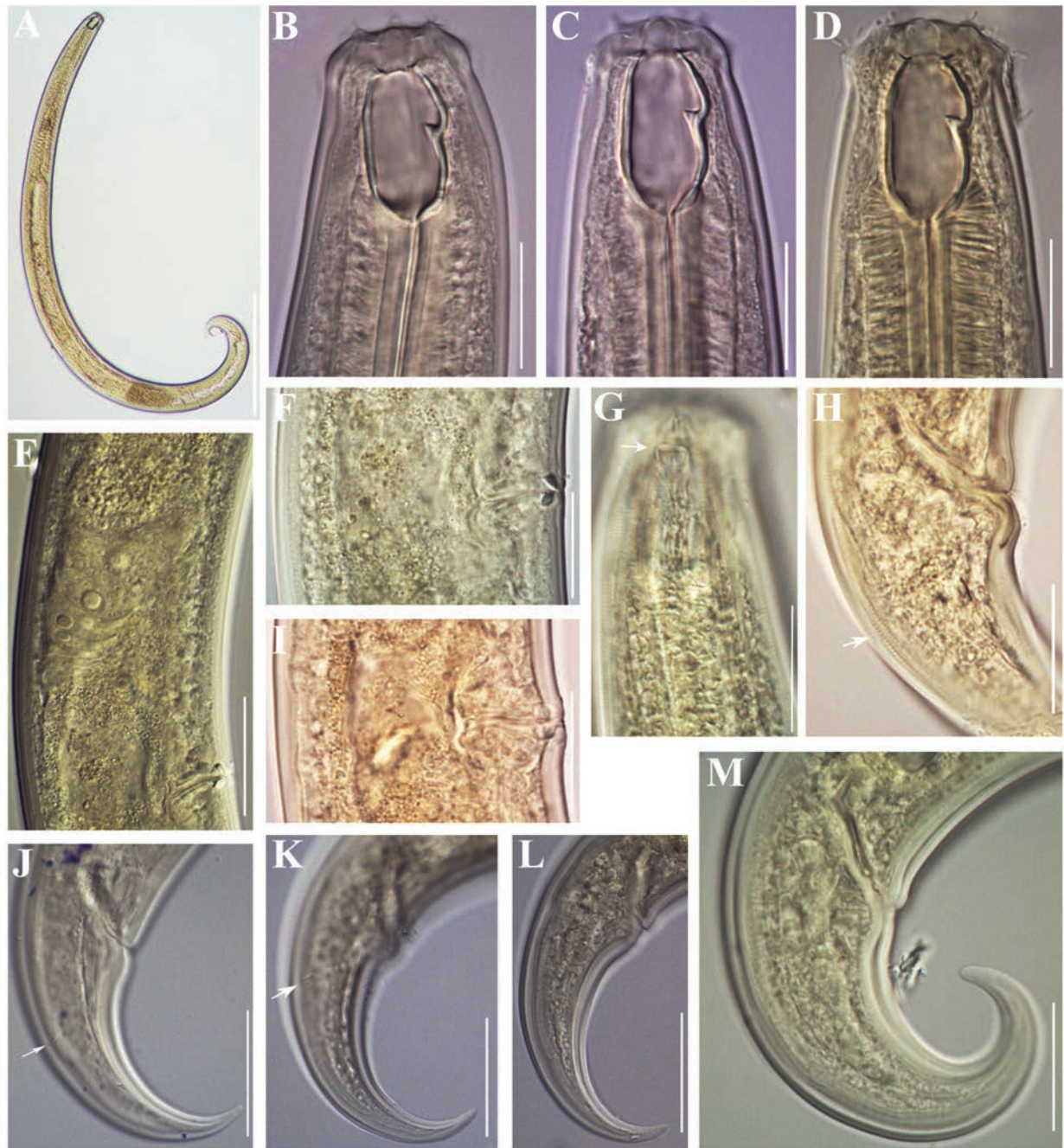


Figure 2. Photomicrographs of *Coomansus parvus* (de Man, 1880) Jairajpuri & Khan, 1977. Female specimens from populations collected from riverbanks of the rivers Lopushnitsa (**A, B, E–G, M**), Vedena (**C, D, H, I, K, L**), and Arda (**J**): **A** entire body **B–D, G** anterior region (amphid opening arrowed in **G**) **E, F, I** reproductive system (**E** anterior genital branch **F, I** vulval region showing *pars refringens vaginae*) **H, J–M** tail (cuticle striation arrowed in **H**; caudal pores arrowed in **J** and **K**). Scale bars: 200 μm (**A**); 20 μm (**B–D, F–I, M**); 50 μm (**E, J–L**).

Genus *Mononchus* Bastian, 1865

Mononchus pseudoaquaticus sp. nov.

<https://zoobank.org/DBD4723B-BBB9-4F7D-BB79-4DDE8CECEC16>

Figs 3–7

Mononchus aquaticus sensu Lazarova et al. (2004) (Syn.)

Mononchus sp. 1 sensu Mejía-Madrid (2018) (Syn.)

Description. Female [Based on 4 specimens from the type-population and 8 voucher specimens from other populations; see Table 3 for measurements.] Body slender ($a = 20.2\text{--}33.6$), almost straight; body diameter at mid-body 44–71. Cuticle smooth under light microscope, 2–2.5 thick along body, 3–3.5 thick in post-anal region. Lip region rounded, almost continuous with adjoining body, 2.4–3.7 as wide as high; papillae small, conical; cephalic papillae somewhat larger than labial. Body at posterior end of pharynx 1.8–2.5 times as wide as body width at lip region. Amphids caliciform, with oval apertures, 4 ± 0.5 (3.5–5.0; $n = 10$), at 8–12 from anterior end; amphid position varying from little anterior to tooth apex to level of anterior end of buccal capsule. Buccal capsule elongate-oval, slightly flattened at base, about twice as long as wide (1.8–2.0; $n = 10$), 1.2–1.3 times as long as the labial diameter; its ventral wall 2–3 thick, dorsal wall posterior to dorsal tooth 3–4 thick. Dorsal tooth strong, its anterior margin 4 ± 0.5 (3–5) wide, located at 6 ± 0.4 (5–6.5) from anterior end of buccal capsule, its anterior margin perpendicular to vertical plane. Buccal capsule with short transverse ridge, small tooth-like projection visible in some specimens in sublateral position ($n = 2$). Ventro-sublateral transverse ribs of buccal capsule weak, situated just posterior to tooth apex. Nerve-ring at 108 ± 8 (96–125) from anterior end of body. Excretory pore small, not well visible, at level of posterior margin of nerve-ring. Reproductive system amphidelphic. Anterior genital branch 171 ± 35 (116–226) long, posterior genital branch 166 ± 32 (120–205) long. Ovaries well developed, anterior ovary 105 ± 39 (65–125; $n = 11$) long, posterior ovary 106 ± 26 (70–135; $n = 11$) long. Oviduct with well-marked *pars dilatata oviductus*, 20–30 wide. Uterus a short tube with thick walls, 25–35 long. Vagina slightly swollen, with straight walls, its length representing 28–38% of corresponding body width; *pars refringens vaginae* as two smooth rhomb-shaped sclerotised pieces 3–6 long and 2–3 wide. Two females were recovered possessing a single large, thin-shelled uterine egg measuring 86–94 × 37–46 (specimens from River Maritsa and Komluka Island). Vulva a transverse slit. Vulva-anus distance equals 2.9–4.2 tail lengths. Tail long, slender, initially conoid, then almost cylindrical (10–13 wide) and slightly swollen at the tip, slightly curved ventrally in the third part; tail length represents 10–14% of body length. Caudal glands moderately developed, arranged in group. Tail tip rounded, with terminal spinneret and one small papilla. One female with abnormal tail, very short and almost straight. **Male.** Not found.

Type habitat and locality. Soil around *Salix* sp. along River Danube at Vetren, Silistra Province, North Bulgaria (44°08'24"N, 27°01'47"E; elevation 20 m a.s.l.)

Other localities. Komluka Island (River Danube), rivers Veleka, Shirokolesha, and Maritsa (see Table 1 for details).

Type material. The holotype female and one paratype female are deposited in the Nematode Collection of the Institute of Biodiversity and Ecosystem Research, Bulgarian Academy of Sciences, Bulgaria, under the accession numbers IBER-BAS NTC 105 and 106. One paratype female is deposited in the Wageningen Nematode Collection (WANECO), Wageningen, the Netherlands (WANECO accession number WT 4037), and one paratype female is deposited in the Nematode Collection of the U.S. Department of Agriculture (USDA), Beltsville, Maryland, USA (USDA accession number T-8065p).

Voucher material. Eight voucher specimens are deposited in the Nematode Collection of the Institute of Biodiversity and Ecosystem Research, Bulgarian

Table 3. Morphometric data for females of *Mononchus pseudoaquaticus* sp. nov. collected in five riparian localities in Bulgaria.

Locality	Vetren, Silistra Province		Komluka Island	Shiroka Laka, Smolyan Province	Brodilovo, Burgas Province	Near Plovdiv, Plovdiv Province ^a
River	Danube (Southern Dobruja)		Danube	Shirokoleshka (Rhodope Mountains)	Veleka (Strandzha Mountains)	Maritsa (Upper Thracian Plain)
Habitat	<i>Salix</i> sp. (soil)		<i>Populus</i> sp. (soil)	<i>Salix</i> sp. (soil)	<i>Alnus glutinosa</i> (soil)	<i>Salix</i> sp. (soil)
<i>n</i>	Holotype	Paratypes (<i>n</i> = 3)	(<i>n</i> = 2)	(<i>n</i> = 1)	(<i>n</i> = 3)	(<i>n</i> = 2)
<i>L</i> (mm)	1.45	1.52, 1.60, 1.23	1.72, 1.88	1.61	1.60, 1.71, 1.69	1.81, 1.50
<i>a</i>	20.2	28.7, 32.0, 28.0	27.7, 33.6	30.9	27.5, 33.5, 28.6	28.3, 29.4
<i>b</i>	4.0	4.5, 4.5, 4.0	4.6, 4.5	4.4	4.4, 4.6, 4.7	4.6, 4.5
<i>c</i>	7.5	–, 8.4, 7.2	8.5, 9.1	8.9	7.8, 8.3, 8.0	10.2, –
<i>c'</i>	5.0	–, 5.8, 5.7	5.3, 5.8	5.3	5.1, 5.8, 5.4	4.7, –
<i>V</i> (%)	48.3	50.7, 49.7, 53.9	49.7, 50.0	50.7	50.8, 50.3, 48.4	48.8, 50.9
<i>G1</i> (%)	12.9	9.9, 9.7, 9.4	12.8, 11.7	9.1	10.1, 8.0, 9.9	12.5, 11.3
<i>G2</i> (%)	13.3	13.3, 10.3, 9.9	11.5, 9.9	8.7	7.5, 7.5, 10.0	11.3, 11.1
Buccal capsule length	29	31, 31, 29	29, 33	32	30, 30, 29	31, 30
Buccal capsule width	16	16, 16, 15	15, 16	16	15, 16, 16	16, –
Tooth apex from anterior end of buccal capsule	6	7, 6, 5	6, 7	7	5, 6, 6	6, 6
Position of tooth apex (%) ^b	21	21, 19, 18	19, 20	20	18, 20, 21	19, 20
Excretory pore from anterior end	118	121, 121, 112	–	126	129, 131, 124	153, 107
Nerve-ring from anterior end	96	102, 106, 99	108, 125	114	109, 111, 101	117, 110
Pharynx length	365	342, 359, 305	371, 420	369	364, 372, 355	392, 335
Lip region height	7	10, 8, 8	8, 10	8	8, 9, 8	9, 8
Lip region width	25	24, 24, 23	25, 26	26	24, 25, 23	26, 24
Amphid from anterior end	9	11, 11, 9	8, 10	12	10, 12, 11	–
Body diameter at pharynx base	62	49, 50, 43	50, 49	48	52, 49, 52	56, 47
Maximum body diameter	72	53, 50, 44	62, 56	52	58, 51, 59	64, 51
Body diameter at mid-body	71	53, 49, 44	59, 52	50	58, 50, 59	63, 51
Body diameter at vagina	72	50, 50, 44	62, 56	52	58, 51, 56	64, 50
Body diameter at anus	39	34, 33, 30	38, 36	34	40, 36, 39	38, 33
Anterior genital branch length	187	151, 155, 116	220, 220	146	162, 137, 167	226, 170

Locality	Vetren, Silistra Province		Komluka Island	Shiroka Laka, Smolyan Province	Brodilovo, Burgas Province	Near Plovdiv, Plovdiv Province ^a
River	Danube (Southern Dobruja)		Danube	Shirokoleshka (Rhodope Mountains)	Veleka (Strandzha Mountains)	Maritsa (Upper Thracian Plain)
Habitat	<i>Salix</i> sp. (soil)		<i>Populus</i> sp. (soil)	<i>Salix</i> sp. (soil)	<i>Alnus glutinosa</i> (soil)	<i>Salix</i> sp. (soil)
<i>n</i>	Holotype	Paratypes (<i>n</i> = 3)	(<i>n</i> = 2)	(<i>n</i> = 1)	(<i>n</i> = 3)	(<i>n</i> = 2)
Posterior genital branch length	194	203, 165, 122	197, 186	140	120, 128, 168	205, 167
Anterior ovary length	124	94, 65, –	193, 140	85	70, 86, 79	135, 77
Posterior ovary length	135	109, 95, –	133, 135	82	70, 85, 71	130, 117
Vagina length	20	19, 18, 15	–, 16	17	19, 18, 16	19, –
Rectum length	26	28, 31, 29	28, 30	26	28, 26, 28	29, 28
Tail length	195	–, 191, 171	201, 207	180	204, 207, 210	177, –

^a Material reported as *M. aquaticus* by Lazarova et al. (2004).

^b Distance from tooth apex to anterior end of buccal capsule as % of buccal capsule length from its anterior end.

Academy of Sciences, Bulgaria, under the accession numbers IBER-BAS NC 5/2, IBER-BAS NC 18/3, IBER-BAS NC 16/6, IBER-BAS NC 18/5, IBER-BAS NC 78/1, IBER-BAS NC 80/1. Photovouchers for the sequenced specimens are provided in Suppl. material 1: fig. S4.

Representative DNA sequences. 28S rRNA gene (GenBank: PP768893 and PP768894); 18S rRNA gene (PP768902).

Etymology. The species is named *Mononchus pseudoaquaticus* because of its similarity with *M. aquaticus*, hence the prefix *pseudo-* meaning false.

Differential diagnosis and relationships. Females of *M. pseudoaquaticus* sp. nov. are characterised and distinguished from the congeners by a combination of features: a medium-sized body (1.23–1.88 mm); an elongate-oval, slightly flattened at the base buccal capsule measuring 29–33 × 15–16 µm, 1.8–2.0 as long as wide and distinctly shorter than 2 labial diameters (1.2–1.3 times as long as the labial diameter); amphid openings located from slightly anterior to dorsal tooth apex to level of anterior end of buccal capsule; a strong dorsal tooth situated at 18–21% of buccal capsule length from its anterior end, its anterior margin being perpendicular to the vertical plane; subventral transverse ribs located just posterior to dorsal tooth apex; didelphic (amphidelphic) reproductive system with *pars refringens vaginae* distinctly sclerotised in the form of two smooth rhomb-shaped pieces; tail (171–210 µm long, *c* = 7.2–10.2, *c'* = 4.7–5.8) slightly curved at its posterior third, spinneret terminal.

Morphologically, *Mononchus pseudoaquaticus* sp. nov. appears most similar to *M. aquaticus*, *M. pulcher* Andrassy, 1993, and *M. caudatus* Shah & Hussain, 2016. However, *M. aquaticus* likely represents a composite species (see also Baqri and Jairajpuri 1972) based on the wide ranges of morphometric variation reported in the literature (see comparative data in Suppl. material 2: table S2). However, it is not possible to revise the identification of these materials because in many cases the findings are not documented properly and important characters such as vaginal characteristics (the shape of *pars refringens vaginae* in particular), buccal capsule shape and length/width ratio, etc., are not described, and the voucher material is inaccessible. Therefore, the species con-

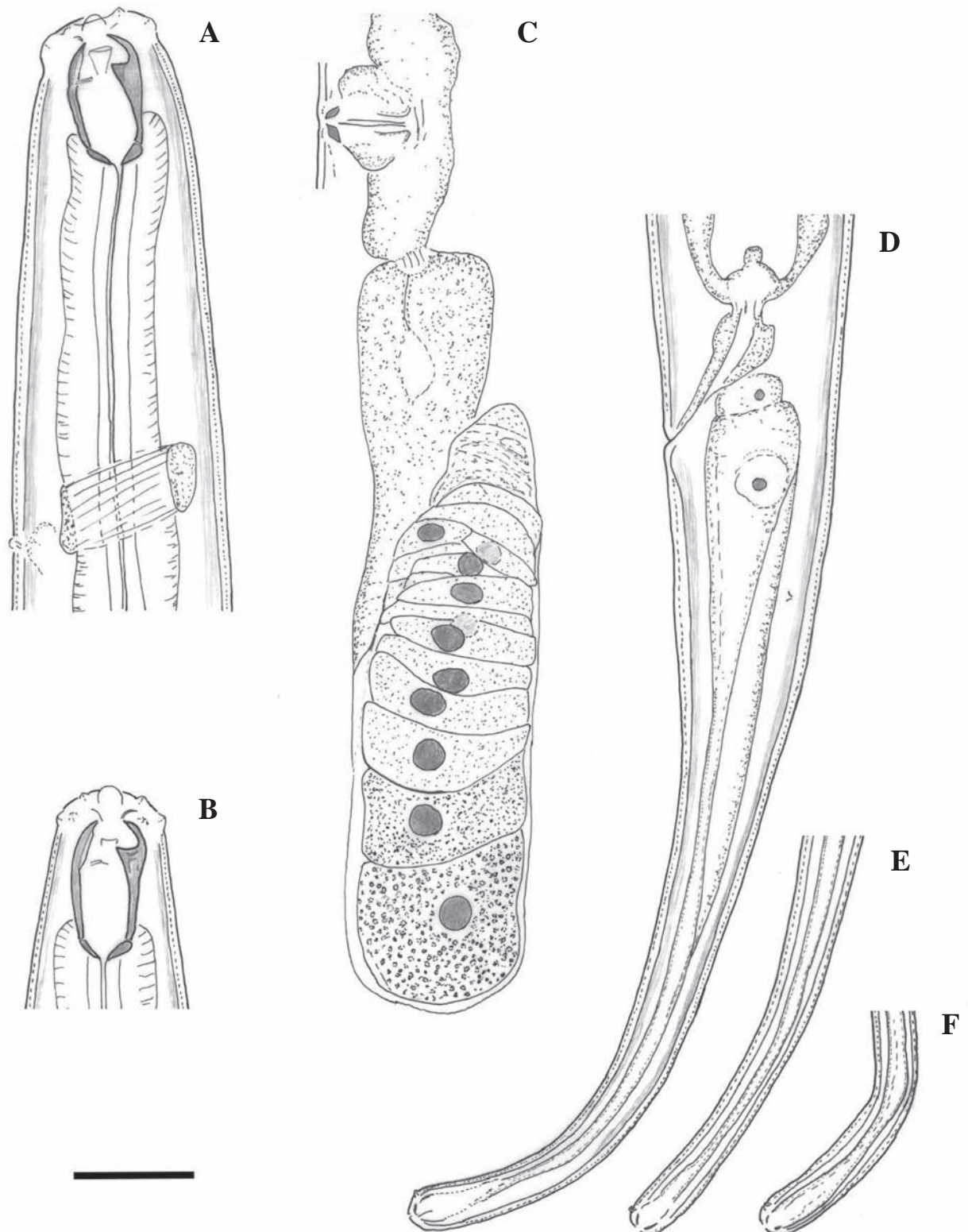


Figure 3. Line drawings of *Mononchus pseudoaquaticus* sp. nov. Holotype female (A, C, D) and paratype specimens (B, E, F): A, B anterior region C posterior genital branch D tail region E, F tail tip. Scale bar: 25 μ m.

cept for *M. aquaticus* (sensu stricto) used in the present comparisons is based on the original description of Coetzee (1968) and the data by Baqri and Jairajpuri (1972) who re-examined and provided metrical data for some paratypes of *M. aquaticus*. This concept was also applied by Andr assy (2011a) in the most

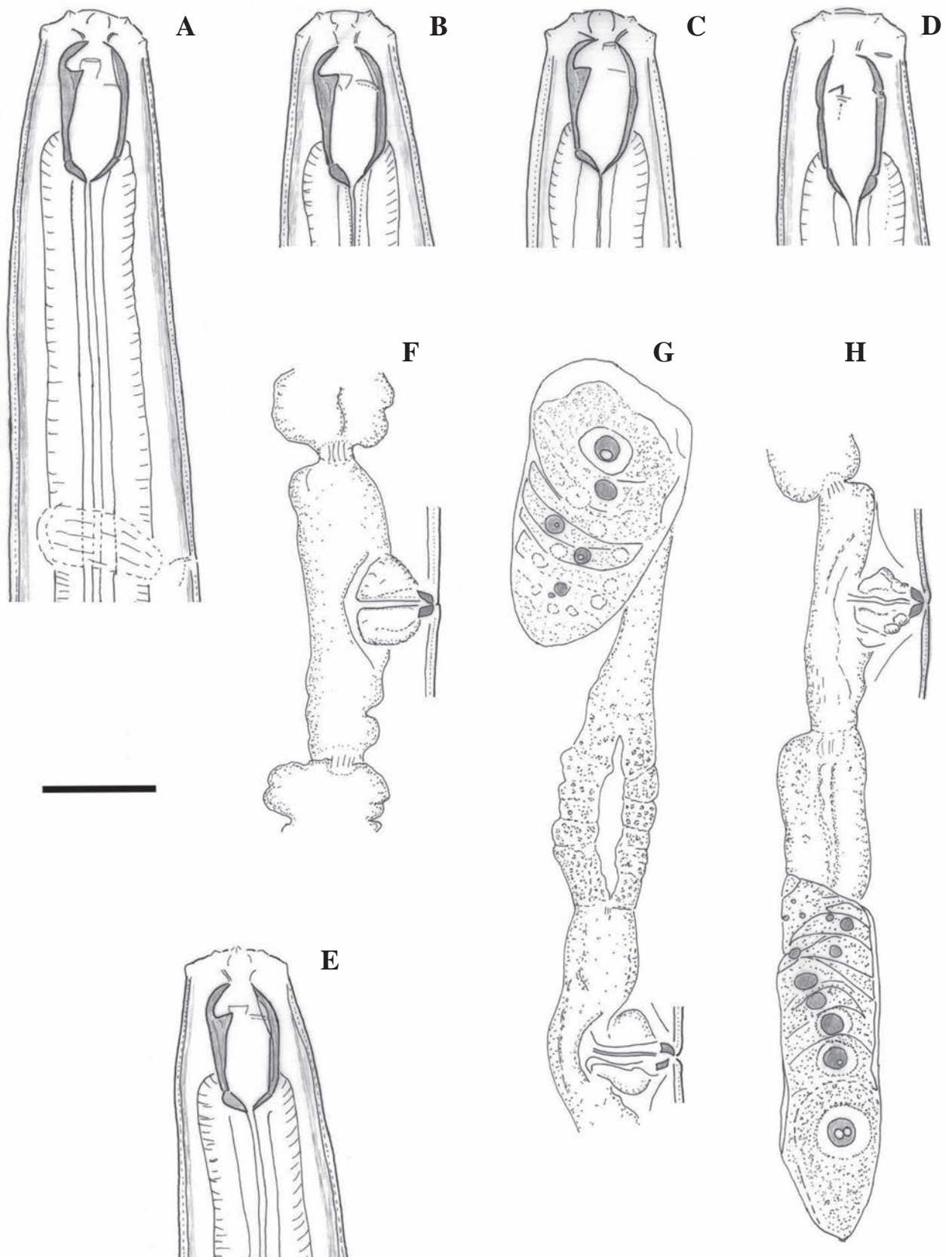


Figure 4. Line drawings of *Mononchus pseudoaquaticus* sp. nov. Paratype females from populations collected from riverbanks of the rivers Shirokoleshka (A, H), Maritsa (B, F), Veleka (E, G) and Danube (C, D): A–E anterior region F vulval region G anterior genital branch H vulval region and posterior genital branch. Scale bar: 25 μ m.

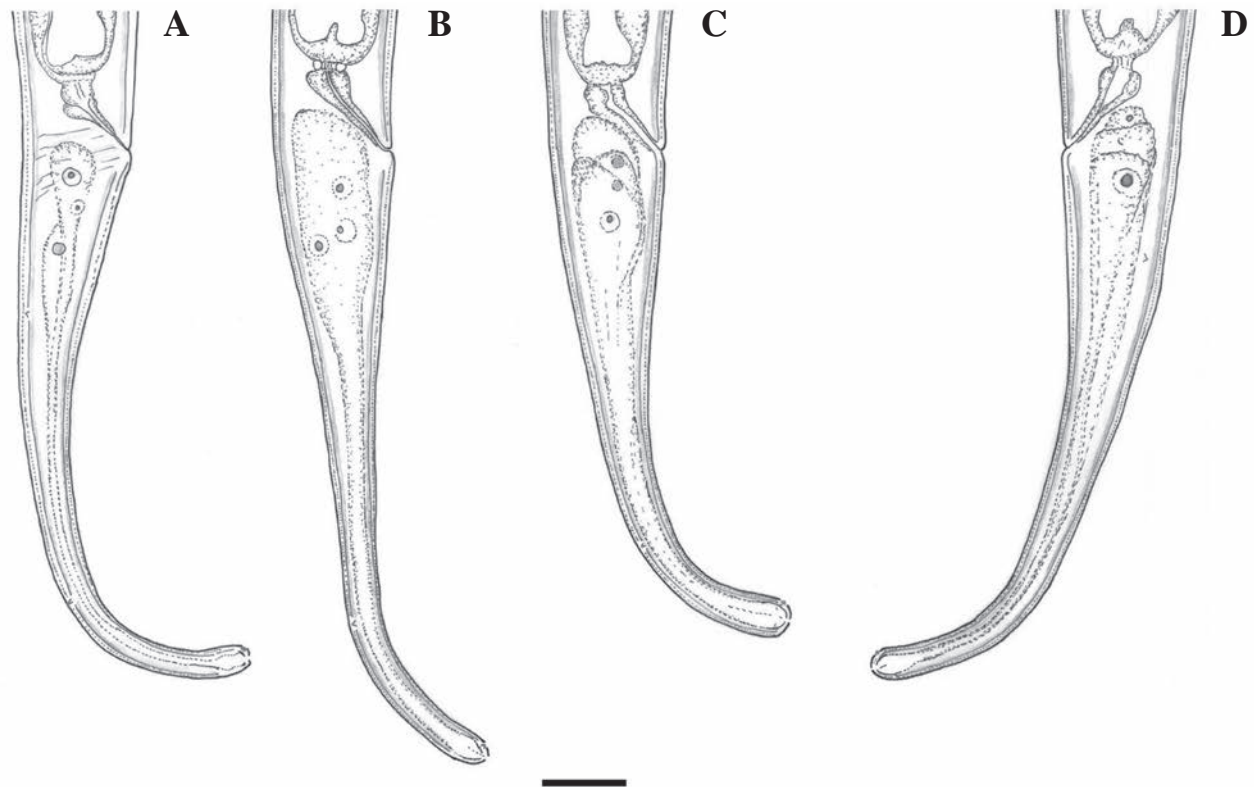


Figure 5. Line drawings of the tail region in females of *Mononchus pseudoaquaticus* sp. nov. from populations collected in Komluka Island (A) and riverbanks of the rivers Veleka (B), Maritsa (C) and Danube (D). Scale bar: 25 µm.

recent key to the species of *Mononchus* (see Suppl. material 2: table S3 for details) and in the updated key to the species of *Mononchus* provided here.

The present material differs from the type material of *M. aquaticus* (Coetzee 1968; Baqri and Jairajpuri 1972) by having: a smaller buccal capsule length/width ratio (1.8–2.0 vs 2.2–2.5); a different shape of the base of the buccal capsule (flattened vs tapering); a different direction of the anterior margin of dorsal tooth (perpendicular to the vertical plane vs oblique); a different shape of the vaginal sclerotised pieces (*pars refringens vaginae*) (rhomb-shaped vs drop-shaped); and a longer tail (171–210 vs 94–156 µm (mean 150 µm) (Suppl. material 2: table S3).

The new species differs from *M. caudatus* by having: a different buccal capsule length/width ratio (1.8–2.0 vs 2.0–2.5); lower a value (20.2–33.6 vs 34–38); more anteriorly situated nerve-ring (96–125 vs 125–134 µm); different arrangement of the caudal glands (in a group vs in tandem); and shorter rectum (26–31 vs 32–36 µm) and vagina (16–20 vs 27–29 µm) (Shah and Hussain 2016; Suppl. material 2: table S3).

Differentiation from *M. pulcher* is more complicated because the original description of Andrassy (1993) is based on two, geographically largely separated populations from Chile and Hungary. However, Andrassy's (1993: fig. 2) illustrations indicate that he probably dealt with different species. Unfortunately, it is impossible to separate the rather incomplete metrical data since Andrassy (1993) provided pooled data for the position of dorsal tooth apex, the length of pharynx, the width of the lip region, the body diameter at mid-body, and tail length (Suppl. material 2: table S3). Still, in addition to the morphological differences (e.g., different shape of the buccal capsule and direction of the dorsal tooth), the Hungarian population is characterised by having a smaller buccal capsule length

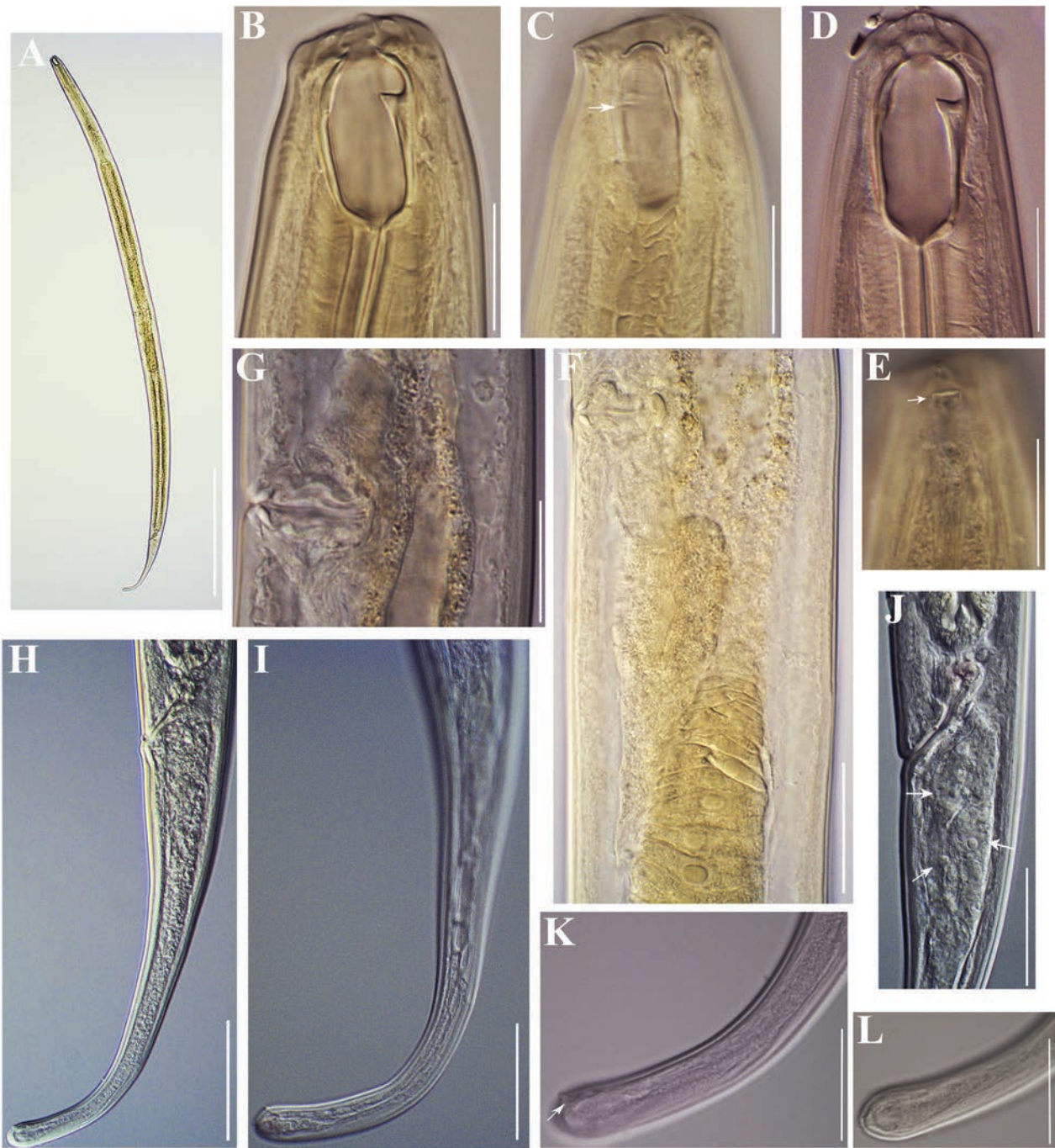


Figure 6. Photomicrographs of *Mononchus pseudoaquaticus* sp. nov. Holotype (A–C, E, F, H, I, L) and paratype (D, G, J, K) females: **A** body, total view **B–E** anterior region (transverse ridge arrowed in **C**; amphid opening arrowed in **E**) **F, G** vulval region showing *pars refringens vaginae* and posterior genital branch (**F**) **H–J** tail (caudal glands arrowed in **J**) **K, L** tail tip showing one small papilla (arrowed in **K**) and terminal spinneret (**L**). Scale bars: 400 μ m (**A**); 20 μ m (**B–E, G, J, K, L**); 30 μ m (**F, I, H**).

(and hence length/width ratio) and an overall smaller body length/tail length ratio (c). The size of the buccal capsule is a feature that varies in rather narrow ranges for a given population/species and is one of the most important differentiating characters for all mononchids. These data indicate that the Hungarian population may represent another species. However, it is impossible to identify this material given the scant data provided in Andr ssy (2011a). Therefore, our

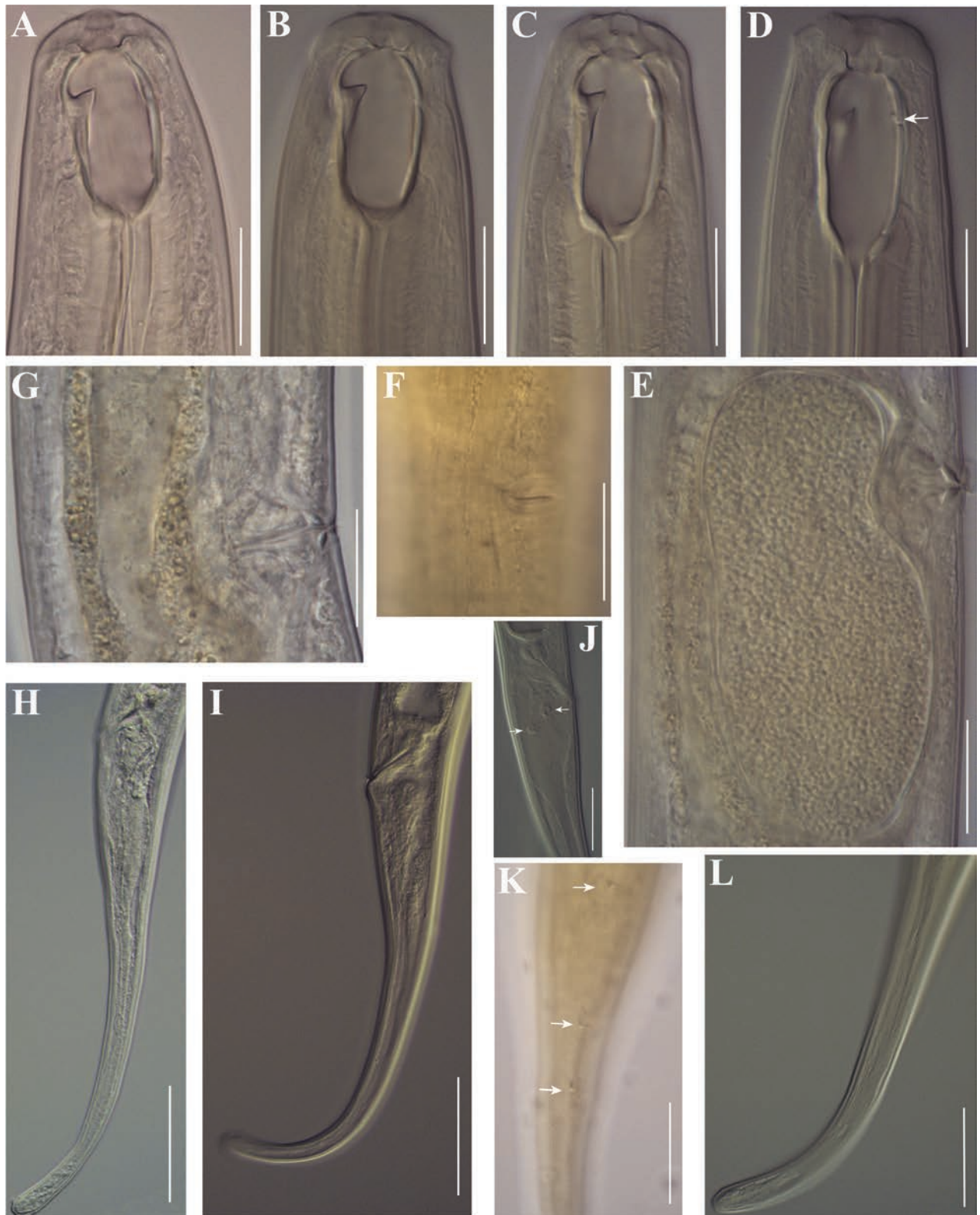


Figure 7. Photomicrographs of *Mononchus pseudoaquaticus* sp. nov. Females from populations collected from riverbanks of the rivers Veleka (**A, G, H**), Danube (**B, D, E, I, J**), Shirokoleshka (**C, L**) and Maritsa (**F, K**): **A–D** anterior region (transverse ridge arrowed in **D**) **E–G** vulval region showing an egg (**E**) vulval opening, subventral view (**F**) and *pars refringens vaginae* (**G**) **H, I** tail **J** caudal glands (arrowed) **K** caudal pores (arrowed) **L** tail tip. Scale bars: 20 µm (**A–G, K**); 30 µm (**J, L**); 50 µm (**H, I**).

comparisons are based on the morphology and metrical data for the type-population of *M. pulcher* from Chile. The new species differs from *M. pulcher* (sensu stricto) by having: a shorter (29–33 vs 35–38 μm) and narrower (15–16 vs 16–18 μm) buccal capsule; lower values for *a* (20–34 vs 35–39); anterior margin of the dorsal tooth perpendicular to the vertical plane vs oblique, vagina not spotted in its anterior part vs spotted, rhomb-shaped *pars refringens vaginae* vs drop-shaped; and smaller egg length (86–94 vs 98–100 μm). Additionally, the upper ranges for body length and tail length are greater in both populations of *M. pulcher* (Suppl. material 2: table S3).

***Mononchus truncatus* Bastian, 1865**

Figs 8, 9

Description. Female [Based on 14 specimens from 6 localities; see Table 4 for measurements.] Body of most specimens straight, with only last part of tail ventrally curved (body C-shaped upon fixation in a few specimens), comparatively slender, body diameter at mid-body 53–71. Cuticle smooth under light microscope, 2–3 thick along most of body, thicker (4–5) in post-anal region. Lip region rounded, continuous with adjoining body, papillae small, cephalic papillae very small and rounded, labial papillae somewhat larger and conical. Body at posterior end of pharynx 1.2–1.4 times as wide as body width at lip region. Amphids with oval apertures, situated at the beginning or middle of buccal capsule, at 11 ± 1 (10–13) ($n = 12$) from anterior end and 40 ± 3 (37–44) ($n = 12$) from posterior end of buccal capsule, aperture 4.5 ± 0.5 (4–5) ($n = 12$) wide. Buccal capsule oval, tapering at base, 2.0–2.3 as long as wide or 1.3–1.7 times as long as lip region width; its ventral wall 2–3 thick, dorsal wall posterior to dorsal tooth ~ 3 –5 thick. Dorsal tooth strong, its anterior margin 5 ± 0.6 (4–6) ($n = 12$) wide, located at 11 ± 0.5 (10–12) from anterior end of buccal capsule. Ventral wall with short, not so well visible rib, ventro-sublateral transverse ribs located at level of tooth apex or slightly more anterior. Nerve-ring at 127 ± 8 (116–144) ($n = 12$) from anterior end of body. Excretory pore weakly marked, posterior to nerve-ring. Reproductive system amphidelphic. Anterior genital branch 193 ± 14 (175–223) long, posterior branch somewhat longer, 204 ± 16 (187–240) long. Ovaries well developed, not reaching uterus-oviduct junction; anterior ovary 107 ± 17 (75–142) ($n = 12$) long, posterior ovary 114 ± 18 (95–146) ($n = 12$) long. Oviduct with marked *pars dilatata oviductus*, 33 ± 7 (20–45) wide. Uteri thick-walled tubes, 40–60 long, length ranges for anterior and posterior uterus almost identical. Vagina with straight walls, 28 ± 3 in length representing 24–33% of corresponding body width; *pars refringens vaginae* as two rounded drop-shaped pieces with smooth surface, 3–5 long and 2–3 wide. Vulva transverse, not protruding. Vulva-anus distance equals 2.3–3.3 tail lengths. Tail long, slender, curved ventrally in second part, length representing 11–13% of total body length, 11–13 μm wide at cylindrical part, with rounded and slightly swollen tip. Caudal glands moderately developed, arranged in group, spinneret terminal. **Male.** Not found.

Voucher material. Ten specimens are deposited in the Nematode Collection of the Institute of Biodiversity and Ecosystem Research, Bulgarian Academy of Sciences, under the accession numbers IBER-BAS NC 5/1, IBER-BAS NC 16/1-6, IBER-BAS NC 17/1, IBER-BAS NC 18/3, IBER-BAS NC 30/13, IBER-BAS NC 311/7-9.

Table 4. Morphometric data for females of *Mononchus truncatus* collected in six riparian localities in Bulgaria.

Locality	Shiroka Laka, Smolyan Province	Teshel, Smolyan Province	Near Primorsko, Burgas Province	Slivarovo, Burgas Province	Near Plovdiv, Plovdiv Province	Vetren, Silistra Province
River	Shirokoleshka (Rhodope Mountains)	Trigradska (Rhodope Mountains)	Dyavolska (Strandzha Mountains)	Rezovska (Strandzha Mountains)	Maritsa (Upper Thracian Plain)	Danube (Southern Dobruja)
Habitat	<i>Salix</i> sp. (soil)	<i>Salix</i> sp. (litter)	<i>Fraxinus excelsior</i> (soil)	<i>Ulmus laevis</i> (soil)	<i>Salix</i> sp. (soil)	<i>Salix</i> sp. (soil)
<i>n</i>	(<i>n</i> = 6)	(<i>n</i> = 1)	(<i>n</i> = 1)	(<i>n</i> = 3)	(<i>n</i> = 1)	(<i>n</i> = 2)
<i>L</i> (mm)	1.94 ± 1.08 (1.83–2.09)	1.89	2.06	1.77, 1.85, 1.84	1.83	1.89, 1.91
<i>a</i>	30.6 ± 2.5 (27–34)	26.5	38.9	32.1, 33.7, 29.2	33.3	33.7, 32.4
<i>b</i>	4.1 ± 0.2 (3.7–4.3)	4.0	3.9	4.0, 4.2, 4.1	4.2	4.0, 4.2
<i>c</i>	8.3 ± 0.2 (8.1–8.7)	8.6	8.2	7.8, 8.0, 8.2	8.2	8.9, 9.3
<i>c'</i>	5.5 ± 0.4 (5.0–6.0)	5.5	6.1	6.7, 6.3, 6.2	6.2	5.0, 5.0
<i>V</i> (%)	55.2 ± 1.3 (53.4–57.3)	54.0	53.9	57.6, 53.1, 53.2	52.6	54.3, 53.8
<i>G1</i> (%)	10.1 ± 0.6 (9.5–10.9)	9.6	10.0	11.3, 9.6, 10.3	10.2	9.7, 9.8
<i>G2</i> (%)	10.4 ± 0.6 (9.7–11.6)	11.4	11.6	11.8, 10.4, 10.2	10.8	9.9, 10.1
Buccal capsule length	43 ± 2 (40–44)	44	44	42, 42, 41	40	42, 42
Buccal capsule width	20 ± 1 (19–22)	21	21	18, 19, 19	19	19, 20
Tooth apex from anterior end of buccal capsule	12 ± 1 (11–12)	11	11	11, 11, 11	10	11, 12
Position of tooth apex (%) ^a	27 ± 1 (26–29)	25	25	26, 27, 27	26	26, 27
Excretory pore from anterior end	148 ± 16 (137–176) (<i>n</i> = 5)	150	–	138, 141, 142	134	156, 146
Nerve-ring from anterior end	126 ± 10 (116–144) (<i>n</i> = 5)	–	140	138, 141, 142	122	129, 129
Pharynx length	479 ± 34 (423–518)	468	525	439, 443, 446	437	468, 450
Lip region height	9 ± 1 (8–11)	9	10	10, 10, 9	10	9, 11
Lip region width	29 ± 1 (28–30)	26	30	26, 26, 25	26	27, 25
Amphid from base of buccal capsule	40 ± 3 (37–44)	41	44	–, 39, 39	37	41, 38
Amphid from anterior end	12 ± 1 (10–13) (<i>n</i> = 4)	10	11	–, 12, 10	13	12, 11
Maximum body diameter	64 ± 6 (55–70)	71	53	55, 55, 63	55	56, 59
Body diameter at pharynx base	58 ± 4 (51–61)	53	52	51, 55, 58	53	53, 56
Body diameter at mid-body	61 ± 4 (53–65)	71	53	55, 55, 63	55	55, 59
Body diameter at vagina	64 ± 6 (55–70)	71	53	53, 54, 60	55	56, 59
Body diameter at anus	42 ± 3 (38–47)	40	41	34, 37, 36	34	42, 41
Anterior genital branch length	196 ± 18 (175–223)	181	206	199, 179, 189	207	182, 188

Locality	Shiroka Laka, Smolyan Province	Teshel, Smolyan Province	Near Primorsko, Burgas Province	Slivarovo, Burgas Province	Near Plovdiv, Plovdiv Province	Vetren, Silistra Province
River	Shirokoleska (Rhodope Mountains)	Trigradska (Rhodope Mountains)	Dyavolska (Strandzha Mountains)	Rezovska (Strandzha Mountains)	Maritsa (Upper Thracian Plain)	Danube (Southern Dobruja)
Habitat	<i>Salix</i> sp. (soil)	<i>Salix</i> sp. (litter)	<i>Fraxinus excelsior</i> (soil)	<i>Ulmus laevis</i> (soil)	<i>Salix</i> sp. (soil)	<i>Salix</i> sp. (soil)
<i>n</i>	(<i>n</i> = 6)	(<i>n</i> = 1)	(<i>n</i> = 1)	(<i>n</i> = 3)	(<i>n</i> = 1)	(<i>n</i> = 2)
Posterior genital branch length	203 ± 13 (190–220)	215	240	208, 193, 187	215	187, 193
Anterior ovary length	98 ± 15 (75–115) (<i>n</i> = 5)	125	120	108, 91, –	142	107, 107
Posterior ovary length	106 ± 16 (95–135) (<i>n</i> = 5)	125	146	100, 109, –	141	101, 120
Vagina length	17 ± 1 (15–17)	17	14	–, 18, 17	17	17, 16
Rectum length	31 ± 1 (29–33)	36	27	29, 32, 31	28	32, 30
Tail length	234 ± 11 (225–254)	218	252	227, 232, 224	211	212, 205

^a Distance from tooth apex to anterior end of buccal capsule as % of buccal capsule length from its anterior end.

Photovouchers for the sequenced specimens are provided in Suppl. material 1: figs S5–S7.

Habitats and localities. Soil around roots of *F. excelsior*, *U. laevis*, *A. glutinosa* and *Salix* sp. and litter around *Salix* sp. along banks of the rivers Shirokoleska, Trigradska, Dyavolska, Rezovska, Veleka, Maritsa, and Danube (see Table 1 for details).

Representative DNA sequences. 28S rRNA gene (GenBank: PP768890–PP768892); 18S rRNA gene (PP768901).

Distribution. According to the abundant published data for materials reported as *M. truncatus*, this species appears to exhibit a worldwide distribution. However, we agree with Andr assy (2011a) who doubted that all of the records referring to *M. truncatus* concern in fact this species. In Bulgaria, *M. truncatus* has been reported from many localities but with no morphological evidence supporting identification. Andr assy (1958) recorded this species for the first time in Rila Mountains and Varna. Subsequently, *M. truncatus* was reported from the North Thracian Plain (Katalan-Gateva 1962) and Pazardzhik Province (Katalan-Gateva 1965) associated with cultivated plants. In aquatic habitats, the species has been reported in sediments from 24 rivers and three lakes (Stoichev 1996; Stoichev and Chernev 2011; Stoichev and Varadinova 2011). The present study is the first to provide morphological and morphometric data for *M. truncatus* in Bulgaria.

Remarks. Morphologically, the present material belongs to and was identified as *M. truncatus*. However, similar to the situation with *M. aquaticus* (sensu lato) considered above, *M. truncatus* also represents a composite species (Andr assy 2011a) based on the wide ranges of morphometric variation reported in the literature (see Suppl. material 2: table S4). Andr assy (2011a) summarised the data from the original description and subsequent re-descriptions of *M. truncatus* and provided novel data for a population from Hungary. This concept of *M. truncatus* (sensu stricto) (“real *M. truncatus*” of Andr assy 2011a) is applied here. Comparative morphometric data for several records deviating from this species concept are also provided in Suppl. material 2: table S4. Typically, these include studies

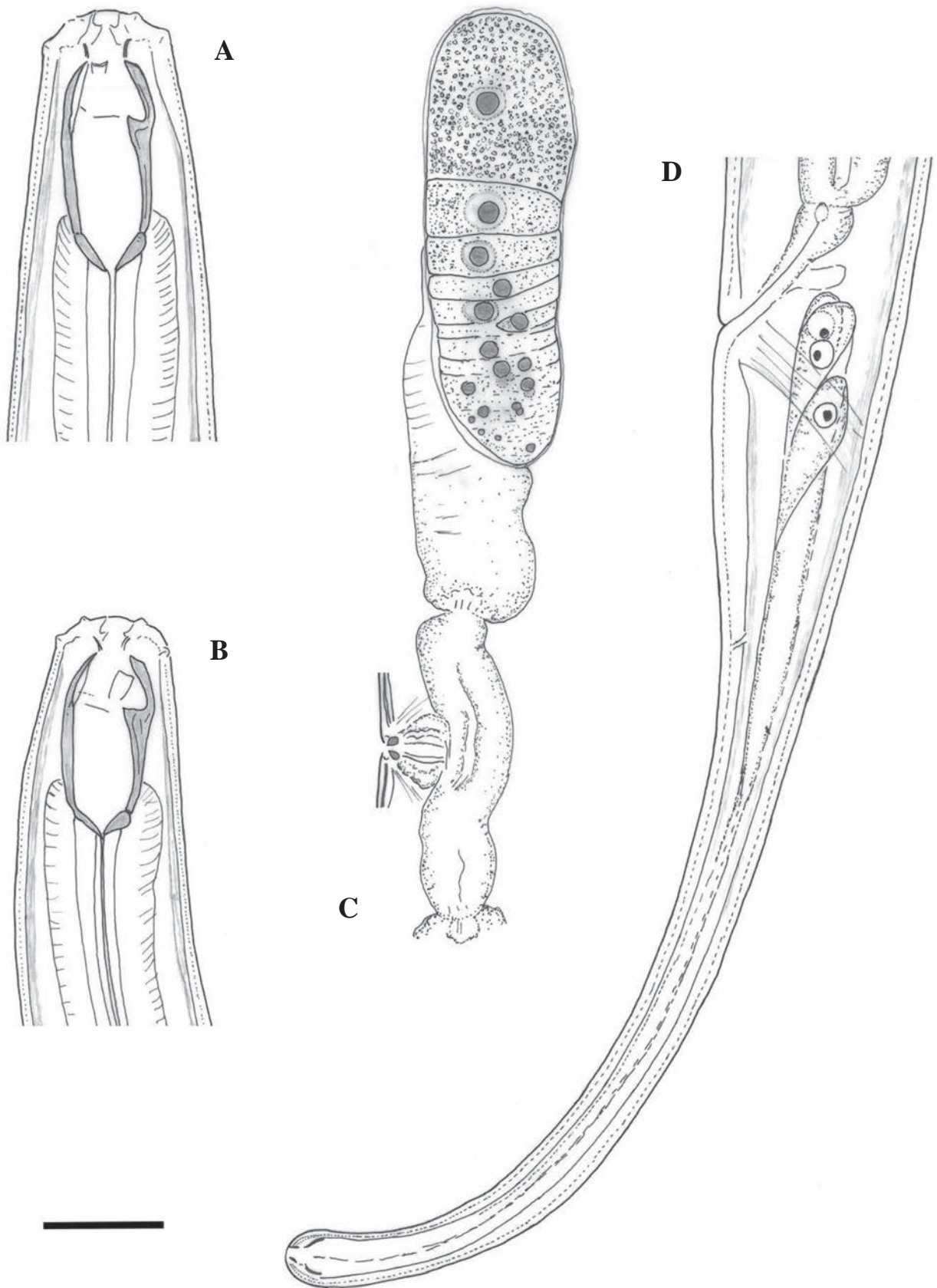


Figure 8. Line drawings of *Mononchus truncatus* Bastian, 1865. Females from populations collected from riverbanks of the rivers Shirokoleshka (**A, C, D**) and Maritsa (**B**): **A, B** anterior region **C** anterior genital branch **D** tail region. Scale bar: 25 μ m.

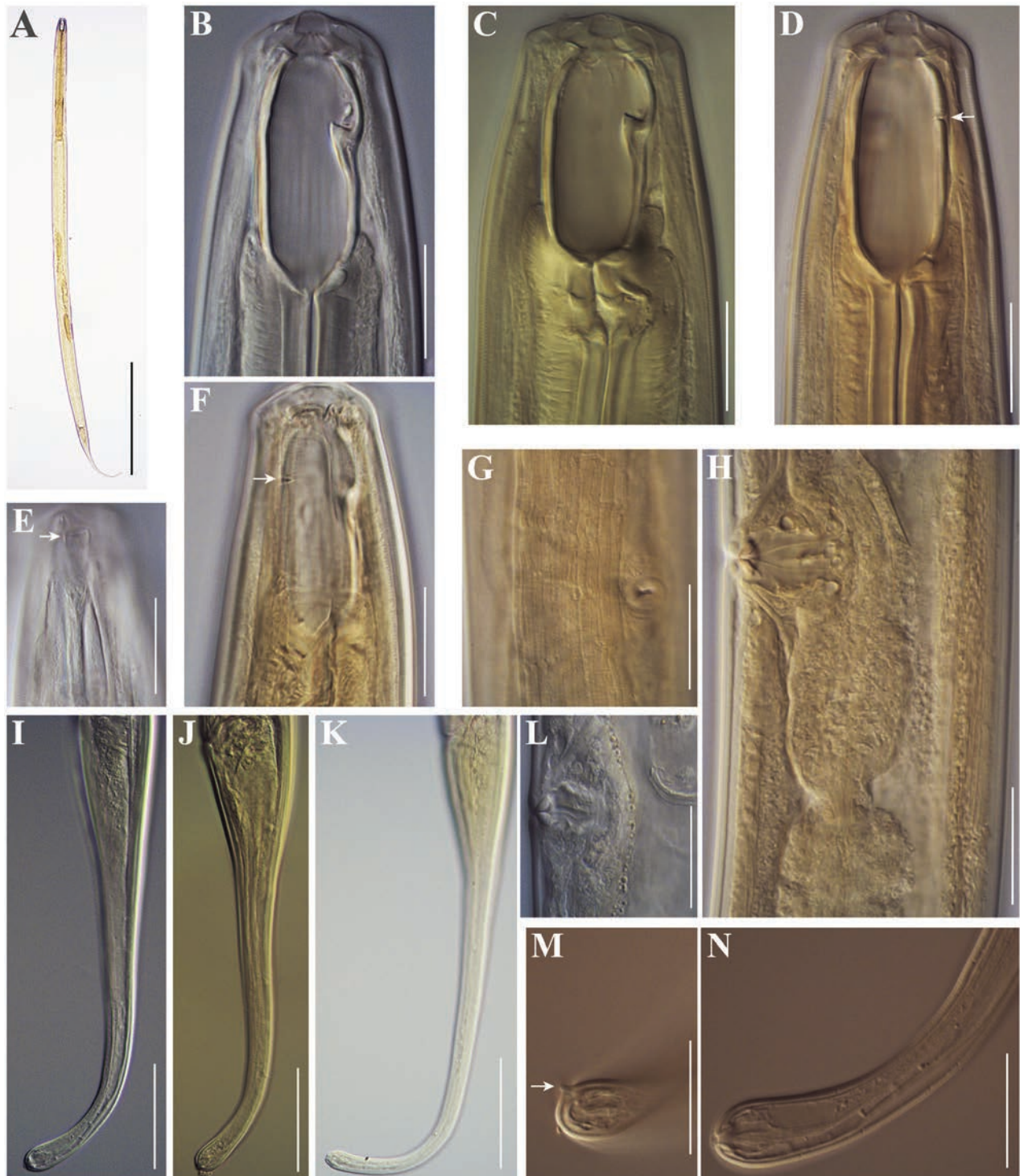


Figure 9. Photomicrographs of *Mononchus truncatus* Bastian, 1865. Females from populations collected from riverbanks of the rivers Rezovska (A, D, F, G, H, K), Danube (B, E, J, L) and Shirokoleshka (C, I, M, N): A body, total view B–F anterior region (ventro-sublateral ribs arrowed in D; amphid opening arrowed in E; transverse ridge arrowed in F) G, H, L vulval region: G vulval opening, ventral view H vulva and part of posterior genital branch (posterior uterus and part of *pars dilatata oviductus*), lateral view L vulval region showing *pars refringens vaginae* I–K tail M, N tail tip showing papilla (arrowed in M) and terminal spinneret (N). Scale bars: 400 μ m (A); 20 μ m (B–H, L–N); 50 μ m (I–K).

providing data (sometimes pooled, e.g., Nakazawa 1999; Eisendle 2008) for nematodes from different localities (e.g., Botha and Heyns 1992; Nakazawa 1999; Eisendle 2008; Farahmand et al. 2009). Thus, the data by Botha and Heyns (1992) show upper ranges above the upper range (b , c , and V) and lower ranges below the lower range of variation in *M. truncatus* (sensu stricto) (buccal capsule width, position of tooth apex, anterior end to pharyngo-intestinal valve, body diameter at mid-body and tail length). Almost all of these differences were recorded in a single sample (Crocodile River) likely containing a misidentified specimen. Similarly, both samples studied by Farahmand et al. (2009) contain specimens with largely deviating morphometric data (Suppl. material 2: table S4).

We are also aware of two other questionable records of *M. truncatus*, not included in Suppl. material 2: table S4: Koohkan et al. (2014) reported as *M. truncatus* nematodes of a population from Ghale Asgar, Kerman Province, Iran, that do not correspond to this species because all important morphometric characters are outside the ranges of the “true” *M. truncatus* sensu Andr assy (2011a). Probably this population represents a yet undescribed species as it cannot be identified using the available keys. Similarly, Rawat and Ahmad (2000) reported *M. truncatus* as a new geographical record for India and provided a brief description based on five females. However, the measurements of some key characters such as the length of the buccal capsule (37–38 vs 42–50 μm), tail length (172–212 vs 232–283 μm) are outside the ranges of the “true” *M. truncatus* and the data provided are insufficient to identify the species. We consider that the records listed above are based on composite material.

We agree with Andr assy (2011a) who considered the description by De Bruin and Heyns (1992) to represent the “real *M. truncatus*” and add to his list of reliable records the data by Coomans et al. (1995). The present material agrees well with the characteristics of *M. truncatus* (sensu stricto) based on the original description, the description and data for the neotype population by Clark (1960), Coomans and Khan (1981), and Baqri and Jairajpuri (1972), and the description by Andr assy (2011a) except for the shorter tail (205 vs 240–283 μm) in a single specimen from Vetren (Table 4), resulting in a greater value for c (9.3 vs 5.8–8.6) (Suppl. material 2: tables S4, S5).

Mononchus truncatus was first reported from Bulgaria by Andr assy (1958) who provided limited metrical data. However, the body length reported by this author is outside the range for *M. truncatus*; additionally, two largely differing measurements (22.3 and 43.3 μm) were given for the length of the buccal capsule in two females of similar size, suggesting that this report is based on more than one species.

***Mononchus* sp.**

Figs 10, 11

Description. Female [Based on 2 females; see Table 5 for measurements]. Body slender, straight, with strongly ventrally curved tail; body diameter 42 at posterior end of buccal capsule and 45–52 at mid-body. Cuticle smooth under light microscope, 3–3.5 thick along body, thicker (4–5) around vulva and posterior to anus. Lip region rounded, continuous with adjoining body; papillae small, cephalic papillae round and somewhat more visible than labial. Body at posterior end of pharynx twice as wide as lip region. Amphids with oval apertures (5 wide),

located between dorsal tooth apex and anterior end of buccal capsule. Buccal capsule oblong, with flattened base, 2.3–2.4 as long as wide or 1.7–1.8 times as long as the labial diameter, its ventral wall around 3 thick, dorsal wall posterior to dorsal tooth 4 thick. Dorsal tooth robust, its anterior margin 4 wide, located at 10–11 from anterior end of buccal capsule. Ventral wall of buccal capsule with short, not well-visible rib, transverse ventro-sublateral ribs located at level of dorsal tooth apex. Excretory pore weakly marked, posterior to nerve-ring. Reproductive system amphidelphic, genital branches short. Ovaries well developed, not reaching uterus-oviduct junction. Oviduct with well-marked *pars dilatata oviductus*, 25 wide. Uteri short, anterior uterus 30 long, posterior uterus 36 long ($n = 1$). Oviduct-uterus junction with moderately developed muscular sphincter. Vagina with straight walls and small spots next to *pars refringens vaginae*, length representing 31% of corresponding body width; *pars refringens vaginae* as two round drop-shaped sclerotised pieces with smooth surface, 4×2 in size; *pars distalis vaginae* well visible, ~ 4 long. Vulval opening round (Fig. 11E), vulva not protruding; vulva-anus distance equals 2.1 tail lengths. Tail long, cylindrical, strongly curved ventrad, length representing 16–18% of body length; cylindrical part of tail ~ 6 wide. Caudal glands moderately developed, arranged in tandem. Tail tip rounded, somewhat asymmetrical, dorsal part better developed, with terminal spinneret and one large setiform papilla. Three pairs of caudal pores present.

Male. Not found.

Voucher material. Two specimens are deposited in the Nematode Collection of the Institute of Biodiversity and Ecosystem Research, Bulgarian Academy of Sciences, under the accession numbers IBER-BAS NC 316/1.

Habitat and locality. Soil around roots of *F. sylvatica* near a waterfall (River Grafaska, inflow of River Kopilovtsi; see Table 1 for details).

Remarks. Morphologically, the specimens resemble most *Mononchus oblongus* Andr ssy, 2011 regarding the shape of the buccal capsule, the actual and relative length of the tail (as percent of body length), and the position of tooth apex (Table 5; Andr ssy 2011a). However, the present specimens exhibit some differences in other morphometric features and proportions such as the total body length (1.31–1.62 vs 1.60–1.88 μm), the length of the buccal capsule (45–47 vs 48–51 μm) and tail (230–263 vs 264–276 μm), the width of the lip region (25–27 vs 22–23 μm), and the ratios buccal capsule length/width (2.3–2.4 vs 2.6–2.8), buccal capsule length/lip region width (1.7–1.8 vs 2.1–2.3) and body at pharynx base/lip region width (1.9–2.0 vs 2.7–2.9).

The present specimens also show similarities with *M. truncatus* and *M. himalayensis* Rawat & Ahmad, 2000. However, *Mononchus* sp. differs from *M. truncatus* in having a shorter body (1.31–1.62 vs 1.7–2.1 mm), a more anterior position of tooth apex (22–23 vs 25–29%), longer tail in relation to body length (16–18 vs 10–13%), smaller vulva-anus length/tail length ratio (2.1 vs 2.4–3.0), a lower *c* value (5.7–6.1 vs 7.5–8.4) and a different shape of the vulva (round vs transverse) (Andr ssy 2011a). Differences between *Mononchus* sp. and *M. himalayensis* include a shorter body (1.31–1.62 vs 1.6–1.9 mm), a more anterior position of tooth apex (22–23 vs 25–31%), lower *a*- and *c*'-values (28–31 vs 33–38 and 7.7–7.9 vs 8.8–10.4, respectively) and absence of pre-vulval papilla (vs presence) (Rawat and Ahmad 2000). Probably the two females represent a species not yet described; however, additional specimens are needed to confirm the identity of the Bulgarian population.

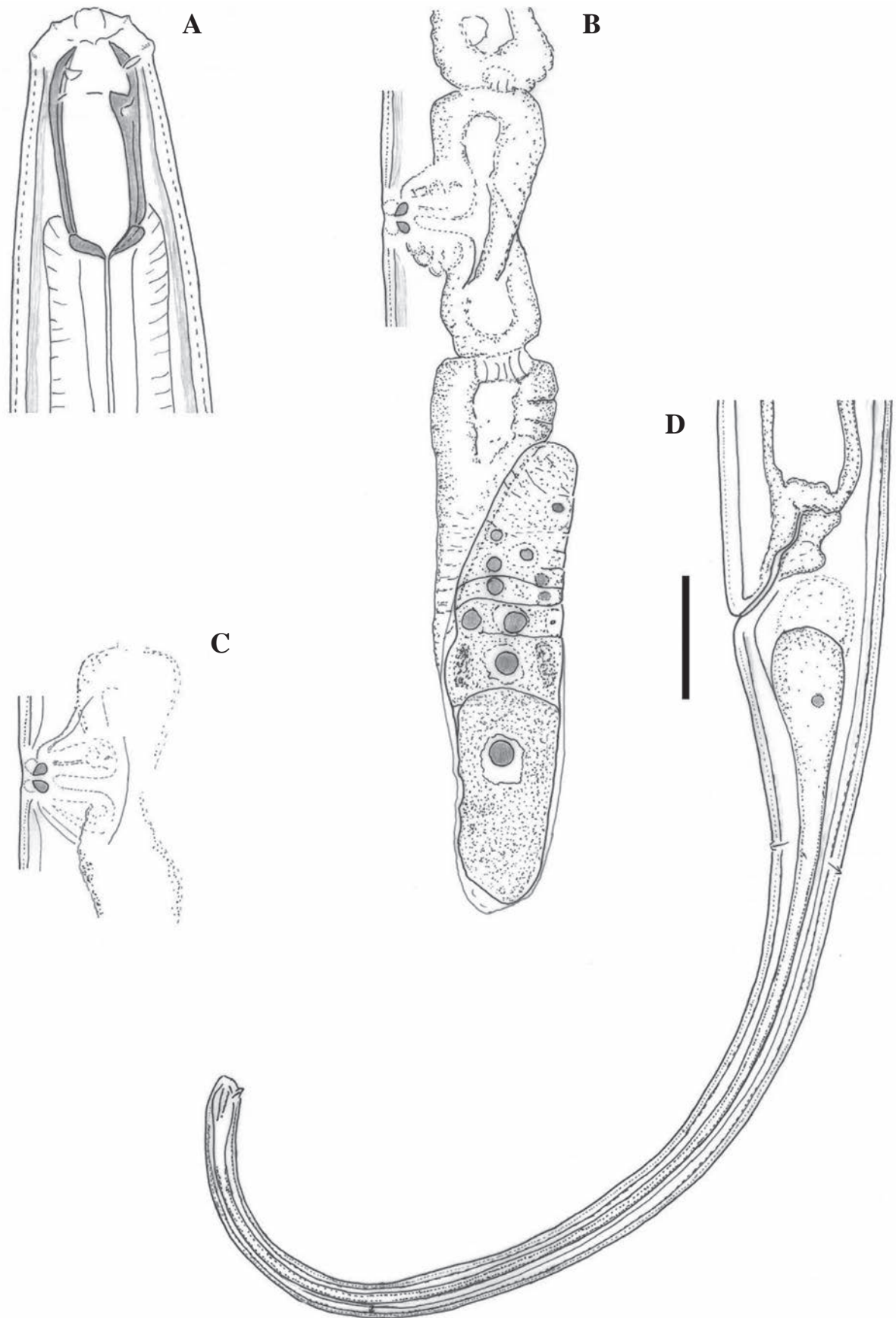


Figure 10. Line drawings of *Mononchus* sp. female: **A** anterior region **B** vulval region and posterior genital branch **C** vulval region **D** tail. Scale bar: 25 μ m.

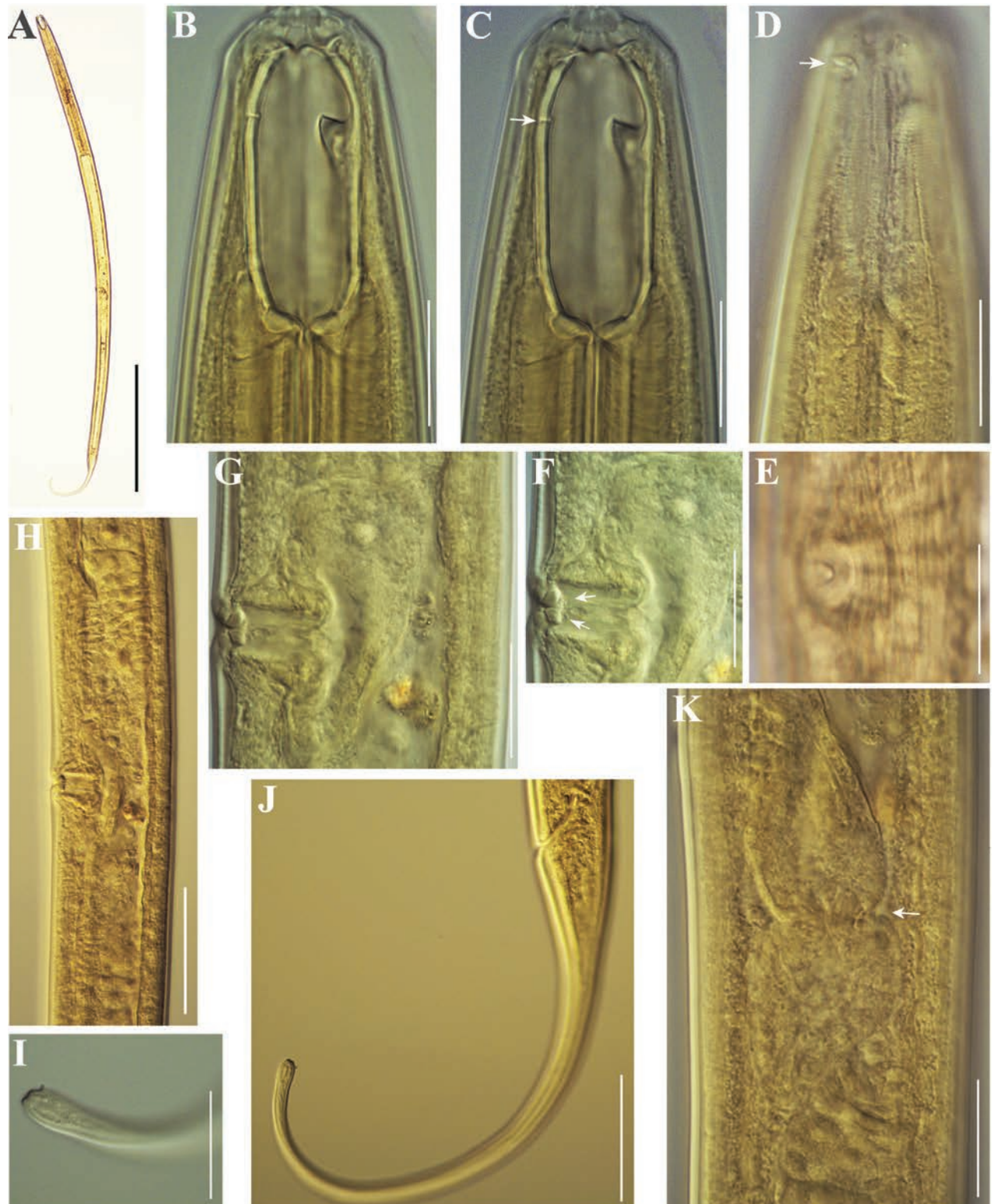


Figure 11. Photomicrographs of *Mononchus* sp. females: **A** body, total view **B–D** anterior region (ventro-sublateral ribs arrowed in **C**; amphid opening arrowed in **D**) **E** vulval opening, subventral view **F, G** *Pars refringens vaginae* (small spots next to it arrowed in **F**) **H** reproductive system **I** tail tip **J** tail **K** sphincter of the oviduct-uterus junction (arrow). Scale bars: 400 μm (**A**); 20 μm (**B–G, I, K**); 50 μm (**H, J**).

Table 5. Morphometric data for females of *Mononchus* sp. and *Mononchus oblongus*.

Species	<i>Mononchus</i> sp.	<i>M. oblongus</i>
Source	Present study	Andrássy (2011a)
Locality	Waterfall “Durshin skok”, near Kopilovtsi, Montana Province	Near Ossés, South of France
River	Grafska (Balkan Mountains)	na
Habitat	<i>Fagus sylvatica</i> (soil)	Liver moss (soil)
<i>n</i>	(<i>n</i> = 2)	(<i>n</i> = 6)
L (mm)	1.31, 1.62	1.60–1.88
<i>a</i>	27.9, 30.6	25–29
<i>b</i>	3.5, 4.1	3.5–3.7
<i>c</i>	5.7, 6.2	6.0–7.1
<i>c</i> '	7.9, 7.7	7.5–8.8
V (%)	51.2, 56.2	52–54
G1 (%)	7.2, 8.3	7.6–9.4
G2 (%)	8.0, 9.2	7.6–9.4
Buccal capsule length	45, 47	48–51
Buccal capsule width	19, 20	18–19
Tooth apex from anterior end of buccal capsule	10, 11	10.0–11.5
Position of tooth apex (%) ^a	22, 23	21–23
Excretory pore from anterior end	123, 139	–
Nerve-ring from anterior end	111, 123	–
Pharynx length	370, 392	450–504
Lip region height	8, 9	7–9
Lip region width	25, 27	22–23
Amphid from anterior end	12, 19	– ^b
Maximum body diameter	47, 53	–
Body diameter at pharynx base	47, 53	60–65
Body diameter at mid-body	45, 52	60–68
Body diameter at vagina	46, 51	–
Body diameter at anus	29, 34	30–36
Anterior genital branch length	94, 135	–
Posterior genital branch length	105, 149	–
Anterior ovary length	40, 88	–
Posterior ovary length	45, 97	–
Vagina length	–, 16	18–21
Rectum length	24, 27	–
Tail length	230, 263	264–276

^a Distance from tooth apex to anterior end of buccal capsule as % of buccal capsule length from its anterior end.

^b “Somewhat posterior to anterior end of buccal capsule.” (Andrássy, 2011a).

Key to the species of *Mononchus*

Since the last identification key to the species of the genus *Mononchus* was published by Andrássy (2011a), eight additional species have been described and one species, *M. intermedius* Tahseen & Rajan, 2009, was not considered by Andrássy (2011a) (see Table 6 for the main morphometric characters of these species). The key by Andrássy (2011a) was, therefore, modified in order to accommodate all 31 species of the genus known to date, including

the new species described here. Examination of recent literature revealed that *Mononchus caudatus* Gagarin & Naumova, 2017 was preoccupied by *Mononchus caudatus* Shah & Hussain, 2016. Therefore, for the species described by Gagarin and Naumova (2017) we propose the replacement name *Mononchus baikalensis* (Gagarin & Naumova, 2017) nom. nov. after the type locality, Lake Baikal.

1	Large species, body 2.4–7.0 mm long.....	2
–	Smaller species, body 0.9–2.1 mm long	13
2	Tail very short, about 2 anal body diameters long	3
–	Tail longer, (3–) 4–9 anal body diameters long.....	6
3	Posterior third of tail digitate, ventrally curved	<i>M. mulveyi</i> Andrásy, 1985
–	Posterior third of tail not digitate, more or less straight.....	4
4	Buccal capsule 100–120 µm long, nearly 3 times as long as wide	
	<i>M. tajmiris</i> Gagarin, 1991
–	Buccal capsule 50–90 µm long, about twice as long as wide	5
5	Buccal capsule 80–90 µm long; spicule 300 µm long.....	
	<i>M. angarensis</i> Gagarin, 1984
–	Buccal capsule about 50 µm long; spicule 120 µm long	
	<i>M. maduei</i> Schneider, 1925
6	Body 5.0–7.2 mm long.....	7
–	Body 2.4–3.7 mm long.....	9
7	Body 5.0–6.4 mm long; tail as long as 5–6 (♂♂ 2.4) anal body diameters... ..	
	<i>M. superbus</i> Mulvey, 1978
–	Body 6.7–7.2 mm long; tail as long as 9 (♂♂ 4.6) anal body diameters	
	<i>M. amplus</i> Gagarin & Naumova, 2017
9	Buccal capsule > 80 µm long;.....	10
–	Buccal capsule 46–74 µm long;.....	11
10	Buccal capsule 80–84 µm long; tail as long as 3–4 anal body diameters... ..	
	<i>M. agilis</i> Gagarin & Mataphonov, 2004
–	Buccal capsule 105–112 µm long; tail as long as 5 (♂♂ 2.9–3.5) anal body diameters	
	<i>M. baikalensis</i> (Gagarin & Naumova, 2017) nom. nov.
11	Dorsal tooth apex at up to 16% of buccal capsule length from its anterior end; tail as long as 3–6 anal body diameters.....	12
–	Dorsal tooth apex at 28–30% of buccal capsule length from its anterior end; tail as long as 8–9 anal body diameters.....	
	<i>M. altiplanicus</i> Andrásy, 2011
12	Body 2.8–3.5 mm long; buccal capsule 46–56 × 20–25 µm; spicules relatively short (134–140 µm)	<i>M. niddensis</i> Skwarra, 1921
–	Body 2.4–2.9 mm long; buccal capsule 65–74 × 28–31 µm; spicules longer (205–215 µm)	<i>M. minutus</i> Naumova & Gagarin, 2018
13	Monodelphic species	<i>M. italicus</i> Andrásy, 1959
–	Didelphic species	14
14	Tail quite short (as long as 1.5–2 anal body diameters); spinneret subdorsal.....	
	<i>M. clarki</i> Altherr, 1972
–	Tail as long as 3 anal body diameters or longer (c' = up to 15); spinneret terminal	15
15	Buccal capsule small, 18–23 µm long.....	16
–	Buccal capsule larger, 26–50 µm long.....	17

16	Buccal capsule very narrow (nearly 3 times as long as wide); dorsal tooth apex quite close to the anterior end of buccal capsule	
 <i>M. tunbridgensis</i> Bastian, 1865	
–	Buccal capsule wider (twice as long as wide); dorsal tooth apex at 28–33% of buccal capsule length from its anterior end	
 <i>M. loofi</i> Winiszewska, 1998	
17	Tail as long as 7–15 (mostly 9–14) anal body diameters	18
–	Tail as long as 3–8 (mostly 4–7) anal body diameters	20
18	Tail 340–390 µm long, as long as 13–15 anal body diameters	
 <i>M. syrmatius</i> Andrásy, 2008	
–	Tail 220–300 µm long, as long as 8–11 anal body diameters	19
19	Buccal capsule 40–47 µm long; one prevulval papilla present	
 <i>M. himalayensis</i> Rawat & Ahmad, 2000	
–	Buccal capsule 28–35 µm long; prevulval papilla absent	
 <i>M. sandur</i> Eisendle, 2008	
20	<i>Pars refringens vaginae</i> not sclerotised <i>M. sinensis</i> Soni & Nama, 1983	
–	<i>Pars refringens vaginae</i> distinctly sclerotised	21
21	Subventral transverse ribs located anteriorly to tooth apex	22
–	Subventral transverse ribs located at level of or posterior to tooth apex	23
22	Lip region relatively wide (24–28 µm); cylindrical portion of tail 10–12 µm thick	
 <i>M. truncatus</i> Bastian, 1865	
–	Lip region narrower (20 µm); cylindrical portion of tail 5–7 µm thick	
 <i>M. medius</i> Andrásy, 2011	
23	Amphid aperture posterior to dorsal tooth	
 <i>M. laminatus</i> Zullini, Loof & Bongers, 2002	
–	Amphid aperture anterior to dorsal tooth	24
24	Tail as long as 3–4 anal body diameters	25
–	Tail as long as 4–7 anal body diameters	26
25	Body 1.6–2.1 mm long; dorsal tooth apex at 22–24% of buccal capsule length from its anterior end; tail 176 µm	
 <i>M. nudus</i> Gagarin, 1991	
–	Body 1.5 mm long, dorsal tooth apex at 30–35% of buccal capsule length from its anterior end; tail 117–122 µm	
 <i>M. oryzae</i> Ishaque, Iqbal, Dawar & Kazi, 2022	
26	Buccal capsule two labial diameters long or longer	27
–	Buccal capsule conspicuously shorter than two labial diameters	28
27	Buccal capsule oblong, 47–50 µm long, labial diameter 22–23 µm	
 <i>M. oblongus</i> Andrásy, 2011	
–	Buccal capsule barrel-shaped, 33–34 µm long, labial diameter 16–17 µm	
 <i>M. prodentatus</i> Shah & Hussain, 2016	
28	Dorsal tooth apex at > 25% of buccal capsule length from its anterior end	29
–	Dorsal tooth apex at < 25% of buccal capsule length from its anterior end	30
29	Buccal capsule 36–44 µm long, $c = 8.7–10.6$; tail 145–182 µm long	
 <i>M. intermedius</i> Tahseen & Rajan, 2009	
–	Buccal capsule 29–43 µm long, $c = 7–8$; tail 193–231 µm long	
 <i>M. labiatus</i> Shah & Hussain, 2016	

- 30 Buccal capsule (33)35–38 μm long, vagina spotted in its anterior part ***M. pulcher* Andrásy, 1993**
 – Buccal capsule 29–33 μm long, vagina not spotted.....**31**
 31 Buccal capsule 1.8–2.0 times as long as wide, *pars refringens vaginae* rhomb-shaped ***M. pseudoaquaticus* sp. nov.**
 – Buccal capsule 2.2–2.5 times as long as wide, *pars rrefringens vaginae* drop-shaped.....**32**
 32 Body 1.2–1.7 mm long, rectum length 24–25 μm
 ***M. aquaticus* Coetzee, 1968**
 – Body 1.7–1.9 mm long, rectum length 32–36 μm
 ***M. caudatus* Shah & Hussain, 2016**

Molecular phylogenies

To assess the associations of the newly generated sequences (4 for *C. parvus* and 5 for *Mononchus* spp.) from the nematode populations sampled in Bulgaria, we carried out an exploratory neighbour-joining (NJ) analysis on an untrimmed 28S rDNA alignment (domains D1-D3), including representative sequences for *Mononchus* spp. (20 sequences) and *Coomansus* spp. (15 sequences). Using pairwise deletion of missing data allowed us to include more taxa and sequences, e.g., several sequences of Schenk et al. (2017), including sequences for *M. aquaticus*, albeit with a short overlap (GenBank codes MF-XXX, D3-D5 region) (Fig. 12). The novel isolates of *C. parvus* formed a reciprocally monophyletic clade with *C. parvus*, *C. batxatensis* Vu, 2021 and *Coomansus* spp. with maximum support; the clade of *Coomansus* spp. was recovered as sister to *C. gerlachei* (de Man, 1904) Jairajpuri & Khan, 1977 (GenBank: KM092524) but with poor statistical support. The isolates of *M. pseudoaquaticus* sp. nov. clustered with maximum support with *Mononchus* sp. 1 sensu Mejía-Madrid (2018) within the strongly supported clade of *Mononchus* spp. comprising the novel and published isolates of *M. aquaticus*, *M. truncatus*, *M. maduei*, *M. tunbridgensis*, and *Mononchus* sp. sensu Schenk et al. (2017) to the exclusion of one isolate identified as *M. aquaticus* (GenBank: MF125523; Schenk et al. 2017). This molecular prospecting analysis confirmed the identification of the novel isolates based on the detailed morphological analysis (see above) and indicated that *Mononchus* sp. 1 sensu Mejía-Madrid (2018) belongs to the new species described here.

Next, we assessed the phylogenetic relationships of the novel isolates with representatives of the suborder Mononchina using two alignments. Upon trimming to the length of the shortest sequence, the 28S rDNA (domains D2-D3) alignment comprised a total of 779 nt positions and contained sequences for representatives of ten genera of the families Anatonchidae (*Anatonchus* Cobb, 1916, *Iotonchus* Cobb, 1916, *Jensenonchus* Jairajpuri & Khan, 1982, *Mulveyellus* Siddiqi, 1984 and *Parahadronchus* Mulvey, 1978), Mononchidae (*Coomansus*, *Mononchus*, *Parkellus* and *Prionchulus* Cobb, 1916) and Mylonchulidae (*Mylonchulus* Jairajpuri, 1969). There were no sequence data for *Miconchus* spp. and *Actus* spp., and the available sequences for *Clarkus papillatus* (Bastian, 1865) Jairajpuri, 1970 (domains D3-D5) could not be used due to the very small overlap. Overall, the topology of the ML tree (Fig. 13) was well resolved

Table 6. Main morphometric data for the nine additional species of *Mononchus* described after 2011 and included in the key to species.

Species	<i>M. amplus</i> Gagarin & Naumova, 2017	<i>M. baikalensis</i> (Gagarin & Naumova, 2017) nom. nov.	<i>M. caudatus</i> Shah & Hussain, 2016	<i>M. intermedius</i> Tahseen & Rajan, 2009	<i>M. labiatus</i> Shah & Hussain, 2016	<i>M. minutus</i> Naumova & Gagarin, 2018	<i>M. oryzae</i> Ishaque et al., 2022	<i>M. prodeniatus</i> Shah & Hussain, 2016	<i>M. pseudoaquaticus</i> sp. nov.
L (mm)	♀ 6.74–7.24 ♂ 6.90	♂ 3.35–3.72 ♀ 3.35	♀ 1.73–1.92	♀ 1.32–1.65	♀ 1.31–1.79	♀ 2.38–2.89 ♂ 2.34–2.83	♀ 1.51–1.53	♀ 1.69–1.76	♀ 1.23–1.88
a	52–61	22–26	34–37	20.5–28.8	30–36	26–33	28.4–31.7	31–33	21–36
b	4.7–4.8	3.4–3.6	4.0–5.0	3.8–4.7	3.0–4.0	3.3–3.7	3.6–3.9	4.0–5.0	4.0–4.6
c	11.3–11.6	11.2–13.0	9.0–10.0	8.7–10.6	7.0–8.0	12.8–15.1	12.3–13.0	8.0–9.0	7.2–10.2
c'	8.9	2.9–3.5	5.0–6.0	3.9–5.8	6.0–7.0	3.3–4.4	3.9–4.2	5.0–6.0	4.7–5.8
V (%)	59	–	48–51	50–55	56–64	56–61	59–61	53–55	48–54
Lip region width	58–60	54–60	24–25	20–26	24–25	35–40	23–24	16–17	23–26
Buccal capsule length	70–78	105–112	30–33	36–44	29–43	65–74	34–35	33–34	29–33
Position of tooth apex (%) ^a	27–29	28–30	18–21	25–30	27–35	9–14	19–20	24–28	18–21
Tail length	595–625	275–300	190–195	145–182	193–231	175–208	117–122	196–200	171–207
Supplements	–	31–32	–	–	–	–	–	–	–
Spicule	–	220–235	–	–	–	–	–	–	–

^a Distance from tooth apex to anterior end of buccal capsule as % of buccal capsule length from its anterior end. References: Gagarin and Naumova (2017); Shah and Hussain (2016); Tahseen and Rajan (2009); Naumova and Gagarin (2018); Ishaque et al. (2022).

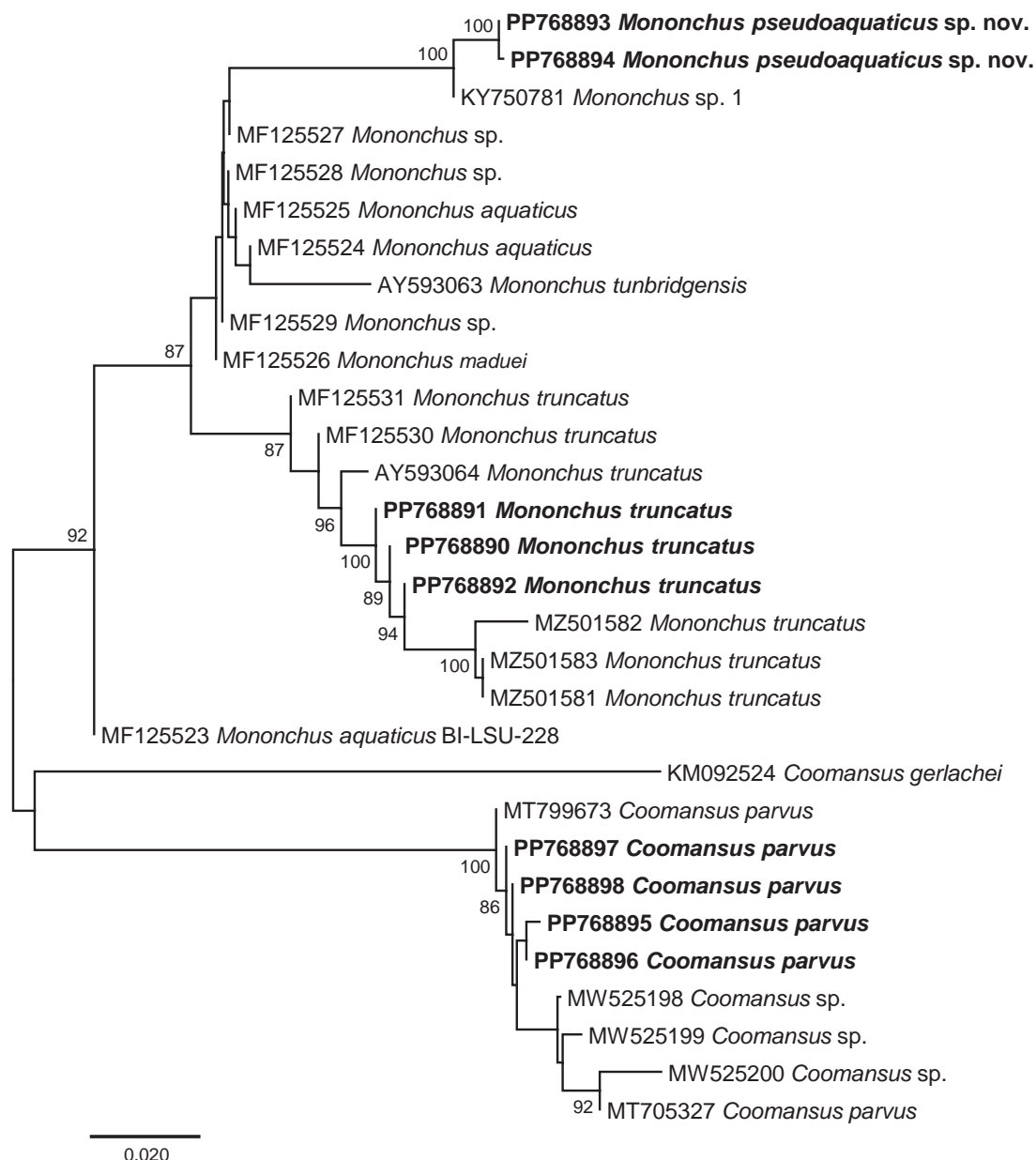


Figure 12. Neighbour-joining tree based on the 28S rDNA (domains D1-D3) dataset (1293 nt positions). The newly generated sequences are indicated in bold. Only bootstrap values > 70% are shown.

with two strongly supported main clades: (i) *Mononchus* spp. (98% supported); and (ii) a large clade (80% supported) comprising the remaining genera except for *Mylonchulus*. Within the *Mononchus* clade, the novel sequences for *M. truncatus* clustered with four published sequences for *M. truncatus* with maximum support and *M. pseudoaquaticus* sp. nov. clustered with a sequence for *Mononchus* sp. 1 sensu Mejía-Madrid (2018), again with maximum support. The second clade had fully resolved internal topology with two large sub-clades, one (100% supported) comprising *Coomansus* spp. (*C. parvus* + *C. batxatensis*) plus representatives of *Jensenonchus*, *Prionchulus*, *Mulveyellus*, and *Parkellus*, and one (74% supported) comprising *C. gerlachei* and representatives of *Anatonchus*, *Iotonchus* and *Parahadronchus*. The relationships of the strongly supported (100%) clade of *Mylonchulus* spp. remained unresolved.

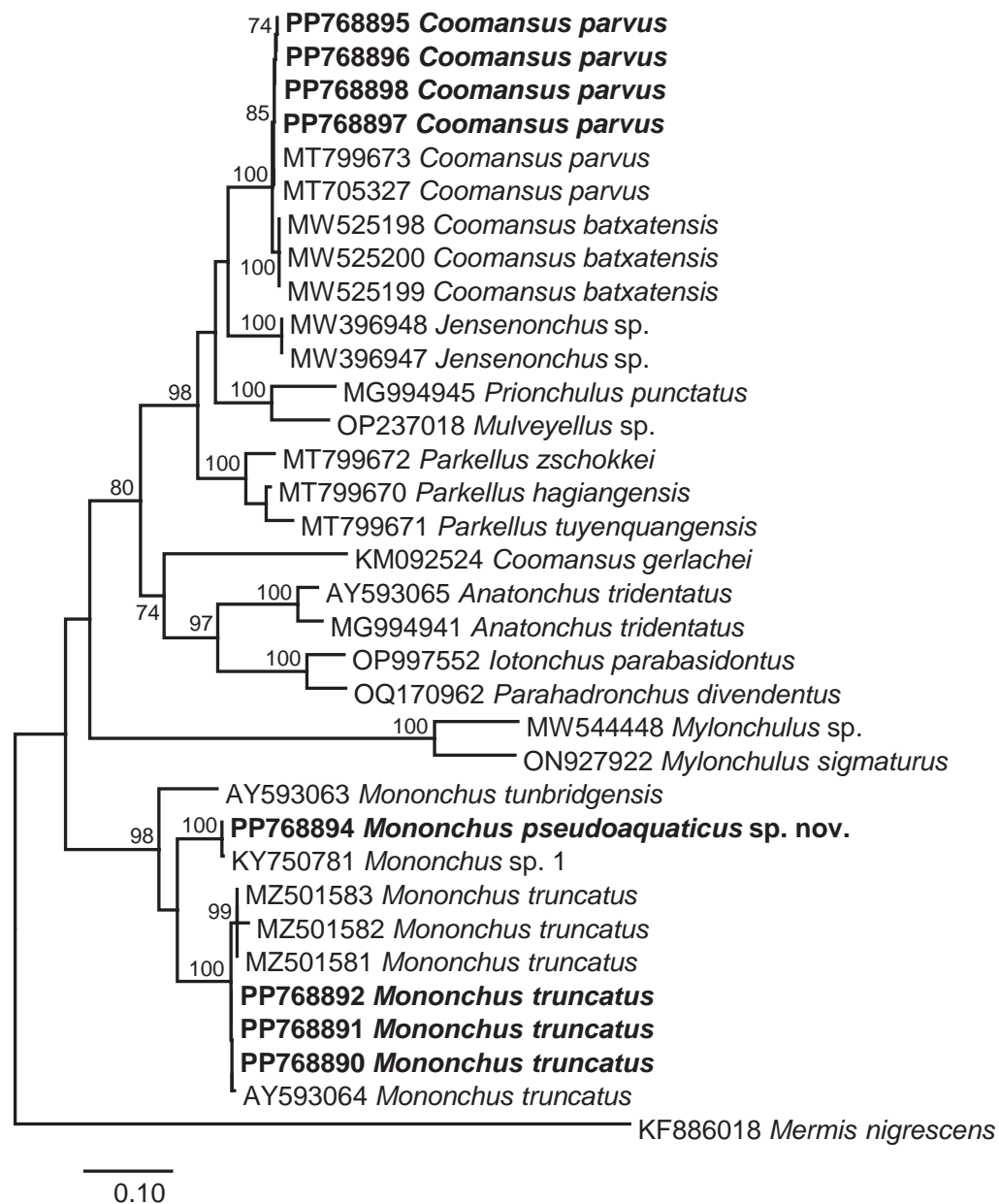


Figure 13. Maximum likelihood phylogeny based on the 28S rDNA (domains D2-D3) dataset (779 nt positions). The newly generated sequences are indicated in bold. Only bootstrap values > 70% are shown.

The 18S rDNA alignment comprised a total of 1636 nt positions after trimming the ends to match the shortest aligned sequences and contained sequences for representatives of ten genera of the families Anatonchidae (*Anatonchus* and *Miconchus* Andr assy, 1958), Mononchidae (*Actus* Baqri & Jairajpuri, 1974, *Clarkus* Jairajpuri, 1970, *Coomansus*, *Mononchus*, *Parkellus*, and *Prionchulus*) and Mylonchulidae (*Granonchulus* Andr assy, 1958 and *Mylonchulus*). The available sequences for representatives of the genera *Iotonchus*, *Jensenonchus*, *Mulveyellus*, and *Parahadronchus* were excluded from the analyses because they were too short and did not exhibit sufficient overlap with the alignment. The topology of the ML tree (Fig. 14) exhibited poorly resolved basal nodes and four strongly supported clades: (i) *Mononchus* spp. (100% supported) (*M. tunbridgensis* + *M. truncatus* + *M. aquaticus* + *M. pseudoaquaticus* sp. nov.

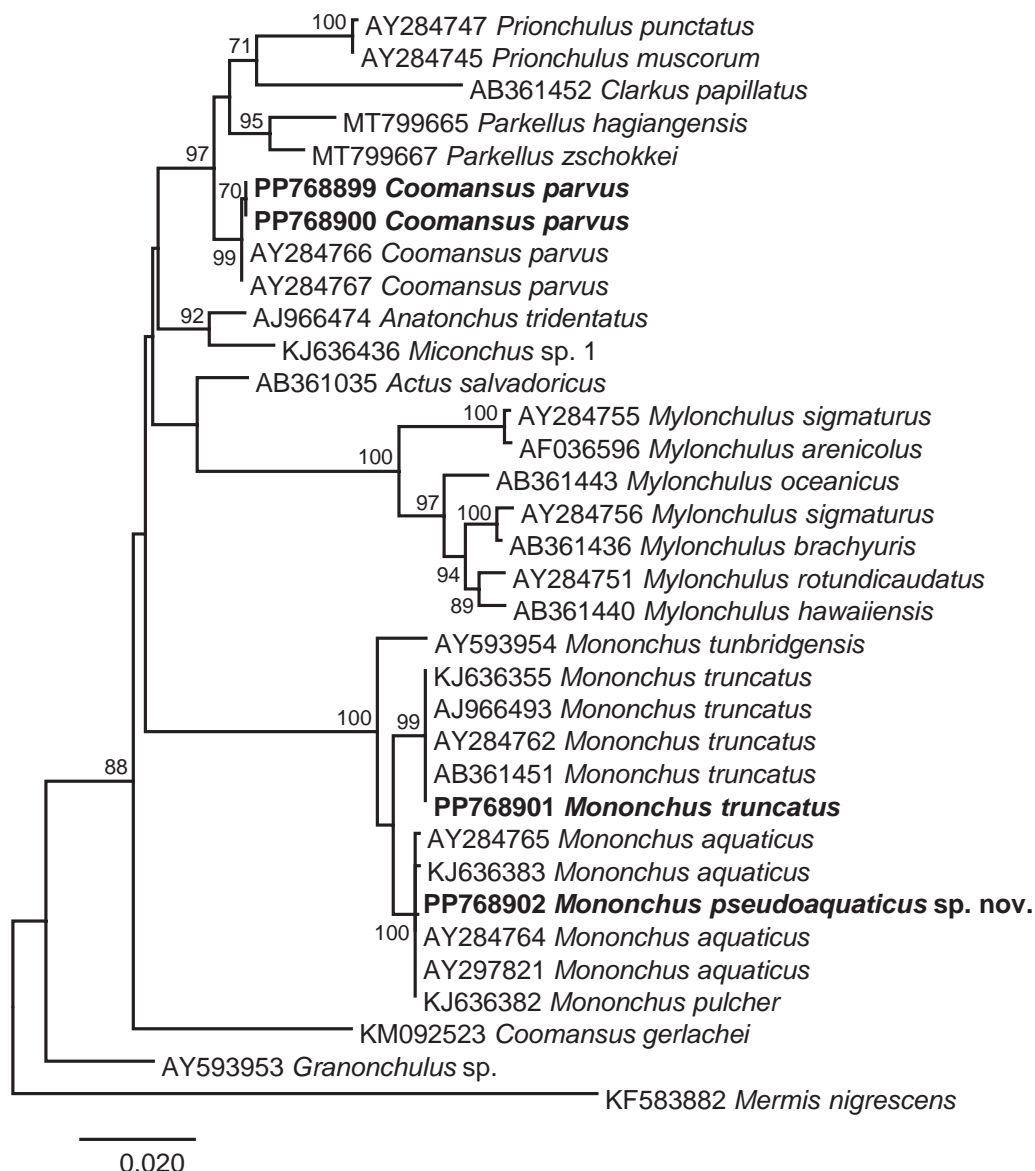


Figure 14. Maximum likelihood phylogeny based on the 18S rDNA dataset (1636 nt positions). The newly generated sequences are indicated in bold. Only bootstrap values > 70% are shown.

+ *M. pulcher*); (ii) the remaining mononchids (*Coomansus* + *Clarkus* + *Parkellus* + *Prionchulus*) (97% supported); (iii) *Mylonchulus* (100% supported); and (iv) *Anatonchus* + *Miconchus* (both Anatonchidae) (92% supported).

At the species level, both phylogenies (18S rDNA and 28S rDNA) supported (i) the identification based on morphology of the novel isolates of *M. truncatus* and *C. parvus* both forming strongly supported reciprocally monophyletic clades, and (ii) the exclusion of *C. gerlachei* from *Coomansus*; this species was recovered as a sister taxon (74% supported) to the representatives of the Anatonchidae in the 28S rDNA phylogeny and as a basal taxon to the remaining taxa except for *Granonchulus* in the 18S rDNA analysis. However, in contrast to the clear delineation of *M. pseudoaquaticus* sp. nov. (100% supported) in the 28S rDNA phylogeny, the 18S rDNA phylogeny did not provide support for the delimitation of *M. aquaticus* (as *M. pulcher* sensu van Megen et al. 2009; GenBank: KJ636382) and *M. pseudoaquaticus* sp. nov.

At the generic level, both phylogenies recovered the three genera represented by two or more species (i.e., *Mononchus*, *Mylonchulus*, and *Parkellus*) as monophyletic with strong support. At the suprageneric level, both phylogenies resolved fewer relationships due to the small number of taxa (10 genera, 5 genera in common) and perhaps the much poorly resolved basal nodes in the 18S rDNA phylogeny. Both phylogenies recovered the Mononchidae as paraphyletic with *Mononchus* placed in a separate basal clade and Mylonchulidae and Anatonchidae nested within the second clade of the Mononchidae despite the different composition of the taxa included in the analyses. However, this is the only concordant result for the two molecular markers. Thus, the Mylonchulidae (represented by *Mylonchulus* alone) was recovered as monophyletic in the 28S rDNA phylogeny but as polyphyletic in the 18S rDNA phylogeny (represented by *Mylonchulus* and *Granonchulus*). Similarly, the Anatonchidae was monophyletic in the 18S rDNA phylogeny (2 genera: *Anatonchus* and *Miconchus*) but paraphyletic in the 28S rDNA phylogeny containing five genera, with *Anatonchus* + *Iotonchus* + *Parahadronchus* recovered in a strongly supported clade (97% supported) and *Jensenonchus* and *Mulveyellus* nested within one of the clades of the Mononchidae.

Comparative sequence analysis

The trimmed alignments of 28S rDNA and 18S rDNA allowed a comparative assessment of the genetic divergence at the level of species (intraspecific) and genus (interspecific) as well as between genera (intergeneric) based on pairwise comparisons. As shown in Table 7, the divergence levels for 18S rDNA are much lower for all three categories of comparisons: up to 10-fold for intraspecific variation, up to ~ 4-fold for interspecific variation, and up to ~ 5-fold for intergeneric variation. The interspecific divergence in 18S rDNA sequences for *M. pulcher* sensu van Megen et al. (2009; GenBank: KJ636382), *M. aquaticus*, and *M. pseudoaquaticus* sp. nov. was particularly low (0–1 nt positions; 0–0.1%).

Comparative sequence analyses also provided support for the position in the phylogenies of the isolate identified as *C. gerlachei* (GenBank: KM092523 and KM092524) by Elshishka et al. (2015). This isolate differed from *C. parvus* at 70–71 nt positions (4.3–4.4%; 18S rDNA) and from the remaining *Coomansus* spp. at 135–137 nt positions (20.6–20.8%; 28S rDNA), values well above the genetic divergence between congeners. The isolates identified by Kagoshima et al. (2019) (GenBank: LC457639–LC457644; LC457655–LC457661) were found to be associated with high support with the isolate of Elshishka et al. (2015) that also represented the best BLAST hit for all isolates.

Genetic divergence estimates in 28S rDNA also indicated that *C. batxatensis* may be conspecific with *C. parvus* (difference at 6–8 nt positions, i.e., 0.9–1.2%). This difference is distinctly lower than the ranges of interspecific divergence within the genera *Mononchus*, *Coomansus*, *Parkellus* and *Mylonchulus*, i.e., 34–77 nt positions or 5.1–11.8%; Table 7). Furthermore, the otherwise unpublished isolate identified as *M. truncatus* (GenBank: MZ501582) may have been misidentified; this isolate differs from the remaining isolates of *M. truncatus* by 8–15 nt (1.2–2.0%). Finally, the intergeneric divergence between *Coomansus* spp. and *Parkellus* spp. falls within the range of interspecific divergence for both genes (Table 7) and this is in contrast with both model-based phylogenies supporting the distinction of *Parkellus* spp. at the generic level (Figs 13, 14).

Table 7. Genetic divergence estimated for the 18S rDNA and 28S rDNA sequence pairs within and between species and between species of different genera compared in this study.

Divergence	Taxa	18S rRNA gene		28S rRNA gene	
		Differences (nt)	p-distance (%)	Differences (nt)	p-distance (%)
Intraspecific	<i>Mononchus truncatus</i>	0	0	0–7 ^a	0–1.1 ^a
	<i>Mononchus aquaticus</i>	0–2 ^b	0–0.1 ^b	1	0.2
	<i>Coomansus parvus</i>	0–1	0–0.1	0–2	0–0.3
Interspecific	<i>M. truncatus</i> vs <i>M. aquaticus</i>	13–14	0.8–0.9	59–70	8.9–10.5
	<i>Mononchus</i> spp.	13–23 ^b	0.8–1.4 ^b	59–77	8.9–11.8
	<i>Coomansus</i> spp.	70–71 ^c	4.3–4.4 ^c	6–8 ^d	0.9–1.2 ^d
	<i>Parkellus</i> spp.	24	1.5	34–54	5.1–8.2
	<i>Mylonchulus</i> spp.	3–52	0.2–3.2	69	10.1
Intergeneric	<i>Mononchus</i> spp. vs <i>Coomansus</i> spp.	76–80	4.7–4.9	140–158 ^d	21.2–22.8 ^d
	<i>Coomansus</i> spp. vs <i>Parkellus</i> spp.	27–35 ^e	1.7–2.2 ^e	64–74 ^d	9.7–11.2 ^d

^a *M. truncatus* (GenBank: MZ501582; unpublished) excluded from the comparison (differs from the remaining isolates of *M. truncatus* at 8–15 nt positions, i.e., 1.2–2.0%).

^b *M. pulcher* (GenBank: KJ636382) included in the comparison (differs from *M. aquaticus* at 0–1 nt positions, i.e., 0–0.1%).

^c Genetic divergence between *C. parvus* and *C. gerlachei*.

^d *C. gerlachei* (GenBank: KM092524) excluded from the comparison (differs from the remaining *Coomansus* spp. at 135–137 nt positions, i.e., 20.6–20.8%).

^e *C. gerlachei* (GenBank: KM092523) excluded from the comparison.

Discussion

To the best of our knowledge, the present study is the first to apply an integrative taxonomic approach to the diversity of mononchid nematodes in European riparian ecosystems. Our extensive, focused sampling in a range of riverine habitats in Bulgaria revealed a wide geographical distribution and altitudinal ranges of three species of the family Mononchidae of which one represents a species new to science; these were also associated with a range of tree species of seven genera (*Alnus*, *Carpinus*, *Fagus*, *Fraxinus*, *Populus*, *Salix*, and *Ulmus*). The integration of molecular and morphological data for these three species provided support for their distinct species status. Thus, our study is the first to provide taxonomically verified 18S rDNA and 28S rDNA sequences for *C. parvus*, *M. truncatus* (sensu stricto), and *M. pseudoaquaticus* sp. nov.

At the species level, phylogenetic analyses revealed that the newly sequenced isolates of *M. truncatus* (sensu stricto) and *C. parvus* consistently clustered together with published sequences for these species irrespective of the ribosomal locus (Figs 13, 14) or region of the 28S rRNA gene (Figs 12, 13). However, the 18S rDNA phylogeny did not allow delimitation of *M. pseudoaquaticus* sp. nov. and *M. aquaticus* (Fig. 14). Whereas *M. pulcher* sensu van Megen et al. (2009) (GenBank: KJ636382) not used in the analysis by these authors and by Holterman et al. (2008) is likely a misidentification, the morphological differentiation of *M. aquaticus* and *M. pseudoaquaticus* sp. nov. was strongly supported in the 28S rDNA phylogeny, suggesting that the 18S rRNA gene does not allow reliable differentiation of closely related species at least within the genus *Mononchus*. Lower resolution of the 18S rRNA gene was reported in a comparative barcoding/metabarcoding study by Schenk et al. (2020); out of 22 nematode species identified using morphology in their study, 20 species were delineated using the

28S rDNA marker and only 12 species were detected using the 18S rDNA marker. Our comparative sequence (Table 7) and phylogenetic (Fig. 14) analyses suggest that the utility of the 18S rRNA gene for species delimitation is rather limited at least for some species complexes within the genus *Mononchus*.

An alternative hypothesis for the phylogenetic results based on 18S rDNA is that the specimens of *M. aquaticus* sequenced by van Megen et al. (2009) (GenBank: KJ636382 and KJ636383), Holterman et al. (2006) (GenBank: AY284764 and AY284765) and Oliveira et al. (2004) (GenBank: AY297821) actually represent *M. pseudoaquaticus* sp. nov. However, because of the lack of sequence data for the 28S rRNA gene and deposited voucher material for these sequenced isolates, neither of these hypotheses can be tested.

We highlight that the new species described here could be clearly distinguished morphologically from *M. aquaticus* (sensu stricto) and that currently *M. aquaticus* likely represents a composite species and this may result in misidentifications of the isolates subjected to sequencing. For example, in the 28 rDNA tree of Schenk et al. (2017) the six specimens identified as *M. aquaticus* ($n = 3$), *M. maduei* and *Mononchus* sp. juv. ($n = 3$) formed a reciprocally monophyletic clade with high support (97%). However, in the present NJ analysis (Fig. 12) one isolate (GenBank: MF125523) was resolved as clearly distinct from the other two isolates of *M. aquaticus* sequenced, and in fact, from all isolates of *Mononchus* spp. (Fig. 12), thus questioning the identification of this isolate. The above considerations highlight the need for generating taxonomically verified 18S rDNA and 28S rDNA sequences for *M. aquaticus* (sensu stricto).

The isolate of *C. gerlachei* sequenced by Elshishka et al. (2015) (GenBank: KM092523 and KM092524) was not associated with the *C. parvus* clade (18S rDNA; Fig. 14) or with *C. parvus* + *C. batxatensis* clade (28S rDNA; Fig. 13) and exhibited genetic divergence levels well above the levels observed between species of the mononchid genera *Coomansus*, *Mononchus*, *Mylonchulus*, and *Parkellus* considered here (Table 7). Taken together, our comparative sequence and phylogenetic analyses strongly suggest that the isolates sequenced by Elshishka et al. (2015) and Kagoshima et al. (2019) should be distinguished at the generic level.

At the generic and suprageneric level, the present 18S and 28S phylogenies both recovered the Mononchidae as paraphyletic (as in Holterman et al. 2008 and van Megen et al. 2009). Further, a comparison with the phylogenies of the Mononchida based on 18S rDNA by Holterman et al. (2008) and van Megen et al. (2009) revealed that all four sub-clades identified by these authors (denoted M1-M4 in Holterman et al. 2008) were supported in the present phylogeny: *Mylonchulus* (sub-clade M1); *Mononchus* (sub-clade M2); *Clarkus* + *Prionchulus* + *Coomansus* (sub-clade M3); and *Anatonchus* (sub-clade M4). The differences between the present and published phylogenetic hypotheses represent (i) the recovery of the Anatonchidae as monophyletic in the present phylogeny vs paraphyletic in Holterman et al. (2008) and van Megen et al. (2009), and (ii) the lack of support for a sister-group relationship between *Mylonchulus* (sub-clade M1) and *Mononchus* (sub-clade M2) in the present phylogeny. Finally, the poorly represented Mylonchulidae (2 genera: *Mylonchulus* and *Granonchulus*) was recovered as polyphyletic in the present 18S rDNA phylogeny as in Holterman et al. (2008) and van Megen et al. (2009). These results are due to a single sequence for *Granonchulus* sp. (AY593953) by Holterman et al. (2008). Unfortunately, no

voucher specimen exists to support the identification of the sequenced nematode. Further sequencing of *Granonchulus* spp., and preferably, of species from the other genera of the family, will help develop a natural hypothesis for the relationships within the Mylonchulidae and the Mononchida in general.

Additional information

Conflict of interest

The authors declare that they have no competing interests.

Ethical statement

Not applicable.

Funding

This study was partially funded by a PhD grant to Stela Altash (Institute of Biodiversity and Ecosystem Research, Bulgarian Academy of Sciences).

Author contributions

Stela Altash: Investigation, Formal analysis, Visualisation, Writing – original draft, Writing – review and editing, Funding acquisition. Aneta Kostadinova: Conceptualization, Methodology, Data curation, Formal analysis, Supervision, Writing – review and editing. Vlada Peneva: Conceptualization, Methodology, Data curation, Visualisation, Funding acquisition, Supervision, Writing – review and editing.

Author ORCIDs

Aneta Kostadinova  <https://orcid.org/0000-0001-7070-4968>

Data availability

All data generated or analyzed during this study are included in this published article and its supplementary files. The newly generated sequences were submitted to the GenBank database under the accession numbers PP768899–PP768902 (18S rRNA gene) and PP768890–PP768898 (28S rRNA gene).

References

- Ahmad W, Jairajpuri MS (2010) Mononchida: The predaceous nematodes. In: Hunt DJ, Perry RN (Eds) *Nematology Monographs and Perspectives*; v. 7. Brill Academic Publishers, Leiden-Boston, 298 pp. <https://doi.org/10.1163/ej.9789004174641.i-298.2>
- Aleksiev A, Budurova L, Baicheva O (1998) Biomonitoring investigations of the phytonematode communities in the rhizosphere of *Quercus frainetto* in the region of Debelt (Burgas District). *Biotechnology, Biotechnological Equipment* 12(1): 109–115. <https://doi.org/10.1080/13102818.1998.10818976>
- Andrássy I (1958) Erd-und Süßwasser nematoden aus Bulgarien. *Acta Zoologica Academiae Scientiarum Hungaricae* 4: 1–88.
- Andrássy I (1993) A taxonomic survey of the family Mononchidae (Nematoda). *Acta Zoologica Hungarica* 39: 13–60.
- Andrássy I (2009) *Free-living Nematodes of Hungary: Nematoda Errantia*, v. 3. Hungarian Natural History Museum, Budapest. <https://books.google.bg/books?id=WZEAYAAA-CAAJ>

- Andrássy I (2011a) Three new species of the genus *Mononchus* (Nematoda: Mononchida), and the “real” *Mononchus truncatus* Bastian. *Journal of Natural History* 45(5–6): 303–326. <https://doi.org/10.1080/00222933.2010.524947>
- Andrássy I (2011b) Three new species of the genus *Coomansus* Jairajpuri & Khan, 1977 from the southern hemisphere (Nematoda: Mononchida). *Journal of Nematode Morphology and Systematics* 14: 27–37. <https://revistaselectronicas.ujaen.es/index.php/jnms/article/view/797>
- Archidona-Yuste A, Palomares-Rius JE, Clavero-Camacho I, Cantalapiedra-Navarrete C, Liébanas G, Castillo PA (2023) Blind-identification test on *Criconema annuliferum* (de Man, 1921) Micoletzky, 1925 species complex corroborate the hyper-cryptic species diversity using integrative taxonomy. *Plants* 12(5): 1044. <https://doi.org/10.3390/plants12051044>
- Baqri SZ, Jairajpuri MS (1972) Studies on Mononchida of India V. Some observations on the morphology of *Mononchus aquaticus* Coetzee, 1968 with remarks on its status. *Iranian Journal of Nematology* 2: 105–116.
- Bardgett RD, Anderson JM, Behan-Pelletier V, Brussaard L, Coleman DC, Ettema C, Moldenke A, Schimel JP, Wall DH (2001) The influence of soil biodiversity on hydrological pathways and the transfer of materials between terrestrial and aquatic ecosystems. *Ecosystems (New York, N.Y.)* 4(5): 421–429. <https://doi.org/10.1007/s10021-001-0020-5>
- Bongers T, Ferris H (1999) Nematode community structure as a bioindicator in environmental monitoring. *Trends in Ecology & Evolution* 14(6): 224–228. [https://doi.org/10.1016/S0169-5347\(98\)01583-3](https://doi.org/10.1016/S0169-5347(98)01583-3)
- Botha A, Heyns J (1992) Further records and descriptions of nematodes from rivers in the Kruger National Park (Orders Enoplida, Chromadorida, Monhysterida, Mononchida and Araeolaimida). *Koedoe* 35(2): 11–25. <https://doi.org/10.4102/koedoe.v35i2.401>
- Briar SS, Culman SW, Young-Mathews A, Jackson LE, Ferris H (2012) Nematode community responses to a moisture gradient and grazing along a restored riparian corridor. *European Journal of Soil Biology* 50: 32e38. <https://doi.org/10.1016/j.ejsobi.2011.11.006>
- Clark WC (1960) Redescription of *Mononchus truncatus* Bastian, *M. papillatus* Bastian and *Prionchulus muscorum* (Dujardin) (Enoplida, Nematoda). *Nematologica* 5(3): 184–198. <https://doi.org/10.1163/187529260X00352>
- Coetzee V (1968) Southern African Species of the genera *Mononchus* and *Prionchulus* (Mononchidae). *Nematologica* 14(1): 63–76. <https://doi.org/10.1163/187529268X00651>
- Coomans A, Khan S (1981) Mononchida from Mount Kenya. *Biologisch Jaarboek Dodonaea* 49: 64–75.
- Coomans A, Rashid F, Heyns J (1995) On some predatory nematodes from the Okavango Delta, Botswana. *Hydrobiologia* 302: 119–131. <https://doi.org/10.1007/BF00027037>
- De Bruin S, Heyns J (1992) Mononchida (Nematoda) of Southern Africa: Genera *Mononchus* Bastian, 1865, *Clarkus*, Jairajpuri, 1970 and *Coomansus* Jairajpuri & Khan, 1977. *Phytophylactica* 24: 61–73. https://journals.co.za/doi/pdf/10.10520/AJA03701263_1459
- De Ley P, De Ley IT, Morris K, Abebe E, Mundo-Ocampo M, Yoder M, Heras J, Waumann D, Rocha-Olivares A, Jay Burr AH, James G, Baldwin JG, Kelley Thomas W (2005) An integrated approach to fast and informative morphological vouchering of nematodes for applications in molecular barcoding. *Philosophical Transactions of the Royal Society of London, Series B, Biological Sciences* 360(1462): 1945–1958. <https://doi.org/10.1098/rstb.2005.1726>

- De Man JG (1876) Onderzoekingen over vrij in de aarde levende nematoden. *Nederlandsch Tijdschrift voor Dierkunde*, 78–196.
- De Man JG (1880) Die Eingheimischen, frei in der reinen erde und im süßen wasser lebends Nematoden. *Nederlandsch Tijdschrift voor Dierkunde* 5: 1–104.
- Décamps H, Naiman RJ, McClain ME (2009) Riparian zones. In: Likens GE (Ed.) *Encyclopedia of inland waters*. Academic Press, London, 396–403. <https://doi.org/10.1016/B978-012370626-3.00053-3>
- Eisendle U (2008) Description of *Mononchus sandur* n. sp. (Nematoda: Mononchidae) and remarks on *M. truncatus* Bastian, 1865 and *M. aquaticus* Coetzee, 1968 from a glacial floodplain reach (Grossglockner region, Hohe Tauern, Austria). *Nematology* 10(6): 809–818. <https://doi.org/10.1163/156854108786161481>
- Elshishka M, Lazarova S, Radoslavov G, Hristov P, Peneva VK (2015) New data on two remarkable Antarctic species *Amblydorylaimus isokaryon* (Loof, 1975) Andrassy, 1998 and *Pararhysocolpus paradoxus* (Loof, 1975), gen. n., comb. n. (Nematoda, Dorylaimida). *ZooKeys* 511: 25–68. <https://doi.org/10.3897/zookeys.511.9793>
- Farahmand S, Eskandari A, Orselli L, Karegar A (2009) Some known species of the genera *Mononchus* Bastian, 1865 and *Mylonchulus* (Cobb, 1916) Alther, 1953 (Nematoda: Mononchina) from Semnan province, Iran. *Nematologia Mediterranea* 37: 145–154. <https://journals.flvc.org/nemamedi/article/view/86996>
- Ferris H (2005) Carbon channels and food web structure. *Journal of Nematology* 37: 369.
- Ferris H, Bongers T, de Goede RGM (2001) A framework for soil food web diagnostics: Extension of the nematode faunal analysis concept. *Applied Soil Ecology* 18(1): 13–29. [https://doi.org/10.1016/S0929-1393\(01\)00152-4](https://doi.org/10.1016/S0929-1393(01)00152-4)
- Gagarin VG, Naumova TV (2017) Description of the two new nematode species of the genus *Mononchus* Bastian, 1865 (Nematoda, Mononchida) from Lake Baikal. *Amur Zoological Journal* 9(3): 121–130. <https://doi.org/10.33910/1999-4079-2017-9-3-121-130>
- Hodson AK, Ferris H, Hollander AD, Jackson LE (2014) Nematode food webs associated with native perennial plant species and soil nutrient pools in California riparian oak woodlands. *Geoderma* 228–229: 182–191. <https://doi.org/10.1016/j.geoderma.2013.07.021>
- Holterman M, Van der Wurff A, Elsen S, Megen H, Bongers T, Holovachov O, Bakker J, Helder J (2006) Phylum-wide analysis of SSU rDNA reveals deep phylogenetic relationships among nematodes and accelerated evolution toward crown clades. *Molecular Biology and Evolution* 23(9): 1792–1800. <https://doi.org/10.1093/molbev/msl044>
- Holterman M, Rybarczyk K, van den Elsen S, van Megen H, Mooyman P, Peña Santiago R, Bongers T, Bakker J, Helder J (2008) A ribosomal DNA-based framework for the detection and quantification of stress-sensitive nematode families in terrestrial habitats. *Molecular Ecology Resources* 8(1): 23–34. <https://doi.org/10.1111/j.1471-8286.2007.01963.x>
- Iliev I, Ilieva Z (2014) Nematode communities in beech forests in “Strandzha” Natural Park, Bulgaria. 1. Species composition. *Bulgarian Journal of Agricultural Science* 20: 143–150.
- Iliev I, Ilieva Z (2016) New data on species of order Mononchida (Nematoda) from Rila and the Rhodopes Mountains, Bulgaria. *Silva Balcanica* 17: 63–84.
- Ishaque U, Iqbal E, Dawar S, Kazi N (2022) Description of *Mononchus oryzae* n. sp. with observation on *Coomansus parvus* (De Man, 1880) Jairajpuri and Khan, 1977, (Mononchida: Mononchidae) from Pakistan. *Pakistan Journal of Zoology* 1–4. <https://doi.org/10.17582/journal.pjz/20211005081044>
- Kagoshima H, Maslen R, Kito K, Imura S, Niki H, Convey P (2019) Integrated taxonomy combining morphological and molecular biological analyses of soil nematodes from maritime Antarctica. *Polar Biology* 42(5): 877–887. <https://doi.org/10.1007/s00300-019-02482-8>

- Katalan-Gateva S (1962) Studies on the phytonematode fauna of some cultural and wild plants in Thrace – Bulgaria. *Annuaire de l'Université de Sofia UV-IV*: 145–156. [In Bulgarian, English summary]
- Katalan-Gateva S (1965) Study on soil and plant parasitic nematodes in Pazardzhik region. *Annuaire de l'Université de Sofia 'Kliment Ohridski', Faculté de Biologie, Livre 1 – Zoologie. Physiologie et Biochimie des Animaux* 58: 151–184. [In Bulgarian, English summary]
- Katalan-Gateva S (1968) Soil nematodes in Bulgaria. *Annuaire de l'Université de Sofia, Livre 1 – Zoologie. Physiologie et Biochimie des Animaux* 60(1965–1966): 139–146. [In Bulgarian, English summary]
- Katalan-Gateva S, Tzenkova M, Choleva B (1981) The phytonematode fauna in the roots and rhizosphere of the rose (*Rosa damascena* Mill.) in Bulgaria. *Helmintologia* 12: 12–53.
- Kim J, Kim T, Ryu SH, Joong-Ki Park J-K (2018) *Prionchulus oleksandri* (Nematoda: Mononchida) from Korea. *Animal Systematics, Evolution and Diversity* 34: 194–198. <https://doi.org/10.5635/ASED.2018.34.4.194>
- Koohkan M, Shokoohi E, Abolafia J (2014) Study of some mononchids (Mononchida) from Iran with a compendium of the genus *Anatonchus*. *Tropical Zoology* 27(3): 88–127. <https://doi.org/10.1080/03946975.2014.966457>
- Kumar S, Stecher G, Tamura K (2016) MEGA7: Molecular Evolutionary Genetics Analysis version 7.0 for bigger datasets. *Molecular Biology and Evolution* 33(7): 1870–1874. <https://doi.org/10.1093/molbev/msw054>
- Lazarova S, Peneva V, Nedelchev S (2004) New records of plant nematodes from Bulgaria. *Dokladi na Bulgarskata Akademiã na Naukite* 57: 97–98.
- Littlewood DTJ, Curini-Galletti M, Herniou EA (2000) The interrelationships of Proseriata (Platyhelminthes: Seriata) tested with molecules and morphology. *Molecular Phylogenetics and Evolution* 16(3): 449–466. <https://doi.org/10.1006/mpev.2000.0802>
- Mejía-Madrid HH (2018) Soil nematode abundance and diversity from four vegetation types in Central Mexico. *Nematology* 20(1): 15–32. <https://doi.org/10.1163/15685411-00003119>
- Nakazawa K (1999) Morphological characteristics and ecological survey of three species of the genus *Mononchus* from wet soil in Gunma prefecture. *Japanese Journal of Nematology* 29: 16–23. https://doi.org/10.3725/jjn1993.29.2_16
- Naumova TV, Gagarin VG (2018) *Prodorylaimus baikalensis* sp. n. and *Mononchus minutus* sp. n. (Nematoda) from Lake Baikal, Russia. *Zootaxa* 4459(3): 525–534. <https://doi.org/10.11646/zootaxa.4459.3.6>
- Neher DA (2001) Role of nematodes in soil health and their use as indicators. *Journal of Nematology* 33: 161–168.
- Oliveira CMG, Hübschen J, Brown DJF, Ferraz LCCB, Wright F, Neilson R (2004) Phylogenetic relationships among *Xiphinema* and *Xiphidorus* nematode species from Brazil inferred from 18S rDNA sequences. *Journal of Nematology* 36: 153–159.
- Palomares-Rius JE, Cantalapiedra-Navarrete C, Castillo P (2014) Cryptic species in plant-parasitic nematodes. *Nematology* 16(10): 1105–1118. <https://doi.org/10.1163/15685411-00002831>
- Palomares-Rius JE, Archidona-Yuste A, Clavero-Camacho I, de la Fuente JAC, Rey A, Viñepla B, Liébanas G, Cantalapiedra-Navarrete C, Castillo P (2022) DNA barcoding and morphometry reveal further cryptic bio-diversity within the pin nematode genus *Paratylenchus* (Nematoda: Tylenchulidae). *Plants* 11(23): 3385. <https://doi.org/10.3390/plants11233385>

- Rawat VS, Ahmad M (2000) Mononchida of Garhwal Himalayas (U.P.) India II. Two known and one new species of the genus *Mononchus* Bastian, 1865 (Nematoda: Mononchida). *Iranian Journal of Nematology* 30: 62–66.
- Schenk J, Hohberg K, Helder J, Ristau K, Traunspurger W (2017) The D3-D5 region of large subunit ribosomal DNA provides good resolution of German limnic and terrestrial nematode communities. *Nematology* 19(7): 821–837. <https://doi.org/10.1163/15685411-00003089>
- Schenk J, Kleinbölting N, Traunspurger W (2020) Comparison of morphological, DNA barcoding, and metabarcoding characterizations of freshwater nematode communities. *Ecology and Evolution* 10(6): 2885–2899. <https://doi.org/10.1002/ece3.6104>
- Seinhorst JW (1959) A rapid method for the transfer of nematodes from fixative to anhydrous glycerin. *Nematologica* 4(1): 67–69. <https://doi.org/10.1163/187529259X00381>
- Shah AA, Hussain A (2015) Description of *Prionchulus multidentatus* sp. n. and *Coomansus prodentus* sp. n. (Nematoda: Mononchida) from Jammu and Kashmir, India. *International Journal of Nematology* 25: 26–34.
- Shah AA, Hussain A (2016) Descriptions of three new species of *Mononchus* (Nematoda: Mononchida) from Jammu and Kashmir State, India. *International Journal of Nematology* 26: 29–40.
- Shokoohi E, Moyo N (2022) Molecular character [sic] of *Mylonchulus hawaiiensis* and morphometric differentiation of six *Mylonchulus* (Nematoda; Order Mononchida; Family Mylonchulidae) species using multivariate analysis. *Microbiology Research* 13(3): 655–666. <https://doi.org/10.3390/microbiolres13030047>
- Stoichev S (1996) On the free-living nematode fauna from Bulgarian inland waters, Dinkelscherben. *Lauterbornia* 25: 22–30.
- Stoichev S, Chernev N (2011) Contribution to the study of free-living fresh water nematode fauna (Nematoda, Nemathelminthes) from Sinapovska River, Sakar mountain, South-East Bulgaria. *Annuaire de l'Université de Sofia Livre 1 Zoologie. Physiologie et Biochimie des Animaux* 99: 13–19.
- Stoichev S, Varadinova E (2011) Hydrobiological and faunistic investigation of the nematode fauna (Nematoda, Nemathelminthes) from Bulgarian stretch of the Veleka River (South-East Bulgaria). *Annuaire de l'Université de Sofia Livre 1 Zoologie. Physiologie et Biochimie des Animaux* 99: 21–32.
- Tabolin SB, Kolganova TV (2020) Characterisation of *Coomansus parvus* (de Man, 1880) from Russia with the first report of males. *Russian Journal of Nematology* 28: 131–134.
- Tahseen Q, Rajan P (2009) Description of *Mononchus intermedius* sp. n. (Mononchidae: Nematoda). *Nematologia mediterranea* 37: 161–167. <https://journals.flvc.org/nemamedi/article/view/86998>
- Tkach VV, Littlewood DTJ, Olson PD, Kinsella JM, Swiderski Z (1999) Molecular phylogenetic analysis of the Microphalloidea Ward, 1901 (Trematoda: Digenea). *Systematic Parasitology* 56(1): 1–15. <https://doi.org/10.1023/A:1025546001611>
- van Megen H, van den Elsen S, Holterman M, Karssen G, Mooyman P, Bongers T, Hollovachov O, Bakker J, Helder J (2009) A phylogenetic tree of nematodes based on about 1200 full-length small subunit ribosomal DNA sequences. *Nematology* 11(6): 927–950. <https://doi.org/10.1163/156854109X456862>
- van Rensburg CJ, Fourie H, Ashrafi S, Rashidifard M (2021) Description of *Prionchulus jonkershoekensis* n. sp. (Nematoda: Mononchida), a new predatory species from South Africa. *Journal of Nematology* 53(1): e2021–e2039. <https://doi.org/10.21307/jofnem-2021-039>

- Vu TTT (2021) Description of a new species *Coomansus batxatensis* (Mononchida, Mononchidae) from Vietnam, with an updated key to species. *Journal of Helminthology* 95: e28. <https://doi.org/10.1017/S0022149X21000201>
- Vu TTT, Rybarczyk-Mydlowska K, Susulovsky A, Kubicz M, Flis Ł, Le TML, Winiszewska G (2021a) Descriptions of two new and one known species of *Parkellus* Jairajpuri, Tahseen & Choi, 2001 (Nematoda: Mononchidae) and their phylogenetic position among Mononchida. *Journal of Nematology* 53(1): e2021–e2076. <https://doi.org/10.21307/jofnem-2021-076>
- Vu TTT, Le TML, Nguyen TD (2021b) Morphological and molecular characterization of *Iotonchus lotilabiatus* n. sp. (Nematoda: Iotonchidae) from Lao Cai Province, Vietnam. *Journal of Nematology* 53(1): e2021–e2066. <https://doi.org/10.21307/jofnem-2021-066>
- Young-Mathews A, Culman SW, Sánchez-Moreno S, Toby O'Geen A, Ferris H, Hollander AD, Jackson LE (2010) Plant-soil biodiversity relationships and nutrient retention in agricultural riparian zones of the Sacramento Valley, California. *Agroforestry Systems* 80(1): 41–60. <https://doi.org/10.1007/s10457-010-9332-9>
- Zullini A, Peneva V (2006) Order Mononchida. In: Eyualem-Abebe, Traunspurger W, Andrassy I (Eds) *Freshwater Nematodes: Ecology and Taxonomy*. CABI Publishing, Wallingford, 468–496. <https://doi.org/10.1079/9780851990095.0468>
- Zullini A, Loof PAA, Bongers T (2002) Free-living nematodes from nature reserves in Costa Rica 2. Mononchida. *Nematology* 4(6): 1–23. <https://doi.org/10.1163/156854102760396548>

Supplementary material 1

Photomicrographs of sequenced specimens of *Coomansus parvus*, *Mononchus pseudoaquaticus* sp. nov., and *M. truncatus*

Authors: Stela Altash, Aneta Kostadinova, Vlada Peneva

Data type: pdf

Copyright notice: This dataset is made available under the Open Database License (<http://opendatacommons.org/licenses/odbl/1.0/>). The Open Database License (ODbL) is a license agreement intended to allow users to freely share, modify, and use this Dataset while maintaining this same freedom for others, provided that the original source and author(s) are credited.

Link: <https://doi.org/10.3897/zookeys.1206.124237.suppl1>

Supplementary material 2

Comparative morphometric data for females of *Coomansus parvus*, *Mononchus aquaticus*, *M. pseudoaquaticus* sp. nov., and *Mononchus truncatus*

Authors: Stela Altash, Aneta Kostadinova, Vlada Peneva

Data type: pdf

Copyright notice: This dataset is made available under the Open Database License (<http://opendatacommons.org/licenses/odbl/1.0/>). The Open Database License (ODbL) is a license agreement intended to allow users to freely share, modify, and use this Dataset while maintaining this same freedom for others, provided that the original source and author(s) are credited.

Link: <https://doi.org/10.3897/zookeys.1206.124237.suppl2>

DNA barcoding reveals a taxonomic fraud: Note on validity of *Propomacrus muramotoae* (Coleoptera, Scarabaeidae)

Seunghyun Lee^{1,2}, Seulmaro Hwang³, Minhyeuk Lee^{4,5}, Jinbae Seung⁵, Woong Choi⁶, Ming Bai^{1,7}

1 Key Laboratory of Animal Biodiversity Conservation and Integrated Pest Management, Institute of Zoology, Chinese Academy of Sciences, Beijing, 100101, China

2 Department of Life Sciences, Natural History Museum, London, UK

3 Department of Science Contents, Visang Education, Gwacheon, Republic of Korea

4 National Institute of Agricultural Sciences, Wanju, Republic of Korea

5 Insect Biosystematics Laboratory, Department of Agricultural Biotechnology, Seoul National University, Seoul, Republic of Korea

6 305-403, Sechangsamsunhwan-ro, Namdong-gu, Incheon, Republic of Korea

7 University of Chinese Academy of Sciences, Beijing, China

Corresponding author: Ming Bai (baim@ioz.ac.cn)

Abstract

Until the early 2000s, the genus *Propomacrus* was known to comprise two species, occurring in the Eastern Mediterranean and Southeast China. The discovery of *Propomacrus muramotoae* Fujioka in Tibet and subsequently in Bhutan and Nepal, might play a crucial role in bridging the geographical distribution gap of the Euchirini tribe between the Mediterranean and Central China, offering profound insights into its evolution and biogeography. However, all specimens, including the holotype specimen, were sourced from a single insect vendor, with no further specimens found or catalogued in museum collections thereafter. During our examination of a *P. muramotoae* specimen from a private collection in South Korea, we found its COI gene sequence to be identical to that of *P. bimucronatus* (Pallas) from Turkey, a species known for its wide distribution and genetic variability across regional populations. This overlap in genetic identity raised significant doubts, further compounded by our detection of deliberate modifications in essential diagnostic features during morphological examination. All three specimens we examined showed crude modifications, including staining and artificial grinding. Despite our inability to access the *P. muramotoae* type specimens for direct examination—a challenge we attempted to overcome through various means—it is evident that significant fraudulent tampering has occurred with the *P. muramotoae* specimens. Therefore, a new synonymy is proposed: *Propomacrus bimucronatus* Pallas, 1781 = *P. muramotoae* Fujioka, 2007 (**syn. nov.**). We also advocate for a straightforward verification of the type specimen through molecular analysis of the COI barcode region and morphological re-examination under a microscope for those who have access to the type specimens.

Key words: DNA barcoding, Euchirini, long-armed scarab, manipulated specimen, new synonymy



Academic editor: Andrey Frolov

Received: 8 April 2024

Accepted: 28 May 2024

Published: 8 July 2024

ZooBank: <https://zoobank.org/60626DA3-9459-42E0-ACE5-7231E05C9D8B>

Citation: Lee S, Hwang S, Lee M, Seung J, Choi W, Bai M (2024) DNA barcoding reveals a taxonomic fraud: Note on validity of *Propomacrus muramotoae* (Coleoptera, Scarabaeidae). ZooKeys 1206: 181–190. <https://doi.org/10.3897/zookeys.1206.124932>

Copyright: © Seunghyun Lee et al.
This is an open access article distributed under terms of the Creative Commons Attribution License (Attribution 4.0 International – CC BY 4.0).

Introduction

The beetle tribe Euchirini is characterized by their large size and notably elongated forelegs in males (Young 1989). These species are distributed widely across the Mediterranean, Indo-Asian Continental, and Southwest Pacific Insular regions (Young 1989). The tribe encompasses three genera: *Cheirotonus* Hope, 1841; *Euchirus* Burmeister & Schaum, 1840; and *Propomacrus* Newman, 1837. While *Euchirus* are confined to Southeast Asia and *Cheirotonus* spans Southeast Asia to the Indo-Himalayan region, *Propomacrus* exhibits the broadest yet distinctly disjunct distribution (Young 1989). *Propomacrus bimucronatus* (Pallas 1781), originally described from Turkey, has been recorded across a range of countries including Macedonia, Bulgaria, Greece, Turkey, Syria, Lebanon, Israel, Iran and Iraq (Young 1989; Muramoto 2012; Bezděk 2016; Ibrahim and Fayq 2022). *Propomacrus davidii* Deyrolle, 1874, was described from central China, with its distribution is still restricted to that region. Alexis and Makris (2002) described *Propomacrus cypriacus*, distinguishing it by male protibiae shape and ornamentation, which was later relegated to a subspecies based on mitochondrial DNA analyses, morphological reassessment and ecological data (Sfenthourakis et al. 2017).

A notable discovery within this genus was *Propomacrus muramotoae* Fujioka, 2007, found in Tibet, with subsequent findings from Bhutan and Nepal (Muramoto 2012). This species would bridge the distribution gap between the Mediterranean and Central China, offering invaluable insights into the evolution and biogeography of *Propomacrus* and the tribe Euchirini. However, *P. muramotoae* was morphologically similar to *P. bimucronatus* and was described based on subtle morphological characters like the blunt lateral margin of the pronotum and a ventral groove on the abdomen (Fujioka 2007). Also, all specimens of *P. muramotoae*, including the type specimens, were obtained from Li Jingke, a beetle collector and seller known for altering locality labels (see Discussion). These circumstances raised significant doubts about the validity of this species, particularly given the absence of any subsequent findings. On the other hand, Sfenthourakis et al. (2017) provided extensive genetic resources for *P. bimucronatus* and a few DNA sequences of other Euchirini species, revealing broad genetic variation within *P. bimucronatus* and even the *P. b. cypriacus* population from Cyprus displayed multiple COI haplotypes. This suggests that confirming the validity of *P. muramotoae* could be straightforward with sequencing and comparison to existing public sequences.

This study aims to clarify the status of *P. muramotoae* by analyzing samples labeled as being collected from “Tibet” and “Nepal”.

Material and methods

Three *P. muramotoae* specimens, deposited in the second author’s (S.H.) collection, one pair labeled as being collected from “Tibet” and one from “Nepal”, were used in this study. Specimens were examined with an Olympus SZ61 stereomicroscope and photographed with a DMC 5400 digital camera attached to a Leica Z16 APO motorized macroscope. Serial images were combined using Zerene Stacker.

Genomic DNA from all three samples was extracted from both thoracic muscle and labial palpi of each specimen, using the DNeasy Blood & Tissue kit (Qiagen, Hilden, Germany), following the manufacturer’s protocol. The

examined specimens were deposited in the private collection of the second author, and the collection labels' details are provided in Figs 1, 2.

For compatibility with public sequences, we targeted the cytochrome oxidase subunit I (COI), previously utilized in a *Propomacrus* study (Sfenthourakis et al. 2017), to integrate our de novo data with the public data available on GenBank (<https://www.ncbi.nlm.nih.gov/genbank/>). As our samples were not in optimal condition, we initially retrieved all available COI sequences from GenBank and designed four new *Propomacrus bimucronatus*-specific primer sets. PCRs were performed using AccuPower® PCR PreMix (Bioneer, Daejeon, Korea) and sent to BLONICS Co., Ltd (Seoul, Korea) for sequencing. Public sequences used in this study, PCR primers, and PCR conditions are described in Suppl. material 1: tables S1–S3.

We utilized MAFFT ver. 7 online (Kato et al. 2019) for multiple sequence alignment, and the final alignment was visualized in GENEIOUS (Kearse et al. 2012) to determine the position of each sequence. The amino acid translation option in MEGA X (Kumar et al. 2018) was used for the final sequence assessment. The phylogenetic analysis was conducted using the maximum likelihood method (ML) with IQ-TREE (Nguyen et al. 2015). Haplotype network analysis was performed

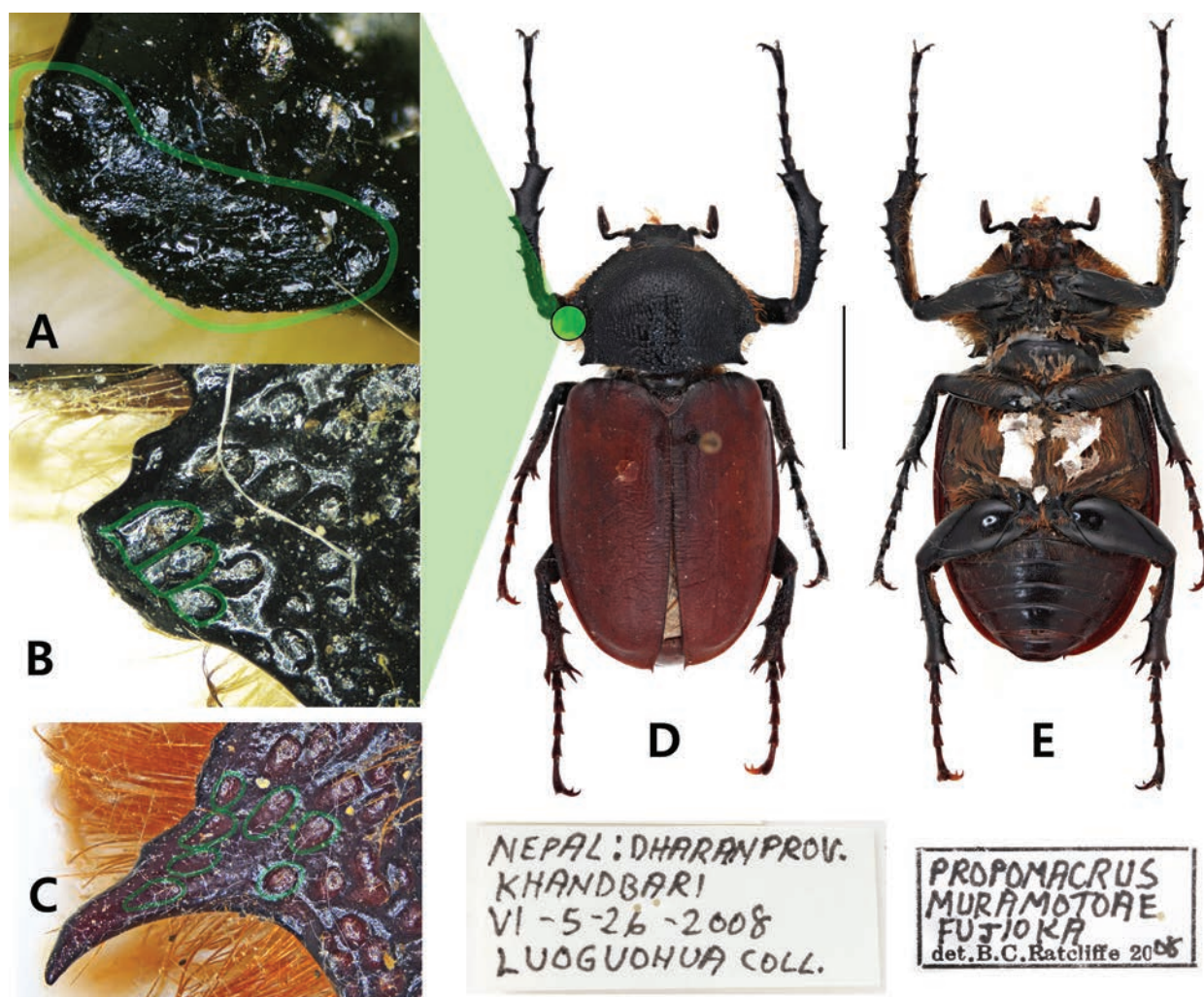


Figure 1. *Propomacrus muramotoae* labeled as being collected from Nepal **A** lateral margin of pronotum, dorsolateral view. Light green lines highlight artificial grinding **B** lateral margin of pronotum, dorsal view. Light green lines highlight a punctation cut in the middle **C** lateral margin of pronotum of *P. bimucronatus* **D** dorsal habitus **E** ventral habitus.

using the TCS algorithm (Clement et al. 2000) implemented in PopART ver. 1.7 (Leigh and Bryant 2015). Sequences were categorized into six groups, representing each taxonomic unit (*Propomacrus muramotoae*, *P. bimucronatus bimucronatus*, *P. bimucronatus cypriacus*, *P. davidis*, *Euchirus dupontianus* and *E. longimanus*).

Results

Morphological examination

The three specimens labeled as "*Propomacrus muramotoae*" exhibited unusual morphological features (Figs 1, 2). Firstly, *P. muramotoae* labeled as being collected in "Nepal" exhibited notably blunt lateral pronotal processes as described in the original species description (Fig. 1D). The development of the elytral lon-

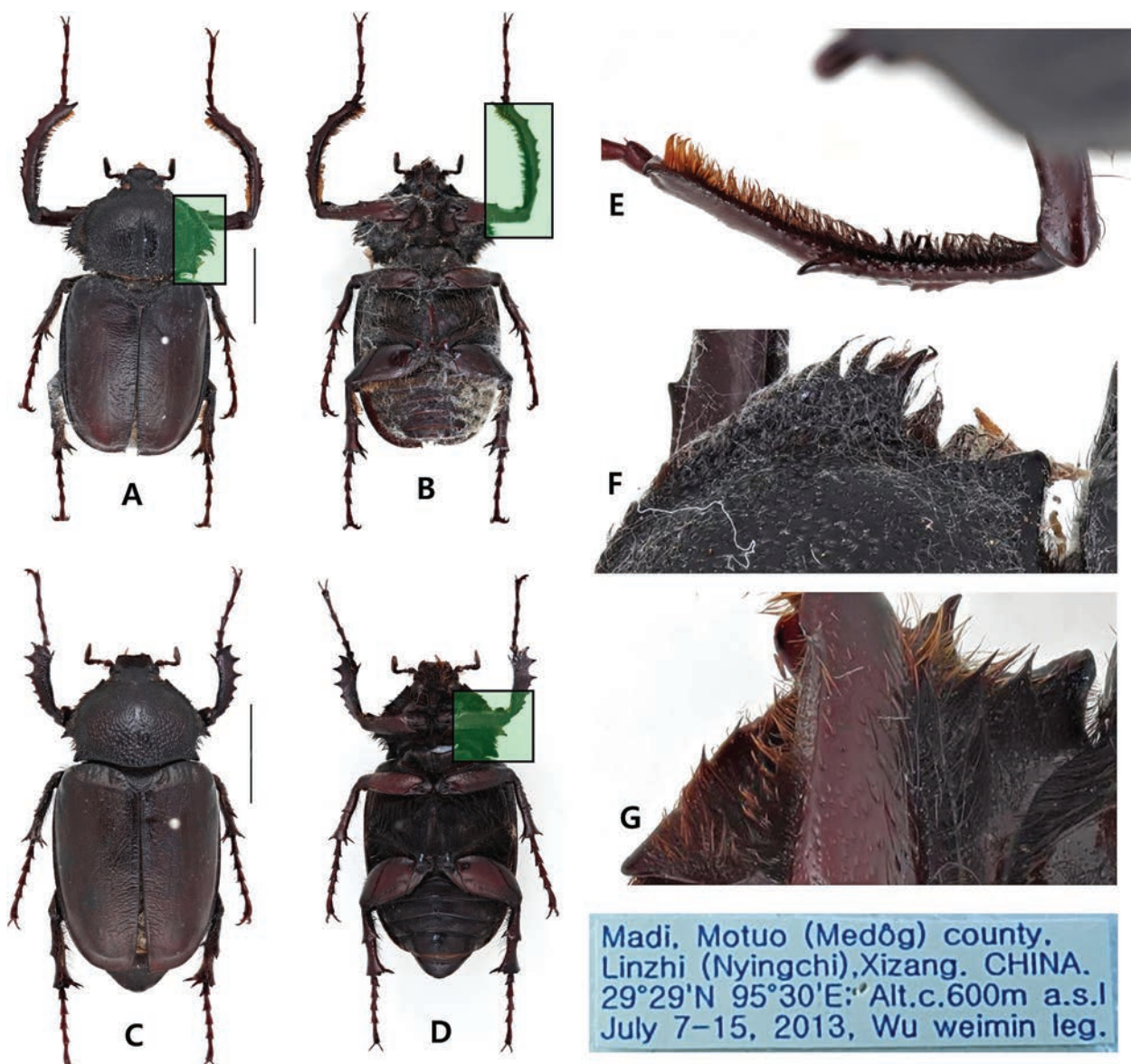


Figure 2. *Propomacrus muramotoae* labeled as being collected from Tibet **A** dorsal habitus, male **B** ventral habitus, male **C** dorsal habitus, female **D** ventral habitus, female **E** forefemur of male with black stain **F** lateral margin of pronotum, dorsal view **G** lateral margin of pronotum, ventral view.

gitudinal costa was weak, and a ventral longitudinal groove was absent. However, microscopic analysis of the blunted areas on the lateral pronotal process indicated clear signs of artificial grinding. When observed from the side, the edges of the areas subjected to grinding were not smooth but were instead bluntly truncated throughout (Fig. 1A). The punctation on the plate was cut in the middle with a straight line across the area suspected of having been ground (Fig. 1B). The *P. muramotoae* specimens labeled as being collected from “Tibet” displayed a mottled black coloring across both sexes, appearing to be artificially dyed (Fig. 2A–G). Each specimen featured sharply developed lateral pronotal processes (Fig. 2F), with the elytral longitudinal costa weakly developed and a ventral longitudinal groove absent (Fig. 2B, D). These specimens have the diagnostic characters of *P. bimucronatus*, with the exception of their coloration.

Molecular analyses

In the network analysis, we identified a total of 17 haplotypes within the *P. bimucronatus* species complex (*P. b. bimucronatus* + *P. b. cypriacus*). Within these, *P. b. cypriacus* exhibited notable diversity, presenting 14 distinct haplotypes. Conversely, only two haplotypes were observed in *P. b. bimucronatus*. Notably, a predominant haplotype, designated as haplotype A, was shared by the majority of individuals studied. This haplotype was particularly significant in our analysis of *P. muramotoae*; all five sequences examined were identical to haplotype A. In terms of haplogroups, *P. b. cypriacus* formed a distinct group, while the remaining sequences recovered polyphyletic (Fig. 3).

Furthermore, monophyly of *P. bimucronatus* species complex was recovered with strong Ultrafast Bootstrap Support (UBS = 100) within the maximum likelihood (ML) tree. In the phylogenetic tree, *P. muramotoae* was clearly nested within the *P. bimucronatus* clade. The clade, which included five *P. muramotoae* specimens was monophyletic with a branch length of zero and high support values (UBS = 99). Consistent with the network analysis, the *P. b. cypriacus* clade formed monophyletic groups with high supporting values (UBS = 90), reinforcing the results observed in the haplotype analysis (Fig. 3).

Discussion

Our DNA analysis showed a variety of haplotypes of *P. b. cypriacus* among the extensive samples from the small island of Cyprus. Conversely, *P. b. bimucronatus*, with a distribution over a significantly larger area, has a disproportionately small number of sequences uploaded to GenBank relative to its range, with all specimens collected in Turkey. Therefore, widely distributed *P. b. bimucronatus* should exhibit higher genetic diversity than *P. b. cypriacus*, as a wider range correlates with greater genetic diversity in close congeners (Cole 2003; Leffler et al. 2012; Hague and Routman 2016). Furthermore, existing studies of the genus *Cheirotonus*, which is closely related to *Propomacrus* (Yu et al. 2023), demonstrate significant intraspecific variation in genetic diversity correlated with its species' distribution patterns: *Cheirotonus gestroi* Pouillaude, 1913, which has a wide distribution, shows a broad range of genetic variation (Yang et al. 2020), in contrast to *Cheirotonus formosanus* Ohaus, 1913, which has a narrower distribution and exhibits lesser genetic variation (Huang et al. 2024). It is particularly unconvinc-

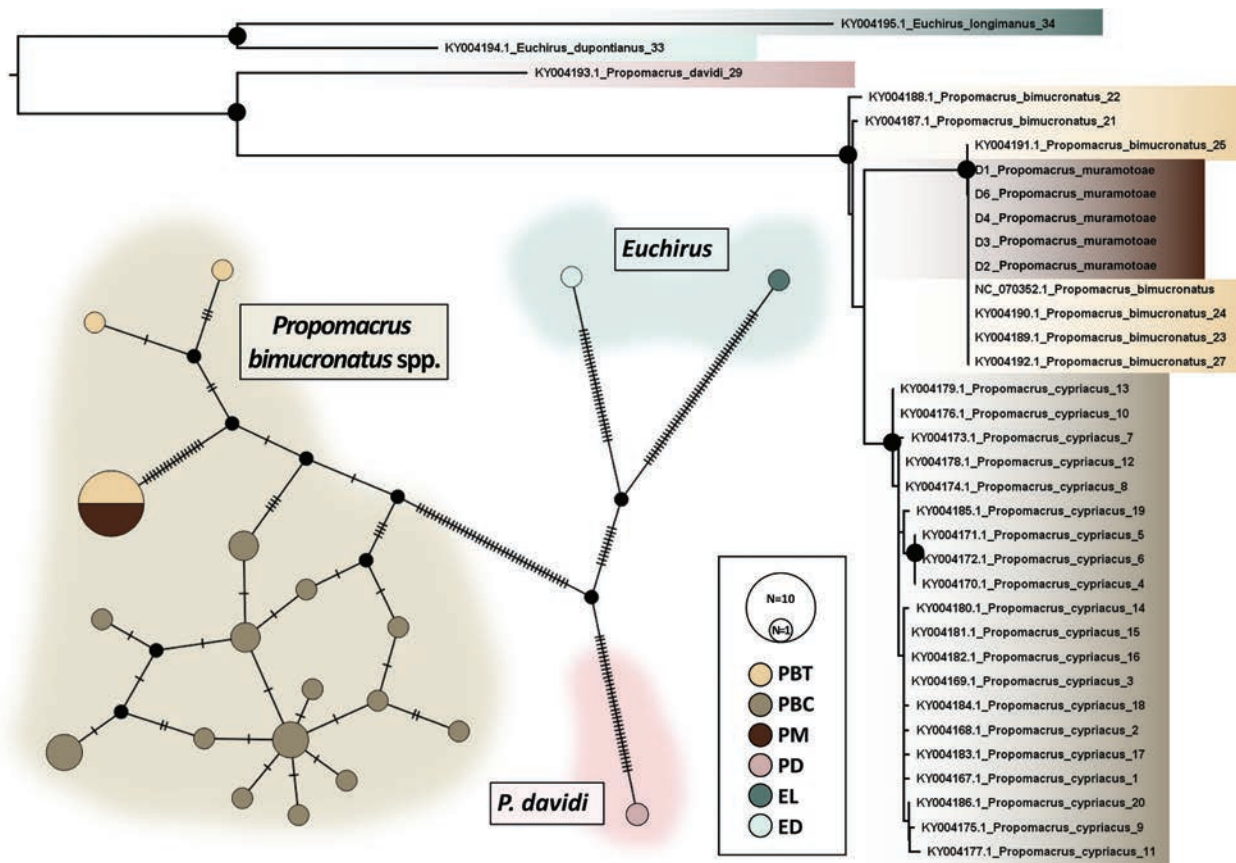


Figure 3. Genetic analyses using COI gene. **Lower left.** Haplotype network analyses. Abbreviations PM: *Propomacrus muramotoae*, PBT: *P. bimucronatus bimucronatus*, PBC: *P. bimucronatus cypriacus*, PD: *P. davidis*, ED: *Euchirus dupontianus*, and EL: *E. longimanus*. **Right.** Phylogenetic relationships of *Propomacrus* resulting from IQtree. High Ultrafast bootstrap support values (≥ 90) are marked with black circles.

ing that individuals found with the labels “Nepal” and “Tibet” possess a COI haplotype identical to the most common haplotype identified in Turkey populations, raising suspicions about the uniformity of sequences between the individuals.

The morphological characteristics of the species are also notably ambiguous. The lateral pronotal process considered a distinctive feature of *P. muramotoae*, was only observed in one specimen, where it appeared to have been artificially modified. This modification is particularly prominent in a sharply cut punctuation along the lateral margin. The presence of the elytral longitudinal costa, a trait often found in *P. bimucronatus*, adds to the ambiguity, along with the absence of the abdominal longitudinal groove in all specimens examined. The remaining two specimens, labeled as from Tibet, were indistinguishable from *P. bimucronatus* in both DNA and morphological aspects and lacked any diagnostic features of *P. muramotoae* according to the original description.

It is essential to recognize that all specimens of *P. muramotoae* were exclusively provided by an insect dealer, Li Jingke (personal communications with the second author). Li Jingke has a well-documented reputation as a fraudster (Suppl. material 2: fig. S1) even though his fraudulent activities have rarely been formally reported (Han et al. 2017). Probably, the specimens were reared from larvae or obtained from common sources, such as bred population from Turkey, and subsequently altered to sell at high prices. Surprisingly, in several advertising emails from Li Jingke that we received, we found descriptions of specimen

variations that appeared completely random, such as white lines on the elytral margin, wider elytra, and a bleached posterior half (Suppl. material 2: fig. S2). Specimens advertised as having these ‘unique features’ were sold at very high prices (Suppl. material 2: fig. S2). Such practices, though inconceivable within the scientific community, unfortunately do exist. Direct manipulation of specimens is rarely documented in entomology (Braby and Eastwood 2019). The morphological alterations by the fraudster were carelessly executed in this case, and fortunately, DNA barcode amplification was successful. However, it should be noted that such verification may not always be possible.

Based on genetic and morphological analysis, coupled with indirect data discussed above, we believe that the type of *P. muramotoae* is an altered specimen of *P. bimucronatus*. Therefore, we propose that *P. muramotoae* Fujioka, 2007, is a junior synonym of *P. bimucronatus* Pallas, 1781. A significant limitation of our study, however, is the absence of examination and genetic analysis of the type specimens. The type specimens of *P. muramotoae* are housed at the National Museum of Nature and Science in Tokyo, Japan, according to the original description. However, we were unable to find the types for our research; they were not deposited at the National Museum of Nature and Science and it is presumed they remain within the collection of the original describer. All authors tried to contact him in various ways but failed to access the type specimens. The lack of genetic divergence from *P. bimucronatus* and clear evidence of morphological manipulation strongly indicate that *P. muramotoae* represents a significant taxonomic deception. Our research indicates that verification of the type specimen is feasible and straightforward and we suggest those with access to the holotype conduct official taxonomic verification of *P. muramotoae*: simply amplify and do molecular analyses using the COI barcode region and examine external morphology under a microscope.

Taxonomic account

Tribe Euchirini Hope 1840

Genus *Propomacrus* Newman, 1837

Porropus Laporte 1840: 113.

Protomacrus Hope 1841: 595.

Macropopus Agassiz 1846: 309.

Type species. *Scarabaeus bimucronatus* Pallas, 1781: 13.

Propomacrus bimucronatus bimucronatus Pallas, 1781

Scarabaeus bimucronatus Pallas, 1781: 13.

Propomacrus arbaces Newman, 1837: 256.

Propomacrus muramotoae Fujioka, 2007: 99. (syn. nov.)

Material examined. **TURKEY** • 1 male, 2 females; Mersin province 1500 m nr. Köseçobanlı village dead in old pollarded oaks; 2017; Serder Göktepe leg.; BMNH{E} 2018-74; Natural History Museum London (NHM hereafter) • 1 male;

Smyrna; NHM • 1 male; Asia Minor; 1910; G.a. Tellalian; NHM • 1 female; Asia Minor; NHM • 1 male, 2 females; Fry coll.; As Min Smyrne; 1905-100; NHM • 1 female; Besika Bay; G.C.C. Champion; 1927-409; NHM • 3 males, 1 female; Smyrne; 1906; Chinese Academy of Sciences • 2 males, 2 females; Hatay; Jun. 2007; private collection of Woong Choi. **SYRIA** • 2 females; Syria; 80.53; NHM • 1 female; Aleppo, Syria; G Lewis; 1915-38; NHM.

Additional material with falsified labels. **NEPAL** 1 female; Khandbari, Dharan Prov.; 5 Jun. 2008; LUOGUOHUA leg.; private collection of Seulmaro Hwang; **CHINA** 1 male, 1 female; Madi (Medog) county, Linzhi (Nyingchi), Xizang; 29°29'N, 95°30'E; alt. c. 600 m; 7–15 Jul. 2014; Wu Weimin leg.; private collection of Seulmaro Hwang.

***Propomacrus bimucronatus cypriacus* Alexis & Makris, 2002**

Propomacrus cypriacus Alexis & Makris, 2002: 103.

Material examined. **CYPRUS** • 1 male; Alethriko, Larnaca; 34°51.54'N, 33°29.38'E; 15. viii. 2006; Aristos Aristophanous leg.; BMNH{E}2015-88; NHM • 1 female Alethriko, Larnaca; 34°51.54'N, 33°29.38'E; 5 ix 2008; Aristos Aristophanous leg.; BMNH{E}2015-88; NHM.

Additional information

Conflict of interest

The authors have declared that no competing interests exist.

Ethical statement

No ethical statement was reported.

Funding

This work was supported by Basic Science Research Program through the National Research Foundation of Korea (NRF) funded by the Ministry of Education (RS-2023-00237795); National Key R&D Program of China (Nos. 2022YFC2601200, 2023YFC2604904); the Survey of Wildlife Resources in Key Areas of Tibet (ZL202203601); and the National Science & Technology Fundamental Resources Investigation Program of China (Nos. 2023FY100301, 2022FY100500).

Author contributions

Conceptualization: SL. Data curation: SL, WC, ML, JS, SH. Formal analysis: SL. Funding acquisition: MB, SL. Investigation: WC, SH, JS, ML. Resources: SH, MB, WC. Supervision: MB. Visualization: SL. Writing - original draft: SL. Writing - review and editing: MB, SH, JS, ML, WC, SL.

Author ORCIDs

Seunghyun Lee  <https://orcid.org/0000-0001-6318-4116>

Minhyeuk Lee  <https://orcid.org/0000-0002-5667-9097>

Jinbae Seung  <https://orcid.org/0000-0001-9115-1733>

Ming Bai  <https://orcid.org/0000-0001-9197-5900>

Data availability

All of the data that support the findings of this study are available in the main text or Supplementary Information.

References

- Alexis R, Makris C (2002) *Propomacrus cypriacus* sp. n. from Cyprus (Coleoptera: Scarabaeidae, Euchirinae). *Biocosme Mésogéen* 18(3): 103–108.
- Bezděk A (2016) Tribe Euchirini Hope, 1840. In: Löbl I, Löbl D (Eds) *Catalogue of Palaearctic Coleoptera. Volume 3, Scarabaeoidea, Scirtoidea, Dascilloidea, Buprestoidea, Byrrhoidea*. Revised and updated edition. Brill, Leiden; Boston, 214–214.
- Braby MF, Eastwood R (2019) Revised taxonomic status of *Pseudalmenus barringtonensis* Waterhouse, 1928 stat. rev. (Lepidoptera: Lycaenidae): uncovering Australia's greatest taxonomic fraud. *Invertebrate Systematics* 33(3): 530–543. <https://doi.org/10.1071/IS18071>
- Clement M, Posada DCKA, Crandall KA (2000) TCS: A computer program to estimate gene genealogies. *Molecular Ecology* 9(10): 1657–1659. <https://doi.org/10.1046/j.1365-294x.2000.01020.x>
- Cole CT (2003) Genetic variation in rare and common plants. *Annual Review of Ecology, Evolution, and Systematics* 34(1): 213–237. <https://doi.org/10.1146/annurev.ecolsys.34.030102.151717>
- Fujioka M (2007) A new species of the genus *Propomacrus* Newman, 1837 from Tibet, China. *Kogane, Tokyo* 8: 99–102.
- Hague MT, Routman EJ (2016) Does population size affect genetic diversity? A test with sympatric lizard species. *Heredity* 116(1): 92–98. <https://doi.org/10.1038/hdy.2015.76>
- Han T, Park IG, Kim KK, Ivanov S, Park H (2017) Identification of the South Korean hermit beetle (Coleoptera: Scarabaeidae: Cetoniinae). *Korean Journal of Applied Entomology* 56(3): 229–239. <https://doi.org/10.5656/KSAE.2016.08.0.036>
- Huang JP, Wu SP, Chen WY, Pham GJ, Kuan YH (2024) Genomic data revealed inbreeding despite a geographically connected stable effective population size since the Holocene in the protected Formosan Long-Arm Scarab beetle, *Cheirotonus formosanus*. *The Journal of Heredity* 115(3): esae006. <https://doi.org/10.1093/jhered/esae006>
- Ibrahim HA, Fayq AF (2022) The first record of *Propomacrus bimucronatus* (Pallas, 1781) (Coleoptera, Scarabaeidae) from Iraq, with notes on its distribution and phenology in the Near East. *Biodiversity Data Journal* 10: e96601. <https://doi.org/10.3897/BDJ.10.e96601>
- Katoh K, Rozewicki J, Yamada KD (2019) MAFFT online service: Multiple sequence alignment, interactive sequence choice and visualization. *Briefings in Bioinformatics* 20(4): 1160–1166. <https://doi.org/10.1093/bib/bbx108>
- Kearse M, Moir R, Wilson A, Stones-Havas S, Cheung M, Sturrock S, Buxton A, Cooper A, Markowitz S, Duran C, Thierer T, Ashton B, Meintjes P, Drummond A (2012) Geneious Basic: An integrated and extendable desktop software platform for the organization and analysis of sequence data. *Bioinformatics (Oxford, England)* 28(12): 1647–1649. <https://doi.org/10.1093/bioinformatics/bts199>
- Kumar S, Stecher G, Li M, Knyaz C, Tamura K (2018) MEGA X: Molecular evolutionary genetics analysis across computing platforms. *Molecular Biology and Evolution* 35(6): 1547–1549. <https://doi.org/10.1093/molbev/msy096>
- Leffler EM, Bullaughey K, Matute DR, Meyer WK, Segurel L, Venkat A, Andolfatto P, Przeworski M (2012) Revisiting an old riddle: What determines genetic diversity levels within species? *PLOS Biology* 10(9): e1001388. <https://doi.org/10.1371/journal.pbio.1001388>

- Leigh JW, Bryant D (2015) PopART: Full-feature software for haplotype network construction. *Methods in Ecology and Evolution* 6(9): 1110–1116. <https://doi.org/10.1111/2041-210X.12410>
- Muramoto R (2012) A catalogue of Euchirinae (Coleoptera, Scarabaeidae). *Kogane* 13: 87–102.
- Nguyen LT, Schmidt HA, Von Haeseler A, Minh BQ (2015) IQ-TREE: A fast and effective stochastic algorithm for estimating maximum-likelihood phylogenies. *Molecular Biology and Evolution* 32(1): 268–274. <https://doi.org/10.1093/molbev/msu300>
- Sfenthourakis S, Hadjiconstantis M, Makris C, Dimitriou A (2017) Revisiting the saproxyl-ic beetle *Propomacrus cypriacus* Alexis & Makris, 2002 (Coleoptera: Euchiridae) using molecular, morphological and ecological data. *Journal of Natural History* 51(17–18): 1021–1034. <https://doi.org/10.1080/00222933.2017.1319521>
- Yang C, Zhu EJ, He QJ, Yi CH, Wang XB, Hu SJ, Wei SJ (2020) Strong genetic differentiation among populations of *Cheirotonus gestroi* (Coleoptera: Euchiridae) in its native area sheds lights on species conservation. *Mitochondrial DNA, Part A, DNA Mapping, Sequencing, and Analysis* 31(3): 108–119. <https://doi.org/10.1080/24701394.2020.1741565>
- Young RM (1989) Euchirinae (Coleoptera: Scarabaeidae) of the world: distribution and taxonomy. *Coleopterists Bulletin* 43: 205–236.
- Yu Y, Lee S, Jin L, Bai M (2023) Mitochondrial genome of *Euchirus longimanus* (Coleoptera: Scarabaeidae) and phylogenetic relationship of Euchirini. *Journal of Asia-Pacific Entomology* 26(4): 102156. <https://doi.org/10.1016/j.aspen.2023.102156>

Supplementary material 1

Public sequences, PCR primers, and PCR conditions

Authors: Seunghyun Lee, Seulmaro Hwang, Minhyeuk Lee, Jinbae Seung, Woong Choi, Ming Bai

Data type: xlsx

Copyright notice: This dataset is made available under the Open Database License (<http://opendatacommons.org/licenses/odbl/1.0/>). The Open Database License (ODbL) is a license agreement intended to allow users to freely share, modify, and use this Dataset while maintaining this same freedom for others, provided that the original source and author(s) are credited.

Link: <https://doi.org/10.3897/zookeys.1206.124932.suppl1>

Supplementary material 2

Deceptive practices of Li Jingke and sales email from him

Authors: Seunghyun Lee, Seulmaro Hwang, Minhyeuk Lee, Jinbae Seung, Woong Choi, Ming Bai

Data type: pdf

Copyright notice: This dataset is made available under the Open Database License (<http://opendatacommons.org/licenses/odbl/1.0/>). The Open Database License (ODbL) is a license agreement intended to allow users to freely share, modify, and use this Dataset while maintaining this same freedom for others, provided that the original source and author(s) are credited.

Link: <https://doi.org/10.3897/zookeys.1206.124932.suppl2>

A new species of holothuroid from the Labrador Sea (eastern Canada): *Pseudothyone labradorensis* sp. nov. (Echinodermata, Holothuroidea, Dendrochirotida, Sclerodactylidae)

Antonina Kremenetskaia¹, Tom Alvestad², Heather D. Penney^{3,4}, Jean-François Hamel⁵, Bárbara de Moura Neves⁶, David Côté⁶, Annie Mercier³

1 Shirshov Institute of Oceanology, Russian Academy of Sciences, Moscow, Russia

2 Department of Natural History, University Museum of Bergen, University of Bergen, Bergen, Norway

3 Department of Ocean Sciences, Memorial University, St. John's, Newfoundland and Labrador, Canada

4 Aquatic Resources Program, St. Francis Xavier University, Antigonish, Nova Scotia, Canada

5 Society for the Exploration and Valuing of the Environment (SEVE), St. Philips, Newfoundland and Labrador, Canada

6 Northwest Atlantic Fisheries Centre, Fisheries and Oceans Canada, St. John's, Newfoundland and Labrador, Canada

Corresponding author: Antonina Kremenetskaia (antonina@ocean.ru)

Abstract

A new species of holothuroid, *Pseudothyone labradorensis* sp. nov. (order Dendrochirotida and family Sclerodactylidae), was discovered off the coast of Labrador (eastern Canada) at a depth of 740–969 m. Two specimens were described based on morphological and genetic parameters. Distinctive characters included pinkish body colour, presence of tube feet on a 'tail', supporting rod-shaped ossicles in the tube feet, and rod-shaped ossicles in the tentacles. To investigate its phylogenetic relationships, partial sequences of COI were obtained for the new species as well as for the type species *P. raphanus* and another North Atlantic species *P. serrifera*. According to the phylogenetic analysis, *P. labradorensis* sp. nov. appeared in a well-supported clade with *P. raphanus* and *P. serrifera*. Molecular data also suggest polyphyly of the genus, showing the Northeast Pacific species *Pseudothyone belli* recovered outside of the clade containing the type species. *Pseudothyone labradorensis* sp. nov. is the first species of the genus from the Northwest Atlantic. A key to the North Atlantic *Pseudothyone* is provided.

Key words: Bathyal fauna, distribution, Northwest Atlantic fauna, sea cucumbers, taxonomy



Academic editor: Didier Vanden Spiegel

Received: 19 March 2024

Accepted: 13 June 2024

Published: 8 July 2024

ZooBank: <https://zoobank.org/13D643CF-1841-4C11-B1FB-7B6737A943A2>

Citation: Kremenetskaia A, Alvestad T, Penney HD, Hamel J-F, de Moura Neves B, Côté D, Mercier A (2024)

A new species of holothuroid from the Labrador Sea (eastern Canada):

Pseudothyone labradorensis sp. nov.

(Echinodermata, Holothuroidea,

Dendrochirotida, Sclerodactylidae).

ZooKeys 1206: 191–206. <https://doi.org/10.3897/zookeys.1206.123364>

<https://doi.org/10.3897/zookeys.1206.123364>

Copyright: This is an open access article distributed under the terms of the CC0 Public Domain Dedication.

Introduction

The genus *Pseudothyone* was established by Panning (1949) for *Thyone raphanus* Dübén & Koren, 1846 within the new subfamily Sclerodactylinae. Apart from the type species, Panning assigned five other species to this genus: *P. belli* (Ludwig 1886), *P. mosaica* (Koehler & Vaney, 1910), *P. poucheti* (Barrois, 1882), *P. argillacea* (Sluiter, 1910), *P. buccalis* (Stimpson, 1855) and *P. trachyplaca* (Clark, 1924). The latter two species were later assigned to other genera, whereas *P. poucheti* was synonymized with *P. raphanus* according to Théel (1886), and *P. argillacea* with *P. belli* according to Deichmann (1954).

Pseudothyone currently includes seven species characterized by a wide range of morphological characters. The original diagnosis by Panning (1949) included the following: ten tentacles, undivided pieces of calcareous ring and its radial pieces with two fork-shaped processes of medium length undivided or consisting of few large pieces, and body-wall ossicles composed of only plates. Later investigations of this genus added more variations to taxonomic characters (Lambert and Oliver 2001; Martins 2019): tentacles ten equal-sized (in *P. levini* Lambert & Oliver, 2001) or eight bigger and two ventral smaller in all other species; body-wall ossicles smooth plates and knobbed buttons (*P. belli*), or smooth plates only (all other species); tube feet ossicles tables and end plates (*P. belli* and *P. mosaica*), rods and end plates (*P. sculponea* Cherbonnier, 1958, *P. serrifera* (Östergren, 1898) and *P. levini*), or end plates only (*P. raphanus* and *P. furnestini* Cherbonnier, 1969); radial pieces of calcareous ring with short posterior processes (*P. levini*), or of medium length (all other species), with posterior processes undivided (*P. raphanus*), or divided into several pieces (*P. belli*, *P. mosaica*, *P. sculponea*).

Most species of *Pseudothyone* are distributed in the Atlantic Ocean (Fig. 1). *Pseudothyone furnestini*, *P. raphanus*, and *P. serrifera* occur in the Northeast Atlantic, and the latter two are also known from the Mediterranean. *Pseudothyone sculponea* is known only from the Mediterranean, and *P. belli* is from the Western Atlantic (Atlantic US coast, Caribbean and Brazil). Moreover, two species are known outside the Atlantic: *P. mosaica* from the Persian Gulf, and *P. levini* from the northeastern Pacific. Bathymetric distribution also differs between the species. The shallowest is *P. belli* occurring at sublittoral depths from the low-tide mark to 37 m (Pawson et al. 2010). Among shallow-water representatives are also *P. levini* occurring from the intertidal to 70 m depth and *P. sculponea* reported from 21 to 41 m (GBIF.org 2023). *Pseudothyone raphanus* and *P. serrifera* occur deeper, at 10–1200 m and 200–1200 m, respectively (Madsen and Hansen 1994; Fernández-Rodríguez et al. 2019). The deepest-dwelling species is *P. furnestini* reported from 440–1347 m (Fernández-Rodríguez et al. 2019). *Pseudothyone mosaica* is known from a single record at 97 m.

Phylogenetic relationships of species within the genus *Pseudothyone*, as well as the latter's position within Sclerodactylidae, remain unclear. The taxon was originally described by Panning (1949) as Sclerodactylinae, a subfamily of Cucumariidae. Later, Pawson and Fell (1965) upgraded its status to the family Sclerodactylidae with two subfamilies, Sclerodactylinae and Cladolabinae. Thandar (1989) restricted the diagnosis of Sclerodactylidae and described a new subfamily, Sclerothyoninae. Smirnov (2012) recognized the subfamilies Cladolabinae and Sclerothyoninae as separate families. Available molecular data (Miller et al. 2017) partly support the system of Smirnov, showing no sister relationships between sclerothyonins *Afrocucumis africana* (Semper, 1867) and *Euthyonidiella huwi* O'Loughlin in O'Loughlin et al., 2014 and sclerodactylins *Pachythyone rubra* (Clark, 1901) and *Sclerodactyla briareus* (Lesueur, 1824).

In this study we describe a new species, *Pseudothyone labradorensis* sp. nov., from the bathyal depths of the Labrador Sea (Northwest Atlantic Ocean) based on morphological and molecular data. Using molecular data on partial sequences of the mitochondrial gene cytochrome c oxidase subunit I (COI), we examined phylogenetic relationships of *P. labradorensis* sp. nov. with two Atlantic congeners, *P. raphanus* (type species of the genus) and *P. serrifera*, for which we

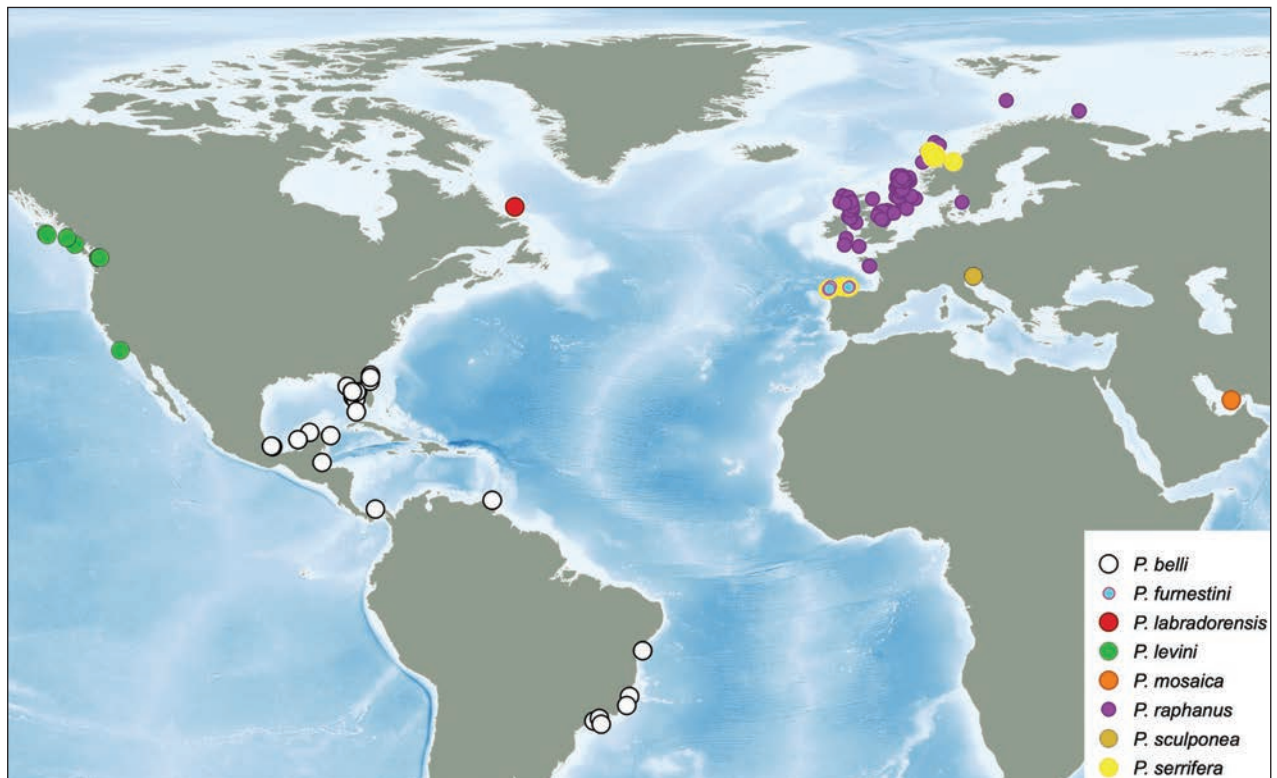


Figure 1. Distribution of *Pseudothyone labradorensis* sp. nov. and other species in the same genus, based on published records and GBIF (2023). Map was prepared using QGIS 3.16.5-Hannover.

obtained additional genetic data, as well as with the Northeast Pacific species *P. levini*. COI is commonly used for recovering relationships within the genera of Holothuroidea (O’Loughlin et al. 2014; Li et al. 2018; Ogawa et al. 2022; Ogawa et al. 2023). To test monophyly of *Pseudothyone* we included available data on the representatives of Sclerodactylidae sensu Smirnov (2012) as well as *Pentamera calcigera* (Stimpson, 1851), as close relationships of *Pentamera* to Sclerodactylidae has been shown previously (Arndt et al. 1996; Miller et al. 2017).

Material and methods

Two specimens of *Pseudothyone labradorensis* sp. nov. were collected together in the same location (North Atlantic Fisheries Organization NAFO, Zone 2J <https://www.marineregions.org/gazetteer.php?p=details&id=23382>) using a rock dredge deployed during the ISECOLD scientific expedition aboard the research icebreaker CCGS *Amundsen* on 30 August 2020 (Table 1). The rock dredge net had a 7 mm mesh. Due to the large volume of mud collected at this station, a fourth of the material was sieved through a 2 mm sieve and the rest was scanned for larger individuals through a 17 mm diameter mesh sieve. The specimens later identified as *Pseudothyone* were preserved in 100% ethanol for morphological and molecular analysis.

The specimens of *P. raphanus* and *P. serrifera* had previously been collected in 2006–2016 with a Van Veen grab, Triangular dredge and Agassiz trawl deployed from the research vessels R/V *Gunnerus*, R/V *Håkon Mosby* and R/V *Hans Brattström* (Table 1). They were preserved and subsequently stored in 96% ethanol.

Table 1. Voucher information for which molecular data were obtained in this study. Additional data can be obtained from corresponding BOLD Process ID pages.

Identification	Voucher	GenBank Acc.	BOLD Process ID	Catalog Number	Storing Institution*	Collection Date	Region	Latitude	Longitude	Depth (m)
<i>Pseudothyone labradorensis</i> sp. nov.	AMLAB-02	PP047583	AMLAB002-21	ECH02801	IORAS	30/08/2020	coast of Labrador (eastern Canada)	56.500	-58.084	740–969
<i>Pseudothyone labradorensis</i> sp. nov.	PT1210	PP047582	PSSP001-23	ECH02802	IORAS	30/08/2020	coast of Labrador (eastern Canada)	56.500	-58.084	740–969
<i>Pseudothyone raphanus</i>	Sletvik2016_87	OR974836	ECHNO258-16	NTNU-VM-72185	NTNU	25/10/2016	Norway, Trondheimsfjorden	63.67830	9.79612	122
<i>Pseudothyone raphanus</i>	ZMBN_120538	OR974833	ECHNO400-18	ZMBN 120538	ZMBN	08/06/2014	Norway, Halsnøyfjorden	59.75777	5.49778	60
<i>Pseudothyone raphanus</i>	ZMBN_120547	OR974839	ECHNO409-18	ZMBN 120547	ZMBN	02/05/2006	Norway, Kobbaleia, Bergen area	60.314	5.156	22–42
<i>Pseudothyone serrifera</i>	Sletvik2016_111	OR974842	ECHNO197-16	NTNU-VM-72204	NTNU	25/10/2016	Norway, Trondheimsleia	63.657	9.634	260–278
<i>Pseudothyone serrifera</i>	Sletvik2016_88	OR974838	ECHNO259-16	ZMBN 155233	ZMBN	24/10/2016	Norway, Trondheimsfjorden	63.586	9.846	280–102
<i>Pseudothyone serrifera</i>	Sletvik2016_89	OR974840	ECHNO260-16	NTNU-VM-72186	NTNU	24/10/2016	Norway, Trondheimsfjorden	63.586	9.846	280–102
<i>Pseudothyone serrifera</i>	Sletvik2016_90	OR974837	ECHNO261-16	NTNU-VM-72187	NTNU	24/10/2016	Norway, Trondheimsfjorden	63.586	9.846	280–102
<i>Pseudothyone serrifera</i>	Sletvik2016_91	OR974834	ECHNO262-16	NTNU-VM-72188	NTNU	25/10/2016	Norway, Trondheimsleia	63.657	9.634	260–278
<i>Pseudothyone serrifera</i>	Sletvik2016_92	OR974835	ECHNO263-16	ZMBN 155234	ZMBN	25/10/2016	Norway, Trondheimsleia	63.657	9.634	260–278
<i>Pseudothyone serrifera</i>	Sletvik2016_86	OR974841	ECHNO271-16	ZMBN 155235	ZMBN	26/10/2016	Norway, Trondheimsleia	63.594	9.508	56–45

*Institution abbreviations:

IORAS: Shirshov Institute of Oceanology, Russian Academy of Sciences, Moscow, Russia

NTNU: Department of Natural History, University Museum of Norwegian University of Science and Technology, Trondheim, Norway

ZMBN: Natural History Collections, University Museum of Bergen, Bergen, Norway

Morphological examination, dissection and photographing were performed using a Leica M205C stereomicroscope equipped with a Leica FLEXACAM C1 digital camera. To extract ossicles, small fragments of the body wall, introvert, tube foot and tentacle skin were digested in a domestic bleach water solution followed by several rinses in distilled water. For light microscopy, ossicles were transferred onto a glass slide, dried using a heating stage and mounted in Canada Balsam. For scanning electronic microscopy (SEM), ossicles were dried with 96% ethanol, mounted on a stub and sputter coated with gold. Ossicles were examined and photographed under a light microscope (Olympus BX43) with a TouPCam U3CMOS08500KPA digital camera and SEM examination was performed using a TESCAN Vega 3.

To evaluate phylogenetic relationships of *Pseudothyone labradorensis* sp. nov. within the genus, partial sequences of cytochrome c oxidase, subunit I (COI) were obtained from two examined specimens. Additionally, COI data were obtained for three specimens of *P. raphanus* and seven specimens of *P. serrifera* (Table 1). Some of these specimens were collected close to their type localities (Bergen area and Trondheimsfjorden, respectively). Also, three sequences of *Pseudothyone*, publicly available in GenBank, were used in the analysis: *P. raphanus* (MG934913) and *P. levini* (MH242951 and MH242950). To test monophyly of *Pseudothyone*, published sequences of Sclerodactylidae sensu Smirnov (2012) were analysed (Table 2). A COI sequence of *Pentamera calcigera* (Phyllophoridae) was also included in

Table 2. Data on sequences obtained from Genbank.

Identification	Current family attribution	Voucher	GenBank Acc.
<i>Eupentacta quinquesemita</i>	Sclerodactylidae	BIOUG<CAN>:BAM00127	HM542177
<i>Eupentacta quinquesemita</i>	Sclerodactylidae	no data	U32218
<i>Eupentacta pseudoquinquesemita</i>	Sclerodactylidae	BMBM-0776	MH242754
<i>Eupentacta</i> sp.	Sclerodactylidae	ECHINO_001_091	MK037199
<i>Eupentacta</i> sp.	Sclerodactylidae	USNM:IZ:1503386	MZ580563
<i>Eupentacta</i> sp.*	Sclerodactylidae	isolate CZ1	MK562383
<i>Havelockia</i> sp.	Sclerodactylidae	NMV_F151829	KF142167
<i>Pachythyone rubra</i>	Sclerodactylidae	SIO:BIC:E6676	KX874387
<i>Pentamera calcigera</i>	Phylloporidae	BIOUG<CAN>:HLC-30032	HM543053
<i>Pseudothyone levini</i>	Sclerodactylidae	BFHL-1914	MH242950
<i>Pseudothyone levini</i>	Sclerodactylidae	BMBM-1095	MH242951
<i>Pseudothyone raphanus</i>	Sclerodactylidae	Echin 6852V	MG934913
<i>Sclerodactyla briareus</i>	Sclerodactylidae	SIO:BIC:E6814	KX874342
<i>Stichopus horrens</i>	Stichopodidae	isolate SHP3	KY986418

*Identification according Turanov et al. (2024)

the analysis as it was recovered in a sister clade to the sclerodactylid *Pachythyone rubra* (Miller et al. 2017). *Stichopus horrens* was set as an outgroup. GenBank accession numbers of the sequences used in the analysis are listed in the Table 2.

Molecular work was carried out in two laboratories applying two different protocols. Genetic data on *Pseudothyone labradorensis* sp. nov. (voucher AM-LAB-02), *P. raphanus* and *P. serrifera* were obtained at the Canadian Centre for DNA Barcoding, University of Guelph following protocols by Ivanova et al. (2006), Ratnasingham and Hebert (2007), and deWaard et al. (2008). Data on another specimen of *P. labradorensis* sp. nov. (voucher PT1210) was generated at IORAS using the following methods: DNA was extracted using QuickExtract™ DNA Extraction Solution (Lucigen) following the manufacturer protocol; PCR amplification was conducted using Encyclo Plus PCR kit (Evrogen, Moscow) according the manufacturer protocol with annealing temperature set at 48 °C; PCR products were purified from agarose gel using HiPure Gel DNA Mini Kit (Magen); the purified samples were sequenced using the Sanger method on Applied Biosystems ABI 3900 (ThermoFisher Scientific) by Evrogen (Moscow, Russia). All PCR amplifications and sequencing were carried out using the LCOech1aF1 (5'-TTTTTTC-TACTAAACACAAGGATATTGG-3'; D. Eernisse unpublished) and HCO2198 (5'-TA-AACTTCAGGGTGACCAAAAATCA-3'; Folmer et al. 1994) primers.

Contigs were assembled from forward and reverse chromatograms using the MUSCLE algorithm implemented in Geneious v.10.0.9 and then manually edited. Sequences were aligned in MEGA 7 (Kumar et al. 2016) also using the MUSCLE algorithm, and then checked for stop-codon presence. The final dataset included 840 aligned positions. Phylogenetic analysis was performed using maximum-likelihood (ML) and Bayesian inference (BI) approaches. PartitionFinder 2 (Lanfear et al. 2017) was used for selecting best-fit partitioning schemes and models of nucleotide evolution. The defined models were TRNEF+I+G for positions 1 and 2, and GTR+G for position 3. ML tree search and bootstrapping was conducted in RAxML-NG (Kozlov et al. 2019) using auto MRE option with cutoff=0.03; the analysis converged after 12950 replicates. BI

analysis was performed using MrBayes v.3.2 (Ronquist et al. 2012). The analysis was conducted in two runs, four chains (one cold and three heated) with trees and parameters sampled every 500 generations. The traces were analysed in Tracer v.1.7.1, and then 10% of the trees were discarded as burn-in. Run convergence was evaluated by analysing sump output parameters in MrBayes *log* file and Tracer v.1.7.1. Genetic distances were calculated using Kimura 2-parameter model (K2P; Kimura 1980) implemented in MEGA 7.

Taxonomy

Order Dendrochirotida Grube, 1840

Family Sclerodactylidae Panning, 1949 sensu Smirnov, 2012

***Pseudothyone* Panning, 1949**

***Pseudothyone labradorensis* sp. nov.**

<https://www.zoobank.org/B4110DB7-0589-4A96-BC32-344F56ABF794>

Figs 2, 3

Type material. Holotype. CANADA • 9.5 mm in length; Labrador Sea, 56.500, -58.084, depth 740–969 m (between bottom and recovery); 30 Aug. 2020; Station ISECOLD -0-1000; rock dredge; substratum primarily mud with sparse rocks; IORAS ECH02801, ID AMLAB-02. **Paratype.** CANADA • 14 mm in length, collected at same time and locality as holotype; IORAS ECH02802, ID PT1210. Both holotype and paratype are preserved and stored in 96% ethanol.

Diagnosis. Body curved, cylindrical, tapered at anterior and posterior ends. Body colour in vivo pinkish. Tentacles 10, two ventral tentacles smaller. Tube feet arranged in several rows along radii, also present in interradii and on tapered posterior part of body. Body-wall ossicles slightly concave plates of irregular shape with smooth margins and perforations. Ossicles of tube feet rod-shaped; terminal plate irregular in shape; rods not numerous, smooth, with enlarged tuberculous ends. Tentacle ossicles rods with enlarged perforated ends. Segments of calcareous ring with undivided posterior projections.

Description. Body curved towards dorsal side, wider and cylindrical in the middle, anterior end tapered towards terminal mouth, posterior end tapered to a 'tail' towards terminal anus, 'tail' short, more prominent in paratype and short in holotype (Fig. 2A–D). Body colour pinkish in living specimens (Fig. 2A, B), tentacles, tube feet and 'tail' more brightly coloured; colour in ethanol uniformly greyish, tentacles and tube feet whitish or greyish (Fig. 2C, D). Body length 9.5 mm in holotype, 14 mm in paratype. Body-wall skin thin, rough, non-transparent, with dense layer of scale-like ossicles (Fig. 2G). Tentacles (examined in holotype, in paratype they were partly retracted) ten, two ventral tentacles remarkably smaller in size. Tube feet small (Fig. 2F), non-transparent in ethanol, arranged in several rows along radii and also scattered in interradii; tube feet more numerous on mid body, along ventrolateral and mid-ventral radii; on 'tail' tube feet smaller and less numerous, arranged in double rows (Fig. 2E). Anal papillae five (Fig. 2E). Pieces of calcareous ring up to 1.6 mm in length, united at most their length, radial segments with undivided posterior projections, with forked grooved anterior projections; interradial segments with grooved anterior projections (Fig. 2H, I). Retractor muscles undivided, not flat, broader anteriorly

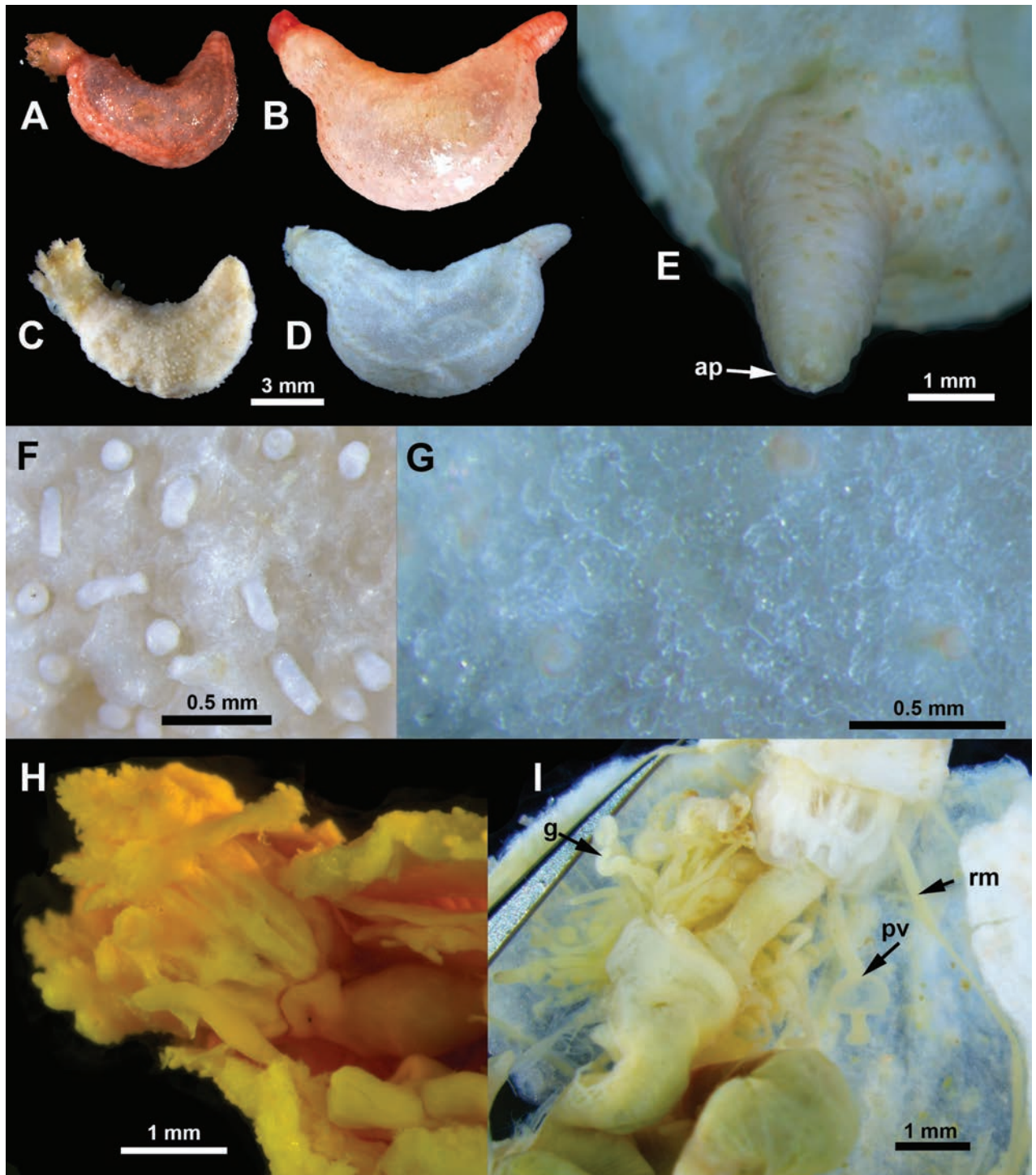


Figure 2. *Pseudothyone labradorensis* sp. nov., external and internal morphology **A, C** holotype, before preservation (**A**) and preserved in ethanol (**C**) **B, D** paratype, before preservation (**B**), in ethanol (**D**) **E** tapered posterior body part in paratype **F** tube feet in holotype **G** body-wall skin with dense layer of ossicles **H** segments of calcareous ring in holotype **I** dissected anterior part in paratype. Labels: ap anal papillae, g gonad, pv Polian vesicle, rm retractor muscle.

(Fig. 2I). Polian vesicle single, non-divided (Fig. 2I). Gonad in a tuft (Fig. 2I), gonad tubules in paratype with oocytes of different size.

Body-wall ossicles in a single dense overlapping layer, laying their concave side out; body-wall ossicles small perforated plates, usually do not exceed 200 μm in length, slightly concave, mostly irregular in shape, smooth; perforations with

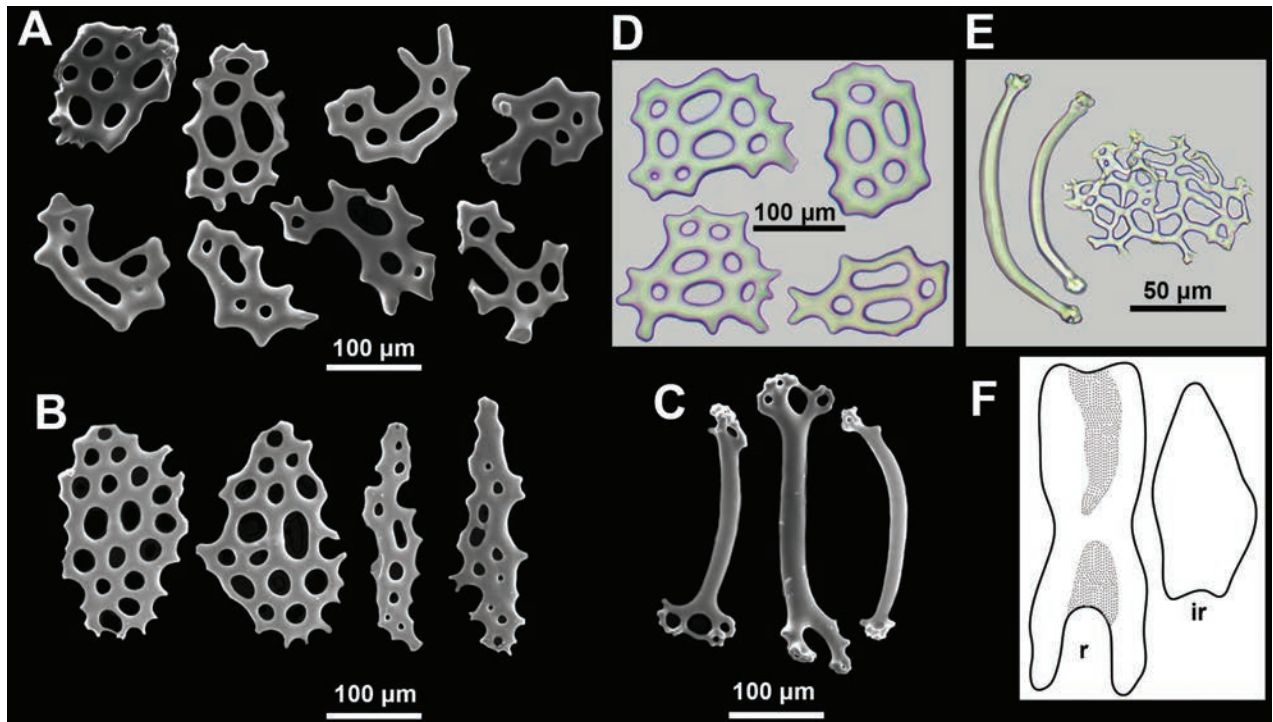


Figure 3. Ossicles of *Pseudothyone labradorensis* sp. nov. **A, D** body-wall perforated plates **B** introvert perforated plates **C** tentacle rods **E** tube foot rods and terminal plate **F** right dorsal radial (r) and interradial (ir) segments of calcareous ring. **A, B, C** SEM images **D, E** light microscope images **F** drawing.

smooth margins, from rounded to oblong in shape, their size and shape can vary even on a same plate (Fig. 3A, D). Introvert with bigger flat plates, plates often narrow and elongated (Fig. 3B). On tube feet supporting rod-shaped ossicles, not numerous, curved in shape, with slightly enlarged perforated ends, length 100–130 µm; terminal plate delicate, irregular in shape, ~70 µm in diameter (Fig. 3E). Tentacle ossicles curved rods, most ossicles ranged 100–480 µm in length, bigger in proximal part of tentacles; smaller rods sometimes enlarged in the middle; bigger rods often with enlarged spatulated and/or bifurcated ends (Fig. 3C).

Differential diagnosis. *Pseudothyone labradorensis* sp. nov. can be distinguished from other species by a combination of the following characters: pinkish body colour (may disappear after preservation in ethanol); tube feet arranged in double rows on tapered posterior end; body-wall ossicles only perforated plates with smooth perforation margins; introvert ossicles perforated plates; tube foot ossicles rods and terminal plate of irregular shape.

Distribution. Canada, Labrador Sea, depth 740–969 m.

Etymology. The species is named after its type locality.

Environmental information

A CTD cast and drop camera deployment took place at 494 and 218 m respectively from the rock dredge recovery location. Bottom water temperature at 990 m was 3.7 °C, salinity 34.8 psu. These conditions are associated with Labrador Sea Water, and are in contrast to colder and less saline conditions found on the adjacent continental shelf (Côté et al. 2019). Modelled bottom water velocities (GIOPS daily historical 3D data extracted from <https://navigator.oceansdata.ca/public/>

for 2022) for this collection location average 0.13 m s^{-1} (range: $0.02\text{--}0.23 \text{ m s}^{-1}$). Other fauna collected in the rock dredge deployment included soft corals *Duva florida* (Rathke, 1806), sea pens (Pennatuloidae), fragments of the gorgonians *Primnoa resedaeformis* (Gunnerus, 1763), *Paragorgia arborea* (Linnaeus, 1758), *Acanella arbuscula* (Johnson, 1862), and the mushroom coral *Anthomastus* Verill, 1878. Sponges, bivalves, and a small grenadier were also present, highlighting a diverse range of bottom type requirements. The seafloor imagery further corroborates the dominance of soft sediment in the study area, with sparse gravel and rocks. Based on 42 seafloor images (along a 1.1 km long transect), 98% of the primary sediment was classified as fine sediment, and only 2.4% as gravel.

Molecular data

Both examined specimens of *Pseudothyone labradorensis* sp. nov. formed a single, well-supported clade [bootstrap (BS) 99, posterior probability (PP) 1, Fig. 4]. The sequences of the holotype and paratype were assigned to the same Barcode

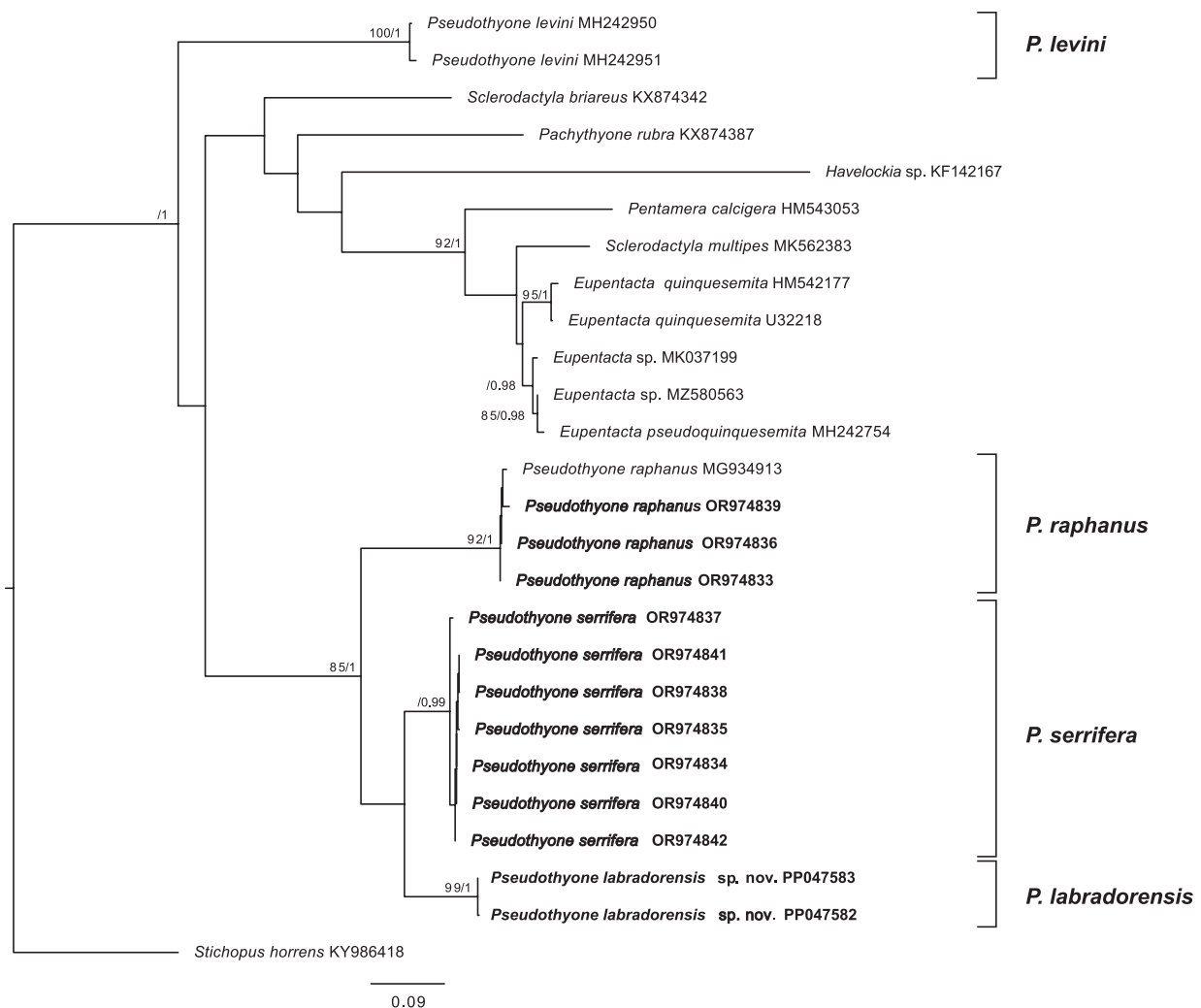


Figure 4. Phylogenetic relationships inferred using maximum-likelihood (ML) and Bayesian (BI) analyses of the COI dataset (840 bp). Topology corresponds to best-scoring ML tree; node values are bootstrap scores ($\geq 75\%$) / BI posterior probabilities (≥ 0.95). Taxa examined in this study are in bold. *Stichopus horrens* KY986418 was set as outgroup.

Index Number (BIN, AEH8268) and showed little genetic divergence (K2P-distance 0.003). Based on the COI data, the closest taxa to *P. labradorensis* sp. nov. were *P. serrifera* (K2P-distance 0.10) and *P. raphanus* (K2P-distance 0.162). Phylogenetic analysis recovered *P. labradorensis* sp. nov. in a sister clade with *P. serrifera*, although this clade was weakly supported (BS 50, PP 0.84). A clade of *P. raphanus*, *P. serrifera* and *P. labradorensis* sp. nov. (*raphanus* clade) was well-supported in the BI analysis and averagely supported by ML (BS 85, PP 1). *Pseudothyone levini* was sister to the clade with all other species of the dataset showing no close relationships with the *raphanus* clade nor with other examined sclerodactylids. The analysis showed no close relationships of the *raphanus* clade with examined sclerodactylid representatives.

Discussion

Molecular data supported close relationships of *Pseudothyone labradorensis* sp. nov. to the type species of the genus, *P. raphanus*, and to the Northeast Atlantic species *P. serrifera*. According to body-wall ossicle morphology, *P. labradorensis* sp. nov. is most closely related to *P. raphanus* (Fig. 5A), from which it differs by its pinkish body colour, presence of tube feet on the 'tail', absence of fern-like ossicles on the tentacles, and by the presence of rod-shaped ossicles in the tube feet. From the genetically closest species, *P. serrifera* (Fig. 5B), the new species differs by the pinkish body colour, absence of S-shaped rods on tentacles, and by the smooth margins and perforations of body-wall ossicles. From another Northeast Atlantic species, *P. furnestini*, the new species differs by body colour and body-wall ossicles. *Pseudothyone furnestini* is characterized by whitish colouration and thick body-wall ossicles that are from rounded to oval in shape and often possess solid, unperforated extensions. Also *Pseudothyone furnestini* lacks rod-shaped ossicles in the tube feet.

According to molecular data, *Pseudothyone levini* was not closely related to the species of the *raphanus* clade. This species has ten tentacles that are equal in size, whereas other species of *Pseudothyone* have two ventral tentacles smaller than others. From species of the *raphanus* clade, it also differs by a less prominent 'tail', less perforated body-wall plates and by more robust rod-shaped ossicles on tube feet.

Some other species of *Pseudothyone* also have remarkable morphological differences. Apart from plates, the body-wall ossicles of *P. belli* include knobbed buttons and plates with handles, which do not occur in *P. raphanus* and most other species of the genus. Also *P. belli* differs by the ossicles from the tentacles, which are plates and rosettes (not rods as in *P. raphanus* and other species), by introvert ossicles pillared tables and plates, and by tube feet ossicles arched pillared tables. Therefore, *P. belli* differs remarkably from *P. raphanus* in most ossicle types. Marked differences in ossicle types are also noted for *P. mosaica*. This species is characterized by large rounded plates on the body wall and arched pillared tables on its tube feet.

The present results suggest that the taxonomy of *Pseudothyone* requires further investigation. Particularly, the generic affiliation of *P. levini*, *P. belli* and *P. mosaica* may require additional evaluation. The taxonomic position of the genus also remains unclear. Based on COI data, the *raphanus* clade (*P. raphanus* + *P. serrifera* + *P. labradorensis* sp. nov.) does not form any well-supported

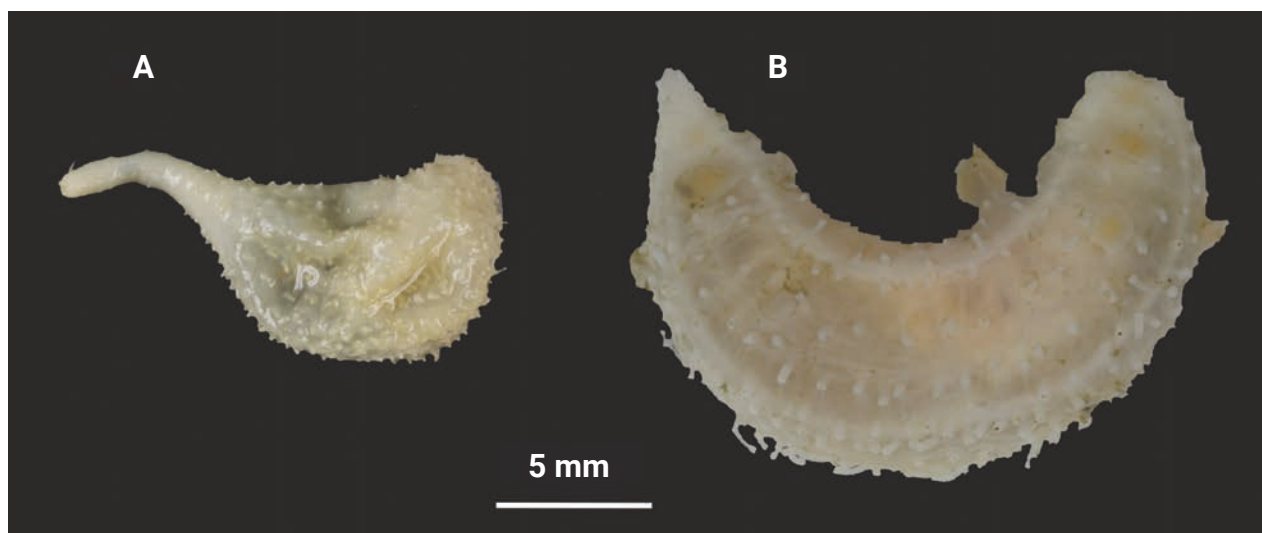


Figure 5. *Pseudothyone raphanus* (A) and *P. serrifera* (B) collected from the type locality areas. A ZMBN 120547 B NTNU-VM-72187. Collection data is given in Table 1. Image courtesy of Katrine Kongshavn.

clade with other examined representatives of Sclerodactylidae sensu Smirnov (2012). More data, both morphological and molecular, are needed to analyze the phylogenetic relationships of *Pseudothyone*.

Scientific collections of fauna in the Labrador Sea are extremely limited so the distribution of this species is yet to be resolved. *Pseudothyone labradorensis* sp. nov. is known from a single locality in the Labrador Sea, at a depth between 740–969 m. Metabarcoding surveys of the ISECOLD transects in the Labrador Sea (Côté et al. 2023) did not detect this species but several other holothuroids were detected over benthic habitats at a depth of 1026 m about 300 km to the north (Côté unpubl. data): *Chiridota laevis* (O. Fabricius, 1780), *Benthogone* sp., *Enypniastes* sp., Psolidae gen. sp., and two unresolved species from the orders Dendrochirotida and Apodida.

Apart from *P. labradorensis* sp. nov., three more species of *Pseudothyone* are known from bathyal depths. The type species *P. raphanus* and another Northeast Atlantic species, *P. serrifera*, were reported down to 1200 m (Fernández-Rodríguez et al. 2019), with most of their records obtained shallower than 250 m and 600 m, respectively. The deepest species of the genus, *P. furnestini*, occurred between 440 and 1347 m (ibid.). According to McKenzie (1991), the body colour in *P. raphanus* can be “sometimes a pale pink”. Combined with personal unpublished observations of pinkish specimens of *P. cf. raphanus* off south Iceland, it is possible that *P. labradorensis* sp. nov. may have a wider distribution in the North Atlantic.

Key to the North Atlantic *Pseudothyone*

- 1 Tube feet present on tapered posterior part of body **3**
- Tube feet absent or few on tapered posterior part of body **2**
- 2 Body-wall ossicles surrounding tube feet with elongated non-perforated prolongations; terminal plate in tube feet star-shaped ***P. sculponea***
- Body-wall ossicles lack prolongations; terminal plate of irregular shape or absent ***P. raphanus***

- 3 Body-wall ossicles smooth plates and knobbed buttons *P. belli*
- Body-wall ossicles smooth plates only **4**
- 4 Tube feet ossicle terminal plate only *P. furnestini*
- Tube feet with supporting rods and terminal plate **5**
- 5 Body-wall plate perforations with serrated margins *P. serrifera*
- Body-wall plate perforations smooth *P. labradorensis* sp. nov.

Acknowledgements

We would like to thank Kaitlin Casey, as well as the researchers and crew aboard the CCGS *Amundsen* for their help during the collections. We would also like to thank Torkild Bakken at the NTNU University Museum for arranging the workshop at Sletvik Field Station and the cruise time on R/V *Gunnerus* from which our specimens of *P. raphanus* and *P. serrifera* from Trondheimsfjorden were collected in 2016. We are grateful to Gustav Paulay and Francisco Alonso Solís Marín whose valuable comments helped to improve the manuscript. We are also grateful to Alexander Filippov (IORAS) for technical assistance in SEM observation, and to Katrine Kongshavn for providing photographs of *P. raphanus* and *P. serrifera*.

Additional information

Conflict of interest

The authors have declared that no competing interests exist.

Ethical statement

All applicable international, national, and/or institutional guidelines for animal testing, animal care and use of animals were followed by the authors.

Sampling and field studies

Permission for the field work and sample collections were obtained by the authors from the Department of Fisheries and Oceans Canada.

Funding

This research was partly funded by Discovery and Ship Time grants to AM from the Natural Sciences and Engineering Research Council of Canada (NSERC), with primary ship time on the CCGS *Amundsen* provided by DFO's ISECOLD program. Some of the data collected aboard the vessel were made available by the Amundsen Science program, which is supported through Université Laval by the Canada Foundation for Innovation (CFI) Major Science Initiatives (MSI) Fund. The sequencing of *P. raphanus* and *P. serrifera* was funded by Norwegian Barcode of Life (NorBOL) www.norbol.org. AK was funded by Minobrnauki of Russian Federation, State assignment theme No FMWE-2024-2022.

Author contributions

Study design, Funding acquisition – AM, JFH, AK, DC; Supervision, Administration – AM, JFH; Sampling – BMN; Morphology – AK; Molecular work – TA, HP, AK; Phylogenetic analysis – AK; Writing – AK; Editing – AM, JFH, BMN, DC, HP, TA. The manuscript was read by and approved by all the authors.

Author ORCIDs

Antonina Kremenetskaia  <https://orcid.org/0000-0001-8851-3318>

Tom Alvestad  <https://orcid.org/0000-0003-0204-2936>

Heather Penney  <https://orcid.org/0000-0001-7259-3931>

Jean-François Hamel  <https://orcid.org/0000-0002-0435-4127>

Bárbara de Moura Neves  <https://orcid.org/0000-0003-2316-9223>

David Côté  <https://orcid.org/0000-0002-5805-5077>

Annie Mercier  <https://orcid.org/0000-0003-0807-2378>

Data availability

All data generated during this study are included in this article. Sequences are published in GenBank and BOLD.

References

- Arndt A, Marquez C, Lambert P, Smith MJ (1996) Molecular phylogeny of eastern Pacific sea cucumbers (Echinodermata: Holothuroidea) based on mitochondrial DNA sequence. *Molecular Phylogenetics and Evolution* 6(3): 425–437. <https://doi.org/10.1006/mpev.1996.0091>
- Barrois T (1882) Catalogue des crustacés Podophtalmaires et des échinodermes recueillis à Concarneau durant les mois d'août septembre 1880. Lille, Imprimerie L Danel, 1–68 pp. <https://doi.org/10.5962/bhl.title.53806>
- Cherbonnier G (1958) Note sur *Pseudothyone sculponea* nouvelles espèce d'holothurie dendrochirote de Méditerranée. *Vie et Milieu* 9: 62–66.
- Cherbonnier G (1969) Échinodermes récoltés par la *Thalassa* au large des côtes d'Espagne et du golfe de Gascogne. *Bulletin du Muséum D'Histoire Naturelle*, 2 série 41: 343–361.
- Clark HL (1901) The holothurians of the Pacific Coast of North America. *Zoologischer Anzeiger* 24: 162–171.
- Côté D, Heggland K, Roul S, Robertson G, Fifield D, Wareham V, Colbourne E, Maillet G, Devine B, Pilgrim L, Pretty C, Le Corre N, Lawson JW, Fuentes-Yaco C, Mercier A (2019) Overview of the biophysical and ecological components of the Labrador Sea Frontier Area. DFO Canadian Science Advisory Secretariat Research Document 2018(067): 1–59.
- Côté D, McClenaghan B, Desforges J, Fahner NA, Hajibabaei M, Chawarski J, Roul S, Singer G, Aubry C, Geoffroy M (2023) Comparing eDNA metabarcoding and conventional pelagic netting to inform biodiversity monitoring in deep ocean environments. In: Miller-Saunders K (Ed.) *ICES Journal of Marine Science* 80: 2545–2562. <https://doi.org/10.1093/icesjms/fsad169>
- Deichmann E (1954) The holothurians of the Gulf of Mexico. *Bulletin of the U.S. Fish Commission* 55: 381–410.
- deWaard JR, Ivanova NV, Hajibabaei M, Hebert PDN (2008) Assembling DNA barcodes. Analytical protocols. In: Martin CC (Ed.) *Environmental Genomics. Methods in Molecular Biology* 410. Humana Press, Totowa, 275–293. https://doi.org/10.1007/978-1-59745-548-0_15
- Düben von MW, Koren J (1846) Öfversigt af Skandinaviens Echinodermmer. *Kongliga vetenskaps-akademiens förhandlingar* 1845: 229–328.
- Fernández-Rodríguez I, Arias A, Anadón N, Acuña JL (2019) Holothurian (Echinodermata) diversity and distribution in the central Cantabrian Sea and the Avilés Canyon System (Bay of Biscay). *Zootaxa* 4567(2): 293–325. <https://doi.org/10.11646/zootaxa.4567.2.5>

- Folmer O, Black M, Hoeh W, Lutz R, Vrijenhoek R (1994) DNA primers for amplification of mitochondrial Cytochrome C oxidase subunit I from diverse metazoan invertebrates. *Molecular Marine Biology and Biotechnology* 3: 294–299.
- GBIF.org (2023) GBIF Occurrence. <https://doi.org/10.15468/dl.gnu3qh> [Accessed 27.09.2023]
- Grube AE (1840) Actinien, Echinodermen und Wurmer des Adriatischen und Mittelmeers. Bon JH, Königsberg, 92 pp. <https://doi.org/10.5962/bhl.title.10133>
- Gunnerus JE (1763) Om en søvevt, allevegne ligesom besat med frøehuuse, *Gorgonia resedæformis*. *Det Trondhiemske Selskabs Skrifter* 2: 321–329.
- Ivanova NV, Dewaard JR, Hebert PDN (2006) An inexpensive, automation-friendly protocol for recovering high-quality DNA. *Molecular Ecology Notes* 6(4): 998–1002. <https://doi.org/10.1111/j.1471-8286.2006.01428.x>
- Johnson JY (1862) Descriptions of two corals from Madeira, belonging to the genera *Primnoa* and *Mopsea*. *Proceedings of the Zoological Society of London* 1862(1): 244–246. <https://doi.org/10.1111/j.1469-7998.1862.tb06521.x>
- Kimura M (1980) A simple method for estimating evolutionary rates of base substitutions through comparative studies of nucleotide sequences. *Journal of Molecular Evolution* 16(2): 111–120. <https://doi.org/10.1007/BF01731581>
- Koehler R, Vaney C (1910) Description d'holothuries nouvelles appartenant au Musée Indien. *Records of the Indian Museum* 5: 89–104. <https://doi.org/10.5962/bhl.part.10494>
- Kozlov AM, Darriba D, Flouri T, Morel B, Stamatakis A (2019) *RAxML-NG*: A fast, scalable and user-friendly tool for maximum likelihood phylogenetic inference. *Bioinformatics (Oxford, England)* 35(21): 4453–4455. <https://doi.org/10.1093/bioinformatics/btz305>
- Kumar S, Stecher G, Tamura K (2016) MEGA7: Molecular Evolutionary Genetics Analysis Version 7.0 for Bigger Datasets. *Molecular Biology and Evolution* 33(7): 1870–1874. <https://doi.org/10.1093/molbev/msw054>
- Lambert P, Oliver KL (2001) *Pseudothyone levini*, a new species of sea cucumber (Echinodermata: Holothuroidea) from the Northeastern Pacific. *Proceedings of the Biological Society of Washington* 114: 589–598.
- Lanfear R, Frandsen PB, Wright AM, Senfeld T, Calcott B (2017) PartitionFinder 2: New methods for selecting partitioned models of evolution for molecular and morphological phylogenetic analyses. *Molecular Biology and Evolution* 34: 772–773. <https://doi.org/10.1093/molbev/msw260>
- Lesueur C (1824) Description of several new species of *Holothuria*. *Journal of the Academy of Natural Sciences of Philadelphia* 4: 155–163. <https://www.biodiversitylibrary.org/page/24655269>
- Li YN, Xiao N, Zhang LP, Zhang H (2018) *Benthodytes marianensis*, a new species of abyssal elasipodid sea cucumbers (Elasipodida: Psychropotidae) from the Mariana Trench area. *Zootaxa* 4462(3): 443–450. <https://doi.org/10.11646/zootaxa.4462.3.10>
- Linnaeus C (1758) *Systema Naturae per regna tria naturae, secundum classes, ordines, genera, species, cum characteribus, differentiis, synonymis, locis*. Laurentius Salvius, Holmiae, 824 pp. <https://doi.org/10.5962/bhl.title.542>
- Ludwig H (1886) Die von G. Chierchia auf der Fahrt der Kgl. Ital. Corvette *Vettor Pisani* gesammelten Holothurien. *Zoologische Jahrbücher. Zeitschrift für Systematik. Geographie und Biologie der Tiere* 2(1): 1–36.
- Madsen FJ, Hansen B (1994) Echinodermata Holothuroidea. *Marine Invertebrates of Scandinavia* 9: 1–143.

- Martins L (2019) Ontogenetic variation of the ossicles in *Pseudothyone belli* (Ludwig, 1887) with a description of a new Sclerodactylidae (Echinodermata: Holothuroidea: Dendrochirotida) from Southwestern Atlantic. *Marine Biology Research* 15(7): 434–443. <https://doi.org/10.1080/17451000.2019.1662051>
- McKenzie JD (1991) The taxonomy and natural history of north European dendrochirote holothurians (Echinodermata). *Journal of Natural History* 25(1): 123–171. <https://doi.org/10.1080/00222939100770091>
- Miller AK, Kerr AM, Paulay G, Reich M, Wilson NG, Carvajal JI, Rouse GW (2017) Molecular phylogeny of extant Holothuroidea (Echinodermata). *Molecular Phylogenetics and Evolution* 111: 110–131. <https://doi.org/10.1016/j.ympev.2017.02.014>
- O’Loughlin PM, Mackenzie M, Paulay G, VandenSpiegel D (2014) Four new species and a new genus of Antarctic sea cucumbers with taxonomic reviews of *Cladodactyla*, *Pseudocnus*, Paracucumidae and *Parathyonidium* (Echinodermata: Holothuroidea: Dendrochirotida). *Memoirs of the Museum of Victoria* 72: 31–61. <https://doi.org/10.24199/j.mmv.2014.72.04>
- Ogawa A, Kremenetskaia A, Hiruta SF, Shibata Y, Narimatsu Y, Miki S, Morita T, Tsuchida S, Fujiwara Y, Fujita T (2022) Rehabilitation of two deep-sea holothurian species in genus *Pannychia* from the northwest Pacific Ocean. *Deep-sea Research, Part II, Topical Studies in Oceanography* 202: 105099. <https://doi.org/10.1016/j.dsr2.2022.105099>
- Ogawa A, Kobayashi I, Kohtsuka H, Fujita T (2023) Two new species of the bathyal holothurian genus *Pannychia* (Elasipodida, Laetmogonidae) from Japanese waters. *Zootaxa* 5323(1): 105–125. <https://doi.org/10.11646/zootaxa.5323.1.6>
- Östergren H (1898) Zur Anatomie der Dendrochiroten, nebst Beschreibungen neuer Arten. *Zoologischer Anzeiger* 21: 133–136.
- Panning A (1949) Versuch einer Neuordnung der familie Cucumariidae (Holothuroidea, Dendrochirota). *Zoologische Jahrbücher Abteilung für Systematik* 78: 323–470.
- Pawson D, Fell H (1965) A revised classification of the dendrochirote holothurians. *Breviora* 15: 1–7. <http://www.vliz.be/imis/imis.php?module=ref&refid=29669>
- Pawson DL, Pawson DJ, King RA (2010) A taxonomic guide to the Echinodermata of the South Atlantic Bight, USA: 1. Sea cucumbers (Echinodermata: Holothuroidea). *Zootaxa* 2449(1): 1–48. <https://doi.org/10.11646/zootaxa.2449.1.1>
- Rathke J (1806) *Zoologia danica, seu Animalium Daniae et Norvegiae rariorum ac minus notorum descriptiones et historia*. Havniae MDCCCVI 4: 1–46.
- Ratnasingham S, Hebert PDN (2007) BOLD: The Barcode of Life Data System: Barcoding. *Molecular Ecology Notes* 7(3): 355–364. <https://doi.org/10.1111/j.1471-8286.2007.01678.x>
- Ronquist F, Teslenko M, van der Mark P, Ayres DL, Darling A, Höhna S, Larget B, Liu L, Suchard MA, Huelsenbeck JP (2012) MrBayes 3.2: Efficient Bayesian Phylogenetic Inference and Model Choice Across a Large Model Space. *Systematic Biology* 61(3): 539–542. <https://doi.org/10.1093/sysbio/sys029>
- Semper C (1867–1868) Holothurien. In: Semper C (Ed.) *Reisen im Archipel der Philippinen. Zweiter Theil. Wissenschaftliche Resultate. Erster Band. Holothurien*. W. Engelmann, Leipzig, 1–288. <https://doi.org/10.5962/bhl.title.11687>
- Sluiter CP (1910) Westindische holothurien. *Zoologische Jahrbücher (Supplementheft 11)*: 331–342.
- Smirnov AV (2012) System of the class Holothuroidea. *Paleontological Journal* 46(8): 793–832. <https://doi.org/10.1134/S0031030112080126>
- Stimpson W (1851) Description of *Pentacta calcigera* n. sp. *Proceedings Boston Society Natural History* 4: 67.

- Stimpson W (1855) Descriptions of some new marine Invertebrata. Proceedings. Academy of Natural Sciences of Philadelphia 7: 385–394. <https://doi.org/10.5962/bhl.title.51445>
- Thandar AS (1989) The sclerodactylid holothurians of southern Africa, with the erection of one new subfamily and two new genera (Echinodermata: Holothuroidea). South African Journal of Zoology 24(4): 290–304. <https://doi.org/10.1080/02541858.1989.11448167>
- Théel H (1886) Report on Holothurioidea dredged by H.M.S. Challenger during the Years 1873–76. Part II. Report of the Scientific Results of the Voyage of H.M.S. Challenger. Zoology: Analysis of Complex Systems, ZACS 39: 1–290. <https://www.19thcentury-science.org/HMSC/HMSC-Reports/Zool-39/README.htm>
- Turanov SV, Smirnov AV, Kartavtsev YP (2024) Taxonomic position of holothurian *Eupentacta fraudatrix* (Echinodermata, Holothuroidea). ZooKeys 1197: 237–248. <https://doi.org/10.3897/zookeys.1197.117752>
- Verrill AE (1878) Art. 46. Notice of recent additions to the marine fauna of the eastern coast of North America, No. 2. American Journal of Science and Arts 16: 371–378. <https://doi.org/10.2475/ajs.s3-16.95.371>

Four genera of the subfamily Opiinae Blanchard (Hymenoptera, Braconidae) new for Japan, with the description of two new species

Yunjong Han^{1*}, Cornelis van Achterberg^{2*}, Hyojoong Kim¹

¹ Animal Systematics Laboratory, Department of Biological Science, Kunsan National University, Gunsan, 54150, Republic of Korea

² Naturalis Biodiversity Center, P.O. 9517, 2300 RA Leiden, Netherlands

Corresponding author: Hyojoong Kim (hkim@kunsan.ac.kr)

Abstract

Four genera are reported for the first time from Japan (*Areotetes* van Achterberg & Li, 2013, *Indiopiopus* Fischer, 1966, *Neopiopus* Gahan, 1917 and *Sternaulopiopus* Fischer, 1965), and keys are provided for the species of these genera. Two new species are described and illustrated: *Areotetes convergens* **sp. nov.** and *Sternaulopiopus maculiferus* **sp. nov.**

Key words: *Areotetes*, identification, *Indiopiopus*, Japan, key, *Neopiopus*, new record, new species, parasitoid, *Sternaulopiopus*

Introduction

The large and cosmopolitan subfamily Opiinae Blanchard, 1845 consists of derived cyclostome wasps, with 2000+ described valid species. Members of Opiinae are koinobiont endoparasitoids of dipterous larvae, some of which are agricultural pests, such as leaf-mining and fruit-infesting species. Therefore, opiine parasitoids are potentially valuable for biological control (Wharton 1997; Ovruski et al. 2000; Delrio et al. 2005; Wahyuni et al. 2017). The actual number of genera of Opiinae is 40+, but the boundaries of the genera *Opiopus* Wesm., 1835 and *Eurytenes* Foerster, 1863 are not settled (e.g., Wharton 1987, 1988, 1997; Wharton and Norrbom 2013; van Achterberg 2023). We treat the genus *Sternaulopiopus* Fischer, 1965 as a valid genus by following Wharton (2006) and Sheng et al. (2019).

Materials and methods

The specimens of *Areotetes convergens* **sp. nov.** and *Neopiopus citrinus* were collected in a Malaise trap, while those of *Sternaulopiopus maculiferus* **sp. nov.**, *S. macrophthalmos* and *Indiopiopus chenae* were collected by using a net to sweep herbal vegetation. For identification of the subfamily Opiinae, see van Achterberg (1990, 1993, 1997); for references to the Opiinae, see Yu et al. (2016).

Morphological terminology follows van Achterberg (1988, 1993), including the abbreviations for wing venation. Measurements are taken as indicated by van Achterberg (1988): for the length and the width of a body part, the maxi-



Academic editor:

Francisco Javier Peris Felipo

Received: 18 April 2024

Accepted: 11 June 2024

Published: 8 July 2024

ZooBank: <https://zoobank.org/13AF475B-5FDF-42C1-876B-EA8A6841B0B7>

Citation: Han Y, van Achterberg C, Kim H (2024) Four genera of the subfamily Opiinae Blanchard (Hymenoptera, Braconidae) new for Japan, with the description of two new species. ZooKeys 1206: 207–229. <https://doi.org/10.3897/zookeys.1206.125662>

Copyright: © Yunjong Han et al.

This is an open access article distributed under terms of the Creative Commons Attribution License (Attribution 4.0 International – CC BY 4.0).

* These authors contributed equally to this work.

mum length and width are taken, unless otherwise indicated. The length of the mesosoma is measured from the anterior border of the mesoscutum to the apex of the propodeum and of the first tergite from the posterior border of the adductor to the medio-posterior margin of the tergite.

Observations, photographic images, and descriptions were made either with a digital stereo microscope (VHX-1000, Keyence) and with a LEICA DMC2900 digital camera or with a LEICA M205 C microscope (Leica Geosystems AG). Images were stacked with Helicon Focus v. 7 software (Helicon Soft, Kharkiv, Ukraine). After stacking, illustrations were created using Adobe Photoshop CS5.1.

The type specimens are deposited in the Osaka Museum of Natural History (OMNH) in Osaka.

Systematics

Genus *Areotetes* van Achterberg & Li, 2013

Areotetes van Achterberg & Li, 2013: 39–51. Type species (by original designation): *Areotetes carinuliferus* Li & van Achterberg, 2013.

Diagnosis. Basal carina of inner side of hind tibia long and slightly sinuate (Fig. 10); occipital carina present laterally; hypoclypeal depression distinct (Fig. 7); clypeus obtuse and truncate ventrally; malar sulcus absent; mandible normal and triangular; pronope absent and obsolescent (Fig. 8); precoxal sulcus finely crenulate or smooth (Fig. 4); medio-posterior depression of mesoscutum rather small or absent (Fig. 5); areola of propodeum distinct and with medio-longitudinal carina (Fig. 9); second submarginal cell of fore wing elongated (Fig. 2); vein m-cu of fore wing postfurcal; ovipositor sheath with very long setae (Fig. 6).

Distribution. Palaearctic [China, Japan (new record), South Korea] and Oriental (China).

Biology. Unknown.

Key to species of the genus *Areotetes* van Achterberg & Li

Notes: Modified after Li et al. (2013), with *Opius nepalensis* Fischer, *Utetes laevigatus* Weng & Chen and the species described in this paper added.

- 1 Medio-posterior depression of mesoscutum absent; antenna of ♀ without white apical band; second metasomal tergite smooth; face dark brown or blackish.....2
- Medio-posterior depression of mesoscutum present, but small; antenna of ♀ with white apical or subapical band; second tergite distinctly costate-striate medially; face yellowish-brown or pale yellowish3
- 2 Length of mesosoma 1.4–1.5× its height; propodeum without a medio-longitudinal carina posteriorly; hind femur 5.0–5.4× longer than its maximum width; vein 3-SR of fore wing 2.3–2.4× longer than vein 2-SR; [first metasomal tergite at least partly smooth and shiny]***A. carinuliferus* Li & van Achterberg, 2013**
- Length of mesosoma about 1.7× its height; propodeum with a medio-longitudinal carina posteriorly; hind femur about 4.0× longer than its maximum

- width; vein 3-SR of fore wing about twice longer than vein 2-SR
 **A. laevigatus (Weng & Chen, 2005)**
- 3 Vein 3-SR of fore wing about 1.7× longer than vein 2-SR and nearly straight; head dorsally (except stemmaticum and its surroundings) yellow; apical third of antenna of ♂ pale yellowish; pterostigma comparatively wide and short **A. albiferus Li & van Achterberg, 2013**
- Vein 3-SR of fore wing 2.2–2.7× longer than vein 2-SR and weakly curved; head dorsally (except orbita) dark brown; apical third of antenna of ♂ dark brown; pterostigma comparatively narrow and longer **4**
- 4 Vein r of fore wing emanating from basal 0.2 of pterostigma (Fig. 2); vein m-cu of fore wing distinctly converging towards vein 1-M posteriorly; [pedicel and third antennal segment yellowish; first metasomal tergite 1.6× longer than its apical width; length of hind femur 4.7× its maximum width]..... **A. convergens Han & van Achterberg, sp. nov.**
- Vein r of fore wing emanating from basal 0.3 of pterostigma; vein m-cu of fore wing subparallel with vein 1-M posteriorly..... **5**
- 5 Second metasomal tergite smooth (except for some indistinct striae medio-anteriorly); hind femur about 5.0× longer than its maximum width; vein 3-SR of fore wing about 2.2× longer than vein 2-SR; face more or less brownish; first tergite 1.6× longer than its apical width; apical antennal segments of ♀ ivory (but according to original description apical segments may be blackish); pedicel yellow and third antennal segment brown
 **A. nepalensis (Fischer, 1966), comb. nov.**
- Second tergite finely to moderately striate or costate-striate medially; hind femur about 4.0× longer than its maximum width; vein 3-SR of fore wing about 2.5× longer than vein 2-SR; face largely yellowish; first tergite 1.4× longer than its apical width; apical antennal segments of ♀ brownish; pedicel and third antennal segment brown.....
 **A. striatiferus Li & van Achterberg, 2013**

***Areotetes convergens* Han & van Achterberg, sp. nov.**

<https://zoobank.org/CD30248E-A76B-41C0-878E-D42F3F1BE68A>

Figs 1–13

Type material. *Holotype*, ♀ (OMNH), “Japan (Ryuku): Oganeku, Yamato, Amamioshima Island, Kagoshima, 28.3593°N, 129.3441°E, 25.v.–15.vi.2019, MT [=Malaise trap], A. Yoshikawa & Shunpei Fujie leg., OMNH”.

Diagnosis. Antenna of ♀ with white band (Figs 1, 12, 13; apical sixth segments); second metasomal tergite largely smooth except faintly striate-rugose medio-basally; clypeus 2.3× wider than its maximum height; pronope transverse elliptical; vein r of fore wing emanating from basal 0.2 of pterostigma (Fig. 2); vein m-cu of fore wing distinctly converging towards vein 1-M posteriorly; vein 3-SR of fore wing 2.4× longer than vein 2-SR and curved downward (Fig. 2); propodeum largely shiny and smooth but with a long medio-longitudinal carina and two diverging oblique carinae and area behind carinae with distinct areola (Fig. 9); setose part of ovipositor sheath about as long as first tergite (Fig. 11).

Description. Holotype, female; length of body 1.6 mm, of fore wing 1.9 mm.

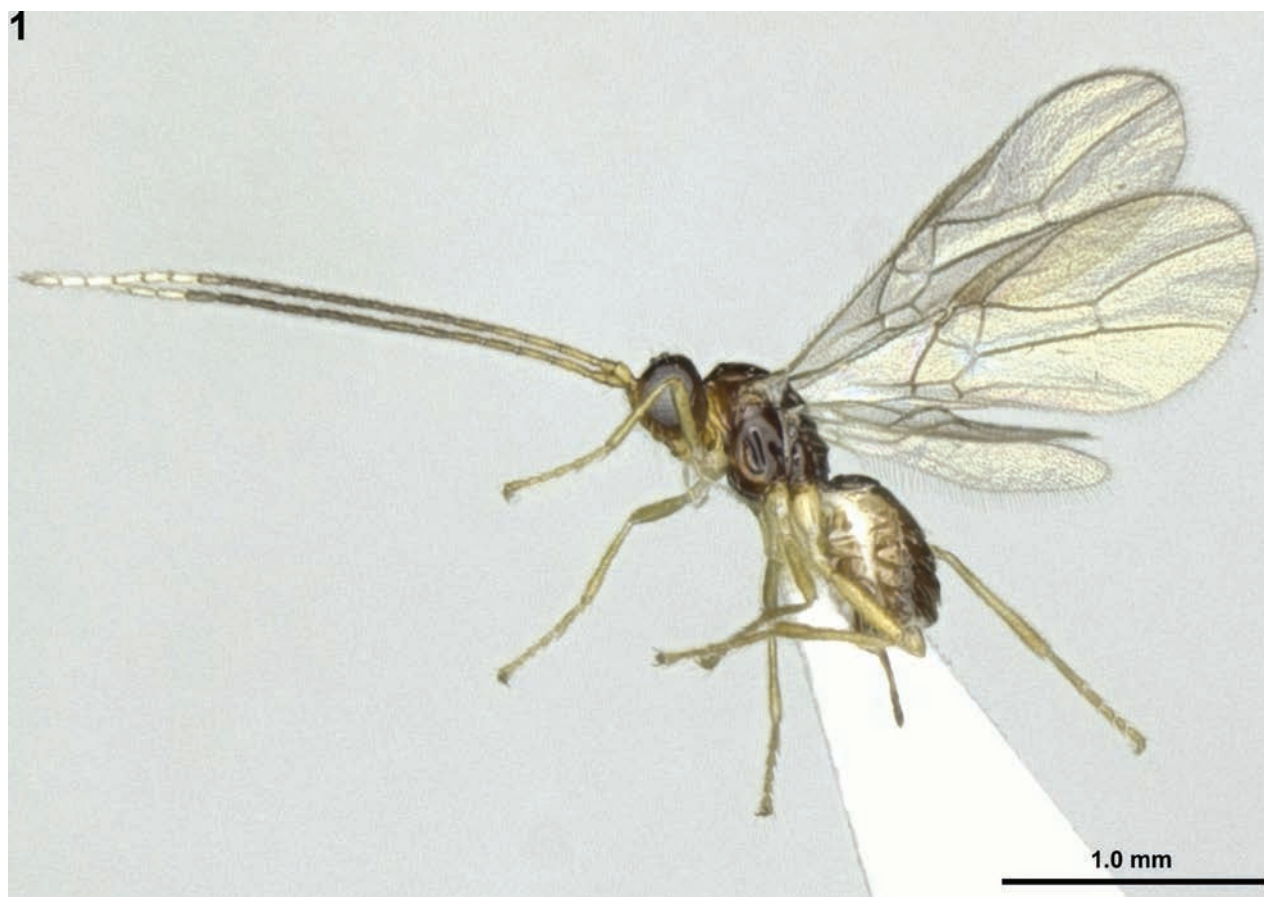
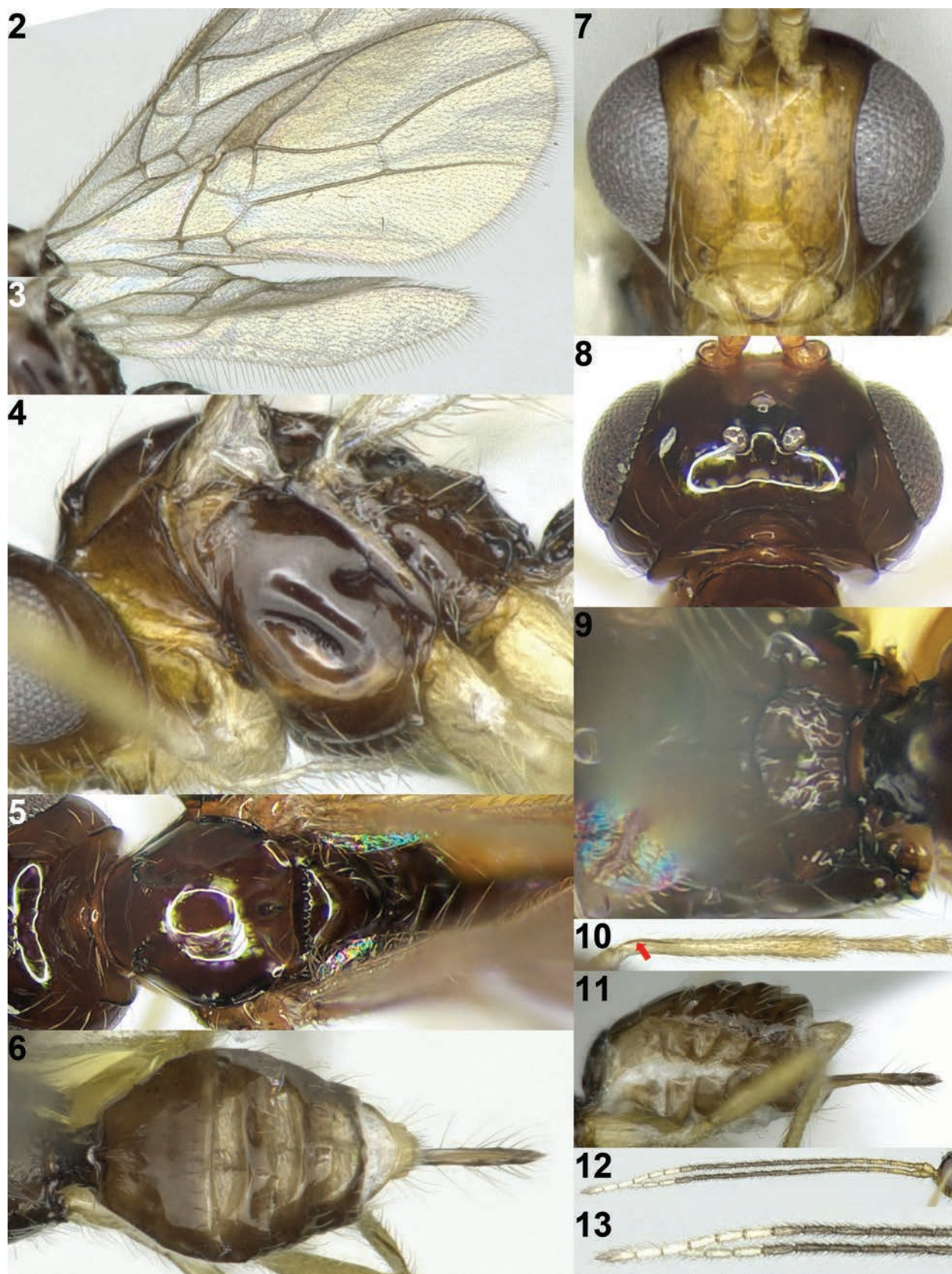


Figure 1. *Areotetes convergens* Han & van Achterberg, sp. nov., holotype, ♀, Japan, habitus, lateral.

Head. Antenna with 20 segments, 1.4× longer than body (Fig. 12); third segment 4.3× longer than its width and 1.3× longer than fourth segment, subapical segments 2.5× longer than its width; eye 2.9× longer than temple in dorsal view (Fig. 8); vertex, frons and occiput smooth and glabrous; face smooth and sparsely long setose (Fig. 7); clypeus 2.3× wider than its maximum height; clypeus shiny, smooth, remotely setose, and rather flat in lateral view, ventral margin of clypeus concave; hypoclypeal depression present; maxillary palp nearly 0.9× as long as height of head; malar sulcus absent; occipital carina interrupted dorsally (Fig. 8); mandible gradually widened basally, moderately setose and slightly twisted in lateral view without acute basal lamella (Figs 4, 7).

Mesosoma. Mesosoma 1.4× longer than its height (Fig. 4); pronope distinct, elliptical (Fig. 5); pronotum smooth and sparsely setose along anterior and lateral margin; pronotal side and propleuron smooth and glabrous (Fig. 4), but smooth transverse carina present ventro-posteriorly; mesopleuron largely smooth and glabrous, but precoxal sulcus crenulate medially, medium-sized and oblique; epicnemial area smooth; mesopleural sulcus smooth; mesosternum smooth and moderately setose; anterior groove of metapleuron smooth, remaining area shiny, smooth and densely setose dorso-anteriorly and ventrally; notauli absent on mesoscutal disc, but a pair of crenulate impressions present anteriorly (Fig. 5); medio-posterior depression of mesoscutum round and shallow; mesoscutum shiny, smooth and sparsely setose; scutellar sulcus narrow and densely crenulate; scutellum smooth and rather flat in lateral view;



Figures 2–13. *Areotetes convergens* Han & van Achterberg, sp. nov., holotype, ♀, Japan. 2 fore wing 3 hind wing 4 mesosoma lateral 5 mesosoma and head dorsal 6 metasoma dorsal 7 head anterior 8 head dorsal 9 propodeum dorsal 10 hind leg inner side 11 metasoma and ovipositor sheath lateral 12 antenna 13 apex of antenna. The arrow indicates carina on inner side of hind tibia.

propodeum smooth, but with a long medio-longitudinal carina and two diverging oblique two transverse carinae and area behind carinae with areola distinct (Fig. 9).

Wings. Fore wing (Fig. 2): Pterostigma narrow elongate triangular, and gradually narrowed apically; vein r very short, angled with vein 3-SR and emanating from basal; veins 1-M and 1-SR+M straight; vein 3-SR curved downward, vein 3-SR 2.7× longer than vein 2-SR and subparallel with vein 2-M apically; r:3-SR:SR1 = 5:71:109; vein SR1 curved upwards; vein m-cu distinctly postfurcal and distinctly converging to vein 1-M posteriorly; second submarginal cell elongated (Fig. 2); first subdiscal cell closed; vein CU1b present. Hind wing (Fig. 3): narrow; vein 1r-m 0.4× longer than vein 1-M; veins m-cu and 2-M absent.

Legs. Length of hind femur 4.7× its maximum width (Fig. 1); basal carina of inner side of hind tibia long and slightly sinuate (Figs 6, 10).

Metasoma. First metasomal tergite 1.6× longer than its apical width, its surface rugose and slightly convex medio-basally in lateral view (Figs 1, 11); dorsope absent; second metasomal suture obsolescent (Fig. 6); second tergite shiny, smooth but faintly striae-rugose anteriorly and with shallow pair of depressions medio-basally; following tergites shiny, smooth and posteriorly setose; setose part of ovipositor sheath 1.6× longer than first tergite and with very long setae (Fig. 11).

Colour. Body generally dark brown (Fig. 1); 6 apical segments of antenna, white; face, clypeus, mandible and pronotal side antero-ventrally, yellowish-brown; scape and basal fifth of antenna and legs, light yellowish; palpi, pale yellowish; pterostigma and vein of wings, light greyish-brown; wings, hyaline.

Distribution. Japan (Ryuku Islands).

Biology. Unknown.

Etymology. From “con-” (Latin for together) and “vergo” (Latin for incline or turn toward) because of the posteriorly converging veins 1-M and m-cu of the fore wing.

Remarks. The new species belongs to the genus *Areotetes* van Achterberg & Li because it has a distinct carina on the inner side of the hind tibia, clypeus slightly concave ventrally with a thick ventral margin, and the propodeum with a long medio-longitudinal carina and a distinct areola. It does not run in the keys by Li et al. (2013) and Tobias (1998). In Fischer (1972, 1987) it runs to the subgenus *Utetes* Foerster and to *O. kamikochiensis* Fischer, 1963 from Japan and *O. sanguanus* Fischer, 1966 from Nepal, respectively.

Opius kamikochiensis Fischer differs from the new species by having the first metasomal tergite about as long as wide apically (1.6× in *A. convergens*), vein 1-SR of fore wing comparatively long (short), antenna with 25 segments (20 segments), vein r of fore wing longer and emanating from near basal third of pterostigma (very short and from basal 0.2 of pterostigma) and pterostigma wider (narrower). *Opius sanguanus* Fischer differs from the new species as follows: vein m-cu of fore wing comparatively far postfurcal (narrowly postfurcal in *A. convergens*), pterostigma wider (narrower), vein r emanating from basal 0.3 of pterostigma (from 0.2 of pterostigma) and third antennal segment brown (yellow). Actually, it is much more similar to *O. nepalensis* Fischer, 1966 from Nepal to which it does not run in Fischer (1987) because of the weird choice of not considering variation between mesosoma 1.4 or 1.5× longer than height in lateral view; the few differences between both species are summarized in the key.

Genus *Indiopus* Fischer, 1966

Indiopus Fischer, 1966: 154–155. Type species (by original designation): *Indiopus humillimus* Fischer, 1966.

Diagnosis. Marginal cell of fore wing open apically (Fig. 15); first subdiscal cell of fore wing open (Fig. 15); veins m-cu and r-m of fore wing absent (Fig. 15); vein cu-a of hind wing absent (Fig. 15); clypeus transverse (Fig. 18); occipital carina entirely absent (Figs 20, 21); first to third metasomal tergites more or less coriaceous or rugulose.

Distribution. Palaearctic including West Palaearctic, East Palaearctic [Japan (new record)] and Oriental.

Biology. Unknown.

Key to species of the genus *Indiopus* Fischer

- 1 Frons with elongate depression between stemmaticum and eyes; vein 2-1A of fore wing not pigmented; vein cu-a of fore wing postfurcal by more than its width; vein 1-R1 about as long as distance between apex of vein 1-R1 and apex of fore wing; India..... ***I. fischeri* Samiuddin & Ahmad, 2009**
- Frons without elongate depression between stemmaticum and eyes, at most with punctures; vein 2-1A of fore wing more or less pigmented; vein cu-a of fore wing postfurcal by its width or interstitial; vein 1-R1 of fore wing 1.2–8.0× longer than distance between apex of vein 1-R1 and apex of fore wing, but about equal in *I. humillimus* and *I. yilmazae*..... **2**
- 2 Vein 1-R1 of fore wing about 1.8× longer than pterostigma and vein 1-R1 of fore wing about 8× longer than distance between its apex and apex of fore wing; posterior margin of pterostigma slightly curved; vein 1-SR absent; Turkmenistan..... ***I. turkmenicus* Tobias, 1986**
- Vein 1-R1 of fore wing 1.0–1.3× longer than pterostigma and vein 1-R1 of fore wing 1.0–4.0× longer than distance between its apex and apex of fore wing; posterior margin of pterostigma straight; vein 1-SR present, but sometimes narrowly so..... **3**
- 3 First metasomal tergite about 1.2× longer than wide apically; between stemmaticum and eyes with a setiferous puncture; antenna of ♀ with about 17 segments; [body brown, but head and mesosoma (except propodeum) and apex of metasoma dark brown]; Vietnam..... ***I. saigonensis* Fischer, 1966**
- First tergite about as long as wide apically; between stemmaticum and eyes without a setiferous puncture; antenna of ♀ with 18–19 segments. **4**
- 4 Vein 1-R1 of fore wing about as long as distance between its apex and apex of fore wing..... **5**
- Vein 1-R1 of fore wing 1.5–3.0× longer than distance between its apex and apex of fore wing..... **6**
- 5 Mesoscutum and head dorsally black; metasoma reddish-brown, but its apex black; antennal segments of ♀ 18; Turkey..... ***I. yilmazae* Fischer & Beyarslan, 2011**
- Mesoscutum and head dorsally yellow; metasoma yellow but its apex dark brown; antennal segments of ♀ 19; India..... ***I. humillimus* Fischer, 1966**

- 6 Width of scutellar sulcus 0.3 times length of scutellum (Fig. 17); fore femur wider than middle femur; [precoxal sulcus distinctly crenulate; face medially paler than dorso-laterally; vein 1-R1 of fore wing about 1.5× longer than distance between its apex and apex of fore wing]; China (Hunan) ***I. chena* van Achterberg & Li, 2013**
- Width of scutellar sulcus 0.1–0.2 times length of scutellum; fore femur about as wide as middle femur **7**
- 7 Vein 1-R1 of fore wing about 1.5× longer than distance between its apex and apex of fore wing; vein 3-SR+SR1 less curved and pointing behind apex of vein 1-R1; notauli indistinctly impressed anteriorly; precoxal sulcus smooth or finely crenulate; [antennal segments of ♀ 18; of ♂ 20]; Mediterranean, Cape Verde Islands..... ***I. cretensis* Fischer, 1983**
- Vein 1-R1 of fore wing about 3× longer than distance between its apex and apex of fore wing; vein 3-SR+SR1 more curved and pointing towards apex of vein 1-R1; notauli distinctly impressed anteriorly; precoxal sulcus distinctly crenulate; [antennal segments of ♀ 18–19]; China (Fujian).....
..... ***I. alutacius* Weng & Chen, 2001**

***Indiopus chena* van Achterberg & Li, 2013**

Figs 14–25

Indiopus chena van Achterberg & Li, 2013: 66–69.

Material. 1 ♂ (OMNH), “Japan (Honshu): Oyamada-chou, Kawachinagano, Osaka, 34.4509°N, 135.5504°E, 23.ix.2017, SW[=collected by sweeping], Shumei Fujie leg., OMNH”; 1 ♀ (OMNH), “Japan (Honshu): Yamazakichou Koudani, Shisou, Hyogo, 35.0238°N, 134.5619°E, 16.ix.2019, SW[=collected by sweeping], Shumei Fujie, OMNH”; 1 ♀ (OMNH), “Japan (Honshu): Oyamada-chou, Kawachinagano, Osaka, 34.4509°N, 135.5504°E, 5.ix.2016, SW[=collected by sweeping], Takao Aoki leg., OMNH”.

Diagnosis. Antenna with 19 segments (Fig. 24); between stemmaticum and eyes sparsely setose without depression; occipital carina entirely absent (Figs 19–21); clypeus 4.3× longer than its maximum height (Fig. 19); mandible gradually widened basally; vein 1-R1 of fore wing 1.7× longer than distance between apex of vein 1-R1 and apex of fore wing; vein cu-a of fore wing interstitial (Fig. 15); maxillary palpi 0.5× as long as height of head; scutellar sulcus robust and distinctly crenulate medially (Fig. 17); fore femur somewhat wider than middle femur; strong dorsal carinae separated up to posterior of first metasomal tergite; first metasomal tergite entirely granulate-rugose (Figs 18, 23).

Re-description. Female; length of body 1.6 mm, of fore wing 1.3–1.6 mm, male; length of body 1.3 mm, of fore wing 1.5 mm.

Head. Antenna with 19 segments, 1.1× longer than body (Fig. 24); third segment 3.1× longer than its width and 1.2× longer than fourth segment (Figs 24, 25); middle flagellar segment 2.9× longer than its width; depression of frons slightly present near antennal sockets; eye as long as temple (Fig. 20); vertex, frons, stemmaticum and occiput smooth and glabrous; face shiny, smooth and moderately setose (Fig. 19); median keel of frons slightly present; clypeus 4.3× wider than its maximum height; clypeus narrow, trap-

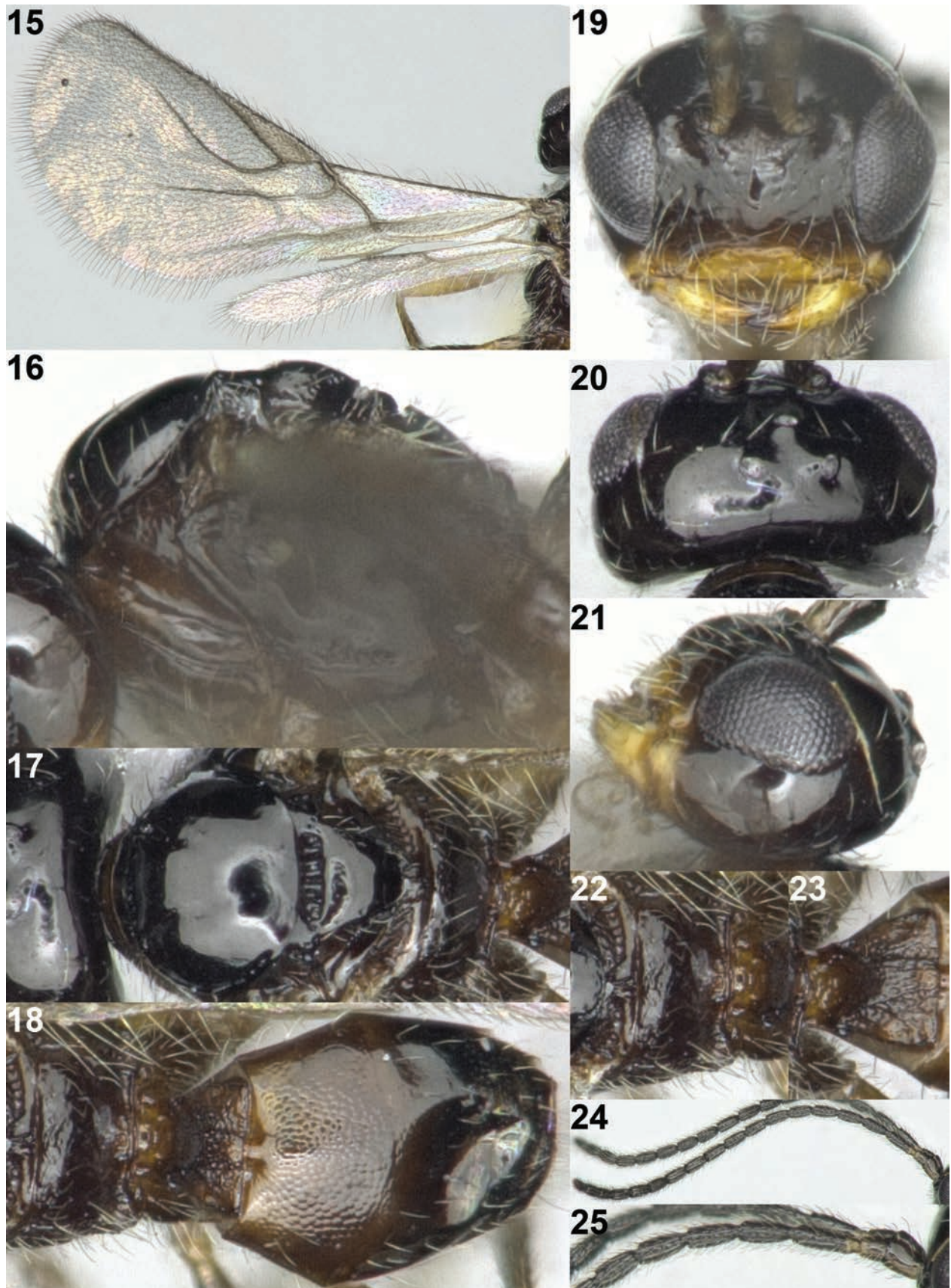


Figure 14. *Indiopius chenaе* van Achterberg & Li, ♂, Japan, habitus, lateral.

ezoid-shaped, shiny, smooth, moderately setose and flat in lateral view, and its ventral margin straight; hypoclypeal depression slightly present; maxillary palpi 0.5× as long as height of head; malar sulcus present and short; occipital carina absent (Figs 20, 21); mandible slightly twisted, moderately setose and slightly widened basally.

Mesosoma. Mesosoma 1.3× longer than its height (Fig. 16); pronope absent; pronotal side smooth, glabrous, and anterior and posterior groove of pronotal side smooth (Fig. 16); propleuron shiny, smooth and rather moderately setose; mesopleuron largely smooth, but precoxal sulcus deeply narrowly crenulate; epicnemial area narrowly crenulate ventrally, remaining area smooth; mesopleural sulcus smooth; mesosternum rather sparsely setose; anterior groove of metapleuron smooth; metapleuron largely shiny, smooth and densely setose posteriorly; notauli absent on disc of mesoscutum, but deeply crenulate anteriorly (Fig. 17); medio-posterior depression of mesoscutum absent; mesoscutum smooth and glabrous; scutellar sulcus straight, relatively short, medium-sized and densely crenulate medially, but reduced laterally; scutellum smooth, glabrous and not protruding above level of mesoscutum in lateral view (Figs 16, 17); propodeum smooth and glabrous without any carinae (Figs 18, 22).

Wings. Fore wing (Fig. 15): Pterostigma triangular; vein 1-M slightly curved; vein 1-SR+M curved downwards; vein 3-SR+SR1 strongly curved and pointing towards apex of vein 1-R1; vein 1-R1 of fore wing about 1.7× longer than distance between its apex and apex of fore wing; vein 3-SR converging with vein



Figures 15–25. *Indiopius chenaе* van Achterberg & Li, ♂, Japan. 15 wings 16 mesosoma lateral 17 mesosoma dorsal 18 propodeum and metasoma dorsal 19 head anterior 20 head dorsal 21 head lateral 22 propodeum dorsal 23 first metasomal tergite dorsal 24 antenna 25 base of antenna.

2-M; vein 1-SR short; vein cu-a interstitial; first subdiscal cell open. Hind wing: entirely narrow and subparallel-sided; vein cu-a absent; vein m-cu absent; vein 2-M pigmented basally and reduced apically.

Legs. Length of hind femur 3.9× its maximum width; fore femur slightly wider than middle femur, nearly 1.1× wider than maximum width of middle femur.

Metasoma. First metasomal tergite as long as its apical width, its surface reticulate-rugose with strong dorsal carinae, and slightly convex medially in lateral view (Fig. 14); dorsope absent; second metasomal suture obsolescent dorsally (Fig. 18); second tergite granulate and glabrous, with pair of triangular depressions basally; third tergite granulate antero-medially and remaining area smooth; following tergites shiny, smooth, and moderately setose posteriorly.

Colour. Body generally dark brown to black (Fig. 14); clypeus and mandible, light brown; pronotal side ventrally and first to third anteriorly metasomal tergites, brown; antenna and legs, dark brown (except legs darker brown dorsally); pterostigma and veins of wings, greyish-brown; wings, hyaline.

Distribution. Japan (Honshu; new record), China (Fujian).

Biology. Unknown.

Genus *Neopius* Gahan, 1917

Neopius Gahan, 1917: 203. Type species (by original designation): *Neopius carinaticeps* Gahan, 1917 (= *Opius rudis* Wesmael, 1835). Synonymized by Quicke et al. (1997) with *Opius* Wesmael, 1835 and restored as valid genus by Li et al. (2013).

Diagnosis. Occipital carina completely crenulate in dorsal and lateral view (Figs 32, 33); frons distinctly granulate (Fig. 32); mandible normal and symmetrically widened basally (Fig. 33); hypoclypeal depression distinct (Fig. 31); precoxal sulcus sculptured (Fig. 28); pronotum sculptured; notauli sculptured at least half of mesoscutum (Fig. 29); medio-posterior depression of mesoscutum present; mesoscutum and mesopleuron largely granulate; ovipositor sheath short.

Distribution. Holarctic, including Japan (new record) and South Korea.

Biology. Endoparasitoids of Agromyzidae larvae (including species *Agromyza megalopsis* Hering, 1933 and *Agromyza nigripes* Meigen, 1830).

Key to species of the genus *Neopius* Gahan

Notes: Modified after Sheng et al. (2019).

- 1 Face yellowish-brown (Fig. 31); notauli gradually reduced posteriorly (Fig. 29); vein m-cu of fore wing shorter than vein 2-CU1 (Fig. 27); occiput comparatively straight in dorsal view (Fig. 32) ***N. citrinus* Sheng & Chen, 2019**
- Face largely dark brown; notauli complete, reaching medio-posterior depression of mesoscutum; vein m-cu of fore wing about 1.5× longer than vein 2-CU1; occiput concave in dorsal view..... ***N. rudis* (Wesmael, 1835)**

***Neopius citrinus* Sheng & Chen, 2019**

Figs 26–36

Neopius citrinus Sheng & Chen, 2019: 592–595.

Material. 1 ♀ (OMNH), “Japan (Honshu): Nakaikemi Wetlands, Kashimagari, Tsuruga, Fukui, 35.6594°N, 136.0884°E, 24.v.–17.vi.2016, MT [=Malaise trap], Asato Noishiki leg., OMNH”.

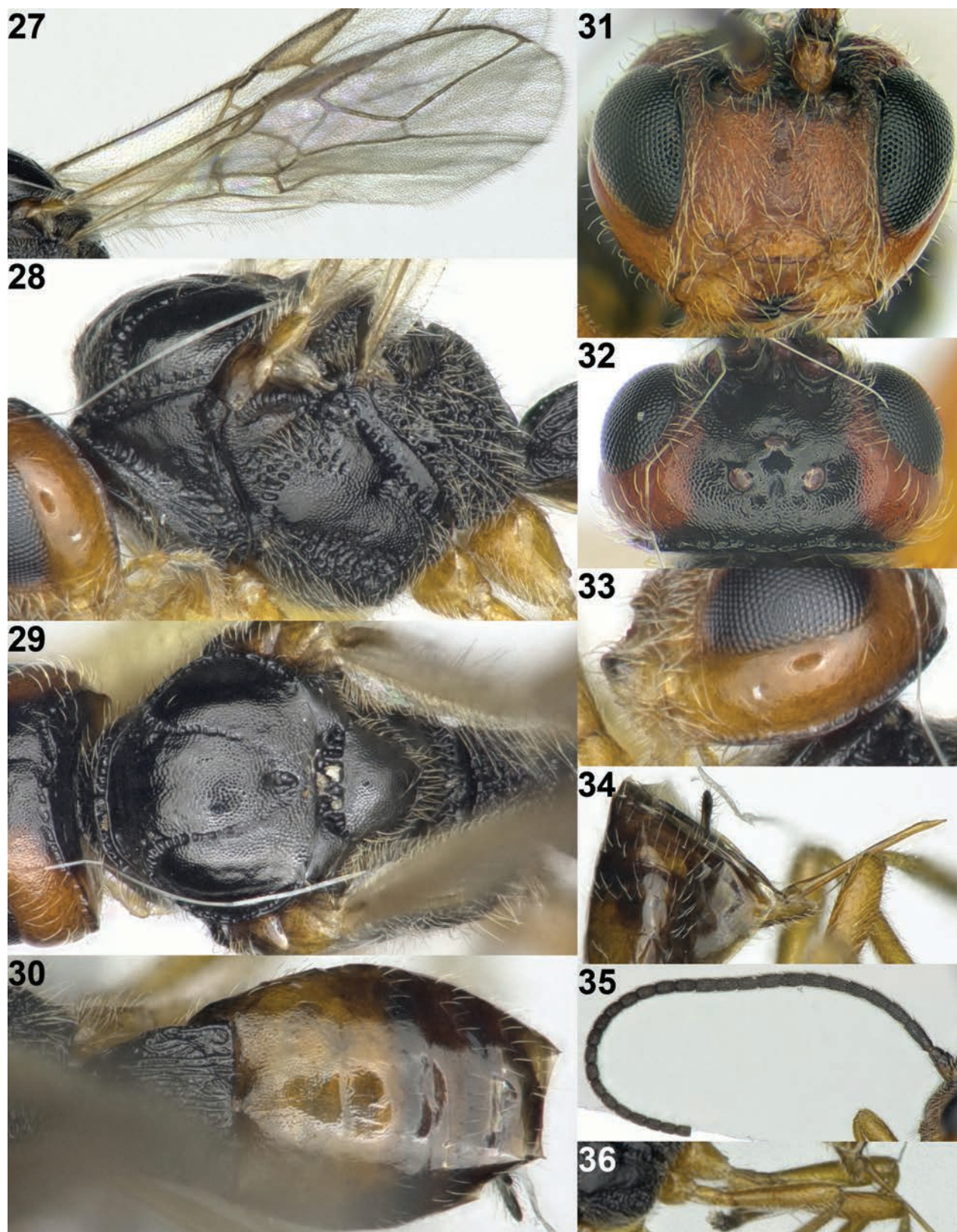
Diagnosis. Face yellow (Fig. 31); notauli nearly complete, gradually reduced posteriorly; occiput comparatively straight in dorsal view (Fig. 32); head largely granulate; scutellar sulcus comparatively robust (Fig. 29); propodeum reticulate-rugose with a medio-longitudinal carina; second and third tergites granulate.

Re-description. Female; length of body 2.8 mm, of fore wing 3.0 mm.

Head. Antenna with 29 segments (Fig. 25; broken and lost); third segment 2.3× longer than its width, 1.2× longer than fourth segment; eye 1.5× longer than temple in dorsal view (Fig. 23); vertex granulate and sparsely setose; frons and occiput shiny and granulate; face densely punctate and setose (Fig. 21); clypeus 2.5× wider than its maximum height; clypeus densely setose, its ventral margin slightly protruding downward; hypoclypeal depression distinct; maxillary palpi nearly 0.7×



Figure 26. *Neopius citrinus* Sheng & Chen, ♀, Japan, habitus, lateral.



Figures 27–36. *Neopius citrinus* Sheng & Chen, ♀, Japan. 27 fore wing 28 mesosoma lateral 29 mesosoma dorsal 30 metasoma dorsal 31 head anterior 32 head dorsal 33 head lateral 34 ovipositor lateral 35 antenna 36 hind femur.

as long as height of head; malar sulcus absent; occipital carina completely present and crenulate, (Figs 29, 32); mandible gradually widened basally, moderately setose and hardly twisted in lateral view without acute basal lamella (Fig. 33).

Mesosoma. Mesosoma 1.3× longer than its height (Fig. 29); pronope absent but transverse crenulated groove and sparsely setose along lateral margin (Fig. 30); pronotal side granulate with ventral crenulated groove; propleuron granulate (Fig. 29); mesopleuron largely coriaceous, but precoxal sulcus crenulate, wide, oblique and reaching anterior area (converging epicnemial area and dorsal crenulate carina); epicnemial area crenulate; mesopleural sulcus crenulate; mesosternum densely setose; anterior groove of metapleuron crenulate, remaining area reticulate-rugose, shiny and densely setose; notauli distinctly crenulate antero-medially, but gradually obsolescent posteriorly (Fig. 29); medio-posterior depression of mesoscutum large, elliptical and deep; mesoscutum coriaceous with few setae along the notaulic course; scutellar sulcus medium-sized, moderately crenulate and gradually narrowed laterally; scutellum granulate and rather flat in lateral view; propodeum entirely reticulate-rugose and densely setose with a short medio-longitudinal carina.

Wings. Fore wing (Fig. 27): Pterostigma triangular and gradually narrowed apically; vein r sublinear with vein 3-SR; vein 1-M nearly straight; vein 1-SR+M straight; vein 2-SR slightly sinuate and oblique; vein 3-SR 1.5× longer than vein 2-SR; r:3-SR:SR1 = 5:18:37; vein SR1 straight; vein m-cu distinctly postfurcal; first subdiscal cell open; vein CU1b short and incomplete. Hind wing (Fig. 28): vein m-cu absent; vein 2-M absent.

Legs. Length of hind femur 4.4× its maximum width (Fig. 36).

Metasoma. First metasomal tergite 0.9× as long as its apical width, its surface striate-rugose and slightly convex medio-basally in lateral view (Figs 26, 30); dorsope absent; second metasomal suture obsolescent (Fig. 30); second tergite shiny and granulate, with shallow pair of depressions medio-basally; third tergite granulate medially and following tergites shiny and smooth, with band of setae posteriorly; setose part of ovipositor sheath 0.5× longer than first tergite (Fig. 34).

Colour. Body generally black (Fig. 26); head yellowish-brown but frons and vertex black medially (Fig. 32); legs and ovipositor, light brown; second and half of basal third tergites, brown; pterostigma and vein of wings, light brown; wings, subhyaline.

Distribution. Japan (Honshu; new record), China (Heilongjiang, Jilin and Liaoning).

Biology. Unknown.

Genus *Sternaulopius* Fischer, 1965

Sternaulopius Fischer, 1965: 311; Wharton, 2006: 317. Type species (monobasic and by original designation). *Sternaulopius bisternaulicus* Fischer, 1965.

Diagnosis. Below precoxal sulcus with a distinct and sculptured second sulcus (= sternaulus; Figs 39, 50); malar space largely smooth, in East Asian species deeply impressed (Figs 43, 54, 56); mandible gradually widened basally and without basal lamella; occipital carina absent medio-dorsally; medio-posterior depression of mesoscutum present as small point-like depression (Afrotropical

spp.) or part of notauli and medium-sized (Asian spp.; Fig. 40); propodeum coarsely reticulate-rugose (Figs 45, 51); dorsope of first tergite deep (van Achterberg 1993, pl. 36) or shallow (Asian sp.; Fig. 41); setose part of ovipositor sheath 0.3–1.0× as long as first tergite.

Distribution. Palaearctic [Japan (new record); China (Jilin)], Oriental [China (Sichuan)] and Afrotropical (Burundi, Cameroon, Democratic Republic of Congo, Kenya, Madagascar) regions. The European records concern *Biophthora* Förster, 1863 and *Sternaulopius* s. str. has not yet been found in Europe.

Biology. Parasitoids of fruit-infesting dipterous larvae of Tephritidae (*Ceratitis* MacLeay, 1829 and *Trirhithrum* Bezzi, 1918).

Key to species of the genus *Sternaulopius* Fischer

- 1 Hypoclypeal depression absent; mesoscutum densely setose; precoxal sulcus and sternaulus gradually converging posteriorly; Afrotropical (Madagascar) ***S. duplicatus* Wharton, 2006**
- Hypoclypeal depression present (Fig. 43); mesoscutum densely or sparsely setose; precoxal sulcus subparallel to precoxal sulcus posteriorly (Fig. 39; van Achterberg 1993, pl. 36)..... **2**
- 2 Posterior half of notauli smooth and shallowly impressed or absent; medio-posterior depression of mesoscutum small, point-like, far removed from notauli (van Achterberg 1993, pl. 36); occipital carina entirely smooth and narrow laterally; dorsope of first tergite deep; malar space without wide depression; distal half of pterostigma slender (van Achterberg 1993, pl. 36); Afrotropical (continental Africa) ***S. bisternaulicus* Fischer, 1965**
- Posterior half of notauli crenulate and deep (Fig. 40); medio-posterior depression of mesoscutum medium-sized and more or less part of notauli (Fig. 40); occipital carina partly crenulate and wide laterally (Fig. 39); dorsope of first tergite shallow (Fig. 41); malar space with wide depression (Fig. 43); distal half of pterostigma robust (Fig. 38); East Palaearctic **3**
- 3 Vein 3-SR of fore wing 1.3–1.4× vein 2-SR; area below pterostigma subhyaline; vein 1-M of fore wing curved; vein m-cu of fore wing postfurcal; length of eye in dorsal view 2.2–2.6× temple..... ***S. macrophthalmos* Sheng & Chen, 2019**
- Vein 3-SR of fore wing as long as vein 2-SR (Fig. 38) area below pterostigma with brownish patch (Fig. 38); vein 1-M of fore wing straight or nearly so (Fig. 38); vein m-cu of fore wing antefurcal; length of eye in dorsal view 1.9× temple (Fig. 44) ***S. maculiferus* Han & van Achterberg, sp. nov.**

***Sternaulopius maculiferus* Han & van Achterberg, sp. nov.**

<https://zoobank.org/D7A31E30-4F94-4B00-86CF-C18117F0D72D>

Figs 37–47

Type material. *Holotype*, ♀ (OMNH), “Japan (Honshu): Nochino, Ono, Fukui, 35.9492°N, 136.6868°E, 5.viii.2011, SW[=collected by sweeping], Shunpei Fujie leg., OMNH”.

Diagnosis. Vein 3-SR of fore wing as long as vein 2-SR (Fig. 38); below pterostigma with brownish patch; first subdiscal cell subparallel-sided (Fig. 38);



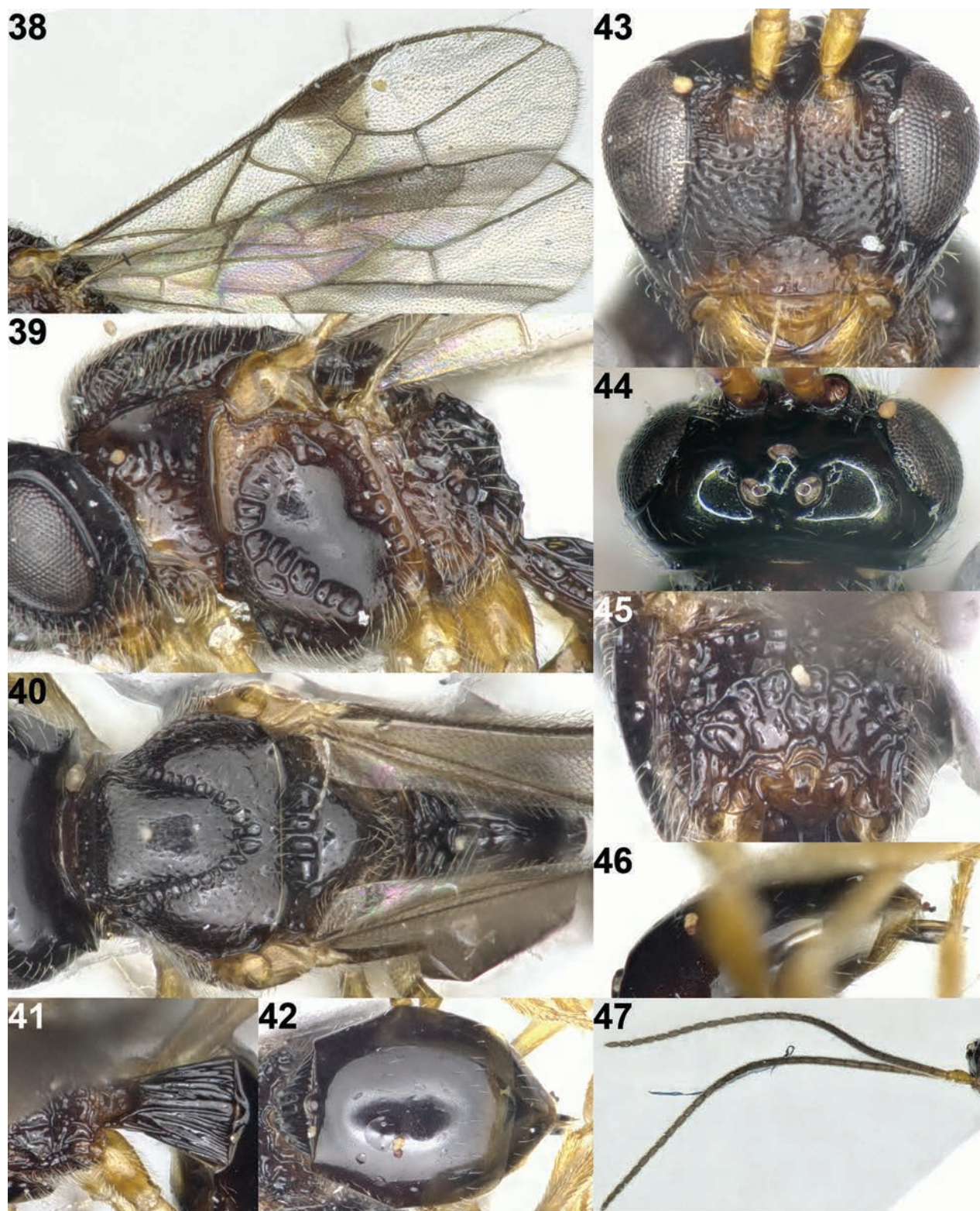
Figure 37. *Sternaulopius maculiferus* Han & van Achterberg, sp. nov., holotype, ♀, Japan, habitus, lateral.

hypoclypeal depression distinct (Fig. 43); eye 1.9× longer than temple in dorsal view (Fig. 44); mesoscutum densely setose (Fig. 40); notauli complete and crenulate; medio-posterior depression of mesoscutum medium-sized and part of notauli (Fig. 40); precoxal sulcus oblique and wide crenulate (Fig. 39); sternaulus crenulate and subparallel-sided with precoxal sulcus; propodeum with short medio-longitudinal carina and transverse carinae, and area behind carinae coarsely reticulate (Fig. 45).

Description. Holotype, female; length of body 3 mm, of fore wing 2.8 mm.

Head. Antenna with 31 segments and as long as body (Fig. 47); third segment 2× longer than wide, 1.3× longer than fourth segment; eye 1.9× longer than temple in dorsal view (Fig. 44); vertex, frons and occiput smooth and glabrous; face densely coarsely punctate and densely setose (Fig. 43); median keel present on face, smooth (Fig. 43); clypeus 2× wider than its maximum height; clypeus faintly punctate, sparsely setose, and protruding in lateral view; hypoclypeal depression present; length of maxillary palpi nearly 0.9× as long as height of head; malar sulcus present; occipital carina interrupted dorsally (Fig. 44); mandible gradually widened basally and densely setose without acute basal lamella.

Mesosoma. Mesosoma 1.4× longer than its height (Fig. 39); pronope absent (Fig. 40); pronotal side with crenulate carina anteriorly and posteriorly (Fig. 39); propleuron rugose and densely setose without oblique carina; mesopleuron largely smooth, but precoxal sulcus crenulate and wide, oblique, reaching anterior part (wide and crenulate area in epicnemial area); sternaulus crenulate and subparallel with precoxal sulcus (Fig. 39); mesopleural sulcus widely crenulate;



Figures 38–47. *Sternaulopius maculiferus* Han & van Achterberg, sp. nov., holotype, ♀, Japan. 38 wings 39 mesosoma lateral 40 mesosoma dorsal 41 first metasomal tergite dorsal 42 metasoma dorsal 43 head frontal 44 head dorsal 45 propodeum dorsal 46 ovipositor lateral 47 antenna.

mesosternum densely setose; anterior groove of metapleuron crenulate and rather densely setose ventrally, remaining area rugose; notauli complete, and crenulate on disc of mesoscutum and reaching mesoscutum posteriorly (Fig.

40); medio-posterior depression of mesoscutum present and part of notauli; mesoscutum rather densely, weakly punctate and densely setose; scutellar sulcus wide, crenulate and curved; scutellum smooth setose and slightly convex in lateral view, but not protruding above level of mesoscutum; propodeum glabrous and reticulate-rugose with short medio-longitudinal carina and diverging oblique two transverse carinae, and area behind carinae coarsely reticulate (Fig. 45).

Wings. Fore wing (Fig. 38): Pterostigma wide, triangular, and slightly convex anteriorly; vein r gradually merging in vein 3-SR; vein 1-M straight; vein 1-SR+M sinuate; vein 2-SR almost straight, as long as vein 3-SR (1.1× longer than vein 3-SR); r:3-SR:SR1 = 5:11:30; vein SR1 straight; vein m-cu distinctly antefurcal and converging to vein 1-M posteriorly; second submarginal cell short (Fig. 38); first subdiscal cell closed and subparallel-sided; vein CU1b present; vein CU1a almost completely pigmented. Hind wing: vein 1r-m 0.8× as long as vein 1-M; vein m-cu pigmented and curved basally; vein 2-M pigmented.

Legs. Length of hind femur 3.1× its maximum width; fore and hind femora robust (Fig. 37).

Metasoma. First metasomal tergite as long as its apical width, its surface densely striate-rugose and in lateral view convex medially (Fig. 41); shallow dorsope present (Figs 39, 41); second metasomal suture absent (Fig. 42); second tergite shiny and smooth, but with pair of shallow depressions medio-basally; following tergites shiny and smooth, with row of setae posteriorly; setose part of ovipositor sheath 0.3× as long as first tergite (Fig. 46).

Colour. Body generally black (Fig. 37); ventral margin of clypeus, dorsal part of epicnemial area, ventral part of pronotal side and anterior part of metapleuron, brown; scape and pedicel of antenna, mandible (except tips of mandible), tegulae and legs, brownish-yellow; palpi, pale yellowish; pterostigma, veins and spot below pterostigma, more or less dark brown; wings, subhyaline.

Distribution. Japan (Honshu).

Biology. Unknown.

Etymology. From “macula” (Lain for patch) and “ferus” (Latin for carrying) because of the brownish patch below the pterostigma.

Remarks. This new species runs to the genus *Sternaulopius* Fischer because of the distinct sternaulus below the precoxal sulcus, the shallow dorsope on the first metasomal tergite, the coarsely rugose propodeum with distinct carinae, and the normal mandible (i.e., without basal lamella or tooth). However, it does not run in the key to *Opius* s.l. by Tobias (1998) by having the medio-posterior depression of mesoscutum connected to the notauli, the distinct hypoclypeal depression, the broadly sculptured precoxal sulcus and the area behind the carinae on the propodeum reticulate and with a short medio-longitudinal carina anteriorly. In the key by Sheng et al. (2019) to *Sternaulopius*, it does not run well either by having the distinct hypoclypeal depression, length of eye 1.9× temple in dorsal view, the densely setose mesoscutum, the distinctly sinuate vein 1-SR+M of the fore wing, and vein 2-SR of fore wing 1.1× longer than vein 3-SR.

***Sternaulopius macrophthalmos* Sheng & Chen, 2019**

Figs 48–57

Sternaulopius macrophthalmos Sheng & Chen, 2019: 595–598.

Material. 1 ♂ (OMNH), "Japan (Honshu): Oyamada-chou, Kawachinagano, Osaka, 34.4509°N, 135.5504°E, 4.xii.2018, SW [=collected by sweeping], Shumei Fujie leg., OMNH".

Diagnosis. Antenna with 24 segments (Fig. 53); hypclypeal depression distinct (Fig. 54); malar space depressed (Figs 50, 54, 56); dorsope slightly impressed (Figs 50, 51); precoxal sulcus and sternaulus distinctly crenulate, absent posteriorly and subparallel posteriorly (Fig. 50); medio-posterior depression rather large and round (Fig. 51); length of eye in dorsal view 2.2× temple (male; Fig. 55); mesoscutum shiny and densely setose (Fig. 51); vein 1-M of fore wing slightly curved (Fig. 49).

Re-description. Male; length of body 2.1 mm, of fore wing 2.2 mm.

Head. Antenna with 24 segments and 1.1× longer than body (Fig. 53); third segment 1.3× longer than fourth segment; eye 2.2× longer than temple (Fig. 55); vertex, frons and occiput smooth and glabrous; face faintly and moderately punctate and sparsely setose (Fig. 54); median keel present on face, smooth; clypeus 1.8× wider than its maximum height; clypeus faintly punctate, and its ventral margin pointed downward; hypclypeal depression present; maxillary palp 0.7× longer than height of head; malar space with a wide depression; occipital carina interrupted dorsally (Figs 55, 56); mandible gradually widened basally.

Mesosoma. Mesosoma 1.4× longer than its height (Fig. 50); pronope elliptical (Figs 51, 55); crenulate carina wide posteriorly on pronotal side (Fig. 50); propleuron smooth and moderately setose; mesopleuron largely smooth with setae dorsally and ventro-posteriorly, but precoxal sulcus crenulate and wide, oblique, reaching anterior part (wide and crenulate carina in epicnemial area); sternaulus crenulate and subparallel with precoxal sulcus (Fig. 50); epicnemial area crenulate; mesopleural sulcus wide and crenulate; mesosternum rather moderately setose; anterior groove of metapleuron crenulate and rather densely setose, remaining area rugose and setose; notauli narrowly crenulate on disc of mesoscutum and partly absent posteriorly, not reaching medio-posterior depression of mesoscutum (Fig. 51); medio-posterior depression of mesoscutum rather large, round and shallow; mesoscutum more or less densely, superficially punctate and densely setose; scutellar sulcus wide and crenulate; scutellum superficially punctate and slightly convex in lateral view, but not protruding above level of mesoscutum; propodeum rugose with indistinctly short medio-longitudinal carina, two diverging oblique transverse carinae behind medio-longitudinal carina, and remaining area reticulate-rugose (Fig. 51).

Wings. Fore wing (Fig. 49): Pterostigma wide, wide elliptical; vein 1-M of fore wing slightly curved basally; vein 1-SR+M almost straight; vein r angled with vein 3-SR; vein 3-SR distinctly longer than vein 2-SR (1.3× longer than vein 2-SR); vein 2-SR slightly sinuate; r:3-SR:SR1 = 1:5:8; vein SR1 slightly curved upward; vein m-cu distinctly postfurcal and sublinear with vein 2-M; second submarginal cell relatively long (Fig. 49); first subdiscal cell closed; vein CU1b present. Hind wing: vein 1r-m 0.7× as long as vein 1-M; vein m-cu short, oblique, pigmented and straight; vein 2-M pigmented.

Legs. Length of hind femur 4.2× its maximum width (Fig. 48).

Metasoma. First metasomal tergite 1.3× longer than its apical width, its surface rugose with striae, convex medially in lateral view (Fig. 51); dorsope present (Figs 50, 51); second tergite shiny and smooth, with pair of narrow depressions basally; third tergite convex posteriorly in lateral view; following tergites shiny and smooth, with band or row of setae posteriorly.

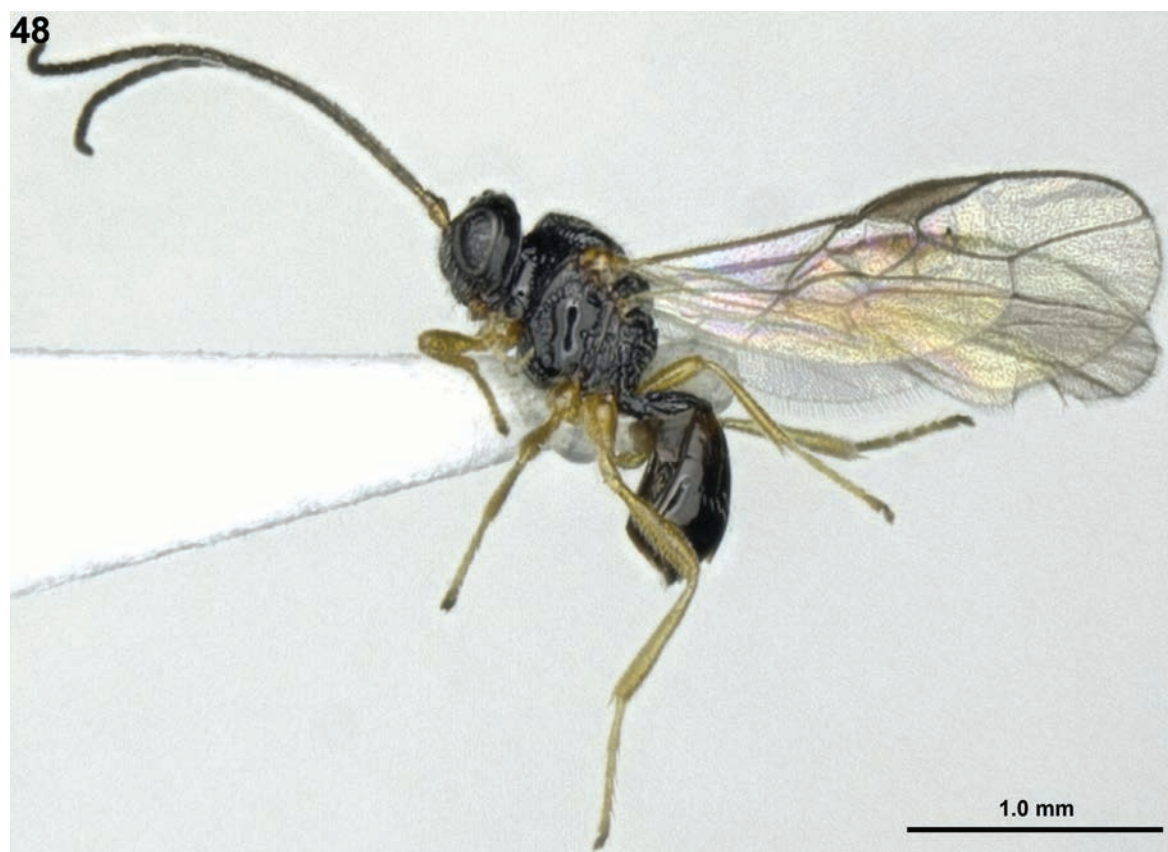


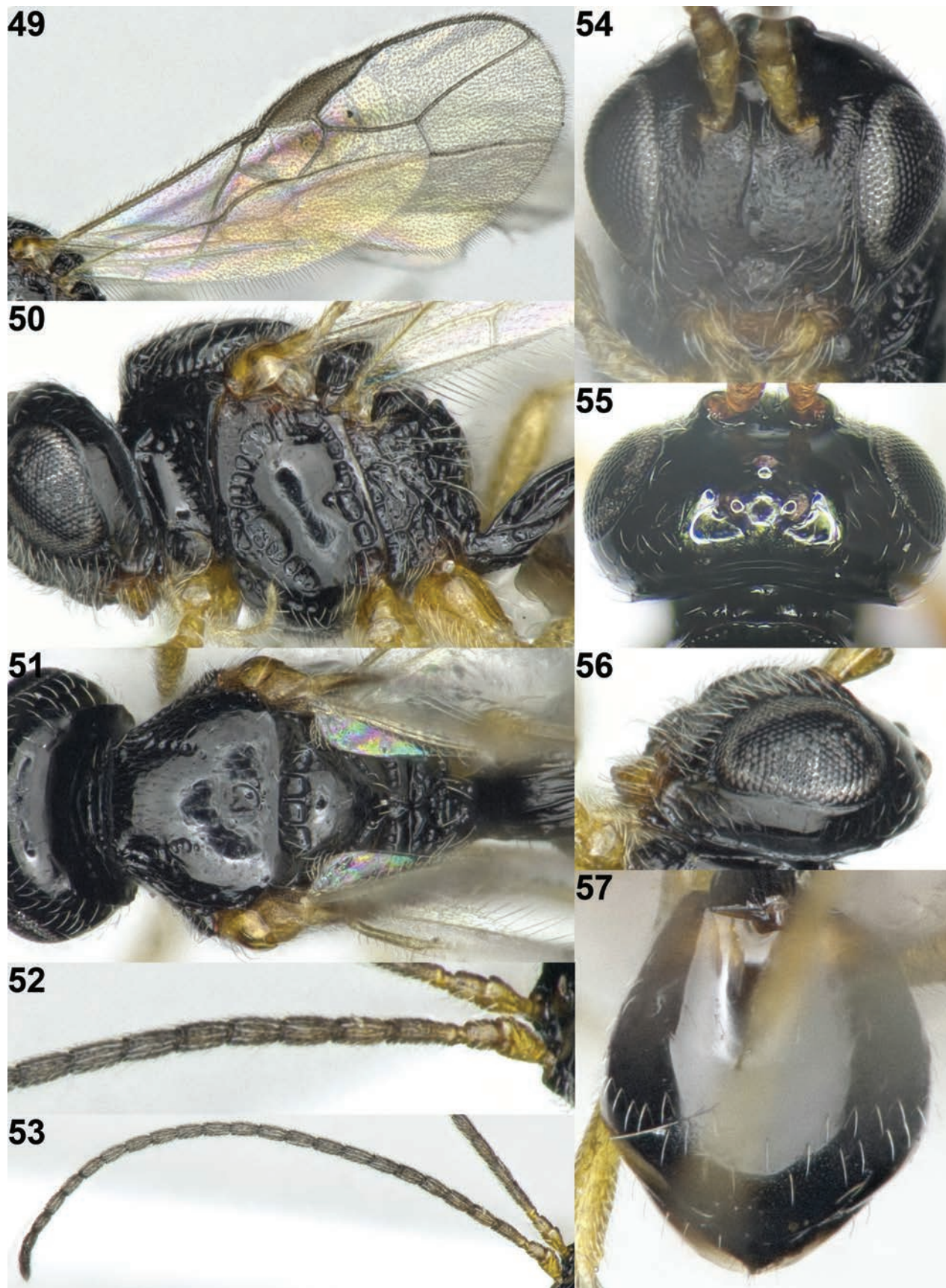
Figure 48. *Sternaulopius macrophthalmos* Sheng & Chen, ♂, Japan, habitus, lateral.

Colour. Body generally black (Fig. 48); socket of antenna, mandible, tegulae and legs, brownish-yellow; palpi, light yellow; basal part of second metasomal tergite, brown; antenna, pterostigma and veins of wings, dark brown; wings, hyaline.

Distribution. Japan (new record), China (Sichuan and Jilin).

Biology. Unknown.

Remarks. This species runs to *Sternaulopius* Fischer in the key by Sheng et al. (2019), specifically to *S. macrophthalmos*, but it differs by having the mesoscutum more setose and less shiny than in the holotype of *S. macrophthalmos*, the somewhat smaller medio-posterior depression of the mesoscutum and less distinct posterior part of notauli, length of eye 2.2× temple in dorsal view (2.8× longer than temple according to description but 2.6× in fig. 34 of the original description), the less curved vein 1-M of fore wing, hind femur 4.2× longer than its width (4.8× longer than its width according to description but 4.3× in fig. 36 of the original description) and second tergite and following tergites shiny and smooth with band or row of setae posteriorly (without distinct band or row of setae). The holotype of *S. macrophthalmos* was collected in alcohol in a Malaise trap and later treated by the AXA method (specimens were chemically treated with a mixture of xylene + alcohol 96% and amyl acetate, respectively (van Achterberg 2009; van Achterberg et al. 2010). The collecting method and the chemical treatment explain the cleanness of specimen, as well as the shinier appearance and loss of dorsal setae. The relative size of the eyes and legs may be related to the difference in sex (the holotype is female); the other differences are not enough to assign the specimen from Japan to a separate species.



Figures 49–57. *Sternaulopius macrophthalmos* Sheng & Chen, ♂, Japan. 49 wings 50 mesosoma lateral 51 mesosoma dorsal 52 base of antenna 53 antenna 54 head anterior 55 head dorsal 56 head lateral 57 metasoma dorsal.

Acknowledgements

We give special thanks to Shunpei Fujie from OMNH for making the Japanese specimens available.

Additional information

Conflict of interest

The authors have declared that no competing interests exist.

Ethical statement

No ethical statement was reported.

Funding

This research was supported by the Basic Science Research Program through the National Research Foundation of Korea (NRF) funded by the Ministry of Education (NRF-2022R1A2C1091308).

Author contributions

Supervision: HK. Writing - original draft: YH. Writing - review and editing: CA.

Author ORCIDs

Yunjong Han  <https://orcid.org/0000-0003-2757-7785>

Cornelis van Achterberg  <https://orcid.org/0000-0002-6495-4853>

Hyojoong Kim  <https://orcid.org/0000-0002-1706-2991>

Data availability

All of the data that support the findings of this study are available in the main text.

References

- Delrio G, Lentini A, Satta A (2005) Biological control of olive fruit fly through inoculative releases of *Opius concolor* Szépl. IOBC/WPRS Bulletin 28(9): 53–58.
- Fischer M (1972) Hymenoptera Braconidae (Opiinae I). (Paläarktische Region). Das Tierreich 91(1973): 1–620.
- Fischer M (1987) Hymenoptera, Opiinae III: Athiopische, orientalische, australische und ozeanische Region. Das Tierreich 104: 1–734. <https://doi.org/10.1515/9783110744965>
- Li X-Y, van Achterberg C, Tan J-C (2013) Revision of the subfamily Opiinae (Hymenoptera, Braconidae) from Hunan (China), including thirty-six new species and two new genera. ZooKeys 268: 1–186. <https://doi.org/10.3897/zookeys.326.5911>
- Ovruski S, Aluja M, Sivinski J, Wharton RA (2000) Hymenopteran parasitoids on fruit-infesting Tephritidae (Diptera) in Latin America and the Southern United States: Diversity, distribution, taxonomic status and their use in fruit fly biological control. Integrated Pest Management Reviews 5(2): 81–107. <https://doi.org/10.1023/A:1009652431251>
- Quicke DLJ, van Achterberg C, Godfray HCJ (1997) Comparative morphology of the venom gland and reservoir in opiine and alysiine braconid wasps (Insecta, Hymenoptera, Braconidae). Zoologica Scripta 26(1): 23–50. <https://doi.org/10.1111/j.1463-6409.1997.tb00407.x>

- Sheng Y-Y, Wu Q, van Achterberg C, Chen X-X (2019) Three newly recorded genera from China (Hymenoptera, Braconidae, Opiinae), with the notes on the genus *Neopius* and descriptions of three new species. *Zootaxa* 4604(3): 4603–4613. <https://doi.org/10.11646/zootaxa.4604.3.13>
- Tobias VI (1998) Alysiinae (Dacnusiini) and Opiinae. In: Ler PA (Ed.) *Keys to the Insects of Russian Far East*. Vol. 4. Neuropteroidea, Mecoptera, Hymenoptera 3. Dal'nauka, Vladivostok, 299–411.
- van Achterberg C (1988) Revision of the subfamily Blacinae Foerster (Hymenoptera, Braconidae). *Zoologische Verhandelingen* 249: 1–324.
- van Achterberg C (1990) Illustrated key to the subfamilies of the Holarctic Braconidae (Hymenoptera: Ichneumonoidea). *Zoologische Mededelingen Leiden* 64(1): 1–20.
- van Achterberg C (1993) Illustrated key to the subfamilies of the Braconidae (Hymenoptera: Ichneumonoidea). *Zoologische Verhandelingen* 283: 1–189.
- van Achterberg C (1997) Revision of the Haliday collection of Braconidae (Hymenoptera). *Zoologische Verhandelingen* 314: 1–115.
- van Achterberg C (2009) Can Townes type Malaise traps be improved? Some recent developments. *Entomologische Berichten* 69(4): 129–135.
- van Achterberg C, Grootaert, Shaw MR (2010) Chapter 17 – Flight interception traps for arthropods. In: Eymann J, Degreef J, Häuser C, Monje JC, Samyn Y, VandenSpiegel D (Eds) *Manual on field recording techniques and protocols for All Taxa Biodiversity Inventories and Monitoring*. *Abc Taxa*, vols 1–2, 421–462.
- van Achterberg C (2023) Illustrated key to the European genera of Opiinae (Hymenoptera, Braconidae), with the description of two new Palaearctic genera and two new species. *ZooKeys* 1176: 79–115. <https://doi.org/10.3897/zookeys.1176.104850>
- Wahyuni S, Supartha W, Ubaidillah R (2017) Functional response of *Opius chromatomyiae* Belokobylskij & Wharton (Hymenoptera: Eulopidae) parasitoid on leaf miner, *Liriomyza sativae* Blanchard (Diptera: Agromyzidae). *International Journal of Entomological Research* 5(1): 17–21.
- Wharton RA (1987) Changes in nomenclature and classification of some opiine Braconidae (Hymenoptera). *Proceedings of the Entomological Society of Washington* 89: 61–73.
- Wharton RA (1988) Classification of the braconid subfamily Opiinae (Hymenoptera). *Canadian Entomologist* 120(4): 333–360. <https://doi.org/10.4039/Ent120333-4>
- Wharton RA (1997) Generic relationships of opiine Braconidae (Hymenoptera) parasitic on fruit-infesting Tephritidae (Diptera). *Contributions of the American Entomological Institute* 30(3): 1–53.
- Wharton RA (2006) The species of *Sternaulopius* Fischer (Hymenoptera: Braconidae, Opiinae) and the braconid sternaulus. *Journal of Hymenoptera Research* 15: 317–347.
- Wharton RA, Norrbom A (2013) New species and host records of new world, mostly Neotropical, opiine Braconidae (Hymenoptera) reared from flower-infesting, stem-galling, and stem-mining Tephritidae (Diptera). *ZooKeys* 349: 11–72. <https://doi.org/10.3897/zookeys.349.5914>
- Yu D, van Achterberg C, Horstmann K (2016) *Taxapad 2016. Ichneumonoidea 2015*. *Taxapad Interactive Catalogue Database on flash-drive*. Ottawa.

Notes on the *Pselaphodes* Westwood complex (Coleoptera, Staphylinidae, Pselaphinae) of Hubei, China, with description of a new species and additional faunistic data

Ting Feng¹, Zi-Wei Yin² 

¹ Shanghai Zoological Park, 2381 Hongqiao Road, Changning District, Shanghai, 200335, China

² Laboratory of Systematic Entomology, College of Life Sciences, Shanghai Normal University, 100 Guilin Road, Xuhui District, Shanghai 200234, China

Corresponding author: Zi-Wei Yin (pselaphinae@gmail.com)

Abstract

The *Pselaphodes* Westwood complex of genera is represented in Hubei Province by four genera and eight species. Recent field work at Wanchaoshan Nature Reserve, Xingshan County revealed a small series of material belonging to this complex. In this paper, we describe *Pselaphodes wanchaoshanus* sp. nov. and provide new faunistic data for *P. nomurai* Yin, Li & Zhao. A key to the hitherto known members of *Pselaphodes* complex that occur in Hubei is provided to facilitate ready species identification.

Key words: Ant-loving beetle, central China, identification key, taxonomy, Tyrini



Academic editor: Adam Brunke

Received: 2 May 2024

Accepted: 25 June 2024

Published: 8 July 2024

ZooBank: <https://zoobank.org/5FD80E14-EE64-4EB7-AB68-EB6BF63128E8>

Citation: Feng T, Yin Z-W (2024)

Notes on the *Pselaphodes* Westwood complex (Coleoptera, Staphylinidae, Pselaphinae) of Hubei, China, with description of a new species and additional faunistic data. ZooKeys 1206: 231–239. <https://doi.org/10.3897/zookeys.1206.126696>

Copyright: © Ting Feng & Zi-Wei Yin.

This is an open access article distributed under terms of the Creative Commons Attribution License (Attribution 4.0 International – CC BY 4.0).

Introduction

The *Pselaphodes* Westwood complex of genera (sensu Hlaváč 2003) is a speciose group including nine morphologically similar, and probably also phylogenetically close, genera (Yin et al. 2013a) of the tribe Tyrini that are diversified primarily in the Oriental Region. As of 1st May, 2024, 179 species of this complex have been described (Newton 2022). The most diverse genus, *Pselaphodes* Westwood, contains 87 species (e.g., Huang et al. 2018a, 2018b; Huang and Yin 2019, 2020; Yin 2019; Yin and Li 2021), followed by *Labomimus* Sharp with 48 species (e.g., Zhang and Yin 2019; Zhang et al. 2019; Li and Yin 2020; Yin and Li 2021), *Linan* Hlaváč with 17 species (e.g., Yin et al. 2011a; Yin and Li 2013a; Zhang et al. 2018; Zhao et al. 2019), *Lasinus* Sharp with 12 species (Bekchiev et al. 2013; Yin et al. 2014), and the other, smaller genera *Nomuraius* Hlaváč (Huang and Yin 2018), *Paralasinus* Hlaváč & Nomura (Hlaváč and Nomura 2001), *Taiwanophodes* Hlaváč (Bekchiev 2010), *Dayao* Yin, Li & Zhao (Yin et al. 2011b, 2013a), and *Indophodes* Hlaváč (Hlaváč 2003), each comprising no more than five species.

Motivated by Prof. Cong Wei of Northwest A&F University, our team recently had an opportunity to visit a few interesting collecting sites at several nature reserves in Hubei, and we successively obtained a short series of pselaphine beetles (c. 80 specimens). An attempt to identify this material revealed a new

species of *Pselaphodes*, which represents the fourth member of the genus in Hubei. Simultaneously collected were two adults of *Pselaphodes nomurai* Yin, Li & Zhao, a well-known species distributed across the Qinling Mountains. This new find is reported in this paper, and a key to aid in the identification of all known species of the *Pselaphodes* complex (nine species) occurring in Hubei is provided.

Materials and methods

The materials treated in this paper are deposited in the Insect Collection of Shanghai Normal University (**SNUC**). The label data of the material is quoted verbatim. Dissected parts were mounted in Euparal on plastic slides pinned with the specimen. The habitus image of the beetle was taken using a Canon EOS R5 camera, equipped with a 5× Mitutoyo M Plan Apo lens, and three 20W UFO LED bulbs (5000 k) were used as the light source. Images of morphological details were produced using a Canon G9 camera mounted to an Olympus CX31 microscope under reflected or transmitted light. Helicon Focus v. 8.2.0 Pro was used for image stacking. All images were modified and grouped into plates using Adobe Photoshop CC 2020.

Measurements were taken as follows: total body length was measured from the anterior margin of the rostrum to the apex of the abdomen; head length was measured from the anterior margin of the rostrum to the head base, excluding the cervical constriction; head width was measured across the eyes; the length of the pronotum was measured along the midline, the width of the pronotum equals the maximum width; the length of the elytra was measured along the suture; the width of the elytra was measured as the maximum width across both elytra; the length of the abdomen is the length of the dorsally exposed part of the abdomen along its midline, the width is the maximum width. The terminology follows Chandler (2001) and Yin (2022). Abdominal tergites and sternites are numbered in Arabic (starting from the first visible segment) and Roman (reflecting true morphological position) numerals, e.g. tergite 1 (IV), or sternite 1 (III). Paired appendages in the description are treated as singular.

Taxonomy

Key to species of *Pselaphodes* complex occurring in Hubei Province, China (males)

- 1 Maxillary palpus small and simple, almost symmetrical, lateral margin of palpomeres 2–4 lacking expansion or projection (Locality: Guanmen-shan) ***Lasinus sinicus* Bekchiev, Hlaváč & Nomura**
- Maxillary palpus asymmetrical, lateral margin of palpomeres 2–4 expanded or projected..... **2**
- 2 Vertexal and frontal fovea indistinct or absent **3**
- Vertexal and frontal fovea distinct **4**
- 3 Frons lacking fovea (Zhang et al. 2018: fig. 1A); antennomere 9 angulate to lateral margin and with small tubercle near apex, 10 simple (Zhang et al. 2018: fig. 2A); mesotibia greatly curved at middle (Zhang et al. 2018: fig. 2G); aedeagus with elongate parameres (Zhang et al. 2018: fig. 2J–L)

- (Locality: Xingdoushan, Changtanhe, Huangjindong).....
-***Linan arcitibialis* Zhang, Li & Yin**
- Frons with small, indistinct fovea (Zhang et al. 2018: fig. 10A); antennomere 9 broadened through length, 10 greatly transverse (Yin et al. 2011a: fig. 11; Zhang et al. 2018: fig. 10B); mesotibia moderately curved at middle; aedeagus with greatly broadened parameres (Yin et al. 2011a: figs 35, 36; Zhang et al. 2018: fig. 10K, J) (Locality: Xingdoushan).....
-***Linan megalobus* Yin & Li, 2011**
- 4 Setose metaventral fovea present; postgenae broadly expanded laterally (Yin and Li 2012: fig. 1B) (Locality: Dabashan)....***Labomimus dabashanus* Yin & Li**
- Setose metaventral fovea absent; postgenae convergent posteriorly**5**
- 5 Body length 2.2–2.4 mm; antennal club simple, lacking modifications (Yin et al. 2011c: fig. 22) (Locality: near Xueluozhai).....
-***Pselaphodes parvus* Yin, Li & Zhao**
- Body length no less than 3.0 mm; antennal club modified.....**6**
- 6 Antennomere 9 subcylindrical, with disc-like projection near apex, antennomere 10 and 11 lacking modifications**7**
- Antennomere 9 subtriangular, lacking disc-like projection, antennomere 10 and 11 greatly modified**8**
- 7 Metaventral processes in lateral view straight, broadened apically and with broad notch at apex (Yin et al. 2013a: fig. 9C); medial lobe of aedeagus extended, with narrowed apex (Yin et al. 2013a: fig. 9J) (Locality: Dabieshan).....***Pselaphodes anhuianus* Yin & Li**
- Metaventral processes in lateral view curved at middle, narrowing apically and with pointed apex (Yin et al. 2013a: fig. 15C); medial lobe of aedeagus extended and broadening toward apex (Yin et al. 2013a: fig. 15J) (Locality: Dabieshan).....***Pselaphodes longilobus* Yin & Li**
- 8 Antennomere 9 subtriangular, lacking large projection (Fig. 1D), 10 round-subquadrate, transverse, dorsal surface broadly impressed (Fig. 1D); metaventral process in lateral view narrowed at apex (Fig. 1E) (Locality: Wanchaoshan).....***Pselaphodes wanchaoshanus* sp. nov.**
- Antennomere 9 subtriangular, greatly projected on inner apical margin (Yin et al. 2010: fig. 92), 10 elongately oblique, mesal surface impressed (Yin et al. 2010: fig. 92); metaventral process in lateral view roundly broadened at apex (Yin et al. 2010: fig. 79) (Locality: Dabashan, Wanchaoshan).....***Pselaphodes nomurai* Yin, Li & Zhao**

***Pselaphodes nomurai* Yin, Li & Zhao, 2010**

Pselaphodes nomurai Yin, Li & Zhao, 2010: 21; Yin et al. 2012 (key); Yin and Li 2012 (distribution); Yin et al. 2013b (distribution). Type locality: China, Shaanxi Prov., Foping County (33°31'28"N, 107°59'26"E), elev. 1,250–1,400 m.

Additional material examined (2 specimens). 2 ♂♂, “China: Hubei, Xingshan County, Wanchaoshan N. R., 31.3217°N, 110.4906°E, 1700 m, 19.viii.2023, Guo-Hao Wei leg., 湖北兴山县万朝山保护区, 魏国豪采” (SNUC).

Distribution. China: Henan, Shaanxi, Hubei, Chongqing, Sichuan. New distributional record in Hubei.

Comments. These two males can be readily identified as *P. nomurai* by the characteristic form of the male antennal club, the apically broadened metaven-tral processes, and the aedeagus with an extended, apically truncate median lobe. In comparison to that of the type locality, the Wanchaoshan population has the inner apical margin of male antennomere 10 being greatly protruding to level above the mesal projection of antennomere 9.

***Pselaphodes wanchaoshanus* Feng & Yin sp. nov.**

<https://zoobank.org/E48B3C8B-AE9F-4B8F-B898-44DBD418707F>

Fig. 1

Chinese common name: 万朝山长角蚁甲

Type material (1 specimen). *Holotype*: CHINA: ♂, “China: Hubei, Xingshan County, Wanchaoshan N. R., 31.3217°N, 110.4906°E, 1700 m, 19.viii.2023, Guo-Hao Wei leg., 湖北兴山县万朝山保护区, 魏国豪采” (SNUC).

Diagnosis. Male. Body length approximately 3.2 mm. Vertex and frontal rostrum with coarse rugose sculpture; maxillary palpomeres 2–4 each roundly protuberant on lateral margin; antenna distinctly clubbed, antennomere 1 with row of dense setae on lateral margin, 7 oblique, 9 subtriangular, 10 broadly impressed on dorsal surface, 11 constricted at base and broadened apically. Center of pronotal disc with large punctures, lacking rugose sculpture, with distinct median longitudinal sulcus. Metaventral process in lateral view short, narrowing apically. Protibia with small apical spur, protrochanter with thin spine, profemur with broad triangular spine; mesotrochanter with one distinct spine and few small denticles, mesofemur with small denticle on ventral margin. Tergite 1 (IV) dorsally more than 3× as long as 2 (V). Aedeagus with broad, extended median lobe, endophallus composed of two long and one short sclerite.

Description. Male. Body (Fig. 1A) length 3.16 mm; head, antennae, pronotum and abdomen dark red brown, elytra reddish-brown, tarsi and mouthparts lighter. Dorsal surface of body covered with short pubescence.

Head (Fig. 1B) roundly triangular, subtruncate at base, slightly longer than wide, length 0.69 mm, width across eyes 0.65 mm; vertex with coarse rugose sculpture, with large, setose vertexal foveae (dorsal tentorial pits), with short medio carina between foveae; rostrum prominent anteriorly, covered with rugose sculpture, with large setose frontal fovea; clypeus sharply descending, its anterior margin carinate and moderately raised. Venter with small, widely separated gular foveae (posterior tentorial pits) in broad and deep impression, lacking median carina. Eyes greatly prominent, each composed of approximately 55 ommatidia. Maxillary palpus (Fig. 1C) four-segmented, palpomere 1 minute, 2 pedunculate in basal half and broadening apically, 3 with short stem at base, apical part broadened and subtriangular, 4 subfusiform, elongate, with elongate apical palpal cone; 2–4 each roundly expanded on lateral margin, with short, dense setae at apex of each expansion. Antenna elongate, length 2.35 mm, with modified antennomeres 7 and 9–11 and distinct club (Fig. 1D); antennomere 1 long and thick, subcylindrical, lateral margin with row of dense, short golden setae, 2–6 each submoniliform, of similar width, with 6 slightly longer than 2–5, 7 oblique, longer than 6, 8 shortest, 9 greatly enlarged, subtriangular, 10 broad, narrower than 9, broadly impressed on dorsal surface and with

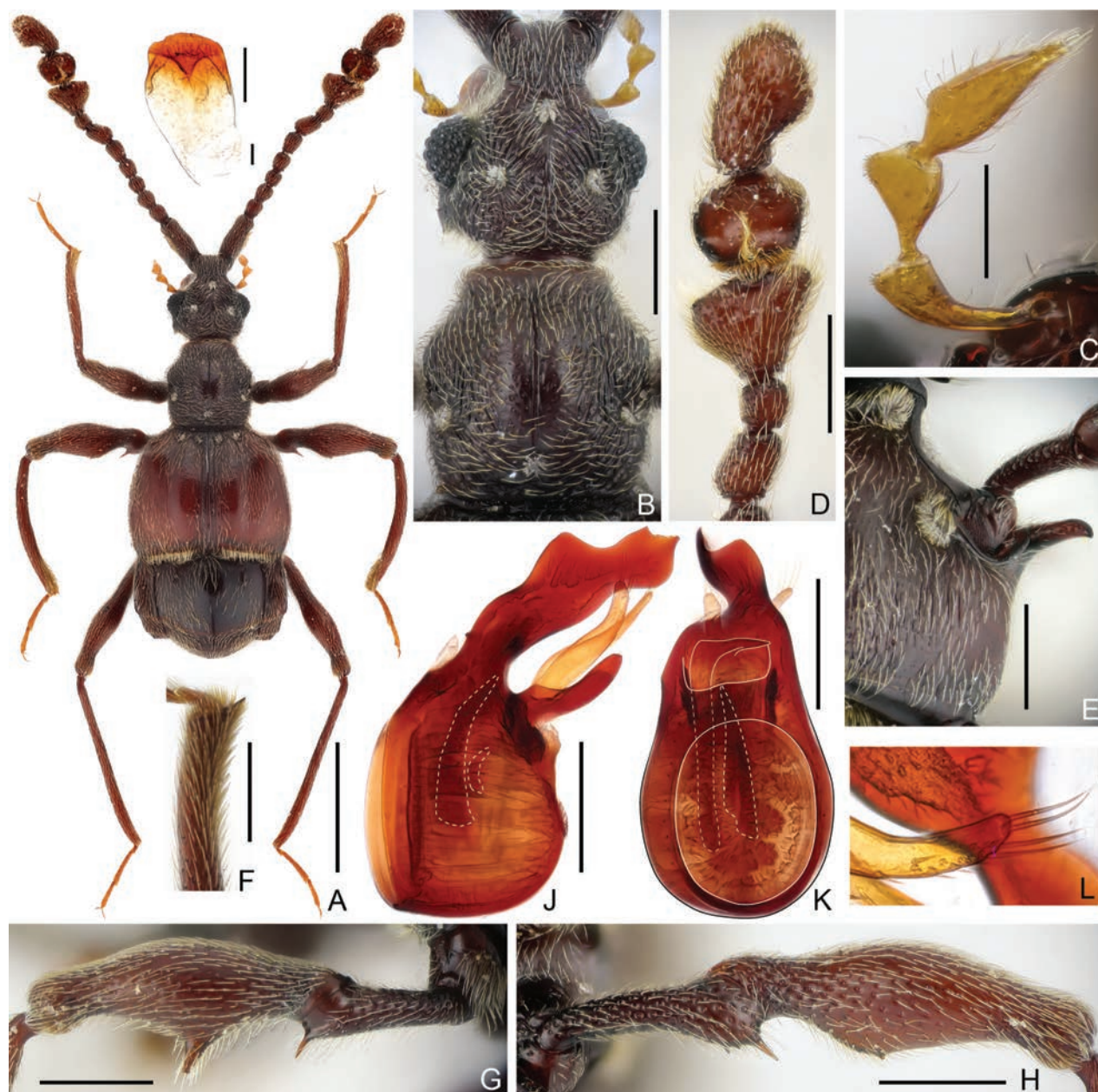


Figure 1. Morphological characters of *Pselaphodes wanchaoshanus* sp. nov. **A** dorsal habitus **B** head dorsum and pronotum **C** maxillary palpus **D** antennal club **E** metaventral process, lateral **F** apex of protibia **G** protrochanter and profemur **H** mesotrochanter and mesofemur **I** sternite 7 (IX) **J, K** aedeagus, lateral (J) and ventral (K) **L** apex of paramere. Scale bars: 1.0 mm (A); 0.3 mm (B, D, E, G, H); 0.2 mm (C, F, J, K); 0.1 mm (I, L).

longitudinal row of setae at middle of impression, 11 asymmetric, constricted for basal 1/5, then obliquely broadening to apex.

Pronotum (Fig. 1B) slightly longer than wide, length 0.69 mm, width 0.66 mm, widest at approximately apical 1/3, sides subparallel posterior to broadest point and convergent apically, with almost straight anterior and posterior margin; disc moderately convex, central portion smooth and with large punctures, rest portion with coarse, rugose sculpture; with distinct median longitudinal sulcus and large, setose median and lateral antebasal foveae. Prosternum with basisternal (precoxal) portion at middle shorter than procoxal rests; with setose lateral procoxal foveae; hypomera fused with sternum, smooth, lacking hypomeral grooves and carinae.

Elytra subquadrate, much broader than long, length 0.91 mm, width 1.26 mm, length/width 0.72; each elytron with two large, setose basal foveae; with complete sutural striae and broad longitudinal discal impressions; humeri roundly prominent, lacking subhumeral foveae or marginal striae; posterior margin with row of dense setae. Metathoracic wings fully developed.

Mesoventrite short, laterally fused with metaventrite; mesanepisterna and anterior region of mesoventrite forming transverse prepectus, posteriorly mesoventrite smoothly broadening, with lateral margins moderately diverging; median mesoventral foveae broadly separated in setose transverse impression, lateral mesoventral foveae large and setose, not forked (straight) internally; intercoxal process blunt and short. Metaventrite weakly impressed at middle, with pair of elongate metaventral processes, laterally each process (Fig. 1E) narrowing toward apex; large, setose lateral mesocoxal foveae present; posterior margin with narrow slit in middle.

Legs elongate; protibia (Fig. 1F) with small apical spur, protrochanter (Fig. 1G) with thin, acute spine and profemur (Fig. 1G) with large, broad triangular spine on ventral margin; mesotrochanter (Fig. 1H) with one long and acute and few small denticles, and mesofemur (Fig. 1H) with single small denticle on ventral margin; hind leg simple.

Abdomen widest at lateral margins of tergite 1 (IV), length 1.08 mm, width 1.18 mm, with well-developed paratergites 1–4. Tergite 1 (IV) in dorsal view approximately 3.3× as long as 2 (V), with broad, setose basal impression, discal carinae broadly separated, extending posterior for approximately 1/4 tergal length, tergite 2 (V) and 3 (VI) each short, subequal in length, 4 (VII) longer than 3, posterior margin angularly convex at middle, 2–4 each with one pair of basolateral foveae, 5 (VIII) transverse, posterior margin narrowed and roundly emarginate at middle. Sternite 2 (IV) longest, with densely setose basal sulcus and one pair of mediobasal and basolateral foveae, 3 (V) to 5 (VII) at middle successively shorter, each with one pair of small basolateral foveae, 6 (VIII) transverse, posterior margin with small emargination at middle, 7 (IX) (Fig. 1I) elongate, semisclerotized in apical portion and membranous basally.

Aedeagus (Fig. 1J, K) 0.61 mm long, dorso-ventrally asymmetric; median lobe with broad basal capsule and large, oval dorsal diaphragm, apical portion broadened and greatly extended, with narrowed apex; endophallus composed of two elongate and one short sclerite; parameres (Fig. 1L) each elongate, membranous, with five small setae along ventral margin in apical part and four long macrosetae at apex.

Female. Unknown.

Comparative notes. This species is placed as a member of the Walkeri group (*sensu* Huang et al. 2018a) based on the asymmetric male antennomeres 7. The subtriangular antennomeres 9 of the male resemble those of *P. anjiensis* Huang, Li & Yin (Zhejiang), *P. antennarius* Huang, Li & Yin (Guizhou), *P. pseudowalkerii* Yin & Li (Zhejiang, Fujian, Jiangxi), and *Pselaphodes walkerii* (Sharp) (Zhejiang), but the new species can be readily separated by the broadly impressed antennomeres 10, basally constricted and apically broadened antennomeres 11, moderately long metaventral processes, the spination of the legs, as well as the configuration of the aedeagus. The antennomeres 11 of this species are also similar to those of *P. nomurai*, but the forms of the antennomeres 9 and 10 are quite different.

Distribution. China: Hubei.

Etymology. The species is named after its type locality, i.e., Wanchaoshan.

Acknowledgements

We are grateful to Cong Wei (魏琮) (Northwest A&F University, Xianyang, China) for logistical support of the field work. Shûhei Nomura (National Museum of Nature and Science, Tsukuba, Japan) and Rostislav Bekchiev (National Museum of Natural History, Sofia, Bulgaria) critically reviewed the draft manuscript.

Additional information

Conflict of interest

The authors have declared that no competing interests exist.

Ethical statement

No ethical statement was reported.

Funding

The field work was supported by the Shennongjia National Park Biodiversity Background Survey Project (SNJNP2022009) and Open Project Fund of Hubei Provincial Key Laboratory on Conservation Biology of Shennongjia Golden Snub-nosed Monkey (SNJGKL2022009). ZWY was also supported by the National Natural Science Foundation of China (32370465).

Author contributions

Conceptualization: ZWY. Funding acquisition: ZWY. Investigation: ZWY. Methodology: TF. Validation: TF. Writing – original draft: TF. Writing – review and editing: ZWY.

Author ORCIDs

Zi-Wei Yin  <https://orcid.org/0000-0001-6659-9448>

Data availability

All of the data that support the findings of this study are available in the main text.

References

- Bekchiev R (2010) Description of the second species of the genus *Taiwanophodes* Hlaváč, 2002 (Coleoptera: Staphylinidae: Pselaphinae) from Vietnam. *Russian Entomological Journal* 19(3): 183–185. <https://doi.org/10.15298/rusentj.19.3.05>
- Bekchiev R, Hlaváč P, Nomura S (2013) A taxonomic revision of Tyrini of the Oriental region. V. Revision of the genus *Lasinus* Sharp, 1874 (Coleoptera, Staphylinidae, Pselaphinae). *ZooKeys* 340: 21–42. <https://doi.org/10.3897/zookeys.340.5980>
- Chandler DS (2001) Biology, morphology, and systematics of the antlike litter beetles of Australia (Coleoptera: Staphylinidae: Pselaphinae). *Memoirs on Entomology International* 15: 1–560.
- Hlaváč P (2003) A taxonomic revision of the Tyrini of the Oriental Region. II. Systematic study on the genus *Pselaphodes* and its allied genera (Coleoptera: Staphylinidae: Pselaphinae). *Annales de la Société Entomologique de France (N.S.)* 38 (3): 283–297.
- Hlaváč P, Nomura S (2001) A taxonomic revision of Tyrini of the Oriental Region I. *Paralasinus* (Coleoptera, Staphylinidae, Pselaphinae), a new genus of Tyrina from Indochina. *Elytra* 29(1): 163–174. [https://coleoptera.sakura.ne.jp/Elytra/29\(1\)163HlavacP_&_NomuraS.pdf](https://coleoptera.sakura.ne.jp/Elytra/29(1)163HlavacP_&_NomuraS.pdf)

- Huang M-C, Yin Z-W (2018) Two new species of *Nomuraius* Hlaváč (Coleoptera: Staphylinidae: Pselaphinae) from southern China. *Zootaxa* 4399(4): 571–578. <https://doi.org/10.11646/zootaxa.4399.4.7>
- Huang M-C, Yin Z-W (2019) The *Pselaphodes* (Coleoptera: Staphylinidae: Pselaphinae) of Nepal. *Revue Suisse de Zoologie* 126(2): 165–196. <https://doi.org/10.5281/zenodo.3463445>
- Huang M-C, Yin Z-W (2020) Validation of five *Pselaphodes* species names in Huang & Yin (2019): The *Pselaphodes* (Coleoptera: Staphylinidae: Pselaphinae) of Nepal. *Revue Suisse de Zoologie* 127(1): 241–242. <https://doi.org/10.35929/RSZ.0016>
- Huang M-C, Li L-Z, Yin Z-W (2018a) Eleven new species and a new country record of *Pselaphodes* (Coleoptera: Staphylinidae: Pselaphinae) from China, with a revised checklist of world species. *Acta Entomologica Musei Nationalis Pragae* 58(2): 457–478. <https://doi.org/10.2478/aemnp-2018-0035>
- Huang M-C, Li L-Z, Yin Z-W (2018b) Four new species of *Pselaphodes* Westwood (Coleoptera: Staphylinidae: Pselaphinae) from Thailand, Laos, and China. *Zootaxa* 4472(1): 100–110. <https://doi.org/10.11646/zootaxa.4472.1.4>
- Li N, Yin Z-W (2020) The first Sri Lankan species of *Labomimus* Sharp (Coleoptera: Staphylinidae: Pselaphinae). *Zootaxa* 4809(2): 397–400. <https://doi.org/10.11646/zootaxa.4809.2.12>
- Newton AF (2022) StaphBase. In: Bánki O, Roskov Y, Döring M, Ower G, Hernández Robles DR, Plata Corredor CA, Stjernegaard Jeppesen T, Örn A, Vandepitte L, Hobern D, Schalk P, DeWalt RE, Ma K, Miller J, Orrell T, Aalbu R, Abbott J, Adlard R, Aedo C et al. *Catalogue of Life Checklist* (Aug 2022). [Last accessed 02 May. 2024] <https://doi.org/10.48580/dfqf-3gk>
- Yin Z-W (2019) Two new species and new records of the *Pselaphodes*-complex of genera from China (Coleoptera: Staphylinidae: Pselaphinae). *Revue Suisse de Zoologie* 126(2): 197–202. <https://doi.org/10.35929/RSZ.0025>
- Yin Z-W (2022) The Batrisini of Tibet: Unveiling an enigmatic ant-loving beetle diversity at Earth's "Third Pole" (Coleoptera, Staphylinidae, Pselaphinae). *Zootaxa* 5111(1): 1–211. <https://doi.org/10.11646/zootaxa.5111.1.1>
- Yin Z-W, Li L-Z (2012) Notes on Michael Schülke's pselaphine collections from China. Tyrini. I. genera *Labomimus* Sharp, *Linan* Hlaváč and *Pselaphodes* Westwood (Coleoptera, Staphylinidae, Pselaphinae). *ZooKeys* 251: 83–118. <https://doi.org/10.3897/zookeys.251.4099>
- Yin Z-W, Li L-Z (2013a) Five new species of the genera *Labomimus* and *Linan* from Guangxi, South China (Coleoptera: Staphylinidae: Pselaphinae). *Acta Entomologica Musei Nationalis Pragae* 53(1): 141–153. https://www.aemnp.eu/data/article-1445/1426-53_1_141.pdf
- Yin Z-W, Li N (2021) Eight new species and additional records of the *Pselaphodes* complex from Laos and Vietnam, with a key to known species (Coleoptera: Staphylinidae: Pselaphinae). *Acta Entomologica Musei Nationalis Pragae* 61(1): 35–53. <https://doi.org/10.37520/aemnp.2021.002>
- Yin Z-W, Li L-Z, Zhao M-J (2010) Taxonomical study on the genus *Pselaphodes* Westwood (Coleoptera: Staphylinidae: Pselaphinae) from China. Part I. *Zootaxa* 2512(1): 1–25. <https://doi.org/10.11646/zootaxa.2512.1.1>
- Yin Z-W, Li L-Z, Zhao M-J (2011a) A review of the genus *Linan* (Coleoptera: Staphylinidae: Pselaphinae). *Acta Entomologica Musei Nationalis Pragae* 51(1): 123–135. <https://doi.org/10.11646/zootaxa.2512.1.1>

- Yin Z-W, Li L-Z, Zhao M-J (2011b) *Dayao* gen. n. of the subtribe Tyrina (Coleoptera, Staphylinidae, Pselaphinae) from South China. *ZooKeys* 141: 45–52. <https://doi.org/10.3897/zookeys.141.1948>
- Yin Z-W, Li L-Z, Zhao M-J (2011c) Taxonomical study on the genus *Pselaphodes* Westwood (Coleoptera: Staphylinidae: Pselaphinae) from China. Part II. *Annales Zoologici* 61(3): 463–481. <https://doi.org/10.3161/000345411X603337>
- Yin Z-W, Li L-Z, Gu F-K (2012) Taxonomic study on the genus *Pselaphodes* Westwood (Coleoptera, Staphylinidae, Pselaphinae) from China. Part III. *Zootaxa* 3189(1): 29–38. <https://doi.org/10.11646/zootaxa.3189.1.2>
- Yin Z-W, Hlaváč P, Li L-Z (2013a) Further studies on the *Pselaphodes* complex of genera from China (Coleoptera, Staphylinidae, Pselaphinae). *ZooKeys* 275: 23–65. <https://doi.org/10.3897/zookeys.275.4571>
- Yin Z-W, Nomura S, Li L-Z (2013b) New species and new records of the *Pselaphodes* complex of genera (Staphylinidae: Pselaphinae: Tyrini) from China *Annales Zoologici* 63 (2): 343–356. <https://doi.org/10.3161/000345413X669595>
- Yin Z-W, Bekchiev R, Li L-Z (2014) A new species of *Lasinus* Sharp (Coleoptera: Staphylinidae: Pselaphinae) from East China. *Zootaxa* 3764(5): 597–600. <https://doi.org/10.11646/zootaxa.3764.5.9>
- Zhang Y-Q, Yin Z-W (2019) Three new species of *Labomimus* Sharp (Coleoptera: Staphylinidae: Pselaphinae) from Taiwan, China, with an updated key for *L. shibatai* Sawada-group. *Zootaxa* 4586(3): 553–561. <https://doi.org/10.11646/zootaxa.4586.3.10>
- Zhang Y-Q, Li L-Z, Yin Z-W (2018) Six new species and a new record of *Linan* Hlaváč in China, with a key to species (Coleoptera, Staphylinidae, Pselaphinae). *ZooKeys* 793: 115–133. <https://doi.org/10.3897/zookeys.793.27661>
- Zhang Y-Q, Li L-Z, Yin Z-W (2019) Fifteen new species and a new country record of *Labomimus* Sharp from China, with a checklist of world species (Coleoptera: Staphylinidae: Pselaphinae). *Zootaxa* 4554(2): 497–531. <https://doi.org/10.11646/zootaxa.4554.2.7>
- Zhao Q-H, Xu W, Yin Z-W (2019) A new species of *Linan* Hlaváč (Coleoptera, Staphylinidae, Pselaphinae) from Shenzhen, China. *ZooKeys* 859: 63–68. <https://doi.org/10.3897/zookeys.859.35465>

A new species of the genus *Luciogobius* Gill, 1859 (Teleostei, Oxudercidae) from Taiwan

Kuan-Hsun Chen¹, Te-Yu Liao¹

¹ Department of Oceanography, National Sun Yat-sen University, Kaohsiung, Taiwan
Corresponding author: Te-Yu Liao (swp0117@gmail.com)

Abstract

A new species, *Luciogobius opisthoproctus* **sp. nov.**, is described based on 18 specimens collected from Daxi Creek (Yilan) and Babian Creek (Taitung) in Taiwan. The new species is characterized by having a yellowish body with scattered spots on the sides, a black blotch on the caudal fin, the absence of free pectoral-fin rays, and more than 40 vertebrae. The new species can be distinguished from congeners by the following combination of characters: AAA distance (anus to anal-fin origin) shorter than twice the body depth at anus, 4.2–7.2% of standard length (SL); pre-anus length 80.0–92.8% of pre-anal-fin length; snout length 39.7–62.7% of AAA distance; abdominal vertebrae 20–22; caudal vertebrae 20–22; first anal-fin pterygiophore usually inserted behind the second haemal spine.

Key words: Actinopterygii, amphidromous, earthworm goby, interstitial habitat, taxonomy, western Pacific



Academic editor: Maria Elina Bichuette
Received: 21 January 2024
Accepted: 17 June 2024
Published: 9 July 2024

ZooBank: <https://zoobank.org/D06F4B8E-D603-45AA-9E12-2CF04BC83F1A>

Citation: Chen K-H, Liao T-Y (2024) A new species of the genus *Luciogobius* Gill, 1859 (Teleostei, Oxudercidae) from Taiwan. ZooKeys 1206: 241–254. <https://doi.org/10.3897/zookeys.1206.118757>

Copyright: © Kuan-Hsun Chen & Te-Yu Liao.
This is an open access article distributed under terms of the Creative Commons Attribution License (Attribution 4.0 International – CC BY 4.0).

Introduction

The earthworm goby genus *Luciogobius* Gill, 1859 of the family Oxudercidae (sensu Nelson et al. 2016) comprises at least 16 valid species distributed along coasts of eastern Russia, Korea, China, Taiwan, Japan, and northern Vietnam (Lindberg and Krasnyukova 1975; Chen et al. 2008; Cho and Choi 2014; Shibukawa et al. 2019, 2020; Ta et al. 2021; Koreeda and Motomura 2022). *Luciogobius* species mostly dwell in the intertidal zones or in estuaries that contain rocky substrates or sandy sediments (Yamada et al. 2009; Shibukawa et al. 2019; Koreeda and Motomura 2022). Their elongated bodies and finely segmented vertebral columns allow them to access various microhabitats (Yamada et al. 2009; Kondo and Kato 2018; Shibukawa et al. 2019, 2020). The most distinguishable characteristics of *Luciogobius*, which set them apart from other oxudercid genera, are their specialized elongate and scaleless bodies with more vertebrae, degenerate eyes, and the absence of the first dorsal fin (Yamada et al. 2009; Nelson et al. 2016; Shibukawa et al. 2019, 2020). However, *Luciogobius* species lack notable morphological characters for distinguishing congeners (Shibukawa et al. 2019). After reviewing the taxonomy of *Luciogobius*, Shibukawa et al. (2019) grouped extant species into five species complexes based on

morphological characters and named them after the earliest described species among each complex: *L. elongatus*, *L. grandis*, *L. guttatus*, *L. platycephalus*, and *L. pallidus* complexes (Shibukawa et al. 2019). However, it is still under debate whether each complex represents only one valid species, as there are still many undescribed and cryptic species (Shibukawa et al. 2019). Among these complexes, the *L. elongatus* complex is the largest and comprises *L. adapel* Okiyama, 2001, *L. elongatus* Regan, 1905, *L. parvulus* (Snyder, 1909), *L. punctilineatus* Koreeda & Motomura, 2022, and nine unnamed species, i.e. *Luciogobius* spp. 8–16, and this complex can be distinguished from *L. grandis*, *L. guttatus*, *L. pallidus* complexes by having an AAA distance of more than half of the body depth at the anus (vs less than half of body depth). It can be further distinguished from *L. guttatus* and *L. pallidus* complexes by having the first anal-fin pterygiophore insertion behind the first haemal spine (vs before the first haemal spine). It can also be separated from *L. grandis* and *L. platycephalus* complexes by having the anteriormost pleural rib attached to the third position (vs second) of the abdominal vertebra (Shibukawa et al. 2019). In the present study, several specimens of an undescribed species of the *L. elongatus* complex were collected from eastern Taiwan. The new species is described here based on morphological and molecular characters.

Material and methods

Specimens were collected from the mouths of the Daxi Creek, Yilan County, and Babian Creek, Taitung County (Figs 1, 2) using a hand-net in water 0–30 cm deep during low tide. The substrate was gravel (5–8 mm in diameter). After sampling, each specimen was photographed, muscle tissues or fin clips were collected, preserved in 95% ethanol solution, and stored at –20 °C for molecular analysis. The specimens were then fixed in 10% neutral buffered formalin and transferred to 70% ethanol solution for permanent preservation. The specimens are deposited in the Department of Oceanography, National Sun Yat-sen University, Kaohsiung (**DOS**), the Academia Sinica Institute of Zoology, Taiwan (**ASIZP**), and the National Museum of Marine Biology and Aquarium (**NMMB-P**), Pingtung. We examined one *L. elongatus* specimen from Osaka Museum of Natural History (**OMNH-P**) for comparison. Meristic counts and morphometric measurements follow Shibukawa et al. (2019), except for the following characters which follow Koreeda and Motomura (2022): AAA was measured from the posterior margin of the anus to the anal-fin origin; body depths were taken at the pelvic-fin origin, anus and anal-fin origin; counts of the abdominal and caudal vertebrae. Other abbreviations: SL, standard length; HL, head length. The series of cephalic sensory papillae on the cheek was based on Shibukawa et al. (2020). The alcian blue–alizarin red staining method (Dingerkus and Uhler 1977) and radiographs were used for counts of the dorsal and anal fin rays, pterygiophores, and vertebrae for all the type specimens. Cyanine blue was used for papillae illustration (Saruwatari and Andrés López 1997).

The GeneMark Easy Tissue & Cell Genomic DNA Purification kit was used for DNA extraction from muscle tissues or fin clips following the manufacturer's protocol. The partial mitochondrial 12S ribosomal RNA (12S) (133 bp) was amplified for molecular analysis. Polymerase chain reactions (PCR) were performed using a 25 µl volume containing 16.47 µl double distilled water, 3.0 µl

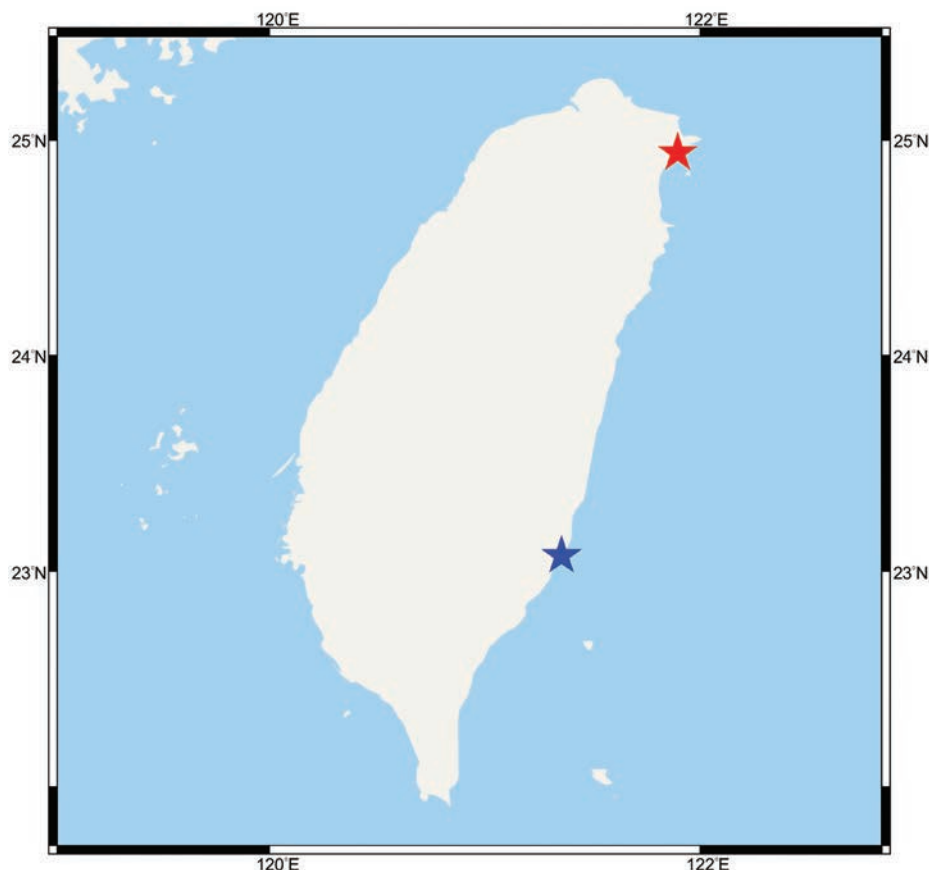


Figure 1. Map of Taiwan showing the collection localities of *Luciogobius opisthoproctus* sp. nov. Red star, Daxi Creek; blue star, Babian Creek.

of 10X Taq Buffer, 2.0 μ l of dNTP mixture at 10 mM, 1.2 μ l of each forward and reverse primers at 5 μ M, 0.125 μ l of Pro Taq Plus DNA polymerase, and 1.0 μ l of template DNA. In some cases, PCR were also performed in a 25 μ l volume consisting of 9.5 μ l double distilled water, 12.5 μ l SuperRed PCR Master Mix (2 \times), 1.0 μ l each of forward and reverse primers at 5 μ M, and 1.0 μ l of template DNA. The mitochondrial 12S rRNA gene was amplified using universal primers MiFishU-F and MifishU-R (Miya et al. 2015), with PCR thermal conditions consisting of an initial denaturation of 95 $^{\circ}$ C for 4 min, followed by 30 cycles of 94 $^{\circ}$ C for 40 s of denaturation, 60 $^{\circ}$ C for 20 s of annealing and 72 $^{\circ}$ C for 20 s of initial extension, and final extension at 72 $^{\circ}$ C for 4–10 min. The PCR products were visualized in 2% agarose gels, purified using SAP-Exo Kit (Jena Bioscience, Jena, Germany) and sent to Genomics S&T (Taipei, Taiwan) for sequencing. Sequences were assembled and edited using SeqMan Pro v. 11.1.0 (DNASTAR Inc., Madison, WI, USA). The obtained 12S sequences were submitted to GenBank under accession numbers OR871675–OR871682 and OR879784. Sequences of *L. elongatus* (LC499453, LC500721, LC579249, LC579251, MH682217), *L. parvulus* (LC717554, LC579254), *L. punctilineatus* (LC677209–LC677214), *L. sp. 8* (LC774564, LC772867), *L. sp. 9* (LC499443, LC579355), *L. sp. 10* (LC499449, LC579264), *L. sp. 11* (LC579262, LC579278), *L. sp. 12* (LC579265), *L. sp. 13* (LC499441, LC579281), *L. sp. 14* (LC499442, LC499450), *L. sp. 15* (LC579275, LC579349), *L. sp. 16* (LC722561, LC722563) were downloaded from GenBank (12S sequence of *L. adapel* is not available). A single sequence of *Inu koma*

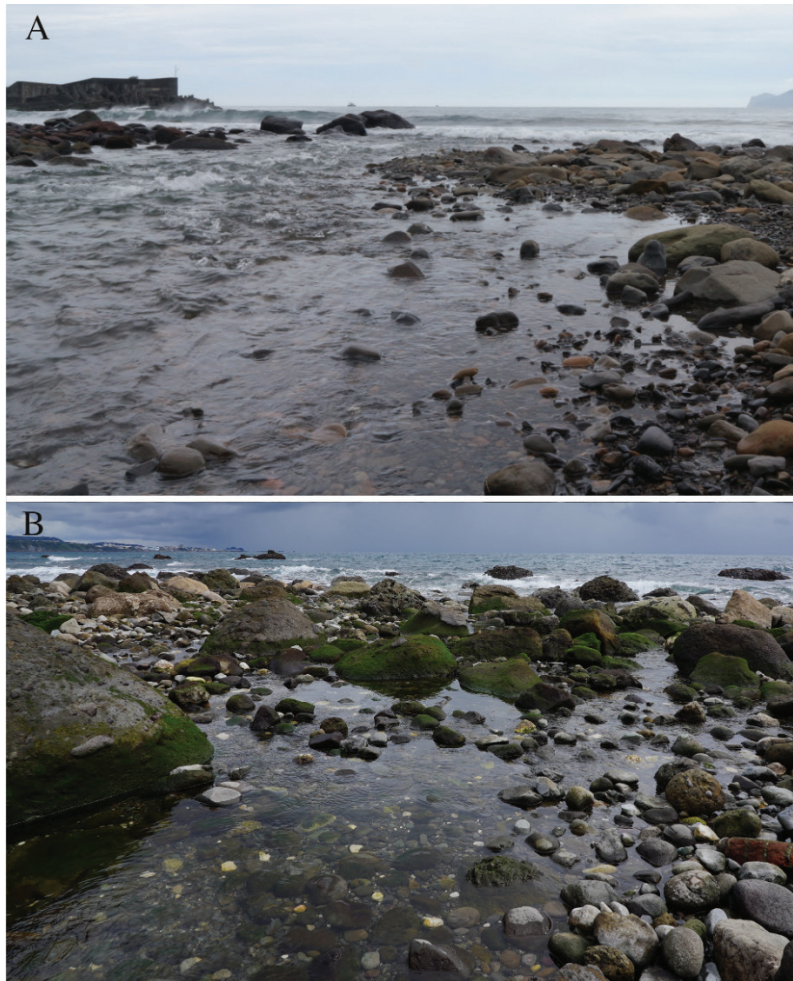


Figure 2. Habitats of *Luciogobius opisthoproctus* sp. nov. **A** river mouth of the Daxi Creek, Yilan County, Taiwan **B** river mouth of the Babian Creek, Taitung County, Taiwan.

(LC579243) was used as an outgroup for tree rooting. Sequences were aligned using MUSCLE (Edgar 2004) alignment in SeqMan v. 11.1.0, and substitution saturation of all sequences was tested using DAMBE v. 6.3.17 (Xia and Xie 2001). The Tamura-3 + G model was selected to reconstruct a maximum-likelihood (ML) tree (Felsenstein 1981) using MEGA v. X (Kumar et al. 2018) with a 1,000 replicates bootstrapping estimation for branch supports. The pairwise distance (p -distance) between each pair of the species was calculated using the Kimura 2-parameter (K2P) model in MEGA v. X (Kumar et al. 2018).

Results

Luciogobius opisthoproctus sp. nov.

<https://zoobank.org/D65F19DD-CC3D-486F-BBC7-7DE41D55226E>

Figs 3–5

New English name: Taiwan Earthworm Goby

Holotype. ASIZP0081790, 25.8 mm SL, TAIWAN, Yilan County, mouth of Daxi Creek, 24°56.48'N, 121°53.72'E, coll. K.H. Chen, 16 February 2023.

Paratypes. 17 specimens (20.6–28.1 mm SL). ASIZP0081791, 22.9 mm SL, ASIZP0081792, 22.9 mm SL, ASIZP0081793, 23.8 mm SL, DOS09993-1,

25.1 mm SL, DOS09993-2, 24.9 mm SL, DOS09993-3, 26.8 mm SL, DOS09993-4, 22.8 mm SL, DOS09993-5, 20.6 mm SL, DOS09993-6, 22.8 mm SL, NMMB-P39322, 22.7 mm SL, NMMB-P39323, 21.44 mm SL, NMMB-P39324, 21.8 mm SL, NMMB-P39325, 23.1 mm SL, NMMB-P39326, 27.5 mm SL, collected with holotype. ASIZP0081794, 27.3 mm SL, DOS09994-1, 24.3 mm SL, NMMB-P39327, 28.1 mm SL, TAIWAN, Taitung County, river mouth of Babian Creek, 23°04.44'N, 121°21.38'E, coll. K.H. Chen, 21 March 2023.

Diagnosis. *Luciogobius opisthoproctus* sp. nov. is diagnosed by the following combination of characters: total vertebrae 41–43; free pectoral-fin rays absent; second dorsal-fin rays 9–12 (usually 11); anal-fin rays 11–14 (11 or 12); pectoral-fin rays 8–12 (10 or 11); pelvic-fin length more than 50% of pectoral-fin length; AAA distance 4.2–7.2% (mean 5.7%) of SL, 72.1–129.7% (mean 99.9%) of body depth at anus; snout length 39.7–62.7% (mean 52.8%) of AAA distance; pre-anus distance 80.0–92.8% (mean 88.6%) of pre-anal-fin length; and anterior-most pterygiophore of anal fin inserted behind the second haemal spine (Fig. 5).

Description. Morphometric measurements and meristic counts are given in Table 1. Body elongate, anteriorly cylindrical, and posteriorly compressed. Head narrowly depressed. Anterior nostril a pair of short tubes; posterior nostril round. Lower jaw slightly projecting; mouth oblique; maxilla extends posteriorly to vertical at front margin of eye. Gill opening narrow, extending from middle of pectoral-fin base to level with posterior end of jaw. Interorbital space narrower than snout length, side compressed, anteriorly swollen. A longitudinal dermal ridge present from below anterior nostril extending to behind eye. Occipital region slightly turgid (swollen) dorsally and laterally. First dorsal fin absent. Origin of second dorsal fin slightly posterior to origin of anal fin. First and second rays of second dorsal fin spinous, remaining rays soft and segmented; posterior margin of second dorsal fin rounded; second dorsal-fin rays 9–12 [9 (3), 10 (5), 11 (8)*, 12 (2)] (* for the number including holotype). Anal fin slightly posterior to anus; first and second rays of anal fin spinous, remaining rays soft and segmented; posterior margin of anal fin rounded; anal fin rays 11–14 [11 (5), 12 (7)*, 13 (4), 14 (2)]. Pectoral-fin fan-shaped and free pectoral-fin rays absent, pectoral-fin relatively small, about 5.5–8.8% of SL; pectoral-fin rays 8–12 [8 (1), 9 (1), 10 (5)*, 11 (6), 12 (5)]. Caudal fin rounded. Pelvic fins round with frenum and complete membrane; pelvic-fin rays I, 5. Segmented caudal-fin rays 15–17 [15 (5), 16 (9), 17 (4)*]. First dorsal pterygiophore inserted between 25th and 26th vertebrae; last dorsal pterygiophore inserted between 31st and 32nd vertebrae; first anal fin pterygiophore inserted behind second haemal spine; insertion pattern not changing with numbers of fin rays; abdominal vertebrae 20–22 (usually 22), caudal vertebrae 20–22 (usually 21).

Cephalic sensory system. The series of cephalic sensory papillae on cheek are illustrated in Fig. 6. Row *a* situated behind eye, extending shortly upwards to orbital area. Row *b* extending from margin behind eye to upper lip. Row *c* starting from posterior of dermal ridge to anterior margin of eye. Single spot *cp* situated under row *c*. Row *d* starting from posterior margin of upper lip to anterior nostril. Row *e* extending from lower margin of preopercle to upper margin of lower jaw. Row *i* extending along weak flap on lower margin of lower jaw to lower part of preopercle. Row *f* in posterior of symphyseal flap on chin. Row *oi* longitudinal, row *ot* and *os* running vertically. Row *oi*, *os*, *ot* separated from each other.

Table 1. Morphometric measurements and meristic counts of *Luciogobius opisthroctus* sp. nov.

	Holotype	Paratypes	
		Daxi Creek (14)	Babian Creek (3)
Standard length (SL; mm)	25.4	20.6–27.5	24.3–28.1
Count			
D ₂ elements	11	9–12	9–11
A elements	12	11–14	11–13
P ₂ elements	6	6	6
P ₁ elements	10	8–12	10–12
C segmented elements	15	16–17	15–16
V	21+22	20–22+20–22	22+21
First D pterygiophore insertion	25–26	25–26	25–26
First A pterygiophore insertion behind	2 nd hs	2 nd hs	2 nd hs
Measurement (%SL)			
HL	14.1	12.7–18.7	13.4–16.6
HD	5.8	3.6–6.5	5.4–6.0
HW	7.1	5.4–8.8	6.8–7.4
SNL	3.1	2.5–3.4	2.6–3.0
IOW	2.9	1.5–2.9	1.7–2.6
BD at P ₂ origin	6	4.3–5.9	5.4–5.8
BD at AN	6.3	4.8–6.5	5.2–6.9
BD at A origin	6.4	4.9–6.3	5.0–6.5
PANL	66.4	60.5–66.4	63.2–65.0
AAA distance	6.6	4.2–7.2	5.0–6.3
CPD	6.6	3.9–5.9	4.1–5.0
CPL	15.8	12.6–16.8	13.2–16.4
PAL	73.8	68.9–73.5	70.0–72.6
PP ₂ L	15.7	15.6–19.0	14.9–16.0
D ₂ L	11	8.3–12.2	9.2–12.3
AL	14.7	10.8–16.5	9.2–13.5
P ₁ L	7.4	5.5–8.8	6.4–7.8
P ₂ L	4.3	3.8–6.1	4.2–5.2
CL	10.4	7.8–15.4	11.1–12.4
PD ₂ L	73.9	69.9–77.8	73.3–74.8
Measurement (% HL)			
HD	40.8	26.0–46.5	33.8–40.5
HW	50.6	39.5–65.3	40.7–52.9
SNL	22.1	16.2–24.8	15.6–20.4
ED	6.4	4.5–10.1	3.6–7.1
IOW	20.4	10.7–19.6	12.5–15.4
SNL (% AAA distance)	52.7	39.7–62.7	45.3–51.5
PANL (% PAL)	90	80.0–92.4	88.2–92.8
P ₂ L (% P ₁ L)	58.5	57.5–84.9	62.1–69.7
AAA distance (% BD at anus)	93.2	72.1–129.7	72.3–121.4

D₂: second dorsal-fin; A: anal-fin; P₂: pelvic-fin; P₁: pectoral-fin; C: caudal-fin; V: vertebrae; D: dorsal; hs: haemal spine; P₁L: pectoral-fin length; BD: body depth; AN: anus; PAL: pre-anal-fin length; AAA distance: distance between anus and anal-fin origin; CPD: caudal-peduncle depth; CPL: caudal-peduncle length; PP₂L: pre-pelvic-fin length; D₂L: second dorsal-fin length; AL: anal-fin length; P₁L: pectoral-fin length; P₂L: pelvic-fin length; CL: caudal-fin length; PD₂L: pre-second dorsal-fin length; PANL: pre-anus length; ED: eye diameter.

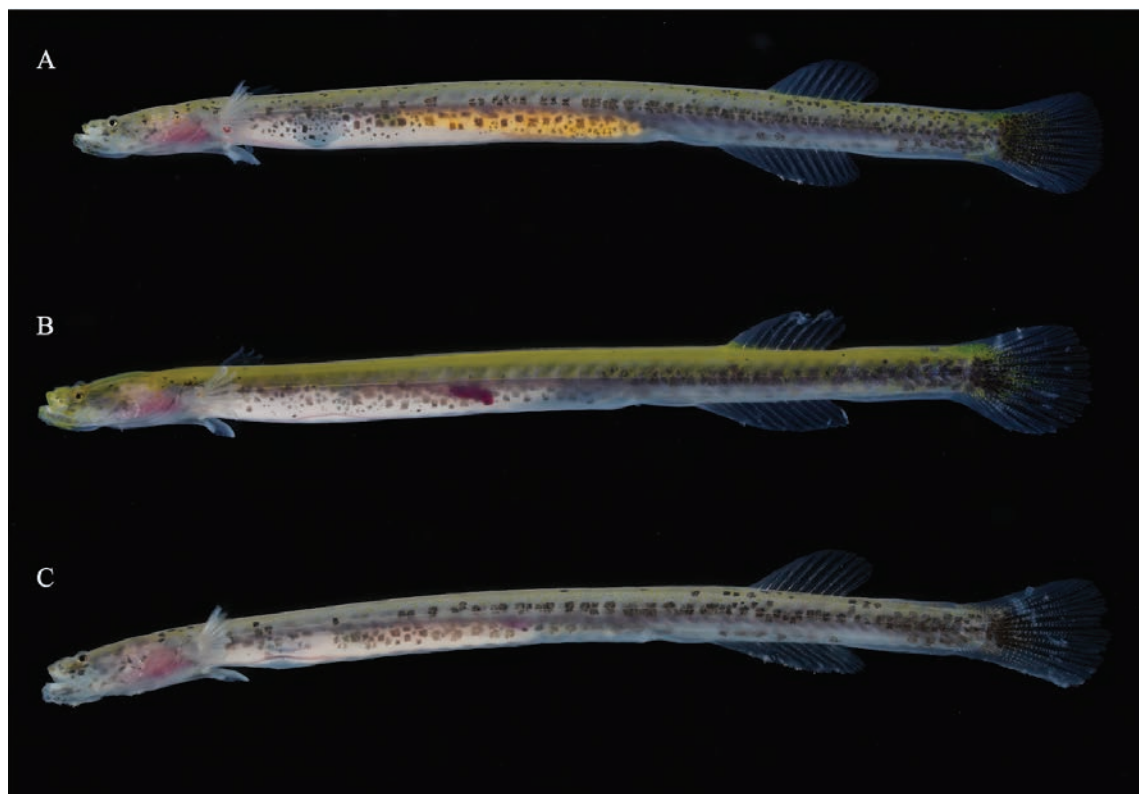


Figure 3. Fresh specimens of *Luciogobius opisthoproctus* sp. nov. **A** holotype, ASIZP0081790, 25.4 mm SL, Daxi Creek, Yilan County, Taiwan **B** paratype, ASIZP0081793, 23.8 mm SL, Daxi Creek, Yilan County **C** paratype, NMMB-P39322, 21.4 mm SL, Daxi Creek, Yilan County, Taiwan.



Figure 4. Live *Luciogobius opisthoproctus* sp. nov. NMMB-P39326, paratype, 27.5 mm SL, Daxi Creek, Yilan County, Taiwan.

Coloration. Body background white, dorsally yellowish, and translucent ventrally. A discontinuous row of black spots on side of body from pectoral-fin to caudal-fin base. Scattered black spots internally embedded in the abdomen and visible through the semi-transparent muscle. Scattered black spots on dorsal surface, highly dense in some individuals. Rays and membranes of dorsal-, pectoral-, pelvic-, and anal-fins transparent and yellowish at base. Caudal fin transparent, with a black, rounded blotch at base. Specimens preserved in 70% ethanol whitish, with the same pattern of black spots when alive.

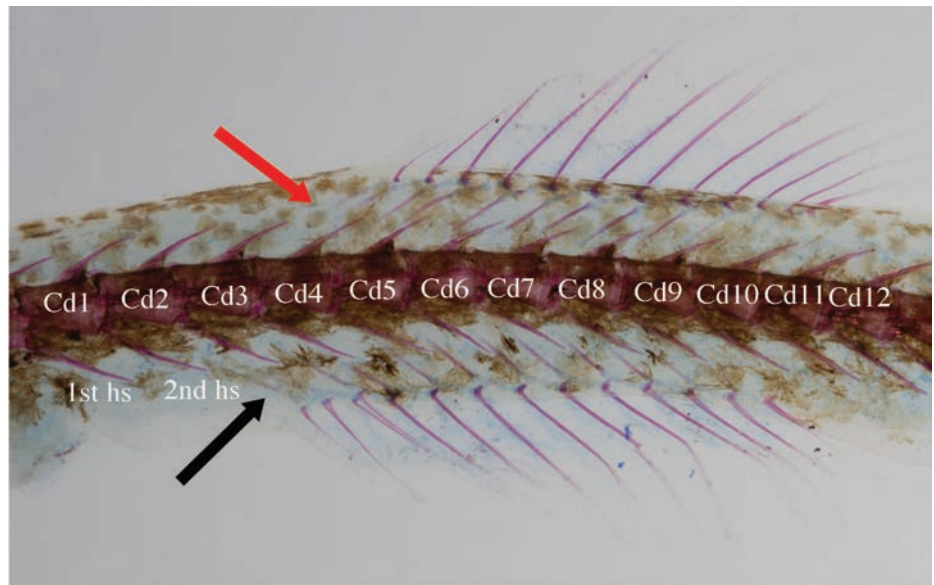


Figure 5. The alcian blue–alizarin red stained specimens of *Luciogobius opisthoproctus* sp. nov. DOS09993-2, paratype, 24.9 mm SL, Daxi Creek, Yilan County, Taiwan, coll. K.H. Chen, 16 February 2023. Cd indicates caudal vertebrae; Hs indicates haemal spine of caudal vertebrae. Both abbreviations are numbered. The red arrow indicates the first dorsal pterygiophore insertion; the black arrow indicates the first anal-fin pterygiophore insertion.

Distribution and habitat. The new species is currently only known from northeastern and southeastern Taiwan. This species mainly inhabits shallow gravel creeks near coastal river mouths.

Etymology. The specific name *opisthoproctus* is from the Greek words *opisthe* (behind) and *proktos* (anus), in allusion to the posteriorly positioned anus (shorter AAA distance).

Molecular analysis. Thirty-nine sequences (133 bp) from 14 species were obtained and used to reconstruct an ML tree (Fig. 7), with *Inu koma* as the outgroup. In the topology of the ML tree, a monophyletic clade consisting of *L. opisthoproctus* sp. nov. was revealed. *Luciogobius opisthoproctus* sp. nov. and *L. sp. 10* are sister species, and these two species are a sister group of a clade comprising *Luciogobius* spp. 8, 13, 14, 15, and 16. The genetic distances between the new species and other members of *L. elongatus* complex are shown in Table 2.

Remarks. Based on the morphological approach, *L. opisthoproctus* sp. nov. belongs to the *L. elongatus* complex (Shibukawa et al. 2019) because of the following characters: absence of free pectoral-fin rays, AAA 72.1–129.7% of body depth at anus, vertebrae 41–43, anterior pleural attaching to third abdominal vertebra, first anal-fin pterygiophore inserted behind second haemal spine, and first to second rays of dorsal- and anal-fin unbranched and spine-like. The new species is most similar to *L. punctilineatus* and *L. sp. 11* in having yellowish coloration, a black blotch on the caudal-fin, a longitudinal line composed of scattered black spots on the sides of body, and similar numbers of dorsal-, anal-, pectoral-fin elements. However, *L. opisthoproctus* sp. nov. can be distinguished from *L. punctilineatus* and *L. sp. 11* by the shorter AAA distance (4.2–7.2% SL vs 11.4–16.9% in *L. punctilineatus*; 9.1–10.4% in *L. sp.11*); longer pre-anus length (80.0–92.8% of pre-anal-fin length vs 75.0–82.0% in *L. punctilineatus*;

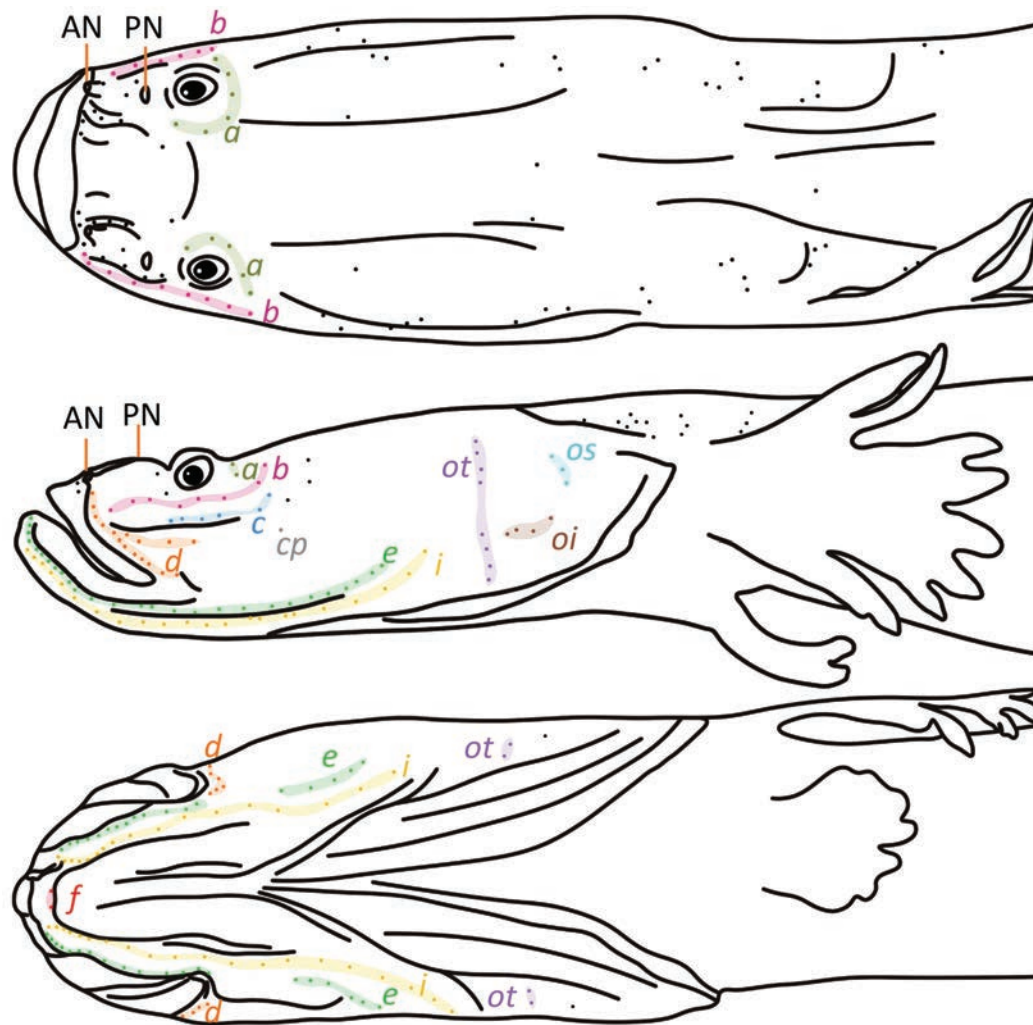


Figure 6. Head cephalic sensory system of *Luciogobius opisthoproctus* sp. nov. ASIZP0081790, holotype, 25.4 mm SL, Daxi Creek, Yilan County, Taiwan. AN, Anterior nostril; PN, Posterior nostril. Color-marked spots with letters indicate the papillae and the name of each row.

84.4–88.8% in *L. sp.11*); longer snout length (39.7–62.7% of AAA distance vs <34.7% in *L. punctilineatus*; 36.7–44.8% in *L. sp.11*); more abdominal vertebrae (20–22 vs 16–18 in *L. punctilineatus*; 17–18 in *L. sp.11*); fewer caudal vertebrae (20–22 vs 22–24 in *L. punctilineatus*; 22–25 in *L. sp.11*); first anal fin pterygiophore usually inserted behind the second haemal spine (vs fifth in *L. punctilineatus*; fourth in *L. sp.11*) (Table 3). The new species can be further distinguished from *L. punctilineatus* in having the AAA distance less than twice the body depth at the anus (vs about twice of the body depth at anus).

Based on the molecular analysis, the topology showed that there is a sister-species relationship between the new species and *L. sp. 10*. However, *L. opisthoproctus* sp. nov. can be distinguished from *L. sp. 10* (Table 3) in having a smaller HL (12.7–18.7% vs 19.5–19.7% SL), more abdominal vertebrae (20–22 vs 14) and more total vertebrae (41–43 vs 36) (Table 4). *Luciogobius opisthoproctus* sp. nov. can be easily distinguished from *L. adapel* and *L. parvulus* by the presence of a pelvic fin (vs absence) and further distinguished from *L. adapel* by the presence of a second dorsal and anal fin (vs absence); from *L. elongatus*, *L. sp. 8*, and *L. sp. 9* by more dorsal-fin rays (9–12 vs usually less

Table 2. Pairwise sequence differences (%: *p*-distance) of 133 bp of 12S ribosomal RNA gene among species of *Luciogobius elongatus* complex. The hyphen “–” indicates that only one sequence is available.

		1	2	3	4	5	6	7	8	9	10	11	12	13	14
1	<i>L. opisthoproctus</i> sp. nov. (8)	0–0.8													
2	<i>L. elongatus</i> (5)	5.9–7.6	0–1.8												
3	<i>L. parvulus</i> (2)	15.1–16.0	12.6–14.3	0											
4	<i>L. punctilineatus</i> (6)	5.9–7.6	4.2–6.7	1.2–1.3	0–1.7										
5	<i>L. sp. 8</i> (2)	5.9–6.7	4.2–5.9	1.3	4.2–5.9	0									
6	<i>L. sp. 9</i> (2)	4.2–17.6	4.2–5.0	13.4–14.3	4.2–5.0	7.6	0								
7	<i>L. sp. 10</i> (2)	4.2–17.6	5.0–7.6	12.6	5.0–7.6	5.0	7.6	1.7							
8	<i>L. sp. 11</i> (2)	4.2–5.9	2.5–3.4	12.6	2.5–3.4	4.2	3.4	1.7–4.2	0						
9	<i>L. sp. 12</i> (1)	12.6–13.4	11.8–13.4	6.7	11.8–13.4	11.8	13.4	10.9–12.6	10.1	–					
10	<i>L. sp. 13</i> (2)	4.2–17.6	3.4–4.2	14.3	3.4–4.2	3.4	6.7	5.0–5.9	3.4	12.6	0				
11	<i>L. sp. 14</i> (2)	5.0–8.4	5.9–6.7	14.3	5.9–6.7	5.0	9.2	5.6–6.7	5.9	13.4	4.2	0			
12	<i>L. sp. 15</i> (2)	8.4–9.2	5.0–5.9	14.3	5.0–5.9	5.9	8.4	6.7–7.6	5.0	13.4	5.0	8	0		
13	<i>L. sp. 16</i> (2)	6.7–7.6	5.0–5.9	14.3	5.0–5.9	4.2	8.4	5.0–5.9	5.0	13.4	3.4	1.7	2.5	0	
14	<i>I. koma</i> (1)	16.8–17.6	16.8–18.5	17.6	16.0–16.8	16.0	18.5	17.6–18.5	16.8	16.8	16.0	1.6	15.1	16.0	–

Numbers in paracenteses for numbers of sequences.

than 9) and anal-fin rays (11–14 vs usually less than 11), and further distinguished from *L. elongatus* and *L. sp. 9* by presence of a well-developed frenum on the pelvic fin (vs absence). The new species can also be distinguished from *Luciogobius* spp. 12–16 by absence of free pectoral-fin rays (vs presence). It can be further distinguished from *L. sp. 12* and *L. sp. 13* by having more vertebrae in total (41–43 vs 38–39), and from *Luciogobius* sp. 14–16 by presence of a black blotch on the caudal-fin (vs absence) (Table 4). *Luciogobius* sp. 3 (sensu Maeda et al. 2008) is also similar to *L. opisthoproctus* sp. nov. in coloration, morphometric measurements, and meristic counts. However, due to the limited information from only one juvenile provided by Maeda et al., further study is needed to verify the relationship of these species. Species within the *L. elongatus* species complex, as defined by Shibukawa et al. (2019), exhibit a unique combination of characters that differentiate them from species in other complexes. However, the presence of a single free pectoral-fin ray of *L. parvulus* and *L. spp. 12–16* of the *L. elongatus* complex is not constant. This trait is apparently not a reliable character to distinguish *L. elongatus* complex from *L. guttatus* complex (vs presence of a free pectoral-fin ray).

Luciogobius opisthoproctus sp. nov. sometimes co-occurs with *L. grandis* Arai, 1970 and *L. guttatus* Gill, 1859 near the mouths of streams. However, *L. opisthoproctus* sp. nov. can be morphologically distinguished by its yellowish body color, differing from the bronze color in *L. grandis* and the brown color in *L. guttatus* (Fig. 8). Additionally, it can also be readily distinguished from other two species by several distinctive features, such as a transparent caudal fin with one black blotch on its base (vs opaque), a pair of fan-shaped pectoral-fin (vs triangular in *L. grandis* and round in *L. guttatus*), absence of pigmentation on pectoral-, anal-, and second dorsal fins (vs presence), and unbranched first to second rays of dorsal- and anal-fins (vs only first ray unbranched).

Table 3. Morphometric measurements and meristic counts between *Luciogobius opisthoproctus* sp. nov. and three morphologically similar species.

	<i>L. opisthoproctus</i> sp. nov. ¹	<i>L. punctilineatus</i> ²	<i>L. sp. 10</i> ³	<i>L. sp. 11</i> ²
Ab V	20–22	16–18	14	17–18
Cd V	20–22	22–24	22	22–25
First A pterygiophore insertion behind	2 nd hs	4–6 (5) th hs	N/A	4 th hs
Measurement				
HL (% SL)	12.7–18.7% (14.5%)	12.7–16.6% (N/A)	19.5–19.7% (N/A)	N/A
AAA distance (% SL)	4.2–7.2% (5.7%)	11.4–16.9% (13.3%)	N/A	9.1–10.4% (9.6%)
AAA distance (% BD at AN)	72.1–129.7% (99.9%)	Twice BD	N/A	N/A
SNL (% AAA)	39.7–62.7% (52.8%)	19.2–34.7% (26.4%)	N/A	36.7–44.8% (40.9%)
PANL (% PAL)	80.0–92.8% (88.6%)	75.0–82.0% (79.3%)	N/A	84.4–88.8% (86.1%)
P ₂ L (% P ₁ L)	57.5–84.9 (69.4%)	42.2%*	N/A	N/A
Reference	Present study	Koreeda et al. 2022	Shibukawa et al. 2019	Koreeda et al. 2022

* Indicates only one specimen is available. N/A: not available. Abbreviation: Ab V: abdominal vertebrae; Cd V: caudal vertebrae; A: anal fin; hs: haemal spine; HL: head length; SL: standard length; AAA distance: distance between anus and anal-fin origin; BD: body depth; AN: anus; SNL: snout length; PANL: pre-anus length; PAL: pre-anal-fin length; P₁L: pectoral-fin length; P₂L: pelvic-fin length. 1 for present study; 2 for Koreeda et al. 2022; 3 for Shibukawa et al. 2019.

Table 4. Selected characters of the species of *Luciogobius elongatus* complex.

	D ₂ element	A element	P ₁ element	Ab V	Cd V	V	Free P ₁ rays	P ₂	P ₂ frenum	Sources
<i>L. adapel</i>	Absent	Absent	9–10	23	26–27	49–50	Absent	Absent	ND	1
<i>L. opisthoproctus</i> sp. nov.	9–12	11–14	8–12	20–22	20–22	41–43	Absent	Present	W-D	2
<i>L. elongatus</i>	6–9	8–10	7–10	19–21	21–23	42–44	Absent	Present	ND	3
<i>L. parvulus</i>	10–12	11–13	11–13	19–21	22–24	41–44	Present*	Absent	ND	4
<i>L. punctilineatus</i>	10–12	12–14	8–12	16–18	22–24	39–42	Absent	Present	W-D	4
<i>L. sp. 3</i>	8–10	11–12	9–10	21–23	19–21	42	Absent	Present	W-D	5
<i>L. sp. 8</i>	7–8	8–10	9–11	20–21	20–23	41–43	Absent	Present	W-D	3
<i>L. sp. 9</i>	7–9	8–11	8–10	20–22	21–23	42–45	Absent	Present	ND	3
<i>L. sp. 10</i>	8	11	11–12	14	22	36	Absent	Present	W-D	3
<i>L. sp. 11</i>	12–13	14–15	8–9	17–18	22–25	40–43	Absent	Present	W-D	3
<i>L. sp. 12</i>	10–12	10–11	14	18–19	20–21	38–39	Present	Present	W-D	3
<i>L. sp. 13</i>	9–11	12–13	13–15	16–17	21–23	38–39	Present	Present	W-D	3
<i>L. sp. 14</i>	10–13	12–15	12–14	19–21	21–23	41–43	Present	Present	W-D	3
<i>L. sp. 15</i>	11–13	13–14	11–14	18–20	21–23	39–42	Present	Present	W-D	3
<i>L. sp. 16</i>	11–13	12–14	10–13	20–21	22–23	22–23	Present*	Present	W-D	3

Abbreviation: D₂: second dorsal-fin; A: anal-fin; P₁: pectoral-fin; P₂: pelvic-fin; Ab V: abdominal vertebrae; Cd V: caudal vertebrae; V: vertebrae; ND: not developed; W-D: well-developed. *=sometimes absent. 1 for Okiyama, 2001; 2 for present study; 3 for Shibukawa et al. 2019; 4 for Koreeda and Motomura 2021; 5 for Maeda et al. 2008.

Comparative material. *L. elongatus*: one specimen, OMNH-P14170, 37.1 mm SL, Nagasaki Coast, Fuke, Misaki, Sennan, Osaka, Japan, coll. Kanai, M., 27 May 2001. *L. grandis*: ten specimens, DOS09990, 30.5–54.1 mm SL, Hualien River, Hualien County, Taiwan, coll. K. H. Chen, 31 January 2022. *L. guttatus*: ten specimens, DOS09988, 38.4–58.7 mm SL, Jinhukun, Yilan County, Taiwan, coll. K.H. Chen, 10 August 2021.

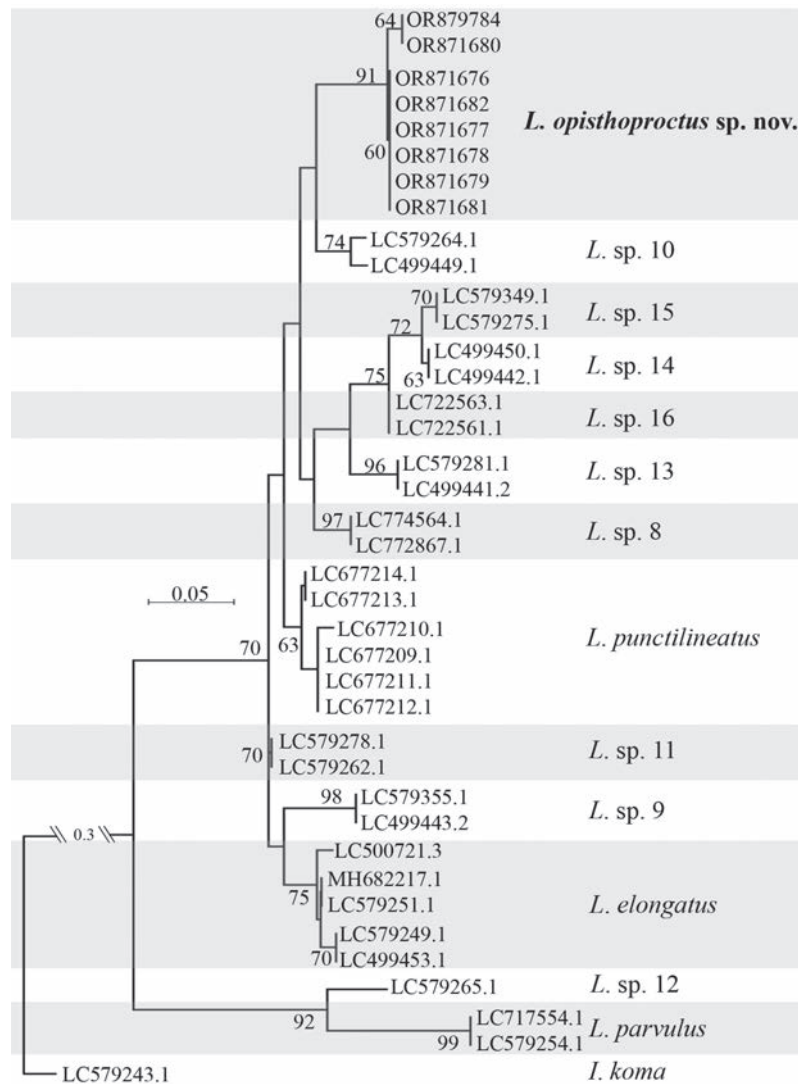


Figure 7. Maximum-likelihood (ML) tree based on 12S ribosomal RNA gene sequences (133 bp) using Tamura-3+G model with 1,000 bootstrap replications. Numbers of branches indicate bootstrap values higher than 60%.



Figure 8. Photos of fresh specimens coexisting with *Luciogobius opisthoproctus* sp. nov. **A** *L. grandis*, DOS09990-2, 53.7 mm SL, Hualien River, Hualien County, Taiwan **B** *L. guttatus*, DOS09988-1, 54.7 mm SL, Jinghukun, Yilan County, Taiwan.

Acknowledgements

We would like to express our gratitude to Wen-Chien Huang and Wei-Cheng Jhuang (NSYSU) for their valuable comments on the manuscript; Rodulf Anthony Balisco (NSYSU) for his assistance in English editing; Shih-Pin Huang (ASIZP) and Po-Na Lee (NMMB-P) for their curatorial assistance; Shoko Matsui (OMNH-P) provided the comparative material. Additionally, our sincere appreciation to the editors and reviewers for their dedication and effort in improving this article.

Additional information

Conflict of interest

The authors have declared that no competing interests exist.

Ethical statement

No ethical statement was reported.

Funding

This study is supported by National Science and Technology Council (112-2321-B-110-003).

Author contributions

K.H. Chen and T.Y. Liao conceptualized, drafted, and edited the manuscript; K.H. Chen collected, photographed, and analyzed the specimens.

Data availability

All of the data that support the findings of this study are available in the main text.

References

- Chen I-S, Suzuki T, Senou H (2008) A new species of gobiid fish, *Luciogobius* from Ryukyus, Japan (Teleostei: Gobiidae). *Journal of Marine Science and Technology* 16(4): 250–254. <https://doi.org/10.51400/2709-6998.2005>
- Cho HG, Choi SH (2014) First record of two gobiid fishes, *Luciogobius elongatus*, *L. platycephalus* (Perciformes: Gobiidae) from Korea. *Animal Systematics, Evolution and Diversity* 30(1): 22–25. <https://doi.org/10.5635/ASED.2014.30.1.022>
- Dingerkus G, Uhler LD (1977) Enzyme clearing of alcian blue stained whole small vertebrates for demonstration of cartilage. *Stain Technology* 52(4): 229–232. <https://doi.org/10.3109/10520297709116780>
- Edgar RC (2004) MUSCLE: Multiple sequence alignment with high accuracy and high throughput. *Nucleic Acids Research* 32(5): 1792–1797. <https://doi.org/10.1093/nar/gkh340>
- Felsenstein J (1981) Evolutionary tree from DNA sequences: A maximum likelihood approach. *Journal of Molecular Evolution* 17(6): 368–376. <https://doi.org/10.1007/BF01734359>
- Gill TN (1859) Notes on a collection of Japanese fishes, made by Dr. J. Morrow. *Proceedings. Academy of Natural Sciences of Philadelphia* 11: 144–150.
- Kondo K, Kato M (2018) Life in coastal pebble sediment: unique interstitial organism community and selective feeding on meiobenthos by interstitial fishes (*Luciogobius*: Gobiidae). *bioRxiv*. <https://doi.org/10.1101/499194>

- Koreeda R, Motomura H (2021) Records of seven temperate and subtropical species of *Luciogobius* from Shimokoshi-shima island, Koshiki Islands, East China Sea, Japan, and the first record of the possible hybrid individuals for *Luciogobius*. *Ichthy. Natural History of Fishes of Japan* 11: 27–52.
- Koreeda R, Motomura H (2022) *Luciogobius punctilineatus* n. sp., a new earthworm goby from southern Japan. *Zootaxa* 5138(2): 137–151. <https://doi.org/10.11646/zootaxa.5138.2.2>
- Koreeda R, Furuhashi R, Yamashita R, Motomura H (2022) First records of *Luciogobius* sp. 16 sensu Shibukawa et al. (2019) from southern Kyushu and the Osumi Islands, Japan with the southernmost records from the latter for the species *Ichthy*. *Natural History of Fishes of Japan* 25: 13–26. [In Japanese]
- Kumar S, Stecher G, Li M, Knyaz C, Tamura K (2018) MEGA X: Molecular Evolutionary Genetics Analysis across Computing Platforms. *Molecular Biology and Evolution* 35(6): 1547–1549. <https://doi.org/10.1093/molbev/msy096>
- Lindberg GU, Krasnyukova ZV (1975) *Fishes of the Sea of Japan and adjacent territories of the Okhotsk and Yellow Sea*. Nauka Publishing, Moscow–Leningrad, 463 pp. [In Russian]
- Maeda K, Yamasaki N, Kondo M, Tachihara K (2008) Occurrence and morphology of larvae and juveniles of six *Luciogobius* species from Aritsu Beach, Okinawa Island. *Ichthyological Research* 55(2): 162–174. <https://doi.org/10.1007/s10228-007-0018-x>
- Miya M, Sato Y, Fukunaga T, Sado T, Poulsen JY, Sato K, Minamoto T, Yamamoto S, Yamanaka H, Araki H, Kondoh M, Iwasaki W (2015) MiFish, a set of universal PCR primers for metabarcoding environmental DNA from fishes: Detection of more than 230 subtropical marine species. *Royal Society Open Science* 2(7): 150088. <https://doi.org/10.1098/rsos.150088>
- Nelson JS, Grande TC, Wilson MVH (2016) *Fishes of the World: Fifth Edition*. Wiley, Hoboken, 707 pp. <https://doi.org/10.1002/9781119174844>
- Okiyama M (2001) *Luciogobius adapel*, a new species of gobiid fish from Japan. *Bulletin of the National Museum of Nature and Science. Series A, Zoology* 27(2): 141–149.
- Saruwatari T, Andrés López J (1997) Cyanine Blue: A Versatile and Harmless Stain for Specimen Observation. *Copeia* 840–841(4): 840. <https://doi.org/10.2307/1447302>
- Shibukawa K, Aizawa M, Suzuki T, Kanagawa N, Muto F (2019) Preliminary review of earthworm gobies of the genus *Luciogobius* (Gobiiformes, Oxudercidae) from Shizuoka Prefecture, Japan. *Bulletin of the Museum of natural and environmental History, Shizuoka* 12: 29–96. [In Japanese]
- Shibukawa K, Aizawa M, Suzuki T (2020) Comparative morphology, validity, and limits of the genus *Inu* Snyder, 1909 (Gobiiformes, Oxudercidae), with comments on the diversification of the related interstice-dwelling goby genera in Japan. *Bulletin of the Museum of natural and environmental History, Shizuoka* 13: 79–116. [In Japanese]
- Ta TT, Tran HD, Dinh LG, Nguyen MH, Tran TT, Ha LM (2021) Planktonic larvae of *Luciogobius* sp. (Gobiidae) in a tropical estuary. *Regional Studies in Marine Science* 48: 102068. <https://doi.org/10.1016/j.rsma.2021.102068>
- Xia X, Xie Z (2001) DAMBE: Software package for data analysis in molecular biology and evolution. *The Journal of Heredity* 92(4): 371–373. <https://doi.org/10.1093/jhered/92.4.371>
- Yamada T, Sugiyama T, Tamaki N, Kawakita A, Kato M (2009) Adaptive radiation of gobies in the interstitial habitats of gravel beaches accompanied by body elongation and excessive vertebral segmentation. *BMC Evolutionary Biology* 9(145): 1–14. <https://doi.org/10.1186/1471-2148-9-145>

A new species of the genus *Hebius* (Squamata, Natricidae) from Yunnan, China

Yu-Hao Xu^{1*}, Dian-Cheng Yang^{2*}, Yan-An Gong², Kai-Chen Ouyang¹, Shi-Yang Weng³, Jun-Dong Deng¹, Song Huang², Li-Fang Peng¹

¹ State Key Laboratory of Plateau Ecology and Agriculture, Qinghai University, Xining 810016, China

² Anhui Province Key Laboratory of the Conservation and Exploitation of Biological Resource, College of Life Sciences, Anhui Normal University, Wuhu 241000, China

³ Tibet Plateau Institute of Biology, Lhasa 850008, China

Corresponding authors: Li-Fang Peng (lifang@qhu.edu.cn); Song Huang (snakeman@ahnu.edu.cn)

Abstract

A new species of the genus *Hebius* Thompson, 1913 is described from Yingjiang County, Dehong Dai and Jingpo Autonomous Prefecture, Yunnan Province, China, based on molecular and morphological evidence. It can be distinguished from its congeners by the following set of characters: (1) dorsal scale rows 19–17–17, feebly keeled; (2) ventrals 146–151; (3) nasal complete, nostril in the middle of the nasal; (4) supralabials 9, the fourth to sixth in contact with the eye; (5) infralabials 10–11, the first 5 touching the first pair of chin shields; (6) preoculars 2; (7) postoculars 3; (8) temporals 3, arranged in two rows (1+2); (9) maxillary teeth 31, the last 4 slightly enlarged, without diastema; (10) tail comparatively long, TAL/TL ratio 0.334 in the male; (11) dorsolateral series of irregular orange or ochre yellow blotches, extending from the neck to the posterior part of the tail; and (12) venter pale orange, tips of ventrals with subrectangular black blotches. All *Hebius* specimens were strongly recovered as monophyletic, in which *Hebius taronensis* (Smith, 1940) and *Hebius venningi* (Wall, 1910) were monophyletic as sister to the Yingjiang County specimens. According to the *p*-distance of cytochrome *b*, the new species differs from its congeners by 9.7–15.4%.

Key words: Cyt *b*, *Hebius citrinoventer* sp. nov., keelback snake, molecular systematics, Natricinae, taxonomy, Yingjiang County



Academic editor: Minh Duc Le

Received: 24 March 2024

Accepted: 24 June 2024

Published: 9 July 2024

ZooBank: <https://zoobank.org/E5C4172E-FD09-48E2-A8EC-C5E109D9674D>

Citation: Xu Y-H, Yang D-C, Gong Y-A, Ouyang K-C, Weng S-Y, Deng J-D, Huang S, Peng L-F (2024) A new species of the genus *Hebius* (Squamata, Natricidae) from Yunnan, China. ZooKeys 1206: 255–274. <https://doi.org/10.3897/zookeys.1206.123841>

Copyright: © Yu-Hao Xu et al.

This is an open access article distributed under terms of the Creative Commons Attribution License (Attribution 4.0 International – CC BY 4.0).

Introduction

The natricine snake genus *Amphiesma* Duméril, Bibron & Duméril, 1854 long represented a genus of small- to medium-sized, semi-aquatic species, widely distributed from South to Southeast Asia (Guo et al. 2014; Zhou et al. 2019; David et al. 2021). Because of interspecific morphological similarities and lack of broader genetic and morphological sampling, the systematic conflict of this group at the genus and species levels long persists. Based on molecular characteristics, Guo et al. (2014) split the genus *Amphiesma* into three genera: *Amphiesma*; *Hebius* Thompson, 1913, which accounts for most of the species; and *Herpetoreas* Günther, 1860. Kizirian et al. (2018) found that the

* These authors have contributed equally to this work.

genera *Parahelicops* Bourret, 1934 and *Pararhabdophis* Bourret, 1934 were junior synonyms of *Hebius* which was also supported by Ren et al. (2018). The molecular data presented by Patel et al. (2023) revealed a new genus, *Sahyadriophis* Patel, Thackeray, Campbell & Mirza, 2023, in which *Hebius beddomei* (Günther, 1864) was included. In addition, the generic assignments of some species have also changed. For example, *Hebius xenura* (Wall, 1907) and *Hebius pealii* (Sclater, 1891) have been assigned to *Herpetoreas*, and *Hebius monticola* (Jerdon, 1853) has been assigned to *Amphiesma* (Kizirian et al. 2018; Ren et al. 2018; Das et al. 2020; Lalronunga et al. 2020; Ren et al. 2022; Patel et al. 2023).

Currently, there are 51 valid species in the genus *Hebius*, of which 26 are known to occur in China (Hauser et al. 2022; Li et al. 2022; Ma et al. 2023; Xu et al. 2023; Uetz et al. 2024). Furthermore, recent morphological and molecular phylogenetic analyses of *Hebius* have shown that the weak species delimitation within this genus may be due to underestimated diversity (Guo et al. 2014; Kizirian et al. 2018; Liu et al. 2018; Zhou et al. 2019; Hou et al. 2021).

Our morphological and molecular results support the presence of a new snake species, based on two specimens collected from Yingjiang County, Yunnan Province, China (Fig. 1) during field surveys in July 2023 and February 2024. The specimens could be identified as members of *Hebius* by having

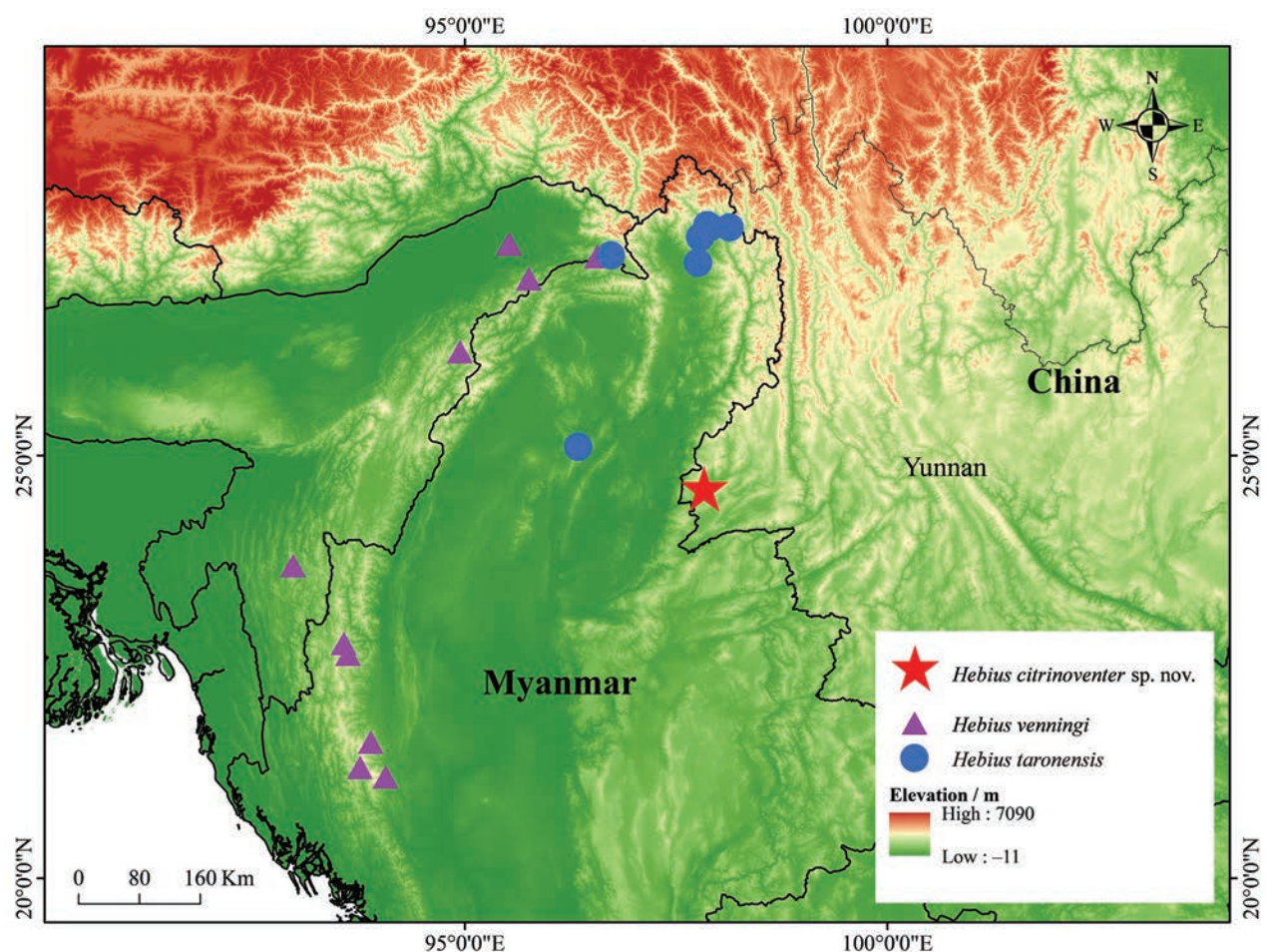


Figure 1. Distribution of selected species of the genus *Hebius*. Red star: *Hebius citrinoventer* sp. nov.; purple triangle: *H. venningi*; blue circle: *H. taronensis*.

the following combination of morphological characters: (1) 2 supralabials in contact with nasal; (2) maxillary teeth in a continuous series, gradually larger posteriorly in the series or the last two teeth abruptly enlarged, the diastema before the distinctly enlarged posterior maxillary teeth absent; (3) internasals broad anteriorly, nostrils lateral; and (4) color pattern usually comprising a dorso-lateral series of dark dots, forming two longitudinal stripes. However, these specimens could not be assigned to any known species (Guo et al. 2014; Ren et al. 2018). Furthermore, molecular analyses also revealed that the Yingjiang County specimens differed from those of other congeners.

Material and methods

Sampling

One drowned adult female and one road-killed subadult male specimens were collected from Yingjiang County, Dehong Dai and Jingpo Autonomous Prefecture, Yunnan Province, China. Sex was determined by tail dissection. Liver tissues were extracted and preserved in 95% ethanol. The specimens were preserved in 75% ethanol, and deposited in the Anhui Normal University Museum (ANU) and Qinghai University Museum (QHU). All sampling and procedures involving snake specimens were performed in accordance with the Wild Animals Protection Law of the People's Republic of China and approved by the Institutional Ethics Committee of Anhui Normal University (protocol code AHNU-ET2021025) and Qinghai University (protocol code SL-2023028).

Molecular phylogeny

Total genomic DNA was extracted from ethanol-preserved liver tissues using the QIAamp DNA Mini Kit (QIAGEN, Changsheng Biotechnology Co. Ltd., Changchun, China). We amplified the fragments of cytochrome *b* (Cyt *b*) by the Polymerase Chain Reaction (PCR), using the primers L14910 (5'-GAC CTG TGA TMT GAA AAC CAY CGT TGT-3') and H16064 (5'-CTT TGG TTT ACA AGA ACA ATG CTT TA-3') (Burbrink et al. 2000). The PCR products were sequenced by Shanghai Map Biotech Co., Ltd. (Shanghai, China). The raw sequences were stitched using SeqMan in the DNASTAR software package (Burland 2000) and the newly generated sequences were submitted to GenBank (accession numbers: PP472750, ANU20230016; PP429724, QHU2024005).

For phylogenetic analysis, 56 sequences were selected (Table 1), among which 54 (No. 3–56) were obtained from the National Center for Biotechnology Information (NCBI), including 51 sequences from 31 *Hebius* species and three outgroups: *Trachischium monticola* (Cantor, 1839), *Herpetoreas platyceps* (Blyth, 1854), and *Herpetoreas burbrinki* Guo, Zhu, Liu, Zhang, Li, Huang & Pyron, 2014, and aligned using MEGA X software (Kumar et al. 2018). Tree inference was performed in IQ-TREE v. 1.6.12 (Nguyen et al. 2015) under the maximum likelihood (ML) model, and 5000 replicates of ultrafast bootstrap were used to estimate the Ultrafast Bootstrap Approximation (UFB) node support. The SH-like approximate likelihood ratio test (SH-aLRT) was conducted with 1000 replicates. In addition, we calculated the uncorrected pairwise distances (*p*-distances) using the MEGA X software (Kumar et al. 2018).

Table 1. GenBank accession numbers, localities, and voucher information for all specimens used in this study.

ID	Species name	Locality	Voucher	Cyt b	Reference
1	<i>Hebius citrinoverter</i> sp. nov.	Yingjiang, Yunnan, China	ANU20230016	PP472750	This study
2	<i>H. citrinoverter</i> sp. nov.	Yingjiang, Yunnan, China	QHU2024005	PP429724	This study
3	<i>H. andreae</i>	Khammouane, Laos	VNUF R.2017.25	MK253674	Ziegler et al. 2019
4	<i>H. annamensis</i>	Laos	FMNH 258637	OK315812	Deepak et al. 2022
5	<i>H. atemporalis</i>	Vietnam	ZMMU NAP-07877	OK315813	Deepak et al. 2022
6	<i>H. atemporalis</i>	Guangdong, China	GP 1626	KJ685680	Guo et al. 2014
7	<i>H. bitaeniatus</i> 1	Guangxi, China	GP 1940	KJ685688	Guo et al. 2014
8	<i>H. bitaeniatus</i> 2	Thailand	AUP-00062	OK315816	Deepak et al. 2022
9	<i>H. boulengeri</i>	Fujian, China	GP 2433	KJ685699	Guo et al. 2014
10	<i>H. boulengeri</i>	Guangdong, China	GP 1789	KJ685684	Guo et al. 2014
11	<i>H. chapaensis</i>	Lao Cai, Vietnam	VNMN 06102	MH778702	Ren et al. 2018
12	<i>H. chapaensis</i>	Lao Cai, Vietnam	VNMN 06103	MH778700	Ren et al. 2018
13	<i>H. clerki</i>	Pianma, Lushui, Yunnan, China	KIZ037714	MZ570478	Hou et al. 2021
14	<i>H. conelarus</i>	Miyakojimashi, Ryukyu, Japan	KUZ R18555	AB989258	Takuma and Toda 2016
15	<i>H. conelarus</i>	Miyakojimashi, Ryukyu, Japan	KUZ R20253	AB989268	Takuma and Toda 2016
16	<i>H. craspedogaster</i>	Guizhou, China	GP 1240	KJ685672	Guo et al. 2014
17	<i>H. deschauenseei</i>	Thailand	AUP-00182	OK315827	Deepak et al. 2022
18	<i>H. igneus</i>	Ha Giang, Vietnam	AMNH 148575	KJ685665	Guo et al. 2014
19	<i>H. ishigakiensis</i>	Ishigakishi, Ryukyu, Japan	KUZ R19251	AB989282	Takuma and Toda 2016
20	<i>H. ishigakiensis</i>	Taketomityo, Ryukyu, Japan	KUZ R33043	AB989292	Takuma and Toda 2016
21	<i>H. jingdongensis</i>	Jingdong, Yunnan, China	CIB 119044	OR285310	Ma et al. 2023
22	<i>H. johannis</i>	Yunnan, China	KIZ014484	MZ570479	Hou et al. 2021
23	<i>H. khasiensis</i>	Kachin state, Myanmar	CAS 221504	KJ685668	Guo et al. 2014
24	<i>H. khasiensis</i>	Kachin state, Myanmar	CAS 221525	KJ685669	Guo et al. 2014
25	<i>H. maximus</i>	Sichuan, China	GP 864	KJ685706	Guo et al. 2014
26	<i>H. maximus</i>	Sichuan, China	GP 2382	KJ685696	Guo et al. 2014
27	<i>H. metusia</i>	Shimian, Sichuan, China	KIZ05178	MZ570480	Hou et al. 2021
28	<i>H. metusia</i>	Sichuan, China	GP 871	KJ685707	Guo et al. 2014
29	<i>H. modestus</i>	Yunnan, China	CAS 234262	KJ685671	Guo et al. 2014
30	<i>H. modestus</i>	Diantan, Tengchong, Yunnan, China	KIZ037715	MZ570481	Hou et al. 2021
31	<i>H. octolineatus</i>	Kunming, Yunnan, China	KIZ026445	MZ570484	Hou et al. 2021
32	<i>H. octolineatus</i>	Kunming, Yunnan, China	KIZ03204	MZ570483	Hou et al. 2021
33	<i>H. optatus</i>	Guizhou, China	GP 1885	KJ685687	Guo et al. 2014
34	<i>H. cf. optatus</i>	Vinh Phuc, Vietnam	AMNH 147155	KJ685662	Guo et al. 2014
35	<i>H. popei</i>	Hainan, China	GP 2169	KJ685692	Guo et al. 2014
36	<i>H. popei</i>	Guizhou, China	GP 2386	KJ685697	Guo et al. 2014
37	<i>H. pryeri</i>	Tokunoshimacho, Ryukyu, Japan	KUZ R34044	AB989124	Takuma and Toda 2016
38	<i>H. pryeri</i>	Ryukyu, Japan	KUZ R34062	AB989126	Takuma and Toda 2016
39	<i>H. sangzhiensis</i>	Hunan, China	SYNU08070350	MK340763	Zhou et al. 2019
40	<i>H. sauteri</i>	Taiwan, China	GP 2549	KJ685701	Guo et al. 2014
41	<i>H. sauteri</i>	Guangdong, China	CIB 118516	OP937178	Li et al. 2022
42	<i>H. septemlineatus</i>	Diantan, Tengchong, Yunnan, China	KIZ037706	MZ570485	Hou et al. 2021
43	<i>H. septemlineatus</i>	Zizhi, Tengchong, Yunnan, China	KIZ037720	MZ570486	Hou et al. 2021
44	<i>H. taronensis</i>	Myanmar	GP 1618	KJ685679	Guo et al. 2014
45	<i>H. taronensis</i>	Myanmar	CAS 224426	OK315828	Deepak et al. 2022
46	<i>H. venningi</i>	KaChin state, Myanmar	CAS 233206	KJ685670	Guo et al. 2014
47	<i>H. vibakari</i>	Liaoning, China	GP 1345	KJ685676	Guo et al. 2014
48	<i>H. vibakari</i>	Heilongjiang, China	GP 1352	KJ685677	Guo et al. 2014
49	<i>H. weixiensis</i>	Weixi, Yunnan, China	KIZ035740	MZ570488	Hou et al. 2021
50	<i>H. weixiensis</i>	Lijiang, Yunnan, China	HSR19088	OQ085074	Xu et al. 2023
51	<i>H. yanbianensis</i>	Yanbian, Sichuan, China	GP 4006	MH532291	Liu et al. 2018
52	<i>H. yanbianensis</i>	Binchuan, Yunnan, China	CIB5334220120	OR215499	Ma et al. 2023
53	<i>H. youjiangensis</i>	Baise, Guangxi, China	ANU20220010	OQ085073	Xu et al. 2023
Out group					
54	<i>Herpetoreas burbrinki</i>	Tibet, China	YBU 071128	GQ281781	Guo et al. 2014
55	<i>H. platyceps</i>	Tibet, China	GP 2096	KJ685690	Guo et al. 2014
56	<i>Trachischium monticola</i>	Tibet, China	GP 1487	JQ687435	Guo et al. 2014

Morphological examination

Morphological characters were described for the newly collected specimen and compared with other key references (Günther 1875; Wall 1910; Wall 1925; Bourret 1934; Taylor 1934; Gressitt 1937; Smith 1940; Dowling 1951a, 1951b; David and Das 2003; Zhao 2006; David and Vogel 2010; Guo et al. 2014; Liu et al. 2018; Ren et al. 2018; Purkayastha and David 2019; Zhou et al. 2019; Ziegler et al. 2019; David et al. 2021; Huang 2021; Hou et al. 2021; Hauser et al. 2022; Li et al. 2022; Ma et al. 2023; Xu et al. 2023). The measurements and scale counts followed those of Dowling (1951a, 1951b), Zhao (2006), and Huang (2021). A ruler with 1 mm accuracy was used to measure the snout-vent length (**SVL**), measured from the tip of the snout to the anterior edge of the vent; tail length (**TAL**), measured from the anterior edge of the vent to the tip of the tail; and total length (**TL**), defined as the sum of the SVL and TAL. All other measurement characteristics were measured to the nearest 0.01 mm using digital calipers: head length (**HL**), measured from the tip of the snout to the posterior margin of the mandible; head width (**HW**), measured from the widest part of the head in dorsal view; and eye diameter (**ED**), measured from the most anterior corner of the eye to the most posterior corner. Scapulation features and their abbreviations are as follows: supralabials (**SL**); infralabials (**IL**); loreals (**LOR**); preoculars (**PRO**); postoculars (**PO**); Chin; infralabials touching the first pair of chin shields (**IFL-1st Chin**); temporals (**TEMP**); supraoculars (**SPO**); and three dorsal scale row (**DSR**) counts: 1) counting from one head length behind the head, 2) at midbody (namely at SVL/2), and 3) at one head length before the vent; ventral scales (**VS**); cloacal plate (**CP**); and subcaudal (**SC**). In addition, we also examined the number of maxillary teeth (**MT**).

Results

Phylogenetic relationships

The ML tree was reconstructed from a fragment of the mitochondrial Cyt *b* gene (Fig. 2). Due to the poor quality at both ends of the newly generated sequences, we cut the sequences to obtain a final length of 725 base pairs (bp). All *Hebius* specimens clustered into one monophyletic group with strong supports (SH 97 / UFB 100). *Hebius taronensis* (Smith, 1940) and *H. venningi* (Wall, 1910) were grouped together (SH 100 / UFB 100), forming a sister clade to specimens from Yingjiang County (SH 82 / UFB 93), then clustering with *H. septemlineatus* (Schmidt, 1925), *H. weixiensis* Hou, Yuan, Wei, Zhao, Liu, Wu, Shen, Chen, Guo & Che, 2021, and the specimen AUP-00062 that was once identified as *H. bitaeniatus* (Wall, 1925). Regarding *p*-distance, the new species differed from its congeners by 9.7% (with *H. venningi*) to 15.4% (with *H. popei* (Schmidt, 1925)) (Table 2), which strongly suggests that the newly collected specimens have distinct genetic differentiation from their congeners. Moreover, morphological data supported the recognition of specimens from Yingjiang County as distinct from all other described species of *Hebius*. Thus, we describe the unnamed specimens as a new species.

Table 2. Uncorrected *p*-distances (%) among the *Hebius* species based on partial mitochondrial Cyt *b* gene.

ID	Species	1-2	3	4	5-6	7	8	9-10	11-12	13	14-15	16	17	18	19-20	21	22
1-2	<i>H. citrinoventer</i> sp. nov.	1.3															
3	<i>H. andreeae</i>	16.5-16.9	-														
4	<i>H. annamensis</i>	14.2-14.5	12.7	-													
5-6	<i>H. atemporalis</i>	12.5-13.7	14.2-15.2	12.5-12.7	6.1												
7	<i>H. bitaeniatus</i> 2	10.0	15.9	12.7	10.7-11.0	-											
8	<i>H. bitaeniatus</i> 1	11.0-11.4	13.7	10.9	9.4-10.5	10.2	-										
9-10	<i>H. boulengeri</i>	13.7-14.5	16.2-16.4	12.2-12.4	11.7-12.2	10.4-10.7	10.4-10.5	1.2									
11-12	<i>H. chapaensis</i>	12.9-13.2	12.7	5.7	11.0-11.4	12.2	10.5	12.0-12.2	0								
13	<i>H. clerki</i>	13.7-14.0	15.5	12.2	10.4-12.2	12.7	11.5	10.5-10.7	11.0	-							
14-15	<i>H. conelarum</i>	14.7-15.0	18.5	14.5	14.0-14.7	13.9	12.9	13.4-13.9	14.0	15.0	0						
16	<i>H. craspedogaster</i>	11.4-11.7	14.7	11.0	9.4-11.2	11.5	3.5	11.2-11.4	10.9	12.0	14.4	-					
17	<i>H. deschauenseel</i>	12.9-13.0	13.4	7.9	12.2-12.5	13.4	11.0	13.2-13.4	6.0	12.4	14.7	11.5	-				
18	<i>H. igneus</i>	13.2-13.4	12.5	5.7	11.4-11.5	12.5	10.9	12.9-13.0	9	11.5	14.5	11.2	5.7	-			
19-20	<i>H. ishigakiensis</i>	12.9-13.2	17.0	12.4	12.0-12.2	12.4	12.2	11.9-12.0	12.5	11.9	12.5	13.2	13.5	12.9	0		
21	<i>H. jingdongensis</i>	11.2-11.5	13.0	10.9	9.9-10.2	10.5	7.4	9.2-9.7	10.5	11.4	13.9	8.5	10.5	10.5	12.2	-	
22	<i>H. johannis</i>	10.4-10.7	14.2	9.7	10.4-10.5	11.0	4.8	10.5-10.7	9.7	11.4	12.9	5.3	11.5	10.2	12.9	9.9	-
23-24	<i>H. khasiensis</i>	14.9-15.2	15.7-16.5	12.4-12.9	11.4-12.7	12.2-12.4	10.7-11.2	7.5-8.0	12.0-12.2	12.2-12.4	14.0-14.4	11.2-11.5	13.0	12.7-13.0	12.9-13.4	9.5-10.7	11.7
25-26	<i>H. maximus</i>	13.9-14.4	13.0-13.2	12.7-13.4	11.2-13.2	12.0-12.2	10.4-10.7	13.2-13.7	11.9	13.0-13.4	14.5-14.9	11.0-11.4	11.7-11.9	11.9-12.0	12.0-12.7	11.9-12.2	12.5-12.7
27-28	<i>H. metusia</i>	10.9-11.4	13.5-13.7	10.2-10.7	9.7-9.9	9.7-10.0	2.8-3.5	10.5-11.2	10.2	11.5-11.7	13.2-16.0	4.7	10.5-10.7	10.4-10.5	12.5-12.7	7.5-8.4	4.5-4.8
29-30	<i>H. modestus</i>	14.2-15.2	13.4-14.2	6.7-7.0	12.0-13.5	13.4-13.7	12.5-12.9	13.5-14.2	5.0-5.3	12.2-12.9	15.7	13.0-13.2	6.2-6.8	4.8	12.4-12.7	11.7-12.0	12.5
31-32	<i>H. octolineatus</i>	11.2-11.5	12.7-12.9	10.5-10.7	9.7-11.0	11.4	4.2-4.3	10.0-10.7	10.5-10.7	11.9-12.0	12.5-13.0	4.7-4.8	11.0-11.4	11.0	12.0-12.2	8.2-8.4	5.2-5.3
33	<i>H. cf. optatus</i>	12.9	15.9	13.5	11.9-12.2	11.5	10.0	10.7-10.9	12.5	12.2	13.5	11.0	12.7	12.5	11.7	11.2	10.5
34	<i>H. optatus</i>	12.7	17.0	13.0	11.5-11.7	11.2	10.4	12.5-12.7	11.2	13.2	13.4	11.0	12.9	11.9	11.7	11.7	11.4
35-36	<i>H. popei</i>	14.2-15.4	15.9-16.5	13.2-13.5	11.0-12.9	13.0-13.4	10.7-11.4	13.5-13.9	13.2-13.5	12.7	15.4-15.7	11.5-12.5	13.2-13.5	13.5-13.9	12.4-13.4	11.4-11.7	12.4-12.5
37-38	<i>H. pryri</i>	14.4-14.7	18.2	14.7	13.5-13.9	13.5	12.5	12.9-13.0	14.5	13.7	9.0	14.2	15.0	15.0	11.5	13.7	13.4
39	<i>H. sangzhiensis</i>	13.0-13.4	14.2	13.0	11.5-12.5	11.5	9.0	12.4-12.5	11.9	13.0	11.7	11.4	12.0	12.2	11.9	11.5	11.0
40-41	<i>H. sauteri</i>	12.0-13.0	14.5-15.5	13.4-13.7	10.9-13.2	11.9-12.4	10.4-11.0	11.9-13.2	12.2-12.5	12.0	14.0	10.4-11.5	12.7-12.9	12.7-12.9	11.4-11.5	9.7-10.7	11.7
42-43	<i>H. septemlineatus</i>	10.0-10.2	15.2-15.5	12.2-12.4	11.0-11.7	4.2	10.0-10.2	10.5-11.4	12.0-12.2	12.4-12.7	13.4-13.5	10.5-10.7	12.4-12.7	12.4-12.7	11.7-12.5	9.5-9.7	10.2-10.7
44-45	<i>H. taronensis</i>	10.7-11.2	14.4-14.5	12.2-12.5	12.2-13.5	10.5-11.0	10.7-11.2	12.7-13.4	11.4-11.7	13.0-13.2	14.4-14.9	10.5-11.0	11.9-12.2	11.7-12.0	12.7-12.9	10.7-11.2	11.0-11.5
46	<i>H. venningi</i>	9.7-10.0	13.2	11.4	11.0-11.2	8.7	9.0	12.7-12.9	10.2	12.5	13.9	10.5	11.7	10.5	12.2	10.2	9.4
47-48	<i>H. vibakari</i>	12.4-12.7	14.4	13.0	10.2-12.5	11.7	9.7	12.7-12.9	11.4	11.7	13.4	11.0	11.9	11.7	12.0	10.0	11.0
49-50	<i>H. weixiensis</i>	11.0-11.5	14.9-15.4	12.2	11.4-12.2	5.7-5.8	9.9-10.2	10.9-11.5	11.5-11.9	12.2-12.7	12.9-13.0	10.2-10.5	12.5-12.9	11.9-12.2	12.2-12.4	9.7-10.2	10.5-10.9
51-52	<i>H. yanbianensis</i>	11.9-12.2	13.7-14.2	11.7-11.9	10.0-10.7	10.7-11.2	3.7-4.2	10.7-11.4	11.0-11.5	12.4-12.7	13.0-13.4	4.8-5.3	11.5-11.7	11.5-11.7	12.4-13.5	9.0-9.5	6.3-6.5
53	<i>H. youjiangensis</i>	14.0-14.2	13.9	6.7	11.7-12.7	13.4	11.5	13.2-13.4	5.2	11.5	15.4	12.2	5.5	4.7	13.0	10.2	12.0

Table 2. Continued.

ID	Species	23-24	25-26	27-28	29-30	31-32	33	34	35-36	37-38	39	40-41	42-43	44-45	46	47-48	49-50	51-52
23-24	<i>H. khasiensis</i>	2.8																
25-26	<i>H. maximus</i>	13.7-14.4	0.7															
27-28	<i>H. metusia</i>	10.9-11.4	10.4-10.9	1.0														
29-30	<i>H. modestus</i>	13.9-14.2	12.5-13.2	12.4-12.9	2.3													
31-32	<i>H. octolineatus</i>	10.7-11.9	10.5-10.9	4.7-4.8	12.2-12.7	0.5												
33	<i>H. cf. optatus</i>	13.5	10.9-11.0	10.9-11.0	13.9-14.0	10.4	-											
34	<i>H. optatus</i>	13.4	10.0-10.4	10.0-10.5	13.7-14.7	10.9-11.4	9.9	-										
35-36	<i>H. popei</i>	12.9-14.0	11.2-12.2	11.2-11.9	13.0-13.9	11.9-12.0	11.4-13.2	10.7-11.2	4.0									
37-38	<i>H. pryevi</i>	14.7	12.9-13.0	12.7-12.9	15.4-16.7	12.4-12.5	14.0	13.5	14.4-14.5	0								
39	<i>H. sangzhiensis</i>	12.5-13.0	6.7-7.0	10.7-11.0	12.5-12.9	9.9-10.0	12.0	12.0	11.4	11.5	-							
40-41	<i>H. sauteri</i>	11.9-13.0	11.2-12.0	10.4-10.7	13.9-14.2	9.7-10.9	11.0-11.7	10.4-10.7	11.2-12.0	13.5-13.9	12.4-13.0	2.3						
42-43	<i>H. septemlineatus</i>	11.7-12.5	11.0-11.5	9.7-9.9	13.0-14.2	10.0-10.2	12.0-12.4	11.4-11.5	12.5-13.7	13.0	10.4-10.7	10.7-11.5	1.0					
44-45	<i>H. taronensis</i>	13.2-14.0	11.7-12.2	10.0-10.9	12.4-13.0	10.0-10.5	12.4-12.9	12.5-13.0	10.9-11.5	13.0-13.4	10.9-11.4	12.5-13.5	9.7-10.2	0.5				
46	<i>H. vanningi</i>	13.0-13.4	12.4-12.7	9.4-9.7	11.4-11.7	9.5-9.9	11.5	12.0	11.4	12.7	10.9	11.7-12.4	8.5-8.8	5.8-6.0	-			
47-48	<i>H. vibakari</i>	12.5	7.9-8.2	10.4-10.5	12.9-13.7	10.4-10.5	12.9	10.4	12.5	13.0	7.2	12.0-12.4	10.2-10.7	11.5-12.0	11.2	0		
49-50	<i>H. weixiensis</i>	12.2-13.0	11.4-11.9	9.9-10.2	12.9-13.5	10.7-11.4	11.7-12.2	10.9-11.0	13.4-13.7	13.4-13.9	10.4-10.9	11.5-12.2	5.0-5.7	9.8-10.9	10.4-10.5	10.4-10.5	0.5	
51-52	<i>H. yanjianensis</i>	11.2-12.5	11.2-11.4	4.5-4.8	13.0-14.0	5.5-6.0	12.2-12.4	11.5	11.7-12.4	12.5-13.5	10.0-10.5	11.2-12.2	9.5-10.4	10.7-11.4	9.8-10.4	10.7-10.9	9.5-10.4	1.8
53	<i>H. youjiangensis</i>	13.2-13.9	12.7-12.9	11.2-11.4	3.7	11.5-11.9	13.5	14.0	13.5	15.4	12.2	12.9-13.2	13.0-13.4	12.4-12.7	12.0	12.5	12.9-13.2	12.7-13.0

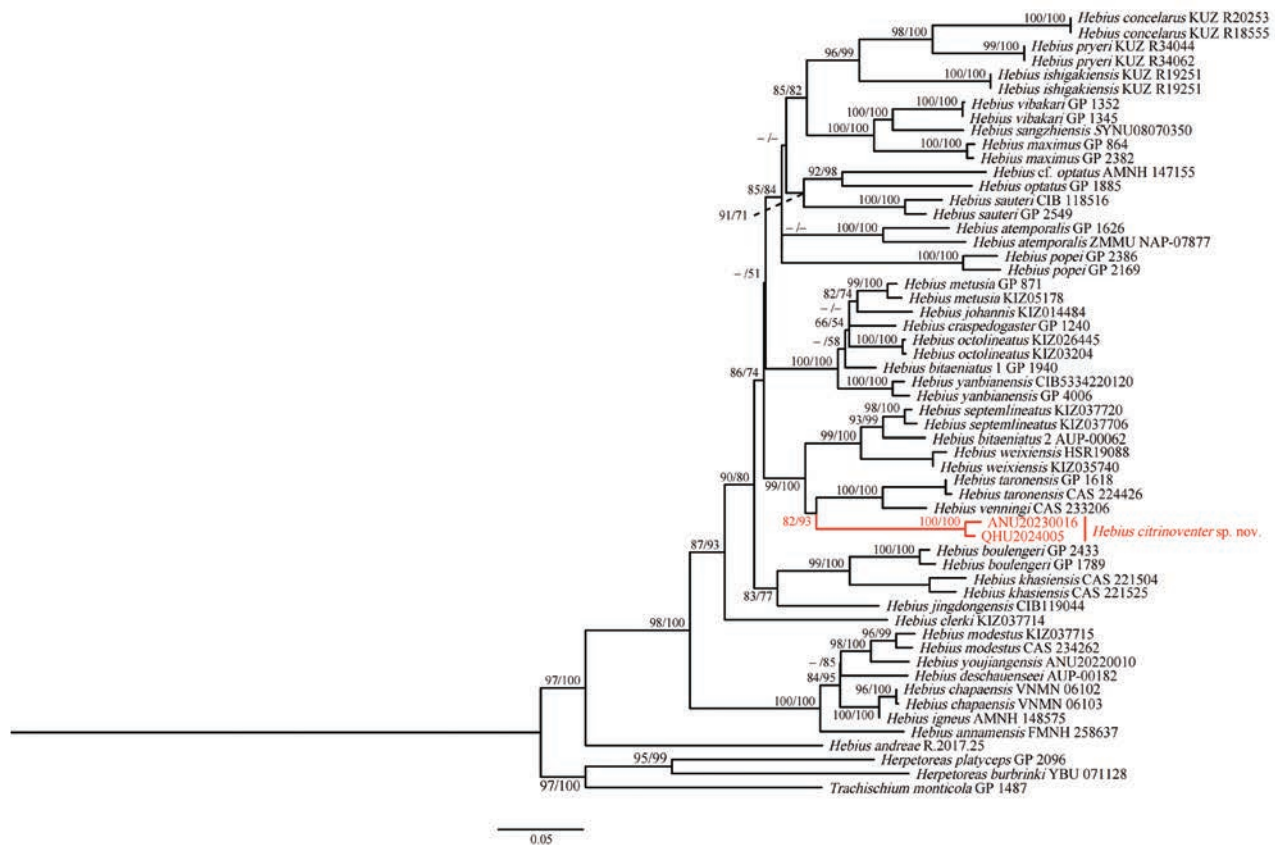


Figure 2. Maximum likelihood tree of the genus *Hebius* inferred from *Cyt b*. The nodes supporting values on branches are presented as SH-like approximate likelihood ratio test (SH) / Ultrafast Bootstrap Approximation (UBF); ones under 50% are omitted. Tips for the new species in the present study are shown in red.

Taxonomic account

Natricinae Bonaparte, 1838

Hebius Thompson, 1913

Hebius citrinoventer Xu, Yang, Ouyang, Huang & Peng, sp. nov.

<https://zoobank.org/EFBD9EA8-897A-46F4-91AD-12E03C26E7F5>

Figs 3–5

Material examined. Holotype. ANU20230016 (field number: HSR23030, Figs 3, 4), an adult female, collected by Diancheng Yang and Jundong Deng on July 18, 2023, in Tongbiguan Town, Yingjiang County, Dehong Dai and Jingpo Autonomous Prefecture, Yunnan Province, China (24°36'30.60"N, 97°39'27.00"E, 1300 m a.s.l.). **Paratype.** QHU2024005 (field number: LFR2024007, Fig. 5), a subadult male, had been crushed to death on the side of the road, collected by Kaichen Ouyang and Lifang Peng on February 5, 2024, in Tongbiguan Town, Yingjiang County, Dehong Dai and Jingpo Autonomous Prefecture, Yunnan Province, China (24°36'03.60"N, 97°39'05.76"E, 1300 m a.s.l.).

Etymology. The specific name *citrinoventer* comprises the Latin words “*citrinus*” (yellowish-orange or orange) and “*venter*” (the belly or underside), based on the pale orange venter of the new species. According to its type locality Yingjiang County, Yunnan Province, China, the name we suggest is Yíng Jiāng Fù Liàn Shé (盈江腹链蛇) in Chinese and Yingjiang Keelback Snake in English.



Figure 3. Fresh specimen of the holotype (ANU20230016) of *Hebius citrinoverter* sp. nov.: dorsal (A), and ventral views (B). Photos by Kai-Chen Ouyang. Scale bars are not shown.

Diagnosis. *Hebius citrinoverter* sp. nov. can be distinguished from its congeners by the following set of characters: (1) DSR 19–17–17, feebly keeled; (2) ventrals 146–151; (3) nasal complete, nostril in the middle of the nasal; (4) supralabials 9, the fourth to sixth in contact with the eye; (5) infralabials 10–11, the first 5 touching the first pair of chin shields; (6) preoculars 2; (7) postoculars 3; (8) temporals 3, arranged in two rows (1+2); (9) maxillary teeth 31, the last 4 slightly enlarged, without diastema; (10) tail comparatively long, TAL/TL ratio 0.334 in male; (11) dorsolateral series of irregular orange or ochre yellow blotches, extending from the neck to the posterior part of the tail; and (12) venter pale orange, tips of ventrals with subrectangular black blotches.

Comparisons. In many characters, *Hebius citrinoverter* sp. nov. is similar to *H. venningi* (Wall, 1910) and *H. taronensis* (Smith, 1940). However, the new species can be distinguished from *H. venningi* by (1) 19 DSR on the anterior part of the body (vs. 17), (2) VS 146–151 (vs. 155–172), (3) TEMP 1+2 (vs. 1 or 1+1); (4) maxillary teeth 31 (vs. 28–30), (5) venter pale orange, tips of ventrals with subrectangular black blotches (vs. venter pink or bright coral red, sometimes yellow). It can be distinguished from *H. taronensis* by (1) 17 DSR at midbody (vs. 19); (2) VS 146–151 (vs. 158–176); (3) TEMP 1+2 (vs. 1 or 1+1); (4) SC 113 (vs. 92–104); (5) tail comparatively longer, TAL/TL ratio 0.334 (vs. TAL/TL ratio 0.254–0.288); and (6) venter pale orange, tips of ventrals with subrectangular black blotches (vs. pale areas of the venter are yellowish-ochre or yellowish-brown). For more detailed information and visual comparisons, please refer to Table 3 and Fig. 6.

Due to the absence of a dark belly, *Hebius citrinoverter* sp. nov. can be distinguished from *H. annamensis* (Bourret, 1934), *H. chapaensis* (Bourret, 1934), *H. deschauenseei* (Taylor, 1934), *H. nigriventer* (Wall, 1925), *H. igneus* David, Vogel, Nguyen, Orlov, Pauwels, Teynié & Ziegler, 2021, and *H. youjiangensis* Yang, Xu, Wu, Gong, Huang & Huang, 2023 (vs. the dark belly present). Moreover, it can be distinguished from *H. deschauenseei* and *H. igneus* by having 17 DSR at midbody (vs. 19); from *H. chapaensis* and *H. nigriventer* by having 19 DSR on the anterior part of the body (vs. 17); from *H. annamensis* by having prefrontals 2 (vs. prefrontal single), VS 146–151 (vs. 158–172), IL 10–11 (vs. up to 10); and from *H. youjiangensis* by having TEMP 1+2 (vs. 1+1), PRO 2 (vs. 1), PO 3 (vs. 2), and dorsolateral series of irregular blotches (vs. a continuous stripe on dorsolateral).



Figure 4. Preserved specimen of the holotype (ANU20230016) of *Hebius citrinoverter* sp. nov. Photos by Yu-Hao Xu. Scale bars: 10 mm.

By having 17 DSR at midbody, *Hebius citrinoverter* sp. nov. can be easily distinguished from the other 35 known species in the genus, which have 19 or 15 rows: *H. andreae* (Ziegler & Le Khac Quyet, 2006), *H. beddomei* (Günther, 1864), *H. bitaeniatus* (Wall, 1925), *H. boulengeri* (Gressitt, 1937), *H. celebicus* (Peters & Doris, 1878), *H. clerki* (Wall, 1925), *H. conelarus* (Malnate, 1963),



Figure 5. Preserved specimen of the paratype (QHU2024005) of *Hebius citrinoverter* sp. nov. Photos by Yu-Hao Xu. Scale bars: 5 mm.

H. craspedogaster (Boulenger, 1899), *H. flavifrons* (Boulenger, 1887), *H. inas* (Laidlaw, 1901), *H. ishigakiensis* (Malnate & Munsterman, 1960), *H. johannis* (Boulenger, 1908), *H. kerinciensis* (David & Das, 2003), *H. khasiensis* (Boulenger, 1890), *H. lacrima* Purkayastha & David, 2019, *H. leucomystax* (David, Bain, Quang Truong, Orlov, Vogel, Ngoc Thanh & Ziegler, 2007), *H. metusia* (Inger, Zhao, Shaffer & Wu, 1990), *H. modestus* (Günther, 1875), *H. miyajimae* (Maki, 1931), *H. nicobariensis* (Sclater, 1891), *H. octolineatus* (Boulenger, 1904), *H. optatus* (Hu & Zhao, 1966), *H. parallelus* (Boulenger, 1890), *H. petersii* (Boulenger, 1893),

Table 3. Comparisons of main morphological characters between *H. citrinoventer* sp. nov., *H. taronensis* and *H. venningi*. Abbreviations as per Material and methods.

Species	TAL/TL	SL	IL	TEMP	DSR	VEN	SC	MT	Venter background coloration
<i>H. citrinoventer</i> sp. nov.	0.334	9	10–11	1+2	19–17–17	146–151	113	31	pale orange
<i>H. taronensis</i>	0.254–0.288	9 (rarely 8)	10	1 or 1+1	19–19–17	158–176	92–104	28–32	yellowish-ochre or yellowish-brown
<i>H. venningi</i>	0.295–0.347	9	9–10	1+1	17–17–17	155–172	115–129	28–30	pink or bright coral red, sometimes yellow

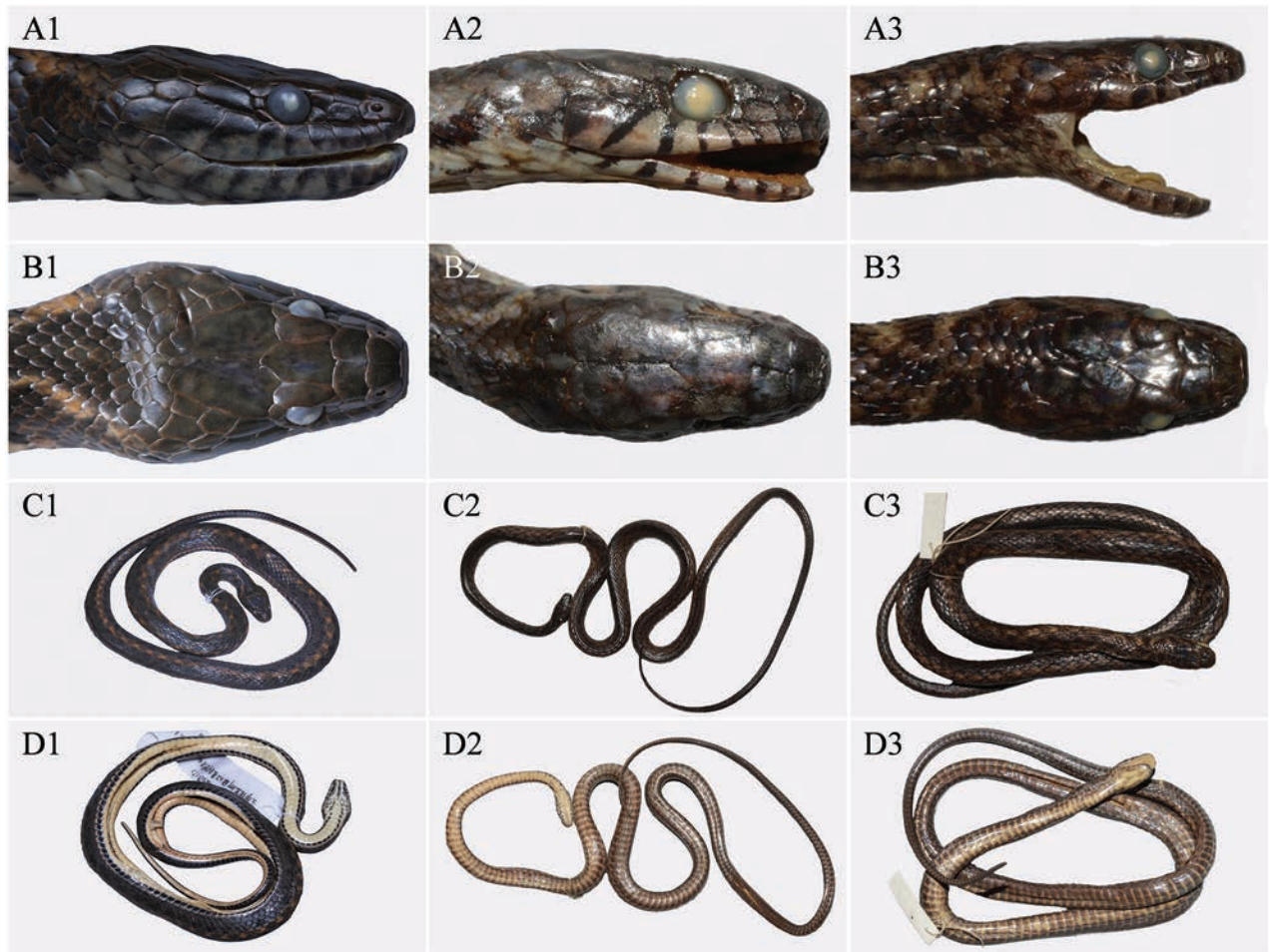


Figure 6. Comparisons of the lateral head (A), dorsal head (B), dorsal overview (C), and ventral overview (D) among the holotypes of *H. citrinoventer* sp. nov. (ANU20230016; **A1–D1**), *H. venningi* (BMNH 1946.1.21.86; **A2–D2**), and *H. taronensis* (BMNH 1946.1.13.55; **A3–D3**). Photos of *H. venningi* and *H. taronensis* were obtained from David et al. (2021), remaining photos by Yu-Hao Xu. Scale bars are not shown.

H. popei (Schmidt, 1925), *H. pryeri* (Boulenger, 1887), *H. sanguineus* (Smedley, 1932), *H. sangzhiensis* Zhou, Qi, Lu, Lyu & Li, 2019, *H. sarasinorum* (Boulenger, 1896), *H. septemlineatus* (Schmidt, 1925), *H. terrakarenorum* Hauser, Smits & David, 2022, *H. vibakari* (Boie, 1826), *H. viperinus* (Schenkel, 1901), *H. weixiensis* Hou, Yuan, Wei, Zhao, Liu, Wu, Shen, Chen, Guo & Che, 2021 and *H. yanbianensis* Liu, Zhong, Wang, Liu & Guo, 2018.

Compared with the other seven congeners that have 17 DSR at the midbody, *Hebius citrinoventer* sp. nov. can be distinguished from *H. arquus* (David & Vogel,

2010), *H. atemporalis* (Bourret, 1934), *H. frenatus* (Dunn, 1923), *H. sarwacensis* (Günther, 1872), *H. sauteri* (Boulenger, 1909), and *H. maximus* (Malnate, 1962) by the 19–17–17 DSR counts (vs. 17–17–15 in *H. arquus* and *H. frenatus*; and 17–17–17 in *H. atemporalis*, *H. sarwacensis*, *H. sauteri* and *H. maximus*), from *H. groundwateri* (Smith, 1922) by the divided cloacal plate (vs. CP entire). Furthermore, this new species differs from *H. arquus* by having a single loreal (vs. the absence of loreal). It differs from *H. atemporalis*, *H. frenatus* and *H. sarwacensis* in terms of SL, namely (9 vs. 6 in *H. atemporalis*, 5–8 in *H. sauteri*, and 8 in *H. frenatus* and *H. sarwacensis*).

Description of holotype. An adult female specimen with SVL 583 mm and incomplete tail (TAL 198+ mm). Body slightly stout and cylindrical; head flattened anteriorly, distinct from the neck, HL 26.1 mm, HW 15.6 mm. Nostril: lateral, round, piercing in the middle of the nasal. Eye large, ED 3.5 mm, pupil round.

Body scalation: DSR 19–17–17, feebly keeled, including the outermost DSR on both sides, not notched at the posterior extremity. VEN 144 (+2 preventrals); SC 80+, all paired; CP divided.

DSR reduction:

3+4→3 (79–80) (right)

19—————17

3+4→3 (78–79) (left)

Dentition: Maxillary teeth 31, gradually enlarged, the last four slightly enlarged, without diastema between last four and anterior teeth.

Head scalation: Rostral pentagonal, wider than high, visible from above; nasal entire, subpentagonal, about twice as wide as high; internasals 2, trapezoidal, in broad contact with each other, narrowing anteriorly; prefrontals 2, pentagonal, wider than long, in contact with loreal; frontal narrow, pentagonal, longer than wide, shield-like, slightly concave in the middle on both sides; SPO 1 on each side, hexagonal, much longer than wide; LOR 1/1, subrectangular, wider than long; PRO 2/2, upper one larger than lower one; PO 3/3; SL 9/9, the first 2 in contact with nasal, the 2nd to 4th in contact with the loreal, 4th to 6th entering orbit, the 7th and 8th largest; TEMP 3/3, arranged in two rows (1+2), the anterior temporal long and trapezoidal; chin shields in 2 pairs, the posterior pair longer than anterior one and separated by several small scales; IL 11/11, first pair in contact behind the mental, 1st to 5th touching the first pair of chin shields, the 5th and 7th largest.

Coloration of the fresh specimen: Dorsal surface of the head is olive-brown and scattered with pale-brown vermiculate stripes or irregular blotches. A pale, irregular yellow-ochre oblique streak is directed upward on both sides of the head, extending from the temporal region to the nape. The upper half of the 1st to 8th SL is olive-brown, the lower half is pale brown, and the 9th is completely olive-brown. Ventral surface of head creamy yellow, the edges of partial scales have irregular black-gray patches.

Body olive-brown, darker on the top than on the sides. A faint, yellow-ochre or rusted dorsolateral stripe extends from the neck to the end of the tail, on the upper part of the 5th to the lower part of the 7th scale rows in the anterior part of the body, and the upper part of the 4th to 6th in the middle and posterior parts of the body, accompanied by a series of conspicuous, pale orange or ochre yellow irregular blotches, about two scales in diameter. The orange or ochre yellow blotches are

not symmetrically distributed on both sides of the body but are arranged in a staggered manner, that is, the blotch on the left side of the body corresponds to the area between the two blotches on the right side of the body, and vice versa. Above and below the orange blotch, there is a slightly smaller, dull blackish-brown irregular blotch. The blackish-brown blotches above are arranged in a staggered pattern in the middle of the body, forming a checkered pattern with the background color.

Ventral anterior pale orange, darker toward the rear, and scattered with a few small black spots. The outermost edge of the ventral is black. Outer one-sixth of the ventrals with subrectangular black blotches on each side, producing an irregular, continuous ventrolateral stripe, which merges with the dark ventral edge in the posterior part of the body. The ventral surface of the tail is uniform pale orange with black-brown edge; a thin, brown-black stripe extends on the ventral part of the tail, formed by the inner margins of the SC, extending from the 1st SC to the end of the tail.

Coloration in preservation: In preservation, the background color of the dorsal body changed to brownish-black, and the checkered pattern on dorsal surface has disappeared or faded. An indistinct pale-brown dorsolateral stripe extends from the neck to the end of the tail and is accompanied by a series of ochre yellow, irregular blotches. Head brownish-black, upper half of the 1st to 8th supralabials brownish-black, lower half gray white, the 9th completely brownish-black. The infralabials mainly black-gray, the left half of the 5th to 11th pale gray, and the right half very dark gray. Ventral surface of the head cream, the edges of the partial scales had irregular very dark gray patches. The ventral surface of the body cream anteriorly, darker toward the rear, and the posterior part is light creamy yellow. In addition, the rest of the color pattern is similar to that seen in life.

Variation. The paratype has a similar coloration in preservation as the holotype, but the subcaudals are almost completely black, with only the inner margins being creamy yellow. In scalation features, there is the following variation: the paratype has fewer infralabials (10 vs. 11) and more ventrals (151 vs. 146). The measurements and scalation features of the series ($N = 2$) are listed in Table 4.

Distribution and habitat. *Hebius citrinoverter* sp. nov. is currently only known from Yingjiang County, Dehong Dai and Jingpo Autonomous Prefecture, Yunnan Province, China: Tongbiguan Town (1300 m a.s.l.) (Fig. 7). The holotype (ANU20230016) was found drowned in a fish-catching cage placed by local



Figure 7. Habitat of *Hebius citrinoverter* sp. nov., Tongbiguan Town, Yingjiang County, Yunnan Province. Photos by Kai-Chen Ouyang.

Table 4. Main morphological characters of *Hebius citrinoventer* sp. nov. Abbreviations as per Material and methods.

Voucher Number	ANU20230016	QHU2024005
	Holotype	Paratype
Sex	Adult female	Subadult male
SVL	583	267
TAL	198+	134
TL	781+	401
TAL/TL	–	0.334
HW	15.6	6.7
HL	26.1	12.6
ED	3.5	1.9
MT	31	–
SL	9/9	9/9
SL-Eye	4 th –6 th	4 th –6 th
IL	11/11	10/10
Chin	2	2
IL-1 st Chin	1 st –5 th	1 st –5 th
LOR	1	1
PRO	2	2
PO	3	3
TEMP	1+2	1+2
DSR	19–17–17	19–17–17
VS	146	151
SC	80+	113
CP	2	2

residents in a wide stream at approximately 7:00 am, and we presume that it may have fallen into the trap the preceding night while attempting to catch fish in the cage. The paratype (QHU2024005) was found road-killed on the side of the road next to a stream after a light rain between 21:00 and 22:00. Both specimens were found in a well-preserved monsoon forest habitat.

Discussion

In this study, we combined morphological and molecular analyses of specimens in the genus *Hebius* to provide robust evidence for the identification of new species. Based on molecular phylogenetic analysis, we found that the sequence KJ685679 (voucher number: GP 1618) from Myanmar clustered together with *H. taronensis* and had a very low *p*-distance of approximately 0.3% in *Cyt b*. However, it was referred to as *Hebius* sp. in Guo et al. (2014) but tentatively as *H. venningi* in David et al. (2021). Because the specimen was not examined, we conservatively assigned it to *H. taronensis*. Additionally, the uncorrected *p*-distance between specimen AMNH 147155 from Vietnam and *H. optatus* was 9.8%, which clearly reached the inter-species level; therefore, we proposed the specimen as *H. cf. optatus*. Likewise, the phylogenetic structure showed that the specimens (GP 1940 and AUP-00062), which were once considered *Hebius bitaeniatus*, clustered in different clades: *H. craspedogaster*, *H. johannis*, *H. metusia* and *H. octolineatus* were clustered together with low support and formed a sister group with specimen GP 1940; the specimen AUP-00062 was clustered with *H. septemlineatus* with high support (SH 93 / UFB 99), and the uncorrected *p*-distance was 4.2%. However,

due to the lack of morphological and molecular data on the topotype, the classification status of these two specimens requires further study.

The new species, *Hebius citrinoverter* sp. nov., has some morphological features common to *H. venningi* and *H. taronensis*, but can still be distinguished from them in the following characters: dorsal scale rows, number of temporal and ventral scales, and venter color pattern. Molecular phylogenetic analysis also separated the new species *H. citrinoverter* sp. nov. and provided strong support for its placement as a sister taxon. Moreover, the new species also possessed a considerable level of genetic divergence from 9.7–10.0% for *H. venningi* and 10.9–11.2% for *H. taronensis* in *Cyt b*. In addition, the new species is geographically isolated by the Hengduan Mountains, which plays an important role as a geographical barrier in speciation.

The genus *Hebius* is a highly diverse group distributed throughout eastern and southern Asia. Owing to the semi-aquatic habitats of this genus, specimen collection is relatively difficult, and the population and distribution data for many species is insufficient, which poses obstacles to conservation. Yingjiang County, where the new species was found, lies in the southwest Yunnan Province and is one of the most biodiverse regions in China. Although the discovery site of this new species is legally protected, the holotype derived from the fish trap and the road-killed paratype clearly indicates that this species is still influenced by human activities. Further surveys and evaluation of the population of the new species should be performed, and further consideration should be given to incorporating it in the local protected animal lists for protection.

In China, most species of *Hebius* are known from Yunnan Province, and the identification of *Hebius citrinoverter* sp. nov. brings the total number of *Hebius* species in China to 27, of which 20 are reported in Yunnan Province. This result further illustrates that reptile diversity in Yunnan is still underestimated. Therefore, more specific surveys may help to better understand the biodiversity in southwest China.

Conclusion

Here, we describe a new species of the genus *Hebius*, *Hebius citrinoverter* sp. nov., based on two specimens collected from Yingjiang County, Dehong Dai and Jingpo Autonomous Prefecture, Yunnan Province, China. The discovery of this new species has brought the total number of known species in the genus *Hebius* to 52. Currently, *Hebius citrinoverter* sp. nov. is only known to be distributed in southwest Yunnan Province, China. Since Yingjiang County is close to the borders of Myanmar, this species also probably occurs in the adjacent area of this country. However, the detailed distribution range, population size, and feeding habits of the new species have not yet been elucidated, and further research and evaluation of the population of the new species should be conducted.

Acknowledgements

We are grateful to Dr Christopher Glasby, Jun-Man Huang (Southern Illinois University), and Editage (www.editage.cn) for English language editing. We thank the reviewers Dr Patrick David and Dr Vinh Quang Luu for valuable and helpful comments.

Additional information

Conflict of interest

The authors have declared that no competing interests exist.

Ethical statement

All sampling and procedures involving snake specimens were performed in accordance with the Wild Animals Protection Law of the People's Republic of China, approved by the Institutional Ethics Committee of Anhui Normal University (protocol code AHNU-ET2021025 and date of approval 7 May 2021) and Qinghai University (protocol code SL-2023028 and date of approval 15 March 2023).

Funding

This research was funded by the National Natural Science Foundation of China (32301325; 31471968), the Project of Qinghai Science & Technology Department (2024-ZJ-965), and the Open Project of State Key Laboratory of Plateau Ecology and Agriculture, Qinghai University (2023-ZZ-08).

Author contributions

YHX, DCY, YAG, HCOY and SYW measured the specimens, analyzed the data, constructed the phylogenetic tree, and prepared the manuscript; LFP and SH provided the funding for the field survey; LFP, JDD and SH conceived and designed the study and reviewed the manuscript before submission. All authors have read and agreed to the published version of the manuscript.

Author ORCIDs

Yu-Hao Xu  <https://orcid.org/0000-0001-6094-6680>

Dian-Cheng Yang  <https://orcid.org/0000-0001-6390-5251>

Yan-An Gong  <https://orcid.org/0000-0002-8155-7024>

Kai-Chen Ouyang  <https://orcid.org/0009-0003-6876-4699>

Song Huang  <https://orcid.org/0000-0001-6786-8523>

Li-Fang Peng  <https://orcid.org/0000-0001-9325-7048>

Data availability

All of the data that support the findings of this study are available in the main text.

References

- Bourret R (1934) Notes herpétologiques sur l'Indochine française. III. Ophidiens d'Annam et du Moyen Laos. Bulletin général de l'Instruction Publique 13e Année (1933–1934) (9 Mai 1934): 167–176. [Separate reprint: 3–12]
- Burbrink FT, Lawson R, Slowinski JB (2000) Mitochondrial DNA phylogeography of the polytypic North American rat snake (*Elaphe obsoleta*): A critique of the subspecies concept. *Evolution; International Journal of Organic Evolution* 54(6): 2107–2118. <https://doi.org/10.1111/j.0014-3820.2000.tb01253.x>
- Burland TG (2000) DNASTAR's Lasergene sequence analysis software. *Methods in Molecular Biology* (Clifton, N.J.) 132: 71–91. <https://doi.org/10.1385/1-59259-192-2:71>

- Das A, Gower DJ, Deepak V (2020) Lost and found: Rediscovery and systematics of the Northeast Indian snake *Hebius pealii* (Sclater, 1891). *Vertebrate Zoology* 70(3): 305–318. <https://doi.org/10.26049/VZ70-3-2020-04>
- David P, Das I (2003) A new species of the snake genus *Amphiesma* (Serpentes: Colubridae: Natricinae) from western Sumatra, Indonesia. *The Raffles Bulletin of Zoology* 51(2): 413–419.
- David P, Vogel G (2010) A new species of the natricine snake genus *Amphiesma* from Borneo (Squamata: Natricidae). *Russian Journal of Herpetology* 17(2): 121–127.
- David P, Vogel G, Nguyen TQ, Orlov NL, Pauwels OSG, Teynié A, Ziegler T (2021) A revision of the dark-bellied, stream-dwelling snakes of the genus *Hebius* (Reptilia: Squamata: Natricidae) with the description of a new species from China, Vietnam and Thailand. *Zootaxa* 4911(1): 1–61. <https://doi.org/10.11646/zootaxa.4911.1.1>
- Deepak V, Cooper N, Poyarkov NA, Kraus F, Burin G, Das A, Narayanan S, Streicher JW, Smith S-J, Gower DJ (2022) Multilocus phylogeny, natural history traits and classification of natricine snakes (Serpentes: Natricinae). *Zoological Journal of the Linnean Society* 195(1): 279–298. <https://doi.org/10.1093/zoolinnean/zlab099>
- Dowling HG (1951a) A proposed system for counting ventrals in snakes. *British Journal of Herpetology* 1(5): 97–99.
- Dowling HG (1951b) A proposed method of expressing scale reductions in snakes. *Copeia* 2(2): 131–134. <https://doi.org/10.2307/1437542>
- Gressitt JL (1937) A new snake from southeastern China. *Proceedings of the Biological Society of Washington* 50: 125–128.
- Günther A (1875) Second report on collections of Indian Reptiles obtained by the British Museum. *Proceedings of the Zoological Society of London*, 1875, 224–234. [Pl. 30–34]
- Guo P, Zhu F, Liu Q, Zhang L, Li JX, Huang YY, Pyron RA (2014) A taxonomic revision of the Asian keelback snakes, genus *Amphiesma* (Serpentes: Colubridae: Natricinae), with description of a new species. *Zootaxa* 3873(4): 425–440. <https://doi.org/10.11646/zootaxa.3873.4.5>
- Hauser J, Smits T, David P (2022) On the distribution of the species of the genus *Hebius* Thompson, 1913 (Squamata: Natricidae) in northern Thailand, including the description of a new species and a discussion on snake diversity of this region. *Zootaxa* 5116(1): 001–039 <https://doi.org/10.11646/zootaxa.5116.1.1>
- Hou SB, Yuan ZY, Wei PF, Zhao GG, Liu GH, Wu YH, Shen WJ, Chen JM, Guo P, Che J (2021) Molecular phylogeny and morphological comparisons of the genus *Hebius* Thompson, 1913 (Reptilia: Squamata: Colubridae) uncover a new taxon from Yunnan Province, China, and support revalidation of *Hebius septemlineatus* (Schmidt, 1925). *Zoological Research* 42(5): 620–625. <https://doi.org/10.24272/j.issn.2095-8137.2021.093>
- Huang S (2021) Sinoophis. The Straits Publishing & Distributing Group, Fuzhou. [In Chinese]
- Kizirian D, Truong NQ, Ngo HT, Le MD (2018) *Parahelicops*, *Pararhabdophis*, *Paraphyly*: Phylogenetic relationships among certain Southeast Asian natricine snakes (*Hebius*). *American Museum Novitates* 3906(3906): 1–8. <https://doi.org/10.1206/3906.1>
- Kumar S, Stecher G, Li M, Knyaz C, Tamura K (2018) MEGA X: Molecular Evolutionary Genetics Analysis across computing platforms. *Molecular Biology and Evolution* 35(6): 1547–1549. <https://doi.org/10.1093/molbev/msy096>
- Lalronunga S, Lalrinchhana C, Vanramliana V, Das A, Gower DJ, Deepak V (2020) A multilocus molecular perspective on the systematics of the poorly known Northeast

- Indian colubrid snakes *Blythia reticulata* (Blyth, 1854), *B. hmuifang* Vogel, Lalremsanga & Vanlalhrima, 2017, and *Hebius xenura* (Wall, 1907). *Zootaxa* 4768(2): 193–200. <https://doi.org/10.11646/zootaxa.4768.2.2>
- Li ML, Ren JL, Huang JJ, Lyu ZT, Qi S, Jiang K, Wang YY, Li JT (2022) On the validity of *Hebius sauteri maximus* (Malnate, 1962) (Squamata, Natricidae), with the redescription of *H. maximus* comb. nov. and *H. sauteri* (Boulenger, 1909). *Herpetozoa* (Wien) 35: 265–282. <https://doi.org/10.3897/herpetozoa.35.e94920>
- Liu Q, Zhong GH, Wang P, Liu Y, Guo P (2018) A new species of the genus *Hebius* (Squamata: Colubridae) from Sichuan, China. *Zootaxa* 4483(2): 385–394. <https://doi.org/10.11646/zootaxa.4483.2.10>
- Ma S, Shi SC, Ayi B, Jiang JP (2023) A New Species of the Genus *Hebius* Thompson, 1913 (Serpentes: Natricidae) from Yunnan, China. *Asian Herpetological Research* 14(3): 1–15. <https://doi.org/10.3724/ahr.2095-0357.2023.0008>
- Nguyen LT, Schmidt HA, Haeseler AV, Minh BQ (2015) IQ-TREE: A fast and effective stochastic algorithm for estimating maximum likelihood phylogenies. *Molecular Biology and Evolution* 32(1): 268–274. <https://doi.org/10.1093/molbev/msu300>
- Patel H, Thackeray T, Campbell PD, Mirza ZA (2023) Systematic assessment of *Hebius beddomei* (Günther, 1864) (Serpentes: Colubridae: Natricinae) with description of a new genus and a new allied species from the Western Ghats, India. *Taxonomy* 3(3): 415–434. <https://doi.org/10.3390/taxonomy3030024>
- Purkayastha J, David P (2019) A new species of the snake genus *Hebius* Thompson from Northeast India (Squamata: Natricidae). *Zootaxa* 4555(1): 79–90. <https://doi.org/10.11646/zootaxa.4555.1.6>
- Ren JL, Wang K, Nguyen TT, Hoang CV, Zhong GH, Jiang K, Guo P, Li JT (2018) Taxonomic reevaluation of the monotypic genus *Pararhabdophis* Bourret, 1934 (Squamata: Colubridae: Natricinae) with discovery of its type species, *P. chapaensis*, from China. *Zootaxa* 4486(1): 31–56. <https://doi.org/10.11646/zootaxa.4486.1.2>
- Ren JL, Jiang K, Huang JJ, David P, Li JT (2022) Taxonomic review of the genus *Herpetoareas* (Serpentes: Natricidae), with the description of a new species from Tibet, China. *Diversity* 14(2): 79. <https://doi.org/10.3390/d14020079>
- Smith MA (1940) The amphibians and reptiles obtained by Mr. Ronald Kaulback in Upper Burma. *Records of the Indian Museum* 43(3): 465–486. [pl. 7] <https://doi.org/10.26515/rzsi/v42/i3/1940/162431>
- Takuma K, Toda M (2016) The biogeographical history of Asian keelback snakes of the genus *Hebius* (Squamata: Colubridae: Natricinae) in the Ryukyu Archipelago, Japan. *Biological Journal of the Linnean Society. Linnean Society of London* 18(2): 187–199. <https://doi.org/10.1111/bij.12726>
- Taylor EH (1934) Zoological results of the third De Schauensee Siamese Expedition, part III. –Amphibians and Reptiles. *Proceedings of the Academy of Natural Sciences of Philadelphia* 86: 281–310. [pl. 17]
- Uetz P, Freed P, Aguilar R, Reyes F, Hošek J (2024) The Reptile Database. <http://www.reptile-database.org> [Accessed 5 February 2024]
- Wall F (1910) A new *Tropidonotus* from the Chin Hills. *Journal of the Bombay Natural History Society* 20(2): 345–346.
- Wall F (1925) Notes on snakes collected in Burma in 1924. *Journal of the Bombay Natural History Society* 30(4): 805–821.
- Xu YH, Yang DC, Gong YA, Wu JX, Huang RY, Liu YJ, Liang SM, Huang TQ, Huang S (2023) A new species of the Genus *Hebius* Thompson, 1913 (Squamata: Colubridae) from Baise, Guangxi, China. *Zootaxa* 5319(1): 076–090. <https://doi.org/10.11646/zootaxa.5319.1.5>

- Zhao EM (2006) Snakes of China. I. Anhui Science and Technology Publishing House, Hefei, 372 pp. [In Chinese]
- Zhou ZY, Sun ZY, Qi S, Lu YY, Lyu ZT, Wang YY, Li PP, Ma JZ (2019) A new species of the genus *Hebius* (Squamata: Colubridae: Natricinae) from Hunan Province, China. *Zootaxa* 4674(1): 068–082. <https://doi.org/10.11646/zootaxa.4674.1.3>
- Ziegler T, Luu QV, Nguyen TT, Ha NV, Ngo HT, Le MD, Nguyen TQ (2019) Rediscovery of Andrea's keelback, *Hebius andreae* (Ziegler & Le, 2006): First country record for Laos and phylogenetic placement. *Revue Suisse de Zoologie* 126(1): 61–71. <https://doi.org/10.5281/zenodo.2619520>

First record of subgenus *Synaldis* Foerster (Hymenoptera, Braconidae, Alysini, *Dinotrema* Foerster) from Chile, with description of ten new species

Francielle Dias de Oliveira¹, Angélica Maria Pentead-Dias²

¹ Programa de Pós-Graduação em Ecologia e Recursos Naturais, Universidade Federal de São Carlos, CP 676, CEP 13 565-905, São Carlos, SP, Brazil

² Universidade Federal de São Carlos, Departamento de Ecologia e Biologia Evolutiva, CP 676, CEP 13 565-905, São Carlos, SP, Brazil

Corresponding authors: Francielle Dias de Oliveira (fdoliveira1@gmail.com); Angélica Maria Pentead-Dias (angelica@ufscar.br)

Abstract

Synaldis is a taxon within the *Aspilota* group with a contentious taxonomic history, currently classified as a subgenus of the genus *Dinotrema*. Species of *Synaldis* were only documented in the Neotropical region in 2017, and until then, the Neotropical fauna of this subgenus was represented by five species from Brazil. In this study, *Synaldis* is reported for the first time in Chile, with the description and illustration of ten new species, namely: *Dinotrema* (*Synaldis*) *acarinareolatum* sp. nov., *D. (S.) brunneum* sp. nov., *D. (S.) chilense* sp. nov., *D. (S.) daltoni* sp. nov., *D. (S.) flavum* sp. nov., *D. (S.) latusdentertium* sp. nov., *D. (S.) perisfelipoi* sp. nov., *D. (S.) pilosicaudatum* sp. nov., *D. (S.) puyehue* sp. nov., and *D. (S.) verae* sp. nov. The studied specimens were collected during expeditions to southern Chile, in the Valdivian temperate rainforest at Parque Nacional de Puyehue. This study also includes a dichotomous identification key for Neotropical species of *Synaldis*, as well as a discussion of the primary morphological characters used to distinguish species within the Neotropical and Nearctic regions.

Key words: Alysini, *Aspilota* group, endoparasitoid wasp, Ichneumonoidea, koinobiont, Neotropical region, parasitoid of Diptera, taxonomy



Academic editor: Filippo Di Giovanni

Received: 1 April 2024

Accepted: 11 June 2024

Published: 10 July 2024

ZooBank: <https://zoobank.org/879E4E4E-8904-4879-8F28-8F6EAD0AE9FC>

Citation: Dias de Oliveira F, Pentead-Dias AM (2024) First record of subgenus *Synaldis* Foerster (Hymenoptera, Braconidae, Alysini, *Dinotrema* Foerster) from Chile, with description of ten new species. ZooKeys 1206: 275–314. <https://doi.org/10.3897/zookeys.1206.124515>

Copyright: © Francielle Dias de Oliveira & Angélica Maria Pentead-Dias. This is an open access article distributed under terms of the Creative Commons Attribution License (Attribution 4.0 International – CC BY 4.0).

Introduction

The subfamily Alysini Leach, 1815 (Hymenoptera, Braconidae) contains koinobiont endoparasitoids exclusively of cyclorrhaphous Diptera larvae (Wharton 1984; van Achterberg 1993). Alysini is morphologically characterized by having exodont mandibles (outwardly directed, non-overlapping even when they are closed), and total loss of the occipital carina (van Achterberg 1993; Wharton 2017). This subfamily is subdivided into two tribes, Alysini and Dacusini, which differ by the presence of the fore wing vein r-m in Alysini and its absence in Dacusini (Shenefelt 1974; Yu et al. 2016).

Within Alysini, the *Aspilota* group (sensu van Achterberg 1988) stands out as a remarkably large and complex group of genera. Members of this group are characterized by having a nearly glabrous apical portion of the ovipositor sheath, with its obtuse apex, and a host-spectrum nearly exclusively comprised

of dipteran Phoridae. They are typically small, with a body length of 1–2 mm (less frequently ~ 3 mm), the body color is predominantly dark brown, and they are often found in decaying organic matter (van Achterberg 1988).

Two of the largest related genera in the *Aspilota* group, *Dinotrema* Foerster, 1863 and *Aspilota* Foerster, 1863 are morphologically distinguished by the size states of the paraclypeal fovea (anterior tentorial pit). In *Dinotrema*, this structure is small and clearly separated from the eye, whereas in *Aspilota*, the paraclypeal fovea is enlarged and almost reaching the margin of the eye (van Achterberg 1988). The genera *Dinotrema*, *Aspilota*, and related taxa are known for being among the most taxonomically complex within Braconidae. In addition to the predominantly small size of their representatives, the complexity is attributed to the limited characteristics used to distinguish species. Moreover, these diagnostic characters exhibit variability, sometimes significant, thereby obscuring the distinctions between closely related taxa (Belokobylskij and Tobias 2007).

Currently, the genus *Dinotrema* comprises three subgenera: the nominative *Dinotrema*, *Synaldis* Foerster, 1863, and *Synaldotrema* Belokobylskij & Tobias, 2002 (Zhu et al. 2017). *Synaldotrema* is distinguished by its anomalous metasomal structure, i.e., clearly narrowed towards the apex (in lateral view), with the apical sternites (and ovipositor) distinctly retracted under the long and protruding apical tergites, and fourth tergite very elongate (Belokobylskij and Tobias 2002, 2007). *Synaldis* differs from *Dinotrema* by the complete absence of vein 2-SR in the fore wing (consequently the first and second submarginal cells are confluent), while in the subgenus *Dinotrema* this vein is present, and the first and second submarginal cells are separated.

With a historically contentious taxonomic status, *Synaldis* was initially proposed as a genus by Foerster (1863). The generic validity of *Synaldis* has been questioned due to the variability in the reduction of certain veins among the Alysiini (Wharton 1980, 2002), including the 2-SR vein in specimens of the *Aspilota* group, as demonstrated by Koenig (1972). In 1988, van Achterberg re-established the genus *Dinotrema* and synonymized the species of “*Synaldis*” (having the paraclypeal fovea separated from the eye) with *Dinotrema*. Alternatively, *Synaldis* continued to be treated as a genus by several authors, and many species were either described in or transferred to it (Fischer 1993a, 1993b, 2003; Papp 1996, 2000; Belokobylskij 2002, 2004; Peris-Felipo et al. 2014a; Peris-Felipo and Belokobylskij 2017). Finally, Zhu et al. (2017) proposed recognizing *Synaldis* as a subgenus of *Dinotrema* for convenience, until a comprehensive phylogenetic study of the genus *Dinotrema* can support the recognition of *Synaldis* as a subgenus or genus, a classification that was employed in this study.

Synaldis has approximately 100 species described worldwide, and its members are often reared from agaric mushrooms and recorded as parasitoids of Phoridae and possibly Drosophilidae larvae (Peris-Felipo and Belokobylskij 2020). Peris-Felipo and Belokobylskij (2017) provided the initial record of *Synaldis* in the Neotropical region, along with an identification key for the previously known Nearctic and Neotropical species of the subgenus. Until then, five Neotropical species had been registered from Brazil: *Dinotrema (Synaldis) brasiliense* (Peris-Felipo, 2017), *Dinotrema (Synaldis) fritzi* (Peris-Felipo, 2017), *Dinotrema (Synaldis) longiflagellaris* (Peris-Felipo, 2017), *Dinotrema (Synaldis) magnioculis* (Peris-Felipo, 2017), and *Dinotrema (Synaldis) novateutoniae* (Peris-Felipo,

2017). In this study, we report the first record of *Synaldis* from Chile, with the description and illustration of ten new species: *Dinotrema (Synaldis) acarinareolatum* sp. nov., *D. (S.) brunneum* sp. nov., *D. (S.) chilense* sp. nov., *D. (S.) daltoni* sp. nov., *D. (S.) flavum* sp. nov., *D. (S.) latusdentertium* sp. nov., *D. (S.) perisfelipoi* sp. nov., *D. (S.) pilosicaudatum* sp. nov., *D. (S.) puyehue* sp. nov., *D. (S.) verae* sp. nov. Additionally, an identification key to the Neotropical species of *Synaldis* is provided.

Materials and methods

The nomenclature of wing venation follows van Achterberg (1993), and body sculpture follows Eady (1968). The other morphological terms and measurements were based on Peris-Felipo et al. (2014b), with additional explanations provided below. Body length: in lateral view, sum of the head extension (Fig. 1B, $he+ew+tp$), mesosoma length (Fig. 1F, msl), and metasoma length (Fig. 1K, $t1l+mtl$). In dorsal view, head width is its maximum width (at eyes or temples), and head length is the midline between frons anteriorly and occiput. For head measurements in lateral view (Fig. 1B), the head was positioned to vertically align the upper base of the mandible with the lateral ocellus (following Wharton 1977). Paraclypeal fovea size: ratio between the maximum diameter of the fovea and the shortest distance from the fovea to the eye (short ≤ 0.40 , middle = $0.45-0.55$) (Fig. 1C). The mandible width is its maximum width (at apex or base) (Fig. 1D); diagonal carina refers to a carina arising from upper tooth (Fig. 9). Antenna length: sum of the lengths of its segments (Fig. 1E). The width of the first flagellar segment (F1) is its apical width, while for the other flagellomeres the width is their maximum width. Maxillary palp length: sum of the lengths of its segments.

Mesosoma width is the maximum width of mesoscutum; prescutellar depression (scutellar sulcus) width is its maximum width (Fig. 1G). Propodeal areola height and width were measured inside the areola (Fig. 1H). Propodeal spiracle size: ratio between the diameter of spiracle (at its outer margin) and the shortest distance from the spiracle to the basal margin of propodeum (small ≤ 0.3 , middle = $0.35-0.50$, large ≥ 0.55), in lateral view (Fig. 1F). Hind femur width is its maximum width and hind tibia width is its subapical width (Fig. 1I). Hind tarsus length: sum of the lengths of its segments. Metasoma length: sum of the first metasomal tergite (T1) length and the distance from anterior margin of the second tergite to the metasomal apex, in lateral view (Fig. 1K; $t1l+mtl$). Metasoma width is its maximum width in dorsal view (Fig. 1L).

The wing veins and cells mentioned in the descriptions and identification key, along with their respective measurements, are depicted in Fig. 2. For these wing veins, the corresponding terminologies from Fischer (1972) and Wharton et al. (2017) are respectively provided, in parentheses, as follows: fore wing – 2-SR (cuqu1, 2SR); r (r1, r); 3-SR (r2, 3RSa); SR1 (r3, 3RSb); cu-a (nv, 1cu-a); hind wing – m-cu (n. rec., m-cu). Additionally, the equivalent terminology of Fischer (1972) for the wing cells is: marginal (radial) cell, first + second submarginal (cubital) cells, and first subdiscal (brachial) cell. The width of the wings corresponds to their maximum width. In the fore wing, the term submarginal cell refers to the first + second submarginal cells. The length of vein (r+3-SR) was measured as the straight-line distance between its intersection with the pterostigma and the r-m vein (Fig. 2A).

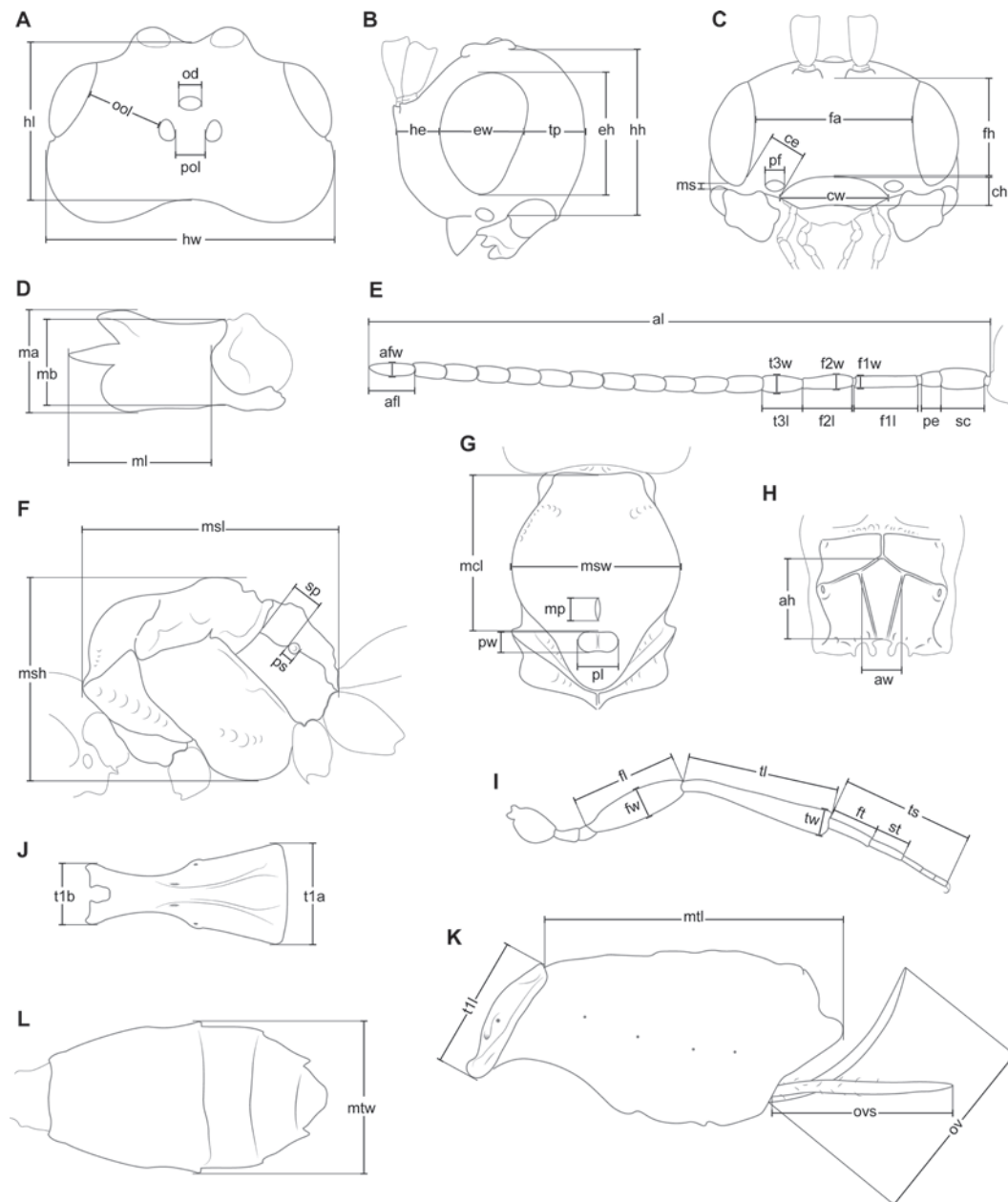


Figure 1. Measurements of head, mandible, antenna, mesosoma, leg, and metasoma **A, B, C** head, dorsal, lateral, and frontal view respectively **D** mandible, lateral view **E** antenna **F** mesosoma, lateral view **G** mesonotum, dorsal view **H** propodeum, dorsal view **I** hind leg **J** first metasomal tergite (T1), dorsal view **K** metasoma, lateral view **L** metasoma (without T1), dorsal view. Abbreviations: afl – apical flagellar segment length, afw – apical flagellar segment width, ah – areola height, al – antenna length, aw – areola width, ce – distance from clypeus to eye, ch – clypeus height, cw – clypeus width, eh – eye height, ew – eye width, f1l – first flagellar segment length, f1w – first flagellar segment width, f2l – second flagellar segment length, f2w – second flagellar segment width, fa – face width, fh – face height, fl – femur length, ft – first segment of tarsus (basitarsus) length, fw – femur width, he – head (partial) extension, hh – head height, hl – head length, hw – head width, ma – mandibular apical width, mb – mandibular basal width, mcl – mesoscutum length, ml – mandible length, mp – mesoscutal pit length, ms – malar space, msh – mesosoma height, msl – mesosoma length, msw – mesosoma width, mtl – metasoma (partial) length, mtw – metasoma width, od – ocellus diameter, ool – ocular-ocellar line, ov – ovipositor length, ovs – ovipositor sheath length, pe – pedicel length, pf – paraclypeal fovea diameter, pl – prescutellar depression length, pol – posterior-ocellar line, ps – propodeal spiracle diameter, pw – prescutellar depression width, sc – scape length, sp – distance from spiracle to base of propodeum, st – second segment of tarsus length, t1a – first metasomal tergite apical width, t1b – first metasomal tergite basal width, t1l – first metasomal tergite length, t3l – third flagellar segment length, t3w – third flagellar segment width, tl – tibia length, tp – temple width, ts – tarsus length, tw – tibia width.

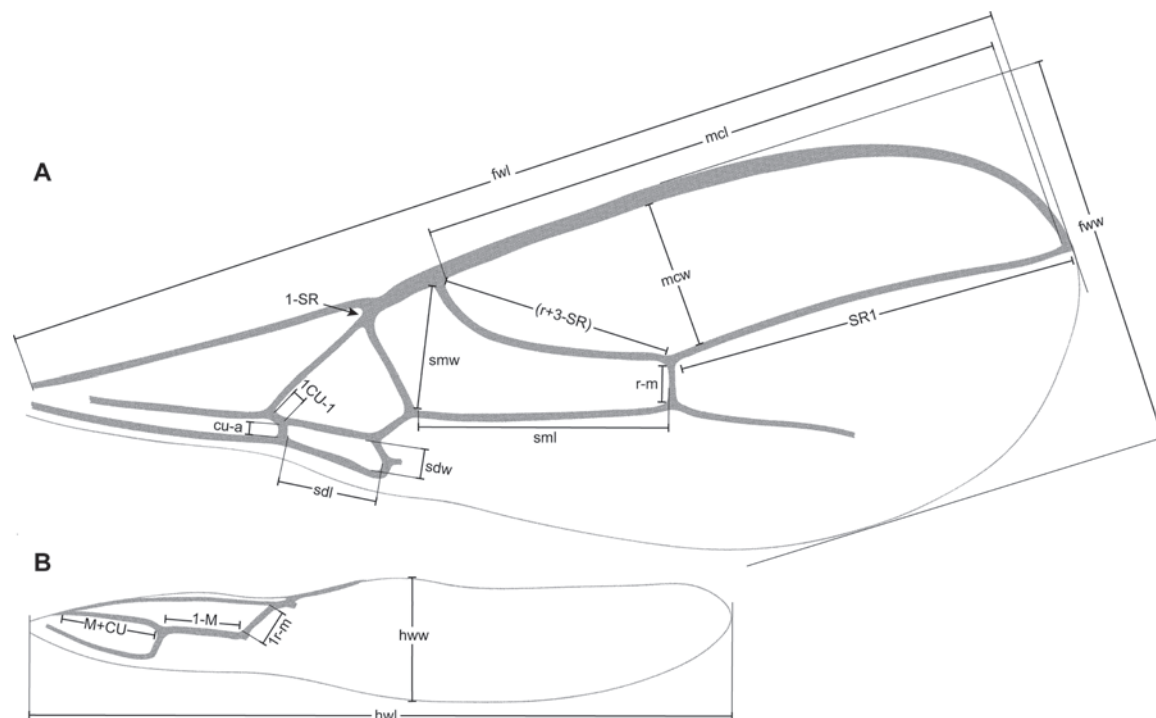


Figure 2. Wing measurements **A** fore wing **B** hind wing. Abbreviations: fwl – fore wing length, fww – fore wing width, hwl – hind wing length, hww – hind wing width, mcl – marginal cell length, mcw – marginal cell width, sdl – subdiscal cell length, sdw – subdiscal cell width, sml – submarginal cell length, smw – submarginal cell width.

Different types of propodeal sculpture and areolation are schematically represented in Fig. 3. The propodeal median longitudinal carina was considered incomplete when it is clearly interrupted (Fig. 3A, F, G), and complete when it crosses the propodeum from the basal to apical margin (Fig. 3B–D, H). Transverse carinae are incomplete when distinctly separated from the lateral parts (sides) of propodeum (Fig. 3A, B), and complete when they extend to the lateral of propodeum, at spiracle margin or lateral carina (Fig. 3C–H). The propodeal surface and the development of carinae were evaluated independently. For instance, the propodeum may exhibit a mainly smooth surface combined with poorly developed carinae (Fig. 3A), or a mainly smooth surface along with a distinct areola and complete carinae (Fig. 3H). A widely sculptured propodeum may exhibit distinct carination (as depicted in Fig. 3D), or the carinae may be lacking or indiscernible.

Digital scanning electronic microscope (SEM) photographs of uncoated specimens were taken with a FEI Quanta 250 SEM in a low vacuum mode. Color digital photographs were taken with a Leica M250C stereomicroscope, using a Leica MC170 HD camera and Leica Application Suite software v. 4.12. Measurements of the specimens were conducted using digital photographs taken with a Leica M165C stereomicroscope, Leica DFC295 HD camera, and Leica Application Suite software v. 3.7. Adobe Illustrator v. 24.1.2 was utilized for illustrations, and Adobe Photoshop CS5 Extended v. 12.1. for minor adjustments to photographs and preparation of the plates.

Abbreviations used throughout the descriptions are as follows: **POL** post-ocellar line (shortest distance between lateral ocelli), **OD** ocellus diameter (maximum diameter of ocellus), **OOL** ocular-ocellar line (shortest distance between lateral ocellus and eye), **F1** first flagellar segment, **F2** second flagellar segment, **F3** third flagellar segment, **AF** apical flagellar segment, **T1** first metasomal tergite.

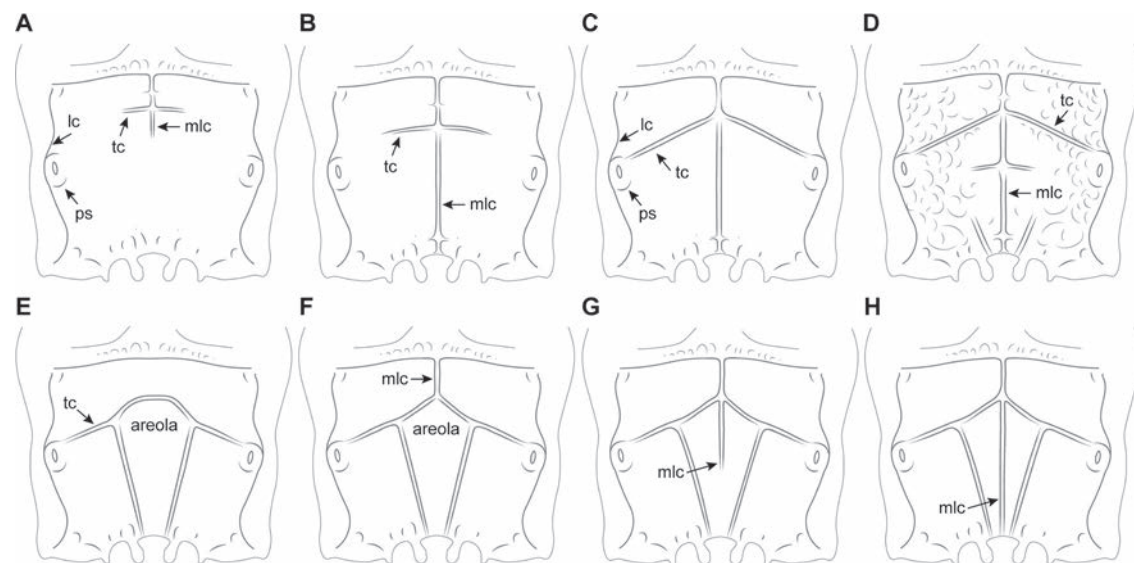


Figure 3. Schematic representation of the various types of propodeal sculpture and areolation in New World species of *Synaldis* **A** propodeum with median longitudinal carina and transverse carinae incomplete, short **B** propodeum with median longitudinal carina complete and transverse carinae incomplete **C** propodeum mainly smooth, with median longitudinal carina and transverse carinae complete **D** propodeum mainly rugose, with median longitudinal carina and transverse carinae complete (areola absent) **E** propodeum with areola and transverse carinae complete (median longitudinal carina absent) **F** propodeum with areola and transverse carinae complete, median longitudinal carina incomplete, basal (not extending inside the areola) **G** propodeum with areola and transverse carinae complete, median longitudinal carina incomplete apically, reaching mid-areola **H** propodeum with areola, median longitudinal carina and transverse carinae complete. Abbreviations: lc – lateral carina, mlc – median longitudinal carina, ps – propodeal spiracle, tc – transverse carina.

Type specimens were collected by Dr D. S. Amorim and Dr V. C. Silva, with loans provided by the former. They originate from collections conducted during expeditions to the southern Chile in Valdivian temperate rainforest at Parque Nacional Puyehue (refer to Amorim et al. 2022). The holotypes and some paratypes are deposited in the Entomology Area of the Museo Nacional de Historia Natural, Santiago, Chile (MNNC), while the remaining paratypes are deposited in the Coleção Taxonômica do Departamento de Ecologia e Biologia Evolutiva, São Carlos, Brazil (DCBU).

Taxonomic account

Subfamily Alysiinae Leach, 1815

Tribe Alysiini Leach, 1815

Genus *Dinotrema* Foerster, 1863

Type species. *Dinotrema erythroga* Foerster, 1863.

Subgenus *Synaldis* Foerster, 1863

Type species. *Bassus concolor* Nees von Esenbeck, 1812 (monobasic).

Foerster 1863: 273 (original designation as genus); van Achterberg 1988: 21 (as synonym of *Dinotrema*); Fischer 1993a: 452 (as genus); Zhu et al. 2017: 38 (as subgenus).

Diagnosis. Mandibles tridentate, teeth of differing shape and length, sometimes upper tooth very small. Paraclypeal fovea small, clearly separated from eye. Precoxal sulcus always present. Pterostigma very long and narrow. Fore wing vein 2-SR always absent, resulting the first and second submarginal cells confluent; break between veins r and 3-SR absent. Vein cu-a often postfurcal, rarely almost interstitial. Metasoma with tergites not very narrowed apically in lateral view, apical sternites and ovipositor not strongly retracted under long apical tergites.

Hosts. Diptera larvae of the family Phoridae and possibly Drosophilidae.

Comments. The subgenus *Synaldis* Foerster, 1863 from the genus *Dinotrema* is recorded in the fauna of Chile for the first time.

***Dinotrema (Synaldis) acarinareolatum* sp. nov.**

<https://zoobank.org/EB2DFDFC-9722-46DB-8CBE-C8C067947E3E>

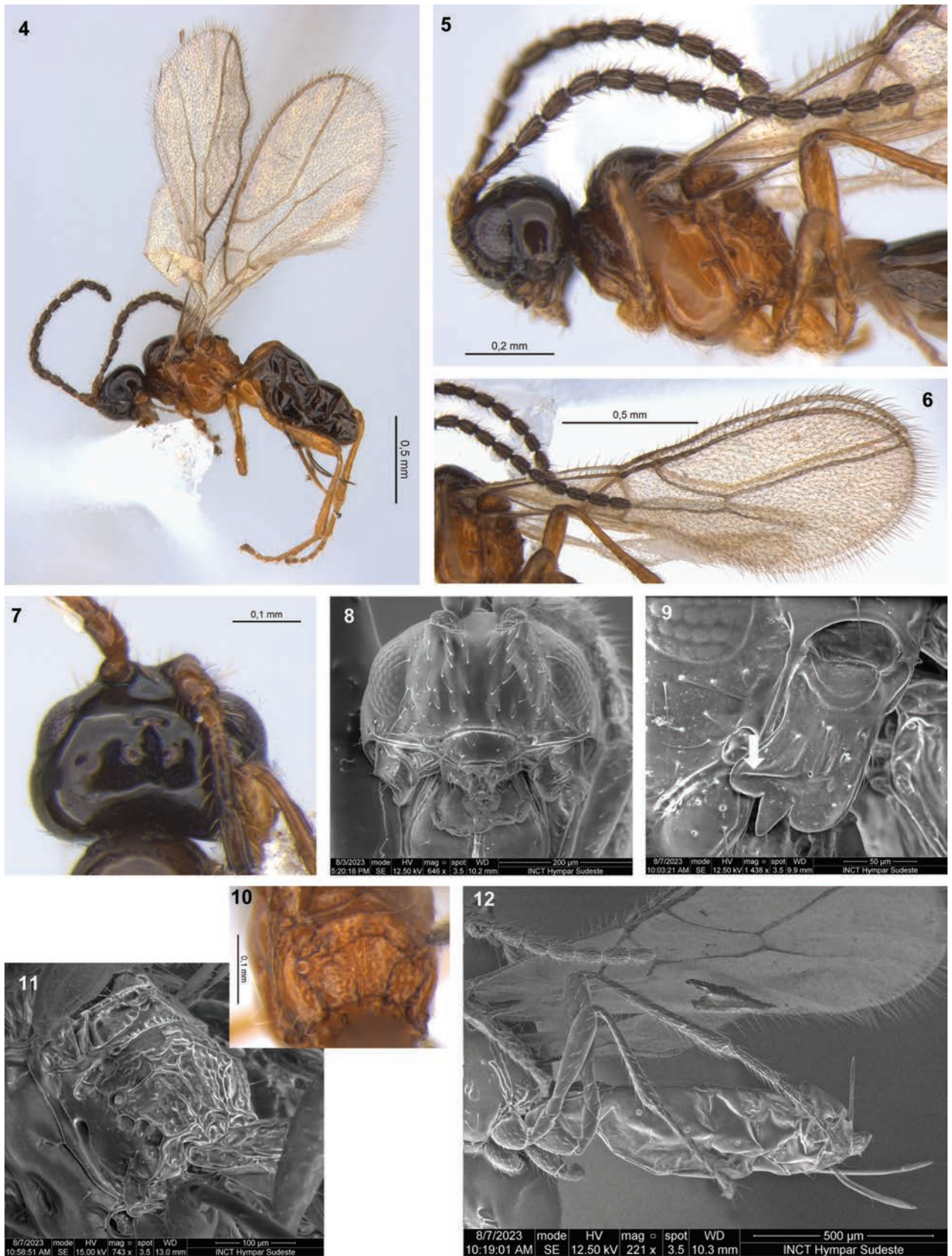
Figs 4–12

Type material. Holotype: CHILE • ♀ (MNNC); Osorno, Parque Nacional Puyehue, Antillanca; 40°46'55"S, 72°12'39"W; alt. 987 m; 9–23 Dec. 2019; D. Amorim and V. Silva leg.; Malaise trap. **Paratypes:** CHILE • 1♀ (DCBU 514718) and 1♂ (MNNC); same data as for holotype.

Diagnosis. This species differs from other New World species of *Synaldis* by the sculpture of the propodeum, with distinct areola and transverse carinae complete, but median longitudinal carina absent (Figs 3E, 10, 11). Additionally, *D. (S.) acarinareolatum* sp. nov. can be differentiated by combination of following characteristics: OOL of ♀ 4.0× as OD (Fig. 7); in lateral view, eye shorter than temple (Fig. 5); mandible with three relatively large teeth, diagonal carina distinct, mandibular apex wider than base (Fig. 9); F1 2.4–2.5× as long as wide (Fig. 5); mesoscutal pit present, but sometimes very weak; fore wing vein cu-a postfurcal, 1-CU1 slightly shorter than cu-a, first subdiscal cell 2.5× as long as wide (Figs 4, 6), hind wing 6.2× as long as wide, vein 1-M 2.3–2.4× as long as 1r-m; hind tibia 8.5–8.7× as long as wide.

Description. ♀. Length. Body: 1.8–1.9 mm. Fore wing: 1.6–1.8 mm. Hind wing: 1.2–1.3 mm.

Head: in dorsal view (Fig. 7), 1.50–1.65× as wide as long, 1.5–1.6× as wide as mesosoma, wider at temples than eyes. Frons smooth. POL 1.5× as OD, OOL 4.0× as OD. In lateral view (Fig. 5), eye 1.4–1.5× as high as wide, 0.6–0.7× as wide as temple. Face 1.8× as wide as high (Fig. 8), 1.8× as wide as clypeus, with a weak longitudinal ridge dorsally. Clypeus 2.4× as wide as high, concave ventrally. Malar space 0.7× as clypeus height. Paraclypeal fovea short. Mandible 1.2–1.3× as long as wide (Fig. 9), diagonal carina present, strong. Mandibular apex 1.2× wide as base. Upper tooth rounded. Middle tooth subacuminate, longer than other teeth. Lower tooth largely rounded, as long as upper tooth. Lower tooth slightly wider than upper, both wider than middle tooth. Antenna with 15–16 segments (Fig. 5), 0.7–0.8× as long as body. Scape 1.7× as long as pedicel. F1 2.4–2.5× as long as wide, 1.1–1.2× as long as F2. F2 1.6–1.8× as long as wide. F3 1.4–1.7× as long as wide. AF 1.8× as long as wide. Maxillary palp 0.8× as long as head height.



Figures 4–12. *Dinotrema (Synaldis) acarinareolatum* sp. nov. (4, 10 holotype ♀, remainder paratypes ♀, except 7, 11 ♂) 4 habitus, lateral view 5 antenna, head and mesosoma, lateral view 6 fore wing 7 head, dorsal view 8 head, frontal view 9 mandible, lateral view, arrow showing the diagonal carina 10, 11 propodeum, dorsal and laterodorsal view 12 hind leg, metasoma and ovipositor, lateral view.

Mesosoma: 1.2–1.3× as long as high (Fig. 5), 2.0–2.1× as long as wide. Mesoscutum approximately as long as wide, notauli absent on horizontal surface of mesoscutum. Mesoscutal pit present, distinct and oval, or very weak and rounded, occupying 0.1× of mesoscutal length. Prescutellar depression 1.9–2.1× as long as wide, with median carina incomplete anteriorly to complete, smooth laterally. Side of pronotum weakly crenulate. Precoxal sulcus crenulate medially, not reaching anterior and/or posterior margins of mesopleuron. Posterior mesopleural furrow smooth. Propodeum mainly rugulose to rugose (Figs 10, 11), with areola 0.9× as high as wide; median longitudinal carina absent; transverse carinae complete. Propodeum with very weak protuberance in lateral view. Propodeal spiracle small (Fig. 5), 0.3× distance from spiracle to base of propodeum.

Wings: fore wing 2.7× as long as wide, vein 1-SR present, (r+3-SR) 5.7–5.8× as long as r-m, SR1 2.40–2.55× as long as (r+3-SR); cu-a postfurcal, 1-CU1 0.9× as long as cu-a. Marginal cell 4.00–4.25× as long as wide, submarginal cell 2.0–2.2× as long as wide, first subdiscal cell 2.5× as long as wide (Figs 4, 6). Hind wing 6.2× as long as wide, vein 1-M 0.6–0.7× as long as M+CU, 2.3–2.4× as long as 1r-m; m-cu absent.

Legs: hind femur 4.0× as long as wide. Hind tibia 8.5–8.6× as long as wide, 1.1× as long as hind tarsus. First segment of hind tarsus 2.0–2.1× as long as second segment (Fig. 12).

Metasoma: 1.7–1.9× as long, and 1.3× as wide as mesosoma. T1 strigose, 1.9× as long as wide, apex 1.4× as wide as base. Ovipositor 0.4× as long as metasoma, 1.5–2.0× as long as T1, 1.1–1.3× as long as hind femur. Ovipositor sheath with some sparse and delicate setae (except on 1/3 apical almost glabrous), 0.3–0.4× as long as metasoma, 1.4× as long as T1 (Figs 4, 12).

Color: head, antennae, pronotum, mesoscutum and metasoma from the second tergite dark brown to brown. Mandibles and side of pronotum light brown. Remaining parts of mesosoma, legs, T1, and ovipositor yellowish. Wings hyaline, veins brown.

Male. Body length 1.6 mm. POL 1.3× OD, OOL 3.0× OD. Face 1.7× as wide as high, 2.1× as wide as clypeus. Clypeus 2.0× as wide as high. Mandible 1.4× as long as wide. Antenna with 18 segments, as long as body. F1 as long as F2. F2 2.0× as long as wide. F3 1.9× as long as wide. Maxillary palp as long as head height. Mesosoma 2.2× as long as wide. Prescutellar depression 1.8× as long as wide. Hind femur 4.2× as long as wide. Hind tibia 8.7× as long as wide. Metasoma 1.5× as long as mesosoma.

Etymology. The epithet is an adjective combining *acarina* (prefix *a-* indicating negation, with *carina* from Latin) and *areolatum* (derived from *areola* in Latin). The species name refers to the sculpture of propodeum, which lacks a median longitudinal carina and has a distinct areola (Figs 10, 11).

Distribution. Chile.

Comments. Based on its eye being shorter than temple, as well as its relatively thickened flagellomeres and legs, *D. (S.) acarinareolatum* sp. nov. appears to be related to the described here *D. (S.) daltoni* sp. nov., *D. (S.) perisfelipoi* sp. nov. and *D. (S.) puyehue* sp. nov., especially to the former. The differences between these species are given in the identification key.

***Dinotrema (Synaldis) brunneum* sp. nov.**

<https://zoobank.org/05E15272-7217-4B01-9F5C-90BA7275B75C>

Figs 13–22

Type material. Holotype: CHILE • ♀ (MNNC); Osorno, Parque Nacional Puyehue, Antillanca; 40°44'06"S, 72°19'47"W; alt. 528 m; 14 Jan.–3 Feb. 2017; D. Amorim and V. Silva leg.; flight intercept trap. **Paratypes:** CHILE • 1♂ (MNNC); same data as for holotype, except 40°44'S, 72°19'W; alt. 440 m; sweeping • 2♀♀ (DCBU 387261, DCBU 387295); same data as for holotype, except 40°44'S, 72°19'W; alt. 440 m; sweeping.

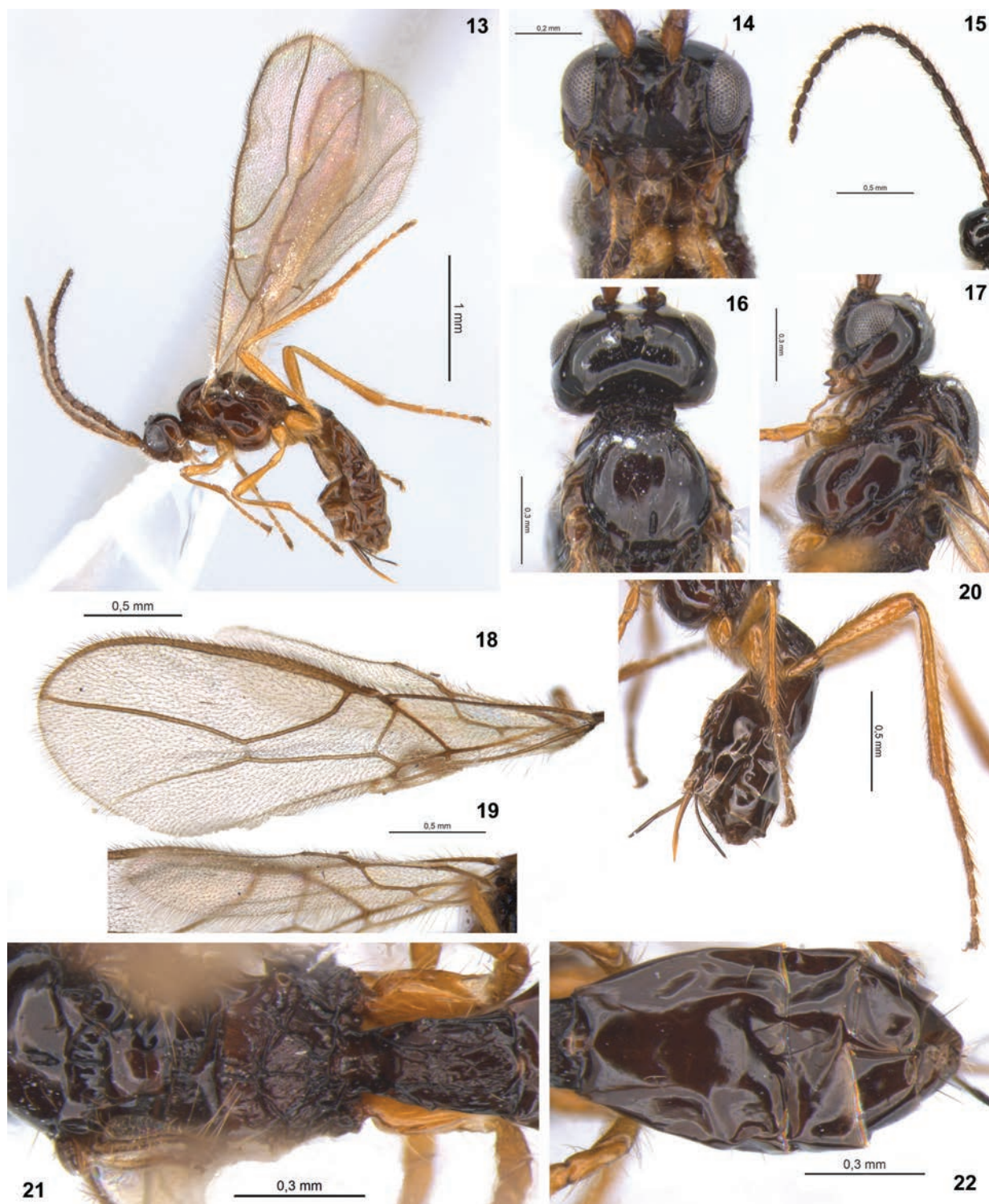
Diagnosis. This species differs from other New World species of *Synaldis* by the combination of the following characteristics: in lateral view, eye wider than temple (Fig. 17); paraclypeal fovea middle size (Fig. 14); mandible with three relatively large teeth, diagonal carina weak, mandibular apex wider than base; F1 2.7–3.3× as long as wide (Fig. 15); mesoscutal pit present, conspicuous (Fig. 16); propodeum with areola, median longitudinal carina and transverse carinae complete (Fig. 21); fore wing vein cu-a postfurcal, 1-CU1 shorter than cu-a (Fig. 18); hind tibia 9.8–10.3× as long as wide (Fig. 20).

Dinotrema (S.) brunneum sp. nov. is similar to *D. (S.) chilense* sp. nov. (see their differences in the identification key) and *D. (S.) verae* sp. nov., from which it can be distinguished by head and mesoscutum brown to dark brown (head dorsally dark brown to brown, but mesoscutum yellowish, lighter than head in *D. (S.) verae* sp. nov., Figs 16, 99), T1 strigose (rugose–foveolate in *D. (S.) verae* sp. nov., Figs 21, 104), fore wing vein (r+3-SR) 5.6–5.9× as long as r-m (4.8–5.1× in *D. (S.) verae* sp. nov., Figs 18, 101), hind femur 4.7–5.0× as long as wide (4.2–4.3× in *D. (S.) verae* sp. nov.), hind tibia 9.8–10.0× as long as wide (8.6–8.9× in *D. (S.) verae* sp. nov., Figs 20, 105).

Description. ♀. Length. Body: 2.5–2.8 mm. Fore wing: 2.6–2.9 mm. Hind wing: 2.0–2.1 mm.

Head: in dorsal view (Fig. 16), 1.7–1.9× as wide as long, 1.3× as wide as mesosoma, as wide at eyes as temples or slightly wider at eyes. Frons smooth or with weak mid groove. POL 1.5× as OD, OOL 2.6× as OD. In lateral view (Fig. 17), eye 1.4–1.5× as high as wide, 1.1–1.2× as wide as temple. Face 1.6× as wide as high (Fig. 14), 1.8–2.0× as wide as clypeus, smooth or punctate, with a weak longitudinal ridge dorsally. Clypeus 1.8–1.9× as wide as high, concave ventrally. Malar space 0.5–0.6× as clypeus height. Paraclypeal fovea middle size. Mandible 1.2–1.4× as long as wide, diagonal carina present, weak. Mandibular apex 1.2× wide as base. Upper tooth rounded. Middle tooth acute, longer than other teeth. Lower tooth rounded or nearly so, as long as upper tooth. Upper tooth ca as wide as lower, wider than middle tooth. Antenna with 18–20 segments (Fig. 15), 0.7–0.9× as long as body. Scape 1.8× as long as pedicel. F1 2.7–3.0× as long as wide, 1.2× as long as F2. F2 1.9–2.2× as long as wide. F3 1.8–2.0× as long as wide. AF 2.1–2.2× as long as wide. Maxillary palp 1.2× as long as head height.

Mesosoma: 1.2–1.4× as long as high (Fig. 17), 2.0–2.1× as long as wide. Mesoscutum as long as wide, notauli absent on horizontal surface of mesoscutum (Fig. 16). Mesoscutal pit present, oval to elongate, occupying 0.1–0.2× of mesoscutal length. Prescutellar depression 2.0–2.2× as long as wide (Fig. 21), with median carina complete, lateral carinae absent or incomplete anteriorly,



Figures 13–22. *Dinotrema (Synaldis) brunneum* sp. nov. (13 holotype ♀, 14–22 paratype ♀) 13 habitus, lateral view 14 head, frontal view 15 antenna 16 head and mesoscutum, dorsal view 17 head and mesosoma, lateral view 18 fore wing 19 hind wing 20 hind leg, metasoma and ovipositor, lateral view 21 prescutellar depression, propodeum and T1, dorsal view 22 metasoma without T1, dorsal view.

very short. Side of pronotum crenulate. Precoxal sulcus crenulate medially, not reaching anterior and/or posterior margins of mesopleuron (Fig. 17). Posterior mesopleural furrow smooth. Propodeum mainly rugulose to rugose (Fig. 21), with areola 0.8× as high as wide; median longitudinal carina complete or nearly

so (interrupted very briefly apically); transverse carinae complete. Propodeum with protuberance in lateral view. Propodeal spiracle small to middle (Fig. 17), 0.3–0.4× distance from spiracle to base of propodeum.

Wings: fore wing 2.8–2.9× as long as wide, vein 1-SR present, (r+3-SR) 5.6–5.9× as long as r-m, SR1 1.8–1.9× as long as (r+3-SR); cu-a postfurcal, 1-CU1 0.6–0.7× as long as cu-a. Marginal cell 4.1× as long as wide, submarginal cell 1.9–2.1× as long as wide, first subdiscal cell 2.8–2.9× as long as wide (Fig. 18). Hind wing 5.4× as long as wide, vein 1-M 0.5–0.6× as long as M+CU, 1.3–1.7× as long as 1r-m; m-cu absent (Fig. 19).

Legs: hind femur 4.7–5.0× as long as wide. Hind tibia 9.8–10.0× as long as wide, 1.1–1.2× as long as hind tarsus. First segment of hind tarsus 1.8–1.9× as long as second segment (Fig. 20).

Metasoma: 1.5–1.7× as long, and as wide as mesosoma (Figs 13, 22). T1 strigose (Fig. 21), 1.7–1.8× as long as wide, apex 1.3–1.6× as wide as base. Ovipositor 0.2–0.3× as long as metasoma, 0.9–1.4× as long as T1, 0.6–0.8× as long as hind femur. Ovipositor sheath with some delicate setae (except on 1/3 apical almost glabrous), 0.2–0.3× as long as metasoma, 0.9–1.2× as long as T1 (Figs 13, 20).

Color: dark brown to brown, except mandibles, legs, and ovipositor yellowish. Wigs hyaline, veins brown.

Male. Body length 2.9 mm, fore wing 3.1 mm, hind wing 2.2 mm. POL 1.4× as OD, OOL 2.3× as OD. Eye 1.3× as wide as temple. Face 1.45× as long as high. Mandibular apex 1.1× as wide as base. Antenna with 25 segments, 1.1× as long as body. F1 3.3× as long as wide, 1.4× as long as F2. F3 2.3× as long as wide. AF 2.5× as long as wide. Propodeum rugose medially. Fore wing 3.1× as long as wide, vein 1-CU1 0.9× as long as cu-a. First subdiscal cell 2.6× as long as wide. Hind tibia 10.3× as long as wide.

Etymology. The epithet is an adjective derived from *brunneus*, which means brown in Latin. The species name refers to its predominantly brown body color (Figs 13–22).

Distribution. Chile.

Dinotrema (Synaldis) chilense sp. nov.

<https://zoobank.org/6C3824F7-549C-47CE-B07E-9D69338D71F5>

Figs 23–33

Type material. Holotype: CHILE • ♀ (MNNC); Osorno, Parque Nacional Puyehue, Antillanca; 40°44'S, 72°19'W; alt. 440 m; 14 Jan.–3 Feb. 2017; D. Amorim and V. Silva leg.; sweeping. **Paratypes:** CHILE • 3♀♀ (MNNC); same data as for holotype • 3♀♀ (MNNC) and 1♂ (MNNC); same data as for holotype, except 40°44'06"S, 72°19'47"W; alt. 528 m; flight intercept trap • 1♀ (DCBU 387163) and 1♂ (DCBU 386948); same data as for holotype • 4♀♀ (DCBU 385728, DCBU 386175, DCBU 386465, DCBU 386544); same data as for holotype, except 40°44'06"S, 72°19'47"W; alt. 528 m; flight intercept trap • 1♀ (DCBU 386168); same data as for holotype, except 40°44'06"S, 72°19'47"W; alt. 528 m; Malaise trap.

Diagnosis. This species differs from other New World species of *Synaldis* by the combination of the following characteristics: in lateral view, eye as wide as or slightly wider than temple (Fig. 31); mandible with three relatively large teeth, diagonal carina present, mandibular apex wider than base (Fig. 28); F1 2.8–3.2×

as long as wide (Fig. 25); mesoscutal pit present, conspicuous; propodeum with areola, median longitudinal carina incomplete apically, transverse carinae complete (Fig. 27); fore wing vein cu-a distinctly postfurcal, 1-CU1 as long as or longer than cu-a (Fig. 29); hind tibia 9.0–9.4× as long as wide (Fig. 32).

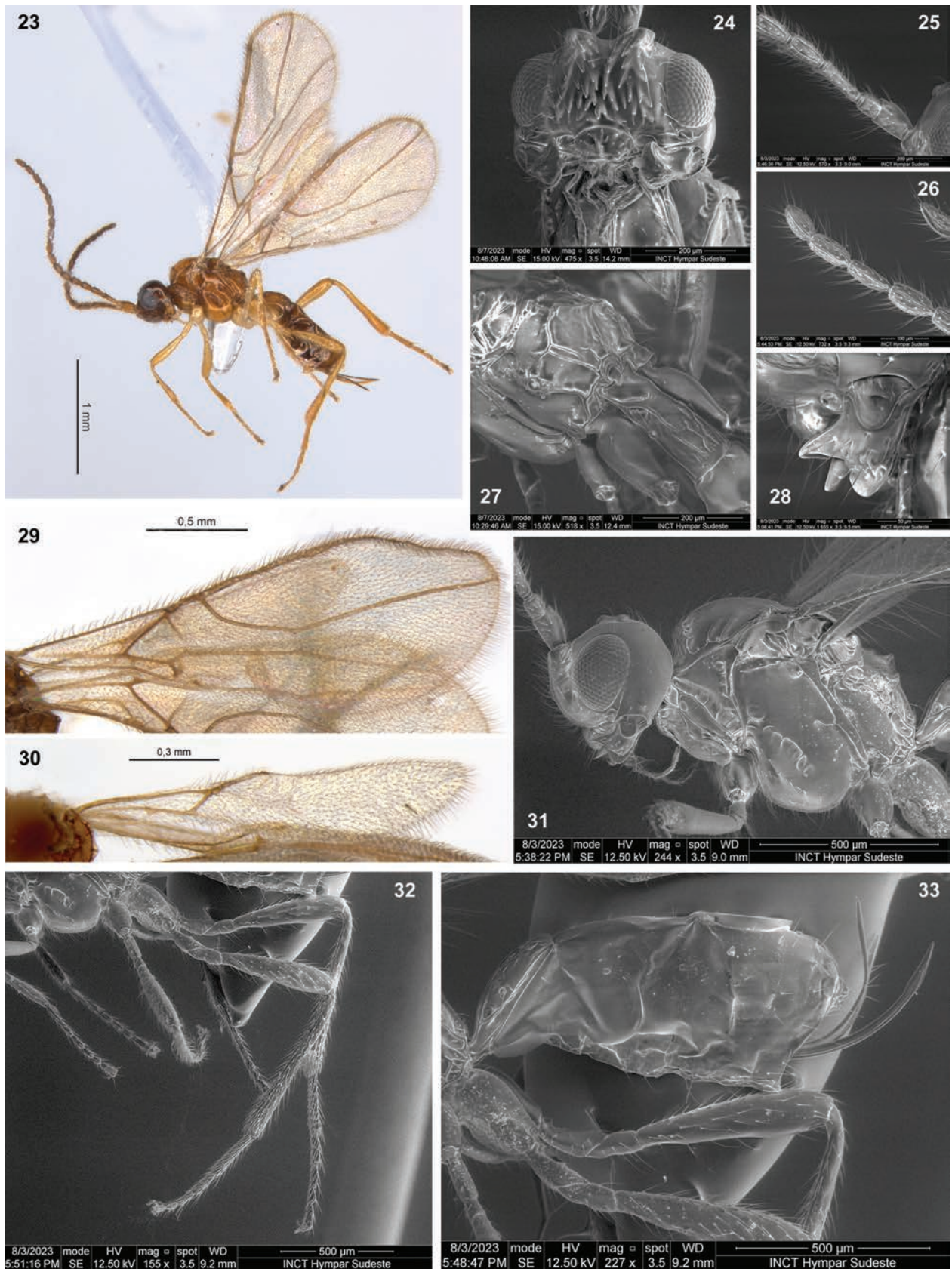
Dinotrema (*S.*) *chilense* sp. nov. is similar to *D.* (*S.*) *brunneum* sp. nov. (see their differences in the identification key) and *D.* (*S.*) *verae* sp. nov., differing from the latter by paraclypeal fovea short size (middle in *D.* (*S.*) *verae* sp. nov., Figs 24, 97), fore wing vein (r+3-SR) 5.6–6.4× as long as r-m (5.1× in *D.* (*S.*) *verae* sp. nov.), 1-CU1 1.0–1.4× as long as cu-a (0.55–0.70× in *D.* (*S.*) *verae* sp. nov., Figs 29, 101), hind wing vein 1-M of ♀ 1.7× as long as 1r-m (1.2× in *D.* (*S.*) *verae* sp. nov.), T1 strigose to rugose (rugose–foveolate in *D.* (*S.*) *verae* sp. nov., Figs 27, 104).

Dinotrema (*S.*) *chilense* sp. nov. is also somewhat similar to *D.* (*S.*) *flavum* sp. nov., from which it can be distinguished by face and clypeus brown to dark brown (yellow in *D.* (*S.*) *flavum* sp. nov.), AF 2.0–2.3× as long as wide (2.7× in *D.* (*S.*) *flavum* sp. nov.), metasoma 0.8× as wide as mesosoma (1.3× in *D.* (*S.*) *flavum* sp. nov.), hind wing 5.6–5.8× as long as wide and vein 1-M 1.4–1.7× as long as 1r-m (6.2× and 2.0× respectively in *D.* (*S.*) *flavum* sp. nov.), hind femur 4.5–4.9× as long as wide (4.2× in *D.* (*S.*) *flavum* sp. nov.), hind tibia 9.0–9.4× as long as wide (10.1–10.4× in *D.* (*S.*) *flavum* sp. nov., Figs 32, 54).

Description. ♀. Length. Body: 1.9–2.6 mm. Fore wing: 2.05–2.65 mm. Hind wing: 1.5–2.0 mm.

Head: in dorsal view, 1.7–2.0× as wide as long, 1.3–1.5× as wide as mesosoma, as wide at eyes as at temples or slightly wider at temples. Frons smooth or with weak mid groove. POL 1.2–1.4× as OD, OOL 2.6–3.0× as OD. In lateral view (Fig. 31), eye 1.2–1.5× as high as wide, 1.0–1.2× as wide as temple. Face 1.4–1.7× as wide as high (Fig. 24), 1.8–2.0× as wide as clypeus, smooth or with a weak longitudinal ridge dorsally. Clypeus 1.8–2.1× as wide as high, slightly concave ventrally. Malar space 0.5–0.6× as clypeus height. Paraclypeal fovea short size. Mandible 1.2–1.4× as long as wide (Fig. 28), diagonal carina present. Mandibular apex 1.2–1.4× wide as base. Upper tooth almost rounded. Middle tooth acute, longer than other teeth. Lower tooth rounded, as long as or slightly longer than upper tooth. Upper tooth ca as wide as lower, wider than middle tooth. Antenna with 17–21 segments, 0.9–1.0× as long as body. Scape 1.80–2.05× as long as pedicel. F1 2.8–3.2× as long as wide (Fig. 25), 1.0–1.2× as long as F2. F2 2.2–2.4× as long as wide. F3 1.9–2.2× as long as wide. AF 2.0–2.3× as long as wide (Fig. 26). Maxillary palp 1.1–1.2× as long as head height.

Mesosoma: 1.2–1.4× as long as high (Fig. 31), 2.05–2.30× as long as wide. Mesoscutum ca as long as wide, notauli absent on horizontal surface of mesoscutum. Mesoscutal pit present, oval–elongate, occupying 0.1–0.3× of mesoscutal length. Prescutellar depression 2.0–2.2× as long as wide, with median carina complete or incomplete anteriorly (very weak), lateral carinae absent to almost complete. Side of pronotum crenulate, sometimes weakly. Precoxal sulcus crenulate medially, not reaching margins of mesopleuron, or almost reaching its anterior margin. Posterior mesopleural furrow smooth. Propodeum mainly smooth to rugulose (except inside areola with some rugae) (Fig. 27), with areola 1.0–1.1× as high as wide; median longitudinal carina incomplete apically, not extending inside areola or reaching at most its middle; transverse carinae complete. Propodeum with protuberance in lateral view. Propodeal spiracle small to middle (Fig. 31), 0.3–0.4× distance from spiracle to base of propodeum.



Figures 23–33. *Dinotrema (Synaldis) chilense* sp. nov. (23 holotype ♀, 24–31 paratypes ♀) 23 habitus, lateral view 24 head, frontal view 25, 26 basal and apical parts of antenna respectively 27 propodeum and T1, dorsal view 28 mandible, lateral view 29 fore wing 30 hind wing 31 head and mesosoma, lateral view 32 hind leg 33 metasoma and ovipositor, lateral view.

Wings: fore wing 2.6–2.9× as long as wide, vein 1-SR present, (r+3-SR) 5.6–6.4× as long as r-m, SR1 2.0–2.2× as long as (r+3-SR); cu-a distinctly postfurcal, 1-CU1 1.2–1.4× as long as cu-a. Marginal cell 4.4–4.6× as long as wide, submarginal cell 2.2–2.5× as long as wide, first subdiscal cell 3.0–3.3× as long as wide (Fig. 29). Hind wing 5.6–5.8× as long as wide, vein 1-M 0.5–0.6× as long as M+CU, 1.7× as long as 1r-m; m-cu absent (Fig. 30).

Legs: hind femur 4.5–4.7× as long as wide. Hind tibia 9.0–9.4× as long as wide, 1.0–1.2× as long as hind tarsus. First segment of hind tarsus 1.9–2.2× as long as second segment (Fig. 32).

Metasoma: 1.4–1.8× as long, and 0.8× as wide as mesosoma (Fig. 23). T1 strigose to rugose (Fig. 27), 1.9–2.2× as long as wide, apex 1.2–1.5× as wide as base. Ovipositor 0.35–0.50× as long as metasoma, 1.20–1.75× as long as T1, 0.7–1.2× as long as hind femur. Ovipositor sheath with some delicate setae (except on 1/4 apical almost glabrous), 0.35–0.50× as long as metasoma, 1.20–1.55× as long as T1 (Figs 23, 33).

Color: head brown to dark brown. Mesosoma light brown to yellow. Mandibles and legs yellowish. Antennae and metasoma brown to yellow. Wings hyaline to slightly darkened, veins light brown to brown.

Variation. The female of this species has two morphological groups, characterized by:

I) fore wing vein (r+3-SR) 5.5–5.9× as long as r-m, OOL 2.6–2.8× as OD, body length 2.2–2.6 mm,

II) fore wing vein (r+3-SR) 6.3–6.4× as long as r-m, OOL 2.9–3.0× as OD, body length 1.9–2.2 mm.

Male. Body length 1.4–2.1 mm, fore wing length 1.5–1.7 mm, hind wing length 1.1–1.7 mm. OOL 2.6–3.4× as OD. Antenna with 18–23 segments, 1.2–1.3× as long as body. F3 2.5× as long as wide. Fore wing vein SR1 2.4× as long as (r+3-SR), marginal cell 4.2× as long as wide. Hind wing vein 1-M 1.4–1.7× as long as 1r-m. Metasoma as wide as mesosoma.

Etymology. The name of species *chilense* is a gentile adjective derived from Latin in reference to Chile, the country where this species was found.

Distribution. Chile.

***Dinotrema (Synaldis) daltoni* sp. nov.**

<https://zoobank.org/F2451134-8798-42F3-AD97-539322A274D8>

Figs 34–45

Type material. Holotype: CHILE • ♀ (MNNC); Osorno, Parque Nacional Puyehue, Antillanca; 40°44'06"S, 72°19'47"W; alt. 528 m; 14 Jan.–3 Feb. 2017; D. Amorim and V. Silva leg.; flight intercept trap. **Paratypes:** CHILE • 1♀ (MNNC); same data as for holotype, except 40°44'S, 72°19'W; alt. 440 m; sweeping • 1♂ (MNNC); same data as for holotype, except 40°46'55"S, 72°12'39"W; alt. 987 m; 23 Dec. 2019–6 Jan. 2020; Malaise trap • 2♀♀ (DCBU 386560, DCBU 386360); same data as for holotype • 1♀ (DCBU 387144); same data as for holotype, except 40°44'S, 72°19'W; alt. 440 m; sweeping.

Diagnosis. This species differs from other New World species of *Synaldis* by the combination of the following characteristics: in lateral view, eye shorter than temple (Fig. 39); mandible with three relatively large teeth, mandibular

apex wider than base (Fig. 37); malar space $0.8\times$ as clypeus height (Fig. 36); F1 $2.3\text{--}2.5\times$ as long as wide (Fig. 38); mesoscutal pit present, although weak (Fig. 41); propodeum with areola, median longitudinal carina incomplete, basal (not extending inside areola), transverse carinae complete (Fig. 42); propodeal spiracle of ♀ large (Fig. 39) and ♂ middle; fore wing of ♀ with vein cu-a almost interstitial to slightly postfurcal, 1-CU1 distinctly shorter than cu-a; hind tibia $8.1\text{--}8.4\times$ as long as wide (Fig. 43).

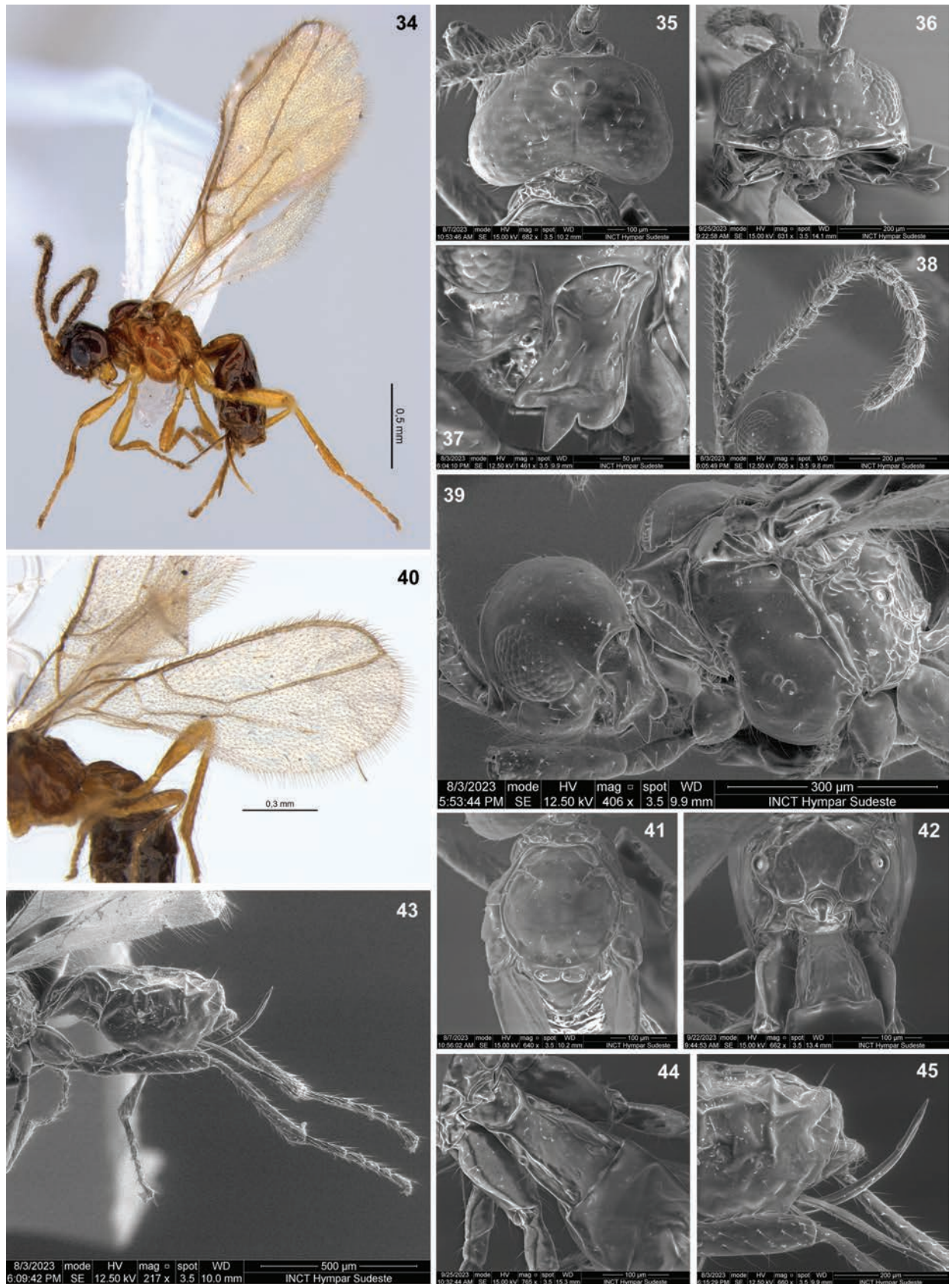
Dinotrema (S.) *daltoni* sp. nov. is similar to *D.* (S.) *perisfelipoi* sp. nov., from which it can be distinguished by fore wing vein (r+3-SR) $5.0\text{--}5.3\times$ as long as r-m ($6.2\text{--}6.3\times$ in *D.* (S.) *perisfelipoi* sp. nov., Figs 34, 69), hind femur $3.7\text{--}4.2\times$ as long as wide ($4.6\text{--}4.8\times$ in *D.* (S.) *perisfelipoi* sp. nov.), hind tibia $8.1\text{--}8.4\times$ as long as wide ($8.9\text{--}9.2\times$ in *D.* (S.) *perisfelipoi* sp. nov., Figs 43, 71), propodeal spiracle of ♀ large and ♂ middle (♀ middle and ♂ small in *D.* (S.) *perisfelipoi* sp. nov., Figs 39, 68). *Dinotrema* (S.) *daltoni* sp. nov. is also similar to *D.* (S.) *puyehue* sp. nov., their differences are given in the identification key.

Description. ♀. Length. Body: $1.5\text{--}1.9$ mm. Fore wing: $1.5\text{--}2.0$ mm. Hind wing: $1.05\text{--}1.40$ mm.

Head: in dorsal view (Fig. 35), $1.6\text{--}2.0\times$ as wide as long, $1.5\text{--}1.6\times$ as wide as mesosoma, wider at temples than eyes. Frons smooth. POL $1.2\text{--}1.3\times$ as OD, OOL $3.4\times$ as OD. In lateral view, eye $1.3\text{--}1.6\times$ as high as wide, $0.6\text{--}0.8\times$ as wide as temple (Fig. 39). Face $1.7\text{--}1.9\times$ as wide as high (Fig. 36), $2.1\times$ as wide as clypeus, with longitudinal ridge dorsally. Clypeus $2.0\text{--}2.2\times$ as wide as high, straight ventrally. Malar space $0.8\times$ as clypeus height. Paraclypeal fovea short size. Mandible $1.2\text{--}1.4\times$ as long as wide, smooth or with diagonal carina weak (Fig. 37). Mandibular apex $1.2\text{--}1.3\times$ wide as base. Upper tooth slightly rounded. Middle tooth subacuminate to slightly acute, longer than other teeth. Lower tooth largely rounded, as long as upper or slightly longer than upper tooth. Upper tooth ca as wide as middle, narrower than lower tooth. Antenna with 14–15 segments (Fig. 38), $0.6\text{--}0.7\times$ as long as body. Scape $1.9\text{--}2.0\times$ as long as pedicel. F1 $2.3\text{--}2.5\times$ as long as wide, $1.1\text{--}1.2\times$ as long as F2. F2 $1.80\text{--}1.95\times$ as long as wide. F3 $1.5\text{--}1.6\times$ as long as wide. AF $2.1\text{--}2.4\times$ as long as wide. Maxillary palp $0.8\text{--}0.9\times$ as long as head height.

Mesosoma: $1.2\text{--}1.3\times$ as long as high (Fig. 39), $2.1\times$ as long as wide. Mesoscutum ca as long as wide, notauli absent on horizontal surface of mesoscutum (Fig. 41). Mesoscutal pit present, weak, rounded or slightly elongate, occupying $0.05\text{--}0.15\times$ of mesoscutal length. Prescutellar depression $2.4\text{--}2.5\times$ as long as wide, with median carina complete, smooth laterally. Side of pronotum weakly crenulate. Precoxal sulcus crenulate medially, short, not reaching anterior and/or posterior margins of mesopleuron (Fig. 39). Posterior mesopleural furrow smooth. Propodeum mainly smooth to rugulose (Fig. 42), with areola $1.1\times$ as high as wide; median longitudinal carina incomplete, not extending inside areola; transverse carinae complete. Propodeum without protuberance in lateral view. Propodeal spiracle large, $0.6\text{--}0.7\times$ distance from spiracle to base of propodeum (Figs 39, 42).

Wings: fore wing $2.8\text{--}2.9\times$ as long as wide, vein 1-SR present, (r+3-SR) $5.0\text{--}5.3\times$ as long as r-m, SR1 $2.4\text{--}2.6\times$ as long as (r+3-SR); cu-a almost interstitial or slightly postfurcal, 1-CU1 $0.3\times$ as long as cu-a. Marginal cell $5.0\times$ as long as wide, submarginal cell $2.2\text{--}2.5\times$ as long as wide, first subdiscal cell $3.1\text{--}3.2\times$ as long as wide (Figs 34, 40). Hind wing $5.5\times$ as long as wide, vein 1-M $0.5\text{--}0.6\times$ as long as M+CU, $1.5\text{--}1.9\times$ as long as 1r-m; m-cu absent.



Figures 34–45. *Dinotrema (Synaldis) daltoni* sp. nov. (34 holotype ♀, 35–45 paratypes ♀) 34 habitus, lateral view 35, 36 head, dorsal and frontal view respectively 37 mandible, lateral view 38 antenna 39 head and mesosoma, lateral view 40 fore wing 41 mesonotum, dorsal view 42 propodeum and T1, dorsal view 43 metasoma and hind leg, lateral view 44 anterior part of metasoma, dorsal view 45 apex of metasoma and ovipositor, lateral view.

Legs: hind femur 3.7–4.0× as long as wide. Hind tibia 8.1–8.4× as long as wide, 1.1–1.2× as long as hind tarsus. First segment of hind tarsus 1.80–1.95× as long as second segment (Fig. 43).

Metasoma: 1.50–1.65× as long, and 1.4× as wide as mesosoma (Fig. 34). T1 smooth to strigose (Fig. 44), 1.7–2.0× as long as wide, apex 1.4–1.5× as wide as base. Ovipositor 0.4–0.8× as long as metasoma, 1.6–2.9× as long as T1, 1.1–1.9× as long as hind femur. Ovipositor sheath with some delicate setae (except on 1/4 apical almost glabrous), 0.4× as long as metasoma, 1.4–1.6× as long as T1 (Figs 43, 45).

Color: dark brown to light brown, except mandibles, mesopleuron, propodeum, T1, and legs yellowish. Wings hyaline, veins brown.

Male. Face 1.5× as wide as high. Clypeus 1.85× as wide as high, slightly concave ventrally. Mandibular middle tooth acute; upper tooth ca as wide a lower, wider than middle tooth. Antenna with 20 segments, 1.1× as long as body. F1 as long as F2. F3 1.7× as long as wide. Mesosoma 1.9× as long as wide. Propodeal spiracle middle size, 0.5× distance from spiracle to base of propodeum. Fore wing 2.6× as long as wide, vein 1-SR absent, SR1 2.3× as long as (r+3-SR), 1-CU1 0.75× as long as cu-a, submarginal cell 2.05× as long as wide. Hind wing 5.6× as long as wide. Hind femur 4.2× as long as wide. First segment of hind tarsus 2.1× as long as second. Metasoma 1.4× as long as mesosoma. T1 with apex 1.6× as wide as base. Head, flagellum and metasoma from the second tergite brown; mandibles, scape, pedicel dark yellow; mesosoma, legs, and T1 yellow.

Etymology. The species name *daltoni* is a genitive noun, named in honor of Dalton de Souza Amorim, one of the collectors and who supplied the type material for this species.

Distribution. Chile.

Comments. *Dinotrema* (*S.*) *daltoni* sp. nov. has enlarged propodeal spiracles, similar to the Nearctic species *Dinotrema* (*Synaldis*) *spiraculosa* (Fischer, 1967). However, unlike *D. (S.) daltoni* sp. nov., in *D. (S.) spiraculosa* the propodeum lacks an areola (despite being sculptured); the eye is as wide as or wider than temple (in lateral view); and the precoxal sulcus sculpture extends to the anterior margin of the mesopleuron (according to Peris-Felipo and Belokobylskij 2017).

***Dinotrema (Synaldis) flavum* sp. nov.**

<https://zoobank.org/3C4BD845-A600-488C-AFB5-8250BD643F91>

Figs 46–54

Type material. Holotype: CHILE • ♀ (MNNC); Osorno, Parque Nacional Puyehue, Antillanca; 40°44'06"S, 72°18'47"W; alt. 528 m; 14 Jan.–3 Feb. 2017; D. Amorim and V. Silva leg.; flight intercept. **Paratype:** CHILE • 1♀ (DCBU 385798); same data as for holotype, except 40°46'28"S, 72°12'41"W; alt. 1054 m; sweeping.

Diagnosis. This species differs from other New World species of *Synaldis* by the combination of the following characteristics: face and clypeus yellow (Fig. 50); in lateral view, eye as wide as temple (Fig. 47); mandible with three relatively large teeth, diagonal carina present, mandibular apex wider than base (Fig. 51); F1 2.7–3.1× as long as wide (Fig. 48); mesoscutal pit present, conspicuous (Fig. 52); propodeum with areola, median longitudinal carina

incomplete apically, transverse carinae complete (Fig. 53); fore wing vein cu-a distinctly postfurcal, 1-CU1 as long as cu-a (Fig. 46); hind wing vein 1-M 2.0× as long as 1-rm; hind tibia 10.1–10.3× as long as wide (Fig. 54).

Dinotrema (S.) *flavum* sp. nov. is similar to *D.* (S.) *chilense* sp. nov. and *D.* (S.) *puyehue* sp. nov. Their distinctions are given, respectively, in the diagnosis of the *D.* (S.) *chilense* and identification key.

Description. ♀. Length. Body: 1.9–2.4 mm. Fore wing: 2.0–2.4 mm. Hind wing: 1.4–1.7 mm.

Head: in dorsal view (Fig. 49), 1.6× as wide as long, 1.50–1.65× as wide as mesosoma, slightly wider at temples than eyes. Frons with weak mid groove. POL 1.1× as OD, OOL 3.0× as OD. In lateral view (Fig. 47), eye 1.4× as high as wide, as wide as temple. Face 1.6× as wide as high (Fig. 50), 1.9–2.0× as wide as clypeus, smooth. Clypeus 2.0–2.1× as wide as high, slightly concave ventrally. Malar space 0.5–0.6× as clypeus height. Paraclypeal fovea short size. Mandible 1.2× as long as wide (Fig. 51), diagonal carina present. Mandibular apex 1.4× wide as base. Upper tooth rounded. Middle tooth acute, longer than other teeth. Lower tooth rounded, as long as upper tooth. Upper tooth ca as wide as lower, wider than middle tooth. Antenna with 18 segments (Fig. 48), as long as body. Scape 1.8–2.0× as long as pedicel. F1 2.7–3.1× as long as wide, 1.1× as long as F2. F2 2.25–2.40× as long as wide. F3 1.8–2.1× as long as wide. AF 2.7× as long as wide. Maxillary palp 1.1× as long as head height.

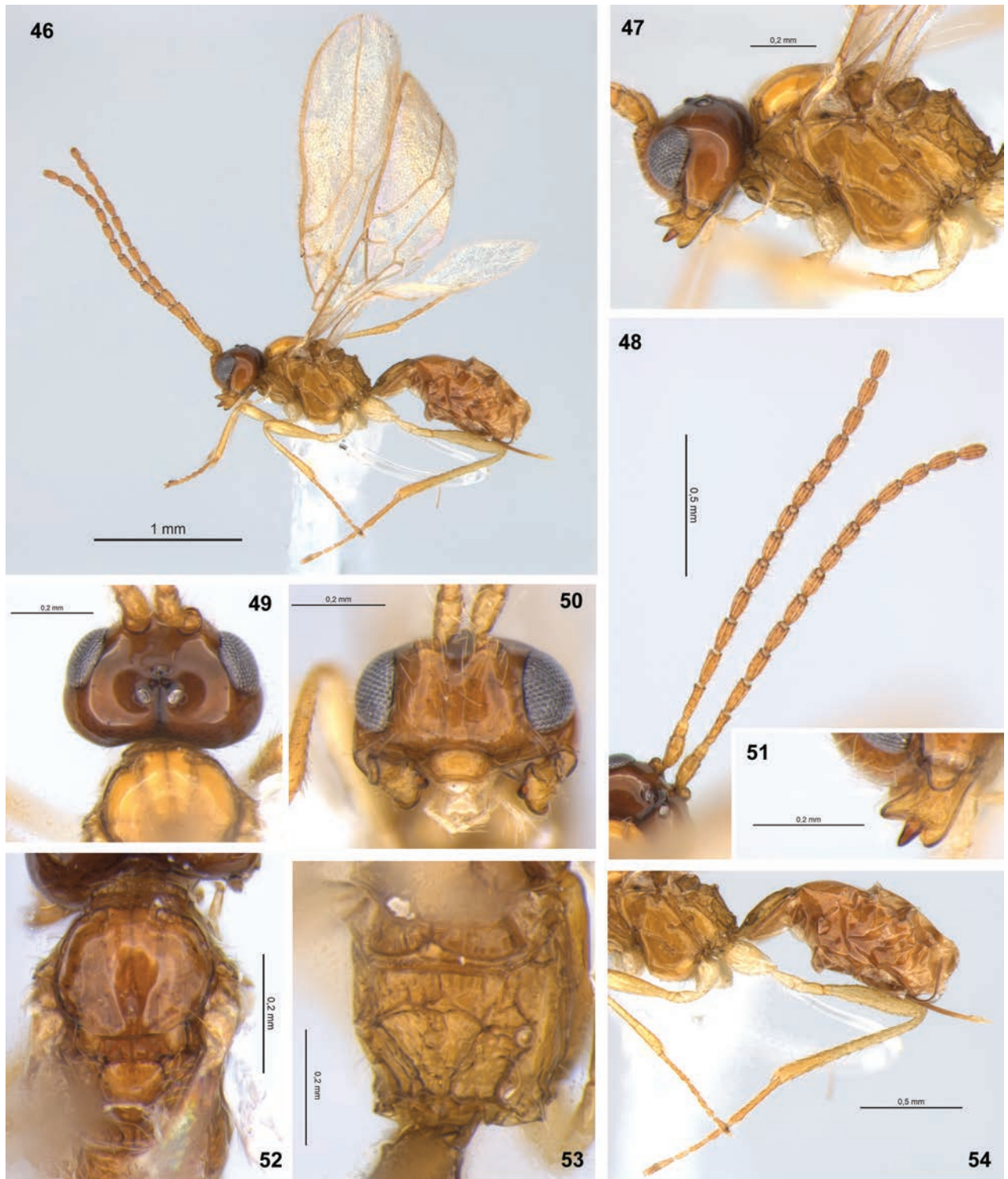
Mesosoma: 1.3× as long as high (Fig. 47), 2.1× as long as wide. Mesoscutum as long as wide, notauli absent on horizontal surface of mesoscutum (Fig. 52). Mesoscutal pit present, oval–elongate, occupying 0.1–0.2× of mesoscutal length. Prescutellar depression 2.5× as long as wide, with median carina complete, lateral carinae almost complete, weak. Side of pronotum crenulate. Precoxal sulcus crenulate medially, not reaching anterior and/or posterior margins of mesopleuron (Fig. 47). Posterior mesopleural furrow smooth. Propodeum mainly rugulose to rugose (Fig. 53), with areola 0.9× as high as wide; median longitudinal carina incomplete, not extending inside areola or reaching its middle at most; transverse carinae complete. Propodeum with protuberance in lateral view. Propodeal spiracle small to middle (Fig. 47), 0.3–0.4× distance from spiracle to base of propodeum.

Wings: fore wing 2.7× as long as wide, vein 1-SR present, (r+3-SR) 4.9–5.0× as long as r-m, SR1 2.1–2.3× as long as (r+3-SR); cu-a distinctly postfurcal, 1-CU1 as long as cu-a. Marginal cell 4.5× as long as wide, submarginal cell 2.4× as long as wide, first subdiscal cell 3.0× as long as wide (Fig. 46). Hind wing 6.2× as long as wide, vein 1-M 0.5× as long as M+CU, 2.0× as long as 1r-m; m-cu absent.

Legs: hind femur 4.1–4.2× as long as wide. Hind tibia 10.1–10.3× as long as wide, 1.1–1.2× as long as hind tarsus. First segment of hind tarsus 2.2× as long as second segment (Fig. 54).

Metasoma: 1.6× as long, and 1.3× as wide as mesosoma (Fig. 46). T1 strigose, 2.15× as long as wide, apex 1.4× as wide as base. Ovipositor 0.4× as long as metasoma, 1.3–1.6× as long as T1, 0.9–1.0× as long as hind femur. Ovipositor sheath with some sparse and delicate setae (except on 1/4 apical almost glabrous), 0.3–0.4× as long as metasoma, 1.20–1.35× as long as T1 (Fig. 54).

Color: mainly yellow, except head dorsally brown to light brown; mesosoma dorsally and flagellum yellow to light brown; metasoma from second tergite light brown; ovipositor sheath brown. Wings hyaline, veins light brown.



Figures 46–54. *Dinotrema (Synaldis) flavum* sp. nov. (holotype ♀, except 52 paratype ♀) 46 habitus, lateral view 47 head and mesosoma, lateral view 48 antenna 49, 50 head, dorsal and frontal view respectively 51 mandible, lateral view 52 mesonotum, dorsal view 53 propodeum, dorsal view 54 hind leg, metasoma and ovipositor, lateral view.

Male. Unknown.

Etymology. The epithet is an adjective derived from *flavus*, which means yellow in Latin. The species name refers to its predominantly yellow body color (Figs 46–54).

Distribution. Chile.

***Dinotrema (Synaldis) latusdentertium* sp. nov.**

<https://zoobank.org/A7DF55C8-8025-4F10-BC68-C5E8D5AC0B3E>

Figs 55–64

Type material. Holotype: CHILE • ♀ (MNNC); Osorno, Parque Nacional Puyehue, Antillanca; 40°46'55"S, 72°12'39"W; alt. 987 m; 16–30 Mar. 2019; D. Amorim and V. Silva leg.; Malaise trap. **Paratype:** CHILE • 1♀ (DCBU 386606); same data as for holotype, except 40°44'S, 72°19'W; alt. 440 m; 14 Jan.–3 Feb. 2017; pan trap.

Diagnosis. This species differs from other New World species of *Synaldis* by the combination of the following characteristics: in lateral view, eye wider than temple, at least slightly (Fig. 60); mandible with three relatively large teeth, diagonal carina present, mandibular apex wider than base (Fig. 57); F1 3.5–3.8× as long as wide (Fig. 59); mesoscutal pit present, conspicuous (Fig. 61); propodeum with areola, median longitudinal carina incomplete to complete, transverse carinae complete (Fig. 62); fore wing vein cu-a distinctly postfurcal, 1-CU1 as long as cu-a (Fig. 63); hind wing 4.9× as long as wide; hind tibia 10.0–10.2× as long as wide (Fig. 64).

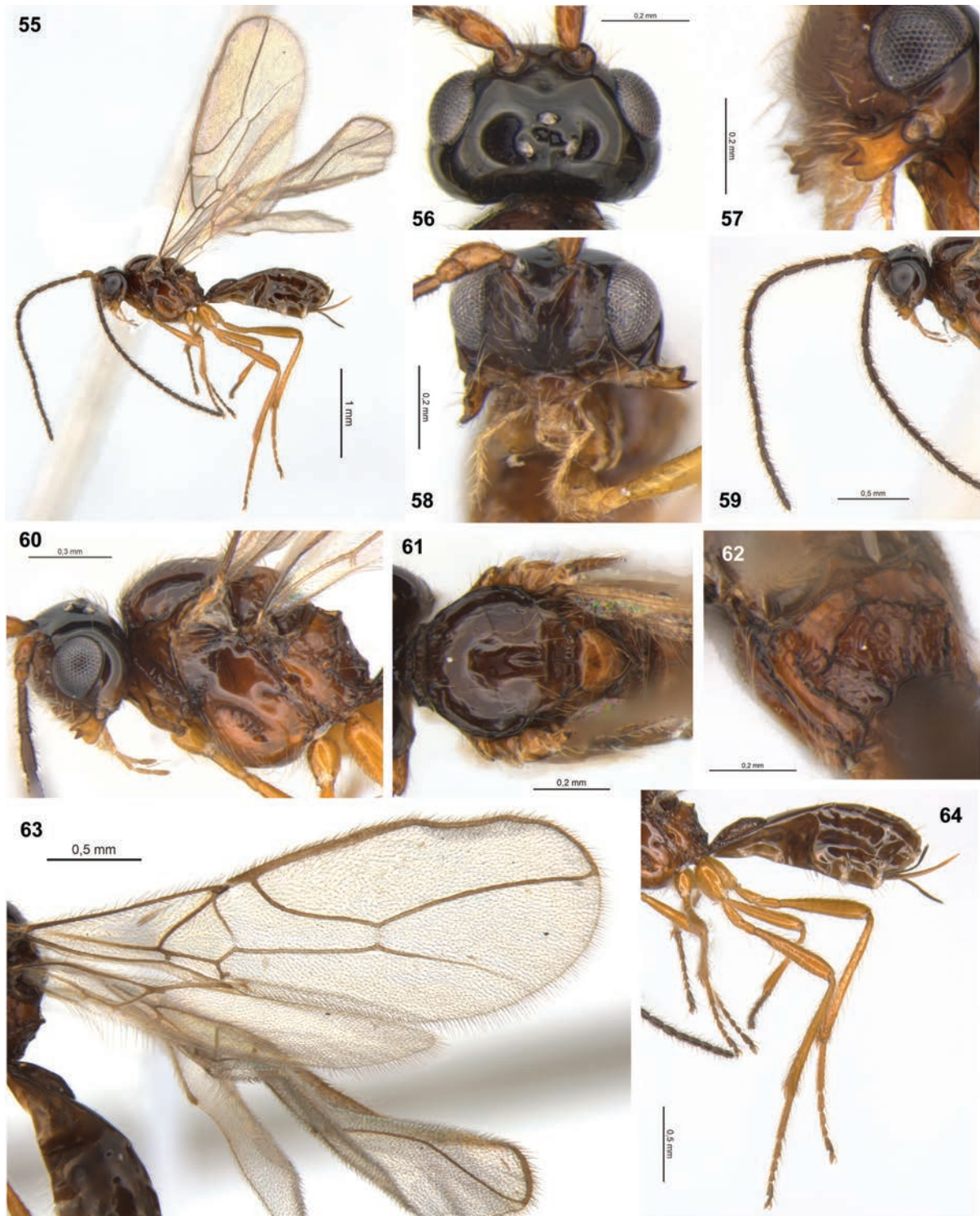
Dinotrema (S.) latusdentertium sp. nov. is similar to *D. (S.) pilosicaudatum* sp. nov., see their distinctions in the identification key.

Description. ♀. Length. Body: 2.6–2.8 mm. Fore wing: 3.05–3.30 mm. Hind wing: 2.3–2.4 mm.

Head: in dorsal view (Fig. 56), 1.8–1.9× as wide as long, 1.2–1.3× as wide as mesosoma, ca as wide at eyes as temples. Frons smooth or with weak mid groove. POL 1.4–1.6× as OD, OOL 2.6–2.7× as OD. In lateral view (Fig. 60), eye 1.4–1.5× as high as wide, 1.1–1.2× as wide as temple. Face 1.6–1.7× as wide as high (Fig. 58), 1.6–1.9× as wide as clypeus, smooth or with a weak longitudinal ridge dorsally. Clypeus 2.1× as wide as high, almost straight ventrally. Malar space 0.5–0.7× as clypeus height. Paraclypeal fovea short size. Mandible 1.5× as long as wide (Fig. 57), diagonal carina present. Mandibular apex 1.2× wide as base. Upper tooth rounded. Middle tooth subacuminate, longer than other teeth. Lower tooth largely rounded, longer than upper tooth. Upper tooth ca as wide as middle, narrower than lower tooth. Antenna with 20–21 segments (Fig. 59), 0.9× as long as body. Scape 1.5–1.8× as long as pedicel. F1 3.5–3.8× as long as wide, 1.2× as long as F2. F2 2.6–2.8× as long as wide. F3 2.0–2.4× as long as wide. AF 2.4–2.6× as long as wide. Maxillary palp 1.4× as long as head height.

Mesosoma: 1.2–1.3× as long as high (Fig. 60), 1.9–2.0× as long as wide. Mesoscutum as long as wide, notauli absent on horizontal surface of mesoscutum (Fig. 61). Mesoscutal pit present, oval–elongate, occupying 0.2× of mesoscutal length. Prescutellar depression 2.1–2.3× as long as wide, with median carina complete, smooth laterally. Side of pronotum crenulate. Precoxal sulcus crenulate medially, not reaching anterior and/or posterior margins of mesopleuron (Fig. 60). Posterior mesopleural furrow smooth. Propodeum mainly rugulose to rugose (Fig. 62), areola 0.9× as high as wide; median longitudinal carina incomplete (interrupted at mid-areola) to complete; transverse carinae complete. Propodeum with protuberance in lateral view. Propodeal spiracle small to middle (Fig. 60), 0.3–0.4× distance from spiracle to base of propodeum.

Wings: fore wing 2.7× as long as wide, vein 1-SR present, (r+3-SR) 6.2× as long as r-m, SR1 1.7–2.0× as long as (r+3-SR); cu-a postfurcal, 1-CU1 as long as cu-a. Marginal cell 4.0× as long as wide, submarginal cell 2.0× as long as



Figures 55–64. *Dinotrema (Synaldis) latusdentertium* sp. nov. (holotype ♀, except 58, 61 paratype ♀) 55 habitus, lateral view 56 head, dorsal view 57 mandible, lateral view 58 head, frontal view 59 antenna 60 head and mesosoma, lateral view 61 mesonotum, dorsal view 62 propodeum, dorsal view 63 wings 64 hind leg, metasoma and ovipositor, lateral view.

wide, first subdiscal cell 2.8× as long as wide (Fig. 63). Hind wing 4.9× as long as wide, vein 1-M 0.5× as long as M+CU, 1.2–1.3× as long as 1r-m; m-cu absent.

Legs: hind femur 4.7–5.0× as long as wide. Hind tibia 10.0–10.2× as long as wide, 1.1–1.3× as long as hind tarsus. First segment of hind tarsus 2.0–2.1× as long as second segment (Fig. 64).

Metasoma: 1.7× as long, and as wide as mesosoma (Fig. 55). T1 strigose to rugose, 1.70–1.85× as long as wide, apex 1.6× as wide as base. Ovipositor 0.4× as long as metasoma, 1.2–1.5× as long as T1, 0.9× as long as hind femur. Ovipositor sheath with some sparse and delicate setae (except on 1/4 apical almost glabrous), 0.3–0.4× as long as metasoma, 1.1–1.4× as long as T1 (Fig. 64).

Color: Head brown to dark brown, except mandibles yellow, scape and pedicel brown to yellowish. Mesosoma brown to light brown, except scutellar disc and tegulae brown to yellow; propleuron, mesopleuron and propodeum orange to yellowish. Legs yellow. Metasoma brown except ovipositor yellow. Wings hyaline, veins brown.

Male. Unknown.

Etymology. The epithet is an adjective derived from Latin, combining *latus* (wide), *den* (from *dens*, Latin for tooth), and *tertius* (third). The species name refers to its lower mandibular tooth wider than upper tooth (Fig. 57).

Distribution. Chile.

Comments. Based on the shape of the mandibles, relative length of the flagellar segments, and the propodeal sculpture, *D. (S.) latusdentertium* sp. nov. can be associated with the Nearctic species *Dinotrema (Synaldis) glabrifovea* (Fischer, 1967). However, in *D. (S.) glabrifovea* the mesoscutal pit is absent, the face and clypeus are relatively wider, and the antenna has 25 segments, among other differences (according to Peris-Felipo and Belokobylskij 2017).

***Dinotrema (Synaldis) perisfelipoi* sp. nov.**

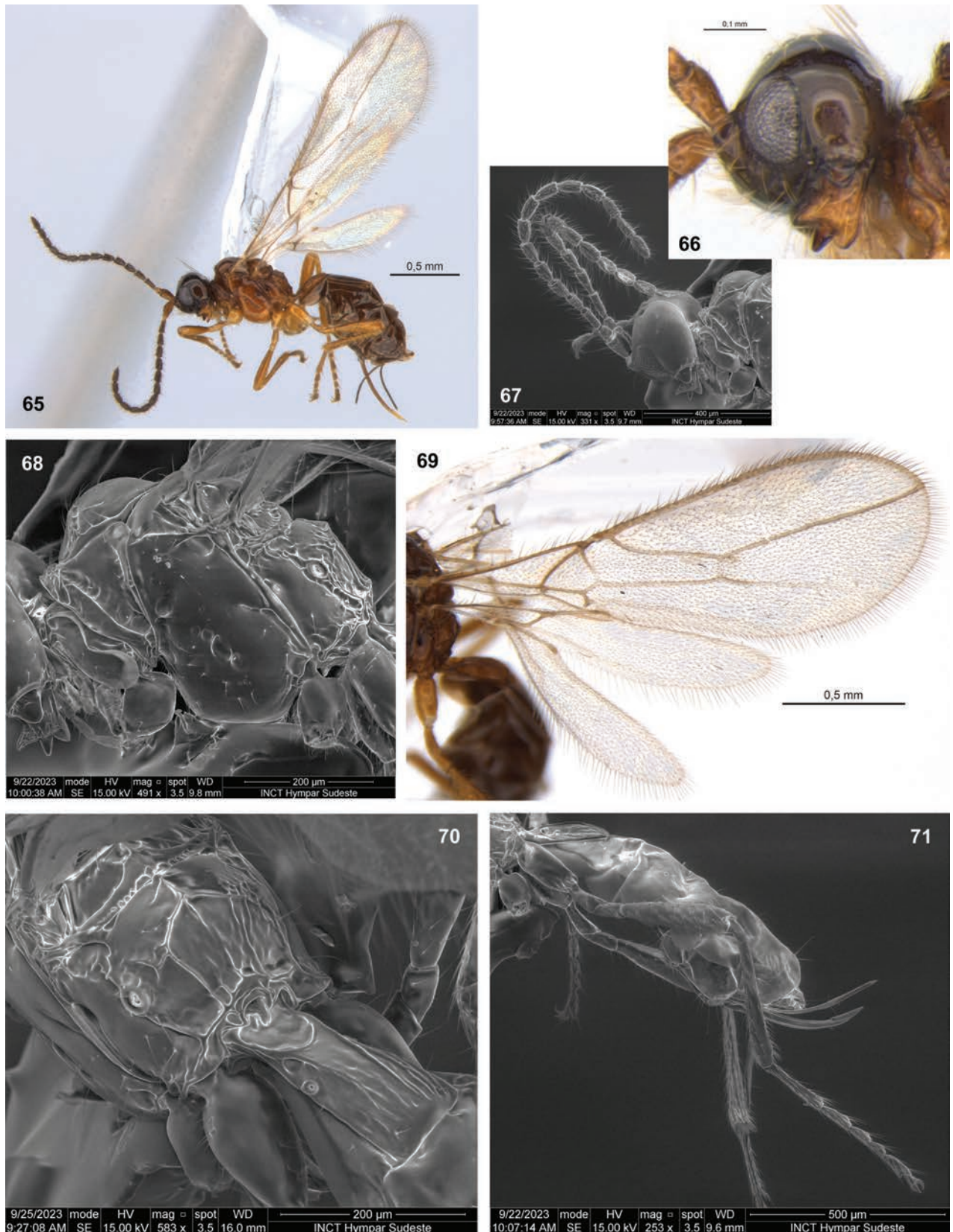
<https://zoobank.org/3123A760-770C-4AAB-BFFE-34634389F62B>

Figs 65–71

Type material. Holotype: CHILE • ♀ (MNNC); Osorno, Parque Nacional Puyehue, Antillanca; 40°46'55"S, 72°12'39"W; alt. 987 m; 16–30 Mar. 2020; D. Amorim and V. Silva leg.; Malaise trap. **Paratypes:** CHILE • 1♀ (MNNC); same data as for holotype, except 40°44'06"S, 72°19'47"W; alt. 528 m; 14 Jan.–3 Feb. 2017; flight intercept trap • 1♂ (MNNC); same data as for holotype, except 11–25 May. 2019 • 1♀ (DCBU 514624); same data as for holotype • 1♀ (DCBU 509530); same data as for holotype, except 9–23 Dec. 2019.

Diagnosis. This species differs from other New World species of *Synaldis* by the combination of the following characteristics: in lateral view, eye shorter than temple (Fig. 66); mandible with three relatively large teeth, diagonal carina present in ♀ (absent in ♂), mandibular apex wider than base; F1 2.4–2.8× as long as wide (Fig. 67); mesoscutal pit present, conspicuous; propodeum with areola, median longitudinal carina incomplete to almost complete, transverse carinae complete (Fig. 70); fore wing vein (r+3-SR) 6.2–6.3× as long as r-m, cu-a postfurcal, 1-CU1 shorter than cu-a (Fig. 69); hind femur 4.6× as long as wide, hind tibia 8.9–9.2× as long as wide (Fig. 71).

Dinotrema (S.) perisfelipoi sp. nov. is similar to *D. (S.) daltoni* sp. nov. (see their distinctions in the diagnosis of the latter) and *D. (S.) puyehue* sp. nov., from which it differs by prescutellar depression smooth laterally (with complete lateral carinae in *D. (S.) puyehue* sp. nov., Fig. 91), fore wing vein (r+3-SR) 6.2–6.3× as long as r-m (5.0–5.2× in *D. (S.) puyehue* sp. nov.), submarginal cell 2.7–2.9× as long as wide (2.05–2.20× in *D. (S.) puyehue* sp. nov., Figs 69, 90), AF 2.5–2.6× as long as wide (1.9–2.2× in *D. (S.) puyehue* sp. nov., Figs 67, 86).



Figures 65–71. *Dinotrema (Synaldis) perisfelipoi* sp. nov. (65, 69 holotype ♀, remainder paratype ♀) 65 habitus, lateral view 66 head and mandible, lateral view 67 antenna 68 mesosoma, lateral view 69 wings 70 propodeum and T1, dorsal view 71 hind leg, metasoma and ovipositor, lateral view.

Description. ♀. Length. Body: 1.7–2.1 mm. Fore wing: 1.8–2.1 mm. Hind wing: 1.2–1.4 mm.

Head: in dorsal view, 1.7× as wide as long, 1.4× as wide as mesosoma, slightly wider at temples than eyes. Frons smooth. POL 1.30–1.45× as OD, OOL 3.2–3.4× as OD. In lateral view (Fig. 66), eye 1.4× as high as wide, 0.7–0.8× as wide as temple. Face 1.7–2.0× as wide as high, 2.0–2.1× as wide as clypeus, smooth or with a weak longitudinal ridge dorsally. Clypeus 1.7–2.0× as wide as high, concave ventrally. Malar space 0.7× as clypeus height. Paraclypeal fovea short size. Mandible 1.2–1.3× as long as wide (Fig. 66), diagonal carina present. Mandibular apex 1.2–1.3× wide as base. Upper rounded or nearly so. Middle tooth subacuminate, longer than other teeth. Lower tooth largely rounded. Upper tooth ca as wide as middle, narrower than lower tooth. Antenna with 15 segments (Fig. 67), 0.6–0.7× as long as body. Scape 1.9–2.1× as long as pedicel. F1 2.4–2.7× as long as wide, 1.0–1.1× as long as F2. F2 2.0–2.3× as long as wide. F3 1.7–2.2× as long as wide. AF 2.5–2.6× as long as wide. Maxillary palp 0.90–1.05× as long as head height.

Mesosoma: 1.2–1.4× as long as high (Fig. 68), 2.1–2.2× as long as wide. Mesoscutum as long as wide, notauli absent on horizontal surface of mesoscutum. Mesoscutal pit present, oval–elongate, occupying 0.1× of mesoscutal length. Prescutellar depression 2.7× as long as wide, with median carina complete (sometimes weak), smooth laterally. Side of pronotum weakly crenulate. Precoxal sulcus crenulate medially, not reaching anterior and/or posterior margins of mesopleuron. Posterior mesopleural furrow smooth. Propodeum mainly smooth to rugulose (Fig. 70), with areola 0.9–1.1× as high as wide; median longitudinal carina incomplete (not extending inside areola) or almost complete (interrupted briefly in mid-areola); transverse carinae complete. Propodeum with very weak protuberance in lateral view. Propodeal spiracle middle (Fig. 68), 0.4–0.5× distance from spiracle to base of propodeum.

Wings: fore wing 2.8–2.9× as wide, vein 1-SR absent or present, (r+3-SR) 6.2–6.3× as long as r-m, SR1 2.0–2.5× as long as (r+3-SR); cu-a postfurcal, 1-CU1 0.4–0.7× as long as cu-a. Marginal cell 4.45–4.90× as long as wide, submarginal cell 2.7–2.8× as long as wide, first subdiscal cell 3.1–3.2× as long as wide (Fig. 69). Hind wing 5.35–5.50× as long as wide, vein 1-M 0.5–0.6× as long as M+CU, 1.50–1.85× as long as 1r-m; m-cu absent.

Legs: hind femur 4.6× as long as wide. Hind tibia 8.9–9.1× as long as wide, 1.0–1.1× as long as hind tarsus. First segment of hind tarsus 2.0–2.1× as long as second segment (Fig. 71).

Metasoma: 1.7–1.9× as long, and 1.4× as wide as mesosoma (Fig. 65). T1 strigose (Fig. 70), 1.4–1.7× as long as wide, apex 1.8× as wide as base. Ovipositor 0.35–0.50× as long as metasoma, 1.5–1.9× as long as T1, 0.9–1.3× as long as hind femur. Ovipositor sheath with some delicate setae (except on 1/4 apical almost glabrous), 0.3–0.4× as long as metasoma, 1.4–1.5× as long as T1 (Fig. 71).

Color: brown to yellow, except head dark brown to light brown, and legs entirely yellow or light brown from trochanter. Wings hyaline, veins brown to light brown.

Male. Head 1.9× as wide as long. Eye 1.5× as high as wide, 0.85× as wide as temple. Face 2.2× as wide as clypeus. Mandible without diagonal carina. Middle tooth acute. Antenna with 21 segments, 1.2× as long as body. F1 2.8× as long

as wide. F2 2.5× as long as wide. F3 2.4× as long as wide. Mesosoma 2.0× as long as wide. Mesoscutal pit occupying 0.2× of mesoscutal length. Prescutellar depression 2.5× as long as wide. Precoxal sulcus almost smooth. Propodeum almost smooth, median longitudinal carina extending to mid-areola. Propodeal spiracle small, 0.25× distance from spiracle to base of propodeum. Fore wing 2.5× as long as wide. Submarginal cell 2.9× as long as wide. Hind femur 4.8× as long as wide. Hind tibia 9.2× as long as wide. Metasoma 1.5× as long as mesosoma. T1 2.4× as long as wide, apex 1.1× as wide as base.

Etymology. The species name *perisfelipoi* is a genitive noun, named in honor of Francisco Javier Peris Felipo, an expert in Alysiinae wasps, who has made significant contributions, particularly in his study of the genus *Dinotrema*.

Distribution. Chile.

***Dinotrema (Synaldis) pilosicaudatum* sp. nov.**

<https://zoobank.org/59D7DEA1-FF88-4DB4-8729-F5173D560940>

Figs 72–82

Type material. Holotype: CHILE • ♀ (MNNC); Osorno, Parque Nacional Puyehue, Antillanca; 40°46'55"S, 72°12'39"W; alt. 987 m; 16–30 Mar. 2020; D. Amorim and V. Silva leg.; Malaise trap. **Paratypes:** CHILE • 1 ♂ (MNNC); same data as for holotype, except 40°46'28"S, 72°12'41"W; alt. 1054 m; 14 Jan.–3 Feb. 2017; sweeping • 1 ♀ (DCBU 514534) and 1 ♂ (DCBU 514551); same data as for holotype.

Diagnosis. This species differs from other New World species of *Synaldis* by the combination of the following characteristics: in lateral view, eye as wider as or slightly wider than temple (Fig. 74); mandible with three relatively large teeth, diagonal carina present, mandibular apex (at least slightly) wider than base (Fig. 74); F1 3.70–3.85× as long as wide (Fig. 76); mesoscutal pit present, conspicuous (Fig. 77); propodeum with areola, median longitudinal carina and transverse carinae complete (Fig. 81); propodeum with a distinct protuberance in lateral view (Fig. 78); fore wing vein cu-a postfurcal, 1-CU1 as long as or shorter than cu-a (Fig. 79); hind tibia 8.9–9.1× as long as wide; T1 rugose-foveolate (Fig. 80); ovipositor sheath with several distinct, erect setae, except on 1/4 apical almost glabrous (Fig. 82).

Dinotrema (S.) pilosicaudatum sp. nov. is similar to *D. (S.) latusdentertium* sp. nov., their distinctions are given in the identification key.

Description. ♀. Length. Body: 2.0–2.2 mm. Fore wing: 2.4 mm. Hind wing: 1.65 mm.

Head: in dorsal view (Fig. 73), 1.7–1.8× as wide as long, 1.4× as wide as mesosoma, ca as wide at eyes as temples. Frons with weak mid groove. POL 1.3× as OD, OOL 2.90–3.15× as OD. In lateral view (Fig. 74), eye 1.4–1.5× as high as wide, 1.0–1.1× as wide as temple. Face 1.6× as wide as high (Fig. 75), 2.0× as wide as clypeus, punctate, with longitudinal ridge dorsally. Clypeus 1.65× as wide as high, slightly concave ventrally. Malar space 0.6× as clypeus height. Paraclypeal fovea short size. Mandible 1.5× as long as wide (Fig. 74), diagonal carina present. Mandibular apex 1.1–1.2× wide as base. Upper tooth almost rounded. Middle tooth acute, longer than other teeth. Lower tooth rounded, as long as upper tooth. Upper tooth as wide as lower, wider than middle tooth. Antenna with 18–20 segments

(Fig. 76), 0.9–1.0× as long as body. Scape 2.0× as long as pedicel. F1 3.7–3.9× as long as wide, 1.3–1.4× as long as F2. F2 2.6× as long as wide. F3 2.1× as long as wide. AF 2.0–2.1× as long as wide. Maxillary palp 1.2× as long as head height.

Mesosoma: 1.2–1.4× as long as high (Fig. 78), 2.1–2.2× as long as wide. Mesoscutum as long as wide, notauli absent on horizontal surface of mesoscutum (Fig. 77). Mesoscutal pit present, oval–elongate, occupying 0.2–0.3× of mesoscutal length. Prescutellar depression 2.0–2.1× as long as wide, with median carina incomplete posteriorly to complete, smooth laterally. Side of pronotum crenulate. Precoxal sulcus crenulate medially, not reaching anterior and/or posterior margins of mesopleuron (Fig. 78). Posterior mesopleural furrow smooth. Propodeum mainly smooth (Fig. 81), with areola as high as wide; median longitudinal carina complete; transverse carinae complete. Propodeum with a distinct protuberance in lateral view (Fig. 78) Propodeal spiracle small, 0.3× distance from spiracle to base of propodeum.

Wings: fore wing 2.5–2.6× as long as wide, vein 1-SR present, (r+3-SR) 5.1–5.4× as long as r-m, SR1 2.0–2.2× as long as (r+3-SR); cu-a postfurcal, 1-CU1 0.7–1.0× as long as cu-a. Marginal cell 4.2–4.3× as long as wide, submarginal cell 2.0–2.2× as long as wide, first subdiscal cell 3.05× as long as wide (Fig. 79). Hind wing 5.8× as long as wide, vein 1-M 0.4× as long as M+CU, 1.2× as long as 1r-m; m-cu absent.

Legs: hind femur 4.9–5.2× as long as wide. Hind tibia 8.9–9.1× as long as wide, 1.1–1.2× as long as hind tarsus. First segment of hind tarsus 1.9–2.1× as long as second segment.

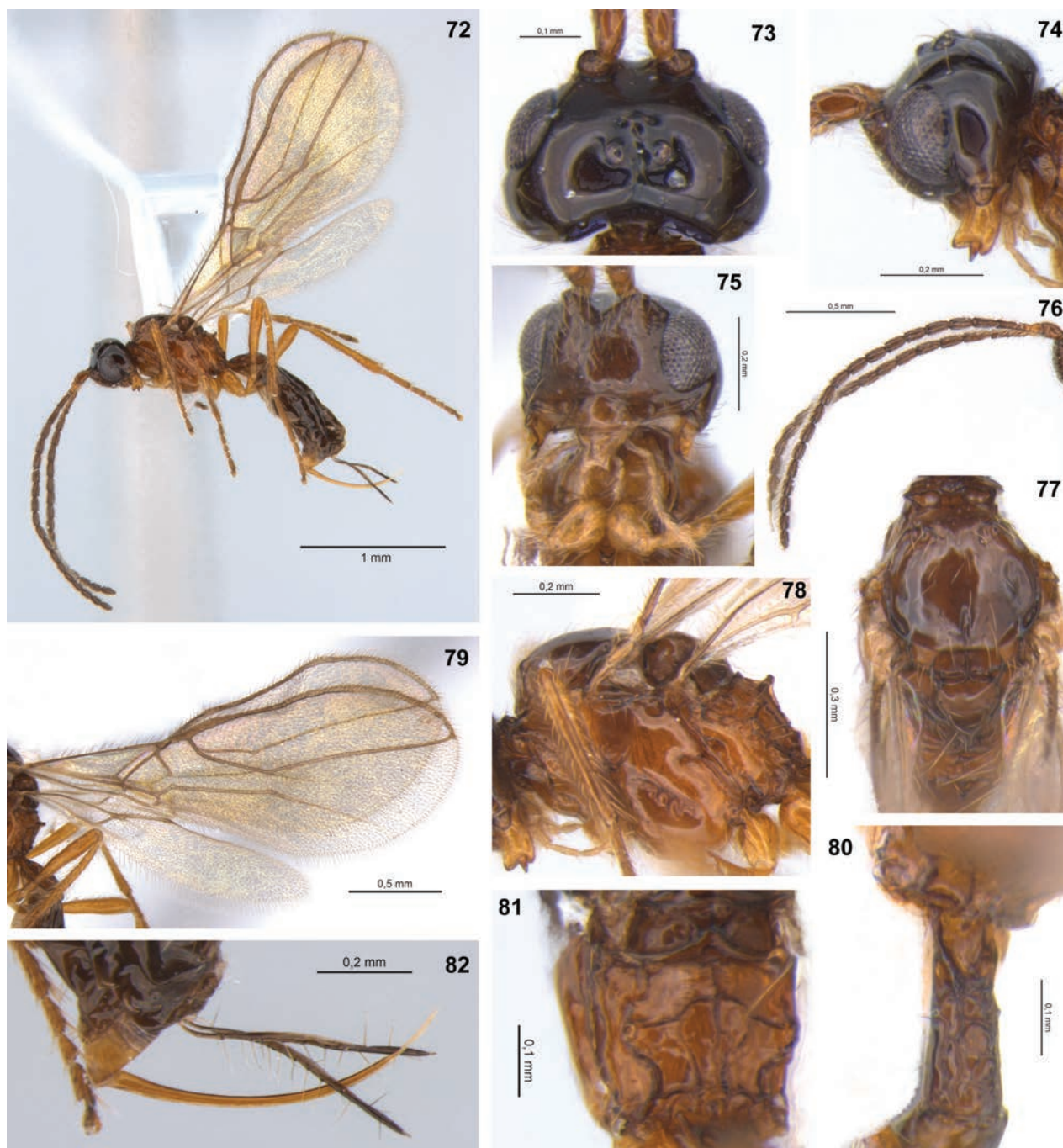
Metasoma: 1.6–1.7× as long, and 0.8× as wide as mesosoma (Fig. 72). T1 rugose–foveolate (Fig. 80), 2.1–2.3× as long as wide, apex 1.2–1.3× as wide as base. Ovipositor 0.6–0.7× as long as metasoma, 2.5× as long as T1, 1.5–1.7× as long as hind femur. Ovipositor sheath with several distinct, erect setae (except on 1/4 apical almost glabrous, Fig. 82), 0.5× as long as metasoma, 1.8× as long as T1 (Fig. 72).

Color: head dark brown, except mandibles and pedicel yellow. Mesosoma orange–yellow, except pronotum, mesoscutum, scutellum, and metanotum brown. Metasoma brown except ovipositor yellow. Wings hyaline, veins brown.

Male. Body length 2.1–2.3 mm. Head 1.3× as wide as mesosoma. POL 1.6× as OD, OOL 2.6× as OD. Face 1.5–1.6× as wide as high, 1.9× as wide as clypeus. Clypeus 1.8× as wide as high. Malar space 0.7× as clypeus height. Mandible 1.4× as long as wide. Antenna with 22 segments, 1.2× as long as body. Scape 1.8× as long as pedicel. F1 1.1–1.3× as long as F2. F2 2.6–2.8× as long as wide. F3 2.3–2.4× as long as wide. AF 2.6× as long as wide. Mesosoma 2.0× as long as wide. Fore wing 2.4× as long as wide, vein SR1 1.8× as long as (r+3-SR). Hind wing 4.65× as long as wide; vein 1-M 0.5× as long as M+CU, 1.3× as long as 1r-m. Hind femur 4.6–5.0× as long as wide. Hind tibia 9.6× as long as wide. Metasoma 1.3–1.5× as long as mesosoma. T1 2.0× as long as wide. Color as in ♀ or brown to dark brown, except mandibles and legs yellow, propleuron, mesopleuron ventrally orange.

Etymology. The epithet is an adjective combining *pilosus* (from *pilosus*, Latin for hairy), *caudatum* (from *cauda*, Latin for tail). The species name refers to its ovipositor sheath with several distinct, erect setae (Fig. 82).

Distribution. Chile.



Figures 72–82. *Dinotrema (Synaldis) pilosicaudatum* sp. nov. (holotype ♀, except 81, 82 paratype ♀) 72 habitus, lateral view 73 head, dorsal view 74 head and mandible, lateral view 75 head, frontal view 76 antenna 77 mesonotum, dorsal view 78 mesosoma, lateral view 79 wings 80 T1, dorsal view 81 propodeum, dorsal view 82 ovipositor and sheath, lateral view.

Comments. *Dinotrema (S.) pilosicaudatum* sp. nov. can be associated with the Nearctic species *D. (S.) glabrifovea* (Fischer, 1967) based on similarities in the shape of mandibles, relative length of the flagellomeres, and propodeal sculpture. However, in *D. (S.) glabrifovea* the mesoscutal pit is absent, the face and clypeus are relatively wider, and the antenna comprises 25 segments, among other distinguishing characteristics (according to Peris-Felipo and Belokobylskij 2017).

***Dinotrema (Synaldis) puyehue* sp. nov.**

<https://zoobank.org/7B39E2B0-9580-4EA3-8C5F-8279FDDD9696>

Figs 83–94

Type material. *Holotype*: CHILE • ♀ (MNNC); Osorno, Parque Nacional Puyehue, Antillanca; 40°46'55"S, 72°12'39"W; alt. 987 m; 9–23 Dec. 2019; D. Amorim and V. Silva leg.; Malaise trap. *Paratypes*: CHILE • 1♀ (MNNC) and 1♂ (MNNC); same data as for holotype • 2♀♀ (DCBU 509931, DCBU 514733) and 1♂ (DCBU 509539); same data as for holotype.

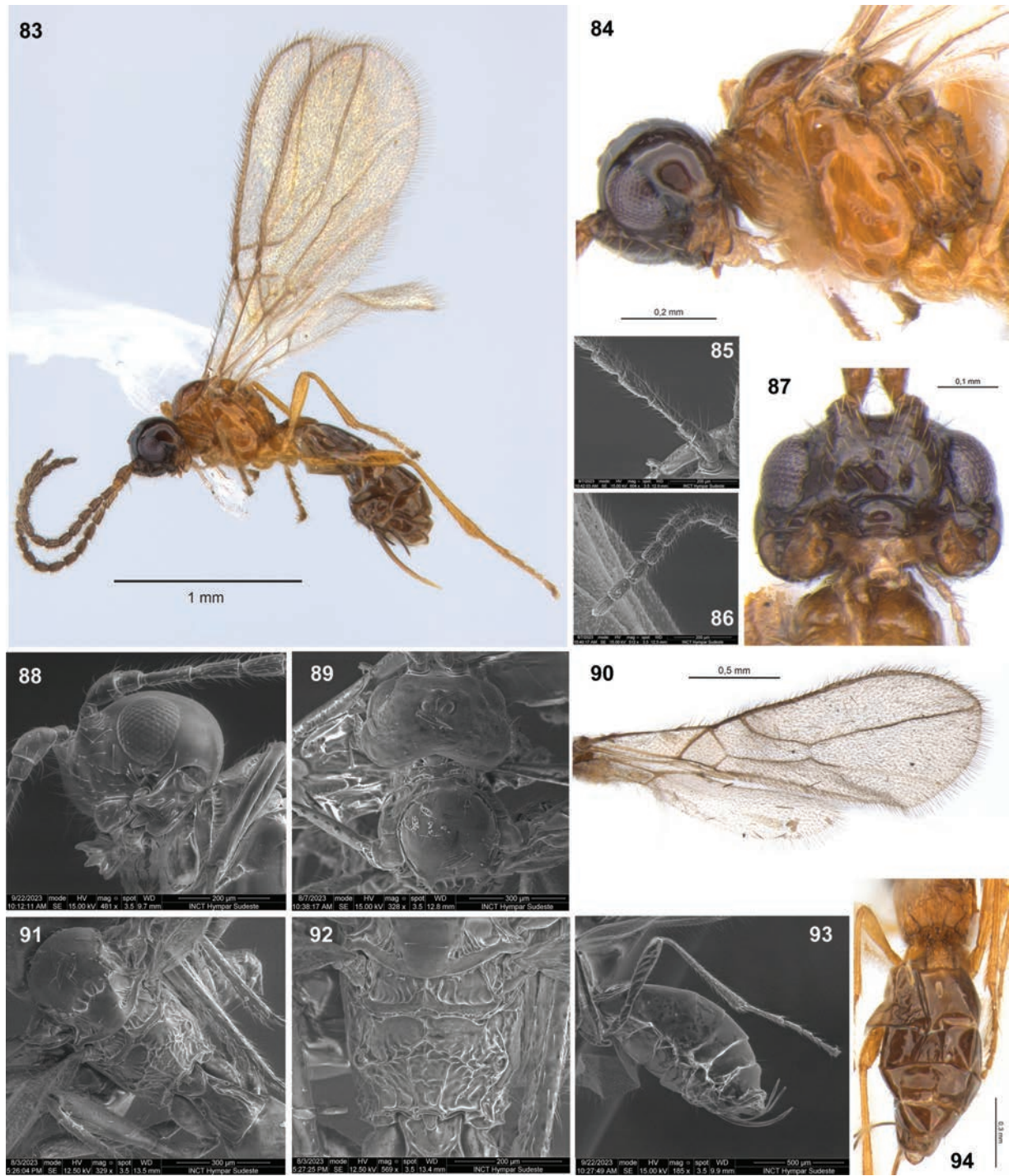
Diagnosis. This species differs from other New World species of *Synaldis* by the combination of the following characteristics: in lateral view, eye shorter than temple, at least slightly (Fig. 84); mandible with three relatively large teeth, diagonal carina present, mandibular apex wider than base (Fig. 88); F1 2.4–2.8× as long as wide (Fig. 85); mesoscutal pit present, conspicuous, prescutellar depression with lateral carinae (Figs 89, 91); propodeum with areola, median longitudinal carina incomplete to complete, transverse carinae complete (Fig. 92); fore wing vein cu-a postfurcal, 1-CU1 shorter than cu-a (Fig. 83); hind tibia 9.4–9.6× as long as wide (Fig. 93); metasoma distinctly wider than mesosoma (Figs 89, 94).

Dinotrema (S.) puyehue sp. nov. is similar to *D. (S.) daltoni* sp. nov., *D. (S.) flavum* sp. nov. (their differences are given in the identification key), and *D. (S.) perisfelipoi* sp. nov. (see their differences in the diagnosis of the latter).

Description. ♀. Length. Body: 2.05–2.50 mm. Fore wing: 2.00–2.15 mm. Hind wing: 1.45–1.60 mm.

Head: in dorsal view (Fig. 89), 1.6–1.7× as wide as long, 1.5× as wide as mesosoma, as wide at eyes as temples. Frons smooth. POL 1.1–1.2× as OD, OOL 2.7–3.1× as OD. In lateral view (Fig. 84), eye 1.30–1.45× as high as wide, 0.7–0.9× as wide as temple. Face 1.6–1.8× as wide as high (Fig. 87), 1.8–2.0× as wide as clypeus, smooth. Clypeus 2.0–2.1× as wide as high, straight ventrally. Malar space 0.6× as clypeus height. Paraclypeal fovea short size. Mandible 1.2–1.3× as long as wide (Figs 84, 88), diagonal carina present. Mandibular apex 1.2–1.3× wide as base. Upper tooth rounded. Middle tooth subacuminate, longer than other teeth. Lower tooth rounded, as long as upper tooth. Lower tooth as wide as or slightly wider than upper, both wider than middle tooth. Antenna with 16–18 segments (Fig. 83), 0.7–0.8× as long as body. Scape 1.9–2.0× as long as pedicel. F1 2.4–2.6× as long as wide (Fig. 85), 0.95–1.10× as long as F2. F2 2.1–2.3× as long as wide. F3 1.6–1.8× as long as wide. AF 2.0–2.2× as long as wide (Fig. 86). Maxillary palp 0.8–0.9× as long as head height.

Mesosoma: 1.1–1.2× as long as high (Fig. 84), 2.1× as long as wide. Mesoscutum as long as wide, notauli absent on horizontal surface of mesoscutum (Fig. 89). Mesoscutal pit present, oval to elongate, occupying 0.1–0.2× of mesoscutal length. Prescutellar depression 2.40–2.65× as long as wide, with median and lateral carinae complete (Figs 89, 91). Side of pronotum almost smooth. Precoxal sulcus crenulate medially, not reaching anterior and/or posterior margins of mesopleuron (Fig. 84). Posterior mesopleural furrow smooth. Propodeum rugulose to rugose (Figs 91, 92), with areola 1.1× as high as wide; median longitudinal carina incomplete (not extending inside areola) to complete; transverse carinae complete. Propodeum with a very weak protuberance in lateral view. Propodeal spiracle middle (Fig. 84), 0.5× distance from spiracle to base of propodeum.



Figures 83–94. *Dinotrema (Synaldis) puyehue* sp. nov. (**83, 84, 87, 94** holotype ♀, remainder paratype ♀) **83** habitus, lateral view **84** head and mesosoma, lateral view **85, 86** basal and apical parts of antenna respectively **87** head, frontal view **88** mandible, lateral view **89** head and mesoscutum, dorsal view **90** wings **91** mesosoma and T1, dorsal view **92** propodeum, dorsal view **93** hind leg, metasoma and ovipositor, lateral view **94** metasoma, dorsal view.

Wings: Fore wing 2.6–2.7× as long as wide, vein 1-SR absent or present, (r+3-SR) 5.0–5.1× as long as r-m, SR1 2.3–2.4× as long as (r+3-SR); cu-a post-furcal, 1-CU1 0.4–0.5× as long as cu-a. Marginal cell 4.5–4.9× as long as wide, submarginal cell 2.2× as long as wide, first subdiscal cell 2.9–3.0× as long as wide (Figs 83, 90). Hind wing 5.3× as long as wide, vein 1-M 0.5–0.6× as long as M+CU, 1.9–2.1× as long as 1r-m; m-cu absent.

Legs: Hind femur 4.0× as long as wide. Hind tibia 9.4–9.6× as long as wide, 1.1–1.2× as long as hind tarsus. First segment of hind tarsus 1.9–2.1× as long as second segment (Fig. 93).

Metasoma: 2.0–2.2× as long, and 1.7× as wide as mesosoma (Figs 83, 89, 94). T1 strigose (Fig. 91), 1.5–1.8× as long as wide, apex 1.45–1.70× as wide as base. Ovipositor 0.4–0.5× as long as metasoma, 1.7–2.1× as long as T1, 0.95–1.40× as long as hind femur. Ovipositor sheath with some sparse and delicate setae (except on 1/3 apical almost glabrous), 0.3× as long as metasoma, 1.3–1.6× as long as T1 (Figs 83, 93).

Color: Head brown to dark brown, except mandibles, scape, and pedicel brown to light brown. Mesosoma light brown to yellow. Legs yellow. Metasoma brown, except T1 light brown and ovipositor yellow. Wings hyaline, veins brown.

Male. Body length 1.7 mm, fore wing 1.7–1.9 mm, hind wing 1.2–1.3 mm. Face with longitudinal ridge dorsally. Antenna 0.9–1.0× as long as body. F1 2.7–2.8× as long as wide. F2 2.3–2.4× as long as wide. F3 2.1× as long as wide. AF 1.9–2.1× as long as wide. Mesosoma 1.3× as long as high. Propodeal areola as high as wide. Propodeal spiracle small, 0.2× distance from spiracle to base of propodeum. Fore wing vein (r+3-SR) 5.2× as long as r-m, SR1 2.05× as long as (r+3-SR), submarginal cell 2.6× as long as wide. Hind wing 5.5× as long as wide, vein 1-M 1.8× as long as 1r-m. Hind femur 4.2× as long as wide. Hind tibia as long as hind tarsus. Metasoma 1.4× as long as mesosoma.

Etymology. The name of species *puyehue* is a noun in apposition in reference to Parque Nacional de Puyehue, the type locality of the species.

Distribution. Chile.

***Dinotrema (Synaldis) verae* sp. nov.**

<https://zoobank.org/2AB7B5DC-D789-46DE-A12E-8211676F7D3F>

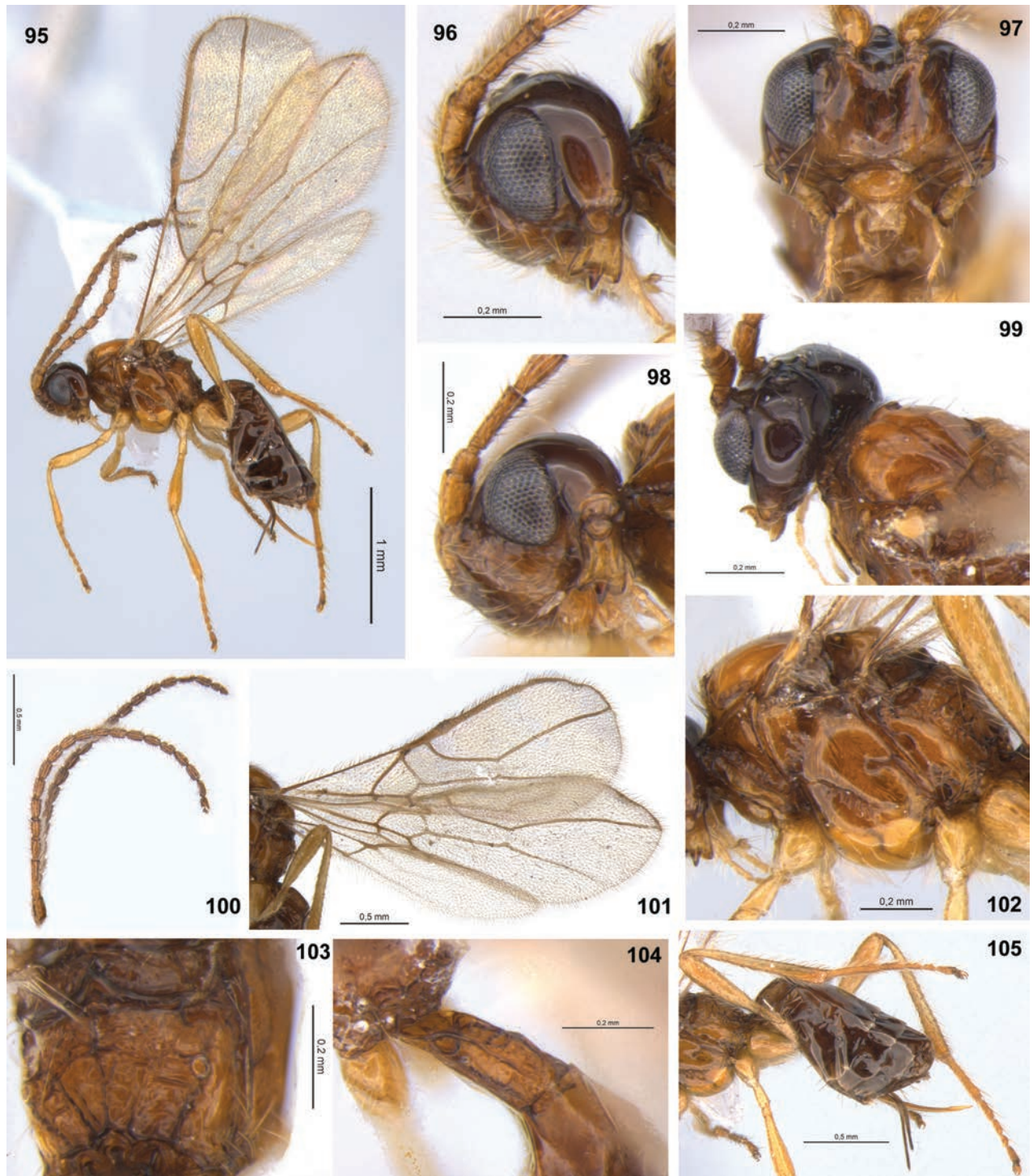
Figs 95–105

Type material. Holotype: CHILE • ♀ (MNNC); Osorno, Parque Nacional Puyehue, Antillanca; 40°44'06"S, 72°18'47"W; alt. 528 m; 14 Jan.–3 Feb. 2017; D. Amorim and V. Silva leg.; flight intercept. **Paratypes:** CHILE • 1♂ (MNNC); same data as for holotype, except 40°44'S, 72°19'W; alt. 440 m; pan trap • 1♀ (DCBU 387214); same data as for holotype, except 40°44'S, 72°19'W; alt. 440 m; sweeping.

Diagnosis. This species differs from other New World species of *Synaldis* by the combination of the following characteristics: in lateral view, eye as wide as or slightly wider than temple (Fig. 96); paraclypeal fovea middle size (Fig. 97); mandible with three relatively large teeth, diagonal carina present, mandibular apex wider than base (Fig. 98); F1 2.7–3.1× as long as wide (Fig. 100); mesoscutal pit present, conspicuous (Fig. 99); propodeum with areola, median longitudinal carina incomplete to complete, transverse carinae complete (Fig. 103); fore wing vein cu-a postfurcal, 1-CU1 shorter than cu-a (Fig. 101); hind tibia 8.6–8.8× as long as wide (Fig. 105); T1 rugose–foveolate (Fig. 104).

Dinotrema (S.) verae sp. nov. is related to *D. (S.) brunneum* sp. nov. and *D. (S.) chilense* sp. nov. Their differences are given in the diagnosis of *D. (S.) brunneum* sp. nov. and *D. (S.) chilense* sp. nov.

Description. ♀. Length. Body: 2.5–2.7 mm. Fore wing: 2.5–2.8 mm. Hind wing: 2.1 mm.



Figures 95–105. *Dinotrema (Synaldis) verae* sp. nov. (holotype ♀, except 99, 100, 104 paratype ♀) 95 habitus, lateral view 96, 97 head, lateral and frontal view respectively 98 mandible, lateral view 99 head and mesoscutum, dorso-lateral view 100 antennae 101 wings 102 mesosoma, lateral view 103 propodeum, dorsal view 104 T1, dorso-lateral view 105 hind leg, metasoma and ovipositor, lateral view.

Head: in dorsal view, 1.6–1.8× as wide as long, 1.3× as wide as mesosoma, slightly wider at temples than eyes. Frons smooth or with weak mid groove. POL 1.2–1.3× as OD, OOL 2.3–2.5× as OD. In lateral view (Fig. 96), eye 1.4–1.5× as high as wide, 1.0–1.1× as wide as temple. Face 1.45–1.60× as wide as high (Fig. 97), 1.9× as wide as clypeus, smooth. Clypeus 1.9× as wide as high,

slightly concave ventrally. Malar space 0.6× as clypeus height. Paraclypeal fovea middle size. Mandible 1.2–1.3× as long as wide (Fig. 98), diagonal carina present. Mandibular apex 1.2–1.4× wide as base. Upper tooth rounded. Middle tooth acute, longer than other teeth. Lower tooth rounded, as long as upper tooth. Upper tooth ca as wide as lower, wider than middle tooth. Antenna with 19–20 segments (Fig. 100), 0.8–0.9× as long as body. Scape 2.0× as long as pedicel. F1 2.7–2.8× as long as wide, 1.2× as long as F2. F2 1.8–2.1× as long as wide. F3 1.7–1.8× as long as wide. AF 1.9× as long as wide. Maxillary palp 1.1× as long as head height.

Mesosoma: 1.3× as long as high (Fig. 102), 2.0–2.2× as long as wide. Mesoscutum as long as wide, notauli absent on horizontal surface of mesoscutum (Fig. 99). Mesoscutal pit present, oval–elongate, occupying 0.2× of mesoscutal length. Prescutellar depression 2.3–2.4× as long as wide, with median carina complete, smooth laterally. Side of pronotum crenulate. Precoxal sulcus crenulate medially, not reaching anterior and/or posterior margins of mesopleuron (Fig. 102). Posterior mesopleural furrow smooth. Propodeum rugulose to rugose (Fig. 103), with areola 0.8–0.9× as high as wide; median longitudinal carina incomplete (not extending inside areola) to complete; transverse carinae complete. Propodeum with weak protuberance in lateral view. Propodeal spiracle small to middle (Fig. 102), 0.3–0.4× distance from spiracle to base of propodeum.

Wings: fore wing 2.8× as long as wide, vein 1-SR present, (r+3-SR) 5.1× as long as r-m, SR1 2.1× as long as (r+3-SR); cu-a postfurcal, 1-CU1 0.55–0.70× as long as cu-a. Marginal cell 4.5× as long as wide, submarginal cell 2.0–2.2× as long as wide, first subdiscal cell 3.1–3.3× as long as wide (Figs 95, 101). Hind wing 5.2× as long as wide, vein 1-M 0.5× as long as M+CU, 1.2× as long as 1r-m; m-cu absent.

Legs: Hind femur 4.2–4.3× as long as wide. Hind tibia 8.6–8.8× as long as wide, 1.2× as long as hind tarsus. First segment of hind tarsus 2.0× as long as second segment (Fig. 105).

Metasoma: 1.5× as long, and as wide as mesosoma (Fig. 95). T1 rugose–foveolate (Fig. 104), 1.9–2.0× as long as wide, apex 1.5× as wide as base. Ovipositor 0.4× as long as metasoma, 1.45× as long as T1, 0.9–1.0× as long as hind femur. Ovipositor sheath with some delicate setae (except on 1/3 apical almost glabrous), 0.3–0.4× as long as metasoma, 1.10–1.45× as long as T1 (Figs 95, 105).

Color: Head dorsally dark brown to brown. Face and clypeus brown to yellowish. Mandibles, antennae, and legs yellow. Mesosoma entirely yellow or parascutellar area and metanotum brown. Metasoma brown to light brown, except T1 brown to yellow and ovipositor yellow. Wings hyaline, veins brown.

Male. Body length 2.8 mm. Head 1.45× as wide as mesosoma. Face 1.8× as wide as clypeus. Clypeus 2.0× as wide as high. F1 3.1× as long as wide. F3 2.05× as long as wide. Prescutellar depression with lateral carinae complete, weak. Fore wing vein (r+3-SR) 4.8× as long as r-m, SR1 1.9× as long as (r+3-SR), marginal cell 4.2× as long as wide, first subdiscal cell 2.9× as long as wide. Hind tibia 8.9× as long as wide. Metasoma 2.0× as long as mesosoma. Head brown, except mandibles yellow; mesosoma and metasoma light brown.

Etymology. The species name *verae* is a genitive noun, named after Vera Cristina Silva, one of the collectors of the type material for this species.

Distribution. Chile.

Key to the Neotropical species of the subgenus *Synaldis* Foerster, 1863

- 1 Propodeum with transverse carinae incomplete, not reaching lateral parts of propodeum (as Fig. 3A, B)..... **2**
- Propodeum with transverse carinae complete, reaching lateral parts of propodeum (as Figs 3C–H, 27, 53, 81)..... **3**
- 2(1) F1 3.5× as long as wide, 1.3× as long as F2. F2 2.3× as long as wide. Middle flagellomeres 1.8–2.0× as long wide. Propodeal spiracle middle size, 0.4× distance from spiracle to base of propodeum. Hind tibia 7.5× as long as wide. Hind wing 5.7× as long as wide. Antenna with 19–26 segments. Body length 1.8–2.0 mm. Brazil
..... ***D. (Synaldis) novateutoniae* (Peris-Felipo, 2017)** ♀♂
- F1 4.0× as long as wide, ca as long as F2. F2 3.2–3.3× as long as wide. Middle flagellomeres 2.5–2.9× as long as wide. Propodeal spiracle small size, 0.1× distance from spiracle to base of propodeum. Hind tibia 8.2× as long as wide. Hind wing 6.5× as long as wide. Antenna with 18–21 segments. Body length 1.5–1.7 mm. Brazil
..... ***Dinotrema (Synaldis) longiflagellaris* (Peris-Felipo, 2017)** ♀♂
- 3(1) Propodeum without distinct areola (as Fig. 3C, D). T1 2.7× as long as wide..... **4**
- Propodeum with areola well defined (as Figs 3E–H, 10, 27, 81). T1 1.4–2.4× as long as wide **5**
- 4(3) Face 1.8× as wide as high. Scape 2.5× as long as pedicel. F2 2.2×, and sixth flagellar segment 1.8× as long as wide in ♀. Hind femur 3.5× as long as wide. Hind tibia 8.8× as long as wide. Antenna with 23–25 segments. Body length 2.4–2.7 mm. Brazil
..... ***Dinotrema (Synaldis) fritzi* (Peris-Felipo, 2017)** ♀♂
- Face 1.2× as wide as high. Scape 2.0× as long as pedicel. F2 2.7×, and sixth flagellar segment 2.5× as long as wide. Hind femur 3.9× as long as wide. Hind tibia 9.6× as long as wide. Antenna with 20 segments. Body length 1.7 mm. Brazil
..... ***Dinotrema (Synaldis) magniocularis* (Peris-Felipo, 2017)** ♀
- 5(3) Mandible not widened towards apex, 1.8× as long as wide. Mandibular teeth relatively small, particularly the upper tooth. Clypeus 3.0× as wide as high. Prescutellar depression 1.1× as long as wide. Eye 1.4× as wide as temple in lateral view. F3 2.7× as long as wide. First segment of hind tarsus 1.5× as long as second segment. Antenna with 20–21 segments. Body length 1.5–1.7 mm. Brazil
..... ***Dinotrema (Synaldis) brasiliense* (Peris-Felipo, 2017)** ♀♂
- Mandible widened to apex (at least weakly), 1.2–1.5× as long as wide. Mandibular teeth relatively large (as Figs 9, 37, 57). Clypeus 1.7–2.2× as wide as high. Prescutellar depression 1.9–2.5× as long as wide. Eye 0.6–1.2× as long as temple in lateral view. F3 1.5–2.4× as long as wide. First segment of hind tarsus 1.8–2.2× as long as second segment..... **6**
- 6(5) Propodeum with areola but completely lacking a median longitudinal carina (Figs 1E, 10, 11). OOL 4.0× (♀), 3.0× (♂) as OD (Fig. 7). Fore wing with first subdiscal cell 2.5× as long as wide (Fig. 4). Hind wing vein 1-M 2.3–2.4× as long as 1r-m. Antenna with 15–18 segments. Body length

- 1.6–1.9 mm. Chile (Figs 4–12)
 ***Dinotrema (Synaldis) acarinareolatum sp. nov.*** ♀♂
- Propodeum with areola and a clear median longitudinal carina, which can be basal (as Fig. 1F) or extend within the areola (as Fig. 1G, H). OOL 2.3–3.4× as OD. Fore wing with first subdiscal cell 2.8–3.3× (♀), 2.3–3.1× (♂) as long as wide. Hind wing vein 1-M 1.2–2.1× as long as 1r-m..... **7**
- 7(6) Eye 0.6–0.8× as wider as temple in lateral view (as Figs 39, 66) **8**
- Eye 0.9–1.2× as wide as temple in lateral view (as Figs 31, 96)..... **10**
- 8(7) Fore wing vein (r+3-SR) 6.2–6.3× as long as r-m (Fig. 69), submarginal cell 2.7–2.9× as long as wide in ♀, 2.9× in ♂. AF 2.5–2.6× as long as wide (Fig. 67). Hind femur 4.6–4.8× as long as wide (Fig. 71). Antenna with 15 segments in ♀, 21 in ♂. Body length 1.7–2.1 mm. Chile (Figs 65–71) ***Dinotrema (Synaldis) perisfelipoi sp. nov.*** ♀♂
- Fore wing vein (r+3-SR) 5.0–5.3× as long as r-m (Figs 34, 90), submarginal cell 2.2–2.3× as long as wide in ♀, 2.0–2.6× in ♂. AF 1.9–2.3× as long as wide (Figs 38, 86). Hind femur 3.7–4.2× as long as wide (Figs 43, 93) **9**
- 9(8) Prescutellar depression without lateral carinae (Fig. 41). Hind tibia 8.1–8.4× as long as wide (Fig. 43). Metasoma of ♀ 1.50–1.65× as long, and 1.4× as wide as mesosoma (Fig. 34). Propodeal spiracle large size in ♀ and middle in ♂ (0.6–0.7× and 0.5× distance from spiracle to base of propodeum respectively, Fig. 39). Antenna with 14–15 segments in ♀, 20 in ♂. Body length 1.5–1.9 mm. Chile (Figs 34–45)
 ***Dinotrema (Synaldis) daltoni sp. nov.*** ♀♂
- Prescutellar depression with distinct lateral carinae (Fig. 91). Hind tibia 9.4–9.6× as long as wide (Fig. 93). Metasoma of ♀ 2.0–2.2× as long, and 1.7× as wide as mesosoma (Figs 83, 94). Propodeal spiracle middle size in ♀ and small in ♂ (0.5× and 0.2× distance from spiracle to base of propodeum respectively, Fig. 84). Antenna with 16–18 segments (Fig. 83). Body length 2.05–2.50 mm. Chile (Figs 83–94)
 ***Dinotrema (Synaldis) puyehue sp. nov.*** ♀♂ (in part 14)
- 10(7) F1 3.5–3.9× as long as wide, F2 2.6–2.8× as long as wide (Figs 59, 76). Mandibular lower tooth wider than upper tooth (Fig. 57) or ovipositor sheath with several distinct erect setae (Fig. 82) **11**
- F1 2.4–3.2× as long as wide, F2 1.8–2.4× as long as wide (as Figs 25, 48). Mandibular lower tooth ca as wide as upper tooth (as Figs 28, 51, 88) and ovipositor sheath with some delicate setae (as Fig. 33) **12**
- 11(10) Mandibular lower tooth wider and slightly longer than upper tooth (Fig. 57). Ovipositor sheath with some delicate setae (Fig. 64), 1.1–1.4× as long as T1. Fore wing vein (r+3-SR) 6.2× as long as r-m (Fig. 63). Hind wing 4.9× as long as wide. T1 strigose to rugose, its apex 1.6× as wide as base. Antenna with 20–21 segments. Body length 2.6–2.8 mm. Chile (Figs 55–64)..... ***Dinotrema (Synaldis) latusdentertium sp. nov.*** ♀
- Mandibular lower tooth ca as wide and as long as upper tooth (Fig. 74). Ovipositor sheath with several distinct and erect setae (Fig. 82), 1.8× as long as T1. Fore wing vein (r+3-SR) 5.1–5.4× as long as r-m (Fig. 79). Hind wing 5.8× as long as wide. T1 rugose–foveolate (Fig. 80), its apex 1.2–1.3× as wide as base. Antenna with 18–22 segments. Body length 2.0–2.3 mm. Chile (Figs 72–80) ***Dinotrema (Synaldis) pilosicaudatum sp. nov.*** ♀♂

- 12(10) Fore wing vein (r+3-SR) 4.9–5.1× as long as r-m (as Figs 90, 101). Hind femur 4.0–4.3× as long as wide (as Figs 54, 93). Prescutellar depression 2.0–2.2× as long as wide **13**
- Fore wing vein (r+3-SR) 5.6–6.4× as long as r-m (Figs 18, 29). Hind femur 4.5–5.0× as long as wide (Figs 20, 32). Prescutellar depression 2.3–2.7× as long as wide **15**
- 13(12) Paraclypeal fovea middle size (Fig. 97, 98). T1 rugose–foveolate (Fig. 104). Hind wing vein 1-M 1.2× as long as 1r-m. Prescutellar depression without lateral carinae (as Fig. 41). Hind tibia 8.6–8.9× as long as wide (Fig. 105). Metasoma as wide as mesosoma. Antenna with 19–20 segments. Body length 2.5–2.8 mm. Chile (Figs 95–105) ***Dinotrema (Synaldis) verae* sp. nov.** ♀♂
- Paraclypeal fovea short size (as Fig. 50). T1 strigose (as Fig. 91). Hind wing vein 1-M 1.8–2.1× as long as 1r-m. Prescutellar depression with lateral carinae, at least incomplete (Figs 52, 91). Hind tibia 9.4–10.3× as long as wide (as Figs 54, 93). Metasoma 1.3–1.7× as wide as mesosoma **14**
- 14(13) Face and clypeus yellow (Fig. 50). Fore wing vein 1-CU1 as long as cu-a (Fig. 46). Metasoma 1.6× as long, and 1.3× as wide as mesosoma. AF 2.7× as long as wide. Hind tibia 10.1–10.3× as long as wide (Fig. 54). Hind wing 6.2× as long as wide. Antenna with 18 segments. Body length 1.9–2.4 mm. Chile (Figs 46–54) ***Dinotrema (Synaldis) flavum* sp. nov.** ♀
- Face and clypeus brown to dark brown (Fig. 87). Fore wing vein 1-CU1 0.4–0.5× as long as cu-a (Fig. 83). Metasoma 2.0–2.2× as long, and 1.7× as wide as mesosoma (Figs 83, 89, 94). AF 1.9–2.2× as long as wide. Hind tibia 9.4–9.6× as long as wide (Fig. 93). Hind wing 5.3–5.5× as long as wide. Antenna with 16–18 segments. Body length 2.05–2.50 mm. Chile (Figs 83–94) ***Dinotrema (Synaldis) puyehue* sp. nov.** ♀♂ (in part 9)
- 15(12) Propodeum brown to dark brown, mainly rugose, with median longitudinal carina complete (or nearly so) (Fig. 21). Paraclypeal fovea middle size (Fig. 14). Fore wing vein 1-CU1 of ♀ 0.6–0.7× as long as cu-a (Fig. 18). Hind tibia 9.8–10.3× as long as wide (Fig. 20). Antenna with 18–20 segments in ♀, 25 in ♂. Body length 1.7–2.8 mm. Chile (Figs 13–22) ***Dinotrema (Synaldis) brunneum* sp. nov.** ♀♂
- Propodeum yellowish, smooth to rugulose, with median longitudinal carina incomplete, clearly lacking apically (Fig. 27). Paraclypeal fovea short size (Fig. 24). Fore wing vein 1-CU1 1.0–1.4× as long as cu-a (Fig. 29). Hind tibia 9.0–9.4× as long as wide (Fig. 32). Antenna with 17–23 segments. Body length 1.4–2.6 mm. Chile (Figs 23–33) ***Dinotrema (Synaldis) chilensis* sp. nov.** ♀♂

Discussion

The extent and type of sculpture on the propodeum, and the presence/absence of a mesoscutal pit are often used to differentiate species of the subgenera *Dinotrema* and *Synaldis* (Fischer 1967, 1972; Belokobylskij 2004; Tobias 2004a, 2004b; Peris-Felipo et al. 2014a, 2014b; Peris-Felipo and Belokobylskij 2017). In addition, characteristics of mandibles were useful diagnostic characters in the taxonomy of the New World fauna of *Synaldis*. Among the Neotropical species,

the development of propodeal transverse carinae and the shape of mandibles allow for the separation of two groups: one containing the species from Brazil, characterized by incomplete propodeal transverse carinae or mandibles with a very small upper tooth (Peris-Felipo and Belokobylskij 2017), and the other consisting of the species from Chile, distinguished by complete propodeal transverse carinae and mandibles with three relatively large teeth. The taxonomic importance of mouth parts in Alysiinae is well-established. Mandibles serve crucial functions in their biology, acting as levers, piercing, or cutting tools for parasitoid to escape from the host puparium and substrate, as well as manipulating substrates during host searching (Griffiths 1964; Wharton 1977, 2017).

On the other hand, most species of *Synaldis* occurring in Nearctic region have mandibles widened towards the apex, with relatively large teeth, like Chilean species (Fischer 1967; Peris-Felipo and Belokobylskij 2017). These Nearctic species exhibit variable propodeal sculpture, but typically lack a distinct areola, differing from Chilean species, which have an areolate propodeum. The exception is *D. (S.) glabrifovea*. This species has an areolate propodeum, with complete median longitudinal and transverse carinae (as depicted in Fig. 3H). Considering its mandibular shape, propodeal sculpture, and relatively elongated flagellomeres, *D. (S.) glabrifovea* appears to be related to *D. (S.) latusdentertium* sp. nov. and *D. (S.) pilosicaudatum* sp. nov. Nevertheless, *D. (S.) glabrifovea* differs from all the Neotropical species of *Synaldis*, including these last ones, by the absence of mesoscutal pit, among other distinguishing characteristics (Peris-Felipo and Belokobylskij 2017).

Differences in propodeal sculpture are commonly used to distinguish species in several genera of Alysiinae. Typically, the propodeum has a median areola with a short median longitudinal carina extending between the areola and its basal margin; however, various transformation series are observed, and in many taxa, the propodeal carination has been completely lost or only a few remnants of it remain. In some groups, the presence of a complete median longitudinal carina appears to result from the gradual narrowing of the areola (Wharton 2002). The ten new species described here have propodea with distinct areolae and complete transverse carinae. In *D. (S.) latusdentertium* sp. nov., *D. (S.) perisfelipoi* sp. nov., *D. (S.) puyehue* sp. nov., and *D. (S.) verae* sp. nov., the median longitudinal carina varied intraspecifically from incomplete to complete. Therefore, the development of this carina be carefully evaluated at both the specific and interspecific levels. In *D. (S.) acarinareolatum* sp. nov., the absence of any median longitudinal carina on the areolate propodeum is a notable characteristic.

The relative width of the eye and temple (in lateral view) is another useful character to distinguish some New World species of *Synaldis*. Most of these species have the eye as wide as or wider than temple, while other species have the eye clearly shorter than temple. In a few species, despite that, the temple varies from slightly wider to as wide as eye (Peris-Felipo and Belokobylskij 2017). Variations in wing veins and cells were also significant, especially in fore wing veins 1CU-1 (which affects the position of cu-a in relation to 1-M), 3-SR in relation to r-m, as well as the relative size of the marginal and submarginal cells.

A diagnostic characteristic of the subgenus *Synaldis* as outlined by Peris-Felipo and Belokobylskij (2020), is the consistent postfurcal positioning of the cu-a vein. However, in *D. (S.) brunneum* sp. nov., *D. (S.) daltoni* sp. nov.,

D. (S.) perisfelipoi sp. nov., *D. (S.) puyehue* sp. nov., and *D. (S.) verae* sp. nov., the 1-CU1 vein exhibited a degree of reduction relative to cu-a. The most extreme reduction was observed in *D. (S.) daltoni* sp. nov., with one of the paratypes having the vein 1-CU1 so short that it is difficult to see, rendering the cu-a almost interstitial. The discovery of this condition in this species led to the expansion of the diagnostic criteria for the subgenus.

Acknowledgements

We are thankful to Dr Dalton S. Amorim and Dr Vera C. Silva for collecting and loaning the studied specimens, to the Museo Nacional de Historia Natural (Chile) for making the material available, and to Dr Luciana Fernandes for taking and editing the photographs. The manuscript was improved thanks to the valuable comments from the reviewers and the subject editor.

Additional information

Conflict of interest

The authors have declared that no competing interests exist.

Ethical statement

No ethical statement was reported.

Funding

This study was financed by Coordenação de Aperfeiçoamento de Pessoal de Nível Superior (CAPES) Finance Code 001 (PROAP/CAPES PPGERN), Fundação de Amparo à Pesquisa do Estado de São Paulo (FAPESP), Conselho Nacional de Desenvolvimento Científico e Tecnológico (CNPq), and Instituto Nacional de Ciência e Tecnologia dos Hymenoptera Parasitoides (INCT-HYMPAR).

Author contributions

Francielle Oliveira: conceptualization (supporting), data curation, formal analysis, investigation, methodology, visualization (lead), writing (original draft, review, and editing). Angélica Penteado-Dias: conceptualization (lead), funding acquisition, project administration, resources, supervision, validation, visualization (supporting), writing (review and editing).

Author ORCIDs

Francielle Dias de Oliveira  <https://orcid.org/0000-0003-4471-4024>

Angélica Maria Penteado-Dias  <https://orcid.org/0000-0002-8371-5591>

Data availability

All of the data that support the findings of this study are available in the main text.

References

Amorim DDS, Elgueta M, González CR, Silva VC, Rafael JA, Valderrama CH, Cea SM, Cea SM, Báez SG (2022) An extensive collection of the insect fauna of the Valdivian forest, in the Parque Nacional Puyehue, southern Chile. *Fly Times* (68): 1–13. <http://www.nadsdiptera.org/News/FlyTimes/issue68.pdf>

- Belokobylskij SA (2002) Eastern Palaearctic species of the braconid wasp genus *Synaldis* Förster (Hymenoptera, Braconidae, Alysiinae). Species without mesoscutal pit. *Entomological Review* 82(4): 404–423.
- Belokobylskij SA (2004) Eastern Palaearctic species of the braconid wasp genus *Synaldis* Förster (Hymenoptera, Braconidae, Alysiinae). Species with mesoscutal pit. I. *Entomological Review* 84(2): 191–215.
- Belokobylskij SA, Tobias VI (2002) New subgenus of the genus *Dinotrema* Foerster (Hymenoptera, Braconidae, Alysiinae) from East Palearctic with description of a new species. *Far Eastern Entomologist = Dal'nevostochnyi Entomolog* 120: 1–7.
- Belokobylskij SA, Tobias VI (2007) Braconidae: Alysiinae. In: Lelej AS (Ed.) *Key to the insects of Russia Far East. Vol. IV. Neuropteroidea, Mecoptera, Hymenoptera. Pt 5.* Dalnauka, Vladivostok, 9–133. [In Russian]
- Eady RD (1968) Some illustrations of microsculpture in the Hymenoptera. *Proceedings of the Royal Entomological Society of London. Series A, General Entomology* 43(4–6): 66–72. <https://doi.org/10.1111/j.1365-3032.1968.tb01029.x>
- Fischer M (1967) Die nearktischen arten der gattung *Synaldis* Foerster (Hymenoptera, Braconidae, Alysiinae). *Polskie Pismo Entomologiczne* 37(3): 431–478.
- Fischer M (1972) Erste gliederung der palaarktischen *Aspilota*-Arten (Hym., Braconidae, Alysiinae). *Polskie Pismo Entomologiczne* 42: 323–459.
- Fischer M (1993a) Zur formenvielfalt der kieferwespen der Alten Welt: über die gattungen *Synaldis* Foerster, *Trisynaldis* Fischer und *Kritscherysia* Fischer gen. nov. (Hymenoptera, Braconidae, Alysiinae). *Annalen des Naturhistorischen Museums in Wien* 94–95(B): 451–490.
- Fischer M (1993b) Eine neue studie über buckelfliegen–kieferwespen: *Synaldis* Foerster und *Dinotrema* Foerster (Hymenoptera, Braconidae, Alysiinae). *Linzer Biologische Beitrage* 25(2): 565–592.
- Fischer M (2003) Ein beitrag zur kenntnis der gattungen *Synaldis* Foerster und *Adelphenaldis* Fischer, gen. nov. (Hymenoptera, Braconidae, Alysiinae). *Linzer Biologische Beitrage* 35(1): 19–74.
- Foerster A (1863) Synopsis der familien und gattungen der Braconen. *Verhandlungen des Naturhistorischen Vereines preussischen Rheinlande und Westphalens* (1862) 19: 225–288.
- Griffiths GCD (1964) The Alysiinae (Hym., Braconidae) parasites of the Agromyzidae (Diptera). I. General questions of taxonomy, biology and evolution. *Beiträge zur Entomologie* 14: 823–914.
- Koenig R (1972) Zur systematik, faunistik, phaenologie und oekologie mitteleuropaeischer Braconiden (Hymenoptera) I. *Faunistisch-Oekologische Mitteilungen* 4: 85–106.
- Nees von Esenbeck CG (1812) *Ichneumonides Adsciti, in genera et familias divisi.* *Magazin Gesellschaft Naturforschender Freunde zu Berlin* 5: 3–37.
- Papp J (1996) Braconidae (Hymenoptera) from Korea, XVIII. *Annales Historico-Naturales Musei Nationalis Hungarici* 88: 145–170. http://publication.nhnm.hu/pdf/annHNHM/Annals_HNHM_1996_Vol_88_145.pdf
- Papp J (2000) Braconidae (Hymenoptera) from Mongolia, XIV: Doryctinae, Helconinae, Meteorinae, Euphorinae, Blacinae, Opiinae and Alysiinae. *Acta Zoologica Academiae Scientiarum Hungaricae* 46(1): 35–52.
- Peris-Felipo FJ, Belokobylskij SA (2017) The genus *Synaldis* Foerster, 1863 (Hymenoptera: Braconidae: Alysiinae) in the Neotropical region: first record, descriptions of new species and a key to the New World taxa. *European Journal of Taxonomy* 386(386): 1–28. <https://doi.org/10.5852/ejt.2017.386>

- Peris-Felipo FJ, Belokobylskij SA (2020) Species of the subgenus *Synaldis* Foerster, 1863 (Hymenoptera: Braconidae: Alysiinae: *Dinotrema* Foerster, 1863) in Papua New Guinea: descriptions of three new species and a key to the Australasian taxa. In: Robillard T, Legendre CV, Leponce M (Eds) *Insects of Mount Wilhelm Papua New Guinea*. Vol. II. Scientifiques du Muséum Historie Naturelle, Paris 2: 191–208.
- Peris-Felipo FJ, Papp J, Belokobylskij SA, Jiménez-Peydró R (2014a) Seven new Spanish species of the genus *Synaldis* (Hymenoptera, Braconidae, Alysiinae) with mesoscutal pit. *Zootaxa* 3764(1): 39–60. <https://doi.org/10.11646/zootaxa.3764.1.3>
- Peris-Felipo FJ, Belokobylskij SA, Jiménez-Peydró R (2014b) Revision of the western Palearctic species of the genus *Dinotrema* Foerster, 1862 (Hymenoptera, Braconidae, Alysiinae). *Zootaxa* 3885(1): 1–483. <https://doi.org/10.11646/zootaxa.3885.1.1>
- Shenefelt RD (1974) Pars 11. Braconidae 7. Alysiinae. In: van der Vecht J, Shenefelt RD (Eds) *Hymenopterorum Catalogus (nova editio)*. Dr. W. Junk, The Hague, 937–1113.
- Tobias VI (2004a) Species of the genus *Dinotrema* Foerster, 1862 (Hymenoptera, Braconidae, Alysiinae) without prescutellar pit and with a widely sculptured propodeum and short mandibles from Russia and neighboring territories. *Entomological Review* 84(2): 216–232.
- Tobias VI (2004b) Two new species of the genus *Dinotrema* Foerster (Hymenoptera, Braconidae, Alysiinae) without prescutellar pit. *Entomological Review* 84(6): 673–676.
- van Achterberg C (1988) The genera of the *Aspilota*-group and some descriptions of fungicolous Alysiini from the Netherlands (Hymenoptera: Braconidae: Alysiinae). *Zoölogische Verhandelingen* 247: 1–88. <https://repository.naturalis.nl/pub/317564/ZV1988247001.pdf>
- van Achterberg C (1993) Illustrated key to the subfamilies of the Braconidae (Hymenoptera: Ichneumonoidea). *Zoölogische Verhandelingen* 283: 1–189. <https://repository.naturalis.nl/pub/317645/ZV1993283001.pdf>
- Wharton RA (1977) New World *Aphaereta* species (Hymenoptera: Braconidae: Alysiinae), with a discussion of terminology used in the tribe Alysiini. *Annals of the Entomological Society of America* 70(5): 782–803. <https://doi.org/10.1093/aesa/70.5.782>
- Wharton RA (1980) Review of the Nearctic Alysiini (Hymenoptera, Braconidae) with discussion of generic relationships within the tribe. *University of California Publications in Entomology* 88: 1–112.
- Wharton RA (1984) Biology of the Alysiini (Hymenoptera: Braconidae), parasitoids of cyclorrhaphous Diptera. *Texas Agricultural Experimental Station* 11: 1–39.
- Wharton RA (2002) Revision of the Australian Alysiini (Hymenoptera: Braconidae). *Invertebrate Systematics* 16(1): 7–105. <https://doi.org/10.1071/IT01012>
- Wharton RA (2017) Subfamily Alysiinae. In: Wharton RA, Marsh PM, Sharkey MJ (Eds) *Manual of the New World Genera of the Family Braconidae (Hymenoptera)* (2nd edn.). International Society of Hymenopterists, Washington, 82–117.
- Wharton RA, Marsh PM, Sharkey MJ (2017) *Manual of the New World Genera of the Family Braconidae (Hymenoptera)* (2nd edn.). International Society of Hymenopterists, Washington, 476 pp.
- Yu DSK, van Achterberg K, Horstmann K (2016) Home of Ichneumonoidea. Taxapad, Ottawa, Ontario. [database on flash-drive]
- Zhu JC, van Achterberg C, Chen XX (2017) An illustrated key to the genera and subgenera of the Alysiini (Hymenoptera, Braconidae, Alysiinae), with three genera new for China. *ZooKeys* 722: 37–79. <https://doi.org/10.3897/zookeys.722.14799>

Low-cost, high-volume imaging for entomological digitization

Dirk Steinke^{1,2*}, Jaclyn T. A. McKeown^{1*}, Allison Zyba¹, Joschka McLeod¹, Corey Feng¹, Paul D. N. Hebert^{1,2}

¹ Centre for Biodiversity Genomics, University of Guelph, 50 Stone Road East, Guelph, Ontario, N1G 2W1, Canada

² Department of Integrative Biology, University of Guelph, 50 Stone Road East, Guelph, Ontario, N1G 2W1, Canada

Corresponding author: Dirk Steinke (dsteinke@uoguelph.ca)

Abstract

Large-scale digitization of natural history collections requires automation of image acquisition and processing. Reflecting this fact, various approaches, some highly sophisticated, have been developed to support imaging of museum specimens. However, most of these systems are complex and expensive, restricting their deployment. Here we describe a simple, inexpensive technique for imaging arthropods larger than 5 mm. By mounting a digital SLR camera on a CNC (computer numerical control) motor-drive rig, we created a system that captures high-resolution z-axis stacked images (6960 × 4640 pixels) of 95 specimens in 30 minutes. This system can be assembled inexpensively (\$1000 USD without a camera) and it is easy to set-up and maintain. By coupling low cost with high production capacity, it represents a solution for digitizing any natural history collection.

Key words: AI, Arthropoda, collections, databases, insects, machine learning, photography



Academic editor: Pavel Stoev

Received: 26 March 2024

Accepted: 10 May 2024

Published: 11 July 2024

ZooBank: <https://zoobank.org/09CCADF4-C991-47EF-B01F-519B43A62AF7>

Citation: Steinke D, McKeown JTA, Zyba A, McLeod J, Feng C, Hebert PDN (2024) Low-cost, high-volume imaging for entomological digitization. ZooKeys 1206: 315–326. <https://doi.org/10.3897/zookeys.1206.123670>

Copyright: © Copyright work is made by His Majesty or by an officer or servant of the Crown in the course of his duties.

This is an open access article distributed under terms of the Creative Commons Attribution License (Attribution 4.0 International – CC BY 4.0).

Introduction

Advances in computational and imaging technologies have stimulated the digitization of specimens in natural history collections (Berents et al. 2010; Vollmar et al. 2010; Moore 2011; Beaman and Cellinese 2012; Mantle et al. 2012; Mathys et al. 2013; Holovachov et al. 2014; Hudson et al. 2015; Mertens et al. 2017; Hedrick et al. 2020). Because the largest collections contain millions of specimens, comprehensive digitization can be a challenge (Blagoderov et al. 2012). This is particularly true for insects, as they dominate most zoological collections (Tegelberg et al. 2014). Consequently, many digitization projects have only captured high-resolution images of a few representative specimens of each species (deWaard et al. 2019).

Projects that seek to digitize entire insect collections require automated image acquisition and processing. Because of the effort in handling individual specimens and the risk of damaging them, some digitization programs have imaged drawers of specimens (Blagoderov et al. 2012; Mantle et al. 2012; Holovachov et al. 2014). This approach has three limitations. First, resolution is often insufficient to allow examination of some morphological traits. Second,

* These authors contributed equally to the work.

dorsal images are captured, so characters only visible with a lateral or ventral view are inaccessible. Third, this approach brings informatics challenges as the drawer image must be decomposed into its component specimen images (Blagoderov et al. 2012; Holovachov et al. 2014). In practice, most of the time required in these digitization projects is spent on image selection and metadata capture (Blagoderov et al. 2012).

Recently, several approaches have been developed to digitize individual specimens in museum collections (Heerlien et al. 2015; Tegelberg et al. 2017; Ströbel et al. 2018) or as part of community sampling and sorting procedures (Ärje et al. 2020; Wühl et al. 2021). Some of these systems generate several images per specimen to facilitate 3-D modelling (Ströbel et al. 2018) or include robotic handling of specimens to accelerate processing (Ärje et al. 2020; Wühl et al. 2021). At this time, most of these systems are elaborate and expensive.

Optimal high-throughput specimen digitization requires combining technologies in novel workflows and is largely driven by purpose (collection digitization versus one component of a multifaceted workflow). This study introduces an imaging system developed to support the specimen-centric workflow employed by the Centre for Biodiversity Genomics (CBG), Guelph, Canada to gather DNA barcode records. Because images are essential to validate DNA barcodes, the CBG photographs every specimen. Small specimens (<5 mm) are each placed into a well in a 96-well plate and are imaged with a high-resolution automated microscope system (Steinke et al. in prep.) before entering molecular analysis. Larger individuals are pinned, arrayed in Schmidt boxes, and then imaged using the digital SLR camera rig described here. This system is easy to install and was designed to provide high production capacity at low cost for operations ranging from small entomology laboratories to large natural history collections.

Material and methods

System hardware

The SLR rig (Fig. 1) employs a Canon 90D camera (32.5 megapixel) with an EF-S 60 mm f/2.8 Macro USM lens (Canon Corp, Irvine, CA, USA). The camera is attached to an OpenBuilds Acro 1010 40" x 40" motor-drive rig (OpenBuilds, New York, NY, USA). Most components for the OpenBuilds Acro 1010 were purchased, but some components were printed (i-Fast; QIDI Technology Official, China) using 3D-models available on the OpenBuilds website (<https://openbuildspartstore.com>). The OpenBuilds Acro 1010 frame is screwed onto a wooden base which is placed on a sturdy table (79 cm from floor). Two 60×60 cm softbox lights (Neewer 24×24, Shenzhen) are stationed to the left and right of the SLR camera motor-drive rig at a height of 165 cm on their stands. A LED light strip is positioned along the circumference of the Acro system facing inwards (Daylight White LED Strip Light; Shenzhen Intellirocks Tech Co. Ltd., Shenzhen, China). The SLR camera is mounted 16 cm above the table's surface and a Kimaru ACK-E6 DR-E6 DC Coupler LP-E6N Dummy Battery AC Power Adapter Kit is used to provide constant power. A USB-A to micro-USB cable connects the camera to the computer (iMac 27-inch, 8GB Ram. 3.4GHz Quad-core Intel-Core i5).



Figure 1. The SLR rig is placed on a heavy-base table to minimize vibration. The inset shows the actual rig area with specimens on the styrofoam base.

Software control

The SLR rig is controlled by a program that employs both a python script (Suppl. material 1) and a G-code script (Suppl. material 2) through an Apple iMac operating system. The system is manually calibrated using OpenBuilds Control (OpenBuilds) integrated into the python script. The camera is controlled using the command line tool Gphoto2 (gphoto2.org). It is set to an ISO value of 100, an aperture value of f/8, and a shutter speed of 1/8s. Focus bracketing to allow z-axis stacking is set to take nine images at different levels of focus. The lens is set to auto-focus, so the first image captures the uppermost of a specimen before eight more images are automatically captured at lower focal planes to allow z-axis stacking. The nine images are combined to generate a single composite in-focus image using Helicon Focus 8 (Helicon Soft Ltd, Kharkov, Ukraine).

Operation

Pinned arthropods are loaded into the SLR rig in batches of 95 after being transferred to a 75 cm by 47 cm foam platform (Fig. 2). This platform has 95 positions for specimen loading, each a slot with a depth of 1.8 cm, a length of

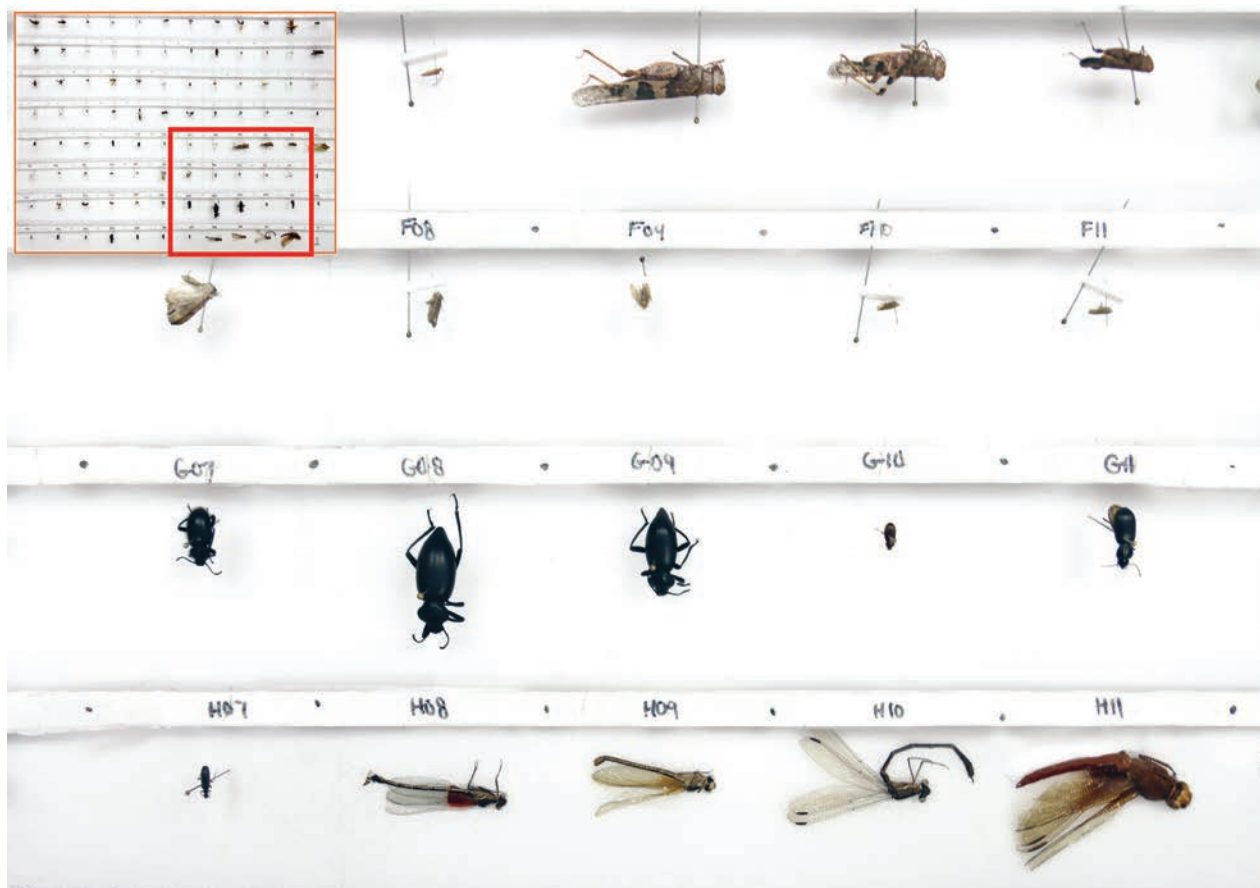


Figure 2. 75 cm by 47 cm foam platform with pinned insects in dorsal and lateral positions.

6 cm, and a width of 5 cm. This count ensures that all specimens in each 96-well micro-plate (95 specimens, 1 negative control) are processed as a batch. The platform is split into 8 rows, each with 12 slots (Fig. 2). Each pinned specimen is placed centrally in a slot where it can be positioned for dorsal or lateral imaging (Fig. 2). Each row has a foam strip (height = 2 cm) that facilitates lateral imaging. Specimens stored in envelopes are removed from them and placed centrally at the base of a slot.

Data handling

Gphoto2 is used to transfer images to the computer for further processing. Z-stacked images are cropped to standardised dimensions with a 4×3 aspect ratio using a machine-learning-based cropping tool (Gharaee et al. 2023). A scale bar is added to each image using the batch action tool of Photoshop 2023 (Adobe Inc., San Jose, USA). Once edited, images are uploaded to the Barcode of Life Database System (BOLD) (Ratnasingham and Hebert 2007) where they are automatically associated with individual specimen records and the DNA barcode sequence of the photographed specimen. A python script (Suppl. material 3) generates a metadata file and compresses it together with packets of 95 images into a zip folder to meet BOLD's requirements for image upload. Similar scripts could be developed to transfer images to any other database.

Results and discussion

Performance and costs

Fig. 3 shows a selection of specimens and their sizes. When using a Canon 90D with the described settings, the resulting image is 6960 × 4640 pixels before cropping. This translates into an average size of 9.5MB for a jpg-file.

The CNC motor activates at a pre-set time, which depends upon the distance between each slot and the dwell time (3.75 s) at each stop, allowing the camera to take nine images and transfer them to the computer. Operating in this mode, the SLR rig images 95 specimens in 30 min and the stacking software requires another 11.5 min to process these images, but this usually occurs while the next batch is being photographed. The transfer of pinned specimens to and off the foam platform takes about 15 min each and is done while the SLR rig is running another batch. The time required to crop and edit each batch varies (15–30 min) with the type of specimens. Operated by one staff member, the SLR rig can image 4000 specimens in a week. The CBG's system has now imaged more than 250,000 specimens and the sole maintenance involved the replacement of a wire leading to one motor.

The SLR rig cost of \$4500 USD reflects three main components: 1) CNC machine kit (\$1000), 2) Apple computer (\$1000), and 3) Canon 90D including lens (\$2500). Costs can be reduced by replacing the computer with a raspberry pi (\$100), but under heavy usage (40 h a week), it will need replacement every six months. Less expensive cameras can be used if they can be controlled with gphoto2. They do have a lower resolution (12–20 megapixels) than the Canon 90D (32.5 megapixels), but this resolution is adequate for many applications. However, it is important to select a camera with a depth stacking function such as focus bracketing (e.g., Canon PowerShot G7 X Mark II, \$900; Olympus OM-D E-M1 Mark II & III, \$920 for body). By careful selection of components, the overall cost can be reduced to about \$2000 (using the CNC kit, a raspberry pi, and a low budget point and shoot camera with depth stacking). The light setup can also vary in cost. The Neewer 24×24 Softbox pair used in our study costs about \$150 but it can be replaced by LED strips (~\$20) attached to the inner part of the CNC frame. Plastic components for the OpenBuilds Acro 1010 are freely available as 3D models so users can modify and 3D-print custom components if such a system is available. One modification made to our SLR rig was the addition of bumpers and a triangular structure to improve wire management during operation (Suppl. materials 4, 5).

Adjustments

The SLR rig can image a wide variety of specimens by adjusting settings as described in this section. The distance between the camera and the specimen dictates the size of the image (focal distance from base = 16 cm). The frame size varies by 0.5 cm in both directions depending upon the depth of the focus point determined by the auto-focus program. This limits the size range of specimens which can be imaged (5–45 mm). As each slot on the platform is designed to fit the camera frame, no specimen should overlap an adjacent space because the cropping tool is likely to malfunction. However, larger specimens can be imaged if the distance between the camera and the specimen is increased as

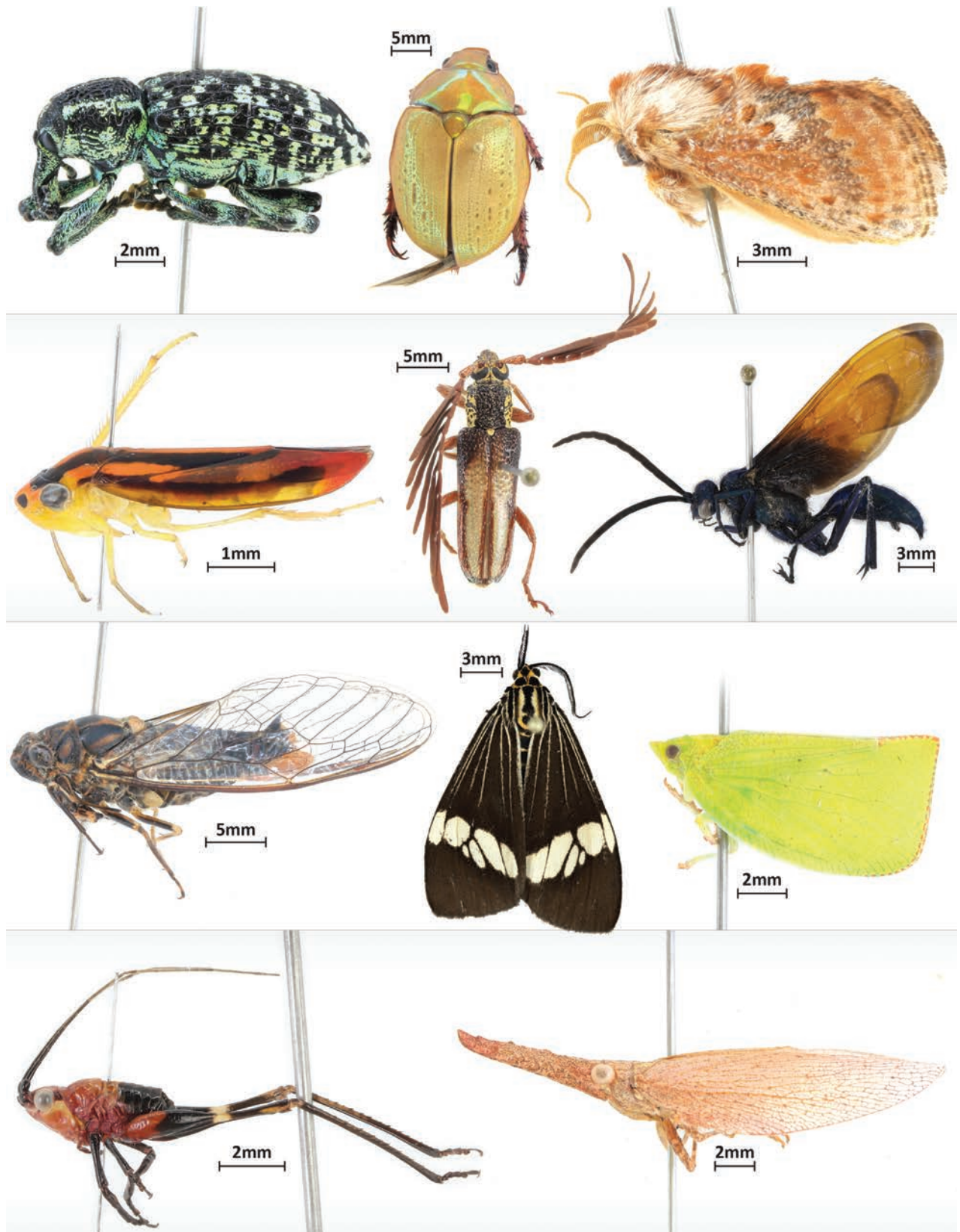


Figure 3. Panel of example images taken with the SLR rig.

this enlarges the size of the frame. Conversely, reducing the camera-specimen distance decreases the size of the frame, allowing smaller specimens (down to 2 mm using the 60 mm macro lens in our setup) to be imaged. Any change

in the camera's operating height is difficult with the described setup as it requires remounting the camera at a higher or lower position on its mount or the exchange of the legs mounted to the rig frame. Future optimization could incorporate legs capable of height adjustment.

Background colour and light settings can also be modified to improve image quality. Dark backgrounds improve the contrast for dark specimens, helping to highlight otherwise subtle features and also help to contrast pale specimens that blend into a white background. To make this adjustment, a second platform can be made of dark foam, or dark strips can be temporarily added to the existing platform. As lighting and whitening settings on the camera must be adjusted to accommodate the change in background colour, all 95 slots must have the same background.

The number of images taken of each specimen can be adjusted with the depth stack function on the camera. Increasing the image count expands the depth range in focus, but increases the time required to capture photographs and to process them in Helicon Focus. The dwell time of the CNC motor system would need to be extended to allow more images to be taken before the camera moves. Conversely, imaging and processing times can be reduced by reducing the number of images taken per specimen. Experimentation with sets of specimens in the target group is the best way to optimize the number of images taken.

Although this CBG's SLR system is primarily used with pinned insects, it is effective in imaging other specimens (e.g., soft-bodied invertebrates in liquid preservatives). In the latter case, the foam platform is simply replaced by a grid structure that holds each specimen vial (Mendez et al. 2018). Focal distance and stack depth often need to be adjusted in such cases (Mendez et al. 2018).

Limitations

Generating an image with enough resolution to allow species identification can be difficult with any automated system given the manifold differences in shape and size of specimens (Blagoderov et al. 2012). Very large individuals that exceed the standard stacking depth can cause the auto-focus program to return an out-of-focus image. The auto-focus function is also vulnerable to vertical protrusions, especially if they contrast with the background. In such cases, the depth stack may begin above the organism's body plane leading to a blurred image. For winged insects, such as Lepidoptera, variation in wing orientation can lead the wingspan exceeding the range of the image stack. In such cases, the resulting image may show a focused wing with an out-of-focus body or an in-focus body with a blurred wing. In such cases, a slight change in the angle at which a specimen is positioned can greatly improve image quality but a switch from lateral to dorsal view is sometimes required. Because reorienting a few specimens requires recapturing an entire set of images, it is often more time-effective to simply accept few imperfect images (Chapman 2005; Ahl et al. 2023). Such specimens could be imaged separately using any setup.

At the CBG, specimens are usually imaged before they are labelled. When labelled specimens are imaged, a small white piece of paper with a slit in the middle is used to cover labels, allowing images of small specimens to remain sharp when cropped. Alternatively, the labels can be removed and reattached to the specimen after photography.

Conclusion

The present SLR rig was designed to photograph terrestrial arthropods that were being analyzed to construct DNA barcode reference libraries. About 90% of these specimens are small enough to be imaged within 96-well plates, but the remainder must be pinned. As the CBG currently barcodes three million specimens annually, it was essential to develop a system capable of imaging the larger specimens in a cost-effective way. This led to the present solution, which can be acquired for \$2000–4500 USD depending on the choice of camera and controller and generates almost 200 high-resolution specimen images per hour.

As the CBG's SLR rig has performed reliably for 2.5 years of heavy use (12h/day), this system is ideal for deployment in settings remote from technical support. Because of its capacity to rapidly generate large numbers of high-quality digital images for online databases, it is also an asset for any large specimen collection.

Acknowledgements

We thank Suzanne Bateson for helping with graphics.

Additional information

Conflict of interest

The authors have declared that no competing interests exist.

Ethical statement

No ethical statement was reported.

Funding

This study was enabled by awards to PDNH from the Walder Foundation, the Ontario Ministry of Economic Development, Job Creation and Trade, the Canada Foundation for Innovation, and by a grant from the Canada First Research Excellence Fund to the University of Guelph's "Food From Thought" research program.

Author contributions

Conceptualization: AZ, DS, JTAM. Data curation: CF, JTAM. Formal analysis: DS. Funding acquisition: PDNDH. Investigation: CF, JM. Methodology: AZ, JM, JTAM. Project administration: DS. Supervision: PDNDH. Validation: CF, AZ, JM. Visualization: DS. Writing – original draft: DS. Writing – review and editing: JTAM, PDNDH, CF, JM.

Author ORCIDs

Dirk Steinke  <https://orcid.org/0000-0002-8992-575X>

Jaclyn T. A. McKeown  <https://orcid.org/0009-0005-7193-2643>

Joschka McLeod  <https://orcid.org/0000-0002-7503-1835>

Corey Feng  <https://orcid.org/0009-0007-7630-7884>

Paul D. N. Hebert  <https://orcid.org/0000-0002-3081-6700>

Data availability

All of the data that support the findings of this study are available in the main text or Supplementary Information.

References

- Ärje J, Melvad C, Rosenhøj Jeppesen M, Agerskov Madsen S, Raitoharju J, Strandgård Rasmussen M, Iosifidis A, Tirronen V, Gabbouj M, Meissner K, Høye TT (2020) Automatic image-based identification and biomass estimation of invertebrates. *Methods in Ecology and Evolution* 11(8): 922–931. <https://doi.org/10.1111/2041-210X.13428>
- Beaman RS, Cellinese N (2012) Mass digitization of scientific collections: New opportunities to transform the use of biological specimens and underwrite biodiversity science. *ZooKeys* 209: 7–17. <https://doi.org/10.3897/zookeys.209.3313>
- Berents P, Hamer M, Chavan V (2010) Towards demand-driven publishing: Approaches to the prioritization of digitization of natural history collection data. *Biodiversity Informatics* 7: 113–119. <https://doi.org/10.17161/bi.v7i2.3990>
- Blagoderov V, Kitching IJ, Livermore L, Simonsen TJ, Smith VS (2012) No specimen left behind: Industrial scale digitization of natural history collections. *ZooKeys* 209: 133–146. <https://doi.org/10.3897/zookeys.209.3178>
- Chapman A (2005) Principles of Data Quality. Global Biodiversity Information Facility. <https://doi.org/10.15468/doc.jrgg-a190>
- deWaard JR, Ratnasingham S, Zakharov EV, Borisenko AV, Steinke D, Telfer AC, Perez KHJ, Sones JE, Young MR, Levesque-Beaudin V, Sobel CN, Abrahamyan A, Bessonov K, Blagoev G, deWaard SL, Ho C, Ivanova NV, Layton KKS, Lu L, Manjunath R, McKeown JTA, Milton MA, Miskie R, Monkhouse N, Naik S, Nikolova N, Pentinsaari M, Prosser SWJ, Radulovici AE, Steinke C, Warne CP, Hebert PDN (2019) A reference library for Canadian invertebrates with 1.5 million barcodes, voucher specimens, and DNA samples. *Scientific Data* 6(1): 308. <https://doi.org/10.1038/s41597-019-0320-2>
- Gharaee Z, Gong Z, Pellegrino N, Zarubiieva I, Haurum JB, Lowe SC, McKeown JTA, Ho CCY, McLeod J, Wei YC, Agda J, Ratnasingham S, Steinke D, Chang AX, Taylor GW, Fieguth P (2023) A step towards worldwide biodiversity assessment: The BIOSCAN-1M insect dataset. *Advances in Neural Information Processing Systems* 37.
- Hedrick BP, Heberling JM, Meineke EK, Turner KG, Grassa CJ, Park DS, Kennedy J, Clarke JA, Cook JA, Blackburn DC, Edwards SV, Davis CC (2020) Digitization and the future of natural history collections. *Bioscience* 70(3): 243–251. <https://doi.org/10.1093/biosci/biz163>
- Heerlien M, van Leusen J, Schnörr S, de Jong-Kole S, Raes R, van Hulsen K (2015) The natural history production line: An industrial approach to the digitization of scientific collections. *ACM Journal on Computing and Cultural Heritage* 8(1): 1–11. <https://doi.org/10.1145/2644822>
- Holovachov O, Zatushevsky A, Shydlovsky I (2014) Whole-drawer imaging of entomological collections: Benefits, limitations and alternative applications. *Journal of Conservation & Museum Studies* 12(1): 9. <https://doi.org/10.5334/jcms.1021218>
- Hudson LN, Blagoderov V, Heaton A, Holtzhausen P, Livermore L, Price BW, van der Walt S, Smith VS (2015) Insect: Automating the digitization of natural history collections. *PLoS one* 10: e0143402. <https://doi.org/10.1371/journal.pone.0143402>
- Ahl LI, Bellucci L, Brewer P, Gagnier P-Y, Hardy HM, Haston EM, Livermore L, De Smedt S, Enghoff H (2023) Digitisation of natural history collections: criteria for prioritization. *Research Ideas and Outcomes* 9: e114548. <https://doi.org/10.3897/rio.9.e114548>
- Mantle BL, Salle JL, Fisher N (2012) Whole-drawer imaging for digital management and curation of a large entomological collection. *ZooKeys* 209: 147–163. <https://doi.org/10.3897/zookeys.209.3169>

- Mathys A, Brecko J, Semal P (2013) Comparing 3D digitizing technologies: What are the differences? Digital Heritage International Congress. Marseille, 201–204. <https://doi.org/10.1109/DigitalHeritage.2013.6743733>
- Mendez PK, Lee S, Venter CE (2018) Imaging natural history museum collections from the bottom up: 3D print technology facilitates imaging of fluid-stored arthropods with flatbed scanners. *ZooKeys* 795: 49–65. <https://doi.org/10.3897/zookeys.795.28416>
- Mertens JEJ, Roie MV, Merckx J, Dekoninck W (2017) The use of low-cost compact cameras with focus stacking functionality in entomological digitization projects. *ZooKeys* 712: 141–154. <https://doi.org/10.3897/zookeys.712.205055>
- Moore W (2011) Biology needs cyber-infrastructure to facilitate specimen-level data acquisition for insect and other hyperdiverse groups. *ZooKeys* 147: 479–486. <https://doi.org/10.3897/zookeys.147.1944>
- Ratnasingham S, Hebert PDN (2007) BOLD: the barcode of life data system (<http://www.barcodinglife.org>). *Molecular Ecology Notes* 7(3): 355–364. <https://doi.org/10.1111/j.1471-8286.2007.01678.x>
- Ströbel B, Schmelzle S, Blüthgen N, Heethoff M (2018) An automated device for the digitization and 3D modelling of insects, combining extended-depth-of-field and all-side multi-view imaging. *ZooKeys* 759: 1–27. <https://doi.org/10.3897/zookeys.759.24584>
- Tegelberg R, Mononen T, Saarenmaa H (2014) High-performance digitization of natural history collections: Automated imaging lines for herbarium and insect specimens. *Taxon* 63(6): 1307–1313. <https://doi.org/10.12705/636.13>
- Tegelberg R, Kahanpää J, Karppinen J, Mononen T, Wu Z, Saarenmaa H (2017) Mass digitization of individual pinned insects using conveyor-driven imaging. 2017 IEEE 13th International Conference on e-Science (e-Science): 523–527. <https://doi.org/10.1109/eScience.2017.85>
- Vollmar A, Macklin JA, Ford LS (2010) Natural history specimen digitization: Challenges and concerns. *Biodiversity Informatics* 7(2): 93–113. <https://doi.org/10.17161/bi.v7i2.3992>
- Wühl L, Pylatiuk C, Giersch M, Lapp F, von Rintelen T, Balke M, Schmidt S, Cerretti P, Meier R (2021) DiversityScanner: Robotic discovery of small invertebrates with machine learning methods. *BioRxiv preprint*. <https://doi.org/10.1101/2021.05.17.444523>

Supplementary material 1

SLR Rig controlling script

Authors: Dirk Steinke, Jaclyn T. A. McKeown, Allison Zyba, Joschka McLeod, Corey Feng, Paul D. N. Hebert

Data type: py

Copyright notice: This dataset is made available under the Open Database License (<http://opendatacommons.org/licenses/odbl/1.0/>). The Open Database License (ODbL) is a license agreement intended to allow users to freely share, modify, and use this Dataset while maintaining this same freedom for others, provided that the original source and author(s) are credited.

Link: <https://doi.org/10.3897/zookeys.1206.123670.suppl1>

Supplementary material 2

G-code control script

Authors: Dirk Steinke, Jaclyn T. A. McKeown, Allison Zyba, Joschka McLeod, Corey Feng, Paul D. N. Hebert

Data type: gcode

Copyright notice: This dataset is made available under the Open Database License (<http://opendatacommons.org/licenses/odbl/1.0/>). The Open Database License (ODbL) is a license agreement intended to allow users to freely share, modify, and use this Dataset while maintaining this same freedom for others, provided that the original source and author(s) are credited.

Link: <https://doi.org/10.3897/zookeys.1206.123670.suppl2>

Supplementary material 3

Image packaging and upload to BOLD

Authors: Dirk Steinke, Jaclyn T. A. McKeown, Allison Zyba, Joschka McLeod, Corey Feng, Paul D. N. Hebert

Data type: py

Copyright notice: This dataset is made available under the Open Database License (<http://opendatacommons.org/licenses/odbl/1.0/>). The Open Database License (ODbL) is a license agreement intended to allow users to freely share, modify, and use this Dataset while maintaining this same freedom for others, provided that the original source and author(s) are credited.

Link: <https://doi.org/10.3897/zookeys.1206.123670.suppl3>

Supplementary material 4

File for 3D printing of bumpers used in system

Authors: Dirk Steinke, Jaclyn T. A. McKeown, Allison Zyba, Joschka McLeod, Corey Feng, Paul D. N. Hebert

Data type: x3d

Copyright notice: This dataset is made available under the Open Database License (<http://opendatacommons.org/licenses/odbl/1.0/>). The Open Database License (ODbL) is a license agreement intended to allow users to freely share, modify, and use this Dataset while maintaining this same freedom for others, provided that the original source and author(s) are credited.

Link: <https://doi.org/10.3897/zookeys.1206.123670.suppl4>

Supplementary material 5

File for 3D printing of triangular wire management piece

Authors: Dirk Steinke, Jaclyn T. A. McKeown, Allison Zyba, Joschka McLeod, Corey Feng, Paul D. N. Hebert

Data type: x3d

Copyright notice: This dataset is made available under the Open Database License (<http://opendatacommons.org/licenses/odbl/1.0/>). The Open Database License (ODbL) is a license agreement intended to allow users to freely share, modify, and use this Dataset while maintaining this same freedom for others, provided that the original source and author(s) are credited.

Link: <https://doi.org/10.3897/zookeys.1206.123670.suppl5>

The tiniest violin: the male of *Loxosceles vallenar* (Araneae, Sicariidae)

Ivan L. F. Magalhaes¹, Hernán A. Iuri¹, Antonio D. Brescovit², Jaime Pizarro-Araya^{3,4,5,6}

¹ División Aracnología, Museo Argentino de Ciencias Naturales “Bernardino Rivadavia” – CONICET, Av. Angel Gallardo 470, C1405DJR, Buenos Aires, Argentina

² Laboratório de Coleções Zoológicas, Instituto Butantan, Av. Vital Brasil, 1500, 05503-900, São Paulo, SP, Brazil

³ Laboratorio de Entomología Ecológica (LEULS), Departamento de Biología, Facultad de Ciencias, Universidad de La Serena, Casilla 554, La Serena, Chile

⁴ Programa de Doctorado en Conservación y Gestión de la Biodiversidad, Facultad de Ciencias, Universidad Santo Tomás, Ejército 146, Santiago, Chile

⁵ Instituto de Ecología y Biodiversidad (IEB), Ñuñoa, Santiago, Chile

⁶ Grupo de Artrópodos, Sistema Integrado de Monitoreo y Evaluación de Ecosistemas Forestales Nativos (SIMEF), Santiago, Chile

Corresponding author: Ivan L. F. Magalhaes (magalhaes@macn.gov.ar)

Abstract

In recent years, several endemic species of *Loxosceles*, violin spiders, have been described from the North-Central Chile biodiversity hotspot, some of which have ambiguous placement within the species groups of the genus. In a recent expedition to the Atacama region, we collected male specimens representing new records of two recently described species: *Loxosceles vicentei* Taucare-Ríos, Brescovit & Villablanca, 2022 and *Loxosceles vallenar* Brescovit, Taucare-Ríos, Magalhaes & Santos, 2017 (Araneae, Sicariidae). Males of the latter are hitherto unknown and are here described for the first time. Examination of the morphology of these species revealed characters such as an embolic keel and digitiform median receptacles, which suggest they do not belong in the *laeta* species group, but rather in the *spadicea* species group, which is briefly re-diagnosed. With carapace lengths smaller than 2 mm, the newly discovered males of *L. vallenar* are the tiniest members of the genus. In addition, males of this species bear strong macrosetae in the clypeus, a sexually dimorphic character not previously reported in *Loxosceles*.

Key words: Atacama, brown recluse spider, Chile, desert, Matorral, sexual dimorphism, taxonomy, violin spider



Academic editor: Cristina Rheims

Received: 7 March 2024

Accepted: 27 May 2024

Published: 11 July 2024

ZooBank: <https://zoobank.org/4CD78168-C16E-4D3D-AAA2-8BF769CC1E65>

Citation: Magalhaes ILF, Iuri HA, Brescovit AD, Pizarro-Araya J (2024) The tiniest violin: the male of *Loxosceles vallenar* (Araneae, Sicariidae). ZooKeys 1206: 327–346. <https://doi.org/10.3897/zookeys.1206.122469>

Copyright: © Ivan L. F. Magalhaes et al.
This is an open access article distributed under terms of the Creative Commons Attribution License (Attribution 4.0 International – CC BY 4.0).

Introduction

Central Chile is renowned as a biodiversity hotspot (Myers et al. 2000; Mittermeier et al. 2011). However, there are knowledge gaps for its arthropod species, specifically referring to Linnean and Wallacean shortfalls, resulting in challenges for regional conservation (Vergara-Asenjo et al. 2023). Regarding spiders, numerous new species have been described in the last decade, partially tackling such shortfalls (e.g., Laborda et al. 2013; Bustamante et al. 2014; Brescovit and Sánchez-Ruiz 2016; Grismado and Pizarro-Araya 2016; Brescovit et al. 2017; Griotti et al. 2022; Taucare-Ríos et al. 2022). In particular, the spider genus *Loxosceles* includes five species endemic to Central Chile: *L. coquimbo*

Gertsch, 1967, *L. diaguita* Brescovit, Taucare-Ríos, Magalhaes & Santos, 2017, *L. pallalla* Brescovit, Taucare-Ríos, Magalhaes & Santos, 2017, *L. vollenar* Brescovit, Taucare-Ríos, Magalhaes & Santos, 2017 and *L. vicentei* Taucare-Ríos, Brescovit & Villablanca, 2022. Four of these have been described in the last decade, indicating that the diversity of this medically important genus has been previously underestimated in Chile.

Loxosceles violin spiders include 149 species occurring naturally mainly in Africa, the Americas and the Mediterranean region (WSC 2024). The genus dates back to the Cretaceous (Binford et al. 2008; Magalhaes et al. 2019), and due to its high morphological and taxonomic diversity, it has been separated into several species groups (Gertsch 1967), most of which have resisted the scrutiny of phylogenetic analyses (Binford et al. 2008). Three of the Central Chile endemics have been placed in the *laeta* species group – *L. coquimbo*, *L. vollenar* and *L. vicentei* – and thus were assumed to be closely related to *Loxosceles laeta* (Nicolet, 1849), a species that may cause serious injury in humans due to the dermonecrotic activity of its venom (Schenone et al. 1989). The other two species have been placed tentatively in the *spadicea* species group (*L. diaguita*) or left unplaced due to its aberrant genital morphology (*L. pallalla*) (see Brescovit et al. 2017). This seems to indicate that the *laeta* species group is the most diverse among Chilean species.

In a recent expedition to Boquerón Chañar (Fig. 1), an area in the Atacama region, Chile (Fig. 2), we collected males of *Loxosceles* that did not fit with any described specimens in the literature, mainly because of the modified clypeal macrosetae (Fig. 3). In the same area, we found a similar-sized female specimen of *Loxosceles vollenar* (Fig. 4B–E), a species hitherto known only by the females, which led us to conclude that the undescribed males are conspecific with them. In addition to describing this male, the new specimens prompted us to re-evaluate the placement of Chilean *Loxosceles* in the different species



Figure 1. Habitat in Boquerón Chañar, Atacama, where *Loxosceles vollenar* and *L. vicentei* were collected.

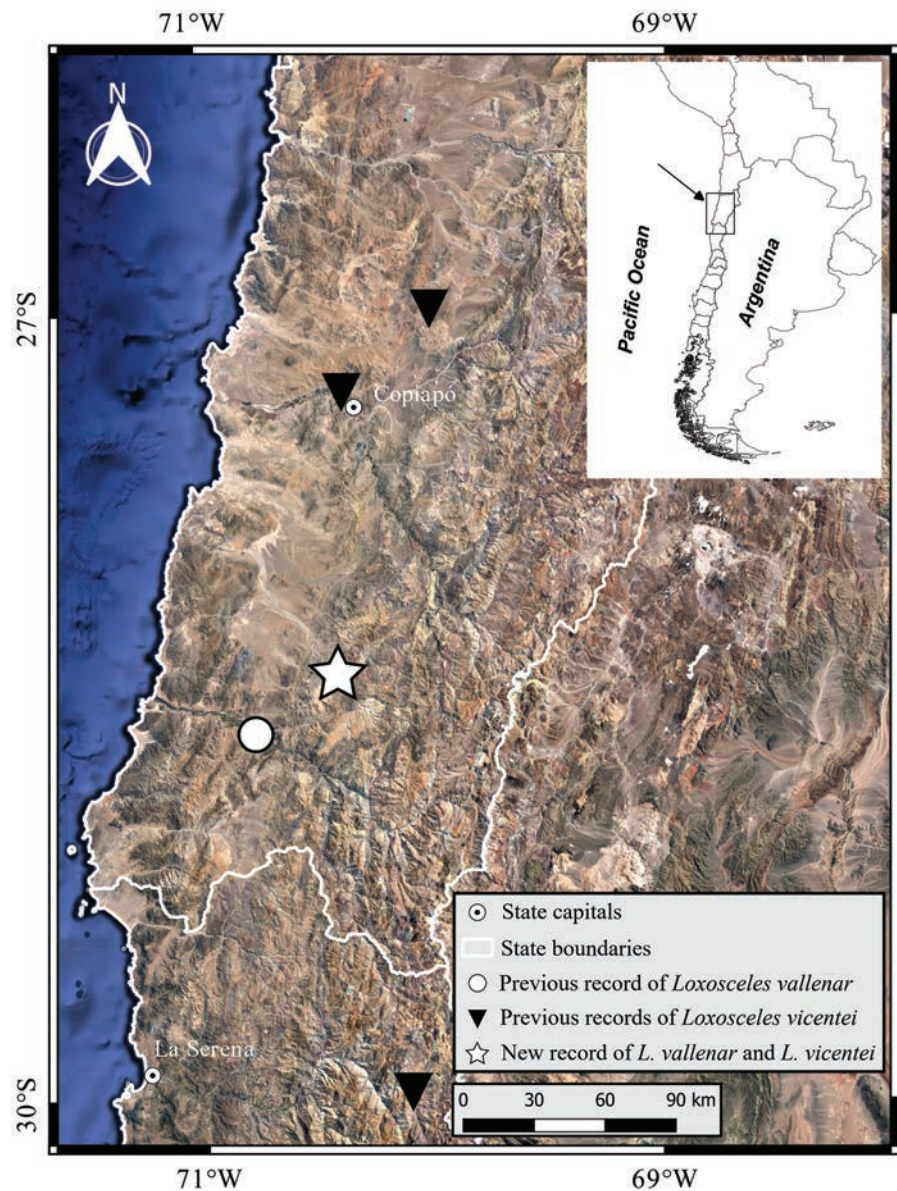


Figure 2. Distribution of *Loxosceles vallenar* and *Loxosceles vicentei*. The star represents a new record for both species in the same locality.

groups, as the newly discovered specimen does not present characters consistent with the *laeta* species group. Finally, we report sexually dimorphic characters that had not been previously described in *Loxosceles*.

Material and methods

Fieldwork

Specimen collection was performed during November 2023 (late spring) in several places of Quebrada Algarrobal, near Boquerón Chañar, in the Atacama region. The specimens were manually collected by searching on the ground at night using a headlight. Photographs of the live specimens were taken with an Olympus Tough TG-5 digital camera.

Microscopy

Endogynes were examined in lactic acid after digestion using pancreatin solution (Álvarez-Padilla and Hormiga 2008). Images of the holotype were taken with a Leica DM4000B Microscope and a Leica M205C stereomicroscope at Instituto Butantan, São Paulo. For other specimens, images in multiple focal planes were taken with a Leica M205C stereomicroscope or an Olympus BH2 compound microscope in Museo Argentino de Ciencias Naturales Bernardino Rivadavia (MACN), Buenos Aires, and then combined with Helicon Focus 7 (HeliconSoft, Kharkiv, Ukraine); a camera lucida was used to make a schematic drawing. Material for scanning electron microscopy was dried in a series of ethanol solutions of increasing concentrations, with a final step of reagent-grade, pure hexamethyldisilazane (Sigma-Aldrich), and then air-dried. Samples were mounted on aluminum stubs and sputter coated with gold-palladium, and then examined under a high vacuum with a Zeiss GeminiSEM 360 scanning electron microscope in MACN.

Description

The format of the description follows Brescovit et al. (2017), with slight modifications; leg measurements are given as total length (femur, patella, tibia, metatarsus and tarsus lengths). Descriptions and lists of examined material were prepared using automated spreadsheets (Magalhaes 2019). Specimens whose geographical coordinates are placed between square brackets were georeferenced by us using Google Earth (Google, Mountain View, USA); coordinates placed between parentheses represent those on the original labels. Geographic coordinates of the collecting sites were recorded using a GPS Garmin eTrex, Vista C. The distribution map was generated using QGIS 3.22.10-Białowieża (distributed under the GNU General Public License, www.gnu.org/licenses) using Land-Sat satellite images (Chávez 1996; Chander and Markham 2003) and supporting cartography from the Instituto Geográfico Militar at a scale of 1:250,000 (IGM 1986).

Collections

The material studied in this paper is deposited in the American Museum of Natural History, New York, U.S.A. (AMNH; curator L. Prendini) and in the Museo Argentino de Ciencias Naturales “Bernardino Rivadavia”, Buenos Aires, Argentina (MACN-Ar; curator M.J. Ramírez).

Taxonomy

Family Sicariidae Keyserling, 1880

***Loxosceles* Heineken & Lowe, 1832**

The *spadicea* species group

Diagnosis. Small to medium-sized *Loxosceles* (body length 2–8 mm). The carapace may be uniform brown or orange (e.g., *L. vallerar*, *L. hirsuta*, *L. diaguita*;

Fig. 4B) or bear distinctive markings (e.g., *L. vicentei*; Taucare-Ríos et al. 2022, fig. 1), and may be distinctly hirsute. The leg formula is usually 2413, but may be 2143 in some females, and 4213 in some species (*L. vicentei* males and females, *L. vollenar* females). The most distinctive features of the group are in the genitalia: the female genitalia have the receptacles separated by two to several times their width at the base, and the receptacles are short and digitiform, usually bearing a small head (Fig. 5); the uterus externus and the interpulmonary fold are not particularly sclerotized or modified. Male palps have the cymbium short and diamond-shaped (Fig. 6B); the bulb is always globose at the base, and the embolus always bears a keel (“wing or carina” sensu Gertsch 1967) (Figs 7–9, arrows); the embolus may be quite short (Fig. 7) to quite long (Brescovit et al. 2017, fig. 7). The first metatarsi of males are unmodified.

Species included. So far, the group encompasses *L. hirsuta* Mello-Leitão, *L. intermedia* Mello-Leitão, *L. spadicea* Simon, *L. anomala* Mello-Leitão and *L. diaguia*. We argue that, based on the diagnosis above, the following species also belong in the group: *L. vollenar*, *L. coquimbo*, *L. vicentei*, and *L. pallalla*.

***Loxosceles vollenar* Brescovit, Taucare-Ríos, Magalhaes & Santos, 2017**

Figs 3–8

Loxosceles vollenar Brescovit, Taucare-Ríos, Magalhaes & Santos, 2017: 14, fig. 8E.

Holotype (examined). CHILE • 1 ♀; Atacama, Prov. Huasco, Vollenar, 3 km S Vollenar; 460 m.a.s.l. [28.601°S, 70.77°W]; 7 Jan. 1985; N Platnick, O Francke leg.; deposited in AMNH.

New records. CHILE • 1 ♂; Atacama, Prov. Huasco, Boquerón Chañar; Algarrobal; 992 m.a.s.l.; (28.3708°S, 70.4128°W); 24–25 Nov. 2022; J Pizarro-Araya, FM Alfaro, JE Barriga, AA Ojanguren-Affilastro, HA Iuri & JE Calderón leg.; IFM-2580; MACN-Ar 44129 • 1 ♂; same collecting data; MACN-Ar 44130 • 1 ♀; same collecting data; MACN-Ar 44131.

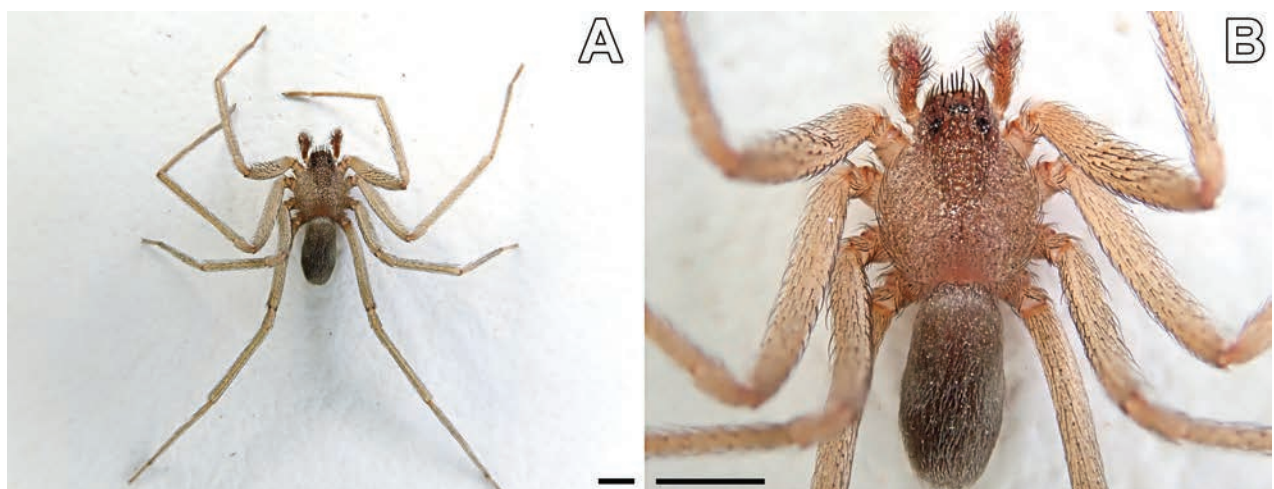


Figure 3. *Loxosceles vollenar*, live male specimen from Boquerón Chañar **A** entire specimen **B** close-up. Notice the clypeal setae. Scale bar: 1 mm.

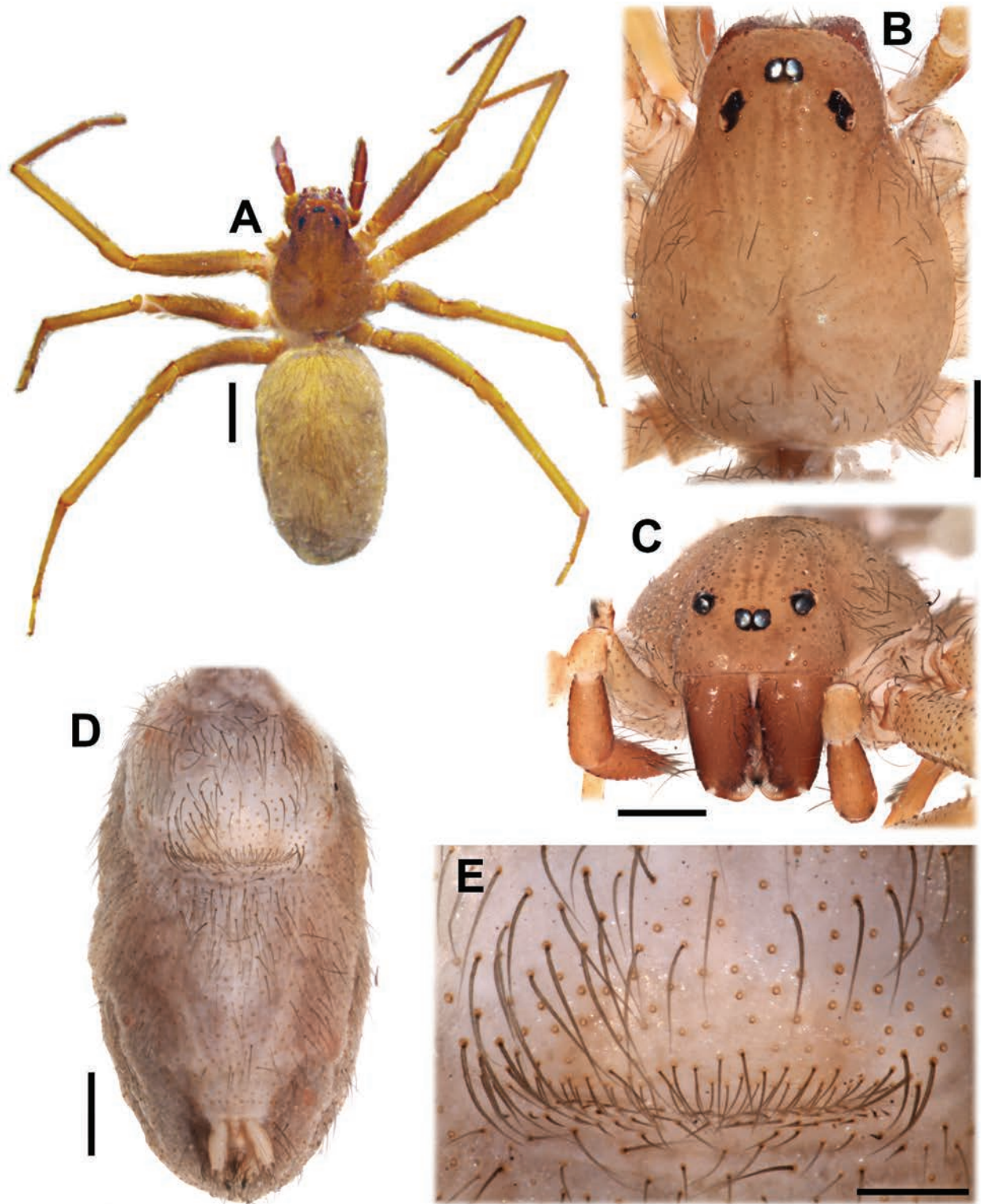


Figure 4. *Loxosceles vallenar* Brescovit, Taucare-Ríos, Magalhaes & Santos, females **A** holotype from Vallenar (AMNH), dorsal **B–E** female from Boquerón Chañar (MACN-Ar 44131) **B** dorsal **C** carapace, anterior **D** abdomen, ventral **E** genital region, ventral. Scale bars: 1000 μm (**A**); 500 μm (**B–D**); 200 μm (**E**).

Remarks. The genitalia of the holotype was incorrectly illustrated by Brescovit et al. (2017), as the digitiform, membranous median receptacles were overlooked. Re-examination of the holotype revealed they are present

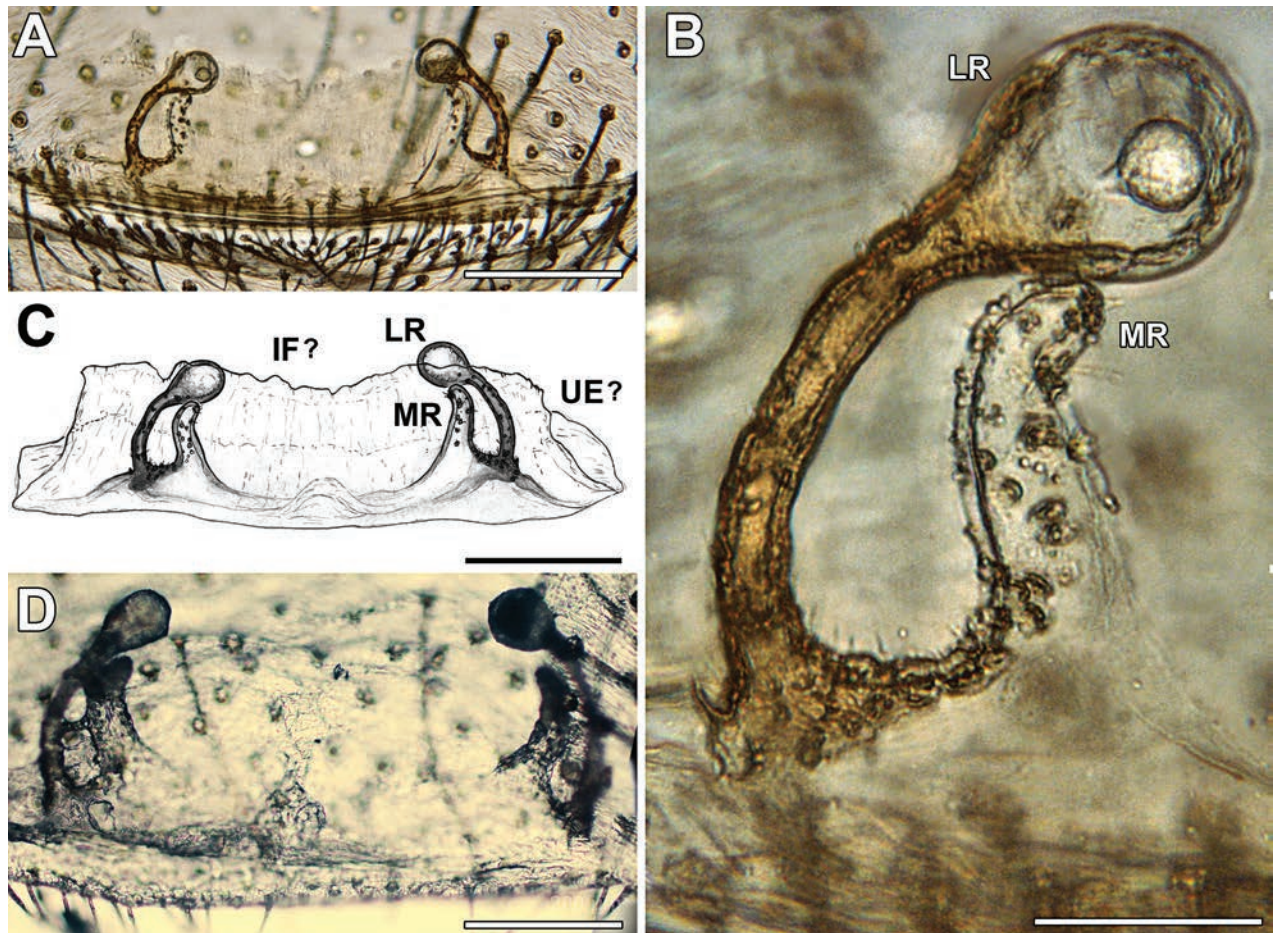


Figure 5. *Loxosceles vallenar*, median and lateral receptacles of the female genitalia **A–C** female from Boquerón Chañar (MACN-Ar 44131) **D** holotype from Vallenar (AMNH). Abbreviations: IF? = putative interpulmonary fold, LR = lateral receptacle, MR = median receptacle, UE? = putative uterus externus; details could not be resolved in light microscopy. Scale bars: 200 µm (**A, C, D**); 50 µm (**B**).

(Fig. 5D). We briefly describe the females collected with the males, especially their endogyne, which is in a better state than that of the holotype. The hitherto undescribed male has a palpal bulb bearing an embolic keel and overall morphology concordant with the *spadicea* species group (Figs 6–8). Thus, the species is moved from the *laeta* species group to the *spadicea* species group.

Diagnosis. Males resemble those of other members of the *spadicea* species group by the subtriangular cymbium in dorsal view (Fig. 6B) and embolus bearing a keel (Fig. 7C), but can be distinguished by the clypeus bearing macrosetae (Figs 3, 6A–C) (vs. clypeus without macrosetae) and by the more piriform, tapering copulatory bulb (Fig. 7B) (vs. bulb clearly globose; Gertsch 1967, figs 1, 4, 9). Females resemble those of other members of the *spadicea* species group by the short and digitiform median receptacle, but differ by the inwards curved base of the lateral receptacle (Fig. 5) (vs. base of the lateral receptacle sinuous to convoluted; Gertsch 1967, figs 11–14).

Description. Male from Boquerón Chañar, Atacama, Chile (MACN-Ar 44130). **Coloration in ethanol** (Fig. 6A). Carapace yellowish-brown with slightly darker pars cephalica, eyes surrounded by black pigment rings. Chelicerae orange brown. Labium light brown. Endites brownish-cream at base, darker

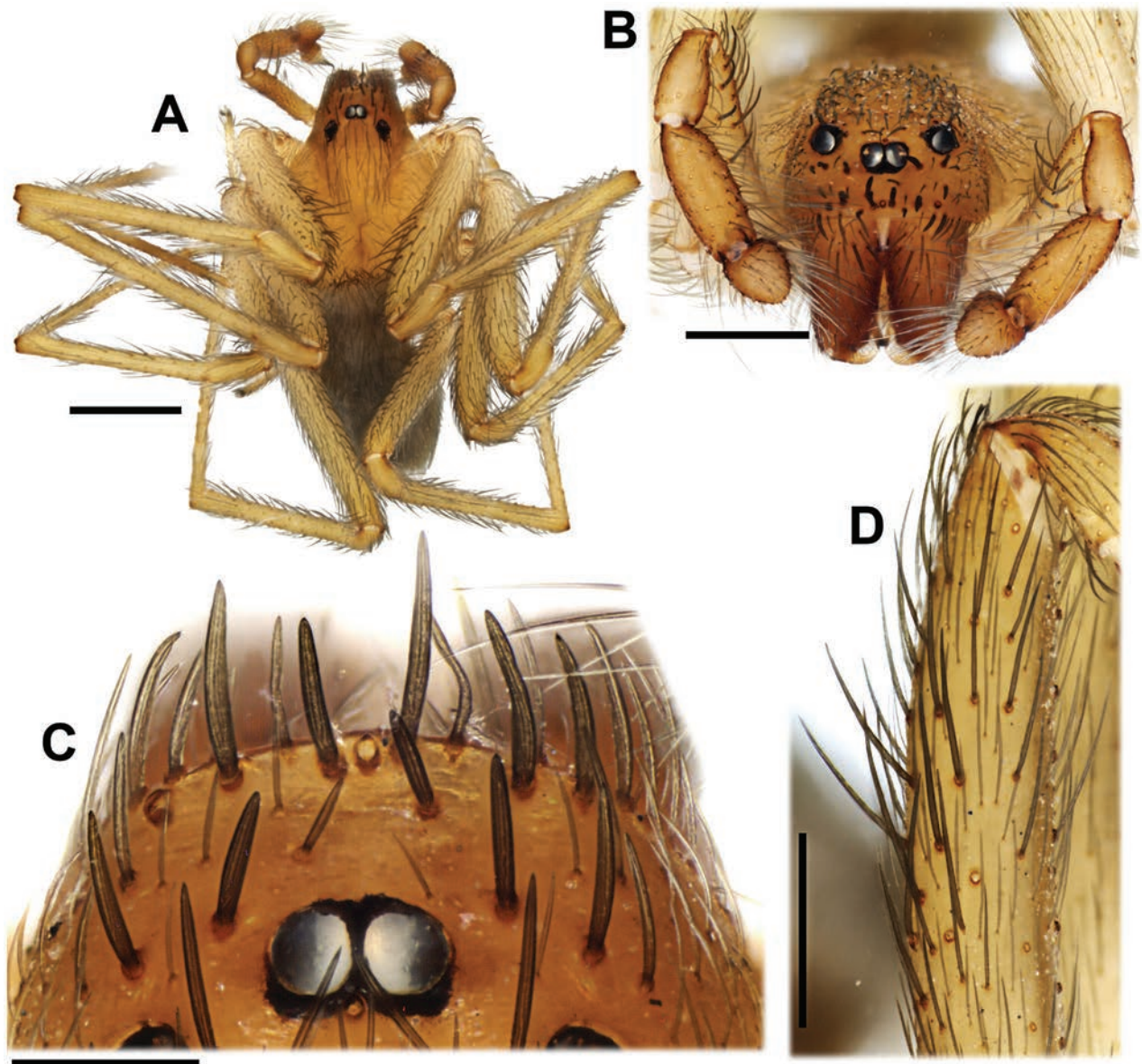


Figure 6. *Loxosceles vallerar*, male from Boquerón Chañar (MACN-Ar 44130) **A** habitus, dorsal **B** clypeus, anterior **C** clypeus, dorsal **D** left femur I, prolateral. Scale bars: 1000 μm (**A**); 500 μm (**B**, **D**); 200 μm (**C**).

at median third, whitish at tip. Palps yellowish-brown, tarsus darkest. Sternum brownish-cream. Legs uniformly light brown. Opisthosoma uniformly brownish-gray. **Measurements.** Total length 3.62. Carapace length 1.92, width 1.48. Clypeus height 0.23. Eye diameters and interdistances: ALE 0.11, PLE 0.12, PME 0.10, ALE–PME 0.13. Sternum length 1.13, width 0.95. Palp: femur length 1.08, height 0.18, tibia length 0.60, height 0.25, tarsus length 0.27. Leg I 8.6 (2.38, 0.58, 2.43, 2.38, 0.83). Leg II 10.11 (2.82, 0.59, 3.03, 2.84, 0.83). Leg III 7.53 (2.23, 0.57, 1.95, 2.14, 0.64). Leg IV 9.88 (2.82, 0.58, 2.75, 2.96, 0.77). Leg formula 2413. Abdomen: length 1.67, width 1.08. Femur I with ~17 prolateral macrosetae in a subdistal patch (Fig. 6D). Metatarsus I unmodified. Clypeus with ~20 macrosetae (Fig. 6C). **Male genitalia** (Figs 7, 8). Palpal femur with 5 prolateral macrosetae in apical third, tibia slightly swollen, with two pronounced condyles apically, cymbium short and subtriangular in dorsal

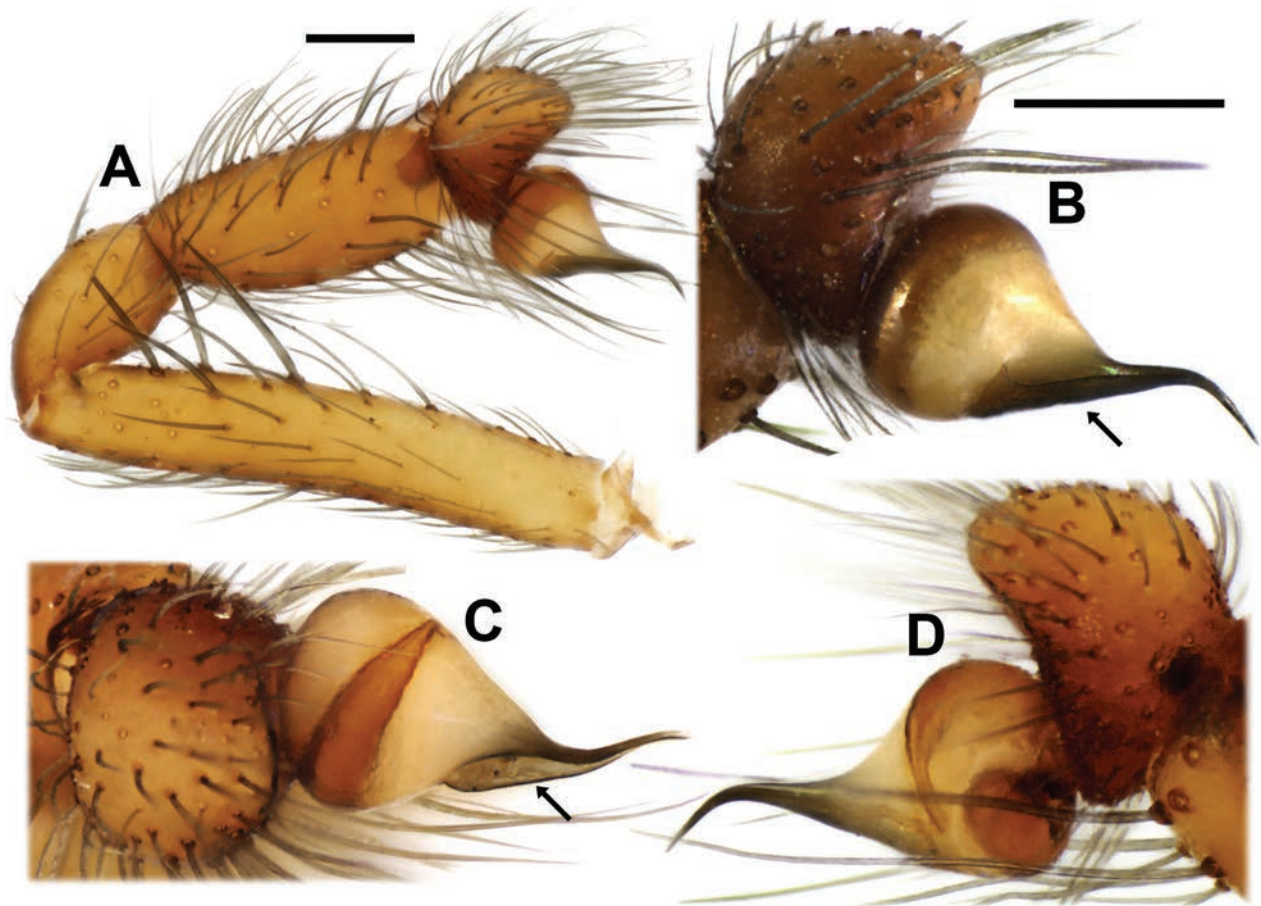


Figure 7. *Loxosceles vallenar*, males from Boquerón Chañar (MACN-Ar 44130) (except B, MACN-Ar 44129, dry specimen before sputter-coating), left palps **A, B** prolateral **C** dorsal **D** retrolateral. Arrows indicate embolic keel. Scale bars: 200 μ m (**B–D** to the same scale).

view, bulb short and rounded, embolus curved and tapering retrolaterally, with a prolateral keel, without micro-spines (Fig. 8). State of the specimen: good; left palp dissected.

Female from Boquerón Chañar, Atacama, Chile (MACN-Ar 44131). Coloration and general structure as in the holotype (Fig. 4). Carapace length 2.20, width 1.68. Genital region externally pubescent but without stronger sclerotization (Fig. 4E). **Endogyne** (Fig. 5). Median receptacle digitiform, slightly sinuous and lightly sclerotized, bearing glandular pores throughout. Lateral receptacle with thin, sclerotized and arched base bearing glandular pores, leading to a rounded, unsclerotized head lacking pores; fold (presumably uterus externus and/or interpulmonary fold) short and membranous. State of the specimen: good; endogyne dissected.

Variation. The two males and two females examined have seemingly identical genitalia. Two males: total length 3.62 to 3.74; carapace length 1.92 to 1.97; tibia I length 2.43 to 2.73. Both females have a carapace length of 2.2 and vary in total length from 5.53 to 6.00.

Natural history. The label data indicates that the holotype was collected “in scrubby mountain-side, under rocks”. The specimens from Boquerón Chañar were collected at night, searching with headlights. The male specimens were actively walking on the ground.

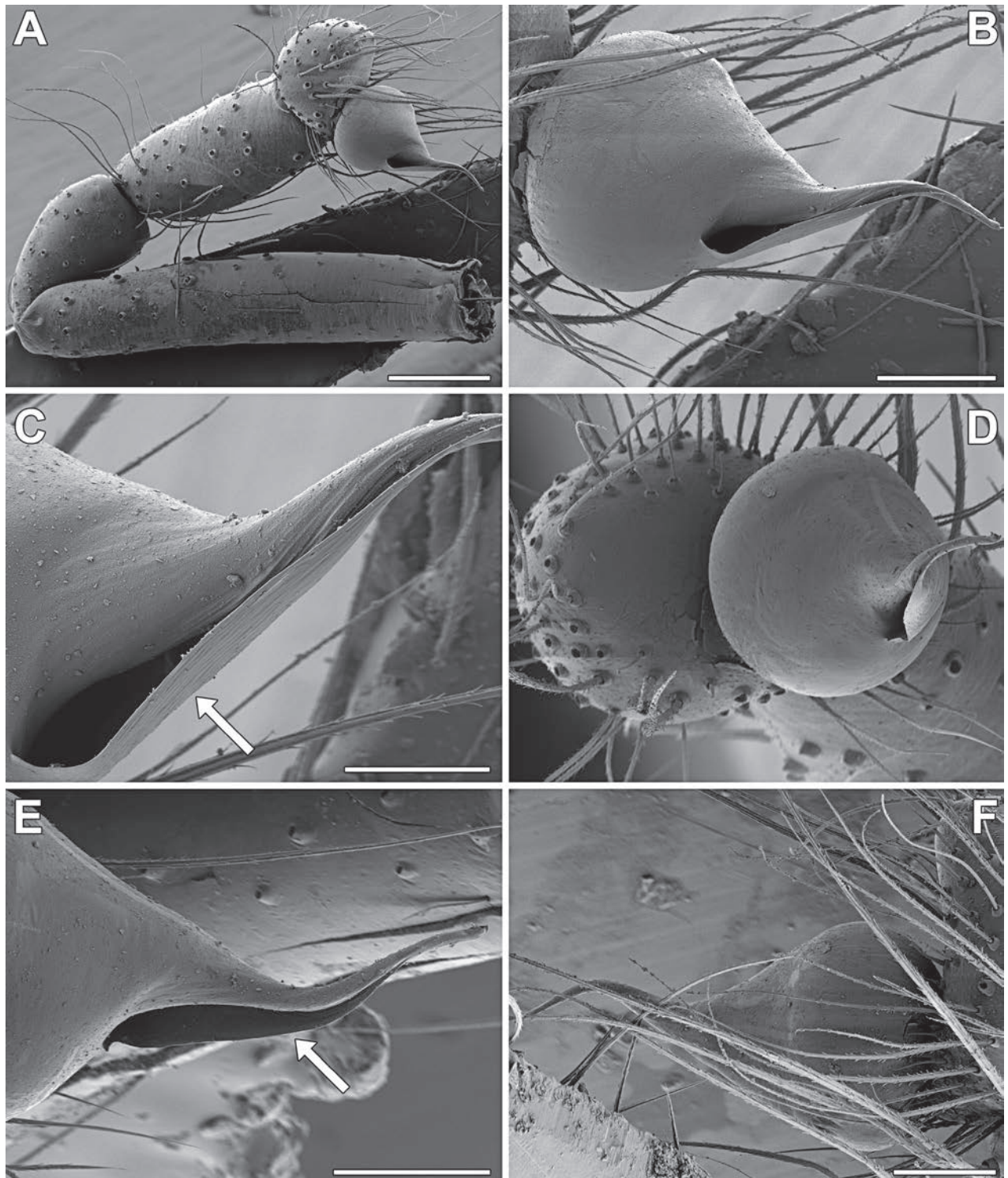


Figure 8. *Loxosceles vallenar*, male left palp (MACN-Ar 44129) under scanning electron microscopy **A** prolateral **B** bulb, prolateral **C** detail of embolic keel **D** bulb, apical **E** bulb, dorsal **F** bulb, retrolateral. Arrows indicate embolic keel. Scale bars: 200 μm (**A**); 100 μm (**B, E, F**); 50 μm (**C**).

Habitat. Specimens of *Loxosceles vallenar* and *L. vicentei* were collected in vegetation zones characterized by an inland Mediterranean-desert shrubland of *Adesmia argentea* Meyen and *Bulnesia chilensis* Gay (Luebert and Plischoff 2006). These areas are defined by an extremely open shrubland with tall shrubs and the

presence of tree species. Shrubs include *A. argentea*, *Bulnesia chilensis*, *Balsamocarpon brevifolium* Clos, *Cordia decandra* Hook. & Arn., *Heliotropium sinuatum* (Miers) I.M. Johnston, *Pintoa chilensis* Gay, and *Proustia ilicifolia* Hook. & Arn. Additionally, low shrubs such as *Caesalpinia angulata* (Hook. & Arn.) Baill., *Encelia canescens* Lam., *Pleurophora pungens* D. Don, and cacti like *Cumulopuntia sphaerica* (C.F. Först.) E.F. Anderson and *Trichocereus coquimbanus* (Molina) Britton and Rose are common. Herbaceous plants abound during the rainy season, including species like *Cruckshanksia pumila* Clos and *Argyria irradian* (L.) D. Don. This entire environment is dominated by trees such as *Neltuma chilensis* (Molina) Hughes & Lewis, *Geoffroea decorticans* (Gillies ex Hook. & Arn.) Burkart, *Acacia caven* (Molina) Molina, and *Schinus polygama* (Cav.) Cabrera (Luebert and Pliscoff 2006) (Fig. 1). The climate in the area is semiarid subtropical Mediterranean in the northern margin and marine subtropical Mediterranean in the southern margin (Novoa and Villaseca 1989). The total precipitation recorded in the study area (Vallenar Station, 28°33'6.11"S, 70°47'25.92"W, 421 m.a.s.l.) in 2022 was 83.8 mm and was concentrated in July (66.5 mm) and June (4.9 mm) (CEAZA-Met 2024).

Distribution. Originally described from Vallenar, the new record extends the distribution of the species about 40 km northeastward. Both points are in Huasco Province, Atacama region, Chile (Fig. 2).

***Loxosceles vicentei* Taucare-Ríos, Brescovit & Villablanca, 2022**

Fig. 9

Loxosceles vicentei Taucare-Ríos, Brescovit & Villablanca, 2022: 158, figs 1A–B, 2A–D, 4A–B.

Holotype (not examined). CHILE • 1 ♂; Coquimbo, Elqui Prov., Vicuña, Fondo El Calvario, near Juntas del Toro, 29°58'30.97"S, 70°6'11.86"W, 2050 m.a.s.l., 14 Oct. 2021, V Villablanca Miranda, J Villablanca Rivera & A Taucare-Ríos leg.; Museo Nacional de Historia Natural, Santiago, CHILE, MNNC 8371.

New record. CHILE • 1 ♂; Atacama, Prov. Huasco, Boquerón Chañar; Algarrobal; 992 m.a.s.l., (28.3708°S, 70.4128°W); 24–25 Nov. 2022; J Pizarro-Araya, FM Alfaro, JE Barriga, AA Ojanguren-Affilastro, HA Iuri & JE Calderón leg.; IFM-2579; MACN-Ar 44128.

Remarks. The new record is about 183 km north of the type locality of *L. vicentei*, but within the distribution of this species presented by Taucare-Ríos et al. (2022). The embolic keel we observed in our specimens (Fig. 9, arrows) was not mentioned in the original description of the species but can nonetheless be seen in their figures (Taucare-Ríos et al. 2022, fig. 2A). The holotype has a slightly longer embolus and a seemingly larger keel; a larger series of specimens must be examined to evaluate the significance of these morphological differences. The presence of an embolic keel, allied with the digitiform median receptacles of the female (Taucare-Ríos et al. 2022, fig. 2D), hints that *L. vicentei* belongs in the *spadicea* species group, rather than in the *laeta* species group. Taucare-Ríos et al. (2022) present a map with four records, but their list of material examined indicated only three localities; the fourth record had been included by mistake (A. Taucare-Ríos, in litt.), and thus, we omit it in our map.

Habitat. See remarks under *L. vollenar* above.

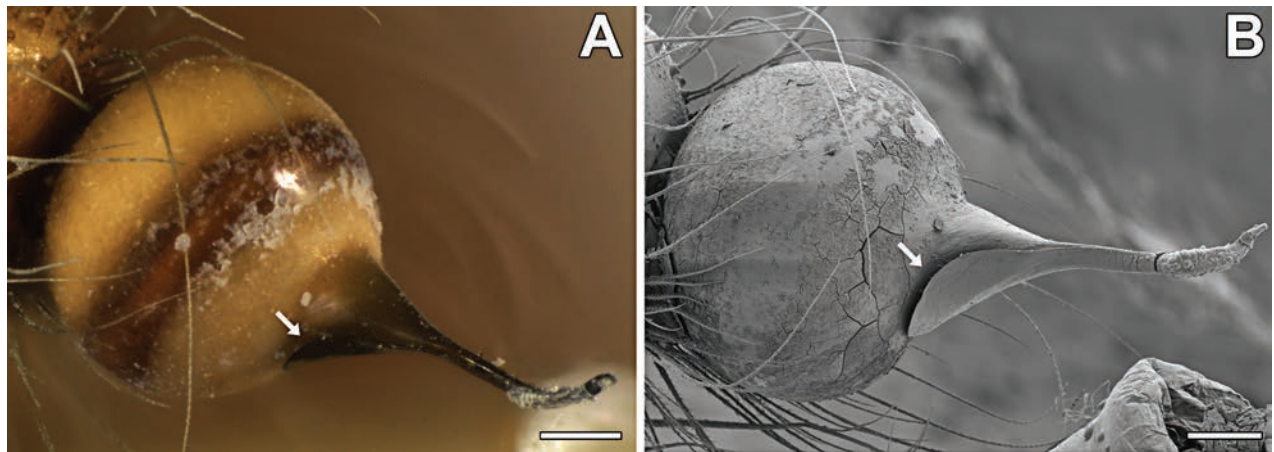


Figure 9. *Loxosceles vicentei* Taucare-Ríos, Brescovit & Villablanca, 2022, male from Boquerón Chañar (MACN-Ar 44128), left bulb, prolateral, in light (A) and scanning electron microscopy (B). Arrows indicate embolic keel. Scale bars: 100 μ m.

Discussion

The newly described male indicates that *Loxosceles vallenar* is the smallest species among violin spiders. With a carapace length between 1.92 and 1.97, males are smaller than those of *Loxosceles dejagerae* Lotz, 2017 from South Africa (carapace lengths of 2.0–3.2; see Lotz 2017: 478), the previously smallest representative. Some other members of the *spadicea* group are also small, such as *L. spadicea* and *L. hirsuta* (carapace length 2.5; see Gertsch 1967).

The male of *Loxosceles vallenar* presents a secondary sexual character that has not been previously reported in the genus: a group of strong macrosetae in the clypeus. Secondary sexual characters in *Loxosceles* males are rare and usually associated with the legs, such as sinuous tibiae or metatarsi (see Brescovit et al. 2017; Bertani et al. 2018) or the presence of sexually dimorphic macrosetae patches (Bertani et al. 2018; Magalhaes et al. 2022). *Loxosceles vallenar* males also present a prolateral patch of macrosetae in the first femur. Presumably, some of these modifications of the legs may serve as clasping spurs during mating; for instance, *L. laeta* males grab the female coxae with their first legs during courtship and mating (Fischer 2007). This behavior is absent in *L. hirsuta* and *L. intermedia* (Fischer and Vasconellos-Neto 2000; Fischer and Silva 2001), whose males have unmodified legs. In these two species, however, males and females touch pedipalps during courtship, a very unusual behavior; we wonder if their embolic keel (see Gertsch 1967, fig. 3) plays a role in this. Regarding the clypeal macrosetae, several other Synspermiata (the clade where Sicariidae belongs) have males with modified clypei, such as *Relictocera* Li & Li (Psilodercidae), *Unicorn* Platnick & Brescovit (Oonopidae) and *Perania* Thorell (Pacullidae) (Lehtinen 1981; Platnick and Brescovit 1995; Chang et al. 2019). In most Synspermiata, the male faces the underside of the female during palpal insertions (see Fischer 2007). In this position, such clypeal modifications may help locking or stimulating the underside of the female. It remains to be tested if this is the case in *L. vallenar*.

We argue that *L. vallenar* and *L. vicentei* belong in the *spadicea* species group rather than in the *laeta* species group. Additionally, we re-examined the male of *Loxosceles coquimbo* described by Brescovit et al. (2017), revealing that its palpal bulb also bears an embolic keel, albeit small (Brescovit et al. 2017, fig.

2B). Together with the similar structure of the endogyne of *L. coquimbo* and *L. vicentei*, this suggests that the former also belongs in the *spadicea* species group. This indicates that the *spadicea* species group has diversified on both sides of the Andes: in Chile, it includes *L. diagueta*, *L. vollenar*, *L. coquimbo*, *L. vicentei*, and *L. pallalla*, which also possesses an embolic keel. East of the Andes, it includes *L. hirsuta*, *L. intermedia*, *L. spadicea* and *L. anomala*. The *laeta* group is thus represented in Chile only by two species: *L. surca* Gertsch, which occurs in Andean areas in the north of the country, and the synanthropic *L. laeta*.

Acknowledgments

We thank Lorenzo Prendini and Lou Sorkin (AMNH) for loan of specimens from the collection under their care. Fabián Tricárico aided in obtaining SEM images. We are indebted to Juan E. Barriga-Tuñón, Andres A. Ojanguren-Afilastro, Fermín M. Alfaro, and Juan E. Calderon for their assistance in the field. J.P-A thanks the Academic Excellence Scholarship (B134) from the Academic Vice-Rector's Office, Research and Postgraduate Studies of Universidad Santo Tomás, Santiago, Chile, and ANID doctoral fellowship 2024 (2024-21241400). Collecting permits were issued by Sistema de Monitoreo de Ecosistemas Forestales Nativos de Chile (SIMEF).

Additional information

Conflict of interest

The authors have declared that no competing interests exist.

Ethical statement

No ethical statement was reported.

Funding

This research was funded by Agencia Nacional de Promoción de la Investigación, el Desarrollo Tecnológico y la Innovación (PICT 2020-1907; ILFM), Consejo Nacional de Investigaciones Científicas y Técnicas (PUE-098; MACN), Conselho Nacional de Desenvolvimento Científico e Tecnológico (PQ 303903/2019-8; ADB), Fundação de Amparo à Pesquisa do Estado de São Paulo (2022/12588-1; ADB), DIDULS PR232128 and DIDULS PEQMEN212124 projects of Universidad de La Serena, La Serena, Chile, and through funding by the Ministry of Education of Chile, through MINEDUC's performance agreement: "Implementation of a competitive model of innovation and creation: preparing the University of La Serena for 2030, ULS19101", and to the project Climate Change and Sustainability in Coastal Zones of Chile (PFUE-RED21992) of the Ministry of Education of Chile.

Author contributions

Conceptualization: ILFM; Methodology: all authors; Formal analysis: ILFM; Investigation: all authors; Data Curation: ILFM; Writing – Original draft: all authors; Writing – Review and Editing: all authors; Funding Acquisition: ILFM, JPA.

Author ORCIDs

Ivan L. F. Magalhaes  <https://orcid.org/0000-0003-3728-3270>

Hernán A. Iuri  <https://orcid.org/0000-0002-8094-9157>

Antonio D. Brescovit  <https://orcid.org/0000-0002-1511-5324>

Jaime Pizarro-Araya  <https://orcid.org/0000-0002-1595-6924>

Data availability

All of the data that support the findings of this study are available in the main text.

References

- Álvarez-Padilla F, Hormiga G (2008) A protocol for digesting internal soft tissues and mounting spiders for scanning electron microscopy. *The Journal of Arachnology* 35(3): 538–542. <https://doi.org/10.1636/Sh06-55.1>
- Bertani R, Von Schimonsky DM, Gallão JE, Bichuette ME (2018) Four new troglomorphic species of *Loxosceles* Heineken & Lowe, 1832: Contributions to the knowledge of recluse spiders from Brazilian caves (Araneae, Sicariidae). *ZooKeys* 806: 47–72. <https://doi.org/10.3897/zookeys.806.27404>
- Binford GJ, Callahan MS, Bodner MR, Rynerson MR, Núñez PB, Ellison CE, Duncan RP (2008) Phylogenetic relationships of *Loxosceles* and *Sicarius* spiders are consistent with Western Gondwanan vicariance. *Molecular Phylogenetics and Evolution* 49(2): 538–553. <https://doi.org/10.1016/j.ympev.2008.08.003>
- Brescovit AD, Sánchez-Ruiz A (2016) Descriptions of two new genera of the spider family Caponiidae (Arachnida, Araneae) and an update of *Tisentnops* and *Taintnops* from Brazil and Chile. *ZooKeys* 622: 47–84. <https://doi.org/10.3897/zookeys.622.8682>
- Brescovit AD, Taucare-Ríos A, Magalhaes ILF, Santos AJ (2017) On Chilean *Loxosceles* (Araneae: Sicariidae): first description of the males of *L. surca* and *L. coquimbo*, new records of *L. laeta* and three remarkable new species from coastal deserts. *European Journal of Taxonomy* 388: 1–20. <https://doi.org/10.5852/ejt.2017.388>
- Bustamante AA, Scioscia CL, Casanueva ME (2014) A new species of *Admesturius* Galiano, 1988 from north Chile (Araneae: Salticidae: Amycoidea). *Zootaxa* 3774: 197–200. <https://doi.org/10.11646/zootaxa.3774.2.7>
- CEAZA-Met (2024) CEAZA-Met. <https://www.ceazamet.cl/> [Accessed on 26 April 2024]
- Chander G, Markham BL (2003) Revised Landsat 5 TM radiometric calibration procedures and post-calibration dynamic ranges. *IEEE Transactions on Geoscience and Remote Sensing* 41(11): 2674–2677. <https://doi.org/10.1109/TGRS.2003.818464>
- Chang W-J, Li F, Li S (2019) On the genera *Qiongocera* and *Relictocera* (Araneae, Psilodercidae) from Southeast Asia. *ZooKeys* 862: 61–79. <https://doi.org/10.3897/zookeys.862.33078>
- Chávez PS (1996) Image-based atmospheric corrections-revisited and improved. *Photogrammetric Engineering and Remote Sensing* 62(9): 1025–1036.
- Fischer ML (2007) Comportamento sexual de *Loxosceles laeta* (Nicolet) (Araneae, Sicariidae): Influência da idade da fêmea. *Revista Brasileira de Zoologia* 24(4): 865–872. <https://doi.org/10.1590/S0101-81752007000400002>
- Fischer ML, Silva EM (2001) Comportamento sexual de *Loxosceles hirsuta* Mello-Leitão, 1931 (Araneae: Sicariidae). *Estudos de Biologia* 47: 7–14.
- Fischer ML, Vasconcellos-Neto J (2000) Comportamento sexual de *Loxosceles intermedia* Mello-Leitão, 1934 (Araneae, Sicariidae). *Revista de Etologia* 2: 31–42.
- Gertsch WJ (1967) The spider genus *Loxosceles* in South America. *Bulletin of the American Museum of Natural History* 136: 121–182. <https://doi.org/10.1038/113141b0>
- Griotti M, Grismado CJ, Roig-Juñent S, Ramírez MJ (2022) Taxonomy and phylogenetic analysis of the South American genus *Petrichus* Simon (Araneae: Philodromidae)

- provide new insights into the running crab spiders' phylogeny. *Invertebrate Systematics* 36(4): 306–353. <https://doi.org/10.1071/IS21068>
- Grismado CJ, Pizarro-Araya J (2016) The spider genus *Cyrioctea* Simon on Chañaral Island (Pinguino de Humboldt National Reserve, Atacama, Chile): Description of a new species, and the male of *Cyrioctea cruz* Platnick (Araneae, Zodariidae). *Zootaxa* 4107(2): 267–276. <https://doi.org/10.11646/zootaxa.4107.2.8>
- IGM (1986) *Cartas de Región de Coquimbo y Región de Atacama*. 1:250.000. Santiago de Chile. Instituto Geográfico Militar de Chile. <https://www.igm.cl/?page=descargas-gratuitas-igm> [Last accessed in 25/04/2024]
- Keyserling E (1880) *Die Spinnen Amerikas. Laterigradae*. [Erster Band]. Bauer & Raspe, Nürnberg, 283 pp. [pl. 1–8] <https://doi.org/10.5962/bhl.title.64832>
- Laborda Á, Ramírez MJ, Pizarro-Araya J (2013) New species of the spider genera *Aysenia* and *Aysenoides* from Chile and Argentina: description and phylogenetic relationships (Araneae: Anyphaenidae, Amaurobioidinae). *Zootaxa* 3731(1): 133–152. <https://doi.org/10.11646/zootaxa.3731.1.6>
- Lehtinen PT (1981) Spiders of the Oriental-Australian region. III. Tetrablemmidae, with a world revision. *Acta Zoologica Fennica* 162: 1–151.
- Lotz LN (2017) An update on the spider genus *Loxosceles* (Araneae: Sicariidae) in the Afrotropical region, with description of seven new species. *Zootaxa* 4341(4): 475–494. <https://doi.org/10.11646/Zootaxa.4341.4.2>
- Lowe RT (1832) Descriptions of two species of Araneidae, natives of Madeira. *The Zoological Journal* 5(19, 1831): 320–323. [pl. 17–18]
- Luebert F, Pliscoff P (2006) *Sinopsis Bioclimática y Vegetacional de Chile*. Editorial Universitaria, Santiago, Chile, 316 pp.
- Magalhaes ILF (2019) Spreadsheets to expedite taxonomic publications by automatic generation of morphological descriptions and specimen lists. *Zootaxa* 4624(1): 147–150. <https://doi.org/10.11646/zootaxa.4624.1.12>
- Magalhaes ILF, Neves DM, Santos FR, Vidigal THDA, Brescovit AD, Santos AJ (2019) Phylogeny of Neotropical *Sicarius* sand spiders suggests frequent transitions from deserts to dry forests despite antique, broad-scale niche conservatism. *Molecular Phylogenetics and Evolution* 140: 106569. <https://doi.org/10.1016/j.ympev.2019.106569>
- Magalhaes ILF, Pérez-González A, Labarque FM, Carboni M, Hammel JU, Kunz R, Ramírez MJ, Solórzano-Kraemer MM (2022) Revision of recluse spiders (Araneae: Sicariidae: *Loxosceles*) preserved in Dominican amber and a total evidence phylogeny of Scytodoidea reveal the first fossil Drymusidae. *Arthropod Systematics & Phylogeny* 80: 541–559. <https://doi.org/10.3897/asp.80.e86008>
- Mittermeier RA, Turner WR, Larsen FW, Brooks TM, Gascon C (2011) Global biodiversity conservation: the critical role of hotspots. In: Zachos F, Habel J (Eds) *Biodiversity Hotspots*. Springer, Berlin, Heidelberg, 3–22. https://doi.org/10.1007/978-3-642-20992-5_1
- Myers N, Mittermeier RA, Mittermeier CG, Fonseca GA, Kent J (2000) Biodiversity hotspots for conservation priorities. *Nature* 403(6772): 853–858. <https://doi.org/10.1038/35002501>
- Nicolet H (1849) *Arácnidos*. In: Gay C (Ed.) *Historia física y política de Chile*. *Zoología* 3: 319–543. [pl. 1–5. Paris, Thunot]
- Novoa SA, Villaseca S (1989) *Mapa agroclimático de Chile* Investigaciones Agropecuarias. INIA, Santiago, Chile, 216 pp.
- Platnick NI, Brescovit AD (1995) On *Unicorn*, a new genus of the spider family Oonopidae (Araneae, Dysderoidea). *American Museum Novitates*. American Museum Novitates 3152: 1–12.

- Schenone H, Saavedra T, Rojas A, Villaroel F (1989) Loxoscelismo en Chile: Estudios epidemiológicos, clínicos y experimentales. *Revista do Instituto de Medicina Tropical de São Paulo* 31(6): 403–415. <https://doi.org/10.1590/S0036-46651989000600007>
- Taucare-Ríos A, Brescovit AD, Villablanca J (2022) A new species of *Loxosceles* Heineken & Lowe, 1832 (Araneae: Sicariidae) from Chile. *Revista Chilena de Entomología* 48(1): 157–164. <https://doi.org/10.35249/rche.48.1.22.15>
- Vergara-Asenjo G, Alfaro FM, Pizarro-Araya J (2023) Linnean and Wallacean shortfalls in the knowledge of arthropod species in Chile: Challenges and implications for regional conservation. *Biological Conservation* 281: 110027. <https://doi.org/10.1016/j.biocon.2023.110027>
- World Spider Catalog (2024) World Spider Catalog. Version 25.0. Natural History Museum Bern. <https://doi.org/10.24436/2> [Accessed on 09 February 2024]